TRANSFER OF CHIRALITY FROM AMPHIPHILES INTO MATERIALS

Wojciech Jakub Saletra

Doctoral Thesis

Programa de doctorat en Quimica

Supervised by:
Prof. David B.Amabilino
Institut de Ciència de Materials de Barcelona (CSIC)

Departament de Química
Facultat de Ciències
Universitat Autònoma de Barcelona

2013

Memòria presentada per aspirar al Grau de Doctor per Wojciech Jakub Saletra

Vist i plau,

El Director
David B. Amabilino

Tutor:
Rosa Maria Ortuño Mingarro

Bellaterra 13/06/2013

Acknowledgments

I would like to thank Prof. David Amabilino for his time and support, his patience, that he was always geyser of great ideas, even when the things were not looking clear to me. I need to acknowledge him for the time he spent the correcting and guiding my work during my PhD time at ICMAB.

I would like to thank the Marie Curie Research Training Network "CHEXTAN" for the financial support, which gave me insight how about an European collaboration project is working, the Spanish Ministry of Science for JAE-predoc fellowship and mobility grant - Estancias Breves, and the Marie Curie 7th Framework – project "RESOLVE".

I would like to thank all of the people from Prof. David Amabilino's Group. Firstly, to Patrizia Iavicoli that guided me in my first days in the lab, Lise Feldborg with whom I shared the desk in my first weeks at ICMAB, Josep Puigmarti with whom we made a side project about porphyrins studied with STM. Francois, Mathieu, Krycha, Filippo, Marta, Angela, Maggie and Arantzazu for sharing lab and group seminars. I would like to thank also the people from Prof. Jaume Veciana's group that in the very beginning of my thesis we were part of, and whit whom we shared the laboratory: Amable – supertechnician, Evelyn, Claudia, Ingrid, Judit, Javi, Lurdes, Nuria, Victor, Pepe, Raphael, Paco, Javi, Witek, Cesar, Elisa and all the others. The collegues from the office: Markos (great cyclist), Luis, Marysia, Magda, Dani, Queralt that made a good environment to share and work.

There is a group of people in ICMAB that contributed in this thesis: RobertaCeravola for measuring samples in DSC and Anna Crespi for X-ray diffractionmeasuments

I would like to thank also all the people that helped me during my stays abroad:

- Group of Prof. Steven de Feyter in Katholieke Universiteit Leuven: Hong Xu that assisted me in my first days with STM measurments and taught me the technique and for their help and support with measurments. Tatiana, Elke, Kunal, Inge and all the other people that helped me during my days in Leuven.
- Group of Prof. Roberto Lazzaroni in University of Mons: Andrea Minoia that was my teacher of modeling and spent a lot of time explaining me how to

perform a properly simulation. Bernard van Averbeke for performing missing dynamics. Mike, Stavros and Juan and all the other people there for their companion during winter days of 2009.

- SYNCOM B.V. from Gronigen the Netherlands, where I had a practice in efficient synthesis and they performed most of the HPLC analysis included in this thesis. So excellent group of people there: Maarten, Wolter, Richard Kellog and many others.
- Prof.Albert Schenning and Floris Helmich for their help in CD measurments and Jian Bin Lin for the HPLC resolution experiment.
- Prof. Judit Telegdi for her warm reception during my stay in Hungarian Academy of Science, working with Langmuir-Bloddget films. The results were not included in this thesis, but I learned a lot from this stay.
- Last but not least Prof. Jordi Esquena from CID-CSIC in Barcelona (this one not abroad), for his patience in explaining me details of SAXS and WAXS measurements and Maria for helping me in the preparation of the samples and and developing the measurements.

Personally I would like to thank all of the people that helped me during those days in ICMAB: Carme Gimeno, Vicente, Mariona, Maria, Piedad, Trini and all the others that I could always ask in case of problems with daylife and smaller bureaucratic issues.

I would like to thantk also people that helped me in my daylife in Catalunya, members of Esglesia Evangelica Bautista de Cerdanyola: Pr. Daniel Banyuls, Ester, Conxita, Rosamari…. I could name all of them as their support was significant in many ways.

Specialne podziękowania dla moich kochanych rodziców, którzy wspierali mnie przez całe moje dzieciństwo i młodość, pomagali mi zrealizować wiele ciekawych pomysłów. Także za ich wsparcie finasowe w czasie moich studiów w Warszawie. No i dla mojego brata Piotra też w sumie podziękowania, bo to niezły luzak.

Last but not least I would like to thank my dear wife Cathia, which took care of me, supported me in good and bad days with her love.

And thanks to God Almighty that is taking care of me, that I managed to finish this work as it is, although I had moment of doubts he always was with me.

THANK YOU ALL

Contents

Chapter 1 Introduction 1

1.1 Nanoscale chirality 1

1.2 Behaviour of racemates in condensed phases 2

1.3 Separation of enantiomers 5

1.4 Study of chirality at interfaces 7

Chapter 2 Objectives 11

Chapter 3 Nanoscale chirality of a family of amphiphilic acids at a solid-liquid interface: Shape, Conglomerates and Racemates 12

3.1 Preamble 12

3.1.1 STM of monolayers 13

3.2 2,7-Naphthalne derived amphiphile 14

3.2.1 Synthesis 14

3.2.2 Self-assembly of acid (*R*)-2,7Naph at the graphite-phenyloctane interface 16

3.2.3 Self-assembly of acid (*S*)-2,7Naph at the graphite-phenyloctane interface 17

3.2.4 Self-assembly of the racemic mixture of acid 2,7Naph at the graphite-phenyloctane interface 19

3.3 2,6-Naphthalne derived amphiphile 21

3.3.1 Synthesis 21

3.3.2 Self-assembly of acid (*R*)-2,6Naph at the graphite-phenyloctane interface 22

3.3.3 Self-assembly of racemic mixture of acid 2,6Naph at the graphite-phenyloctane interface 25

3.4 1,5-Naphthalene derived amphiphile 28

3.4.1 Synthesis 28

3.4.2 Self-assembly of (*S*)-1,5Naph at the graphite-phenyloctane interface 29

3.4.3 Self-assembly of (*R*)-1,5Naph at the graphite-phenyloctane interface 34

3.4.4 Self-assembly of the racemic mixture of acid 1,5Naph at the graphite-1-phenyloctane interface 38

3.5 4,4’-Biphenyl amphiphile 41

3.5.1 Synthesis 41

3.5.2 Self-assembly of acid (*R*)-4,4’Biph at the graphite-1-phenyloctane interface 42

3.5.3 Self-assembly of acid (*S*)-4,4’Biph at the graphite-1-phenyloctane interface 47

3.5.4 Self-assembly of the racemic mixture of 4,4’Biph at the graphite-phenyloctane interface 49

3.6 Hydroquionone-derived amphiphile 53
3.6.1 Synthesis 53
3.6.2 Self-assembly of (*R*)-1,4Ph at the graphite-phenyloctane interface ... 54
3.6.3 Self-assembly of (*S*)-1,4Ph at the graphite-phenyloctane interface 57
3.7 Discussion 60
3.8 Conclusions 63
Chapter 4 Phase behaviour of self-assembled monolayers of mixtures of amphiphiles at the liquid solid interface 65
4.1 Introduction 65
4.2 Self-assembly of (*R*)-2,7Naph (*S*)-2,6Naph 71
4.3 Self-assembly of (*R*)-2,7Naph (*R*)-2,6Naph 76
4.4 Self-assembly of (*R*)-2,7Naph (*R*)-1,5Naph 80
4.5 Self-assembly of (*R*)-2,7Naph (*S*)-1,5Naph 85
4.6 Self-assembly of (*R*)-2,6Naph (*S*)-1,5Naph 91
4.7 Self-assembly of (*R*)-2,6Naph (*R*)-1,5Naph 95
4.8 Discussion 98
4.9 Conclusions 101
Chapter 5 Chiral molecular recognition on an achiral surface 102
5.1 Introduction 102
5.2 Self-assembly of resorcinol derivative 1,3Ph and diaminocyclohexane 103
5.3 Self-assembly of 2,7-Dihydroxynaphthalene derivative 2,7Naph and trans-1,2-diaminocyclohexane 124
5.4 Self-assembly of 1,5-Dihydroxynaphthalene derivative (*S*)-1,5Naph and trans-1,2-diaminocyclohexane 133
5.5 Self-assembly of Hydroquinone amphiphilic derivative (*R*)-1,4Ph and trans-1,2 diaminocyclohexane 137
5.6 Diastereomer complexation experiments with other amines 139
5.6.1 Self-assembly of (*R*)-1,3Ph and cis-1,2 diaminocyclohexane 139
5.6.2 Self-assembly of (*R*)-1,3Ph and trans-1,4-diaminocyclohexane 140
5.6.3 Self-assembly of racemic 1,3Ph and (*R*)-2-methylpiperazine 143
5.6.4 Self-assembly of (*S*)-1,3Ph and Metoprolol 144
5.6.5 Other experiments 153
5.7 Conclusions 153

Chapter 6 Mixtures of amphiphilic acids as resolving agents at the graphite solvent interface 156

6.1 Introduction..... 156

6.2 General procedure..... 156

6.3 Self-assembly of (*R*)-2,7Naph (*S*)-1,5Naph (*R*,*R*)-DACH 157

6.4 Self-assembly of (*R*)-2,7Naph (*S*)-1,5Naph (*S*,*S*)-DACH 162

6.5 Self-assembly of (*S*)-2,7Naph (*R*)-1,5Naph (*R*,*R*)-DACH 165

6.6 Self-assembly of (*R*)-2,7Naph (*R*)-1,5Naph (*R*,*R*)-DACH..... 166

6.7 Self-assembly of (*R*)-2,7Naph (*R*)-2,6Naph (*R*,*R*)-DACH..... 168

6.8 Self-assembly of (*R*)-2,6Naph (*R*)-1,5Naph (*R*,*R*)-DACH..... 170

6.9 Self-assembly of (*R*)-2,7Naph (*R*)-1,3Ph (*R*,*R*)-DACH 172

6.10 Discussion..... 174

6.11 Conclusions 176

Chapter 7 Bulk phase behaviour of supramolecular diastereoisomers of the complex formed between a chiral amphiphilic acid and diaminocyclohexane. 177

7.1 Introduction..... 177

7.2 Sample preparation 178

7.3 Summary of qualitative observations of aged samples under heating. 179

7.4 (*R*)-1,3Ph acid (*R*,*R*)-diaminocyclohexane 186

7.5 (*R*)-1,3Ph acid, (*R*,*R*)-diaminocyclohexane and (*S*,*S*)-diaminocyclohexane (2:0.75:0.25) 190

7.6 (*R*)-1,3Ph acid and (rac) diaminocyclohexane (2:1)..... 193

7.7 (*R*)-1,3Ph acid and (*R*,*R*)-diaminocyclohexane(*S*,*S*)-diaminocyclohexane (2:0.25:075) 198

7.8 (*R*)-1,3Ph acid and (*S*,*S*)-diaminocyclohexane (2:1) 202

7.9 (*S*)-1,3Ph acid and (*R*,*R*)-diaminocyclohexane (2:1)..... 205

7.10 (*S*)-1,3Ph acid(*R*)-1,3Ph acid and (*R*,*R*)-diaminocyclohexane (1.5:0.5:1) 208

7.11 (rac)-1,3Ph acid and (*R*,*R*)-diaminocyclohexane (2:1)..... 212

7.12 (*S*)-1,3Ph acid (*R*)-1,3Ph acid and (*R*,*R*)-diaminocyclohexane (0.5:1.5:1) 215

7.13 Conclusions 218

Chapter 8 General Conclusions..... 220

Chapter 9 Experimental Section 222

9.1 Techniques and instruments 222

9.1.1 Spectroscopy and spectrometry 222
9.1.2 Chromatography 222
9.1.3 Scanning Tunnelling Microscopy 223
9.1.4 Small and Wide Angle X-Ray Diffraction 223
9.1.5 Differential Scanning Calorimetry 223
9.1.6 Optical Microscopy 224
9.1.7 Polarimetry 224
9.1.8 Reactants and solvents 224
9.2 Synthesis 224

9.2.1 (*S*)-Methyl 2-(7-hydroxy-naphthalen-2-yloxy)propionate 224
9.2.2 (*S*)-Methyl 2-(7-octadecyloxy-naphthalen-2-yloxy)propionate 225
9.2.3 (*S*)-2-(7-Octadecyloxy-naphthalen-2-yloxy)-propionic acid 226
9.2.4 (*R*)-Methyl 2-(7-hydroxy-naphthalen-2-yloxy)propionate 226
9.2.5 (*R*)-Methyl 2-(7-Octadecyloxy-naphthalen-2-yloxy)propionate 227
9.2.6 (*R*)-Methyl 2-(7-Octadecyloxy-naphthalen-2-yloxy)-propionic acid 228
9.2.7 (*R*)-Methyl 2-(6-Hydroxy-naphthalen-2-yloxy)propionate 228
9.2.8 (*R*)-Methyl 2-(6-(octadecyloxy)naphthalen-2-yloxy)propionate 229
9.2.9 (*R*)-2-(6-Octadecyloxy-naphthalen-2-yloxy)-propionic acid 229
9.2.10 (*S*)-Methyl 2-(6-hydroxynaphthalen-2-yloxy)propionate 230
9.2.11 (*S*)-Methyl 2-(6-(octadecyloxy)naphthalen-2-yloxy)propionate 231
9.2.12 (*S*) -2-(6-Octadecyloxy-naphthalen-2-yloxy)-propionic acid 231
9.2.13 (*R*)-Methyl 2-(5-hydroxy-naphthalen-1-yloxy)propionate 232
9.2.14 (*R*)-Methyl 2-(5-Octadecyloxy-naphthalen-1-yloxy)propionate 233
9.2.15 (*R*)-2-(5-Octadecyloxy-naphthalen-1-yloxy)-propionic acid 233
9.2.16 (*S*)-Methyl 2-(5-hydroxy-naphthalen-1-yloxy)propionate 234
9.2.17 (*S*)–Methyl-2-(5-octadecyloxy-naphthalen-1-yloxy)propionate 235
9.2.18 (*S*)-2-(5-Octadecyloxy-naphthalen-1-yloxy)-propionic acid 235
9.2.19 (*S*)-Methyl 2-(4'-hydroxy-biphenyl-4-yloxy)propionate 236
9.2.20 (*S*)-Methyl 2-(4'-octadecyloxy-biphenyl-4-yloxy)propionate 237
9.2.21(*S*)-2-(4'-Octadecyloxy-biphenyl-4-yloxy)-propionic acid 237
9.2.22(*R*)–Butyl 2-(4'-octadecyloxy-biphenyl-4-yloxy)propionate 238
9.2.23(*R*)-2-(4'-Octadecyloxy-biphenyl-4-yloxy)-propionic acid 238
9.2.24 1-Benzyloxy-4-octadecyloxy-benzene 239
9.2.25 4-Octadecyloxy-phenol 240
9.2.26 (*R*)-Methyl 2-(4-octadecyloxy-phenoxy)propionate 240
9.2.27 (*R*)-2-(4-Octadecyloxy-phenoxy)-propionic acid 241
9.2.28 (*S*)-Methyl 2-(4-octadecyloxy-phenoxy)propionate 242
9.2.29 (*S*) -2-(4-Octadecyloxy-phenoxy)-propionic acid 242
9.2.30 Bulk complex formed between 1,3-Ph and diaminocyclohexane in Resolution Experiment 243
Chapter 10 Bibliography 244

Chapter 1
Introduction

1.1 Nanoscale chirality

Chirality is a geometric property of things – an object that is chiral is not superimposable with its mirror image. The word *chirality* comes from Greek "χειρ" what translates into "hand", one of the easiest to imagine examples of a chiral object, however chirality can be found in huge variety of objects from the elemental particles to stars and galaxies.[1] Chirality is of special interest in chemistry and biochemistry as over 90% of molecules that form the living organisms are of one handedness, i.e. enzymes, DNA, proteins and sugars.[2] Knowing this fact, it is not surprising that the different chirality of drugs will have different effects in the human body. One of the most typical examples is penicillin, a chiral drug that is able to destroy *D*-alanine peptide links. As the cell walls of bacteria do contain *D*-alanine it works there, while in the human cells are composed exclusively by *L*-amino acids and are therefore left unaffected. Knowing this example which is one of many, it is not surprising to discover that over 50% of drugs sold nowadays are chiral and non-racemic.[3]

The controlled formation and understanding of induction of chirality in nanostructures at interphases is a challenging and exciting area of research, which has led to important discoveries relevant to chiral recognition, catalysis, electronic and magnetic materials. There is a great deal of new science and of technologically relevant discoveries to be made in the emerging area of chirality at the nanoscale.[4] Specifically, molecular and sub-molecular resolution imaging can provide essential and precise insight into how macroscopic phenomena come about as well as uncovering new effects.[5,6] In particular, the study of the role that stereogenic centres have on the packing of molecules, and as a

---

[1] G. H. Wagnière, *On Chirality and the Universal Asymmetry*, Verlag Helvetica Chimica Acta, Zurich, Wiley-VCH, **2007**.
[2] A. Guijarro, M. Yus, *The Origin of Chirality in the Molecules of Life*, RSC Publishing, **2009**.
[3](a) E. Francotte, W. Lindner (eds) *Chirality in Drug Research*, Wiley-VCH, **2006**.
(b) A. Mannschreck, R. Kiesswetter, E. von Angerer, *J. Chem. Ed*., **2007**, *84*, 2012.
[4] (a) J. Zhang, M.T. Albelda, Y. Liu, J. W. Canary, *Chirality*, **2005**, *17*, 404. (b) D. B. Amabilino, Nanoscale Chirality. Special issue of *Chem. Soc. Rev.*, **2009**, *38*, issue 3. (c) D. B. Amabilino, *Chirality at the Nanoscale*, Wiley-VCH, **2009**. (d) Y. Wang, J. Xu, Y. Wang, H. Chen, *Chem. Soc. Rev.*, **2013**, *42*, 2930.
[5] R. Raval, *Chem. Soc. Rev*. **2009**, *38*, 707.
[6] M. Parschau, R. Fasel, K.H. Ernst, *Cryst. Growth Des*., **2008**, *8*, 1890.

consequence their behaviour as a system, is a rewarding area of research, because macroscopic phenomena, such as the spontaneous separation of enantiomers or the formation of low dimensional solid solutions, is an emerging area which may well provide results which aid the interpretation of these phenomena at the macroscopic three dimensional level.[7,8]

1.2 Behaviour of racemates in condensed phases

The arrangement of chiral molecules in a crystalline three dimensional system is possible in several ways (Figure 1.1), the most typical is racemic compound, where both enantiomers are equally represented in the cell unit of the solid. In the case of a conglomerate, crystals are formed exclusively by one or the other enantiomer, but over the whole sample the two enantiomers are present. In solid solutions in each position one can find either one or the other enantiomer. In principle, pseudoracemates can be considered a kind of solid solution, but for the purposes of this thesis we distinguish between the totally random situation and the case where the structure is ordered in one direction (vertical in the Figure 1.1) while in the other direction it equal probable to find each enantiomer.[9] The thermal behaviour of each of the main arrangements is presented in Figure 1.2.

There is a dramatic change of behaviour of racemates of chiral molecules during formation of crystals in different kinds of condensed phases. In three dimensional systems most (over 90% of compounds) form racemic compounds, similar to the situation takes place in one and zero dimensional systems (Figure 1.3). In stark contrast with that, when a racemic mixture forms a two dimensional crystal on single crystal systems, the formation of conglomerates is favoured.

[7] L. Pérez-García, D. B. Amabilino, *Chem. Soc. Rev.*, **2002**, *31*, 342.
[8] L. Pérez-García, D. B. Amabilino, *Chem. Soc. Rev.*, **2007**, *36*, 941.
[9] Note that formally a solid solution is a random mixture of two compounds in a crystal lattice, so that the lattice spacing does not change irrespective of the local composition. A pseudoracemate can be considered a type of solid solution, but in this Thesis it shall be used as a term for a specific case where there is partial ordering of enantiomers (which could be in rows or sheets) but these structures do not repeat in the lattice (Figure 1.1).

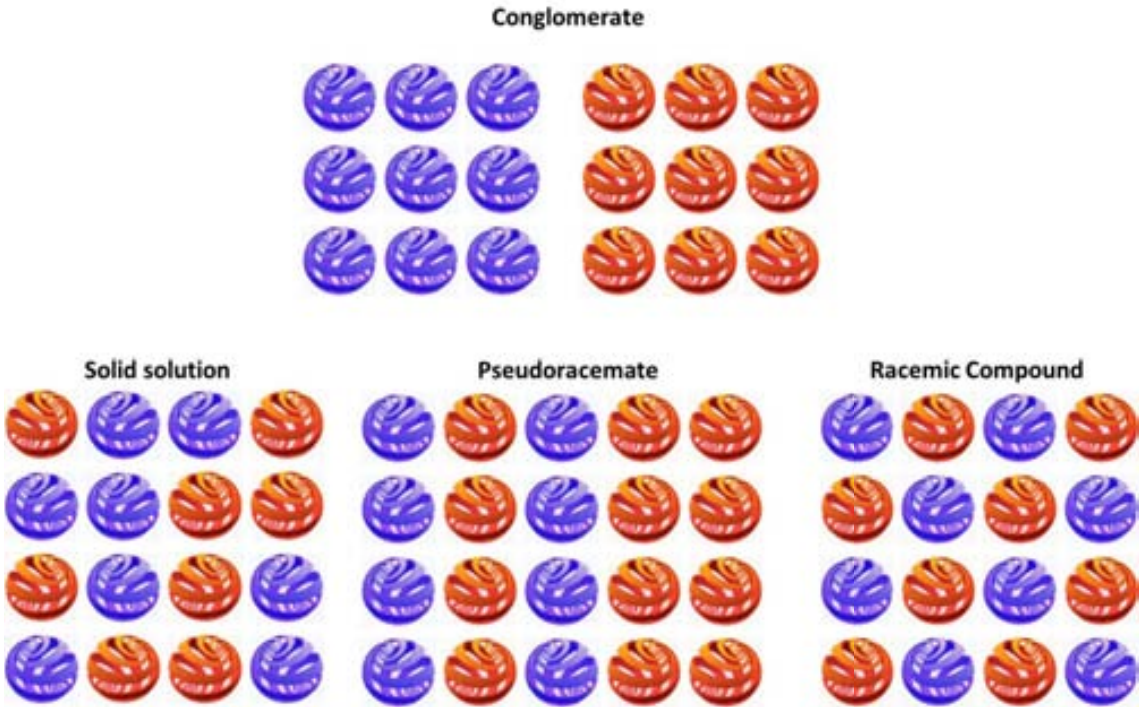

Figure 1.1: *A representation of the packing of different racemates in the condensed phase.*

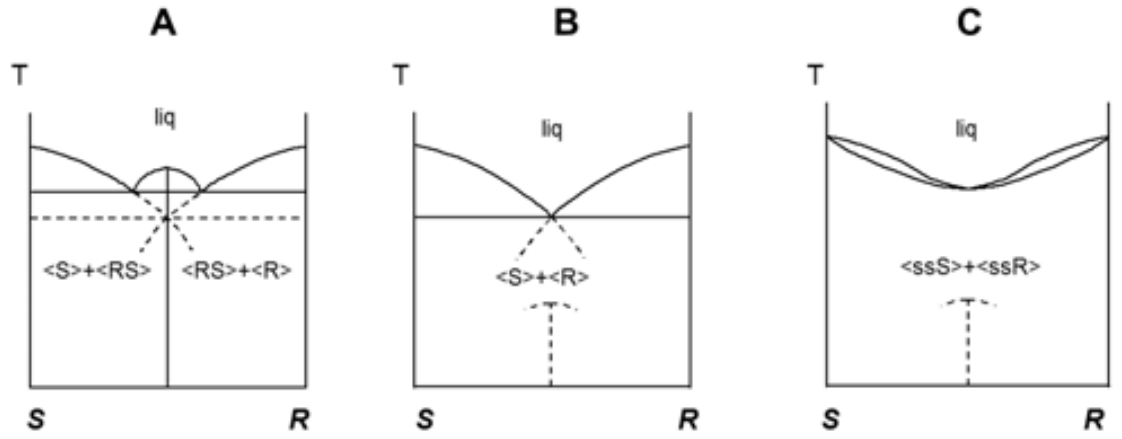

Figure 1.2: *Phase diagrams of chiral compounds. Diagram A for a stable racemic compound. Diagram B for a stable conglomerate. Diagram C for the miscibility in solid state independently of the composition or the temperature of the system.*

A very singular situation takes place in Liquid Crystals (LCs). Until a few years ago the only examples of chiral LCs were produced from enantiomerically enriched liquid crystal samples, until the work of the Walba group reported a remarkable breakthrough:[10] Achiral bent-core molecules can form a chiral liquid crystal phase. The

[10] D. M. Walba, E. Körblova, R. Shao, J. E. Maclennan, D. R. Link, M. A. Glaser, N. A. Clark, *J. Phys. Org. Chem.*, **2000**, *13*, 830.

bent core resorcinol derivative formed two types of arrangement, when placed in electro-optic cells: The majority of molecules formed a racemic arrangement while the minority formed a conglomerate smectic phase.

DIMENSIONALITY	SYSTEM	PROBABILITY
3D	Crystals	Racemate > Conglomerate
	Liquid Crystals	Racemate >>> Conglomerate
2D	Langmuir Monolayers	Racemate >> Conglomerate
	SAMs on Graphite	Racemate <<< Conglomerate
	Chemisorbed molecules on metals	Racemate << Conglomerate
1D	Covalent and Coordination Polymers	Racemate >> Conglomerate
0D	Isolated aggregates in gas, solution or solid	Racemate >> Conglomerate

Figure 1.3: *Comparison of probability of formation of conglomerates in range of systems of different dimensionality.*

When looking at the details of two dimensional systems, one can observe that in case of molecules adsorbed on graphite the percentage of conglomerates is well above 90%. For this reason, understanding the principles that govern the process of formation of self-assembled monolayers on the graphite is an important challenge. A systematic and critical compilation was done by Matzger and his collaborators, as they created two dimensional structural database (2DSD).[11] They have studied and classified over 350 unique examples of two dimensional structures. As in three dimensional systems, two dimensional crystals tend to get the closest possible packing to maximize intermolecular interactions. In 3D crystals the most favoured symmetry element is an inversion centre, that leads to centro-symmetric space groups. This implies that achiral molecules generally crystallize in achiral space groups,[12,13] while racemic mixtures tend to crystallize into arrangements that consist both of enantiomers in the unit cell.[14]

[11] K. E. Plass, A. L. Grzesiak, A. J. Matzger, *Acc. Chem. Res*., **2007**, *40*, 287.
[12] E. Pidcock, *Chem. Comm.,* **2005**, 3457.
[13] T. Matsuura, H. Koshima, *J. Photochem. Photobiol.C-Photochem. Rev.,* **2005**, *6*, 7.
[14] (a) C. P. Brock,W. B. Schweizer, J. D. Dunitz, *J. Am. Chem. Soc.,* **1991**, *113*, 9811. (b) J. Jacques, A. Collet, S. H. Wilen, *Enantiomers, Racemates and Resolutions*, John Wiley & Sons: New York, **1981,** 23.

The situation is very different in 2D systems on graphite, it was found that 2-fold rotation can provide the closest packing and indeed the symmetry groups containing 2-fold rotation are most represented (*p2*, *p2gg* and *p6* together represents over 70% of structures in 2DSD). There are a number of examples of both achiral[15] and chiral[16] molecules that form conglomerates on achiral surfaces. Chiral planar groups represent over 79% of structures, even though many the molecules that form them are not chiral at all, but have chiral conformations once adsorbed to the surface because of the existence of prochiral faces in certain arrangements.

1.3 Separation of enantiomers

The separation of enantiomers is an important step in the production of optically active chemicals used in variety of applications. It is frequently performed using "classical" diastereomeric resolution, one variant of which is Pasteurian resolution.[17] This crystallization process results from the different solubility and crystallization propensity of the diastereomers formed by the enantiomers of a target racemate with a complementary chiral compound – the resolving agent – which forms a complex or a salt with it and where one equivalent of resolving agent is added for each molecule of either enantiomer of the mixture. Alternatively, there are other types of resolution known (Scheme 1.1).

(c) C. P. Price, A. J. Matzger, *J. Org. Chem.*, **2005**, *70*, 1.

[15] (a) D. G. Yablon, L. C. Giancarlo, G. W. Flynn, *J. Phys. Chem. B*, **2000**, *104*, 7627. (b) F. Tao, S. L. Bernasek, *J. Phys. Chem. B*, **2005**, *109*, 6233. (c) A. M. Berg, D. L. Patrick, *Angew.Chem., Int. Ed.*, **2005**, *44*, 1821.

[16] (a) W. Mamdouh, H. Uji-i, A. E. Dulcey, V. Percec, S. De Feyter, F. C. DeSchryver, *Langmuir*, **2004**, *20*, 7678. (b) W. Mamdouh, H. Uji-i, A. Gesquiere, S. De Feyter,; D. B. Amabilino, M. M. S. Abdel-Mottaleb, J. Veciana, F. C. De Schryver, *Langmuir,* **2004**, *20*, 9628. (c) I. Weissbuch, M. Berfeld, W. Bouwman, K. Kjaer, J. Als-Nielsen, M. Lahav, L. Leiserowitz, *J. Am. Chem. Soc.*, **1997**, *119*, 933. (d) S. De Feyter, A. Gesquiere, P. C. M. Grim, F. C. De Schryver, S. Valiyaveettil, C. Meiners, M. Sieffert, K. Mullen, *Langmuir*, **1999**, *15*, 2817.

[17] (a) L. Pasteur *C. R. Acad. Sci.*, **1853**, *37*, 162. (b) L. Pasteur *Ann. Chim. (Paris)*, **1853**, *38*, 437. (c) J. Jacques, A. Collet, S. H. Wilen, *Enantiomers, racemates and resolutions*. Malabar, FL: Krieger Publishing Company, **1994**. (d) E. Fogassy, M. Nógrádi, D. Kozma, G.. Egri, E. Pálovics, V. Kiss, *Org. Biomol. Chem.*, **2006**, *4*, 3011. (e) F. Faigl, E. Fogassy, M. Nógrádi, E. Pálovics, J. Schindler, *Tetrahedron: Asymmetry*, **2008**, *19*, 519.

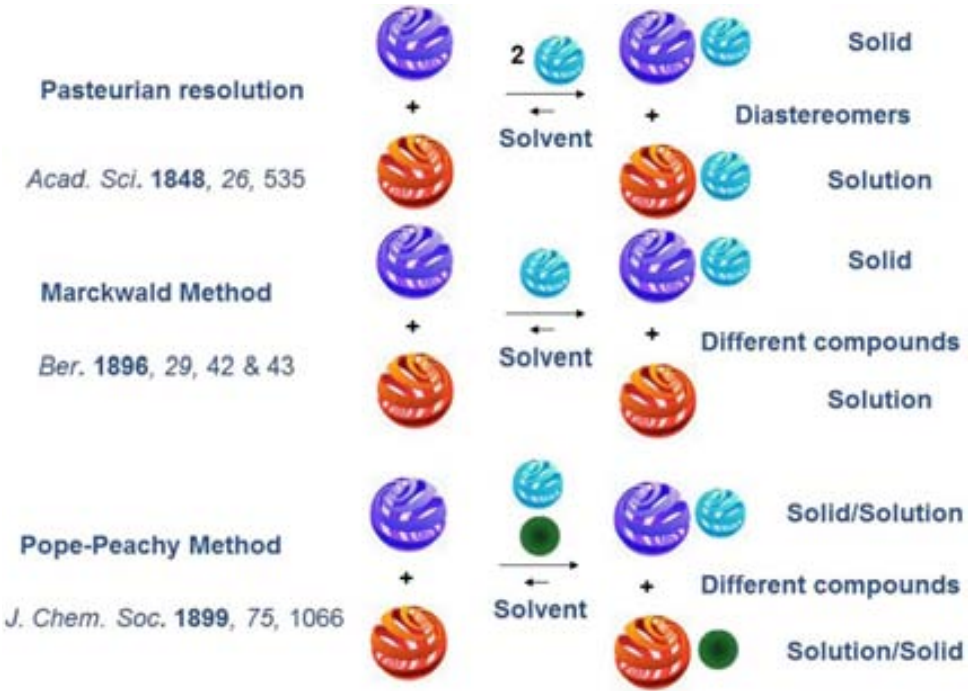

Scheme 1.1: *Different Resolving methods*

In the Marckwald Method,[18] where there is half of the amount of resolving agent used compared with Pasteurain resolution, a complex crystallizes only with one diastereomer between resolving agent and one of the enantiomers in the racemte. The complex is expected to crystalize from the solution, while the other enantiomer stays in the solution. Another possibility is the Pope-Peachy Method,[19] where the racemate is mixed with the resolving agent and an achiral molecule capable of forming a complex. In this case there are two different species formed – the complex of resolving agent with matching enantiomer of resolved compound and complex of achiral molecule with the other enantiomer. In this case also, the difference in solubility of those compounds is used for separation of enantiomers. The identification of the resolving agents that work for a given racemic mixture in this process relies on an empirical screening,[20] although some rationalisation based on phase behaviour or arguments based on supramolecular chemistry and molecular recognition can be invoked largely with the benefit of hindsight.[21] Also there is an important contribution made in the area with introduction

[18] W. Marckwald, A. McKenzie *Ber. Dtsch. Chem. Ges.,* **1899**, *32*, 2130.
[19] W. J. Pope, S. J. Peachy *J. Chem Soc.,* **1899**, *75*, 1066.
[20] D. Kozma, Ed. *CRC Handbook of Optical Resolutions via Diastereomeric Salt Formation*, CRC Press, New York, **2002**.
[21] G.. Coquerel, D. B. Amabilino, *The Nanoscale Aspects of Chirality in Crystal Growth: Structure and Heterogeneous Equilibria* in *Chirality at the Nanoscale* 305-348 D.B Amabilino (Ed.), Wiley-VCH, Weinheim, **2009**.

of Family Approach, known also as Dutch Resolution. In this method family of similar molecules of the same chirality is used as a resolving agent.[22] It was proved that when using a mixture of resolving compounds the probability of resolution is increased significantly.

The study of Pasteurian resolution at surfaces is interesting for a number of reasons, many of which arise from the reduced symmetry possibilities in this low dimensional environment.[23] Unlike the situation in bulk crystals, spontaneous resolution is observed very frequently on crystalline surfaces wherein domains of opposite handedness arise from chiral or achiral adsorbate systems.[7] A notable example is the nanoscale demonstration of Pasteur's triage using STM.[24] While the observation of diastereomeric interactions for the complex formed between phenylglycine and adenine was seen under ultrahigh vacuum conditions on a metal surface,[25] this process originates from the formation of chiral strips of the prochiral base followed by adhesion of the amino acid to it. It is therefore akin to a spontaneous resolution. Transfer of chirality from monolayers to bulk crystals has been used for the selective growth of crystals of one enantiomer in a racemic mixture in solution, which presumably involves diastereomeric interactions between the surface and the crystal nucleus,[26] while for similar cases conglomerates are formed.[27] However, before this work there was no information regarding the formation of two dimensional crystals of diastereomers in a dynamic system in solution.

1.4 Study of chirality at interfaces

Using modern microscopy techniques such as atomic force microscopy (AFM) and especially scanning tunnelling microscopy (STM) one can observe single (chiral) molecules and infer the interactions between them, as well as the nature of their packing

[22] (a) T. Vries, H. van Echten, J. Koek, W. ten Hoeve, R. M. Kellogg, Q. B. Broxterman, A. J.Minnard, S. Van der Sluis, L. Hulshof, J. Kooistra, *Angew. Chem. Int Ed.*, **1998**, *37*, 2249. (b) Q. B. Broxterman, E. van Echten, L. A. Hulshof, Bl Kaptei, R. M. Kellogg, A. J. Minnaard, T. R. Vries, H. Wynberg, *Chemistry Today*, **1998**, *16*, 34. (c) A. Collet, *Angew. Chem. Int Ed.*, **1998**, *37*, 3239. (d) R. M. Kellogg, B. Kaptein, T. R. Vries, *Top. Curr. Chem.*, **2007**, *269*, 159.
[23] (a) I. Weissbuch, I. Kuzmenko, M.Berfeld, L.Leiserowitz, M. Lahav, *J. Phys. Org. Chem.*, **2000**, *13*, 426. (b) I. Weissbuch, M. Lahav, *Chem. Rev.* **2011**, *111*, 3236.
[24] M. Böhringer, W.D. Schneider, R. Berndt, *Surf. Rev. Lett.*, **2000**, *7*, 661.
[25] Q. Chen, N. V. Richardson, *Nature Mat.*, **2003**, *2*, 324.
[26] Y. Mastai, *Chem. Soc. Rev.*, **2009**, *38*, 772.
[27] M. Linares, A. Minoia, P. Brocorens, D. Beljonne, R. Lazzaroni, *Chem. Soc. Rev.*, **2009**, *38*, 806.

in low dimensions at surfaces.[28] A simplified drawing of the STM is presented in Figure 1.4. The non-covalent bonding in these structures – such as hydrogen bonds and Van der Waals interactions – both between the adsorbates themselves as well as between them and the surface determine directly the nature of the assembly on a given substrate.

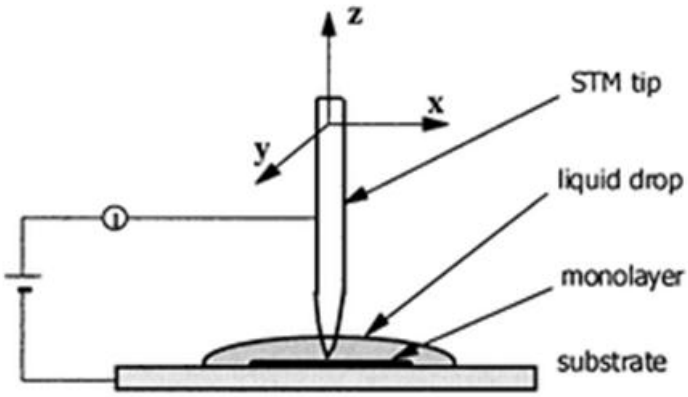

Figure 1.4 *Scanning Tunnelling Microscope scheme. For the measurement presented in this thesis Pt/Ir wire was used as a tip, monolayer was formed on the highly ordered pyrolytic graphite and a solvent was 1-phenyloctane.*

Even more challenging is to find how chirality from single molecules transfers into

[28] (a) M. Böhringer, K. Morgenstern, W. D. Schneider, R. Berndt, *Angew. Chem. Int. Ed.*, **1999**, *38*, 821. (b) M. O. Lorenzo, C. J. Baddeley, C. Muryn, R. Raval, *Nature*, **2000**, *404*, 376. (c) J. D. Mougous, A. J. Brackley, K. Foland, R. T. Baker, D. L. Patrick, *Phys. Rev. Lett.*, **2000**, *84*, 2742. (d) A. Kühnle, T. R. Linderoth, B. Hammer, F. Besenbacher, *Nature*, **2001**, *415*, 891. (e) A. Mugarza, N. Lorente, P. Ordejon, C. Krull, S. Stepanow, M. L. Bockquet, J. Fraxedas, G.. Ceballos, P. Gambardella, *Phys. Rev. Lett.*, **2010**, *105*, 115 702. (f) H. L. Tierney, C. J. Murphy, E. C. H. Sykes, *Phys. Rev. Lett.*, **2011**, *106*, 010 801. (g) J. A. A. W. Elemans, I. De Cat, H. Xu, S. De Feyter, *Chem. Soc. Rev*., **2009**, *38*, 722. (h) R. Gutzler, T. Sirtl, J. F. Dienstmaier, K. Mahata, W. M. Heckl, M. Schmittel, M. J. Lackinger, *J. Am. Chem. Soc.*, **2010**, *132*, 5084. (i) R. Madueno, M. T. Raisanen, C. Silien, M. Buck, *Nature*, **2008**, *454*, 618. (j) D. M. Ceres, J. K. Barton, *J. Am. Chem. Soc*., **2003**, *125*, 14964. (k) D. M. Cyr, B. Venkataraman, G. W. Flynn, *Chem. Mater.* **1996**, *8*, 1600. (l) Q. H. Yuan, C. J. Yan, H. J.Yan, L. J. Wan, B. H. Northrop, H. Jude, P. J. Stang, *J. Am. Chem. Soc.*, **2008**, *130*, 8878. (m) D. P. E. Smith, J. K. H. Horber, G. Binnig, H. Nejoh, *Nature*, **1990**, *344*, 641. (n) S. De Feyter, A. Gesquiere, M. M. Abdel-Mottaleb, P. C. M. Grim, F. C. De Schryver, C.Meiners, M. Sieffert, S. Valiyaveettil, K. Mullen, *Acc. Chem. Res.*, **2000**, *33*, 520. (o) L. Askadskaya, J. P. Rabe, *Phys. Rev. Lett.*, **1992**, *69*, 1395. (q) L. Liu, L. Zhang, X. Mao, L. Niu, Y. Yang, C. Wang, *NanoLett.*, **2009**, *9*, 4066. (r) S. De Feyter, P. . M. Grim, M. Rücker, P. Vanoppen, C. Meiners, M. Sieffert, S. Valiyaveettil, K. Müllen, F. C. De Schryver, *Angew. Chem. Int. Ed.* **1998**, *37*, 1223. (s) V. Humblot, S. M. Barlow, R. Raval, *Prog. Surf. Sci.* **2004**, *76*, 1. (t) S. Romer, B. Behzadi, R. Fasel, K.-H. Ernst, *Chem. Eur. J.* **2005**, *11*, 4149. (u) M. Lingenfelder, G. Tomba, G. Costantini, L. C. Ciacchi, A. De Vita, K. Kern, *Angew. Chem.* **2007**, *119*, 4576--4579; *Angew. Chem. Int. Ed.* **2007**, *46*, 4492. (v) N. Katsonis, E. Lacaze, B. L. Feringa, *J. Mater. Chem.* **2008**, *18*, 2065. (w) I. Paci, *J. Phys. Chem. C* **2010**, *114*, 19425. (w) A. Robin, P. Iavicoli, K. Wurst, M. S. Dyer, S. Haq, D. B. Amabilino, R. Raval, *Cryst. Growth Des.* **2010**, *10*, 4516. (x) E. V. Iski, H. L. Tierney, A. D. Jewell, E. C. H. Sykes, *Chem. Eur. J.* **2011**, *17*, 7205. (y) M. M. Knudsen, N. Kalashnyk, F. Masini, J. R. Cramer, E. Lægsgaard, F. Besenbacher, T. R. Linderoth, K. V. Gothelf, *J. Am. Chem. Soc.* **2011**, *133*, 4896. (z) M. Stöhr, S. Boz, M. Schär, M.-T. Nguyen, C. A. Pignedoli, D. Passerone, W. B. Schweizer, C. Thilgen, T. A. Jung, F. Diederich, *Angew. Chem. Int. Ed.* **2011**, *50*, 9982.

chirality of nanostructures, and gaining control of chirality at the nanoscale would give us a possibility to obtain chiral functionalised systems with potential applications such as stereoselective molecular recognition.

There have been reports about physisorbed self-assembled monolayers (SAMs) at solid-liquid interfaces of relatively big and sophisticated molecules that contain many stereogenic centres,[29] but it is usually challenging to determine what influence the geometry of a single stereogenic centre has on a structure observed on a surface.[30,31] Symmetry breaking at surfaces has been proven,[32] although the role of the stereogenic centres is difficult to pin down.

One of the remarkable studies of molecules absorption at the solid liquid interface was made on achiral oligo(*p*-phenylenevinylene) (OPV).[33] The family of OPV was studied excessively in recent years.[34] In this work the influence of chiral additive on the formation of a monolayer was investigated. Achiral molecules of OPV, when deposited at the 1-octanol-graphite interface form cyclic hexamers stabilized by hydrogen bonds. Two mirror image arrangements (called rosettes, an example is presented in Figure 1.5) were found – either molecule formed clockwise or anticlockwise structures. Moreover the structures are rotated with respect to the graphite substrate either in plus or in minus

[29] (a) A. Gesquiere, P. Jonkheijm, A. P. H. J. Schenning, E. Mena-Osteritz, P. Bauerle, S. De Feyter, F. C. De Schryver, E. W. Meijer, *J. Mater. Chem*., **2003**, *13*, 2164. (b) P. Jonkheijm, A. Miura, M. Zdanowska, F. J. M. Hoeben, S. De Feyter, A. P. H. J. Schenning, F. C. De Schryver, E.W. Meijer, *Angew. Chem. Int. Ed*., **2004**, *43*, 74. (c) A. Miura, P. Jonkheijm, S. De Feyter, A. P. H. J. Schenning, E. W. Meijer, F. C. De Schryver, *Small*, **2005**, *1*, 131. (d) A. Gesquiere, P. Jonkheijm, F.J.M. Hoeben, A.P.H.J. Schenning, S. De Feyter, F. C. De Schryver, E. W. Meijer, *Nano Lett*., **2004**, *4*, 1175. (e) M. Linares, P. Iavicoli, K. Psychogyiopoulou, D. Beljonne, S. De Feyter, D. B. Amabilino, R. Lazzaroni, *Langmuir,* **2008**, *24*, 9566.

[30] D.G. Yablon, J. S. Guo, D. Knapp, H.B. Fang, G. W. Flynn, *J Phys. Chem B*, **2001**, *105*, 4313.

[31] S. De Feyter, A. Gesquiere, P. C. M. Grim, F. C. De Schryver, S. Valiyaveettil, C. Meiners, M. Sieffert, K. Mullen, *Langmuir*, **1999**, *15*, 2817.

[32] (a) F. Stevens, D. J. Dyer, D. M. Walba, *Angew. Chem. Int. Ed.*,**1996**, *35*, 900. (b) P. Qian, H. Nanjo, T. Yokoyama, T. M. Suzuki, *Chem. Lett.*, **1998**, *11*, 1133. (c) P. Qian, H. Nanjo, T. Yokoyama, T. M. Suzuki, K. Akasaka H. Orhui, *Chem. Commun*., **2000**, 2021.

[33] Z. Guo, I. De Cat, B. Van Averbeke, J. Lin, G. Wang, H. Xu, R. Lazzaroni, D. Beljonne, E. W. Meijer, A. P. H. J. Schenning, S. De Feyter, *J. Am. Chem. Soc.***2011**, *133*, 17764.

[34] (a) S. De Feyter, A. Miura, S. Yao, Z. Chen, F. Wurthner, P. Jonkheijm, A. P. H. J. Schenning, E. W. Meijer, F. C. De Schryver, *NanoLett.*, **2005**, *5*, 77. (b) A. Gesquiere, P. Jonkheijm, F. J. M. Hoeben, A. P. H. J. Schenning, S. De Feyter, F. C. De Schryver, E. W. Meijer, Nano *Lett.*,**2004**,*4*, 1175. (c) F. J. M. Hoeben, J. Zhang, C. C. Lee, M. J. Pouderoijen, M. Wolffs, F. Wurthner, A. P. H. J. Schenning, E. W. Meijer, S. De Feyter, *Chem.-Eur. J.*, **2008**, *14*, 8579. (d) P. Jonkheijm, A. Miura, M.Z danowska, F. J. M. Hoeben, S. De Feyter, A. P. H. J. Schenning, F. C. De Schryver, E. W. Meijer, *Angew.Chem., Int. Ed.*, **2004**, *43*, 74. (e) A. Miura, P. Jonkheijm, S. De Feyter, A. P. H. J. Schenning, E. W. Meijer, F. C. De Schryver, *Small*,**2005**, *1*, 131. (f) H. Uji-i, A. Miura, A. Schenning, E. W. Meijer, Z. J. Chen, F. Wurthner, F. C. De Schryver, M. Van der Auweraer, S. De Feyter, *ChemPhysChem*, **2005**, *6*, 2389. (g) A. P. H. J. Schenning, E. W. Meijer, *Chem. Commun.*,**2005**, 3245. (h) Q. Chen, T. Chen, D. Wang, H. B. Liu, Y. L.Li, L. J.Wan, *Proc. Natl. Acad. Sci. U.S.A.*, **2010**, *107*, 2769. (i) D. Gonzalez-Rodríguez, P. G. A. Janssen, R. Martín-Rapun, I. De Cat, S. De Feyter, A. P. H. J. Schenning, E. W. Meijer, *J. Am. Chem. Soc.*, **2010**, *132*, 4710. (j) P. Jonkheijm, P. Van der Shoot, A. P. H. J .Schenning, E. W. Meijer, *Science*,**2006**, *313*, 80.

sense, that is the second expression of the chirality.

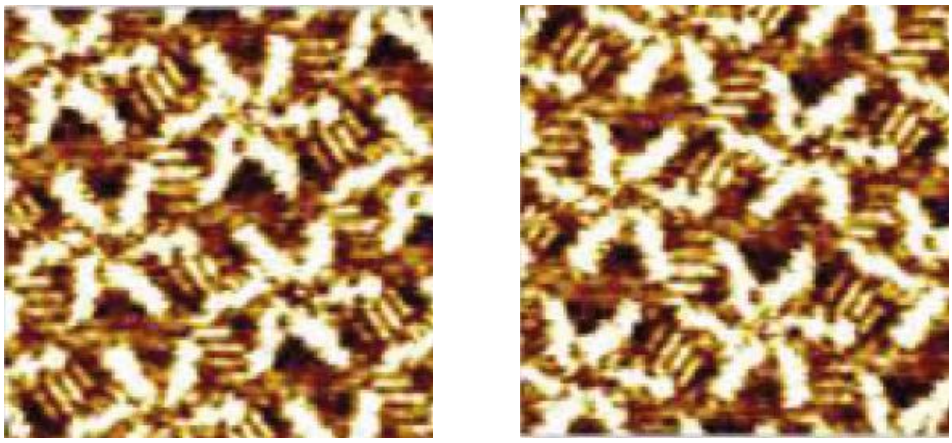

Figure 1.5: *STM image of OPV molecules forming rosettes at graphite-1-octanol interface. The left handed rosettes are presented in the image on the left, and its enatiomer on the right side. The narrow white bright bars correspond to alkyl chain substituents and the thicker white lines to the OPV moieties.*

The molecules of achiral OPV were mixed with either the *L* or *D* enantiomer of thymidine, a nucleoside that does not form on its own any stable monolayer in the experimental conditions and does not interact in solution with molecules of OPV. The investigation proved that there is an equilibrium between rosettes and the formation of two new structures - dimers were observed. Rosettes are formed at the beginning of experiment but the area covered by those structures reduces with time to reach equilibrium after approximately 1h. A study of different ratio of thymidine/OPV was performed to find that with increasing ratio thymidine/OPV one of the structures is preferred over the other. In this way it was proved that Thymidine has a key role in determining chirality of the surface as well as it influences the packing of the molecules.

This example shows the delicate balance between chiral structures on surfaces in a very complex molecule, but information is lacking concerning chiral effects in smaller systems which resolve spontaneously or which are capable of diastereoisomer resolution.

Chapter 2
Objectives

The global main objective of this Thesis is to:

Understand the emergence of chirality in racemates in monolayers, and to use the knowledge for the design of systems where chiral separation can be achieved.

In order to contribute to this goal, the following specific steps were identified:

- Synthesise a family of chiral amphiphilic acids with different aromatic spacers which have a tendency to self-assemble on graphite.
- Determine the effect that rigid aromatic spacers have on the expression of chirality in self-assembled layers by studying their packing arrangements at sub-molecular resolution.
- Reach a hypothesis concerning the role that geometry has on the expression of chirality in this type of two dimensional systems.
- Use the most promising systems to transfer tendency for spontaneous resolution to tendency to act as a good resolving agent by studying the chiral recognition between acid and amine in two dimensional system.
- Determine the behaviour of mixtures of acids in the resolution of compounds in a monolayer system.

In addition, the correlation between these two dimensional systems and three dimensional systems is of interest because it would reveal the importance of the interface as a place for using chirality, so to this end it was decided to:

- Determine the three dimensional phase behaviour of amphiphilic acids used in monolayer systems and their combinations with chiral amines.

Chapter 3

Nanoscale chirality of a family of amphiphilic acids at a solid-liquid interface: Shape, Conglomerates and Racemates

3.1 Preamble

There is presently little knowledge or hypothesis concerning the assembly of molecules and whether they will form condensed phases – a term used here to include solids and colloidal states – where the enantiomers are incorporated into the same fixed structure.

For the purpose of studying the formation of 2D crystals at the graphite-liquid interface, the family of compounds presented in the Scheme 3.1 was synthesized. The molecules consist of an eighteen carbon long alkyl chain on one side and a chiral lactic acid group on the other side, and in between is an aromatic part connected with both side groups via oxygen atoms. Six different members of family have been synthesized, each of them in both of the enantiomeric forms. In the course of this study the influence of size and geometry of each aromatic linker was checked. In the family there are two compounds, **1,3Ph** and **2,7Naph** with angle 120° between the alkoxy chain and the lactate group and other structures has the lactic acid and alkyl chain connected on opposite sides of aromatic part. In the case of **1,4Ph** and **4,4'Biph** those groups are inline, in case of the **2,6Naph** and **1,5Naph**, the groups are a bit shifted, the shift is significantly bigger in **1,5Naph**. This kind of regioisomerism in naphthalene derivatives is known to give rise to different self-organized structures.[35]

[35] S. Yagai, Y. Goto, X. Lin, T. Karatsu, A. Kitamura, D. Kuzuhara, H. Yamada, Y. Kikkawa, A. Saeki, S. Seki, *Angew. Chem. Int. Ed.*,**2012**, *51*, 6643.

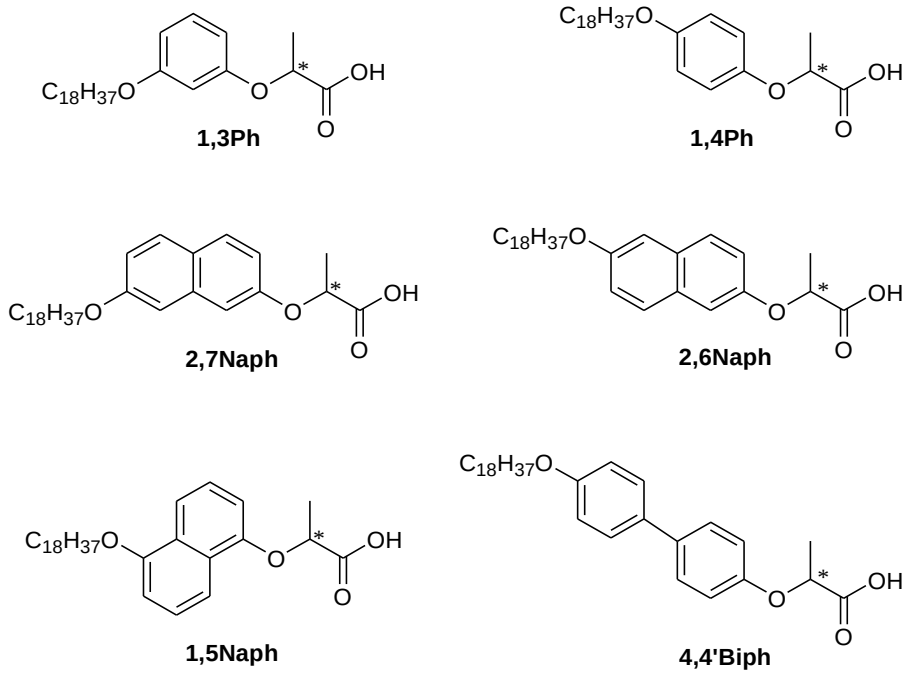

Scheme 3.1: *The family of amphiphiles prepared in this work. The stereogenic centre in each molecule is marked with *.*

3.1.1 STM of monolayers

In order to study the self-assembly of monolayers on a surface, graphite was chosen as the substrate, as it is conductive, chemically inert and atomically flat. Also compounds with long alkyl chains can easily adsorb on the surface. 1-Phenyloctane was the solvent that was used, as it has high boiling point (261-263°C) that permits measuring in air for several hours before the drop evaporates, the compound is stable in experimental conditions and it is good solvent for the studied molecules. Graphite also has the advantage that it can be easily used as a reference for determination of the chirality of the structure with respect to the substrate, simply for each captured image of self-assembled monolayer (SAM) an image of the graphite lying below was captured. The manner of determining chirality of the SAM is presented in the Figure 3.1.

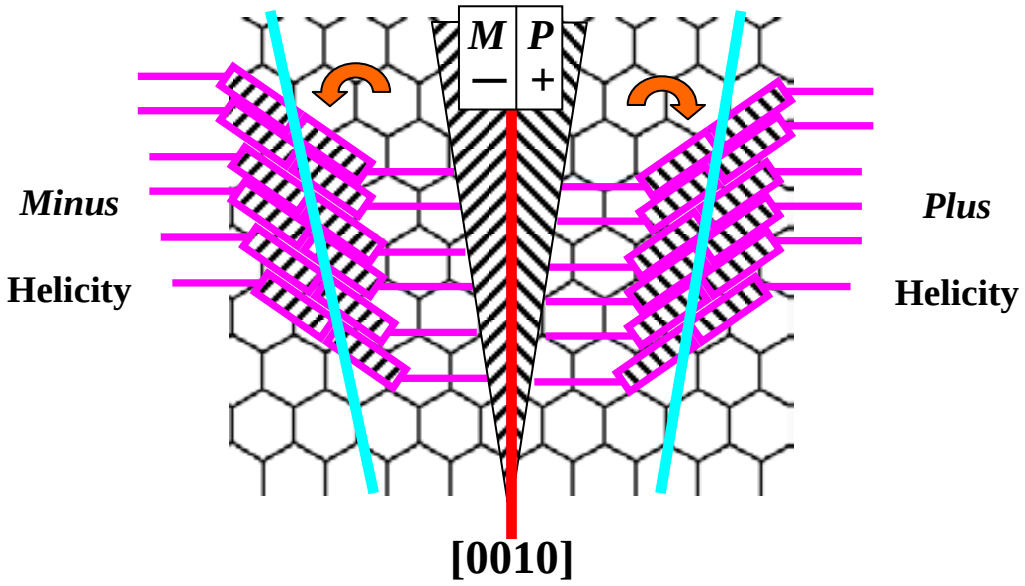

Figure 3.1: *Chirality of a lamellar monolayer is determined with respect to the graphite axis. In the image the structure on the left is defined as minus helicity, because it is rotated anticlockwise with respect to the reference graphite axis marked in the red, while structure on the right is plus helicity, as it is rotated clockwise. The perpendicular to the marked axis is called main graphite axis and is usually used as reference for the structures in this thesis.*

3.2 2,7-Naphthalne derived amphiphile

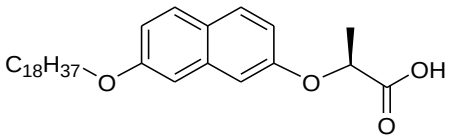

***(S)* -2,7Naph**

3.2.1 Synthesis

The enantiomers of naphthalene derivative **2,7Naph** were synthesised as shown in Scheme 3.3. The first step employed was the reaction of 2,7-dihydroxynaphtalene with either one or the other enantiomer of commercially available methyl lactate using the Mitsunobu protocol[36] where the stereoselective condensation between aromatic and alkyl alcohols is achieved using diisopropylazodicarboxylate in the presence of triphenylphosphine, to obtain compound **11** with 26% of yield for enantiomer (*S*) and 27% of yield in the analogous reaction for the (*R*) enantiomer as well as the bis-lactate substituted compound **11A** after purification by column chromatography. The mono-

[36] O. Mitsunobu, Y. Yamada, *Bull. Chem. Soc. Japan*, **1967**, *40*, 2380.

adduct **11** was reacted with octadecylbromide in the presence of base in refluxing acetonitrile, from which the product **12** of the reaction precipitates after cooling with 57% of yield for the (*S*) product and 64% for (*R*). The last step in the route to the desired amphiphile was the hydrolysis of the ester **12** followed by crystallization of the product, the yield of this step was 59% for acid (*S*) and 66% for acid (*R*). The NMR, IR and chiral HPLC analyses of the compounds confirmed the desired structure.

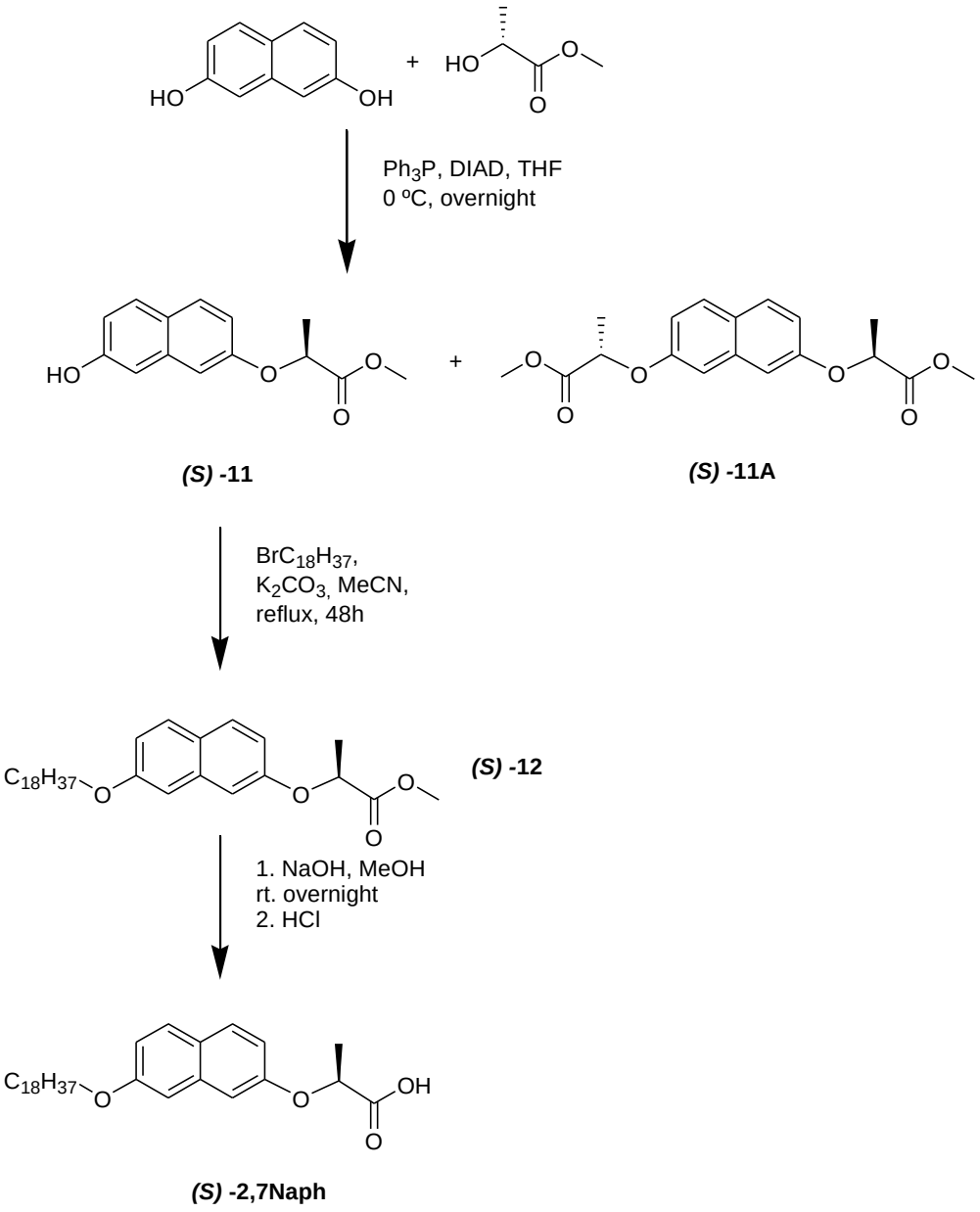

Scheme 3.2**: Synthesis of acid (S)-**2,7Naph

3.2.2 Self-assembly of acid (*R*)-2,7Naph at the graphite-phenyloctane interface

To form a monolayer of the amphiphile **2,7Naph** on the surface, the compound was dissolved in hot 1-phenyloctane and a drop of approximately 10 microliters of the resulting solution was applied to a freshly cleaved surface of highly orientated pyrolitic graphite (HOPG).The graphite was placed inside the Scanning Tunnelling Microscope and the tip was approached. Within a few minutes the monolayer was formed and the STM images were acquired. The image contrast reflects the distance between the tip and the substrate, but is also influenced by the tunnelling current which is higher through aromatic parts of the structures which appear brighter.

Typical STM images of the monolayer of **2,7Naph** are shown in Figure 3.2, there a lamellar structure of the self-assembled monolayer (SAM) can be seen which extends over more than hundred nanometres in every direction. Looking closer at the lamellae in the images, one can spot a bright dot that corresponds to the aromatic part of the molecule and a series of brighter small points, usually nine of them inline, that are attributed to alkyl chains. The number of these points is half compared to the number of carbon atoms in the molecule due to the amplification of the signal of every second carbon atom in the graphite structure. This effect is caused by the shift between the monolayers of graphite. The alkyl chains are interdigitated. The head to head distance in direction of the lamella growth is 1.01 ± 0.06 nm. The heads of the molecules forming dimers via hydrogen bonds are separated by 1.86 ± 0.10 nm and this value is confirmed by the model prepared in HyperChem Pro 6.0, MM+ optimized geometry. The dimers form straight lamellae as is marked in Figure 3.2B. The aromatic parts are in line and a hydrogen bond is formed between molecules marked in the Figure 3.2B, according to the model showed in Figure 3.2C. The dimer is “Z” shaped as marked in the figure. The lamellae thickness is 3.56 ± 0.20 nm. The domain lamellar direction is rotated anticlockwise to the surface and the angle is -7.5 ± 2.7º with respect to the main graphite axis. In Figure 3.2A the unit cell is marked, the parameters are a = 1.01 ± 0.06 nm, b = 3.56 ± 0.20 nm and γ= 90.3 ± 0.6º. In the Figure 3.3 the histogram of angles is presented.

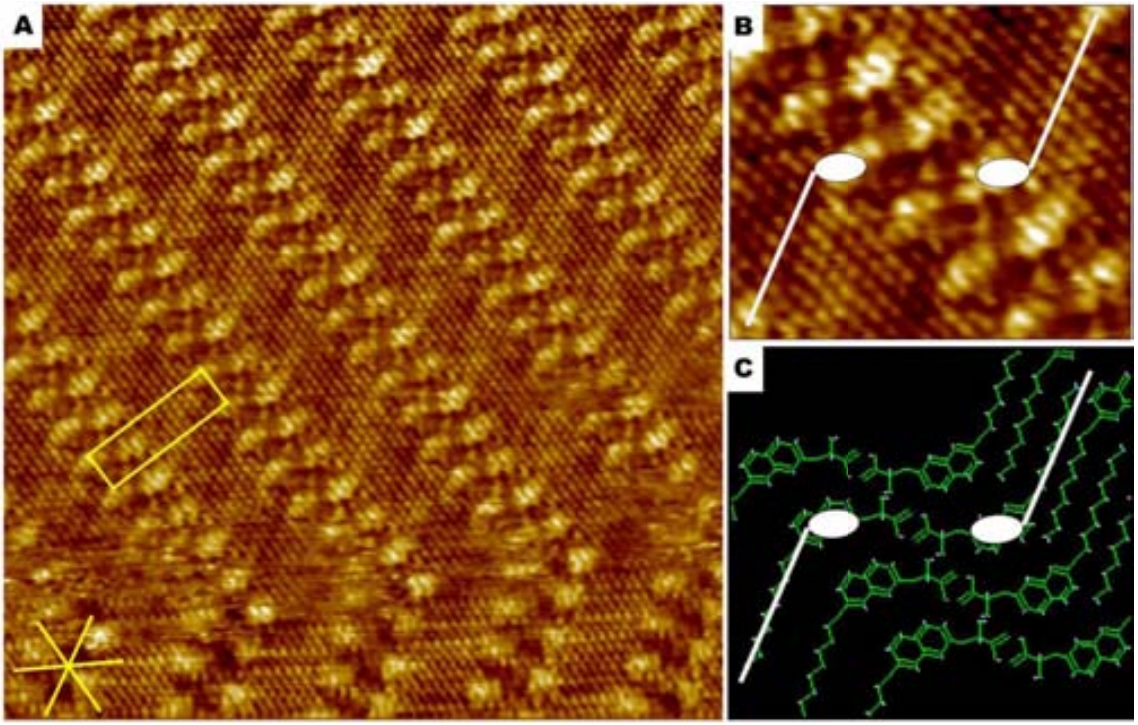

Figure 3.2: *STM images and modelling of a monolayer of (R)-**2,7Naph** at the graphite-1-phenyloctane interface. Image A (18.3 × 18.3 nm; I_{set} = 0.2 nA; V_{bias} = 0.8 V) shows **2,7Naph** at the graphite-1-phenyloctane interface, in yellow the unit cell is marked. Image B shows close up (4.32 x 5.23 nm) of the structure, and the molecules forming dimer are marked. In image C the optimized model prepared using HyperChem, with marked molecules forming dimer.*

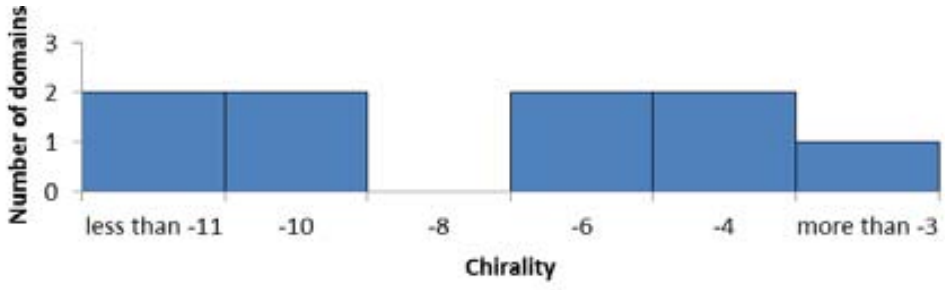

Figure 3.3 *Histogram of angles of (R)-**2,7Naph** Angle measured with respect to the main graphite axes.*

3.2.3 Self-assembly of acid (*S*)-2,7Naph at the graphite-phenyloctane interface

For the enantiomer (*S*)-**2,7Naph** very similar results were obtained with respect to the structure. The compound forms straight and large domains expanding over thousands of square nanometres and the dimers formed are straight and the domain regular. The dimers form an "S" shape, opposite to the "Z" formed by the (*R*) enantiomer. The unit

cell parameters were found to be a= 0.95 ± 0.09 nm, b= 3.41 ± 0.35 nm wide γ= 87.8 ± 1.9º. A typical image is shown in Figure 3.4. Domains are rotated clockwise with respect to the main graphite axis [0010] and the angle measured was +6.0 ± 2.1º. In Figure 3.5 the histogram of angles is presented.

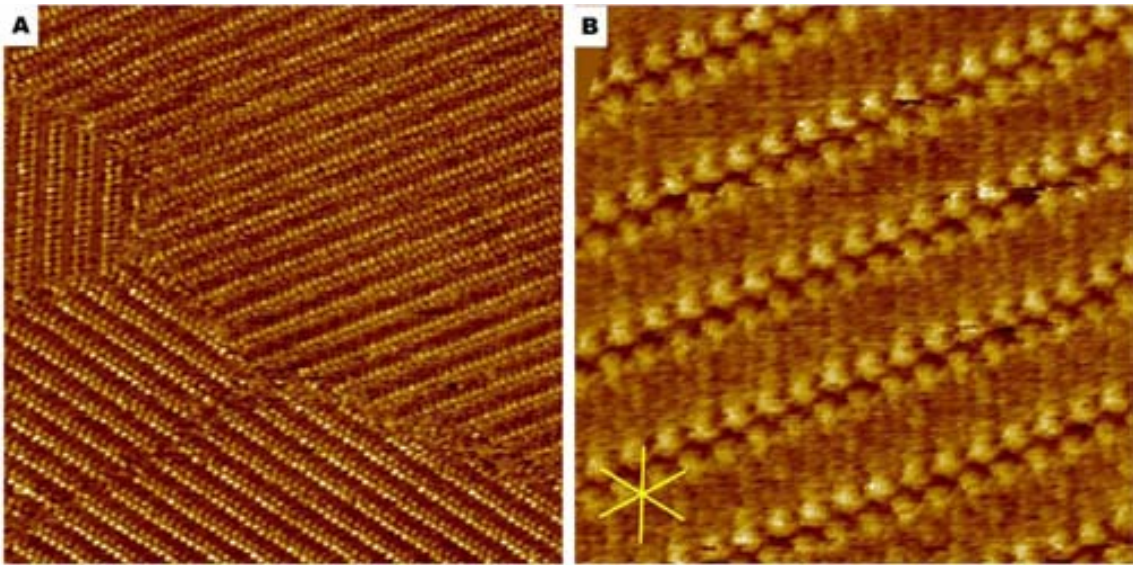

Figure 3.2: *Typical STM images of a monolayer of (S)-**2,7Naph** at the graphite-1-phenyloctane interface. Image A (73.6 x 73.6 nm; I_{set} = 0.2 nA; V_{bias} = 0.8 V) shows the large domain of acid (S)-**2,7Naph** at the graphite 1-phenyloctane interface. In the close up, in image B (16.1 x 16.1 nm; I_{set} = 0.2 nA; V_{bias} = 0.8 V) the "S" shaped structure can be observed, with regular rows of aromatic head groups and interdigitated chains.*

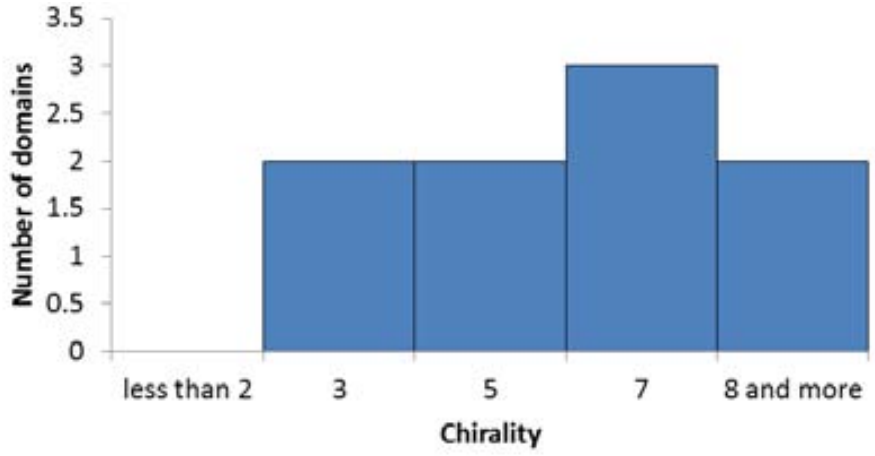

Figure 3.5 *Histogram of angles of (S)-**2,7Naph** Angle measured with respect to the main graphite axes.*

3.2.4 Self-assembly of the racemic mixture of acid 2,7Naph at the graphite-phenyloctane interface

Shortly after the equimolar mixture of the (*R*)-**2,7Naph** and (*S*)-**2,7Naph** in 1-phenyloctane was deposited on the graphite surface, well ordered domains were observed in the monolayer (Figure 3.6).

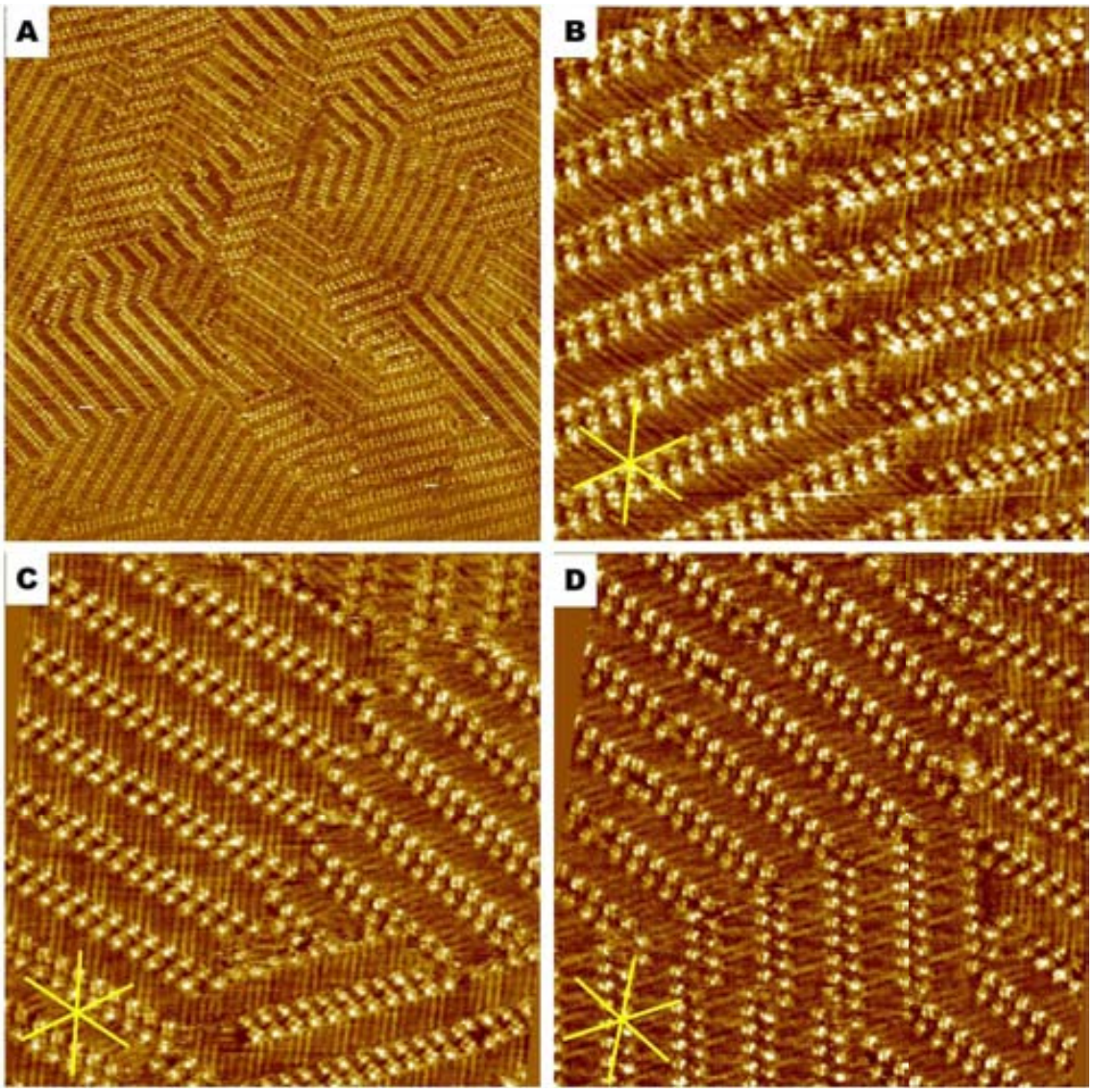

Figure 3.6: *STM image of a monolayer of racemic mixture of compound* ***2,7Naph*** *at the graphite-1-phenyloctane interface. The large scale image A (96.4 x 96.4 nm; I_{set} = 0.2 nA; V_{bias} = 0.8 V) shows the size of the domains. Image B, C and D (24.0 x 24.0 nm, 27.5 x 27.5 nm and 27.4 x 27.4 nm respectively; I_{set} = 0.2 nA; V_{bias} = 0.8 V for all of the images) show the detailed structure of the domains, one can distinguish the "Z" shaped dimers on the left in image B while on the right side the "S" shaped dimers form the monolayer.*

Molecules spontaneously resolve into plus and minus domains, the structures look the same as in the case of the pure enantiomers on graphite and the angle of the lamellae of the structures is, respectively, +4.4 ± 2.6° and -5.5 ± 3.6°. The head-to-head distance and the lamellae width is almost identical as for the pure enantiomers and equals 1.03 ± 0.04 nm (head to head) and 3.43 ± 0.20 nm (width) for the plus domains and 1.03 ± 0.04 nm (head-to-head) and 3.53 ± 0.22 nm (width) for the minus domains. The domains are not as large as in case of the pure enantiomers; the size starts from approximately 10 nm to about 100 nm long lamellae. It is quite easy to distinguish the domains, looking at whether the dimer is "S" or "Z" shaped. Figure 3.6 presents the images where molecules occupy the entire surface and the domain borders are well defined. In Figure 3.7 the histogram of angles is presented. It can be seen clearly that there is higher representation of the domains at +6 than any other, but the histogram for angles in minus is quite similar to the one observed for *(R)* enantiomer of acid. Comparing with combined histograms of both enantiomers, there is higher representation of structures at angles between -3 and +3 for the racemic mixture.

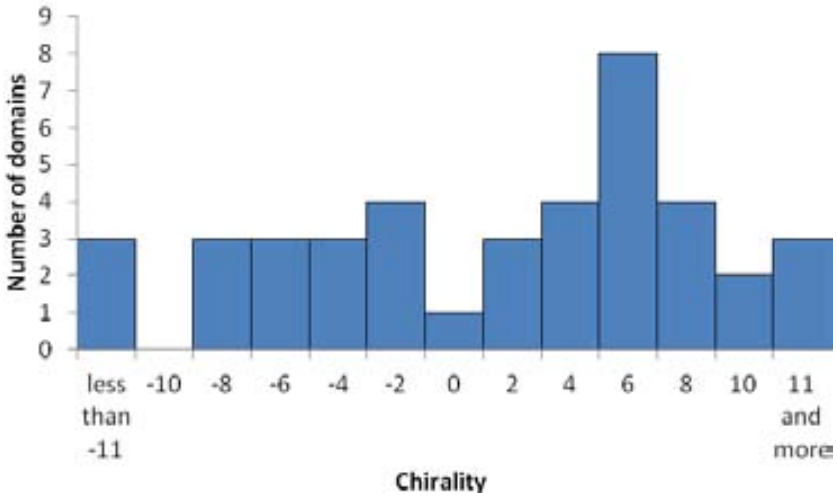

Figure 3.7: *The histogram of angles of domains of racemic* ***2,7Naph*** *at the graphite-1-phenyloctane interface. The angles where measured with respect to main graphite axis. It is clear that there are more domains with chirality close to +5, while in anticlockwise domains surprisingly there is no preferential for any angle, but it might be due to the low number of analysed domains. Still just one domain was found with the angle between -1 and +1.*

3.3 2,6-Naphthalne derived amphiphile[37]

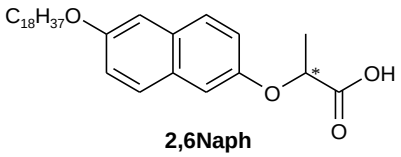

2,6Naph

3.3.1 Synthesis

The enantiomers of the naphthalene derivative **2,6Naph** were synthesised in an analogous manner to its 2,7 regioisomer. The synthetic route is shown in Scheme 3.3. The first step was the Mitsunobu reaction of 2,6-dihydroxynaphtalene with either one or the other enantiomer of the methyl lactate to obtain compound **21** with 24% yield for (*R*) product and 23% yield for (*S*) product, which after separation from the side products of the reaction by column chromatography was used for the next step in which the alkyl chain was attached in the basic conditions (yield of this reaction was 74% for the (*R*) and 65% for the (*S*)). The last step was the hydrolysis of ester followed by crystallization of the product. Yield of the saponification was 69% for both the (*R*) and the (*S*)-**2,6Naph.** The NMR, IR and MS analysis of the compound confirmed the desired structure.

[37] This section was published in: W. J. Saletra, H. Xu, T. Vosch, S. De Feyter, D. B. Amablino, *CrystEngComm,* **2011**, *13*, 5578.

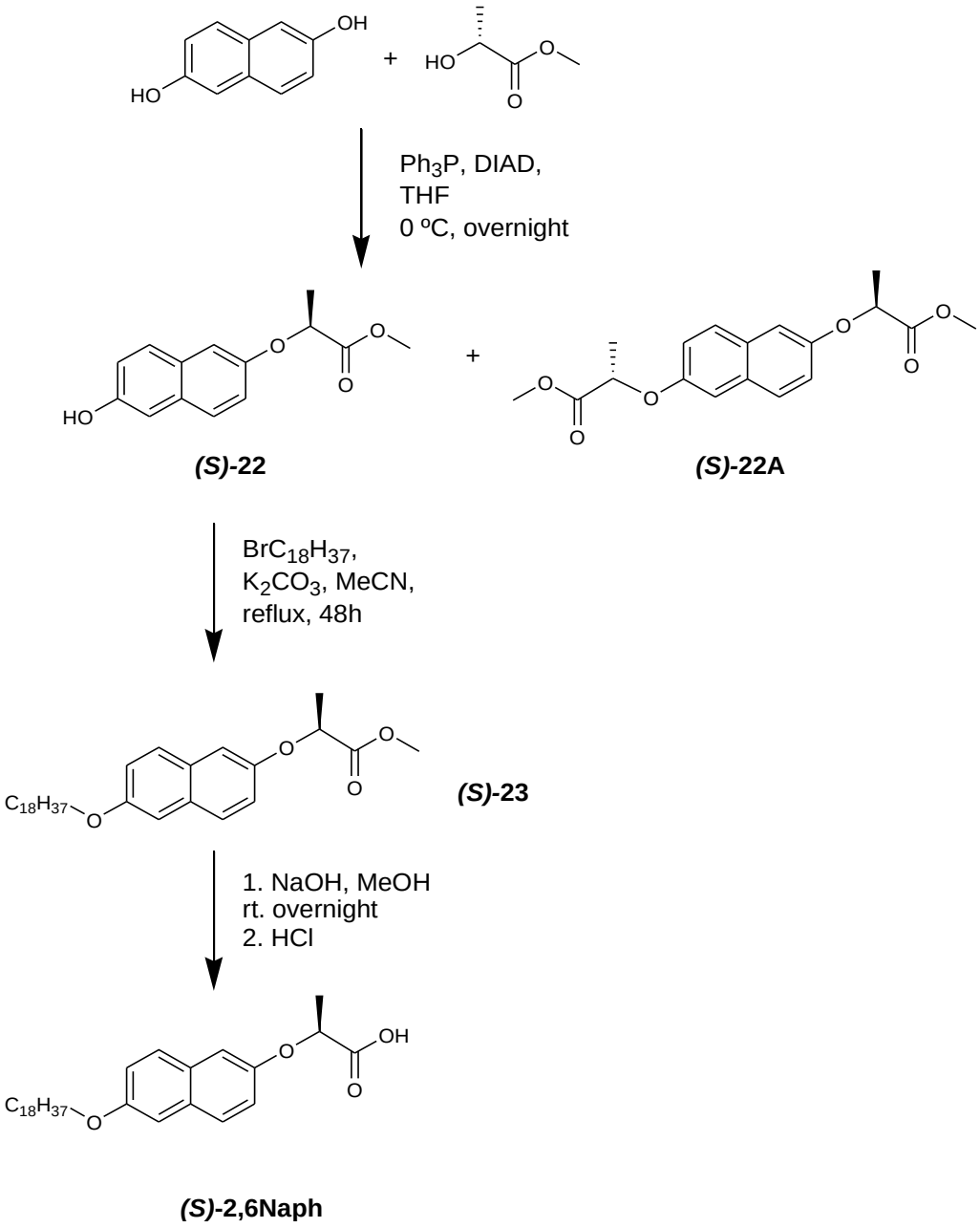

Scheme 3.3: *Synthesis of (S)-**2,6Naph***

3.3.2 Self-assembly of acid (*R*)-2,6Naph at the graphite-phenyloctane interface

The compound was dissolved in 1-phenyloctane and a drop of the warm solution was applied on the surface of freshly cleaved HOPG. The surface was placed in the STM and within minutes the formation of monolayer was observed.

The representative images of the compound **2,6Naph** at the graphite – 1-phenyloctane interface are shown in the Figure 3.8.

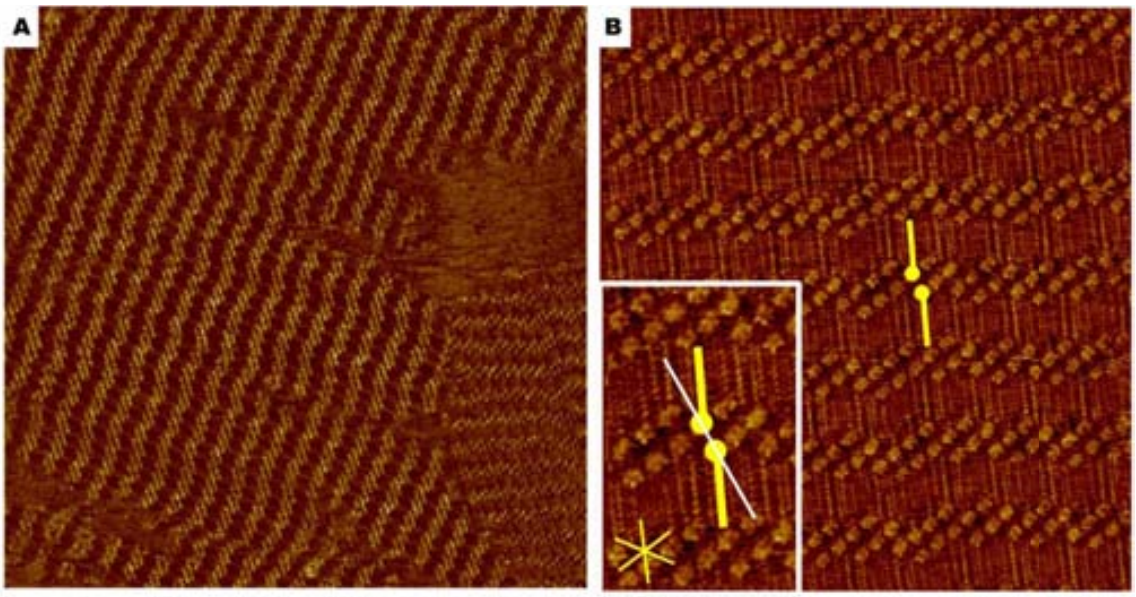

Figure 3.8: *STM images of a monolayer of (R)-**2,6Naph** at the graphite-1-phenyloctane interface. Image A (90.4 × 90.4 nm; I_{set} = 0.25 nA; V_{bias} = 1.0 V) shows a large domain with a boundary. Image B (25.2 × 27.4 nm, I_{set} = 0.25 nA; V_{bias} = 1.0 V) is a smaller-scale image of a single domain. A dimer is indicated in yellow. The head group is represented by a disk, the alkyl chain by a solid line. The white line connecting both head groups of a dimer makes an angle with the long axes of the alkyl chains.*

A lamellar structure is obvious in the images shown, although unlike the majority of structures of this kind observed at the graphite-liquid interface, there are obvious "jumps" in the lamellae. The molecules seem to take a given chiral direction for two or three head-to-head pairs, but then jumps back in the opposite way with respect to the lamella vector. This observation seems to imply that the stereogenic centre in the molecule forces the lamellae into one chiral sense, but the two-dimensional packing restrictions are not compliant, and therefore the pairs of molecules jump back towards the mean lamellar axis. The result of this situation is an ordered structure along the alkyl chain axis, that is there is longitudinal order, but the transversal order is not so strong, and therefore several correlated defects occur. This situation reminds us of the situation in nematic liquid crystals, in which the shape of the molecule determines the superstructure.

An analysis of the regularity of several domains is shown in Figure 3.9. After analysis of five domains containing from 80 to 120 dimers it was found that the most common pattern is the row Up-Down-Up-Down-Up-Down etc., although after the third and fourth regular steps there is higher probability of an irregular step than elsewhere, as

shown in Figure 3.6. The analysis also shows that the SAM of (*R*)-**2,6Naph** has a slight excess of steps up over steps down, and with (*S*)-**2,6Naph** there is an excess of steps down.

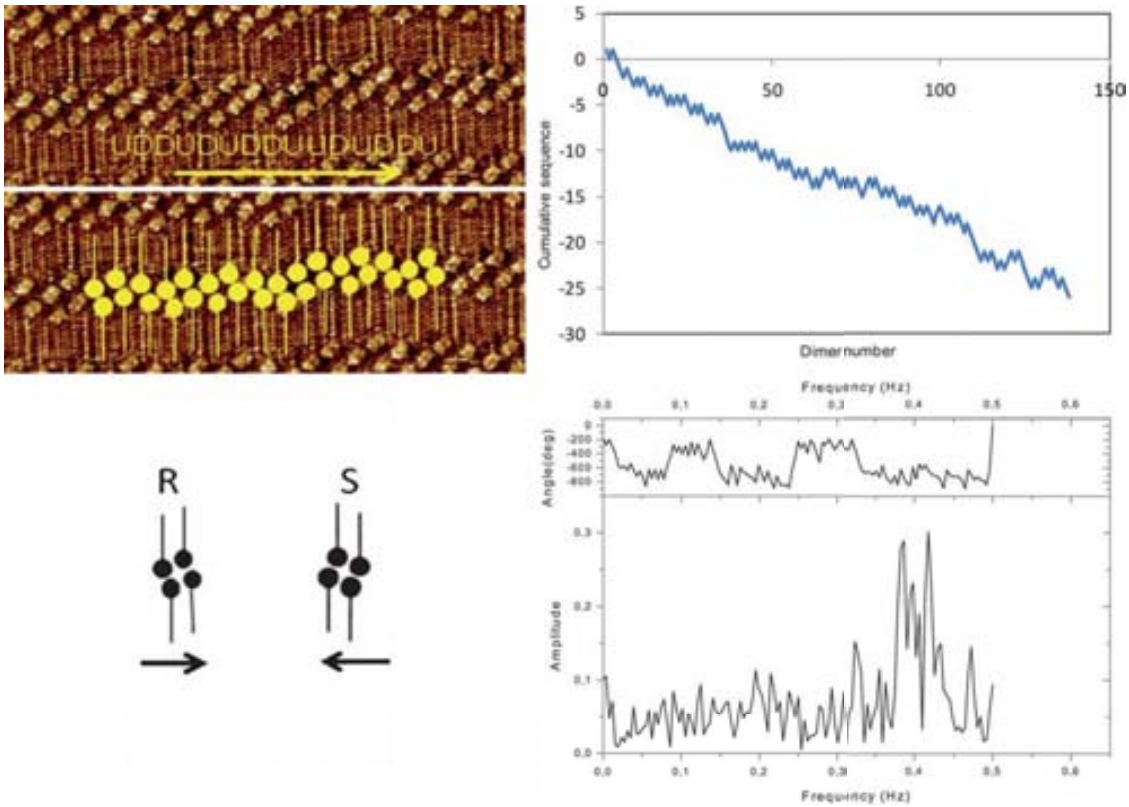

Figure 3.9*: Analysis of irregularity (A) Model for analysis. Looking from left to right: U stands for step up, D stands for step down. (B) Example of irregular domain taken to analysis. (C) Convention of reading the patter from left to right for the (R) enantiomer and from right to left for the (S) one. (D)Frequency of irregularity form pattern U-D-U-D. The peak at 0.4Hz is clear indication of irregularities.*

Apart from the irregularities in the chiral sense of the lamellar packing, some defects in the lamellar structure were also found, albeit infrequently. Most of the molecules form dimers on the surface, but there is an exception from that rule, as shown on Figure 3.10. Here, a pattern is reproduced in every row but one, where three naphthyl units are apparently located in line. This situation cannot allow all the alkyl chains to be located flat on the graphite surface, and it is surmised that the chain attached to the naphthyl ring which is surrounded by others is directed toward the solvent.

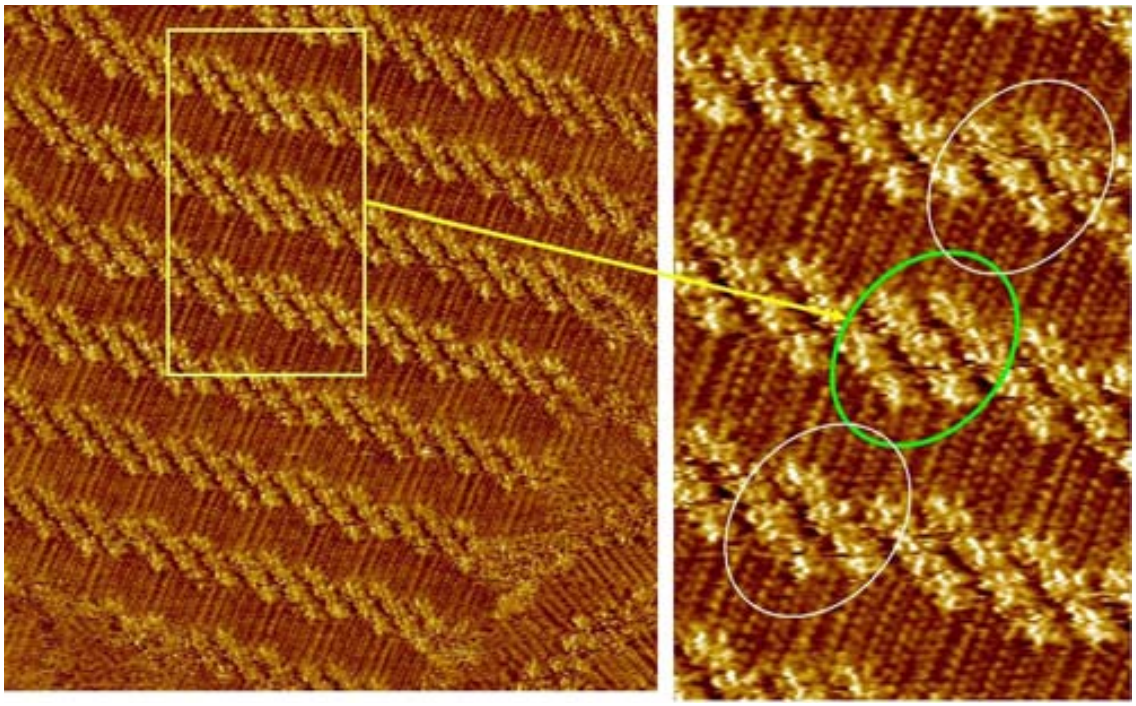

***Figure 3.10**: STM image (26.3 x 26.3 nm, I_{set}: 0.25nA V_{bias}:1.0 V) of a monolayer of (R)-**2,6Naph** at the 1-phenyloctane-HOPG interphase showing a defect in the packing in the form of a naphthalene ring surrounded by six others (middle circle in the lower expanded image).*

3.3.3 Self-assembly of racemic mixture of acid 2,6Naph at the graphite-phenyloctane interface

The influence of the stereogenic centre in the molecule and the chirality of a sample as a whole on the packing can be revealed by comparing the organisation of the racemic sample with that of the enantiopure one. Therefore, the self-assembly of the solution of the equimolar mixture of (*R*)-**2,6Naph** and (*S*)-**2,6Naph** was also investigated by STM at the interface between graphite and 1-phenyloctane, in identical conditions to the enantiopure samples. After deposition of a solution of the racemate on freshly cleaved graphite and a short period of scanning with the tip of the microscope, disordered domains are observed. Again, the STM images show bright spots corresponding to the aromatic head groups and less bright lines arising from the alkyl chains. However, while the molecular contrast is similar to the enantiopure case, it is clear from the large scale STM image in Figure 3.11 that irregular lamellae are formed, which only follow certain well-defined directions over very small areas (around 200 nm^2). However, the alkyl chains – which are interdigitated – seem to follow the same graphite axis over larger areas even though the aromatic head groups are disordered.

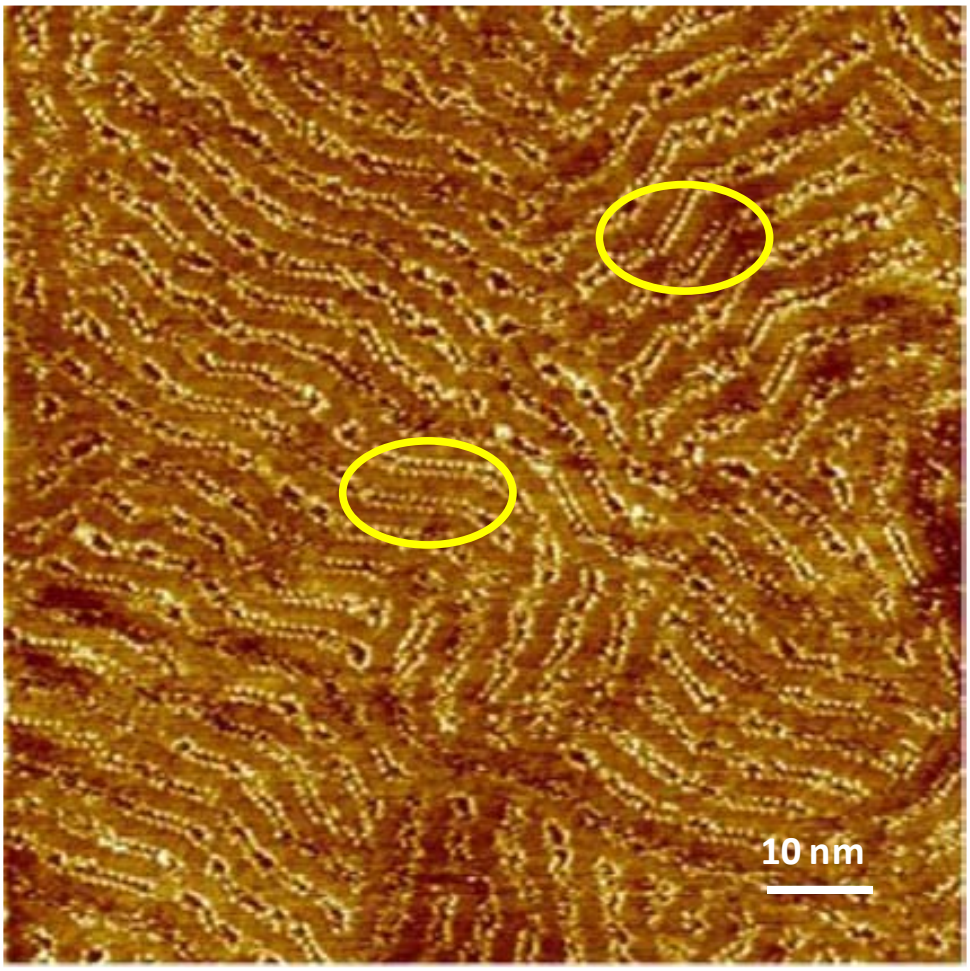

Figure 3.11: *Large scale STM view of the monolayer formed by racemic* ***2,6Naph*** *at the phenyloctane-graphite interface (90.4 x 90.4 nm* I_{set} *= 0.70nA* V_{bias}*=0.8V). In the yellow circles the area where the molecules spontaneously resolve into enantiopure domains.*

In the small more ordered areas, the alkyl chains run parallel to one of the graphite symmetry axes below and the aromatic head groups seem to form a two-dimensional crystalline structure, marked with ellipse in Figure 3.11. This feature might imply that very locally the compound spontaneously resolves in some areas, although in the majority of the monolayer it forms a disordered racemate, with the up-down pattern not formed because of the small size of the domain and the resulting weak overall packing forces. A racemic domain would not be expected to have this characteristic, because of the lack of C_2 symmetry (with the axis perpendicular to the plane of the surface) in the domain, a situation which is favoured for these chiral systems.

Closer images of the monolayer of the racemate (Figure 3.12) reveal that the aromatic head-groups seem to follow an undulating line, rather than the clear and ordered (if not perfectly two-dimensionally periodic) up-down dimer type structure observed in the

enantiopure samples. At the head-to-head point of the lamellae, where the aromatic groups face one another, the centre-to-centre aromatic distance across the apparent gap (where the carboxylic groups must be located) is between 1.35 and 1.60 nm in the racemic monolayer, much larger than the 0.95 to 0.98 nm observed in the pure enantiomers. The distances between aromatic head-groups along the lamellar direction in the racemate are approximately 1.05 nm, similar to the distance in the monolayer of the pure enantiomers. The fuzzy areas in image A in Figure 3.12 probably arise from instability of some conformations on the surface or are caused by the influence of the tip in this relatively poorly packed monolayer.

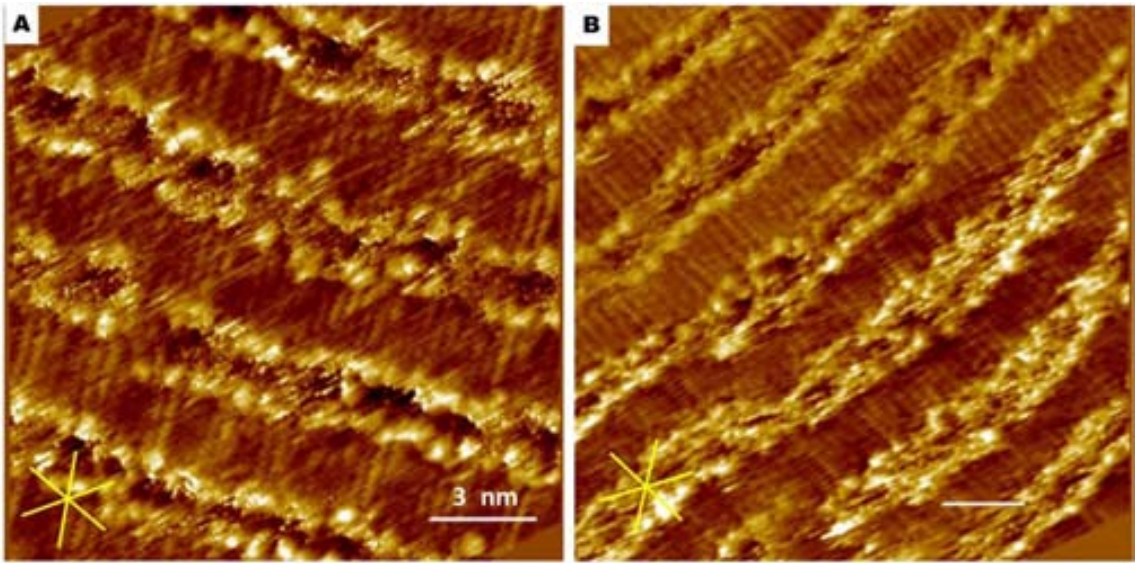

Figure 3.12: *Close-up STM view of the monolayer formed by racemic-**2,6Naph** at the phenyloctane-graphite interface (A 15.8 x 15.8 nm, I_{set}=0.50nA,V_{bias}=0.8V, B 20.5 x 20.5 nm I_{set}=0.50nA V_{bias}=0.8V). The lamellae, although globally keep the direction, locally have a lot of defects. The resolution on aromatic parts is varying a lot, however the alkyl chains have the same contrast and good resolution trough all the images.*

The alkyl chain interactions seem to dominate the packing of the racemic sample, as the (*R*) and (*S*) enantiomers must be distributed throughout the more poorly ordered domains, whereas in the enantiopure samples the homochiral nature of the headgroup forces an ordered structure in the monolayer. Albeit, the influence of the alkyl chain is very strong, as witnessed by the alternating nature of the packing of the head-groups in the enantiopure samples. The ordering of three dimensional crystals using enantiopure samples when compared with racemates has been observed, although in the present case the effect on the structure of the monolayer is dramatic.

3.4 1,5-Naphthalene derived amphiphile

3.4.1 Synthesis

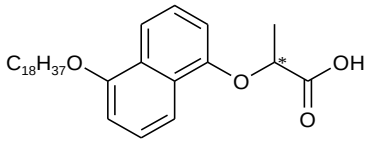

1,5Naph

The enantiomers of naphthalene derivative **1,5Naph** were synthesised in a similar way to the other regioisomers of these acids. The synthetic route is shown in Scheme 3.4. The first step was the Mitsunobu reaction of 1,5-dihydroxynaphtalene with either one or the other enantiomer of the methyl lactate, to obtain compound **31** with 17% yield for the (*R*) enantiomer and 21% of yield of the (*S*) product, which after separation from the side products of the reaction by column chromatography was used for the next step in which the alkyl chain is attached under basic conditions (Yields: 18% for the product (*R*)-**32** and 59% for the (*S*) product). The last step was the hydrolysis of ester followed by crystallization of the product (Yields 54% and 64% for (*S*)-**1,5Naph** and (*R*)-**1,5Naph** respectively). The usual analysis of the compound confirmed the desired structure.

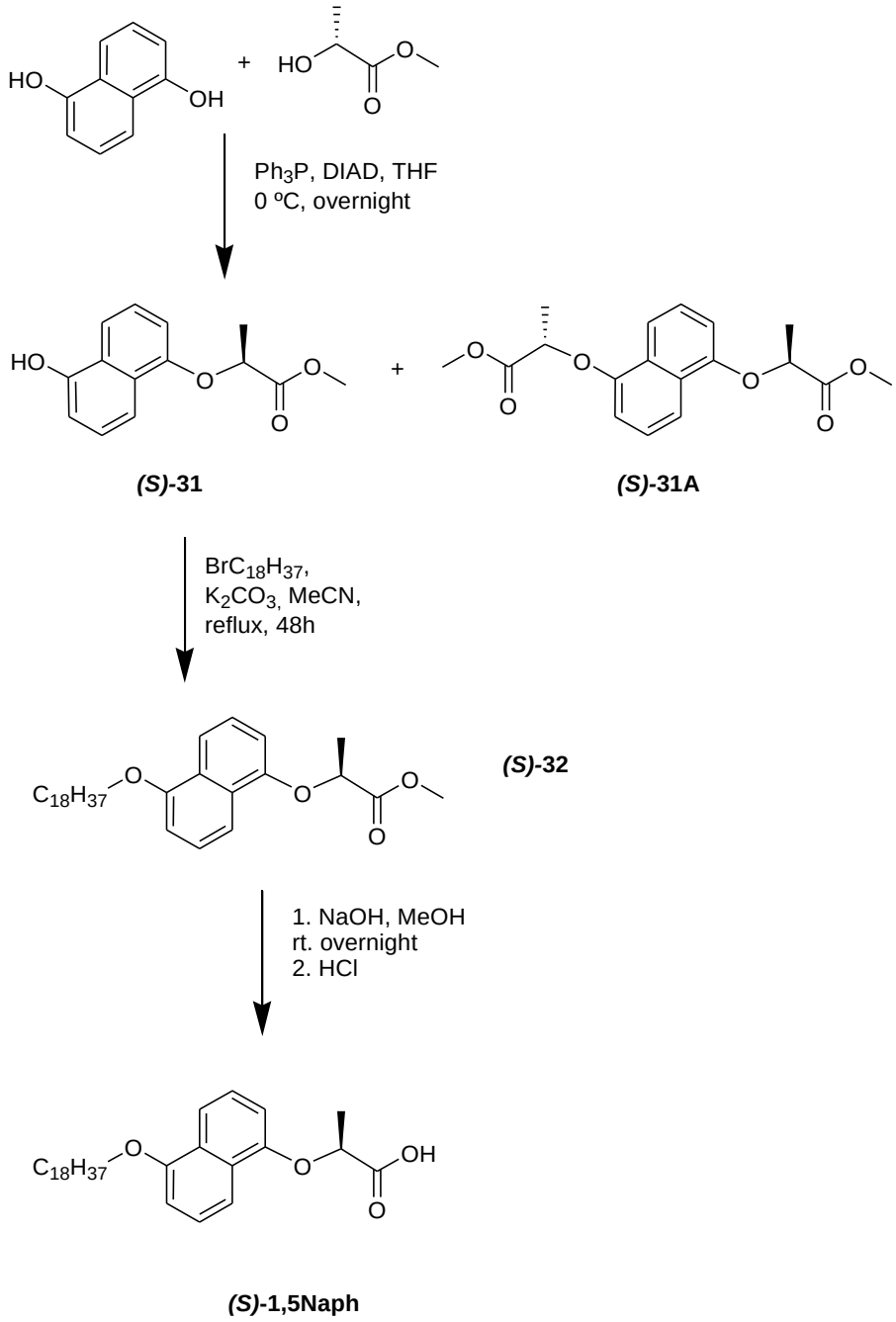

Scheme 3.4: *Synthesis of (S)-**1,5Naph***

3.4.2 Self-assembly of (*S*)-1,5Naph at the graphite-phenyloctane interface

The compound (*S*)-**1,5Naph** was dissolved in 1-phenyloctane and a drop of the warm solution was applied to the cleaved surface of HOPG. Within minutes the self-assembled monolayer was visualised with STM. Typical large scale images of the monoalyer are presented in Figure 3.13. The contrast in the images reflects the distance between the tip and the monolayer. The brightest parts in the images are the aromatic part of molecules,

known for its better conductivity for tunnelling electron when compared with alkyl chains, which appear as duller (dotted) lines. In the case of these molecules, unlike the two previous regioisomers, there are several different structures – surface-based polymorphs, which are precedented for other compounds[38] – that are found in the STM images. The structure has quite a number of defects, marked with the circles in the image 3.13A and others in the image 3.13B, and also apparent aggregates of molecules (white large spots) are observed often. The most common arrangement of the molecules at the graphite-1-phenyloctane interface is a row bright parts – aromatic heads of molecule directed as /////// in the direction of growth of the lamellae (vertical in the image 3.13A). In the STM images one can find two variations of the main arrangement of the molecules, in the image 3.10A the thin yellow line separates them. It is clear that there is difference in angle between the main arrangement (called type 1) that goes almost vertical in this image and inside the marked area (type 2) that is tilted.

A close-up of the main structure, called type 1 is shown in Figure 3.14A and has characteristic stripes of the aromatic parts. It can be seen clearly that the aromatic head groups form straight rows tilted at an angle of approximately 50.9 ± 4.3º to the direction of the lamellae, separated by the dark area where the lactate unit has to be placed. The alkyl chains are interdigitated, but unlike the case of compounds **2,7Naph** and **2,6Naph** the chains seem not to occupy all the area between the aromatic heads, leaving a bit of space on the one side. Having a closer look one can realise that the aromatic parts do not form the ideally straight lamellae, but every second is a bit shifted (left looking at the image orientated as the Figure 3.14A). The unit cell is marked in the image 3.14A and the parameters of the unit are: a= 3.03 ± 0.20 nm, b= 5.34 ± 0.30 nm and γ= 75.6 ± 3.1º. The model of packing is presented in the same image and it is clear that there are 5 molecules forming row of aromatic heads. As in each row of heads three alkyl chains are on one side and two on the opposite side and in next complementary row three are on the opposite side and two on the first. As this pattern is mainly repeated in the domains there are 10 molecules in each unit cell. The structure is chiral itself, the molecules form an asymmetric pattern on the surface. The molecules that form

[38] (a) L. Xu, X. Miao, B. Zha, W. Deng, *Chem. Asian J.*, **2013**, *8*, 926. (b) N. T. N. Ha; T. G. Gopakumar, M. Hietschold, *Surf. Sci.*, **2013**, *607*, 68. (c) J. F. Dienstmaier, K. Mahata, H. Walch, W. M. Heckl, M. Schmittel, M. Lackinger, *Langmuir*, **2010**, *26*, 10708. (d) R. Gutzler, T. Sirtl, J. F. Dienstmaier, K. Mahata, W. M. Heckl, M. Schmittel, M. Lackinger, *J. Am. Chem. Soc.*, **2010**, *132*, 5084. (e) J.-H. Kim, K. Tahara, J. Jung, S. de Feyter, Y. Tobe, Y. Kim, M. Kawai, *J. Phys. Chem. C*, **2012**, *116*, 17082. (f) S. Lei, K. Tahara, F. C. De Schryver, M. van der Auweraer, Y. Tobe, S. de Feyter, *Angew. Chem. Int. Ed.*, **2008**, *47*, 2964.

hydrogen bonds are “S” shaped and the aromatic heads are forming rows of slashes “////” in the direction of growth of the lamella. Another way that the chirality is expressed on the surface is the rotation with respect to the graphite, in this case the structure is rotated anticlockwise with respect to the main graphite axis at an angle of -18.5 ± 3.5º and a histogram of the angles is presented in Figure 3.15.

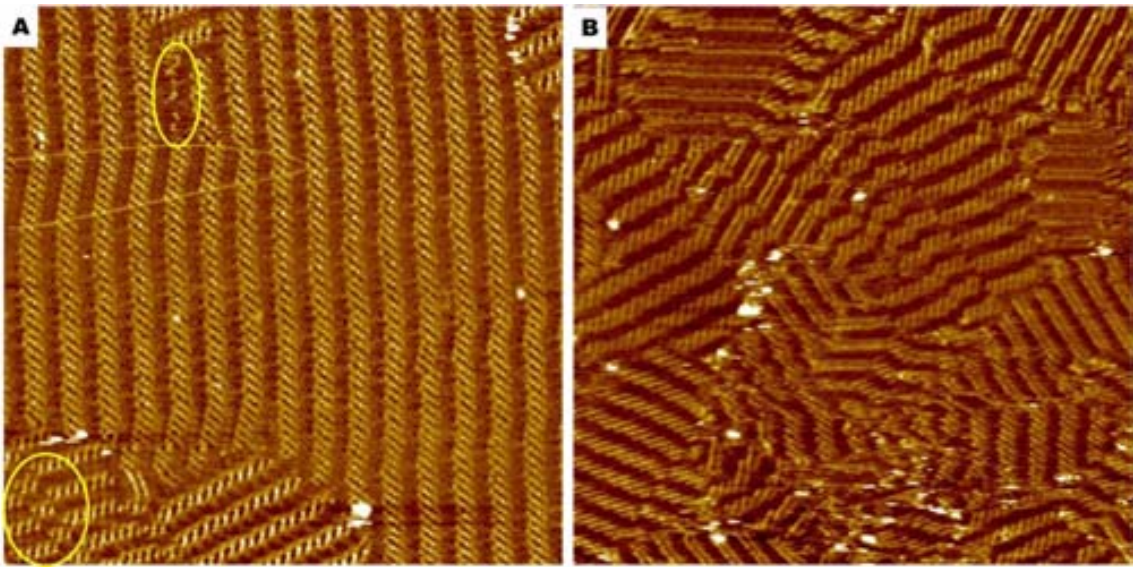

Figure 3.13: *Typical large scale STM images of a monolayer of (S)-**1,5Naph** at the graphite-1-phenyloctane interface. Image A (83.3 x 83.3 nm; I_{set} = 0.2 nA; V_{bias} = 0.8 V) presents the large domain with ordered, regular lamellae type 1, and a surprising defects in the lower left corner of the image marked with the yellow oval, the structure has steps. In the top of the image another defect can be seen: due to the limited space one of the lamella finishes in disordered area marked with oval. In the left part of the image there is domain type 2 marked with thin yellow line. In image B (96.4 x 96.4 nm; I_{set} = 0.2 nA; V_{bias} = 0.8 V) the composition of short domains covers the area. The ability to change from one structure to the other and the different boundary effects can be spotted.*

Variation of this structure, called in this thesis type 2, is observed in Figure 3.13A, marked with thin yellow line, and in close up in Figure 3.14B in left bottom corner. This type of structure is distinguished by having just four aromatic heads of acid in a row, as presented in the model of packing in Figure 3.14B. Also the alkyl chains are interdigitated much better comparing with the other one and domains are much more uniform, it can be appreciated especially in Figure 3.13A. The width of the domains of this type is 4.42 ± 0.28 nm comparing with 5.10 ± 0.21 nm for the type 1, while the chirality of the type 2 structure is -9.8 ± 6.0º (type 1 is -18.5 ± 3.5º). The histogram of

angles of this structure is presented in Figure 3.16. It should be mentioned that structure type 1 and 2 can convert smoothly into other (as in the Figure 3.13A) and it is not always easy to find boundaries between them.

The third type of domain that can be observed in the SAM of (*S*)-**1,5Naph** at the graphite 1-phenyloctane interface is shown in the centre part of the image in Figure 3.14B. The molecules form straight, but short, lamellae in which the alkyl chains are not interdigitated. The aromatic parts of the molecules form straight rows and the brightness of the features from these moieties indicates that they are probably not lying flat on the graphite but are tilted and the naphthyl rings of neighbouring molecules are interacting with each other via π stacking. The only one domain measured with this was 4.9 nm wide and the chirality with respect to the graphite substrate was -13.5º. The lamellas of this type tend to continue into the two main types of domain whenever possible, as observed in Figure 3.14B.

Another, fourth type of domain that was found in the STM images is shown in Figure 3.11D, the molecules form very straight and regular lamellae. The aromatic heads of the molecules can be distinguished easily and the alkyl chains are interdigitated. This kind of domain is not as long as the most common domains. They are usually 10 to 30 nm long and surrounded by the other kinds of lamellae. The molecules seem to form a pattern similar to the SAM made by molecules **2,7Naph –** but it seems that the alkyl chains are almost perpendicular to the domain growth direction in case of (*S*)-**1,5Naph**, while it was clearly at the angle for domains formed by **2,7Naph**. The lamellae thickness equals 3.88 ± 0.10 nm, the head to head distance is 0.80 ± 0.15 nm compared with 3.41 ± 0.30 nm and 0.95 ± 0.09 nm respectively for (*S*)-**2,7Naph**. The structure is rotated clockwise with respect to main graphite axis and the angle is +8.2 ± 8.6º comparing with +6.0 ± 2.1 for (*S*)-**2,7Naph**. It is surprising that the head to head distance is smaller than in **2,7Naph**, as the aromatic spacer in **1,5Naph** is connected in a such way that naphthalene ring cannot be in line with alkyl chain and lactic group.

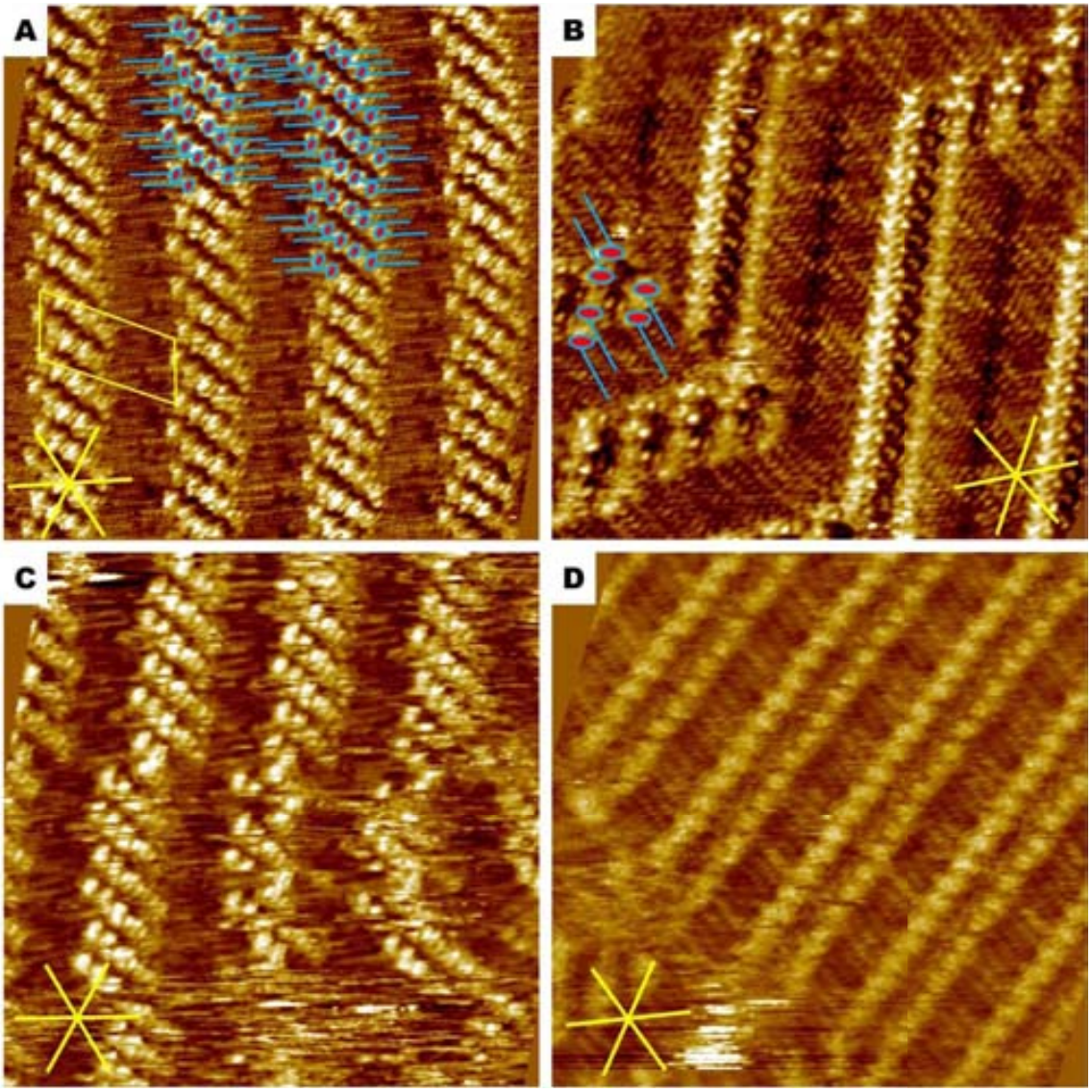

Figure 3.14: *Close-up STM images of a monolayer of (S)-**1,5Naph** at the phenyloctane-graphite interface. Image A (14.4 x 14.4 nm; I_{set} = 0.2 nA; V_{bias} = 0.8 V) shows the most common and most ordered type of domain (type 1), where five aromatic head groups of the molecules form lines that of "///////". The unit cell is marked in the image. In image B (20.4 x 20.4 nm; I_{set} = 0.2 nA; V_{bias} = 0.8 V) another type of structure is found, where the aromatic parts are tilted from the surface and the alkyl chains of the two rows are not interdigitated, while in the left bottom corner of the image the type 2 strucutre is presented also with schematic model of packing. In image C (20.5 x 20.5 nm; I_{set} = 0.2 nA; V_{bias} = 0.8 V) area where domain is losing its order gradually from lamella to lamella from left to right. In image D (16.9 x 16.9 nm; I_{set} = 0.2 nA; V_{bias}= 0.8 V) the third type of structure is presented, with alkyl chains interdigitated and aromatic parts forming long straight rows.*

The analysis of large scale images of (*S*)-**1,5Naph** covering over 50 000 square nanometres gives us an idea of distribution of different structures. 46.6% of area was

covered with main structure type 1, while the second type was covering 23.9% of area. Narrow, noninterdigitated domain (third type) covered 3.4% of area, while narrow interdigitated - 8.8%. 17.3% of area was too noisy to be identified as any specific domain.

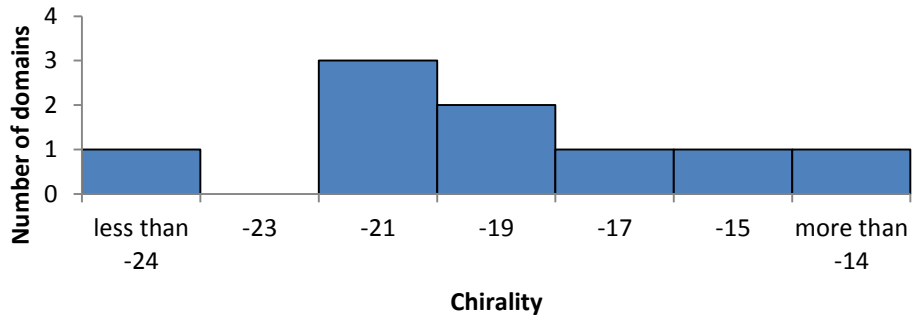

Figure 3.15: *Histogram of angles of main structure type 1. There is clear preference for the anlges between -18 and -22, just one domain is found at lower angles.*

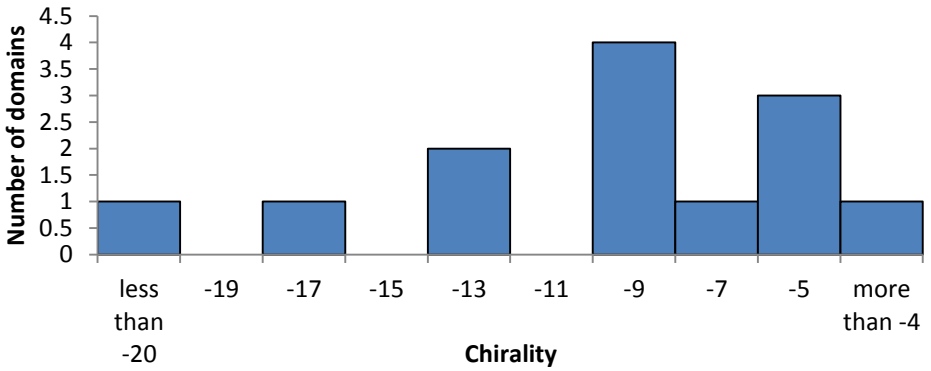

Figure 3.16: *Histogram of angles of main structure type 2. There is preference for the anlges between -4 and -14, just one domain is found at lower angles.*

3.4.3 Self-assembly of (*R*)-1,5Naph at the graphite-phenyloctane interface

For the enantiomer (*R*)-**1,5Naph** similarly as for the mirror image structure four main self-assembled structures were found, and are presented in the Figure 3.17 and 3.18. The most common structure is mirror image of the structure type 2 shown for the enantiomer (*S*), even the bright specks seen in the images are reproduced, but the type 1 is also observed. The details of different structures can be observed in Figure 3.19.

The main structure type 1 is presented in Figure 3.17. The parameters of this kind of domains are: chirality +19.1 ± 5.6º and lamella width 4.82 ± 0.41 nm. Histogram of

angles is shown in Figure 3.20.

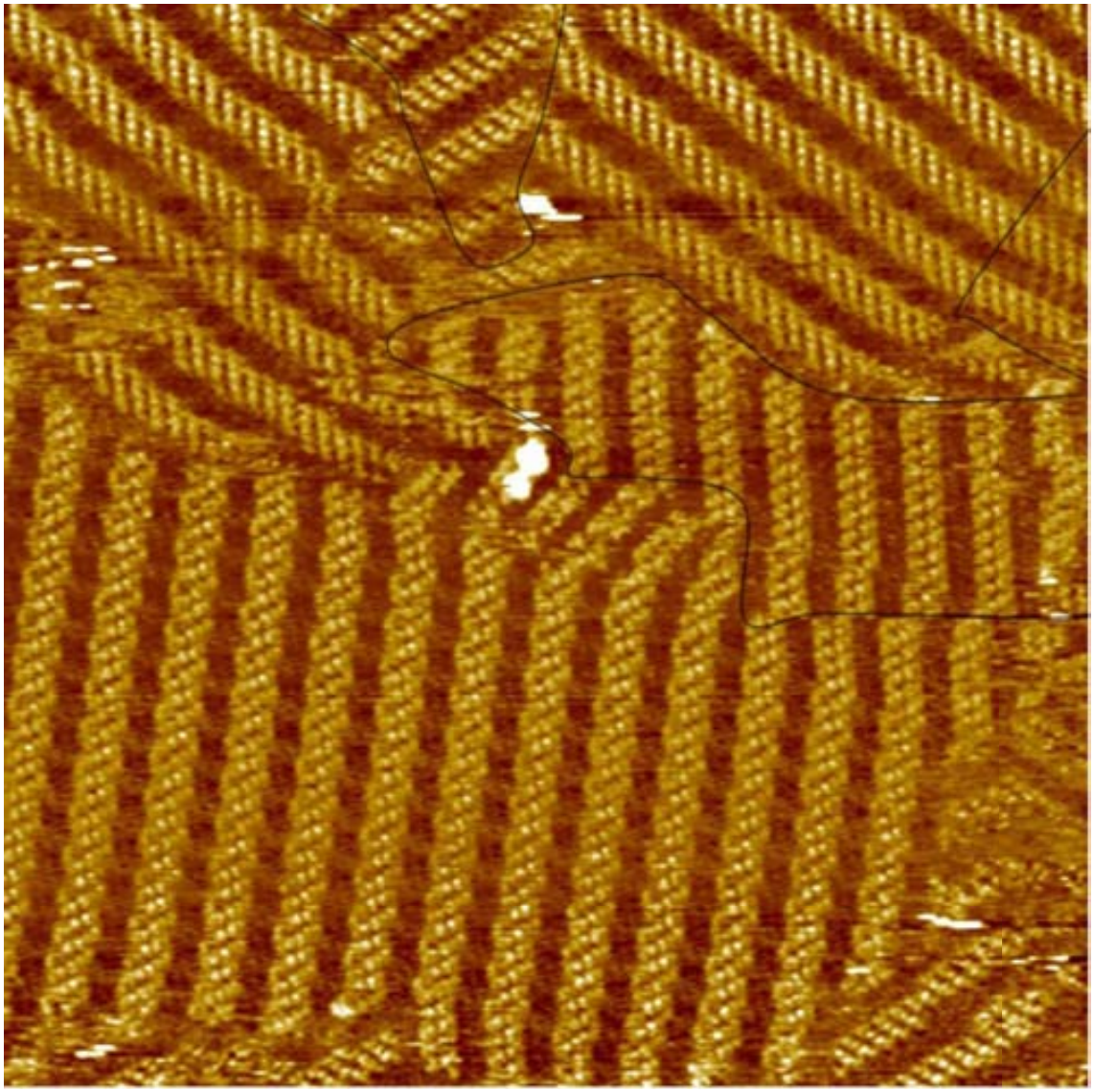

Figure 3.17: *Typical large scale STM images of a monolayer of (R)-**1,5Naph** at the graphite-1-phenyloctane interface. The image (80.1 x 80.1 nm; I_{set} = 0.2 nA; V_{bias} = 0.8 V) shows area with ordered domains. The white spots are the places where aggregates of molecules stick to the surface. Most of the image is covered with main structure type 1 but in the area marked with black line, type 2 domains are observed.*

The other variation of main structure, type 2 is also spotted frequently in this sample. The model of packing of this kind of structure is presented in the Figure 3.19A. Parameters measured for this kind of domains are chirality +6.7 ± 5.3º and width 4.1 ± 0.30 nm. The histogram of angles for this structure is presented in Figure 3.21.

Also, mirror images of the other type of domains shown in Figure 3.14B and 3.14D were found and are presented respectively in the Figure 3.19C and 3.19D. The

parameters of the domains with noninterdigitated alkyl chains are: chirality with respect to main graphite axis equals +8.0 ± 2.4º and the lamella width 5.2 ± 0.1 nm, while for interdigitated structure the angle is -8.2 ± 7.3º and lamella width 3.5 ± 0.2 nm.

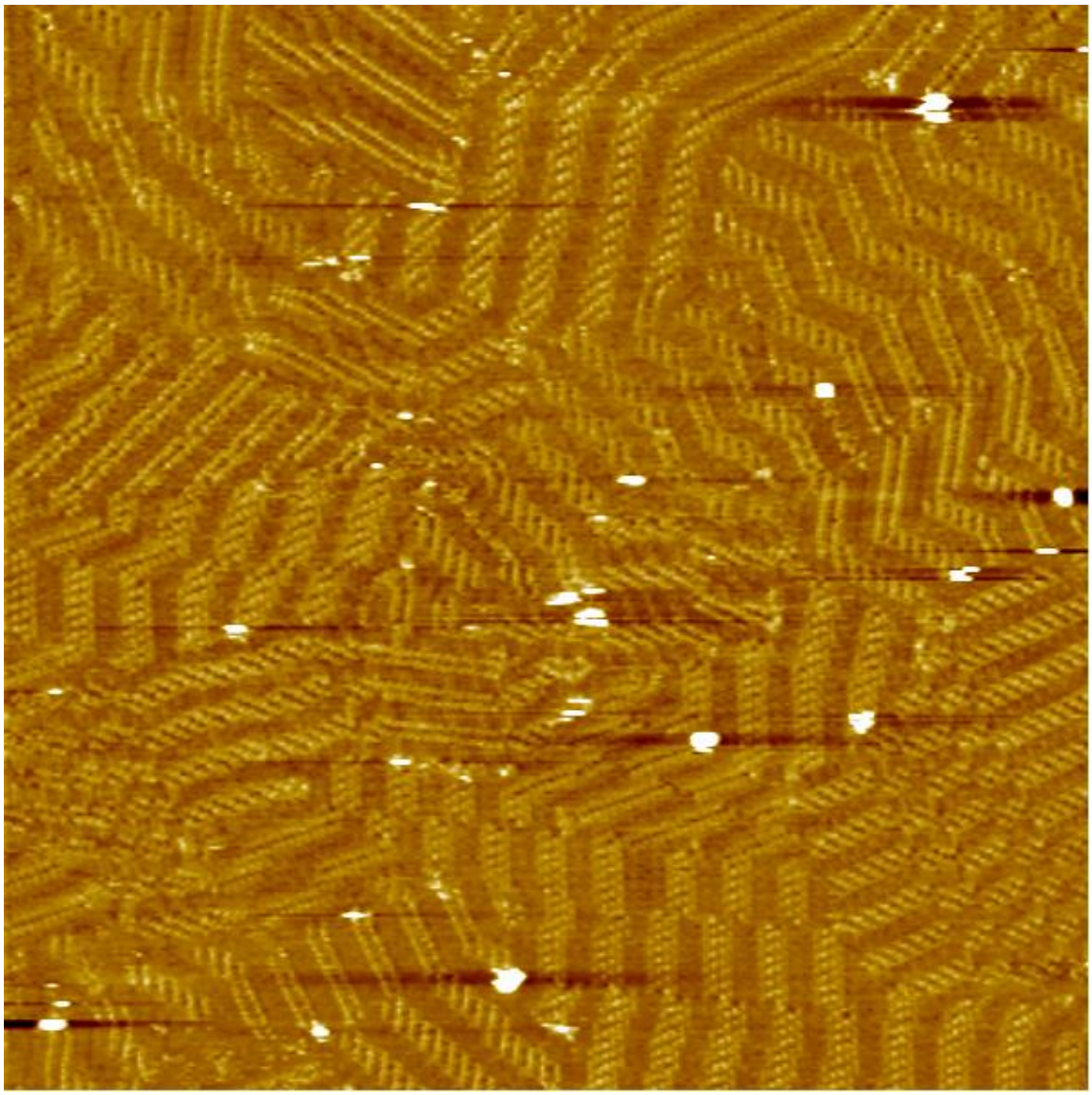

Figure 3.18: *Typical large scale STM images of a monolayer of (R)-**1,5Naph** at the graphite-1-phenyloctane interface. In the image (80.1 x 80.1 nm; I_{set} = 0.2 nA; V_{bias} = 0.8 V) the area with short domains of different type is observed.*

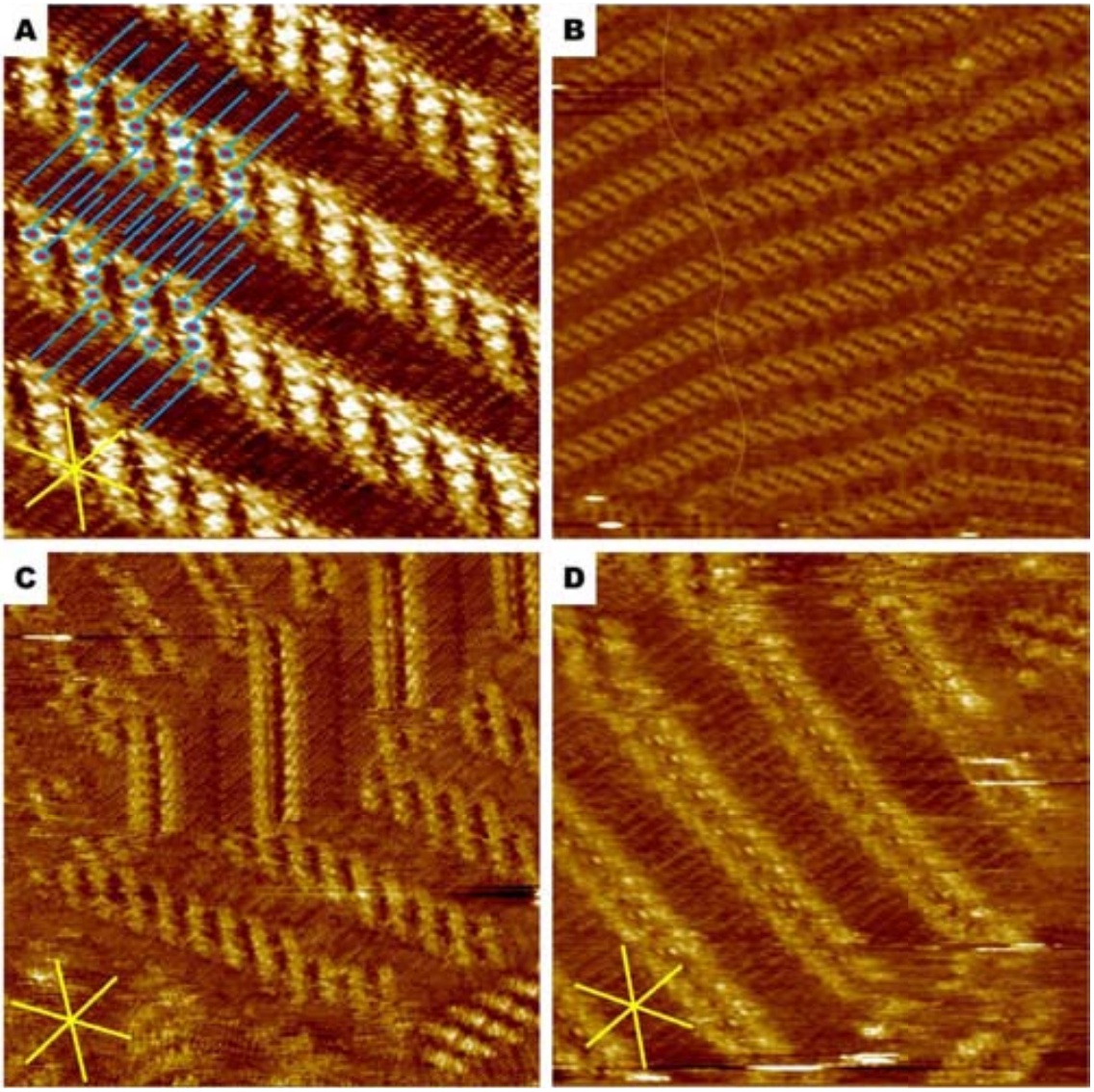

Figure 3.19: *Close-up STM images of a monolayer of (R)-**1,5Naph** at the graphite-1-phenyloctane interface. Image A (14.7 x 14.7 nm; I_{set} = 0.2 nA; V_{bias} = 0.8 V) shows the type 2 domain with aromatic parts forming rows of four head groups and those rows are orientated like "\\\\\\" with respect to the lamella growth direction, alkyl chains are interdigitated. In image B (43.7 x 43.7 nm; I_{set} = 0.2 nA; V_{bias} = 0.8 V) the change between three different type of domains is observed. In the left and top right of the image the type of structure as in image A is observed, then in the centre of the image the contrast of the alkyl chains and the direction of the lamella is changed slightly, to form type 1 domain. The change between 1 and type 2 domains is marked with thin yellow line. In the bottom right part of the image the structure with aromatic parts in line and interdigitated alkyl chains is presented. Image C (21.7 x 21.7 nm; I_{set} = 0.2 nA; V_{bias} = 0.8 V) is where one observe in the upper part of the image domain with aromatic parts tilted from the surface and alkyl chains not interdigitated. In image D (15.0 x 15.0 nm; I_{set} = 0.2 nA; V_{bias} = 0.8 V) domain with interdigitated alkyl chains and aromatic heads forming straight line in lamella growth direction.*

The statistic of area occupied by different structures of acid (*R*)-**1,5Naph** were performed on large scale image covering almost 41 000 square nanometres. The most common structure is main domain type 2 that was found on 43.0% of area, while type 1 was covering 35.2% of surface. The narrow interdigitated domains covered 7.4% of area and non-interdigitated structures covered 5.8% of the surface area. Approximately 8.5% of the area could not be assigned to any of the structures.

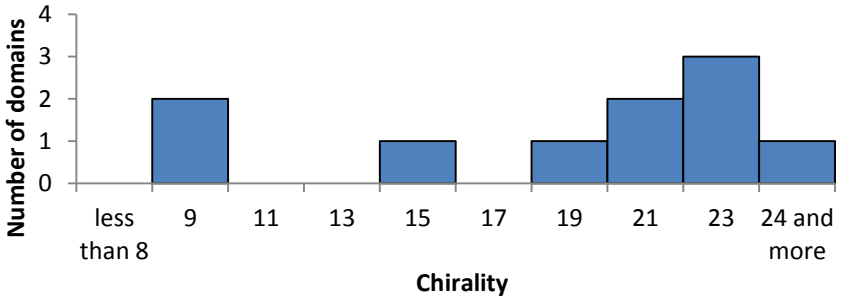

Figure 3.20: *Histogram of angles of the main structure type 1. Most of the domains were found in range <18, 24>, but surprisingly chirality of two domains is below 10 degress with respcet to the main graphtie axis.*

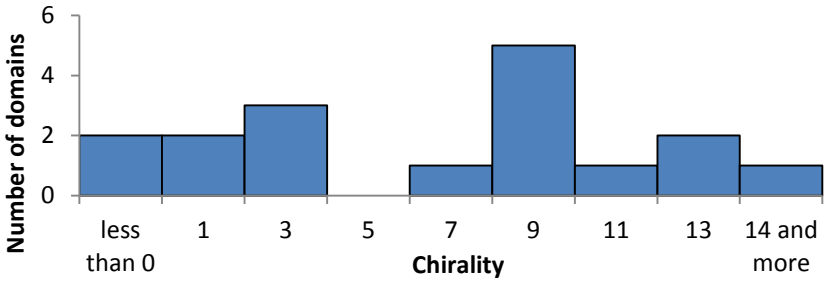

Figure 3.21: *Histogram of angles of the main structure type 2. There is quite a wide range of angles found for this kind of structure, but the most common one is in range <8, 10>.*

3.4.4 Self-assembly of the racemic mixture of acid 1,5Naph at the graphite-1-phenyloctane interface

The racemic mixture of compound **1,5Naph** was also investigated using STM and it was found that the compound forms a monolayer on the surface of graphite within a few minutes of deposition. Typical images are shown in Figure 3.22. In the images it can be seen ordered domains are rather short, usually not longer than 30 nm, and disordered structures. Even in the relatively ordered domains there are many defects and the arrangement of molecules can change within few nanometres several times. It is interesting that the different structures can go smoothly from one to the other. There are

also areas where no resolved monolayer was observed, probably where molecules are not well absorbed on the surface or some reorganization of the SAM was in progress while scanning. The sample is a conglomerate, as the compound apparently spontaneously resolves into domains which can be assigned to the (*S*) and (*R*) enantiomers which appear as "//////////" or "\\\\\\\" patterns, respectively. Still, as there are plenty of areas with defects, or without defined structure, the formation of a poorly ordered racemic compound on the surface cannot be excluded.

The statistics of propensity of different polymorphs was performed on STM images covering over 36 000 square nanometres. The type 1 domains were found in 8.8% of area, type 2 in 11.1%, non-interdigitated straight domains occupied 1.8% of surface while interdigitated 10.0%. Most of the area, exactly 68.3% was too noisy to be assigned to any kind of arrangement.

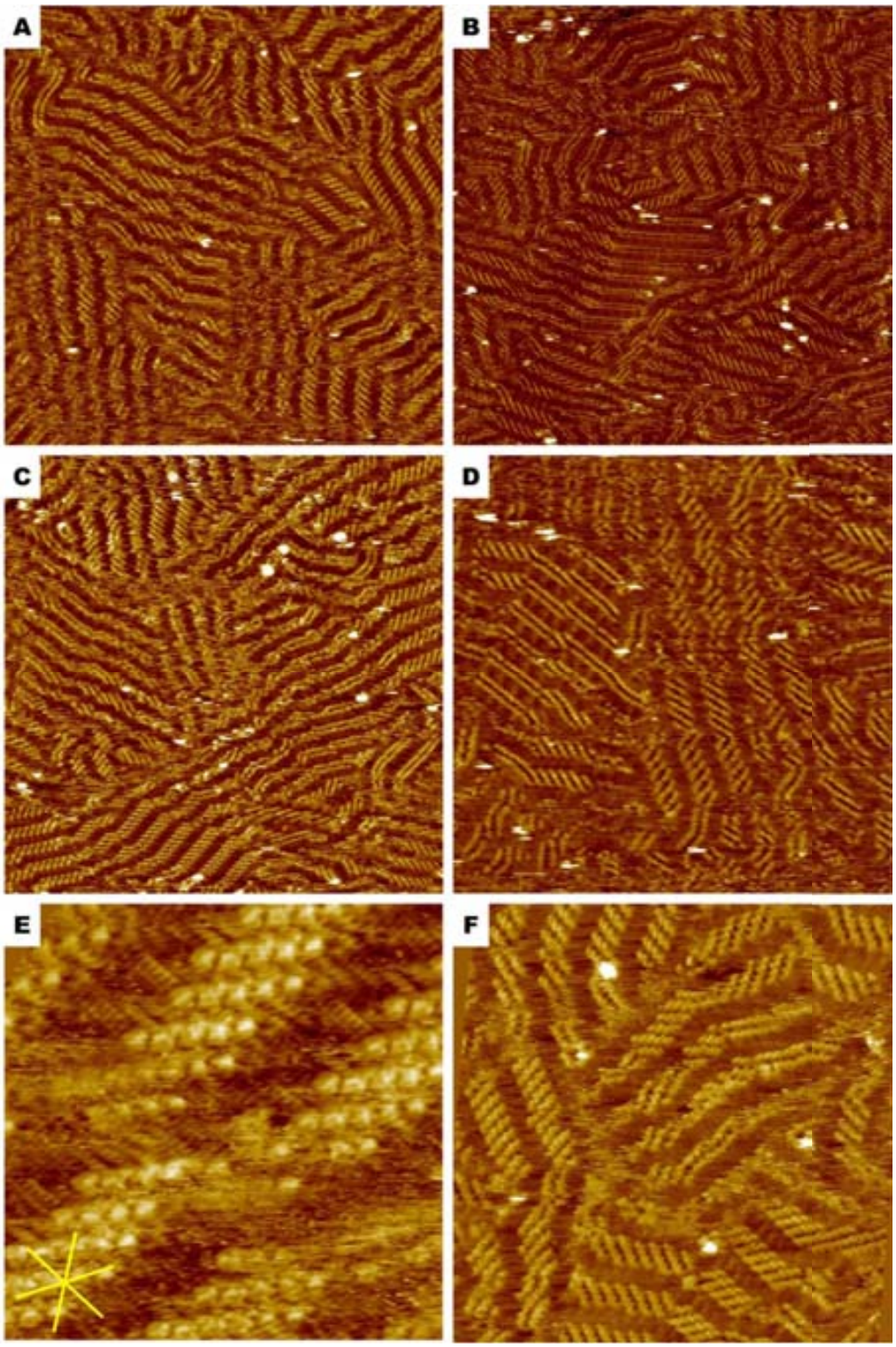

Figure 3.22: *STM of the racemic mixture of compound* ***1,5Naph*** *at the graphite-1-phenyloctane interface. Images A (86.4 x 86.4 nm), B (96.4 x 96.4 nm) C (90.4 x 90.4 nm) and D (62.3 x 62.3 nm) show general view of the monolayer. Images E and F (12.1 x 12.1 nm and 42.6 x42.6 nm) detailed structure of the monolayer is presented. Of particular interest is the lamella in the bottom of image F where the connection between mirror image domains takes place. In image E exceptional resolution of aromatic part is obtained*

3.5 4,4'-Biphenyl amphiphile

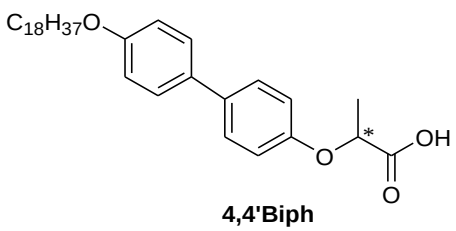

4,4'Biph

3.5.1 Synthesis

The biphenyl derivative (*S*)-**4,4'Biph** was synthesised as shown in Scheme 3.5. The first step was the Mitsunobu reaction of 4,4'dihydroxybiphenyl with (*R*)-methyl lactate to obtain compound (*S*)-**42** with 37% yield, which after separation from the side products of the reaction by column chromatography was used for the next step in which the alkyl chain is attached in the basic conditions, yield of the second step was 68%. The last step was the hydrolysis of ester followed by crystallization of the product, yield of saponification was 41%. The analysis of the compound confirmed desired structure.

The (*R*)-**4,4'Biph** was synthesized in analogical manner, but using (*S*) enantiomer of *n*-butyl lactate, as described previously.[39] The alkylation and saponification was performed in analogical manner as for the other enantiomer with yield 67% and 59% respectively. The NMR, IR and HPLC confirmed the structure of (*R*)-**4,4'Biph.**

[39] D. B. Amabilino, J.-L. Serrano, T. Sierra, J. Veciana, *Mendeleev Commun.* **2004**, 256.

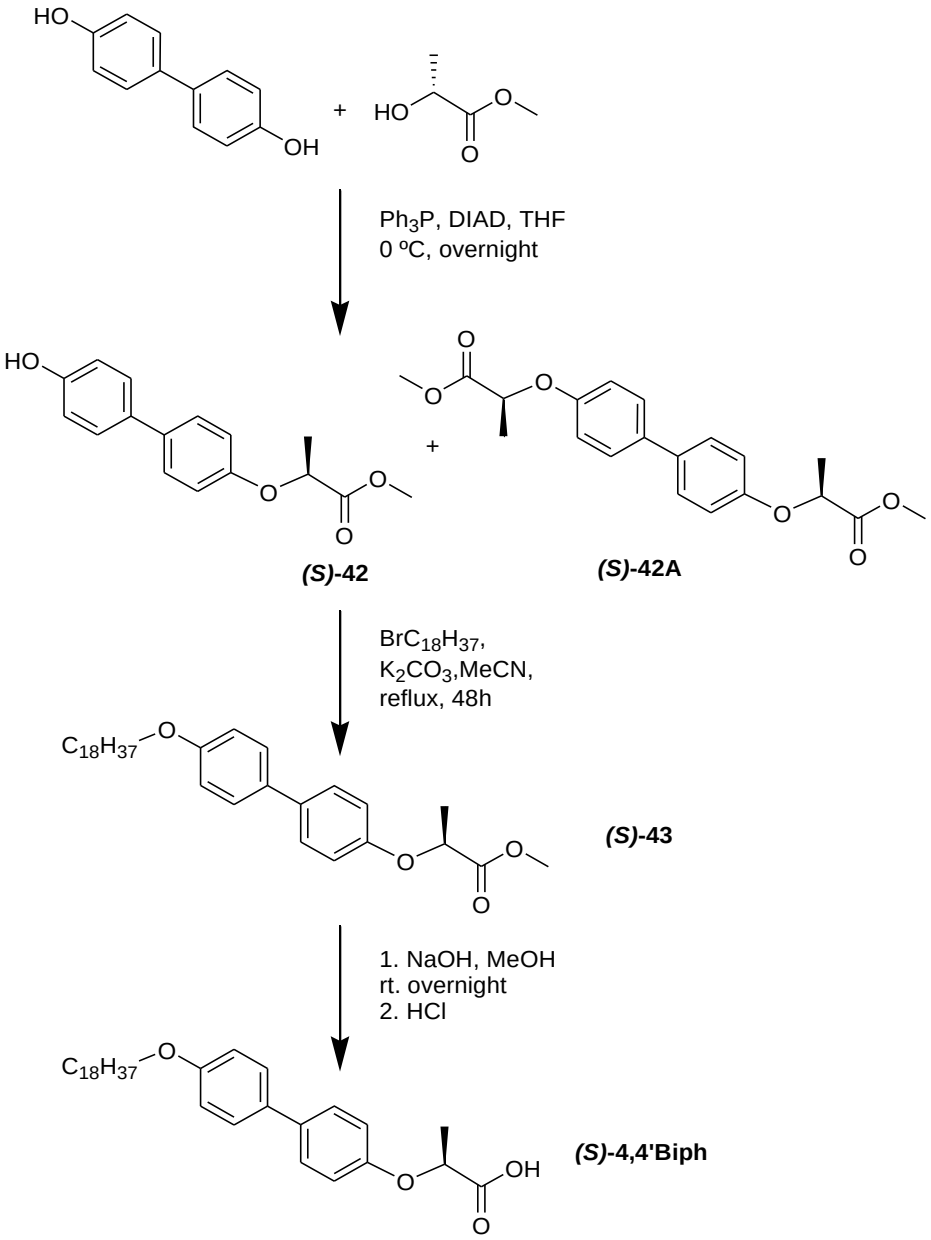

Scheme 3.5**: Synthesis of (S)-**4,4'Biph

3.5.2 Self-assembly of acid (*R*)-4,4'Biph at the graphite-1-phenyloctane interface

The compound was dissolved in the hot 1-phenyloctane and the resulting solution was applied to the surface of freshly cleaved HOPG. Again, as for the other members of this amphiphilic acid family, a few minutes were necessary before being able to visualise the self-assembled structures using STM.

In the STM images of (*S*)-**4,4'Biph** shown in the Figure 3.23 and 3.24 the bright circles that correspond to the biphenyl part of the molecule can be seen clearly, and

darker areas where are a lines of points that correspond to the alkyl chains. Unlike the majority of domains for compounds **2,7Naph**, **2,6Naph**, and **1,5Naph** the alkyl chains are not interdigitated fully, but only the ends of the alkyl chains from two neighbouring lamellae are touching with each other.

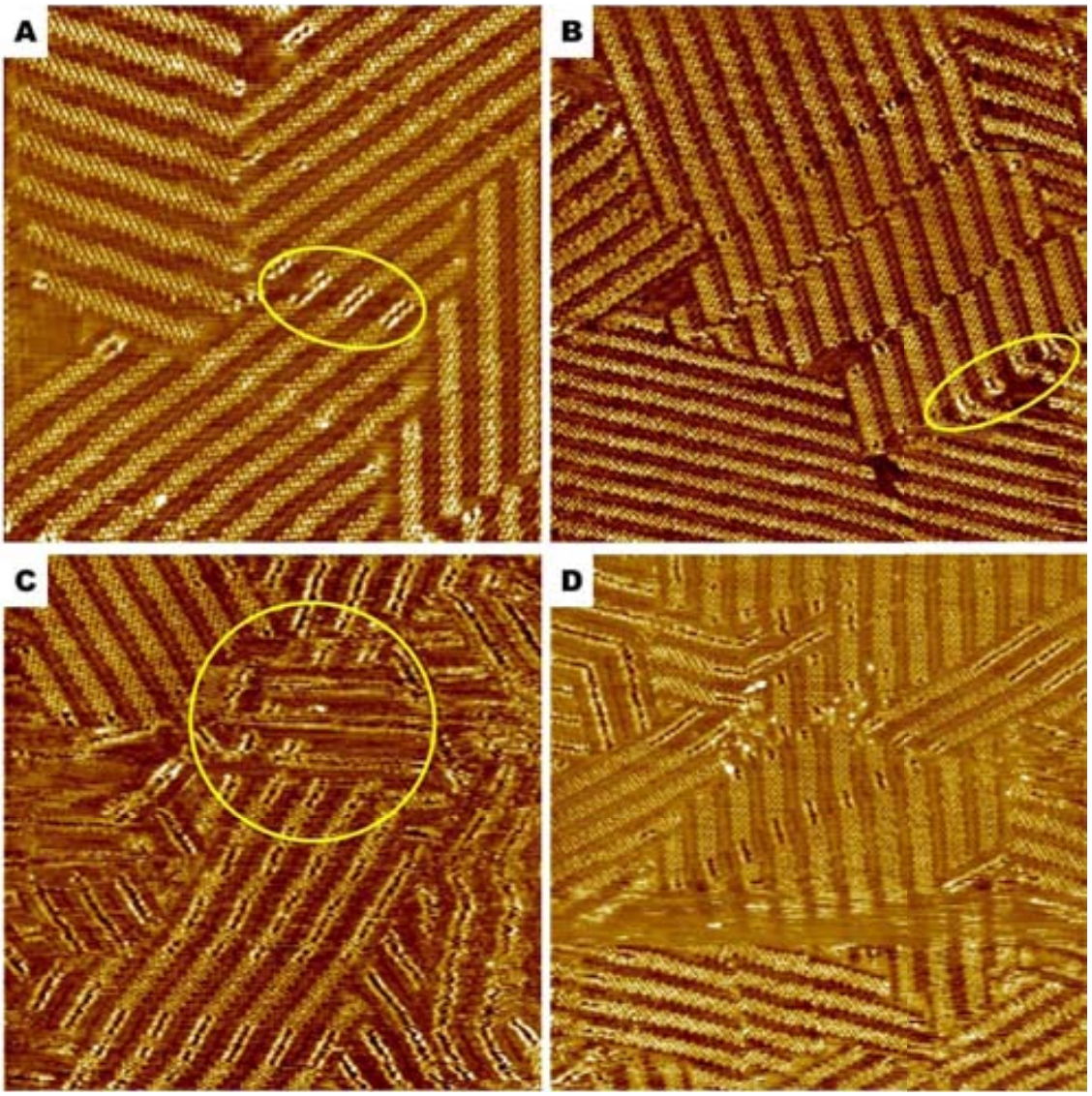

***Figure 3.23**: Typical large scale STM images of a monolayer of (R)-**4,4'Biph** at the graphite-1-phenyloctane interface. The images A and B (90.4 x 90.4 nm and 104 x 104 nm; I_{set} = 0.2 nA; V_{bias} = 0.8 V) show large regular domains. In few places the brighter stripes of other type of domain is observed, two of them marked in yellow. Images C and D (97.1 x 97.1 nm and 104 x 104 nm; I_{set} = 0.2 nA; V_{bias} = 0.8 V) present the shorter domains, where the second type of structure is found in many places. In the area marked in yellow in image C the indication of multilayer is seen, overlaying domains are clearly observed there.*

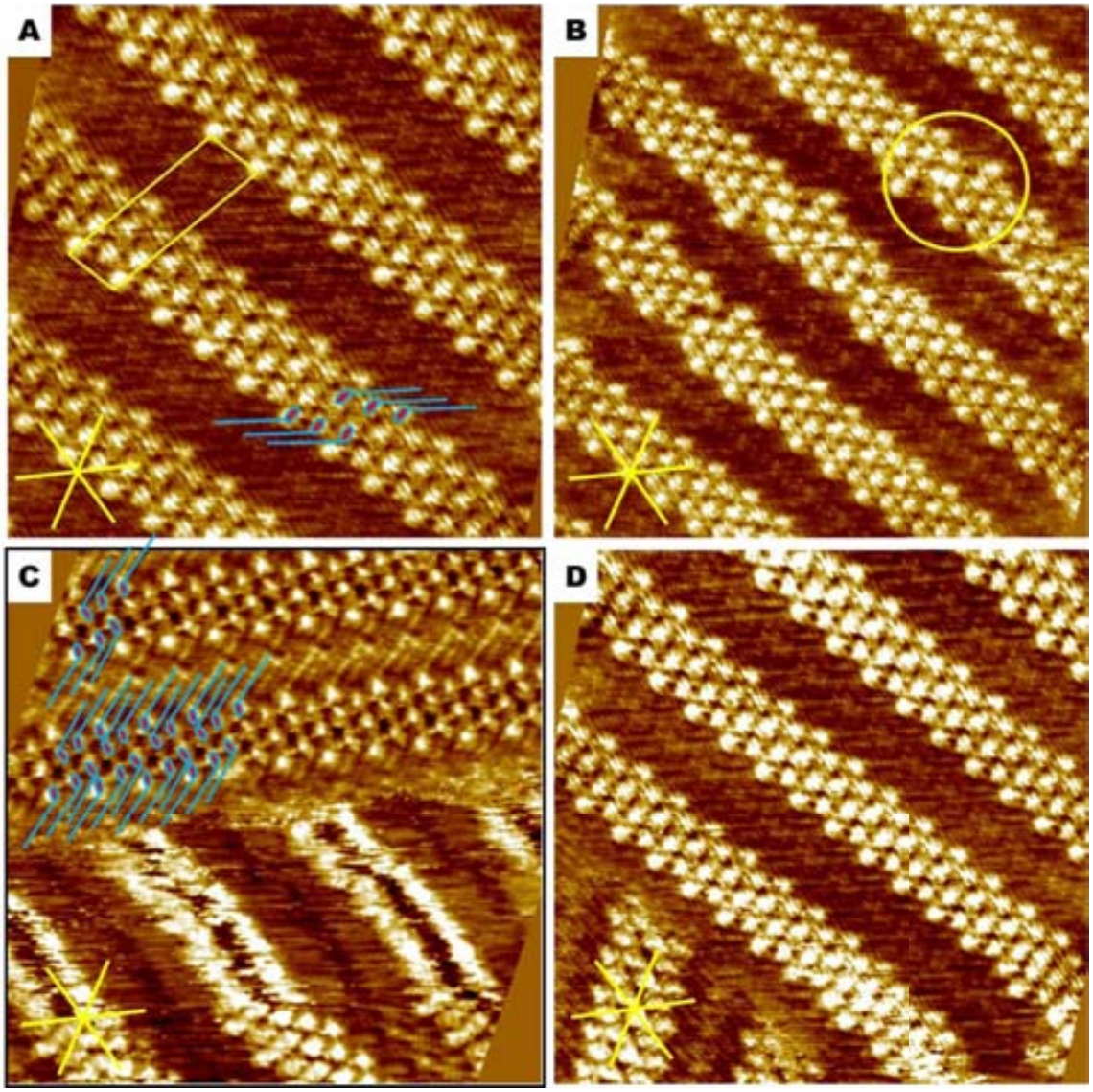

Figure 3.24: *Close-up STM images of a monolayer of (R)-**4,4'Biph** at the graphite-1-phenyloctane interface. Image A (17.9 x 17.9 nm; I_{set}= 0.2 nA; V_{bias} = 0.8 V) shows detailed structure of monolayer. In image A unit cell is marked and block of tree dimers. In image B (23.4 x 23.4 nm; I_{set}= 0.2 nA; V_{bias} = 0.8 V) there is a defect marked in the yellow circle, a different packing, moreover this disturbed packing is repeated in other lamellae in domain. Image C (21.1 x 21.1 nm; I_{set}= 0.2 nA; V_{bias} = 0.8 V) presents the second type of domain in the lower part of the image, where the aromatic parts of the molecules are perpendicular to the surface. In image D (22.2 x 22.2 nm; I_{set}= 0.2 nA; V_{bias} = 0.8 V) boundary of a domain is presented.*

In the close up the structure of monolayer is observed, the alkyl chains are tilted from the perpendicular to the lamella growth direction and do not interdigitated with the alkyl chain of the neighbour lamella. Aromatic head groups form row of three bright spots in direction perpendicular to the lamella growth, each three heads shifted with respect to

the next three either up or down. Lamella is very well ordered, almost without defects, one of the very few observed is shown in Figure 3.24B.

The unit cell is marked in the image 3.24A, in the unit cell there are 6 molecules and the parameters are: a= 1.83 ± 0.08 nm, b= 6.07 ± 0.55 nm and γ= 80.8 ± 3.3º. The distance between the centres of the aromatic heads of molecules that forms dimer, measured as marked in Figure 3.25A was found to be 1.73 ± 0.19 nm what is in agreement compared with distance of 1.82 nm measured in optimized model prepared in HyperChem (Figure 3.25B).

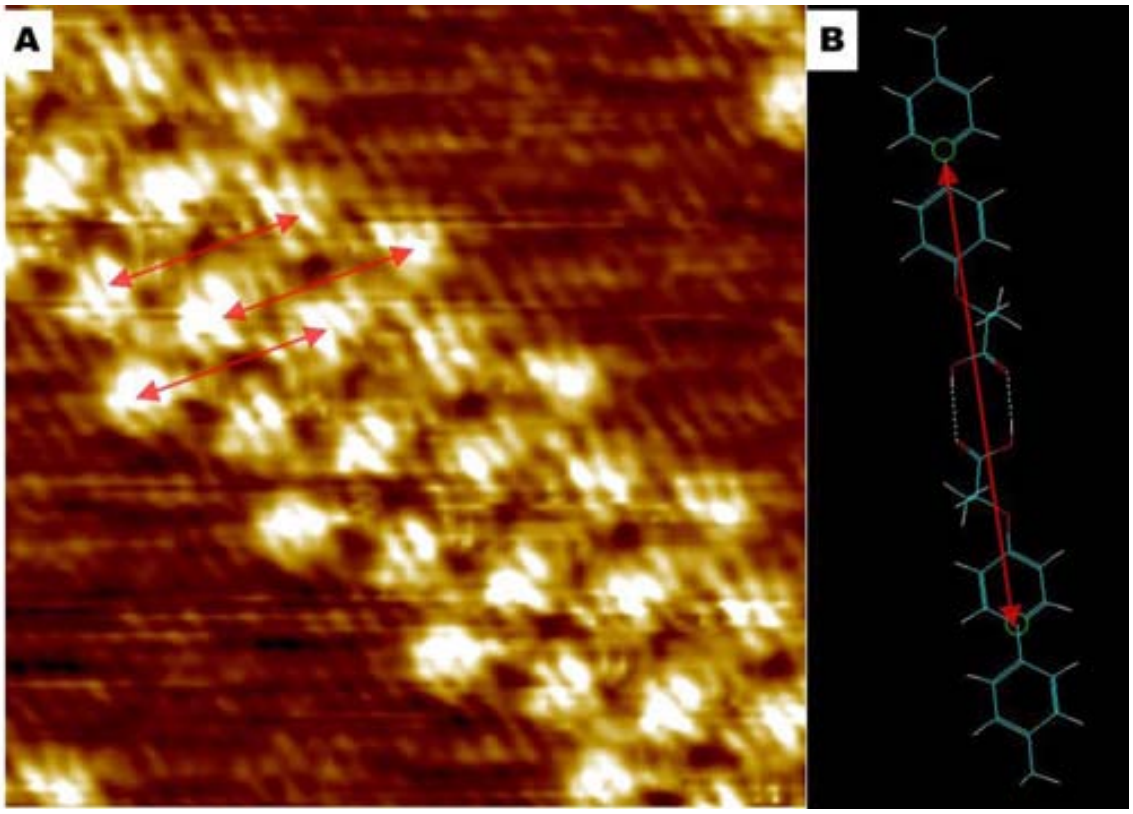

Figure 3.25: *Close-up STM images of a monolayer of (R)-**4,4'Biph** at the graphite-1-phenyloctane interface. The structure in image A (7.27 x 7.27 nm) with marked the distance between aromatic heads that was measured.*

The chirality of the main structure, measured with respect to the main graphite axes equals -7.7 ± 2.7°, and the domain width is 6.00 ± 0.55 nm. The orientation of alkyl chains with respect to the lamella growth direction is like "///////", what is another form of expression of chirality. This type of organization on the surface dominates covering over 89% of surface, although there are a few areas, exactly five found in images covering over 17 000 square nanometres with defects in the lamella structure can be

observed. In image shown in Figure 3.24B there is an area, marked with yellow circle, where the lamellar structure is interrupted clearly. This kind of defect may arise from a molecule that is interacting with a dimer next to it laterally, but not forming the majority kind of dimer. Adjacent to this four dot pattern is a two dot feature, so it appears that one molecule has incorporated into a site which fills the space in the monolayer so that the regular three dot feature cannot be generated. Interestingly, this defect is preserved in the pattern of all other lamellae in the image along a main graphite axis.

Another type of domain found in about 4.5% of area of the sample is shown in Figure 3.24C and is also evident in the centre part of the Figure 3.23A and several parts of the image in Figure 3.23C. All the molecules are in line and it is hardly possible to distinguish between the different head groups: the area corresponding to the aromatic head group shows very high tunnelling current when compared with the flat-lying molecule and this feature is continuous along the lamellae. This kind of STM contrast indicates that the aromatic parts are perpendicular to the surface so molecules occupy less surface area and interactions between aromatic rings of nearby molecules are presumably allowed. This type of structure can smoothly convert into the normal type of lamella as observed in the preceding images, with the change in polymorph conserved and in line perpendicularly to the direction of the lamellae. Unfortunately no high quality images of this kind of structure were captured, and because of that no structural analysis could be performed.

Surface study of over 17 000 square nanometres of domains of (*R*)-**4,4'Biph** at the graphite-1-phenyloctane interface shows that over 89.3% of area is covered with first type of domain, while 4.5% is the second type and 6.2% was too noisy to be assigned.

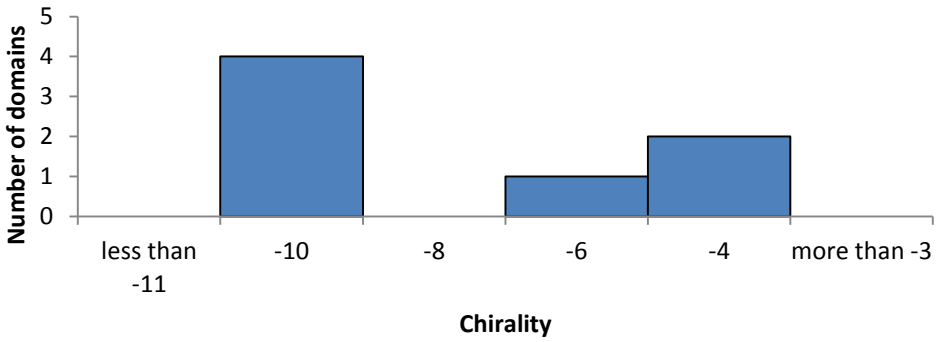

Figure 3.26: *Histogram of angles of main structure of (R)-**4,4'Biph**, measured with respect to the main graphite axis.*

3.5.3 Self-assembly of acid (*S*)-4,4'Biph at the graphite-1-phenyloctane interface

The second enantiomer, (*S*)-**4,4'Biph** was also measured at the graphite 1-phenyloctane interface. In the Figure 3.27 the representative images of the self-assembly monolayer are presented

The structure formed by (*S*)-**4,4'Biph** is very similar to that of its enantiomer, but the orientation of the alkyl chains with respect to the lamella growth direction is like "\\\\\\\\". The chirality of the majority lamellae with respect to the graphite substrate is +5.1 ± 3.2º, while for (*R*)-**4,4'Biph** the domain is rotated anticlockwise at an angle of -7.7 ± 2.7º. Lamella width equals 6.44 ± 0.29 nm, compared with 6.00 ± 0.55 nm for the other enantiomer. Histogram of angles of the (*S*)-**4,4'Biph** is presented in Figure 3.28. The surface covered by one molecule equals 1.73 square nanometres, compared with 1.62 square nanometres for **2,7Naph.**

The defects observed in the (*R*) -**4,4'Biph** are also seen in the monolayers of the (*S*) enantiomer. Another type of defect that is observed in this kind of structure is a jump in lamellae. In the Figure 3.27B in the lamellae at the top right, instead of a majority pattern of up–up-down-up–up-down-up-down-up–up-down molecules, there is (looking from the right edge of the top lamella) an up- down-up-down arrangement. Somehow it looks a bit similar to the case of compound **2,6Naph**, but in this case it is much less common.

The second polymorph is presented in the centre of the image 3.27B in the centre of the image. The lamella width measured for this type of arrangement is 6.41 ± 0.30 nm and chirality measured with respect to the main graphite axis equals -5.7 ± 4.6º. Histogram of angles is presented in figure 3.29. This type of domains was covering 9.7% of area, compared with 68.7% of the main domain. The statistics were performed on almost 57 000 square nanometres and 21.6 % of area was too noisy to be assigned.

In the image 3.27D an area is presented where the lamella contrast changes periodically, which looks like there is a mulitilayer formation, unfortunately this is the only place that this effect was observed and this evidence is not enough to prove the formation of multilayer system.

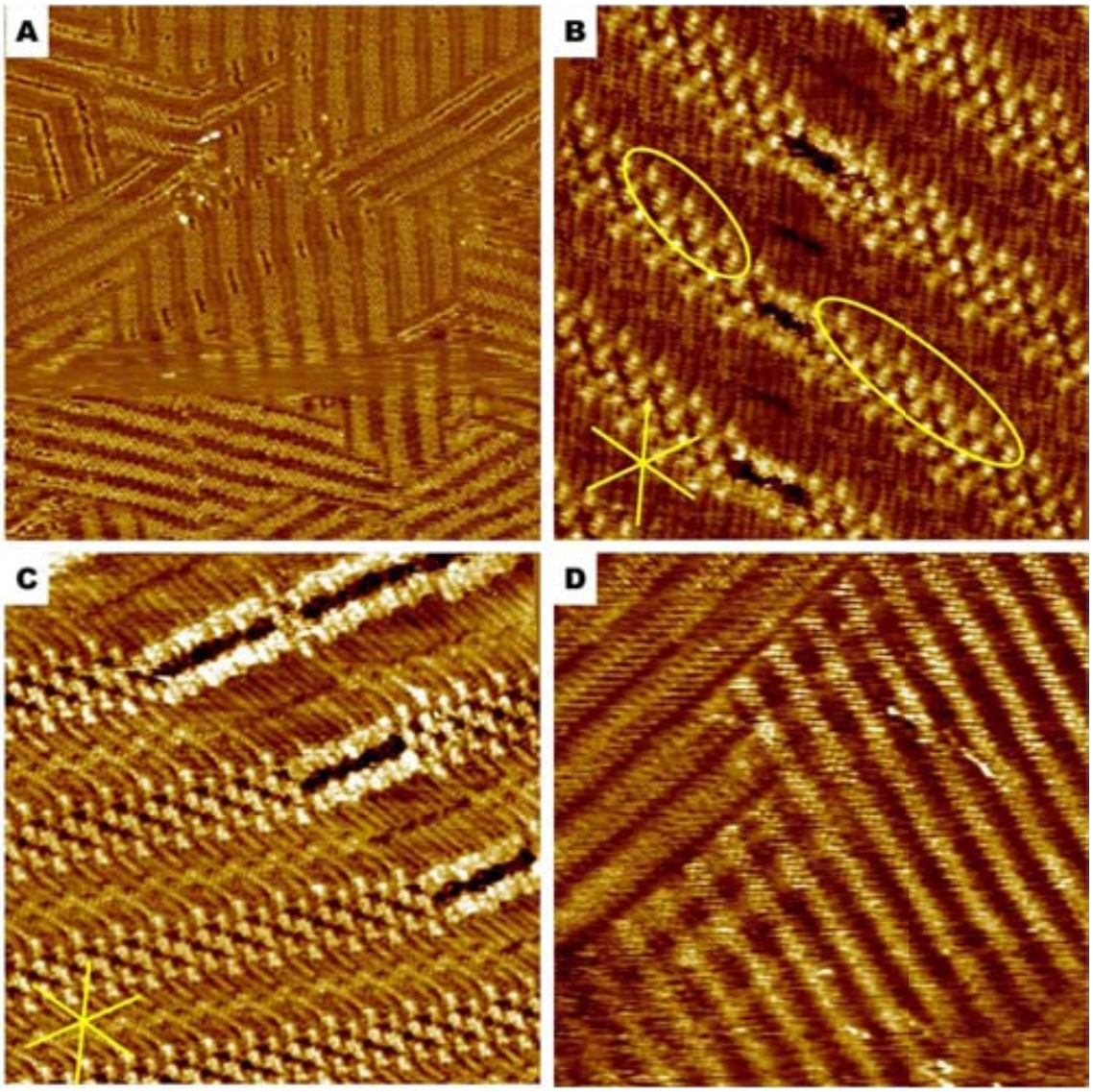

Figure 3.27: *STM images of a monolayer of (R)-**4,4'Biph** at the graphite-1-phenyloctane interface. Image A (104 x 104 nm; I_{set}= 0.2 nA; V_{bias} = 0.8 V) shows general view of the structure of the monolayer. Vertical noise in the lower part of the image is due to problems with tip, perhaps something got attached. In image B and C (21.1 x 21.1 nm; I_{set}= 0.2 nA; V_{bias} = 0.8 V for both of the images) the "Z" shaped dimers can be observed. Also the change of structure inside the same lamella can be observed. In image B there is also a frustration in packing, instead of typical down –up-up-down-up-up (looking from right to the left, marked in the right part of image B) pattern one have up-down –up-down –up-up-down-up-up-down-up-down-up. In image D (69.5 x 69.5 nm; I_{set}= 0.2 nA; V_{bias} = 0.8 V) the surprising change of the contrast, and overlying lines in the centre of the image suggest formation of multilayer.*

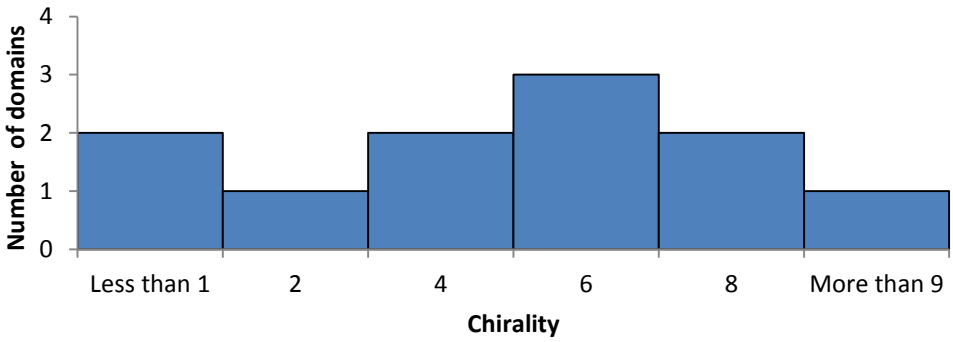

Figure 3.28: *Histogram of angles of the main structure of (S)-**4,4'Biph**, measured with respect to the main graphite axis.*

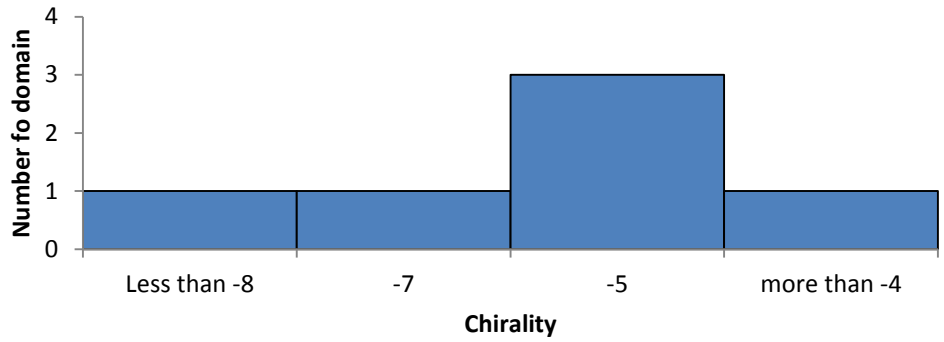

Figure 3.29: *Histogram of angles of the second type domains of (S)-**4,4'Biph**, measured with respect to the main graphite axis.*

3.5.4 Self-assembly of the racemic mixture of 4,4'Biph at the graphite-phenyloctane interface

The racemic mixture of **4,4'Biph** was also studied at the graphite-1-phenyloctane interface and in this case the behaviour is completely different compared with that of the enantiomers. Shortly after the drop was applied to the graphite surface at the beginning of the experiment, the formation of monolayer was observed. The structure, similarly to the enantiopure, samples consist of two different majority structures, although the proportion of the two contrasts with that of the enantiomers. A typical STM image is presented in the Figure 3.30.

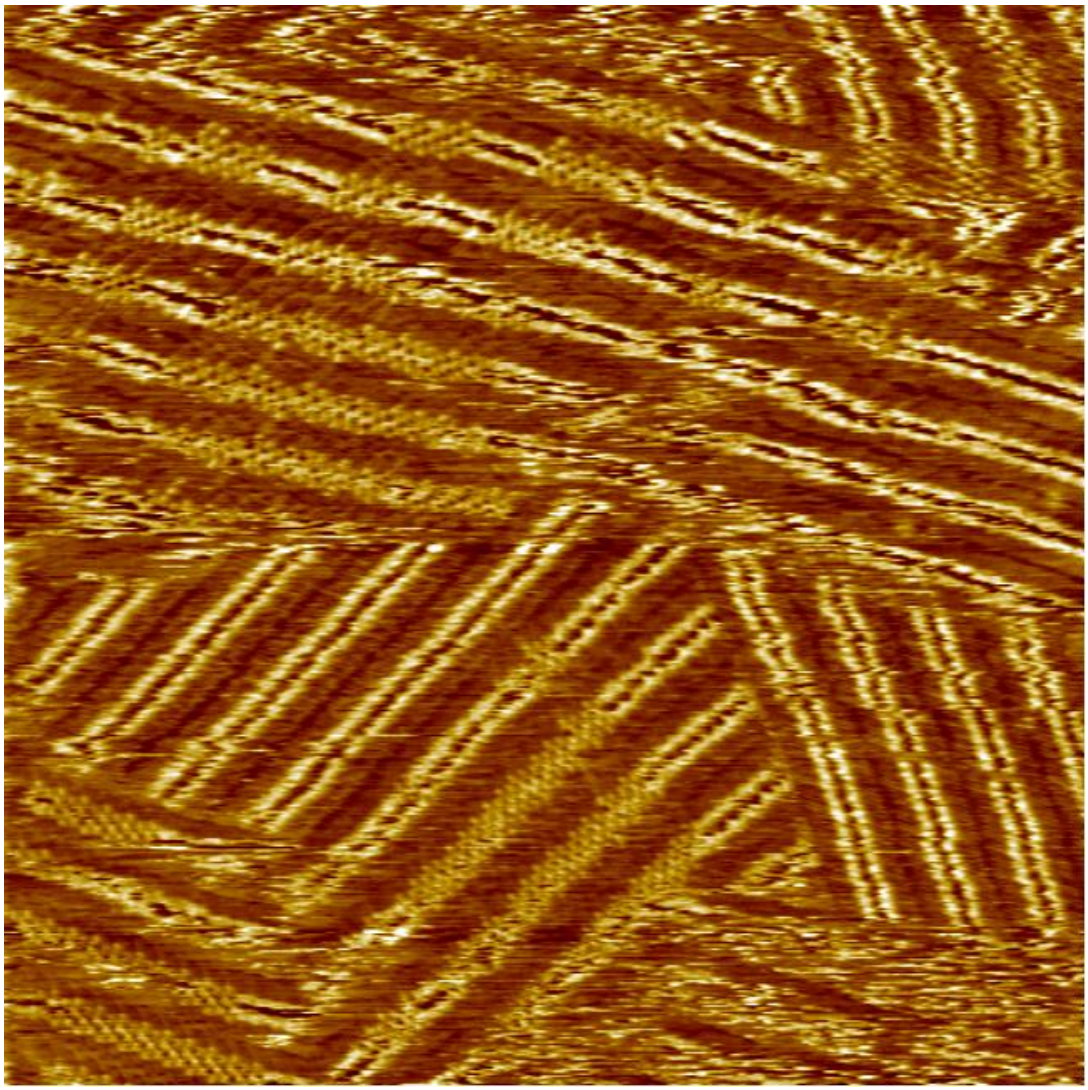

Figure 3.30*: STM images of a monolayer of racemic-**4,4'Biph** at the graphite-1-phenyloctane interface shortly after deposition of solution on the graphite. Image A (90.4 x 90.4 nm; I_{set}= 0.2 nA; V_{bias} = 0.8 V). The formation of separated domains with typical structure observed for the monolayers (as in the Figure 3.24 A, B and D) is observed, but the formation of second type of structure, where the aromatic parts forms bright straight row, is at least as common.*

At the beginning of the experiment both structures were observed clearly, but after approximately 1 hour only the structure with the aromatic parts of the adsorbat tilted from the graphite surface forming straight row was observed. The other polymorph could not be found at all. Instead the (*S*) and (*R*) enantiomers form a monolayer with aromatic parts perpendicular to the surface extending over thousands of square nanometers as presented in Figure 3.31. The domains form well defined edges with the neighbouring ones, and in general there are few large scale defects in the lamellae.

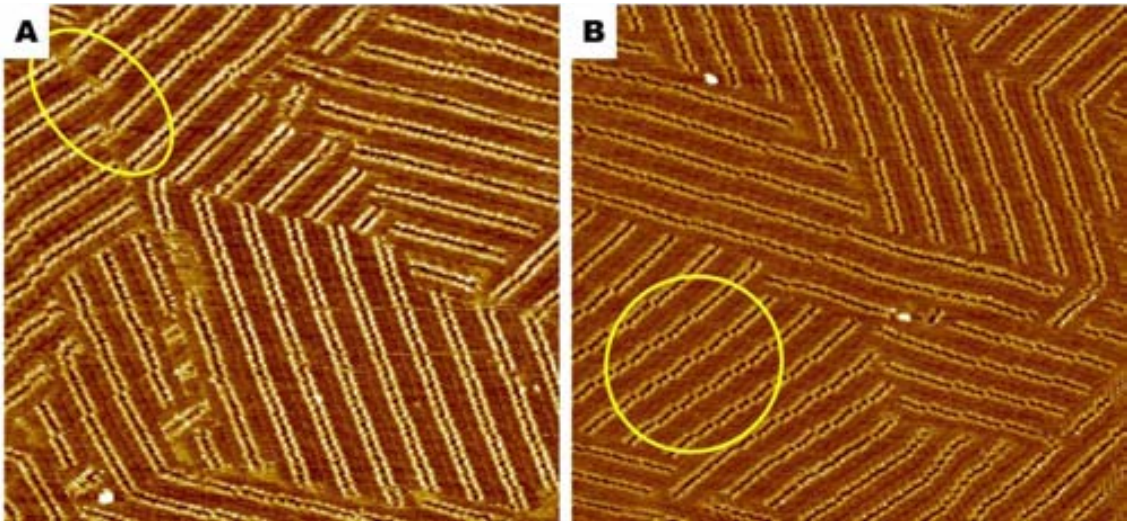

Figure 3.31: *STM images of a monolayer of racemic-**4,4'Biph** at the graphite-1-phenyloctane interface after more than 1 hour. The images (A: 96 x 96 nm, B: 104 x 104 nm; I_{set}= 0.2 nA; V_{bias} = 0.8 V) present large scale organization of the monolayer. In image A there is boundary region marked where the domains of different orientation meet. In image B the defect of monolayers, kind of displacement is marked with the circle.*

Taking a closer view of these self-assembled monolayers, as presented in typical images in Figure 3.32, the aromatic parts of the molecule are not stacked parallel to the graphite, but rather there are at an angle from the substrate. The alkyl chains are straight and not interdigitated. The lamellae are not perfectly straight at this scale, there are frequent incidences where the aromatic parts are shifted. The lamellae are chiral, with alkyl chains tilted at about 60 degrees from lamella growth direction in either a positive or negative angle. Angles of the alkyl chain direction are usually close to 0 with respect to the main graphite axis, average angle equals +1.6 ± 2.0° and the lamella width is 6.76 ± 0.23 nm. Histogram of angles is presented in Figure 3.32.

The changing direction of alkyl chains from (to change from slash to backslash) is unfavourable, as studied in case of 257 lamella more than 89% of cases the neighbour has the same direction just in 11% of cases the neighbour is opposite chirality. This type of pseudoracemate packing at the graphite-liquid interface was reported previously.[40] So, in principle, a conglomerate is formed at the single lamellae level.

[40] S. De Feyter, A. Gesquiére, K. Wurst, D. B. Amabilino, J. Veciana, F. C. De Schryver, *Angew. Chem. Int. Ed.* **2001**, *40*, 3217.

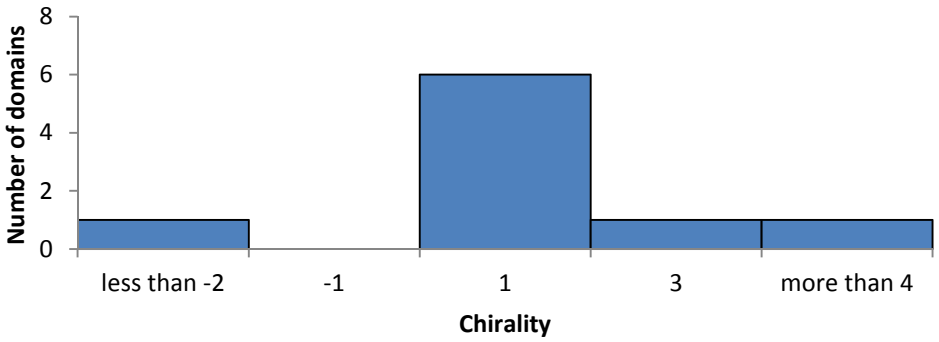

Figure 3.32: *Histogram of angles of the second type domains for the racemic* ***4,4'Biph*** *at graphite – 1-phenyloctane interface measured with respect to the main graphite axis.*

The analysis of surface cover of each polymorph was performed to find that 87.4% of surface is covered with second type domains, shown in Figure 3.33. Just 9.5% of area is assigned to main type of arrangement for pure enantiomers. 3.1% of area was too noisy to be assigned, what proves that racemic mixture of acid **4,4'Biph** packs very well compared with racemic **1,5Naph**, where over 60% of area was too noisy to be identified.

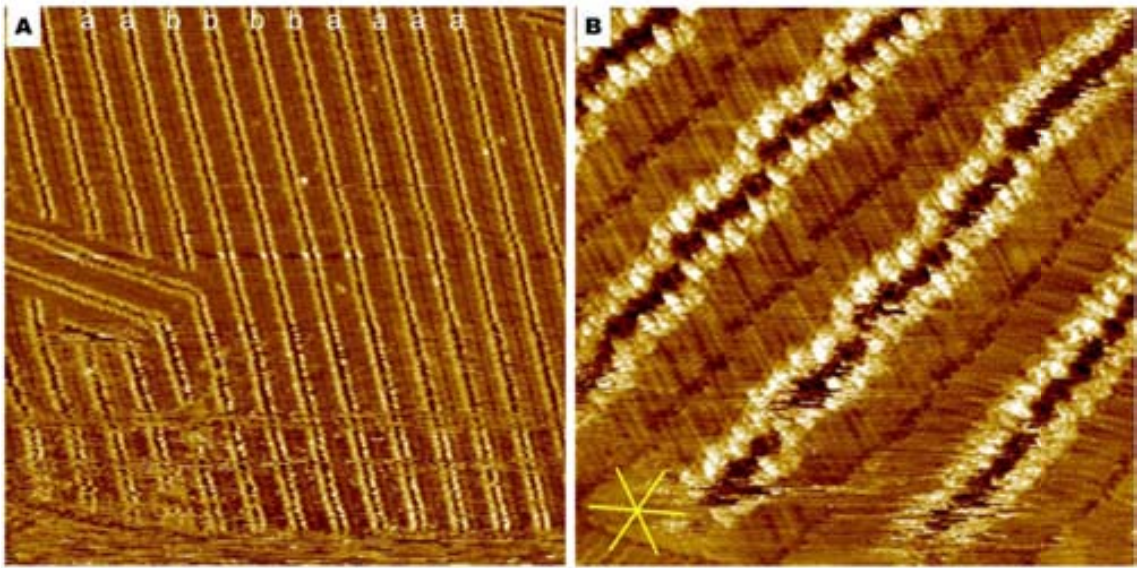

Figure 3.33: *STM images of a monolayer of racemic-****4,4'Biph*** *at the graphite-1-phenyloctane interface (A: 96 x 96 nm, B: 23.0 x 23.0 nm;* I_{set}*= 0.2 nA;* V_{bias} *= 0.8 V). There can be seen a change of the chirality of the domain from left to right in the right part of the image, marked with the letters, a for one direction and b for the other. In the image two changes of chirality between neighbour lamellae. In image B the close-up of the structure is presented, the change of the chirality of lamella is presented.*

3.6 Hydroquionone-derived amphiphile

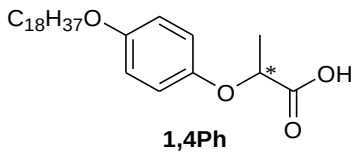

1,4Ph

3.6.1 Synthesis

The enantiomers hydroquinone derivative **1,4Ph** were synthesised as showed in Scheme 3.8. The first step was reaction of 4-(benzoxy) phenol with octadecyl bromide in basic conditions with 89% of yield. In the following step the cleavage of benzyl group was catalysed with Degussa palladium on carbon (54% of yield). Then using Mitsunobu reaction of derivative **52** with either one or the other enantiomer of the lactate ester using the Mitsunobu reaction, to obtain compound **53** with 61% of yield for the (*R*) and 65% for the (*S*) product, which after separation from the side products of the reaction by column chromatography was used for the next step. The last step is the hydrolysis of ester followed by crystallization of the product. The yield of the products were 55% for (*S*)-**1,4Ph** and 59% for (*R*)-**1,4Ph**. The analyses of the compounds confirmed the desired structure.

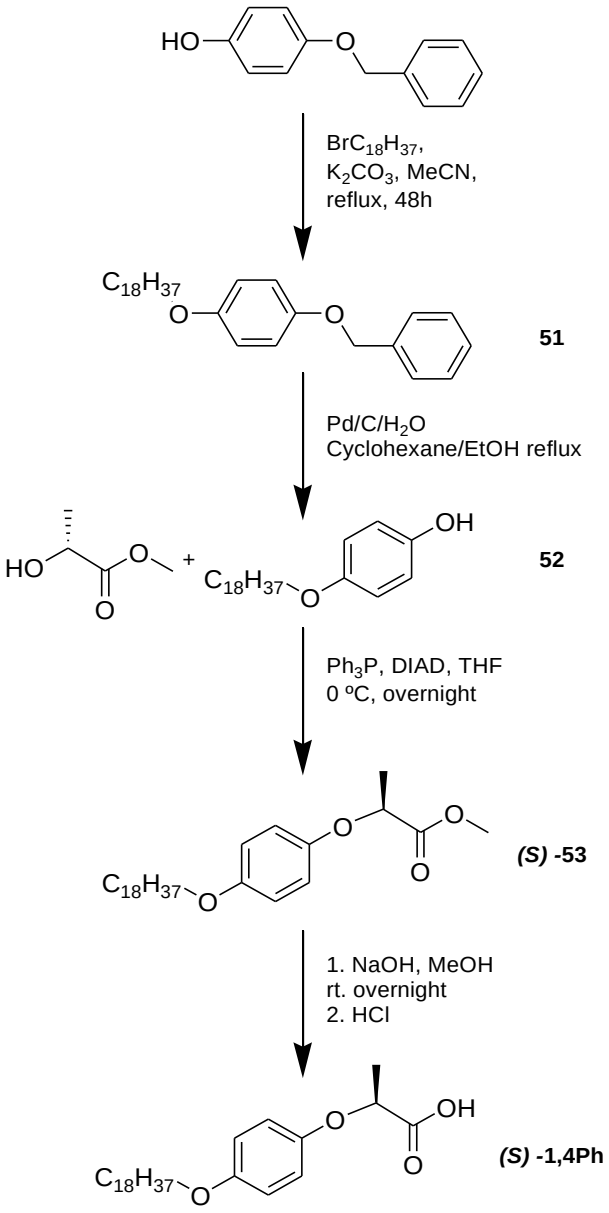

Scheme 3.8**: Synthesis of (S)-**1,4Ph

3.6.2 Self-assembly of (*R*)-1,4Ph at the graphite-phenyloctane interface

The compound (*R*)-**1,4Ph** was dissolved in hot 1-phenyloctane, and was drop cast at the freshly cleaved surface of HOPG, but unlike with the other amphiphiles from the family, more than one hour passed before any images of monolayer were seen. The molecules seem not to absorb very well, as most of the STM images were blurry. The aromatic parts of the compound could be distinguished from the areas where the alkyl chains are located by the contrast, but due to the movement of the molecules it was impossible to distinguish aromatic parts of separate molecules. In some areas we tried to

visualise the structures, but the resolution was lost during scanning due either to molecules attaching to the tip or the movement or even desorption of molecules from the graphite. No good quality large scale images could be captured during the measurement and the best close-up images are showed in the Figure 3.34. The compound presents a variety of packing structures at the graphite-phenyloctane interface. What is in common for all the observed structures is the non-interdigitation between alkyl chains. In the structure shown in Figure 3.34A the alkyl chains are tilted at approximately 60º from the lamella growth direction. Alkyl chains are not interdigitated, and the chains on the both sides of the lamellae have the same direction, although another structure where the alkyl chains on two sides of aromatic parts are directed differently were also observed. The alkyl chains and the lamellae growth direction follow the main graphite axis and lamellae are 6.31 ± 0.62 nm wide. The average chirality of this structure was +5.7 ± 10.4. A different situation was observed in the image presented in Figure 3.34C; here some fluctuations in lamella direction were observed. Also, different contrast in aromatic parts can be appreciated, where a dark area separates the head groups that form dimers, a feature that is reminiscent of the structure formed by racemic **4,4'Biph**. In the lamella shown in Figure 3.34C some local defects - changes of direction are observed. In one other place there was different organization observed, as presented in the figure 3.34D. Here the molecules in the same row are displaced with respect to the neighbour. This structure reminds one of the monolayer composed by enantiomers of **4,4'Biph**.

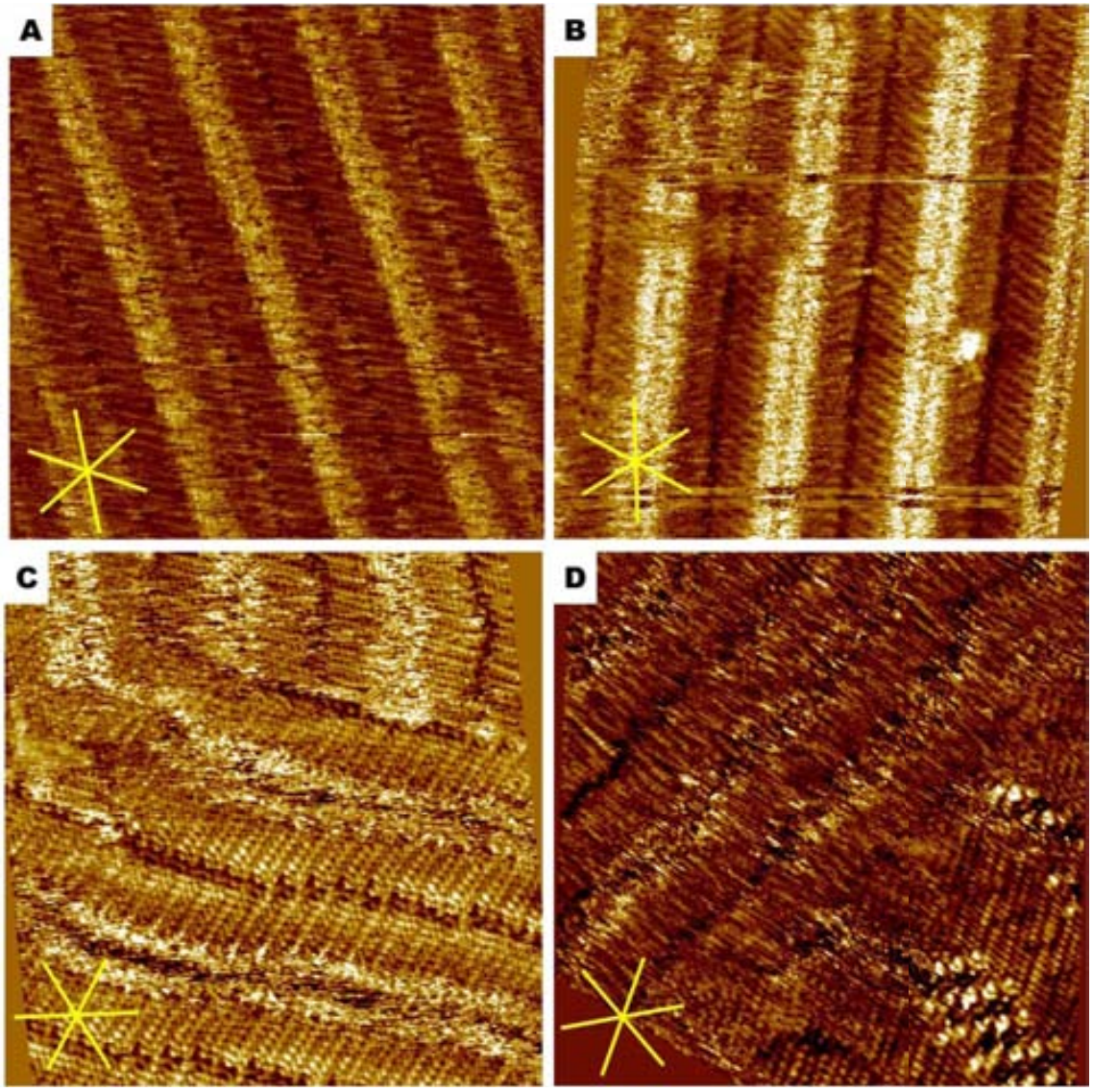

Figure 3.34: *STM images of a monolayer of (R)-**1,4Ph** at the liquid graphite-1-phenyloctane interface (A: 23.7 x 23.7 nm, B: 23.5 x 23.5 nm; C: 20.3 x 20.3 nm, D 20.2 x 20.2 nm, I_{set}= 0.2 nA; V_{bias} = 0.8 V). In image A straight lamellae with alkyl chains in one direction, aromatic parts form almost homogenous bright area in the image. In image B, structure with alkyl chains pointing in different directions on two sides of stripe of aromatic heads, there is darker area between aromatic heads that form dimers. In image C domain with excellent resolution on alkyl chains, but with blurry head groups, which might imply that the aromatic parts are not fixed to the surface as well as the alkyl chains. The lamellae are not perfectly straight. In image D in bottom right corner there is a structure where each of the aromatic groups is visualised as bright dot, no interdigitation of the alkyl chains is witnessed. In the rest of image D domain with a poorly defined structure.*

3.6.3 Self-assembly of (*S*)-1,4Ph at the graphite-phenyloctane interface

A slightly different situation was found in the sample of (*S*)-**1,4Ph** when compared with its enantiomer, it was much easier to capture a few good quality images of this compound. The typical large scale images are presented in Figure 3.35. The compound forms domains that can reach up to 80 nm in width, but the majority of observed domains are shorter than 50 nm. There are at least two different type of packing of the SAM observed in the case of this sample, one with aromatic parts forming bright stripes ”\\\\\\” other one with blurry aromatic parts.

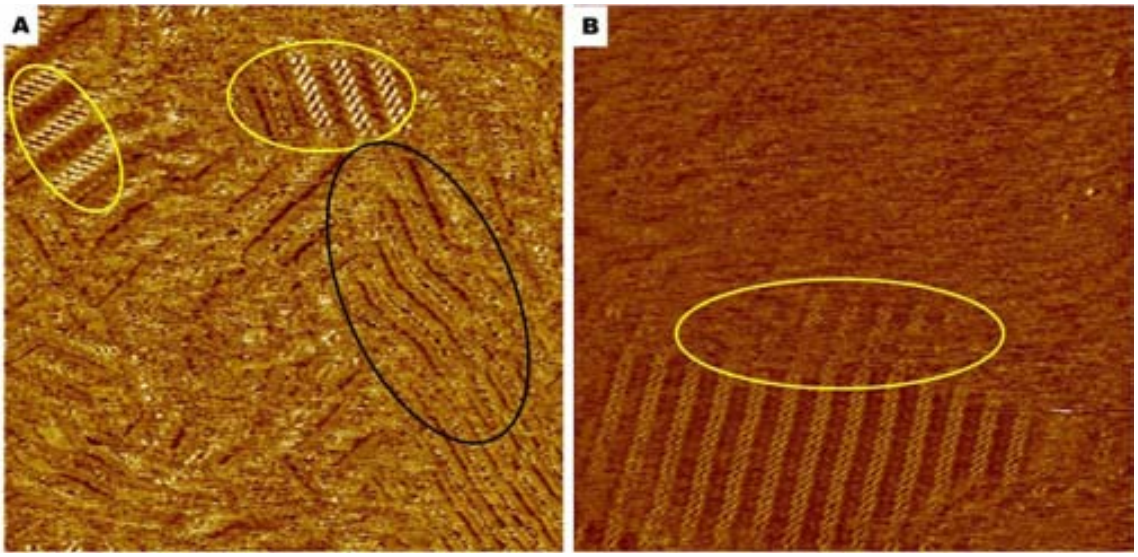

Figure 3.35*: STM images of (S) -**1,4Ph** at graphite 1-phenyloctane interface (A: 90.4 x 90.4 nm, B: 104 x 104 nm; I_{set}= 0.2 nA; V_{bias} = 0.8 V). In image A the general view of monolayer is presented. The structure similar to the acid **4,4’Biph** can be observed in image A (marked with yellow circle) and in the lower part of image B. In image A the short domains are separated by disordered domains. The domains in right part of image A (marked with black oval) are not perfectly ordered, there are changes in lamella direction and the alkyl chains are separated by thin dark area. In image B there is area marked with yellow oval where there organized domain is overlaid by blurry area, which might be an indication of multilayers.*

The close-up of the structure is presented in the Figure 3.36. The two main types of self-assembly monolayers were distinguished:

- Monolayer as presented in the images 3.36A, C and D. The aromatic parts are blurry, in this case the resolution on the aromatic part of the molecule is not as good, but one can see very well the alkyl chains. The structure is chiral because of

the tilt of alkyl chains, all are tilted in the same direction at the angle of approximately 50º. The alkyl chains follow the main graphite axis, and the lamellae rotation with respect to the graphite substrate is clockwise at the angle of +6.7 ± 2.0º. What is a intriguing in this monolayer is the gap between the alkyl chains, it is around 0.5-0.8 nm between the last visualised atoms. In some images there is a curious effect of pairing of alkyl chains, as in the image 3.36D. The lamella width equals 5.41 ± 0.26 nm.

- Monolayer with aromatic parts forming short stripes tilted with respect to the lamella growth direction like "\\\\\" no interdigitation of alkyl chains. The head to head distance is 1.43 nm, the lamella width is 6.32 ± 0.10 nm. The domain has chiral packing, but the lamella growth direction follows almost exactly lays over the main graphite axis, measured angle equals +0.3 ± 0.7º. The typical images are presented in the Figure 3.35B and 3.36B.

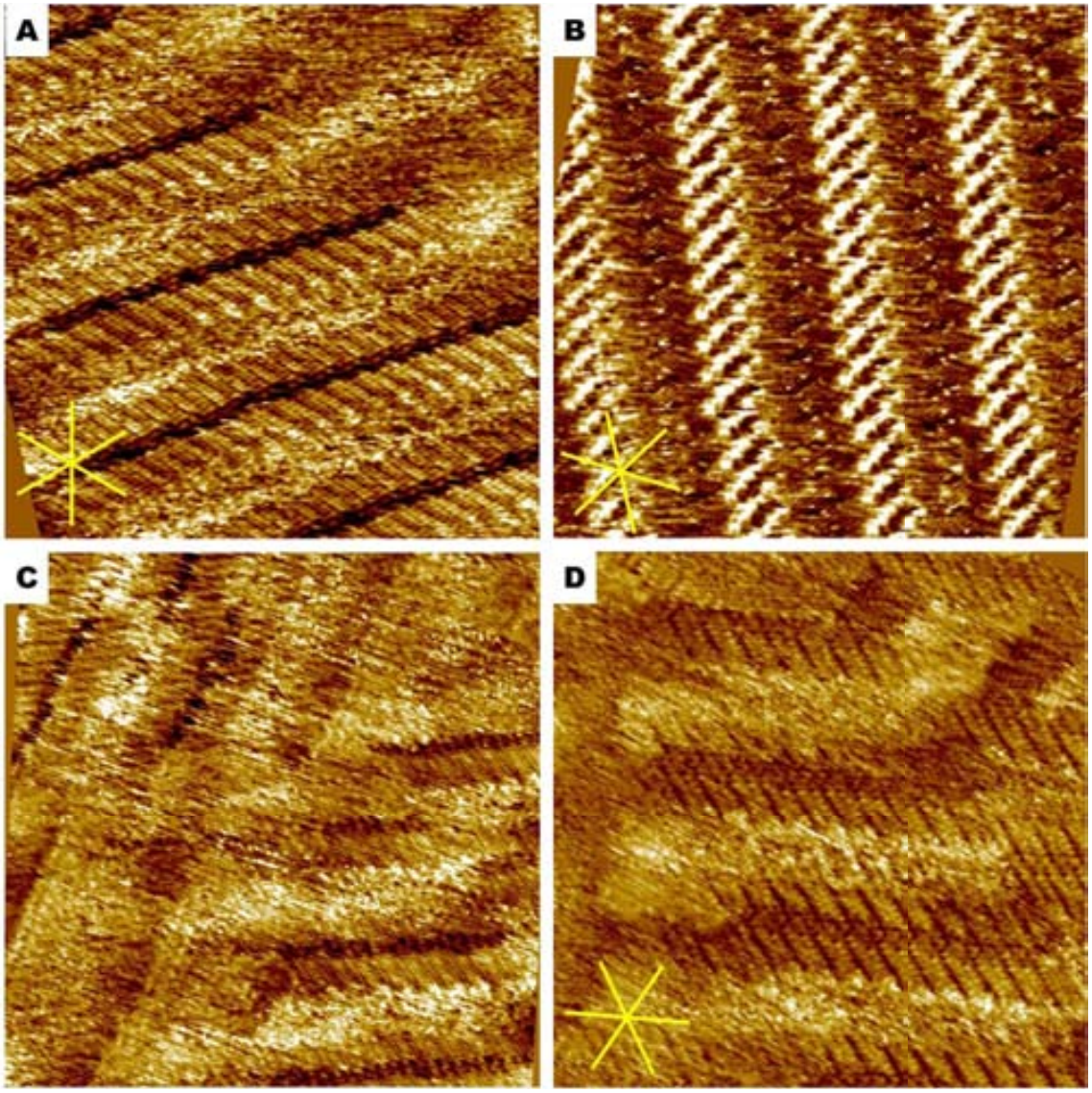

Figure 3.36: *Close-up STM images of (S)* ***-1,4Ph*** *at graphite 1-phenyloctane interface (A: 20.1 x 20.1 nm, B: 24.9 x 24.9 nm, C: 23.2 x 23.2 nm, D: 18.0 x 18.0 nm;* I_{set} *= 0.2 nA;* V_{bias} *= 0.8 V). In image A the molecules forms straight lamella with alkyl chains tilted with respect to the lamella growth direction, aromatic parts are blurry. The alkyl chains of two parallel rows are separated by dark area. Image B shows other type of structure, where aromatic parts of molecules form row of slashes "\\\\\\\", alkyl chains are not interdigitated. In image C there is presented an area where surprising contrast suggest existence of multilayers. In image D there is an area of domain as presenter in image A, but here there is curious effect of pairing alkyl chains.*

Due to the problems with visualising each enantiomer the experiment with racemic mixture was cancelled.

3.7 Discussion

It is clear that very small changes in the structure of the molecule results in completely different arrangement of the molecules at the graphite-1-phenyloctane interface. Each measured molecule forms a different pattern. In Table 3.1 the summary of the parameters of the monolayers is presented. No data is presented for the **2,6Naph**, due to the irregularity of the structure formed by this compound. In Figure 3.37 the comparison of the STM images of the structures is presented.

The similarity of SAMs formed by **2,7Naph** and its resorcinol analogue is clear. [41] The angle between the lactic chiral group and alkyl chain equals 120 degrees and the only difference, apparently not influencing packing is the size of the aromatic spacer. Conversely, there is not much analogy between these structures and those formed by the other acids from the family of amphiphiles. **1,4Ph** and **4,4'Biph** have the same linear geometry at the molecular level, but the structures formed at the graphite 1-phenyloctane interface are very different, **4,4'Biph** has six molecules in the unit cell, with alkyl chains tilted and not interdigitated, while in **1,4Ph** there is whole variety of structures observed, but just in one (Figure 3.34D) a structural similarity is found with the one observed for **4,4'Biph**. At the same time the second observed structure for **4,4'Biph**, (presented in the Figures 3.23C, 3.24C and especially in 3.27C) seems to be common with the one observed for **1,4Ph** (Figure 3.34A and C, Figure 3.36A, C and D) and **1,5Naph** (Figure 3.19C). Just in the case of compound **2,6Naph**, where also the lactic group and aromatic part is attached on the opposite sides of naphthalene ring, no structure with aromatic rings tilted from the surface is observed. It could be explained by high stability, both thermodynamically and kinetically, of the main structure of the amphiphile **2,6Naph**.

[41] P. Iavicoli, H. Xu, T. Keszthelyi, J. Telegdi, K. Wurst, B. Van Averbeke, W. J. Saletra, A. Minoia, D. Beljonne, R. Lazzaroni, S. De Feyter, D.B. Amabilino, Chirality, 2012, 24, 155

Table 3.1: *Comparison of the structures formed by different molecules.*

	Chirality[1]	Lamellae width[nm]	Head to head distance[2] [nm]	Interdigitation of alkyl chains	Percentage of polymorph[3]	Number of domains
(*R*)-2,7Naph	-7.5±3.4	3.56±0.21	1.01±0.06	Yes	100%	9
(*S*)-2,7Naph	+6.0±2.1	3.41±0.35	0.95±0.09	Yes	100%	9
rac-2,7Naph	-5.5±3.6	3.53±0.22	1.03±0.04	Yes	39.0%	16
	+4.4±2.6	3.43±0.20	1.03±0.04	Yes	58.5%	24
(*R*)-4,4'Biph	-7.7±2.7	6.01±0.55	1.83±0.08	No	89.3%	8
	Nd	6.43±0.48	Nd	No	4.5%	3
(*S*)-4,4'Biph	+4.4±6.1	6.94±0.56	Nd	No	68.7%	11
	-5.7±4.6	6.41±0.30	Nd	No	9.7%	6
rac-4,4'Biph	Nd	6.22±0.03	1.83±0.08	No	9.5%	2
	+1.6±2.0	6.76±0.23	Nd	No	87.4%	9
(*R*)-1,5Naph	+19.1±5.6	4.82±0.41	3.04±0.21	Partially	35.2%	10
	+6.7±5.3	4.10±0.30	Nd	Yes	43.0%	17
	-8.2±2.4	5.18±0.09	Nd	No	5.8%	3
	+8.0±2.4	3.50±0.33	Nd	Yes	7.4%	4
(*S*)-1,5Naph	-18.5±3.5	5.10±0.21	Nd	Partially	46.6%	9
	-9.8±6.0	4.42±0.28	Nd	Yes	23.9%	13
	-13.5*	4.9*	Nd	No	3.4%	1
	+8.2±8.6	3.88±0.10	Nd	Yes	8.8%	5
rac-1,5Naph	+20.9*	5.1*	Nd	Partially	8.8%	1
	-17.3±4.9	5.1±0.2	Nd	Partially		2
	+8.8±2.7	4.5±0.3	Nd	Yes	11.1%	5
	-3.45±5.4	4.8±0.1	Nd	Yes		2
	+19.1*	4.9*	Nd	No	1.8%	1
	-3.8±12.0	3.9±0.5	Nd	Yes	10.0%	6
(*R*)-1,4Ph	+5.7±10.4	6.31±0.62	Nd	No	Nd	5
	+9.9	6.87	Nd	No	Nd	1
(*S*)-1,4Ph	+6.7±2.0	5.41±0.26	1.03±0.02	No	Nd	6
	+0.3±0.7	6.32±0.10	1.43*	Partially	Nd	2

*[1]Chirality is measured with the respect to the main graphite axis ,[2]Measured in the lamella growth direction [3]Alkyl angle is measured with respect to the lamellae growth direction.[3]Percetnage of polymorph was checked on large scale images *Mesured in only one image.*

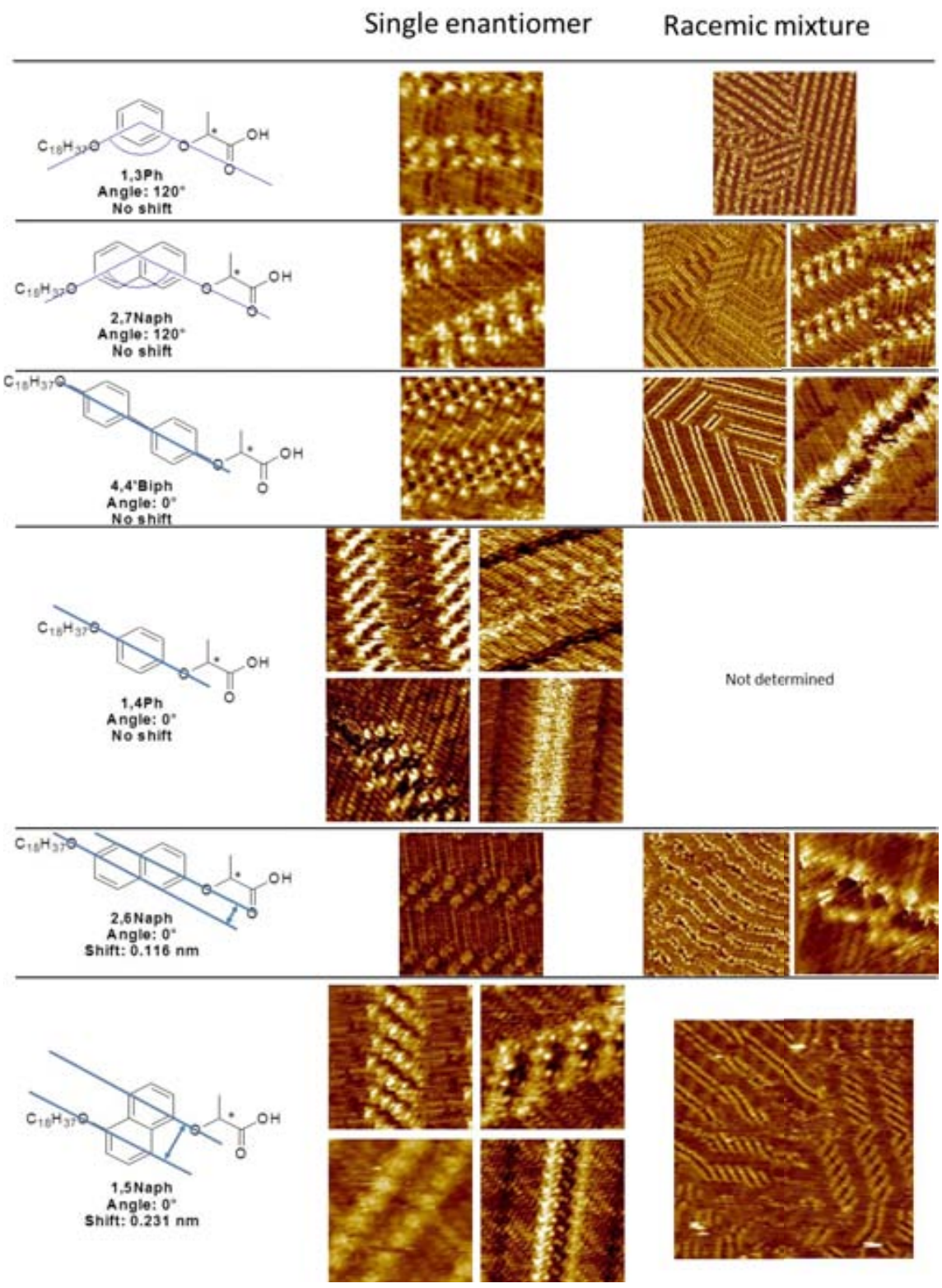

Figure 3.37: *Comparison of structures of acid and their packing*

3.8 Conclusions

Each member of the amphiphile family of acids is capable of forming a stable monolayer at the graphite-1-phenyloctane interface thanks to the presence of the octadecyl chain.

The geometry of the molecule is a key factor in determining the structure of the SAMs. Bent core molecules **1,3Ph** and **2,7-Naph** form one stable type of domains, while different polymorphs were discovered in case of compounds with linear geometry **1,5Naph**, **4,4'Biph** and **1,4Ph**. 1D crystals are formed by **2,6Naph.**

The racemic mixtures of the compounds show very contrasting behaviour: **2,7Naph** is a conglomerate, **4,4Biph** a pseudoracemate and disordered domains with locally ordered structures are present in the SAMs of **1,5Naph** and **2,6Naph**. It is remarkable in this series of compounds that for both **2,6Naph** and **1,5Naph** the racemic mixtures generate monolayers which are less ordered than the enantiopure materials. This situation is, in general, the opposite to bulk racemates, in which ordered racemic compounds are very common in crystalline samples (although, obviously, poorly ordered structures are not generally published or deposited in the Cambridge Crystallographic Data Centre database). Racemic compound **4,4'Biph** fits this scenario better, by changing its conformation on the surface - when compared with the enantiopure material - to give a pseudoracemate. This change is unusual however, because the aromatic parts of the molecule sit edge-on to the graphite. Thus, simple changes in spacer constitution allow one to tailor surface organisation, even if for now predicting the behaviour is out of sight. The bent head group does, however, favour conglomerate formation.

It should be noted that all of the experiments carried out have been performed only at room temperature because of the absence of a temperature control unit on the STM. Therefore, while the equilibrium between monolayer and supernatant solution is possible, many of the structures formed are clearly not thermodynamic minima as can be seen by the small size of domains and high number of domain frontiers. The interaction of the naphthalene ring with the surface would appear to favour this situation, which is not observed in the amphiphiles bearing phenyl rings, although 2,7Naph does show a well ordered conglomerate, so this picture is not complete. Also, interestingly, the substrate is completely covered in all cases, no significant spaces are

formed, and therefore although disordered the layers still fulfil the normal situation in this kind of system where the monolayer is complete or not observable by STM. Variable temperature studies would certainly help to clarify the physicochemical processes at play in the formation of these layers.

Chapter 4

Phase behaviour of self-assembled monolayers of mixtures of amphiphiles at the liquid solid interface

4.1 Introduction

The phase diagrams for pure simple aliphatic acids in solution, the solid state, or at interfaces are expected to be relatively simple, although as demonstrated in the previous chapter complications can arise because of polymorphism, a feature seen when comparing three dimensional crystals and Langmuir films in aliphatic systems.[42] The same is true of totally different crystallising systems which show the formation of diastereomeric salts. Yet in the context of our work, the use of mixtures – which is expected to complicate phase behaviour – can be beneficial. The idea of the Family Approach to resolution of enantiomers[22] – more colloquially referred to as Dutch Resolution – was that having a mixture of chiral molecules with very similar structure as a resolving agent the process of enantioselection could be more effective than each molecule separately. Although perhaps counterintuitive, this approach, which is reminiscent of combinatorial chemistry, is a result of the different roles that molecules can take on during the crystallisation process, and therefore can influence the phase diagram of the system. For example, components might act as nucleating agents, as formers of solid solutions which show enhanced stereoselection, as crystal growth inhibitors, or as solubilising agents for certain enantiomers. It was shown that the chance of diastereomeric salt formation grows from 20-30% to 90% using the Family Approach.[43]

In the forthcoming chapters, we shall see that for our goals the study of mixtures of acids as resolving agents is of interest, especially at the interface between graphite and a non-polar and non-volatile solvent. In order to understand better what takes place in those experiments, mixtures of two acids have been studied in order to investigate their phase behaviour. The dihydroxynaphthalene derivatives **2,7Naph**, **2,6Naph** and **1,5Naph** were chosen for the study because all of them form stable and different

[42] M. Lundquist, *ChimicaScripta*, **1971**, *1*, 197.
[43] R. M. Kellogg, J. W. Nieuwenhuijzen, K. Pouwer, T. R. Vries, Q. B. Broxterman, R. F. P. Grimbergen, B. Kaptein, R. M. La Crois, E. de Wever, K. Zwaagstra, A. C. van der Laan, *Synthesis*, **2003**, *10*, 1623.

monolayer structures on the surface of graphite, so it is easy to distinguish each component.

The phase behaviour of mixtures of common fatty acids and other amphiphiles has been studied both in the bulk and in monolayers, but exclusively at the air-water interface in Langmuir layers[44,45,46] (and especially involving hydrogen and fluorine containing amphiphiles)[47,48] where molecular scale imaging of structure is virtually impossible. As far as we are aware, the use of scanning probe microscopy to look at mixtures of different amphiphiles (enantiomers apart) has not been performed, and therefore this study has additional interest and novelty.

In all experiments with STM, the mixtures were prepared in 1-phenyloctane and a drop of the mixture was placed on freshly cleaved surface of HOPG.

In order to test for a correlation between mixing and separation in the monolayers with the intrinsic mixing ability in the bulk, the thermal properties of macroscopic mixtures of acids were studied by Differential Scanning Calorimetry (DSC) and X-ray powder diffraction (XRD). All of the samples for DSC and XRD were prepared in the same manner, the compounds were mixed as a solid, then dissolved with THF, evaporated and melted again in an oil bath at 100°C, and then left to cool down slowly inside oil bath. Usually 2 to 3 mg of each mixture was used for the calorimetry measurement. The sample of pure acid was measured on crystals prepared as described in experimental part. It is worth mentioning that the observed peaks correspond to phase transitions.

In the Figures 4.1, 4.2 and 4.3 DSC and XRD of pure acids used in the mixtures studied in this chapter are presented. In the DSC shown in Figure 4.3 one can observed that acid **1,5Naph** melts homogenously at 104 and 103°C in first and the second cycle of heating respectively. On the other hand the other two acids measured, **2,6Naph** and **2,7Naph** show more complicated behaviour. In the DSC of the acid **2,7Naph**, presented in the Figure 4.1 there are three peaks during the first sweep, at 68°C, 86°C and 89°C that indicates that there are possibly three different phases before melting. In the second heating there is small negative peak observed at about 55°C that indicates there is exothermic change of structure, and then at 82°C the material melts. The DSC of the

[44] K. Ekelund, E. Sparr, J. Engblom, H. Wennerström, S. Engström. *Langmuir* **1999**,*15*,6946
[45] A. K. Panda, K.Nag, R.R. Harbottle, F. Possmayer, N.O. Petersen *Colloids Surfaces A* **2004**, *247*, 9
[46] B. M. Ocko, M. S. Kelley, A. T. Nikova, D. K. Schwartz *Langmuir* **2002,** *18*, 9810
[47] H. J. Lehmler, M. Jay, P. M. Bummer, *Langmuir* **2000**,*16*, 10161
[48] S. E. Qaqish, S. G. Urquhart, U. Lanke, S. M. K. Brunet, M. F. Paige *Langmuir* **2009**, *25*, 7401

2,6Naph is presented in the Figure 4.2. In the first heating all of the material melts at 107°C, while in the second cycle of heating the peaks appear at 91°C and 100°C.

In the X-ray diffractograms all three of the compounds show clear and well resolved peaks, indicating their crystallinity. The acid **2,7Naph** shows peaks at the angles of 3.56, 7.22, 10.88, 14.44 degrees that correspond to laminar system with the distance between the layers of 2.45 nm and apart the other, less pronounced peaks at around 16-25 degrees, with the most significant peak at 19.02, which correspond to distance of 0.47 nm. The acid **2,6Naph** (Figure 4.2) shows peaks at 4.58, 6.88, 9.18, 11.46, 13.86 and 16.16 degrees which correspond to laminar system with the distance between the layers of 3.80 nm plus one more peak at angle of 21.24 degrees what corresponds to the distance of 0.42 nm. The acid **1,5Naph** (Figure 4.3) shows the structure with the peaks at 3.9, 5.9 and 7.9 degrees which correspond to the laminar structure with 4.4 nm between the layers. The peak at 7.74 corresponds to distance of 1.14 nm.

The XRD results are generally as to be expected for molecules with long alkyl chains that are usually stretched and interdigitated, and as is known from the crystal structure of **1,3Ph**[40] and the STM images molecules of acid are around 3.6-3.8 nm long what suits well the distance observed for the acid **2,6Naph** but there is considerably longer distance 4.4 nm observed for **1,5Naph**, probably because of bulky head- group perpendicular (or at least not in line with the alkyl chain) what force the aromatic part not to stay in the same plane, but shifted with respect to the others. That hypothesis would explain why the layer is longer by approximately 0.8 nm than the size of aromatic part of the molecule. On the contrary the molecules of **2,7Naph** show a shorter distance between the layers (2.45 nm) than the other compounds, this might be caused by a contrasting conformation of the alkyl chains to that observed in STM. The other observed peaks, are the peaks of the head to head distance, in the case of molecules of acids **2,7Naph** and **2,6Naph** the distance is smaller (0.47 and 0.42 nm respectively) than for the **1,5Naph** (1.14 nm). This feature is due to the angle between aromatic moiety and the alkyl chain, the close packing observed for the other two acids for **1,5Naph** is apparently challenged. Also the difference between **2,7Naph** and **2,6Naph** can be easily explained by the change of geometry of the molecule – in the **2,6Naph** the alkyl chain and lactic unit are connected on the two sides of molecule, in the same direction with a slight shift between them (approximately 0.12 nm), while in the **2,7Naph** there is an angle of 120 degrees between the direction of aromatic part and

alkyl chain, that makes molecule a bit wider when stretched compared with **2,6Naph**.

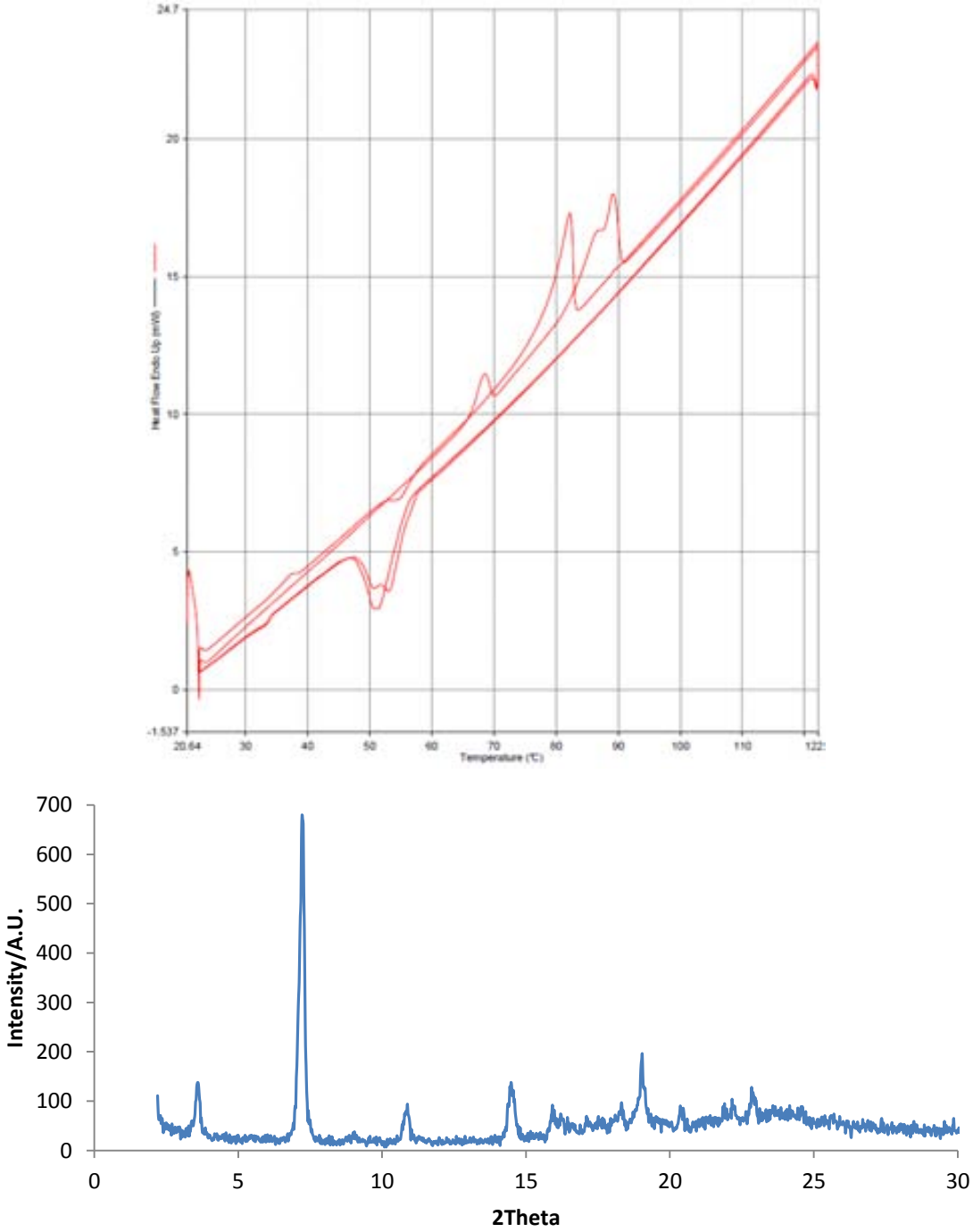

***Figure 4.1**: DSC (top) and XRD (bottom) data of (R)-**2,7Naph**. In the first cycle of DSC the phase changes occur at 68°C, 86°C and 89°C, the last, double peak represents melting of the material. In the second cycle of heating there are negative peaks that appears at 55°C, and then at 82°C material melts which indicates that after heating arrangement of molecules is different. In X-ray diffractogram the peaks are characteristic for laminar structure with distance between the layers 2.45 nm.*

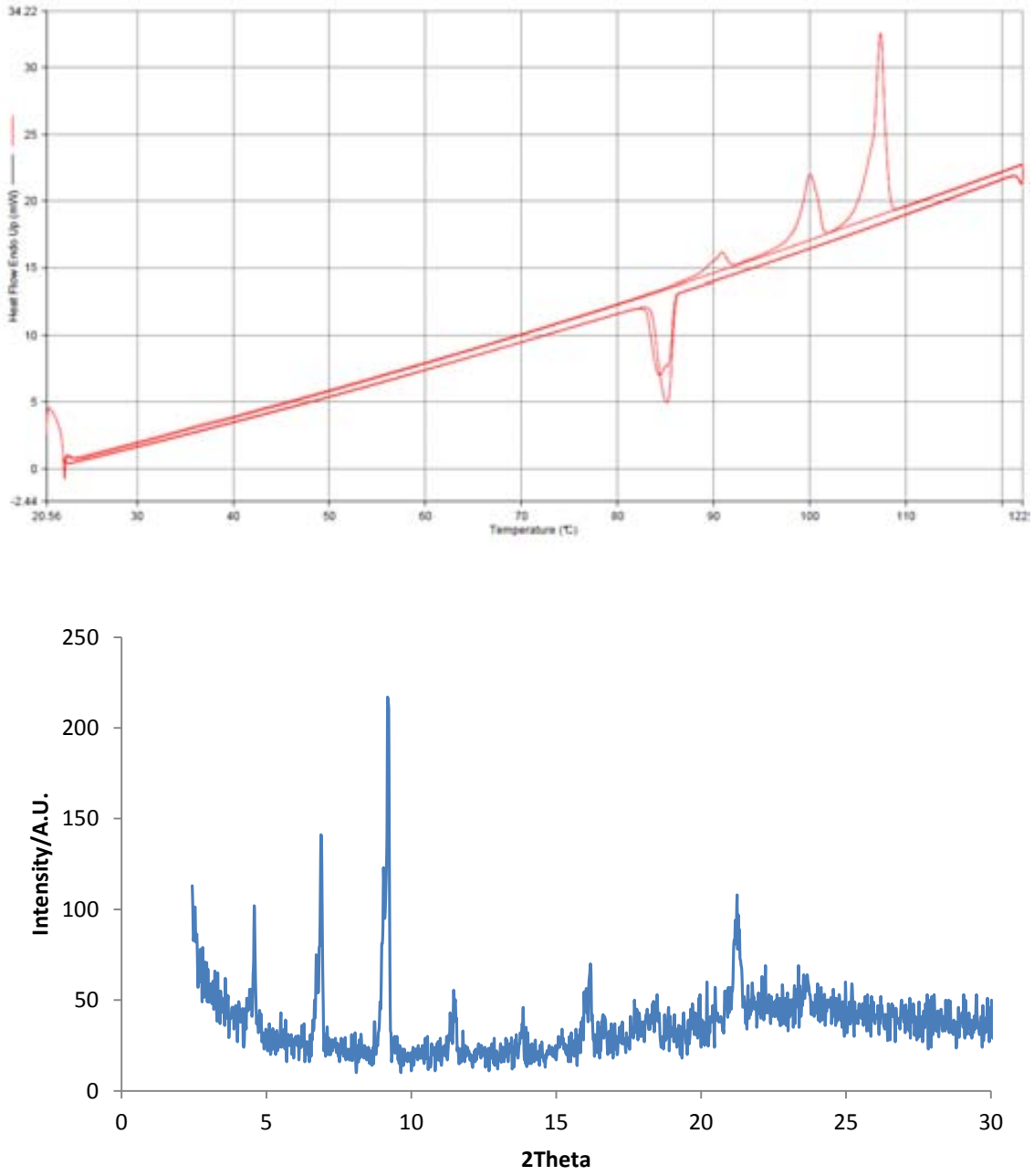

***Figure 4.2**: DSC data (top) and X-ray diffractogram (bottom) of (R)-**2,6Naph**. In the first DSC cycle the phase melting takes place at 107°C. In the second cycle of heating the peaks appear at 91°C and 100°C that there are possibly two different phase after heating and cooling quickly. In the X-ray diffractogram the peaks are characteristic for laminar structure with distance between the layers 3.80 nm.*

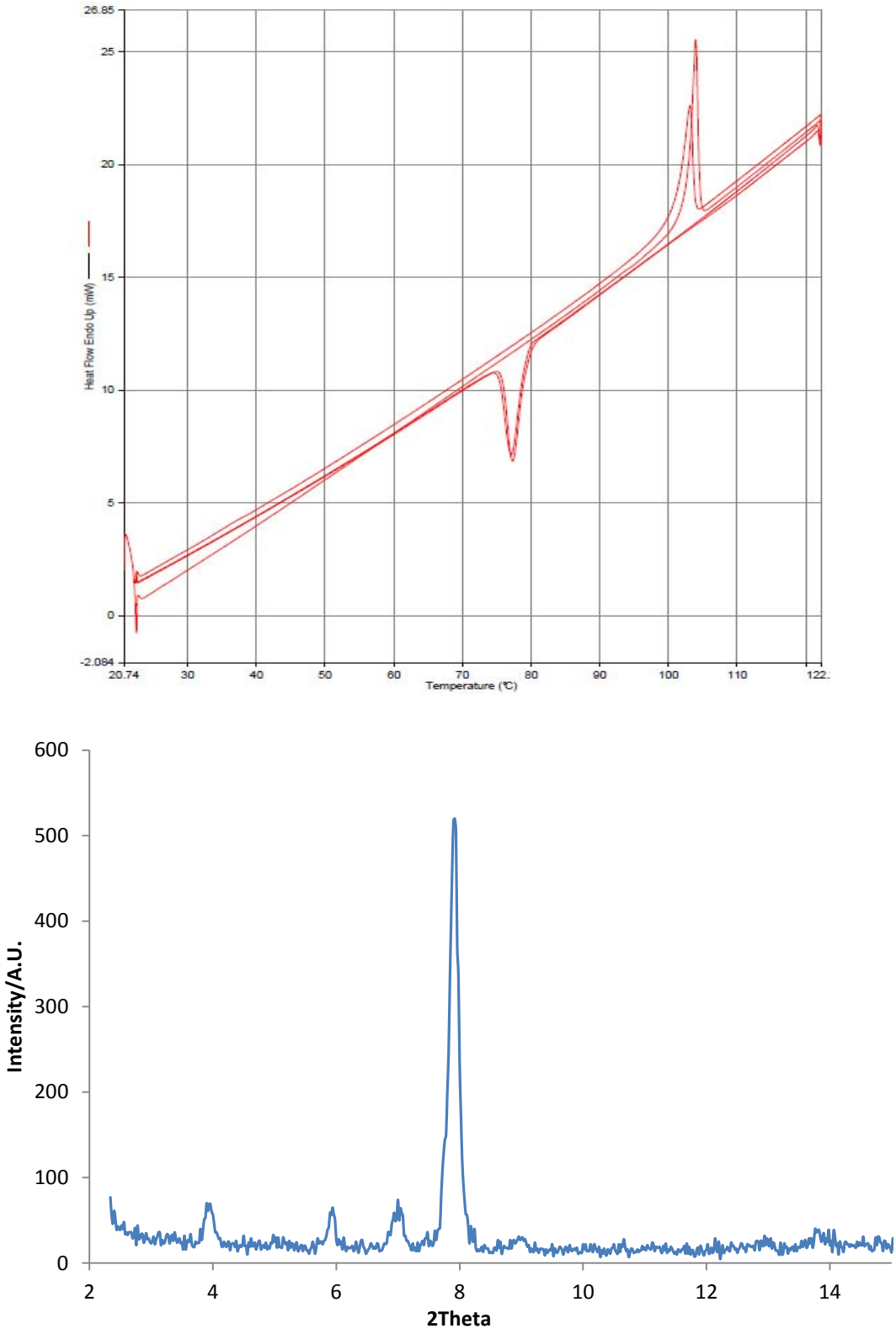

***Figure 4.3**: DSC of (S)-**1,5Naph** (top). In the both cycles the melting takes place homogenously at 104°C and 103°C respectively for first and second cycle. In X-ray diffractogram (bottom) the peaks are characteristic for laminar structure with distance between the layers 4.4 nm.*

4.2 Self-assembly of (R)-2,7Naph (S)-2,6Naph

The mixture of the unlike enantiomers of lactic acid derivatives **2,7Naph** and **2,6Naph** in 1-phenyloctane formed monolayers on graphite after a few minutes of scanning the STM tip in the solution, and a typical image is shown in Figure 4.4. A lamellar structure is clear in the monolayer, as seen by the bright and dark areas corresponding to higher and lower tunnelling current, respectively. And yet, unlike the pure compounds on the surface, in most of the areas the image appears blurred and the lamellae are not very straight and are quite disordered, although some minority areas characteristic of the pure compounds are observed of very small dimensions (less than 300 nm^2, whereas domains of the pure compounds are typically an order of magnitude larger). The fact that the lamellae bend and fuse, separate, widen and shrink is an indication that the composition of the lamellae changes, and that adjacent lamellae do not coincide in their distribution of components which leads to these effects.

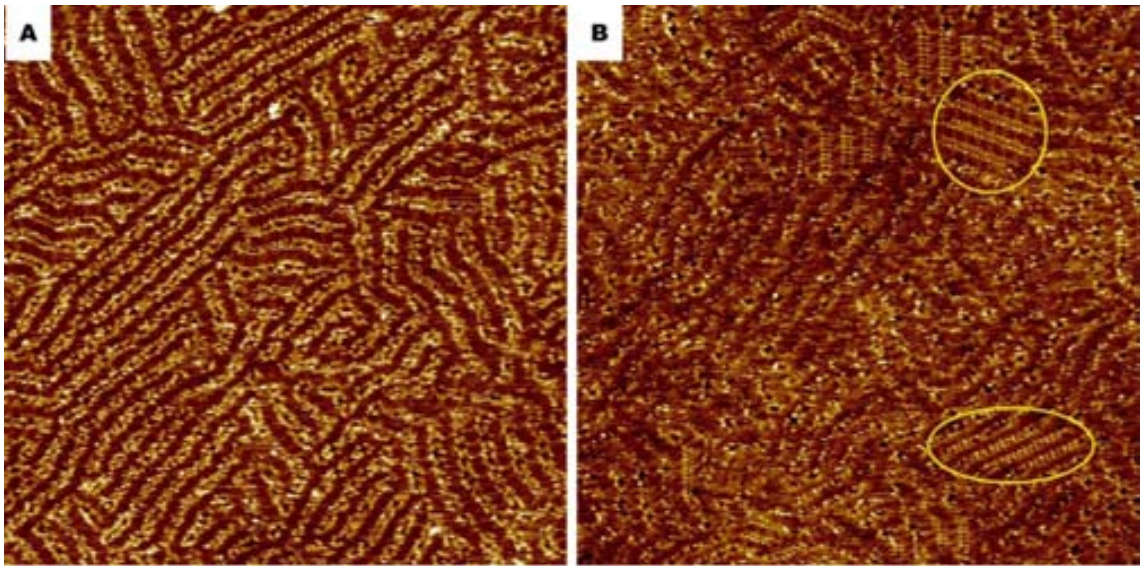

Figure 4.4: *Large scale STM images of a 1:1mixture of amphiphiles (R)-**2,7Naph** and (S)-**2,6Naph** at the 1-phenylooctane graphite interface (both A and B: 96.4 x 96.4 nm; I_{set} = 0.7 nA; V_{bias} = 0.8 V). The lamellar-based self-assembled monolayer is formed, but there is certain level of disorder; lamellae are not straight, many defects can be found all around the area. In image B the areas where a few tens of molecules of acid form well-ordered domains are marked in yellow and a few other smaller organized domains can be observed.*

A closer view of a perceived domain in the monolayer (which is defined by the orientation of the alkyl chains) shows that the octadecyl moieties all point along the

same direction (Figure 4.5). In contrast, the head groups occupy multiple arrangements, where the aromatic groups are apparently closer together, in a straight "head-on" configuration or forming an S or Z-type dimer, or apart generating a tiny "hole" in the lamella. Defects or holes between the lamellae are generally not correlated along neighbouring lamellae in the perpendicular direction to the rows, pointing to a very local disorder effect.

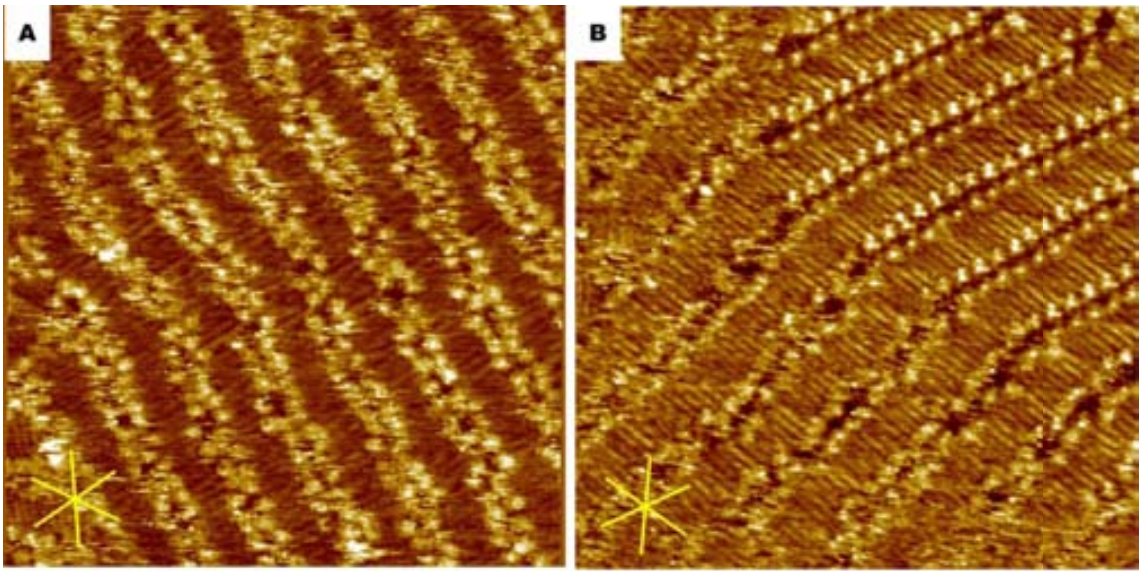

Figure 4.5: *Close-up STM images of a 1:1 mixture of amphiphiles (R)-**2,7Naph** and (S)-**2,6Naph** at the 1-phenylooctane-graphite interface (A: 30.1 x 30.1 nm and B: 28.5 x 28.5 nm; I_{set} = 0.7 nA; V_{bias} = 0.8 V for both). In the top part of image A either admolecules are atop the monolayer or molecules are not absorbed completely, this causes noisy areas and bright specks in the image, and in the lower part the aromatic heads of the molecules can be distinguished in some areas (though not everywhere). The aromatic heads are sometimes separated in a manner that the distance between them is too great for there to be hydrogen bonds. In image B a very regular domain is found in the upper right part of the image whose structure is identical to the one formed exclusively by (R)-**2,7Naph**. In the left part of the image, a noisy area probably occupied by mixed domain is observed. A clear difference in the orientation and resolution of the two types of domain is evident and also it is patent that one type of domain can smoothly convert into the other one. In this image it is also clear that in mixed monolayer alkyl chains are interdigitated.*

The structures that are observed in the images indicate that the monolayer is formed by a mixture of the two component compounds mainly, and the alkyl chains are interdigitated. At the same time as the lamellae are not periodic in any way, a kind of two-dimensional liquid-crystal-like structure on the surface is formed, in that there is

orientational order of the molecules, but positional disorder. The average lamellae width is 4.44 ± 0.28 nm and the rotation with respect to the main graphite axis is anticlockwise and equals -24.6 ± 9.5°, which is significantly different comparing with parameters of the components: (*R*)-**2,7Naph** forms domains that are 3.56 ± 0.21 nm wide and rotated at -7.48 ± 3.41 degrees with respect to the main graphite axis, while for **2,6Naph** the lamella width is 4.14 ± 0.16 nm and the chirality cannot be determined because of the irregularity of the structure, although as presented in the previous chapter the chirality is closer to zero (with respect to the perpendicular to the main graphite axis [0010]) the longer the domain region considered. A histogram of angles of this mixture is presented in the Figure 4.6. Looking at these values it seems that the packing in this mixed monolayer is not as good as in pure monolayer, in that irregularity exists and the lamellar width is larger, leading to a lower density of the structure. It is intriguing that the domain angle is larger than in either case individually, meaning that structural chirality can be enhanced by using a mixture of compounds with unlike chirality: This counter-intuitive result could arise because of the distinct head group geometry of the components.

Areas can be identified which are formed exclusively by molecules of acid (*R*)-**2,7Naph**, as shown in Figure 4.5B (top right). It was checked that the inter-molecule distances, and chirality of this packing structure is the same as that observed in a pure sample of (*R*)-**2,7Naph** on the surface. The few domains of this type that were encountered were rather small; the biggest one was composed by little more than 100 molecules, and the next biggest one by around 80, and a few of around 40 molecules were observed. No domains formed exclusively by acid (*S*)-**2,6Naph** were found. Therefore the mixed monolayer is preferred under the conditions that have been employed.

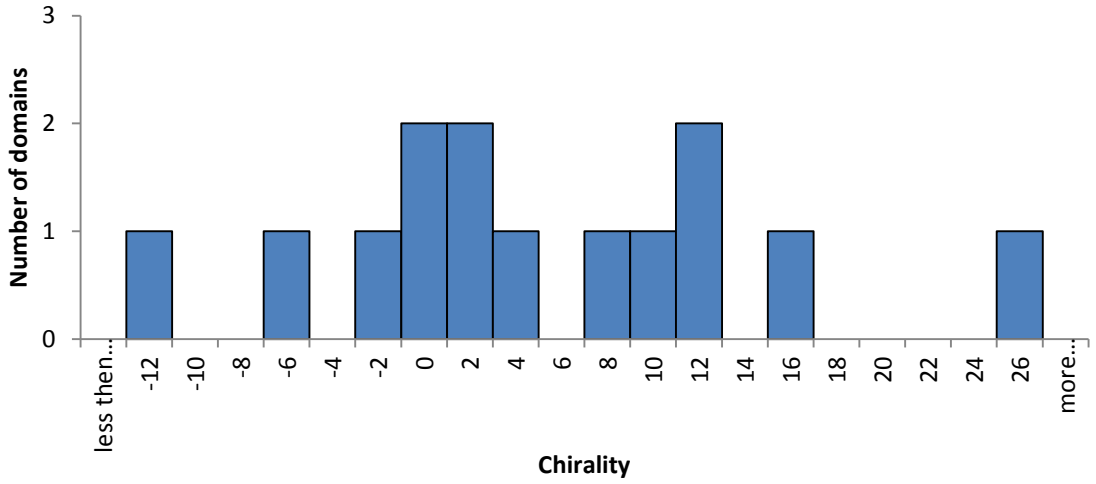

Figure 4.6: *Histogram of angles measured in STM images of a 1:1 mixture of amphiphiles (R)-**2,7Naph** and (S)-**2,6Naph** at the 1-phenylooctane-graphite interface*

In Figure 4.7 the DSC and XRD of mixture of (*R*)-**2,7Naph** and (*S*)-**2,6Naph** is presented. The melting peak observed in the DSC is clear and sharp at 91°C and as the melting occurs in between the melting points for individual acids (89 and 107°C for **2,7Naph** and **2,6Naph** respectively), one can assume that there is homogenous mixture of two acids because of the single intense transition. In the cooling there are a number of peaks, which means that during solidifying some phase separation might take place, at temperatures different to those of the pure compounds (75°C for **2,6Naph** and 53°C for **2,7Naph**) which is an indication of the formation of a mixture in the solid state.

In the X-Ray diffractogram one can observe the peak at angle of 2.46 degree that corresponds to a distance of 3.57 nm, that is the length of the molecule of either of acids. The other five observed peaks are much less intense and corresponds to distance of 0.57 to 0.37 nm, just one of them, at 21.44 is similar to the one observed at 21.03 in acid **2,6Naph**. Notice there are no peaks between 5 and 10 as there were in the component compounds. This observation means that most probably there is new, mixed structure, observed also with X-ray diffraction, which confirms results obtained with DSC.

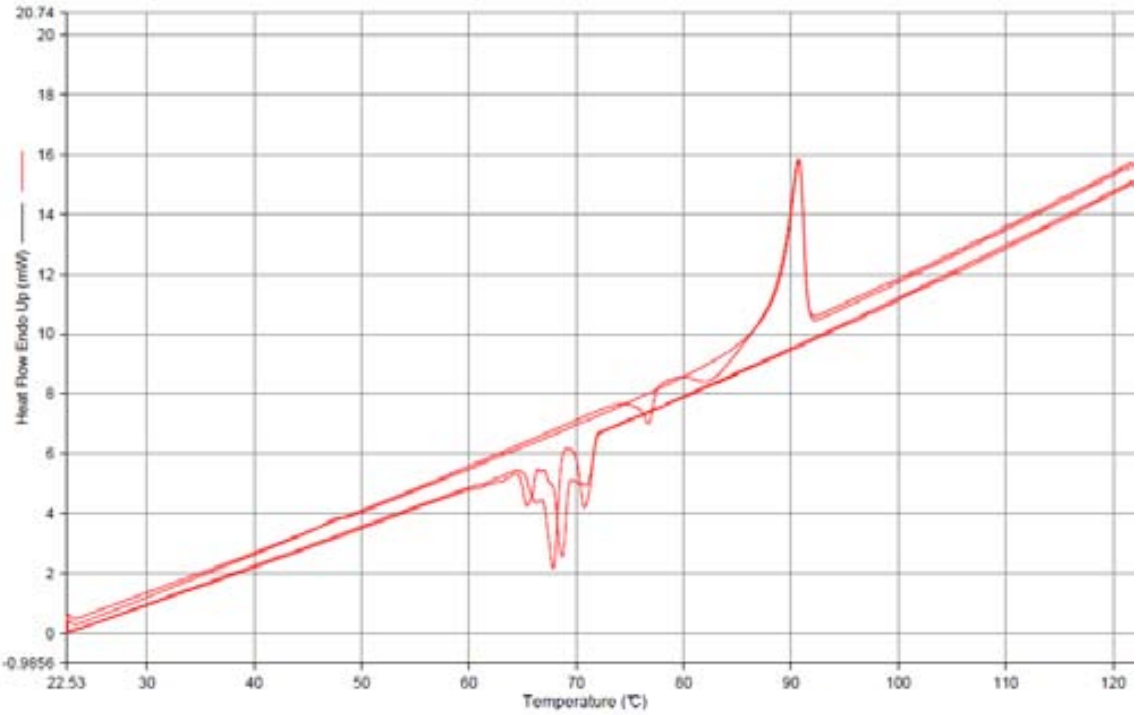

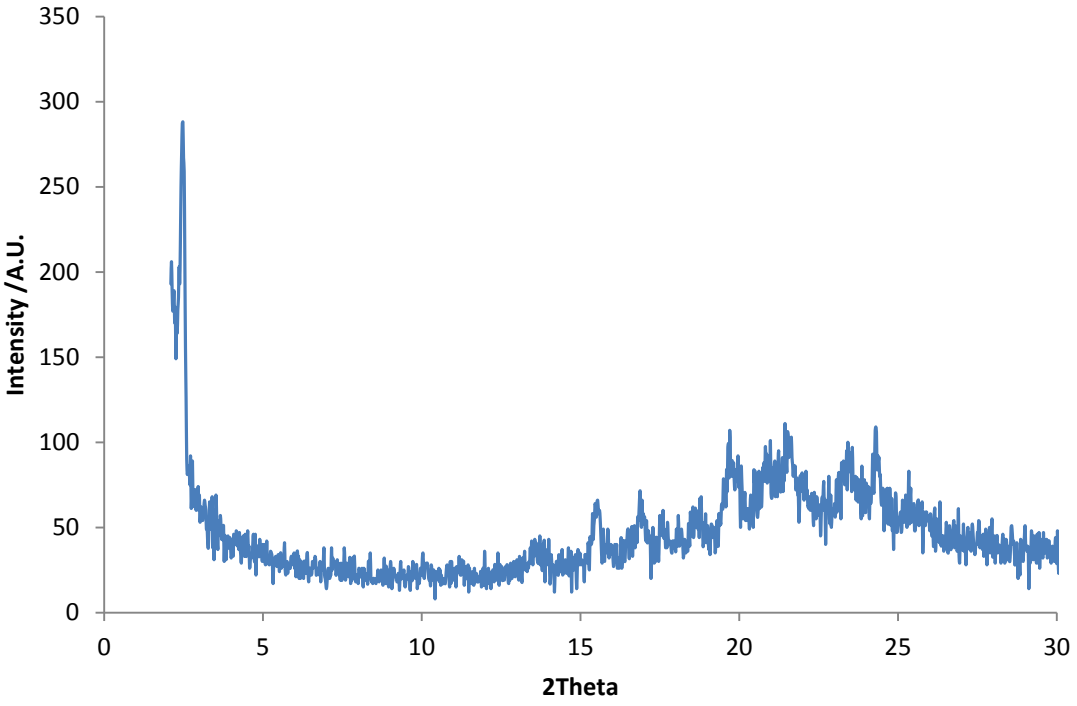

Figure 4.7: *DSC and X-ray diffractogram of a 1:1mixture of acids (R)-**2,7Naph** and (S)-**2,6Naph**. In the both first and second cycle the phase melting occurs at 91°C. In the second cycle there are two small negative peaks at 76°C and 83°C, some exothermic rearrangement of crystal structure occurs then. X-Ray diffractogram of the mixture shows peaks at angle of 2.47 (3.57 nm) and less intense peaks at 15.56 (0.57 nm), 16.88 (0.52 nm) 19.7 (0.45 nm), 21.44 (0.41 nm), 24.3 (0.37 nm).*

Therefore, this mixture produces a complex mixture of phases in a material containing a combination of the two acids both as a monolayer on graphite as well as in the bulk state.

4.3 Self-assembly of (R)-2,7Naph (R)-2,6Naph

The mixture of the acids **2,7Naph** and **2,6Naph**with identical lactate group chirality–(*R*) was prepared by dissolving the in 1-phenyloctane and was studied at the liquid graphite interface using the STM as in the previous cases. In the images shown in Figure 4.8 it is clear that again the lamellar structure of the monolayer is preserved, but there is a lot of movement of the molecules on the surface as witnessed by the fuzzy appearance. The molecules form rows, with the head groups of one row facing those of the next. There is a significant geometrical difference between molecules of acid **2,7Naph** and **2,6Naph**, and it is perhaps for this reason that a stable monolayer is not formed, although it is a little surprising that phase separation does not occur if this is the case. Chirality also plays a defining role, because the structure is completely different to that formed by the unlike enantiomers. It seems that the major driving force in the formation of this monolayer is the interaction between the alkyl chains and the graphite substrate and between the alkyl chains of different molecules. The lamella width observed on few structures was 4.2 ± 0.20 nm, compared with 3.9 ± 0.26 nm for **2,6Naph** and 3.57 ± 0.20 nm for **2,7Naph**, in both of those cases the interdigitation of alkyl chains can be observed in detail in the STM images unlike the present case. There are only a few very small areas in which the structure looks exactly like the lamellae formed by molecules of acid **2,7Naph**, the biggest one observed was composed of approximately 30 molecules.

The sample of these acids was difficult to measure; the images were rather noisy, probably because the STM tip was interacting strongly with the molecules on the surface and moving them. For this reason the noise in the images is mainly in the horizontal direction which is the one of the Raster scanning in all of the measurements. This effect is seen most clearly at the bottom of Figure 4.8B and in Figure 4.9. In the latter, the great degree of disorder in the system can also be appreciated. Despite this fact, areas do appear where head groups can apparently be discerned with non-regular

packing, although the distance between lamellae is remarkably constant.

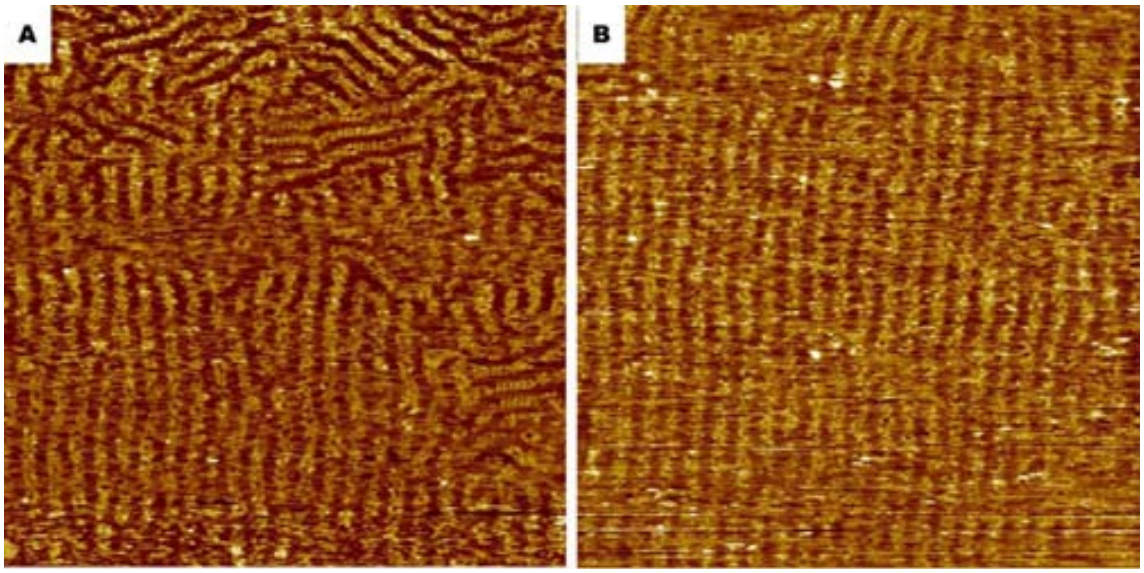

***Figure 4.8**: STM Image of 1:1mixture of acids (R)-**2,7Naph** and (R)-**2,6Naph** (A and B: 96.4 x 96.4 nm; I_{set} = 0.7 nA; V_{bias} = 0.8 V) at the graphite-1-phenyloctane interface. The disordered structure of lamellae in image A is seen clearly, although very small ordered domains of acid (R)-**2,7Naph** can be observed on the right side, close to the edge of the image and in the upper part of the image. In image B large domains with relatively straight lamellae, although with poor definition, are shown.*

The structures that were found were 4.2 ± 0.1 nm wide and the lamella growth direction was almost perpendicular to the main graphiteaxis-28.9 ± 4.8. The instability of the monolayer meant that high quality images of this mixture were not attainable. However, since the experimental conditions were apparently the same as the other combinations of compounds it can be concluded that the overall structure is distinct from the other mixtures because the STM images are qualitatively very different. In a way, they remind one of a smectic A liquid crystal, in which the molecules have orientational order and yet positional disorder within the layers, and where motion is possible. The situation is far from the “two dimensional crystals” usually observed for these monolayers.

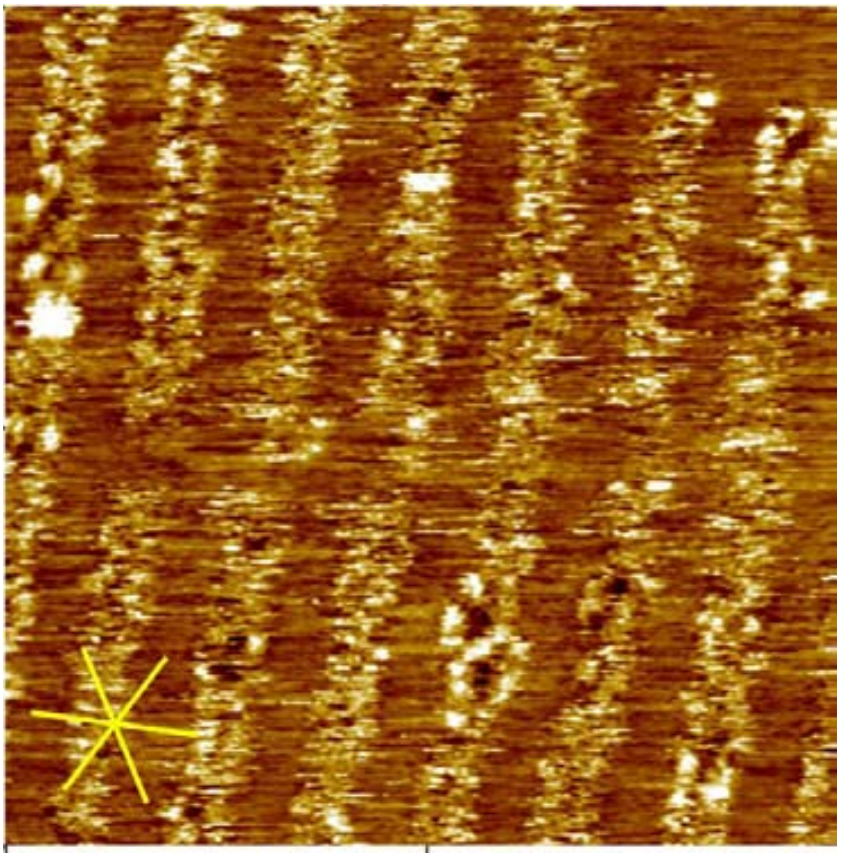

Figure 4.9*: Close up STM image of mixture 1:1 of acids (R)-**2,7Naph** and (R)-**2,6Naph** (28 x 28 nm; I_{set} = 0.7 nA; V_{bias} = 0.8 V)at the graphite-1-phenyloctane interface. There is a constant movement of the molecules on the surface, which makes impossible high resolution imaging with STM. At the bottom in the centre one can see bright molecules, this might be caused by molecules tilted up from the surface.*

In the bulk, the DSC (Figure 4.10) measurements also show that more than one possible arrangement of the molecules is available in the three dimensional systems Two distinct peaks at 88°C and 98°C are observed during the first heating (perhaps an indication of separation of the two components in the bulk) and three distinct ones 71°C, 75°C and 79°C, slightly lower temperature in the second melting. In XRD the peaks observed are at 6.66 and 9.1 degree are very similar to the signals found for lamellar structure of the acid **2,6Naph** (6.88 and 9.18), with the other peaks corresponding to small distances at around 0.41-0.48 nm in the same range as the peaks of the pure acid **2,6Naph**.

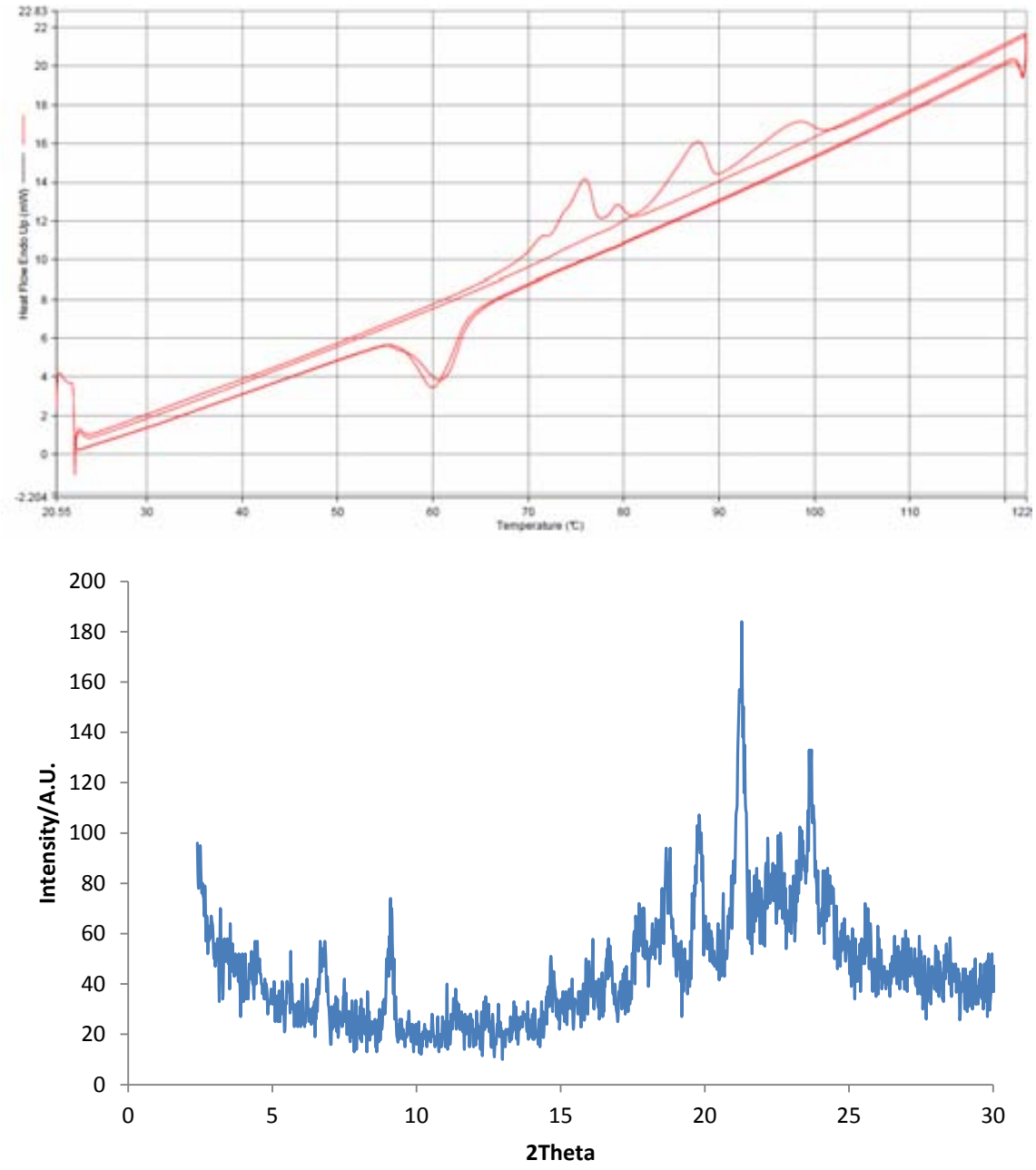

***Figure 4.10**: DSC and X- ray diffractogram of a 1:1 mixture of acids (R)-**2,7Naph** and (R)-**2,6Naph**. In the first cycle the phase changes occurs at 88°C and 98°C, the second peak is melting of the material. In the second cycle of heating the peaks appear at 71°C, 75°C and 79°C, which indicate that there is different phase after heating. In the X-ray diffractogram two peaks are observed at similar angle as for **2,6Naph**, but also few others in the range 15-25 degrees.*

Therefore, in this sample the totally mixed layer on graphite is not mirrored in the bulk state, where better defined phases are formed than in the case where the enantiomers are opposite.

4.4 Self-assembly of (R)-2,7Naph (R)-1,5Naph

The equimolar mixture composed of acids (*R*)-**2,7Naph** and (*R*)-**1,5Naph** in 1-phenyloctane deposited as a hot drop on graphite, as for the other samples, presents an ordered monolayer covering the entire surface (Figure 4.6). The lamellae are straight, although closer inspection reveals that there are quite a lot of defects and the domains sometimes change directions. In Figure 4.11A a domain with straight lamellae coming from the upper left corner of the STM image can be observed, but, following the domain in the direction to the centre of the area scanned, a clear deviation from the main direction is seen, followed by a return to the original direction. This defect does not run perpendicular to the domain as a result of a translational error in packing, but rather propagates as a wave through the structure.

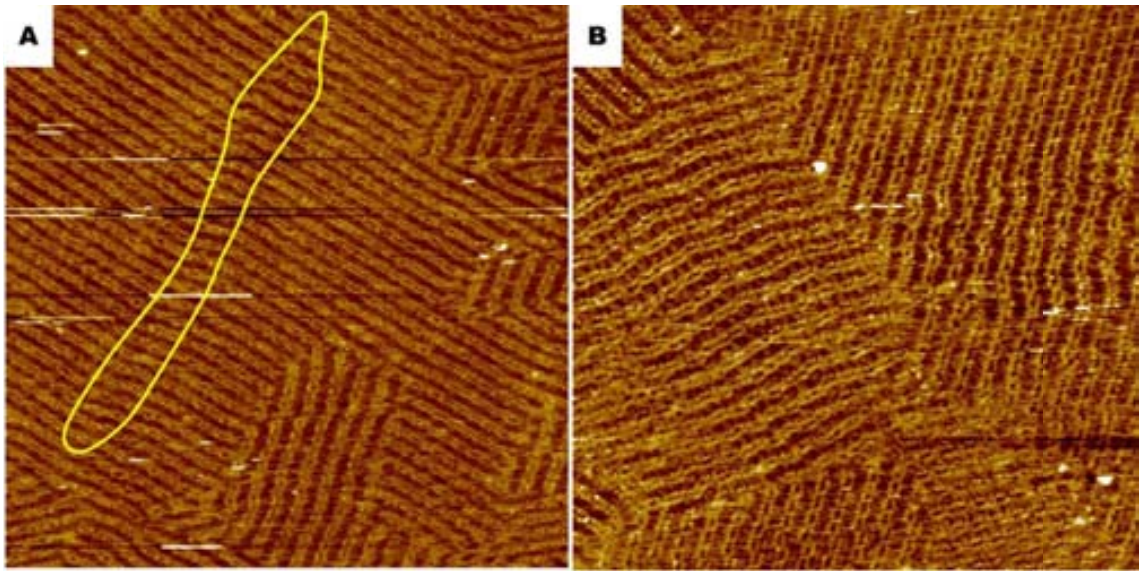

Figure 4.11: *STM images of a1:1 mixture of acids (R)-**2,7Naph** and (R)-**1,5Naph** (A: 96.4 x 96.4 nm; B: 88.6 x 88.6 nm; A and B: I_{set} = 0.7 nA; V_{bias} = 0.8 V) at the graphite-1-phenyloctane interface. In image A the straight lamellae are present in most of the image, but there is an area with a surprising "jump" in the direction (marked in a yellow outline). In the bottom left corner of the image there is an interesting defect –lamella changing direction by approximately30°. In image B one can see the domain composed mostly by molecules of acid **2,7Naph** in the right upper part but the lower down the image the more defects can be found.*

There is also a different kind of domain in the bottom-centre part of image A, where a more disordered region is observed. The wave-like defect structure is also seen more frequently in other areas of the surface, as shown in Figure 4.11B.

In the close-up images of this surface a wide range of packing structures can be observed. These range from the domains composed exclusively of the molecules of acid **2,7Naph**, where the molecules appear with a well-defined shape with few defects that do not influence the global arrangement of the surface, to domains in which the head groups are so disordered that it is not possible to distinguish clearly the nature of the aromatic parts of each molecule. Figure 4.13 C and D show examples of the different domains.

The packing parameters of the lamellae were checked in order to assess their purity. Those areas with a majority of acid (*R*)-**2,7Naph** have a lamella width of 3.48 ± 0.13 nm, the head to head distance is 1.01 ± 0.13 nm and the angle with respect to the main graphite axis is +6.3 ± 15.6°. Those values are similar to the parameters of monolayer of pure (*R*)-**2,7Naph**: lamella width is 3.56 ± 0.21 nm, head to head distance is 1.01 ± 0.06 nm, and chirality angle is -7.5 ± 3.4, parameters of monolayer of **1,5Naph** width is 4.46 ± 0.44 nm, and angle equals +11.3 ± 9.0°. It is clear the average angle for observed structure is different than for the each acid on its own. In the histogram shown in Figure 4.12 the distribution of angles is presented.

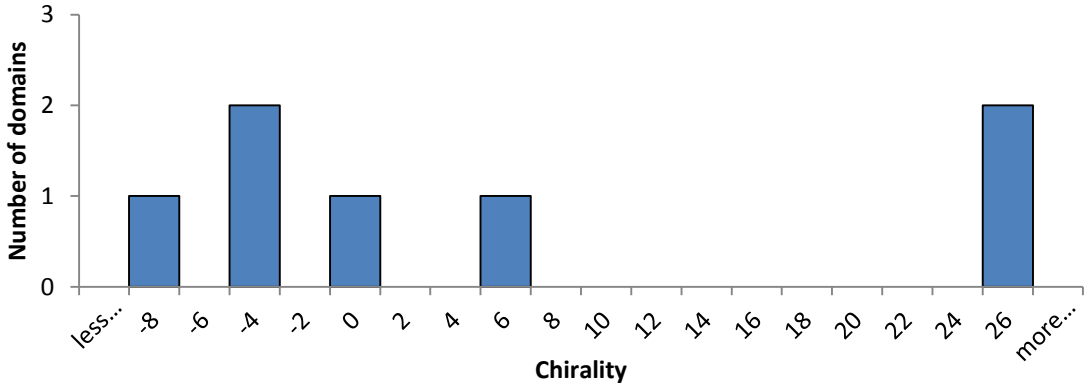

Figure 4.12: *Histogram of angles for structures similar to the observed for* ***2,7Naph*** *measured in STM images of a 1:1 mixture of amphiphiles (R)-****2,7Naph*** *and (R)-****1,5Naph*** *at the 1-phenylooctane-graphite interface*

For the relatively less ordered domains, where the head group of each molecule cannot be clearly distinguished, the lamellae are also rotated anticlockwise with respect to the main graphite axis and the angle measured on the two domains found was -9.7 ± 6.8°. The lamella-lamella repeat distance is 3.99 ± 0.30 nm.

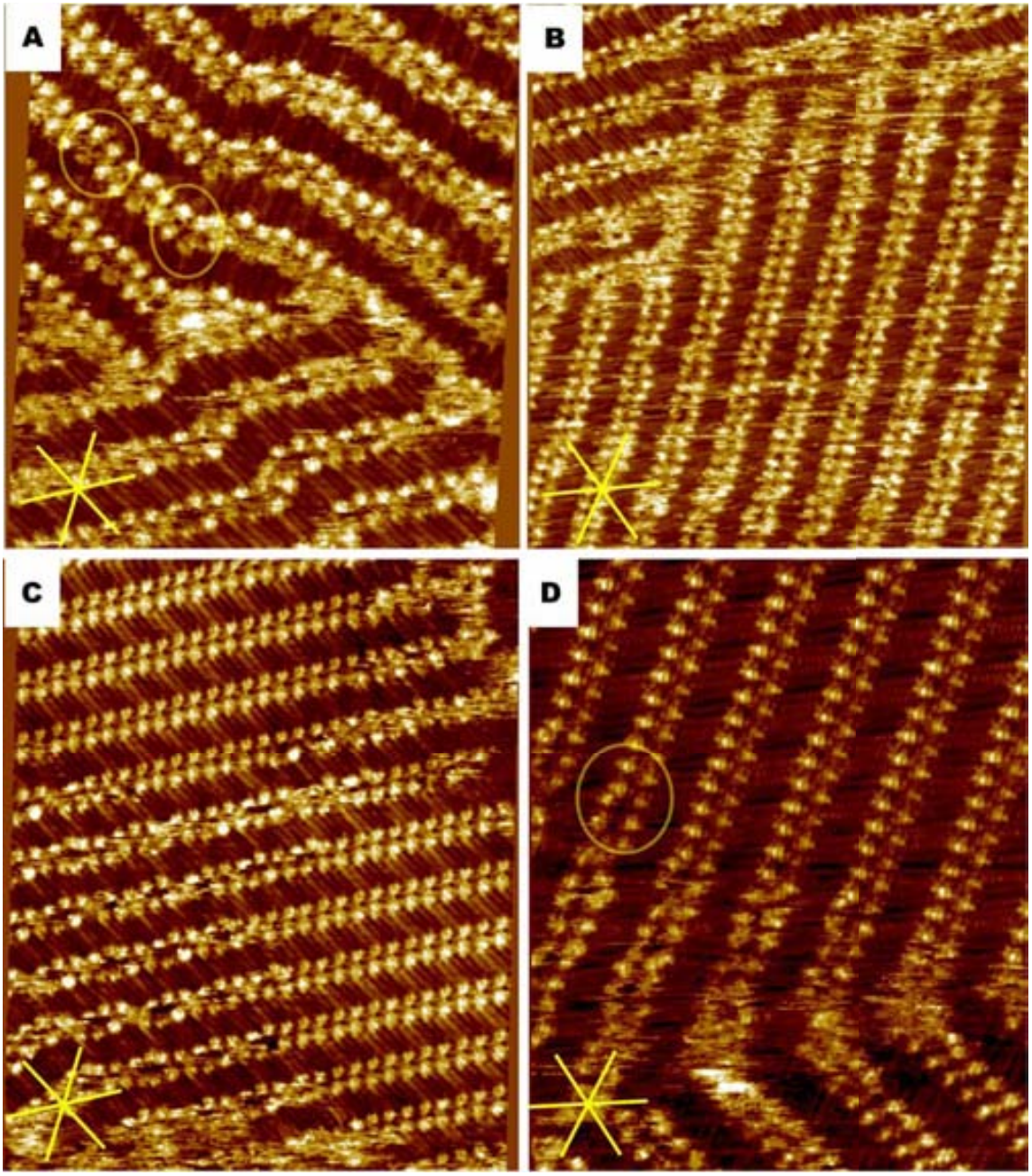

Figure 4.13: *STM images of a 1:1 mixture of acids (R)-**2,7Naph** and (R)-**1,5Naph** (A: 25.2 x 23.4 nm; B: 38.7 x 33.7 nm; C: 35.9 x 30.1 nm D: 25.5 x 20.7 nm; I_{set} = 0.7 nA; V_{bias} = 0.8 V) at the graphite-1-phenyloctane interface. Images A and B show less ordered structures, especially in the left -bottom part of image A. In images C and D one can observe regular rows of molecules of acid in top part of image D and top –left and bottom right part of image C, but there is an area with quite some disorder in the centre left part of image C, the head groups are not exactly in line. Areas where there is an intriguing change of contrast of one head group in the lamella are marked with a circle.*

The formation of domains of the SAM of **2,7Naph** is observed, while no SAM region formed exclusively by acid **1,5Naph** was observed. There are a lot of mixed domains in

which some molecules of **2,7Naph** seem to be substituted in the lattice by molecules of **1,5Naph**. These molecules are apparent because of clear changes in the contrast of the head groups. It seems, therefore, that this mixture is an example of a partial solid solution in a monolayer, where molecules of acid **2,7Naph** act as the solvent and the molecules of **1,5Naph** can be incorporated into the structure of the monolayer without changing the lattice dimensions. In the lamellae where there are a significant amount of molecules of **1,5Naph** the structure is slightly different, the aromatic parts seems not to layflat on the graphite, probably not all of them are able to form hydrogen bonds and the lamellae direction vary locally. There are also domains that although visualized by STM, cannot be analysed in detail because of the movement of the aromatic part of the molecule during scanning. In this case only the direction of the lamellae and the alkyl chains can be seen, but the head groups of the molecules are blurry. Probably these structures are mixed with a significant amount of the two components, and it is not energetically favourable to form well defined structure on the surface. Nevertheless, it seems that the surface proportion of the acids is not the same as that present in solution. This conclusion is surprising taking in account that **1,5Naph** is less soluble in 1-phenyloctane than **2,7Naph**.

In DSC (Figure 4.14) two peaks are observed both in the first and in the second melting, at 78°C and 92°C. The only difference in the scans is the presence of small negative peak in the second heating, probably it represents change of some part of material from metastable structure after the first melting into the principal one. None of the peaks comes exactly at the temperature observed for the acids, although the depression of melting point might be expected in a mixture.

In XRD there are no clear peaks that indicate a laminar system; this effect might be caused by irregularity and defects of the structure. The few observed peaks at around 12-24 degrees indicates that head groups stay in range of 0.7-0.4 nm between them, peaks at 12.58 and 13.74 were found also in the XRD of **1,5Naph**.

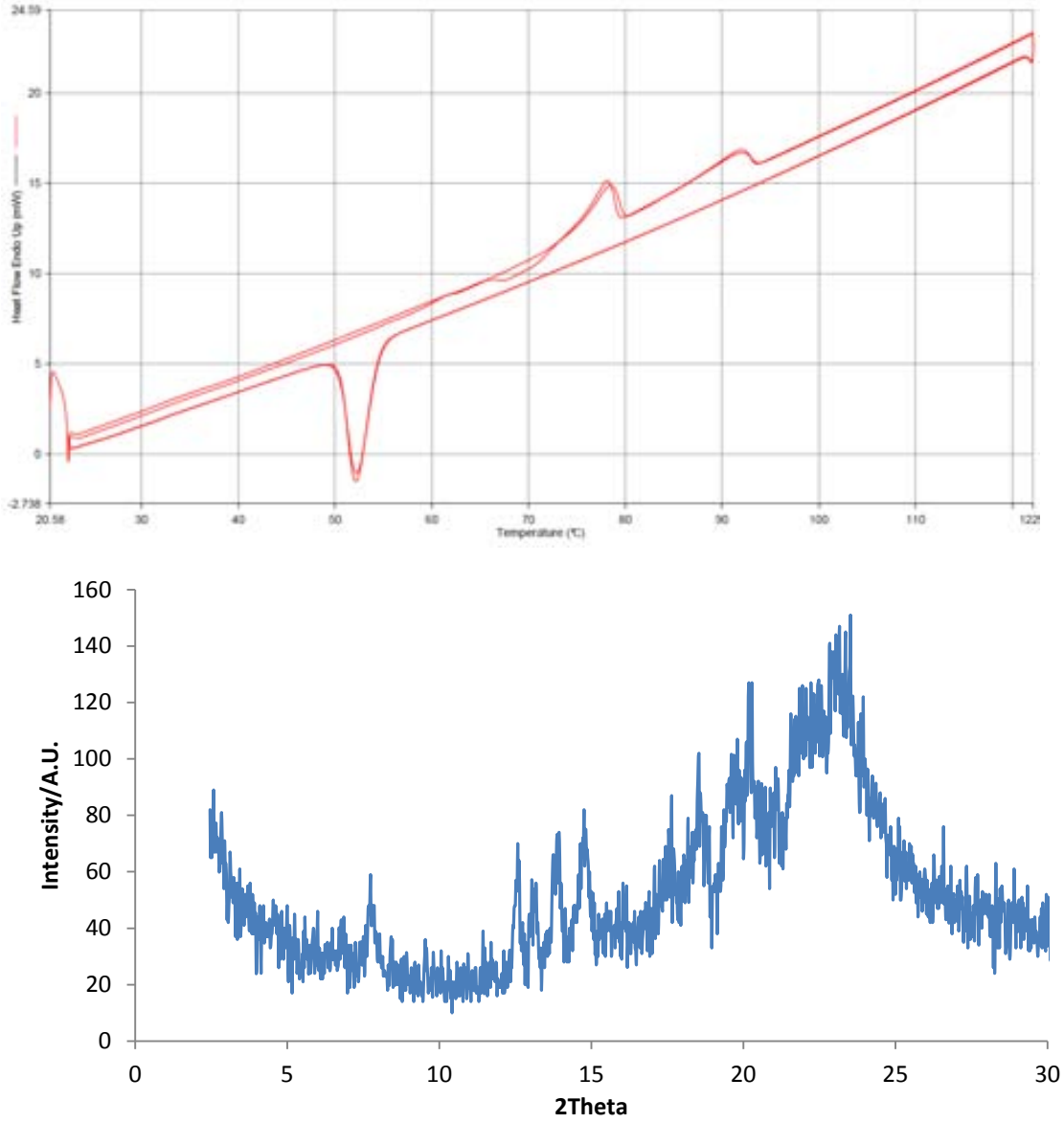

***Figure 4.14**: DSC and XRD of a 1:1mixture of acids (R)-**2,7Naph** and (R)-**1,5Naph**. In the first cycle the phase changes occurs at 78°C and 92°C, the second peak is melting of the material. In the second cycle is almost exactly the same as the first one, with just one slight difference, just before the start of first transition there is negative peak what indicates crystallization of some part of sample. In X-ray diffractogram there are peaks observed for the structure but laminar structure is lost. Just peaks that correspond to distance 0.70 and 0.64 nm observed for **1,5Naph** are seen.*

Therefore, in this sample the separation of phases of the materials seems relatively favoured. In the monolayer system, the formation of the **2,7Naph** layer is clearly preferred. In the bulk phase separation appears to take place as indicated by the melting behaviour.

4.5 Self-assembly of (R)-2,7Naph (S)-1,5Naph

Representative STM images of the 1:1 mixture of acids(*R*)-**2,7Naph** and (*S*)-**1,5Naph** are shown in the Figure 4.15. The surface is completely covered with a self-assembled monolayer of amphiphiles. There are domains that cover thousands of square nanometres and others that are rather small, covering an area smaller than 20 x 20 nm. Moreover, having closer look at the STM images, different type of arrangements of molecules in the domains can be observed. The most highly ordered areas of the monolayer are apparently composed exclusively of molecules of acid **2,7Naph**. In Figure 4.15A this kind of domain is found in the top left corner of the image, at the top edge close to the right corner and in the bottom part in the centre. One can identify each single molecule in the lamellae, their aromatic part appearing as a bright dot. The rest of the surface is covered with domains that possess a certain degree of disorder. In Figure 4.15A the domain at the bottom of the image on the right side has a structure in which each molecule can almost be distinguished, but the molecules do not form a straight row. There are a number of defects and jumps in the lamellae.

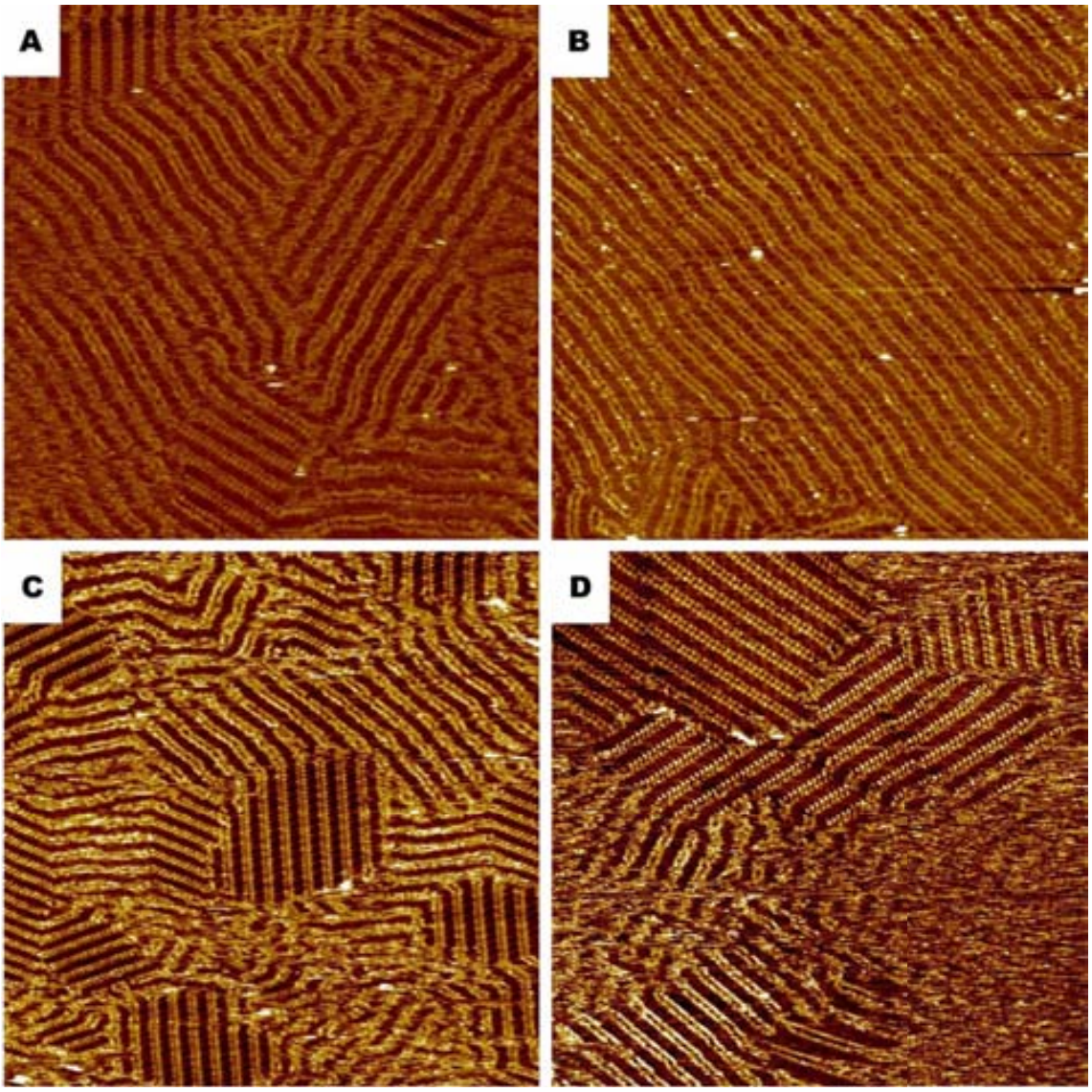

Figure 4.15: *STM images of a 1:1 mixture of acids (R)-**2,7Naph** and (S)-**1,5Naph** (A: 90.4 x 90.4 nm; B, C and D: 96.4 x 96.4 nm; all of the images: I_{set} = 0.7 nA; V_{bias} = 0.8 V) at the graphite-1-phenyloctane interface. The lamellar structure of the monolayer can be seen, in image A there are ordered domains composed of acid **2,7Naph** in the top left corner, at the top edge close to the right corner and in the bottom part in the centre. In image B a mixed domain is spread over almost all the image. The direction of the lamellae can vary locally but the general growth direction is preserved in the whole area. In image C there are smaller domains formed by molecules of **2,7Naph** as in the centre of the image and in the left upper corner, but mixed and disordered structures can be observed in most of the area. In image D there is one of the largest regular domains of **2,7Naph** in the left upper corner. The disordered areas in the lower right hand corner of image D are where there is no stable monolayer formed. It is worth noting the contrast between domains formed by **2,7Naph** and mixed domains like the one in the bottom left part of the image, apparently the mixed domains is brighter, presumably because the aromatic rings are tilted from the surface.*

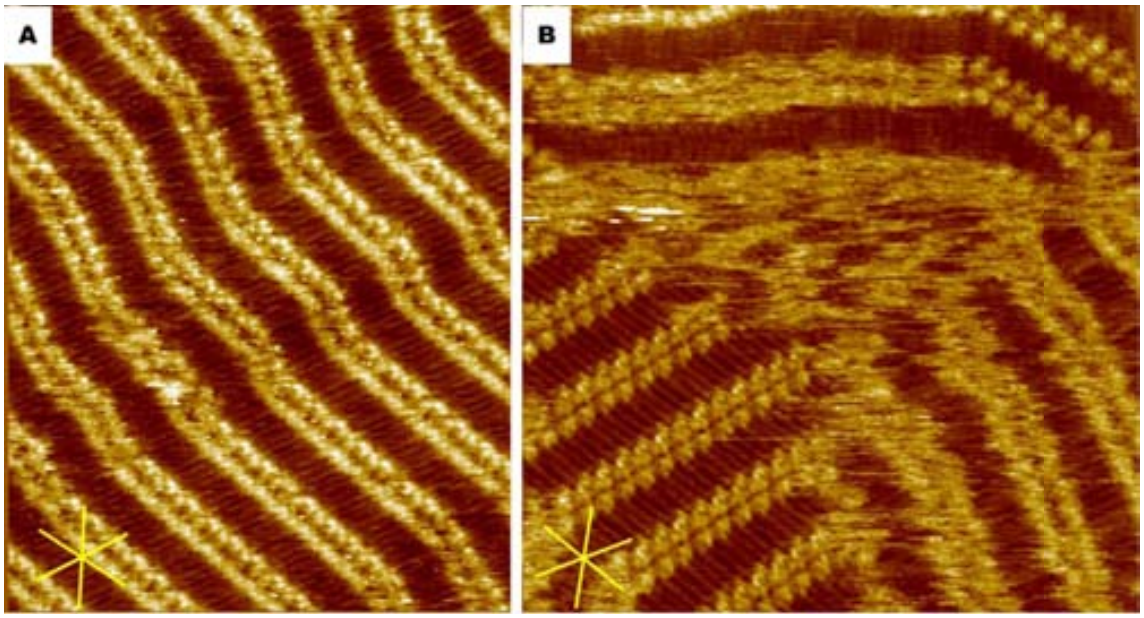

Figure 4.16: *STM images of a 1:1 mixture of acids (R)-**2,7Naph** and (S)-**1,5Naph** (A: 32.2 x 26.8 nm; B: 27.9 x 28.4 nm; A and B: I_{set} = 0.7 nA; V_{bias} = 0.8 V) at the graphite-1-phenyloctane interface. The different type of domains can be observed, in image A it can be seen the mixed lamella, with a changing growth direction. There is also an intriguing change in contrast of the aromatic parts, in the bottom right part of the image the molecules are brighter than the molecules closest to the right bottom corner and lamellae that change direction. In image B the domain of acid **2,7Naph** can be observed in the left lower part of the image, and a disordered domain on the right side of the image. On the top there is a domain that goes almost vertically and however one can observe the alkyl chains well, it is not possible to distinguish the aromatic part of each molecule.*

In Figure 4.16 close-up images of typical domains on the surface are displayed. For this study three different types of self-assembly monolayers could be defined:

- Straight lamella with well separated and resolved aromatic part of each molecule, seen as a bright dot, similar to the monolayer structure of pure acid (*R*)-**2,7Naph**. An example is shown in Figure 4.16B at the bottom of the image. This type of domain is rotated anticlockwise and the angle with respect to the main graphite axis is -4.4 ± 2.9° (see histogram in Figure 4.17). The lamella width is 3.72 ± 0.15 nm, and those values are close to the ones for the monolayer formed by pure (*R*)-**2,7Naph**: chirality -7.5 ± 3.4° and lamella width 3.56 ± 0.21 nm. The alkyl chains are like slash \\\\\\\ with respect to the lamella growth direction.

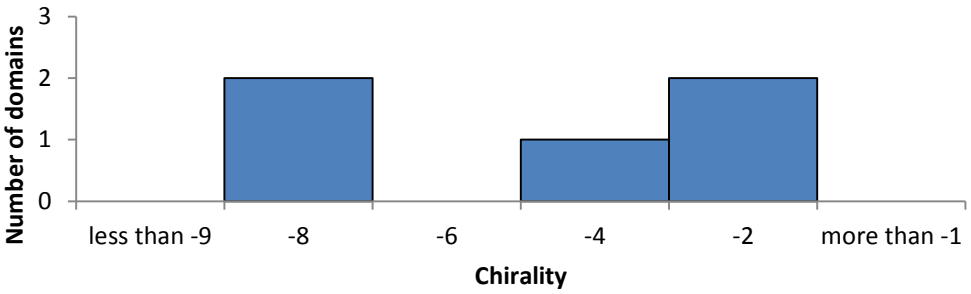

Figure 4.17: *Histogram of angles of domains of acid* ***2,7Naph*** *measured in STM images of a 1:1 mixture of amphiphiles (R)-****2,7Naph*** *and (S)-****1,5Naph*** *at the 1-phenylooctane-graphite interface*

- Straight lamella where the aromatic moieties form continuous straight rows of bright tunnelling current, but in which each molecule is not resolved from the next in the image, as shown in Figure 4.16A. This type of domain is rotated clockwise and the average angle with respect to the main graphite axis is +3.1 ± 4.2 °. The lamella width is 4.24 ± 0.10 nm (see histogram in Figure 4.18). Possibly aromatic head groups of the molecules do not lay flat on the surface which gives more space to the molecules and also makes possible π-π stacking between aromatic parts of the acids. This arrangement is clearly different from the lamellae of the acid (*R*)-**2,7Naph** (parameters as written above), but also different form domains formed by molecules of (*S*)-**1,5Naph**, that, depending on arrangement lamellae, shows tapes that are 4.69 ± 0.35 nm or 3.88 ± 0.19 nm thick with chirality -15.9 ± 5.0° and +8.2 ± 8.8°, respectively, for domains with no interdigitation of alkyl chains and for domains with interdigitation. Also the alkyl chains form rows of backslashes ////// in contrast to the structure of acid **2,7Naph.**

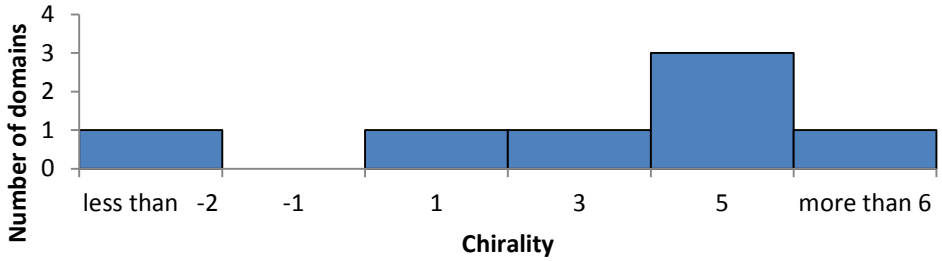

Figure 4.18: *Histogram of angles of straight mixed domains measured in STM images of a 1:1 mixture of amphiphiles (R)-****2,7Naph*** *and (S)-****1,5Naph*** *at the 1-phenylooctane-graphite interface.*

- Disordered lamellae, where the component molecules cannot be distinguished clearly, as seen in Figure 4.16B on the left side. The aromatic parts of the molecules are blurred and do not form straight lamellae. Molecules are not in a fixed periodic position, making high resolution imaging of these moieties very challenging using STM. The rotation with respect to the graphite axis is clockwise and average angle was +27.7 ± 8.8° for the three domains that could be determined. The average lamella width is 4.41 ± 0.43 nm. The parameters of this monolayer indicate that the interaction of alkyl chains with graphite has the greatest influence on the assembly of this domain in the monolayer, and the head groups have more space comparing with other type of domains.

This classification indicates the contrasting cases, and there are also packing structures in between those of these three extremes. Moreover, the domains can smoothly evolve from one type to another.

When compared with the previous sample, where both of the acids where of the same chirality (*R*), there is quite a remarkable change. In the samples where both of the molecules were (*R*)-domains of **2,7Naph** were observed, but also a solid solution of **1,5Naph** in **2,7Naph**. The structure was in general very well ordered with each molecule of acid well visualised. In contrast, in the mixture of opposite enantiomers of acids there is quite polarized situation observed: either there is ordered lamella of acid **2,7Naph** or one of two disordered structures, composed of a mixture of components. Therefore the change of chirality blocks the possibility of formation of solid solution and instead the formation of disordered mixture of domains is observed.

In the DSC diagram (Figure 4.19) it can be observed that the mixture of compounds is homogeneous, just one peak is observed when melting, this result indicates that in the bulk structure mixed packing is favourable, either there is a solid solution or a packing where in each unit cell both of the acid are present in ratio 1:1, the formation that is called quasiracemate. This situation is in total contrast to the mixture of like enantiomers of these two compounds. In the XRD there are very sharp peaks observed, that indicates that the structure, or mixture of structures, is well ordered. There are no peaks of lamellar structure of either one acid or other, but some of the peaks observed in the range 14- 27 degrees (distance 0.6-0.32 nm) correspond to those seen in the sample of **1,5Naph**.

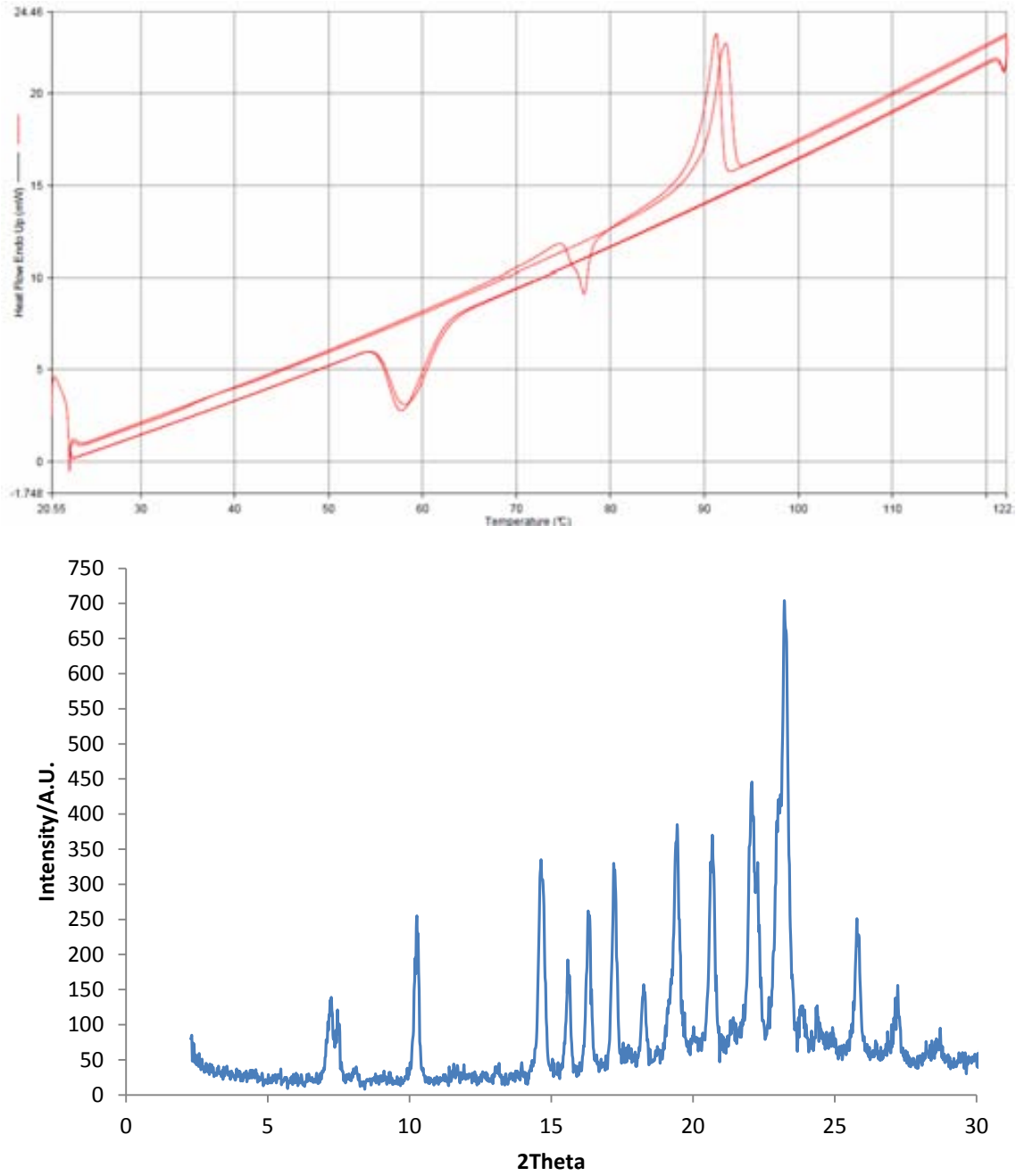

Figure 4.19: *The Differential Scanning Calorimetry (top) and X-ray Diffractogram (bottom) of the mixture shows just one melting peak, at 92°C for the first cycle and 91°C for the second cycle. What is surprising is the negative peak observed at approximately 77°C in the second cycle, it seems to be exothermic rearrangement of the molecules in the crystal structure, which leads to the principle structure. In the cooling crystallization occurs at 58°C. In X-ray diffractogram the peaks characteristic for laminar structure of* ***2,7Naph*** *are found. No signals from laminar structure of* ***1,5Naph*** *were found, but the peaks at 15.6 and 16.3 that correspond to distance 0.57 and 0.54 nm are similar to those observed for the sample of acid* ***1,5Naph****.*

Therefore, the bulk material shows a combination of the two components in an

apparently well-ordered structure (in contrast to the mixture of like enantiomers where separate phases are present), which may be a solid solution at a eutectic composition given the well-defined DSC curves or quasiracemate. In the monolayer system, the formation of the **2,7Naph** layer is again preferred, although mixed structures of many types are also present in the monolayer, in contrast to the bulk system.

4.6 Self-assembly of (R)-2,6Naph (S)-1,5Naph

The 1:1 mixture of (*R*)-**2,6Naph** and (*S*)-**1,5Naph** was studied under the same conditions as for the other combinations of compounds. As with the other mixtures, this one also was dissolved in hot 1-phenyloctane and then a drop was applied to the freshly-cleaved graphite surface. Typical STM images of the monolayer that results are shown in Figure 4.20. The surface is covered with a mixture of small and large domains, with the smallest ones about 10 nm long, most of them 20-60 nm long, but some of the domains exceed 100 nm in length. The lamellar structure of the monolayer is obvious, although the lamellae are not completely straight. There are a number of bends that change the direction of virtually all of the lamellae. What is more there are also changes in the directions, the domains can make turns changing direction by 60 degrees, so that the alkyl chains maintain their direction along one of the graphite axes. Also the organization of molecules inside the lamellae seems not to be constant all along the rows, as large variations in tunnelling current are observed and no well resolved spots corresponding to the naphthyl rings are registered. In Figure 4.21 the structure of the domains can be seen in greater detail. The most representative in terms of population on the surface is shown in B, where one can see that the alkyl chains are interdigitated and are perpendicular to the lamellar propagation direction. The aromatic parts of the molecules do not form straight rows, possibly because there is some kind of mismatch between (*R*)-**2,6Naph** and(*S*)-**1,5Naph** when forming the dimer on the surface. In the image in Figure 4.21A there is a domain that was observed in only one place, where there is no interdigitation of alkyl chains and the aromatic parts form a straight continuous row. The rotation of this unique domain is anticlockwise and the angle with the main graphite axis is -23.4° and the lamellar width is 4.73 nm, while in general the more abundant disordered domains shown in Figure 4.21B are rotated clockwise with the respect to the main graphite axis with on angle of -5.5 ± 9.1° and the lamellar width

is 4.22 ± 0.42 nm. Histogram of angles is presented in Figure 4.22.

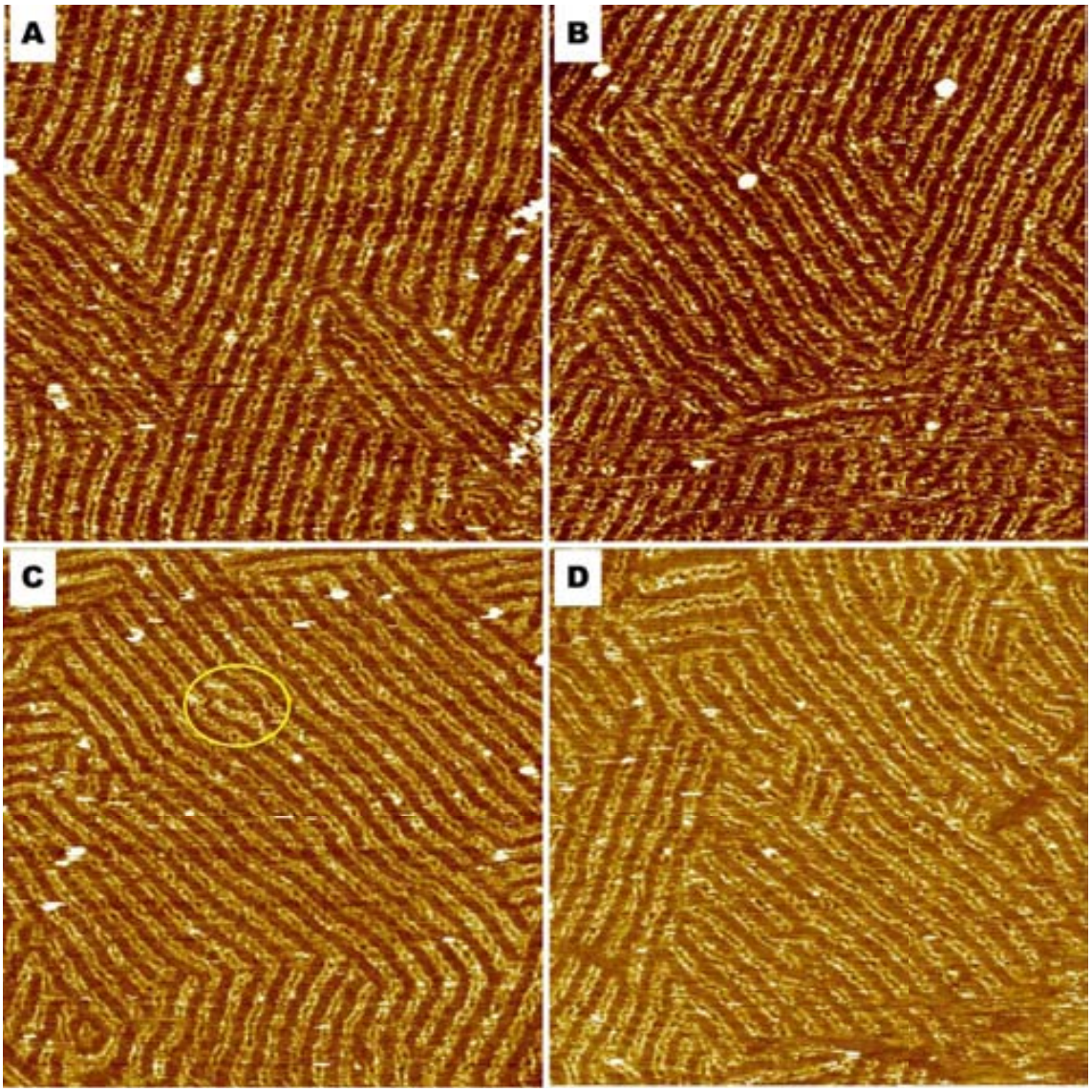

Figure 4.20: *STM images of a 1:1 mixture of acids (R)-**2,6Naph** and (S)-**1,5Naph** (both of the images: 96.4 x 96.4 nm; I_{set} = 0.7 nA; V_{bias} = 0.8 V) at the graphite-1-phenyloctane interface. Images present the structure of different areas of the monolayer on the graphite surface. The white spots on the images are the places where clusters of molecules are hit by the passing tip of STM. In image C there is surprising defect marked in the yellow circle; the lamella is split in two for few nanometres.*

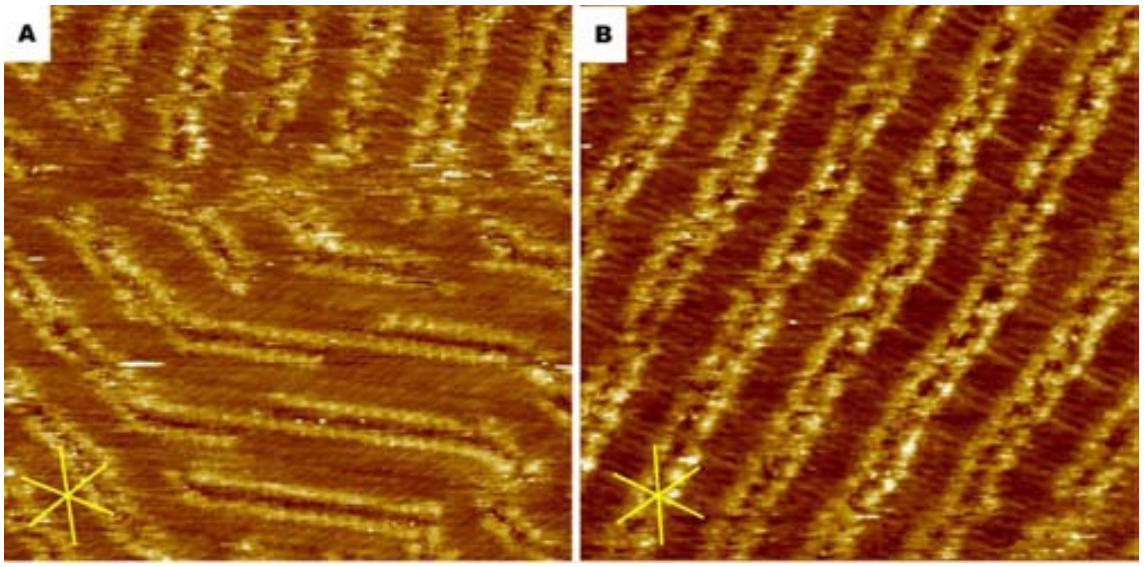

***Figure 4.21**: STM Images of a 1:1 mixture of acids (R)-**2,6Naph** and (S)-**1,5Naph** (A: 27.9 x 28.6 nm; B: 23.1 x 23.3 nm; I_{set} = 0.7 nA; V_{bias} = 0.8 V) at the graphite-1-phenyloctane interface. Images A and B present close up views of the different structures on the surface. In image B there is a typical mixed monolayer. In image A it can be observed an unusual domain with no interdigitation.*

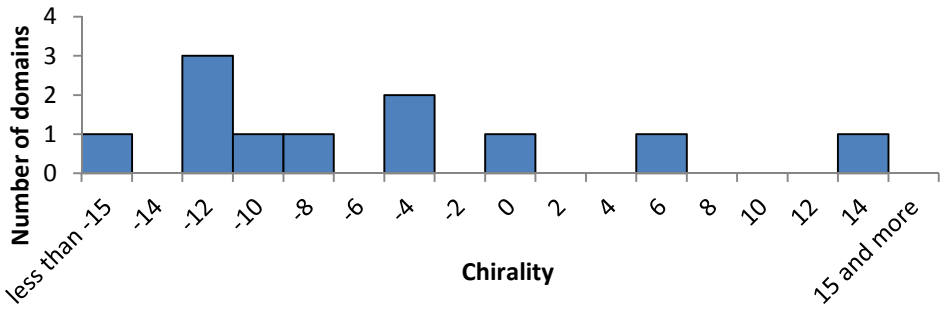

***Figure 4.22:** Histogram of angles of disordered domains measured in STM images of a 1:1 mixture of amphiphiles (R)-**2,6Naph** and (S)-**1,5Naph** at the 1-phenylooctane-graphite interface*

The DSC experiment shows that also in three dimensions there is more than one possible arrangement of the molecules into the material. In the first cycle of heating there are two peaks observed, at 95°C and 101°C (with a shoulder at higher temperature), while in the second one the first peak dominates (this time with maximum at 94°C) and the second one is barely present. The lower melting point of this mixture compared to the pure compounds could point to a solid solution. In the second cycle of heating there is a negative peak observed that indicates that there is an exothermic process taking place, possibly a rearrangement in the solid. This result shows us that there is equilibrium in this sample between structures with higher melting point, more

stable thermodynamically and other one kinetically stable. In both cycles, the material solidifies at approximately 74 ºC, the highest temperature observed for this process in this series of compounds.

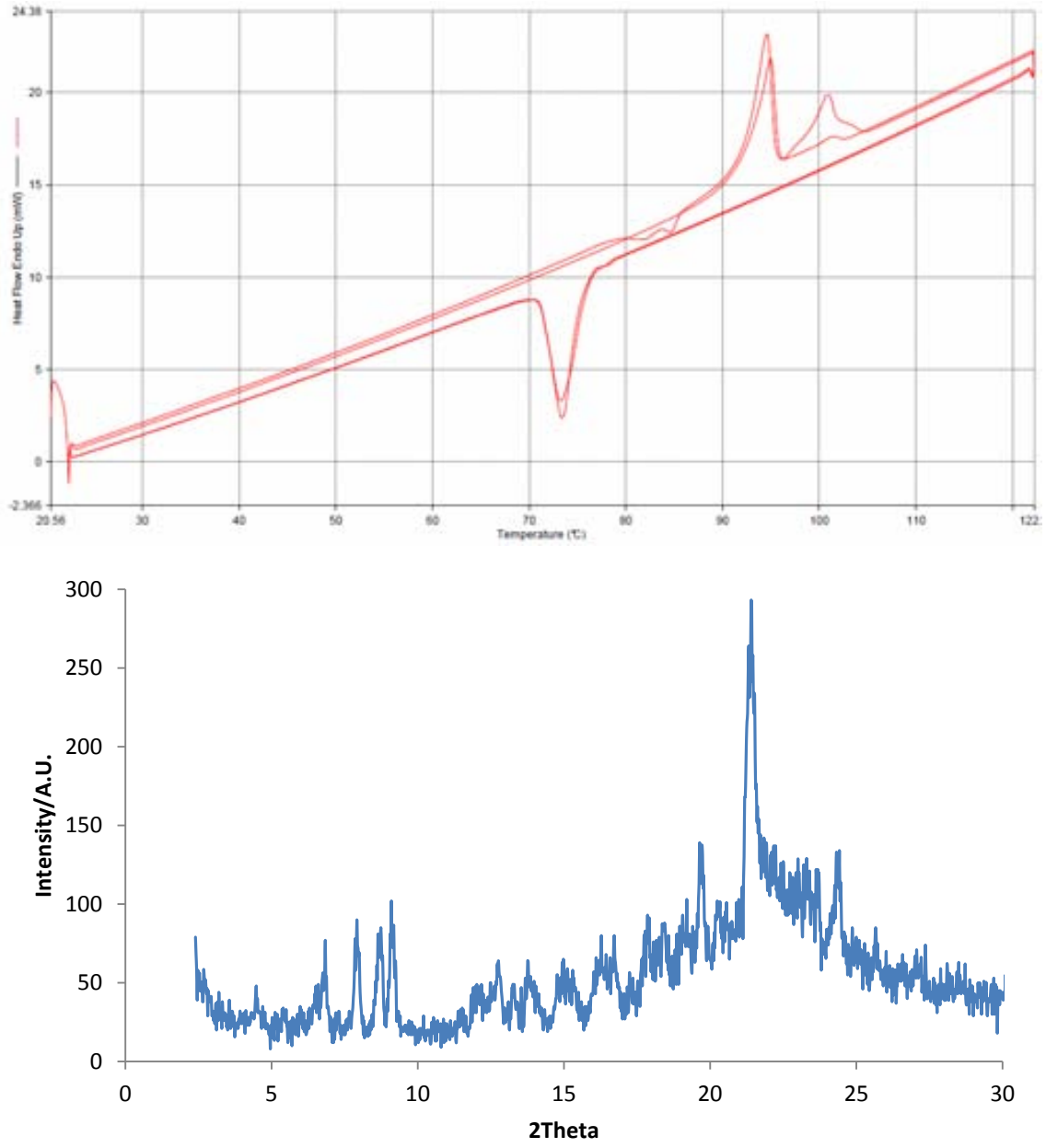

Figure 4.23: *DSC and XRD measurement of a mixture of (R)-**2,6Naph** and (S)-**1,5Naph**. In DSC two peaks are observed in the first cycle, one at 95°C and other, broad one at 101°C. In the second cycle there is surprising negative peak at about 81-85°C, probably the structure of crystal is changing into more stable, effect is similar to the one presented in Figure 4.14. Also in the second cycle it seems that just one type phase is dominating, melting at 94°C, the second peak is barely observed. In XRD no peaks observed for laminar structure of either one or the other acid is observed.*

In XRD no peaks characteristic for laminar structure of either **2,6Naph** or **1,5Naph** were found, but there are peaks in the range 6.8 -9.1 degree that correspond to 1.29-0.97 nm what is head-head distance then few less pronounced peaks until there is a peak observed at 21.5 degree, that corresponds to 0.415 nm.

Therefore, these compounds apparently form mixed crystallites both in the solid and in the monolayers, in the latter case with poor order in the head group orientation and position.

4.7 Self-assembly of (R)-2,6Naph (R)-1,5Naph

When acids (*R*)-**2,6Naph** and (*R*)-**1,5Naph** were dissolved in hot 1-phenyloctane and a drop applied to the freshly cleaved surface of HOPG, the resulting STM images again shown the formation of complete monolayers. In Figure 4.24 one can appreciate that the molecules forms large monolayers, extending sometimes over 100 nm in each direction, but at the same time short domains that are less than 20 nm long are also present, making sure that the whole surface is covered. The lamellae run along a preferred direction with respect to the graphite, but locally there is a lot of fluctuation. Domains may convert smoothly from one direction into another. In Figure 4.25 a detail of the structure of the lamellae can be seen, but due to the movement of the molecules on the surface blurring of the head groups occurs. The alkyl chain interdigitation is clear but the conformation of the aromatic heads cannot be determined with the STM. The variety of aromatic head group structures is absolutely clear though. The chirality of the structure is -24° and the average lamellae size is 4.14 ± 0.25 nm.

Unfortunately, the instability of the tip in the experiment meant that only a few images of the monolayer were captured and more work is necessary to reach a statistically reliable conclusion.

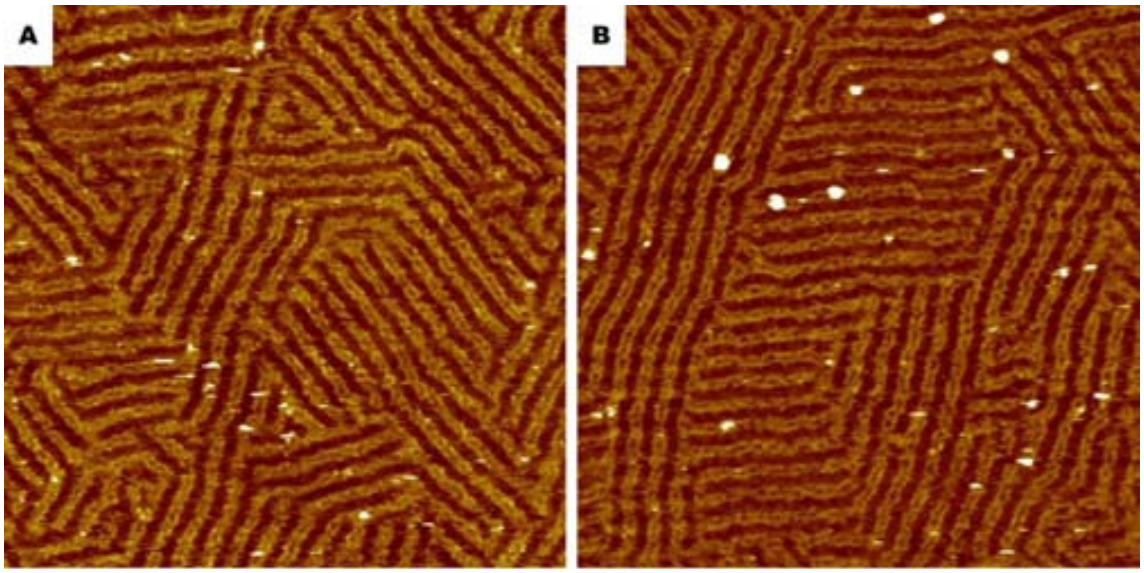

Figure 4.24: *STM Images of a 1:1 mixture of acids (R)-**2,6Naph** and (R)-**1,5Naph** (A: 95.1 x 95.1 nm; B: 98 x 98 nm; I_{set} = 0.7 nA; V_{bias} = 0.8 V) at the graphite-1-phenyloctane interface. Images A and B present the structure of the monolayer on the surface. White dots are places where the tip hit the aggregates of molecules on the surface.*

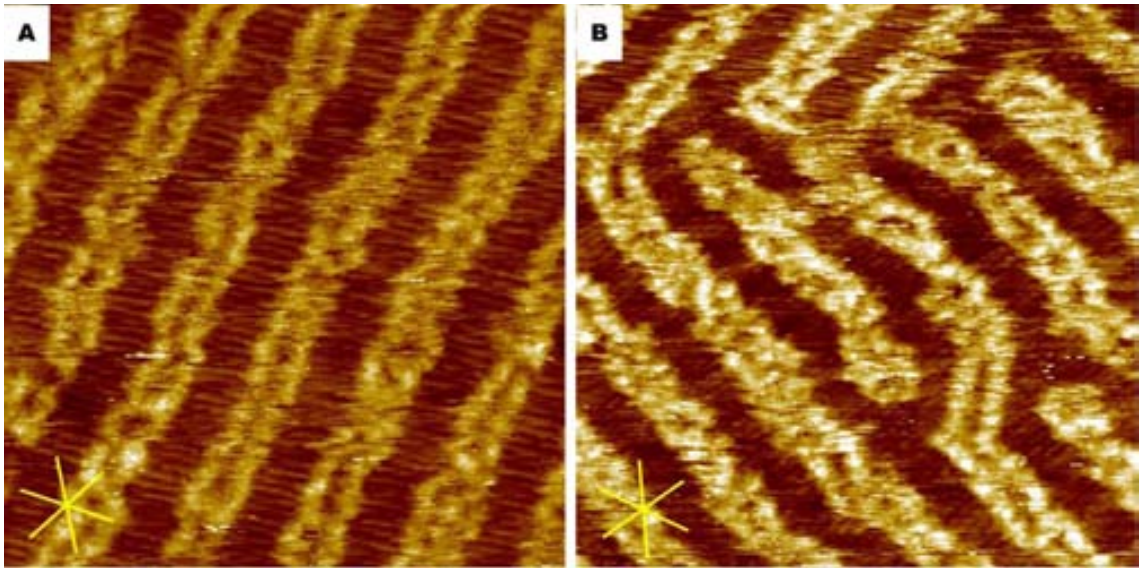

Figure 4.25*: STM Images of a 1:1 mixture of acids (R)-**2,6Naph** and (R)-**1,5Naph** (A: 22.4 x 22.4 nm; B: 22.5 x 22.5 nm; I_{set} = 0.7 nA; V_{bias} = 0.8 V) at the graphite-1-phenyloctane interface. Images present a close up of the structure where the alkyl chains are visualised clearly yet the aromatic head groups are poorly defined. In image B some of the defects are observed, as the molecule linking two parallel lamellae.*

In DSC (Figure 4.26) there is just one peak for each cycle of heating, in first cycle at 94°C. In the second cycle the melting takes place at lower temperature, 81°C, probably sample need more time to rearrange to the structure with higher melting point. What is

remarkable is that the mixture of acid melts much lower than each acid separated (106°C and 104°C for respectively **2,6Naph** and **1,5Naph**) and much lower than the mixture of unlike enantiomers. Thus the homochiral system seems less stable than the racemate-like one.

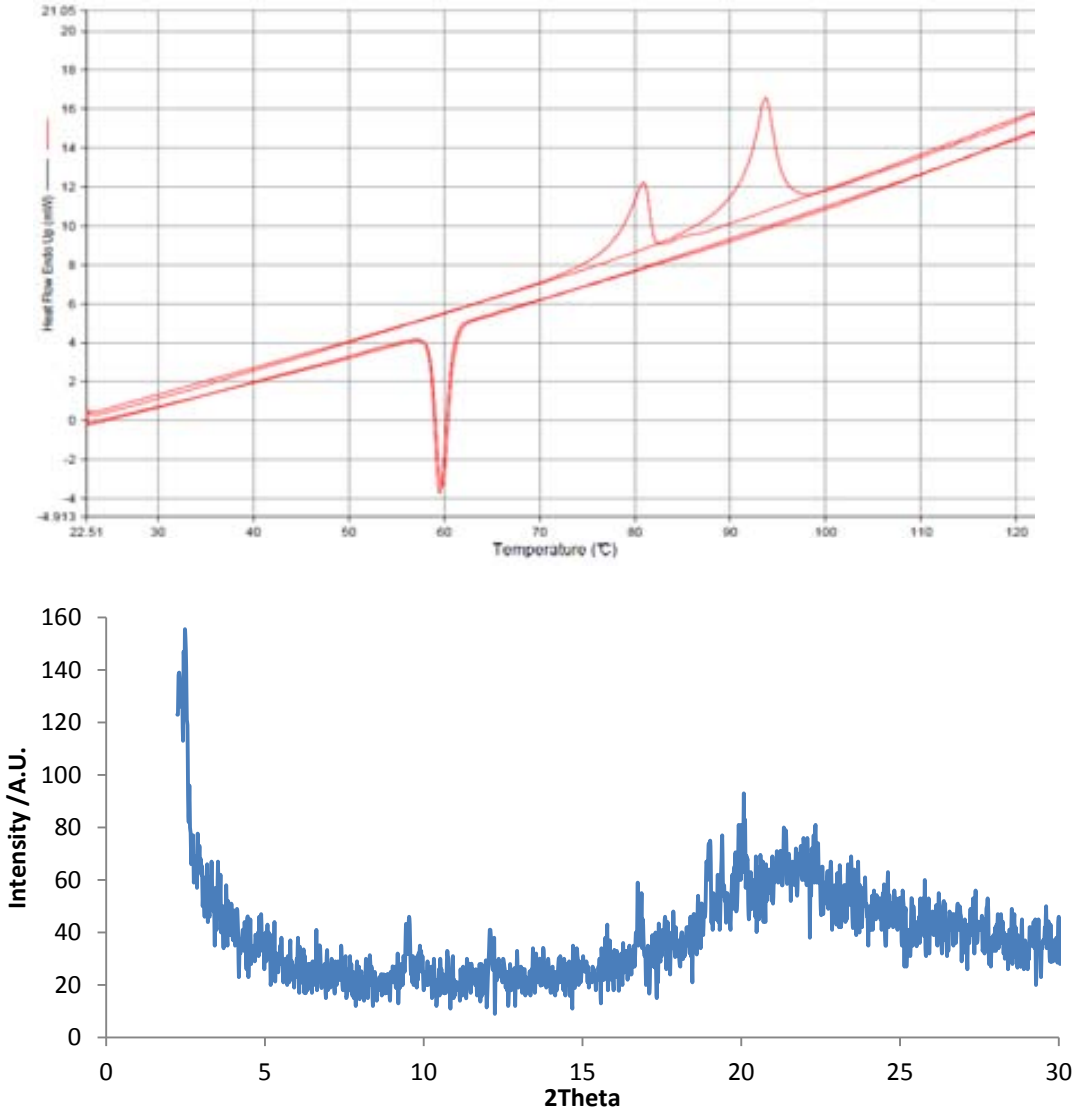

Figure 4.26: *DSC (top) and XRD (bottom) measurement of a mixture of (R)-**2,6Naph** and (R)-**1,5Naph**. In DSC one peak is observed in the first cycle, at 94°C. In the second cycle melting takes place at 81°C. In X-ray diffractogram the first and most intense peak is observed at 2.48 degree (3.56 nm). Other less pronounced peaks appear at 9.46 (0.94 nm), 12.08 (0.73 nm), 16.74 (0.53 nm), 19.02 (0.47 nm), 19.4 (0.46 nm), 20.08 (0.44 nm).*

In X-ray diffractogram (Figure 4.26) there is one intense peak at angle of 2.48 degree that correspond to the distance of 3.56 nm and few other at the angles from 9.46 to 20.08 degrees, but none of them could be identified on the diffractograms of either

2,6Naph or **1,5Naph**. This leads to the conclusion that there is a new, mixed phase – probably a solid solution - observed in X-ray diffraction and no separated phases of acid is observed. This observation is confirmation of the behaviour observed with both DSC and STM that this combination of compounds mixes well.

Therefore, as in the mixture of the unlike enantiomers, these compounds apparently form mixed crystallites both in the solid and in the monolayers. In the bulk case, this mixing is more thorough than in the previous case, with well-defined melting.

4.8 Discussion

The mixed monolayers formed by combinations of two aliphatic acids show a variety of phase behaviours, from phase separated domains to solid solutions and liquid-crystalline-like mixtures. In any case, it is positive that all the mixtures form monolayers, none of them remain in solution despite possible effects of the solubility of the components.

The influence of each molecule on the structures formed is different, as is demonstrated for the case of all mixtures containing acid **2,7Naph** in which it was possible to find small domains apparently composed exclusively by molecules of this acid. It therefore seems that this molecule forms the most stable well-ordered monolayers on the graphite surface when compared with the other similar compounds in this series. However, the mixed monolayer is predominant in all the cases, which may indicate that spontaneous separation of molecules on the surface is not favourable under these conditions. In the mixtures of acids (*R*)-**2,6Naph** and (*S*)-**1,5Naph** the structure shown in Figure 4.22A was observed in one place, which is similar to the structure found once in acid (*S*)-**1,5Naph**, although more evidence is necessary to prove that this is the same type of arrangement. The most common monolayer is a mixed one for all of the combinations, where the orientation of the alkyl chain seems to be the driving force for absorption on the surface. In the four out of six samples the lamella direction is close (± 6°) to the normal to the main graphite axis [0010], which indicates that alkyl chains are lying along the main graphite axis, although they waver away from it presumably as a result of the non-optimum packing of the head groups.

Table 4.1 *Comparison of parameters of mixed SAMs with pure acid domains.*

	Lamella width [nm]	Chirality	Composition
(*R*)-**2,7Naph**/(*S*)-**2,6Naph**	**3.45***	**-3.6±1.8**	(*R*)-**2,7Naph**
	4.44±0.28	**-24.6±9.5**	(*R*)-**2,7Naph**/(*S*)-**2,6Naph**
(*R*)-**2,7Naph**/(*R*)-**2,6Naph**	**4.20±0.20**	**-28.9±4.8**	(*R*)-**2,7Naph**/(*R*)-**2,6Naph**
(*R*)-**2,7Naph**/(*R*)-**1,5Naph**	**3.48±0.13**	**-13.7±15.6**	(*R*)-**2,7Naph**
	3.99±0.30	**-9.7±6.8**	(*R*)-**2,7Naph**/(*R*)-**1,5Naph**
(*R*)-**2,7Naph**/(*S*)-**1,5Naph**	**3.72±015**	**-4.4±2.9**	(*R*)-**2,7Naph**
	4.24±0.10	**+3.1±4.2**	(*R*)-**2,7Naph**/(*S*)-**1,5Naph**[a]
	4.41±0.43	**+27.7±8.8**	(*R*)-**2,7Naph**/(*S*)-**1,5Naph**[b]
(*R*)-**2,6Naph**/(*S*)-**1,5Naph**	**4.22±0.42**	**-5.5±9.1**	(*R*)-**2,6Naph**/(*S*)-**1,5Naph**
(*R*)-**2,6Naph**/(*R*)-**1,5Naph**	**4.14±0.25**	**-24***	(*R*)-**2,6Naph**/(*R*)-**1,5Naph**
(*R*)-**2,7Naph**	**3.56±0.21**	**-7.5±3.4**	(***R***)-**2,7Naph**
(*S*)-**2,7Naph**	**3.41±0.35**	**+6.0±2.1**	(***S***)-**2,7Naph**
(*R*)-**1,5Naph**	**4.82±0.41**	**+19.1±5.6**	(***R***)-**1,5Naph**[c]
	4.10±0.30	**+6.7±5.3**	(***R***)-**1,5Naph**[d]
	3.50±0.33	**-8.2±7.3**	(***R***)-**1,5Naph**[e]
	5.18±0.09	**+8.0±2.4**	(***R***)-**1,5Naph**[f]
(*S*)-**1,5Naph**	**5.10±0.21**	**-18.9±3.5**	(***S***)-**1,5Naph**[c]
	4.42±0.28	**-9.8±6.0**	(***S***)-**1,5Naph**[d]
	3.90±0.10	**+8.8±6.3**	(***S***)-**1,5Naph**[e]
	4.93*	**-13.5***	(***S***)-**1,5Naph**[f]

*[a]For the straight disordered structures. [b]For the wavy disordered structures .[c]For the partialy interdigitated domains [d]For the interdigitated dashed domains [e]For the interdigitated straight domains [e]For the non-interdigitated straight domains *Measured in just one image. Chirality was measured with respect to the main graphite axis.*

The situation where there are two different molecules randomly located in a monolayer on the surface and its molecular level imaging has, as far as we know, not been reported in the scientific literature. The molecules forms some kind of two-dimensional liquid crystal-like state where there is a certain degree of freedom but the main direction of the molecules is the same, so there is orientational order but positional disorder at a local level, with domains which fuse at random orientations. Intriguingly, the main structural director in these layers seems to be the alkyl chains and the aromatic head groups can adopt different orientations, whereas in liquid crystals the rigid aromatic parts are the ordering part of the structure. This effect is surely a result of the symmetry requirements of the packing of the alkyl chains on the graphite surface, whereas the aromatic head groups do not have a very well defined positioning,

presumably because of the promiscuity of the aromatic stacking interaction.[49]

Comparing the DSC of all of the mixtures with the DSC of pure acids there is quite a complex structure with various phase transition observed in some cases, while the others have seems to form mixed phase: (*R*)-**2,7Naph** with (*S*)-**2,6Naph**, (*R*)-**2,7Naph** with (*S*)-**1,5Naph** and (*R*)-**2,6Naph** with (*R*)-**1,5Naph**. In the XRD it is clear that laminar structure characteristic for each compound is lost, just in case of one sample there are signals that could be assigned to lamellar structure of acid **2,6Naph**. In other compounds there are many signals corresponding to short range order, in the length range of approximately 0.4-1 nm, but no laminar structure is found. In general the measurement of bulk shows that mixed phase is more stable than separated acids and this goes in line with the observation of STM, where mixed domains are observed for all of the compounds.

The results highlight the rich gamma of possibilities open to mixtures of organic compounds in the solid state either in the bulk or when organised in monolayers. There is no correlation between the two in the samples that have been studied here, presumably because of the great influence that the graphite-alkyl chain interaction has on the packing in the monolayers. In general, it appears that this interaction favours the formation of mixed domains but with a poor degree of order. It should be pointed out, however, that the monolayer structures are formed from a cooling solution near room temperature, while the bulk experiments are a result of heating and melting at much higher temperature, a difference which may influence the order observed in the packing. The dramatic influence that both lactate absolute configuration and naphthalene constitution have on the phase behaviour is in any case remarkable.

[49] C. A. Hunter, J. K. M. Sanders, *J. Am. Chem. Soc*. **1990**, *112*, 5525.

4.9 Conclusions

The naphthalene derivatives are capable of forming mixed monolayers at the liquid solid interface. Moreover the mixed monoalyers seems more stable than separated ones all of the experiments mixed ones were formed. Just in three experiments out of six separated domains were observed, and it was in case of mixtures of **2,7Naph** that forms very stable and regular monolayer, with either opposite chirality molecules (**2,6Naph** and **1,5Naph**). Another case was mixture of same chirality of 1,5Naph and 2,7Naph, where three different arrangements were observed, including two dimensional solid solution.

In bulk the lamellar structure of each acid is lost and a mixed phase is more stable as witnessed by DSC and XRD. Just in one case the peaks of acid **2,6Naph** where found in X-ray diffractogram. In DSC there are various phase transition observed, mixtures show strong hysteresis, and in some cases an equilibrium between phases can be observed.

Chapter 5

Chiral molecular recognition on an achiral surface

5.1 Introduction

In this chapter the in situ observation of Pasteurian resolution of a racemate upon diastereoselective adsorption on an *achiral* surface via surface-mediated complex formation in a liquid is demonstrated. STM, supported by molecular modelling,[27] was used to visualize and explain the adsorption process and the chiral resolution at the nanoscale. The strategy was just like a classical resolution: Upon mixing a racemate and a resolving agent pairs of diastereomers are expected to form in solution or at the liquid-solid interface and show a pronounced difference in their affinity for adsorption onto the achiral substrate. Ideally, only one diastereomer adsorbs preferentially to the solid surface, leaving the other diastereomer completely in solution.

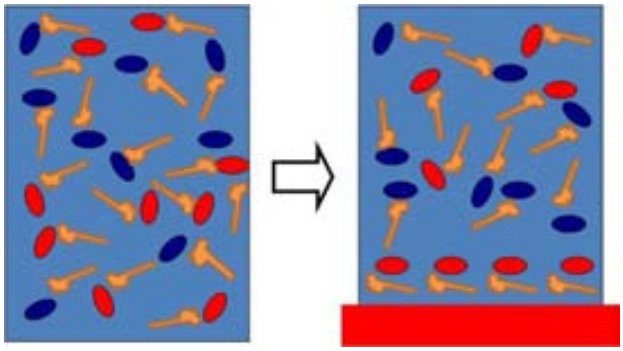

Scheme 5.1*: A cartoon depicting diastereoselective crystallisation at the liquid-solid interface. The orange hammer-like features symbolize the enantiopure resolving agents. The red and blue ovals represent the enantiomers of the racemate to be resolved.*

STM is well suited for the exploration of stereochemical aspects of monolayers and nanostructures with sub-molecular resolution on a conductive, atomically flat surface (also termed the substrate). It is one of the very few techniques that allow monolayer chirality identification, and can even allow assignment of the absolute configuration of the molecules involved in some cases.[50] Various phenomena related to surface chirality

[50] (a) K. H. Ernst, *Top. Curr. Chem*., **2006**, *265*, 209. (b) V. Demers-Carpentier, G. Goubert, F. Masini, R. Lafleur-Lambert, R., Y. Dong, S. Lavoie, G. Mahieu, J., Boukouvalas, H. L. Gao, A. M. H. Rasmussen, L. Ferrighi, Y. X. Pan, B. Hammer, P. H. McBreen, *Science*, **2011**, *334*, 776. (c) T. E. Jones, C. J. Baddeley, *Surf. Sci.* **2002**, *519*, 237. (d) Y. Wei, K. Kannappan, G. W. Flynn, M. B. Zimmt, *J. Am. Chem. Soc.* **2004**,

have been revealed with the technique, but apparently none of them deal with diastereomeric resolution via surface-mediated diastereomeric complex formation in solution.

5.2 Self-assembly of resorcinol derivative 1,3Ph and diaminocyclohexane[51]

The preliminary results of chiral recognition between the resorcinol derivative **1,3Ph** and *trans*-1,2 diaminocyclohexane (DACH, Figure 5.1)were shown in the doctoral thesis of Patrizia Iavicoli, defended in December 2008 in ICMAB –CSIC. The aim of this work was to confirm the phenomenon and get a better understanding of the processes of chiral recognition on the surface

The alkylated resorcinol derivative **1,3Ph** with a lactate moiety – the source of chirality – was selected as the potential resolving agent, as the compound itself displays spontaneous resolution on HOPG which can be observed by STM. The octadecyloxy chains favour monolayer formation by physisorption through [C-H$\cdots\pi$] interactions with HOPG and van der Waals interactions between those chains. *Rac-trans*-1,2-diaminocyclohexane (a 1:1 mixture of (*R,R*)- and (*S,S*)-1,2-diaminocyclohexane) was chosen as the compound to be resolved because the amine groups can interact with the hydrogen-bond donors in the acid group of the resolving agent and a 2:1 complex between the acid and diamine would fulfil the C_2 symmetry which is a very common feature of self-assembled monolayers on HOPG.[11]

126, 5318. (e) N. Liu, S. Haq, G. R. Darling, R. Raval, *Angew. Chem. Int. Ed.* **2007**, *46*, 7613. (f) W. Xiao, X. Feng, P. Ruffieux, O. Gröning, K. Müllen, R. Fasel, *J. Am. Chem. Soc.* **2008**, *130*, 8910. (g) U. Schlickum, R. Decker, F. Klappenberger, G. Zoppellaro, S. Klyatskaya, W. Auwärter, S. Neppl, K. Kern, H. Brune, M. Ruben, J. V. Barth, *J. Am. Chem. Soc.* **2008**, *130*, 11778. (h) S. Haq, N. Liu, V. Humblot, A. P. J. Jansen, R. Raval, *Nat. Chem.* **2009**, *1*, 409. (i) L. Burkholder, D. Stacchiola, J. A. Boscoboinik, W. T. Tysoe, *J. Phys. Chem. C* **2009**, *113*, 13877. (j) P. Iavicoli, H. Xu, L. N. Feldborg, M. Linares, M. Paradinas, S. Stafström, C. Ocal, B. Nieto-Ortega, J. Casado, J. T. López Navarrete, R. Lazzaroni, S. De Feyter, D. B. Amabilino, *J. Am. Chem. Soc.* **2010**, *132*, 9350. (k) M. E. Cañas-Ventura, K. Aït-Mansour, P. Ruffieux, R. Rieger, K. Müllen, H. Brune, R. Fasel, *ACS NANO* **2011**, *5*, 457. (l) F. Masini, N. Kalashnyk, M. M. Knudsen, J. R. Cramer, E. Lægsgaard, F. Besenbacher, K. V. Gothelf, T. R. Linderoth, *J. Am. Chem. Soc.* **2011**, *133*, 13910. (m) J. Liu, T. Chen, X. Deng, D. Wang, J. Pei, L. J. Wan, *J. Am. Chem. Soc.* **2011**, *133*, 21010. (n) K. Tahara, H. Yamaga, E. Ghijsens, K. Inukai, J. Adisoejoso, M. O. Blunt, S. De Feyter, Y. Tobe, *Nat. Chem.* **2011**, *3*, 714. (o) I. De Cat, Z. Guo, S. J. George, E. W. Meijer, A. P. H. J. Schenning, S. De Feyter, *J. Am. Chem. Soc.* **2012**, *134*, 3171

[51] This section was published in: H. Xu, W. J. Saletra, P. Iavicoli, B. van Averbeke, E. Ghijsens, K. S. Mali, A. P. H. J. Schenning, D. Beljonne, R. Lazzaroni, D. B. Amablino, S. de Feyter, *Angew. Chem. Int. Ed.*, **2012**, *51*, 11981.

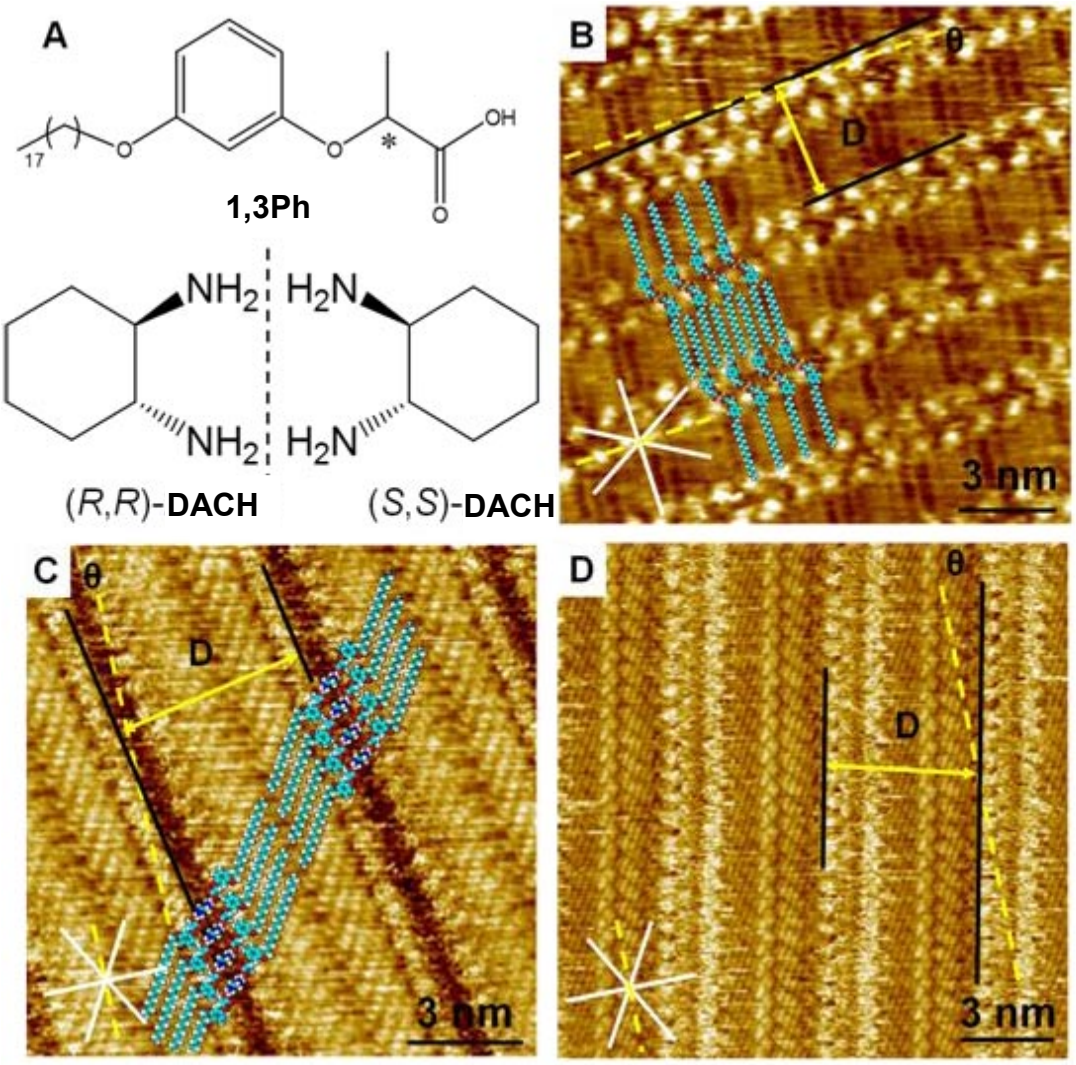

Figure 5.1: *Chemical structures of the chiral resorcinol derivative* ***1,3Ph*** *and 1,2-DACH A: * indicates the location of a stereogenic centre. STM images of monolayers at the 1-phenyloctane - HOPG interface formed by B:* ***1,3Ph*** *(I_{set} = 0.70 nA; V_{set} = 0.50 V); C and D upon premixing* ***1,3Ph*** *and DACH at a 2:1 ratio. Concentration of acid is 7.6×10^{-3} M. C: (R)-**1,3Ph**: (R,R)-DACH (2:1) (I_{set} = 0.25 nA; V_{set} = 1.00 V); D: (S)-**1,3Ph** : (S,S)-DACH (2:1) (I_{set} = 0.20 nA; V_{set} = 1.00 V). White solid lines indicate graphite main symmetry axes. Yellow dashed lines indicate the selected graphite reference axis running perpendicular to one of the main symmetry axes. Black solid lines indicate the direction of molecular rows. Double-headed yellow arrows show the width D of the bi-component rows. In a tentative molecular model, resorcinol and diamine molecules are superimposed on the STM image to highlight their respective location. E: Molecular model for the self-assembled monolayer of (R)-**1,3Ph** and (R,R)-DACH .*

The enantiomers of **1,3Ph** form mirror image monolayers on HOPG when adsorbed from 1-phenyloctane, and the enantiomers resolve spontaneously under these conditions.[40] The individual resorcinol residues can be identified by STM, showing that

nearest neighbour molecules of different rows form dimer structures which are most probably stabilized by hydrogen bonding (Figure 5.1B). These dimers form into lamellae-type patterns over large areas (up to several square microns). The lamellae are predominantly oriented at a small angle (θ) with respect to one of the three symmetry-related directions of the substrate. The alkyl chains are fully extended, adsorbed on the surface, and interdigitated with those of adjacent rows. The width of a row (D) is about 3.7 nm. Diaminocyclohexane does not self-assemble into a monolayer at the 1-phenyloctane-HOPG interface under the conditions used here for the STM imaging.

Upon premixing like enantiomers of **1,3Ph** and amine in solution and deposition on the substrate, a new packing pattern is observed on the HOPG surface by STM. Figure 5.1 C and D show typical STM images of such a monolayers formed by (*R*)-**1,3Ph** and (*R,R*)-diaminocyclohexane**,** and (*S*)-**1,3Ph** and (*S,S*)-diaminocyclohexane at a solution ratio of 2:1 of the components. In both cases, a similar pattern is formed which differs from the monolayer structures formed by **1,3Ph** itself. Molecules order into rows again, but their width (D) is about 5.3 nm, which is much larger than for enantiopure **1,3Ph** (3.7 nm). In addition to the alkyl chains, STM images sometimes reveal 'blobs' which often appear brighter than the alkyl chains and contain streaks parallel to the raster scanning direction (Figure 5.1D). Also, in some images (e.g. Figure 5.1C) the molecular rows are separated by dark (apparent) troughs.

As suggested by the STM contrast, especially at the level of the alkyl chains, rows consist of abutted tail-to-tail molecules of **1,3Ph**. The alkyl chains are not interdigitated, but this feature explains only in part the increased width of the rows. Although molecules of the DACH are not easily visualised in the STM images (under different stoichiometries they can occasionally, see Figure 5.10 below), the best fit of the molecular models with the STM images requires the formation of a **1,3Ph**-diaminocyclohexane-**1,3Ph** complex, the DACH being located between two lactate groups (Figure 5.4). Based on the orientation and packing of the alkyl chains, the distance between resorcinol groups of adjacent molecules along the propagation directions of the rows is only about 0.7 nm. This distance is significantly less than that for the enantiopure **1,3Ph** alone (ca. 1.0 nm), and indicates that the aromatic part of **1,3Ph** does not lie flat on the surface, but must be tilted up away from it. Such a conformation is consistent with the streaky features observed in the STM images, which arise from the tip knocking the molecular segments standing above the plane of the

alkyl chains in the monolayer. In contrast to the enantiopure layers of the pure acids where the alkyl chains are oriented quasi-perpendicular to the lamellar direction, the two-dimensional chirality of the monolayers of the **1,3Ph**-diaminocyclohexane-**1,3Ph** complex can clearly be determined by the orientation of the alkyl chains with respect to the molecular propagation direction. For the complex of (*R*)-**1,3Ph** with (*R,R*)-diaminocyclohexane the alkyl chains are rotated clockwise (CW) with respect to the normal of the row propagation direction and anticlockwise (ACW) in the (*S*)-**1,3Ph** and (*S,S*)-amine case. These features can also be envisaged as S and Z shapes, respectively. In addition, the monolayer chirality is also established by the relative orientation of the row propagation directions with respect to the graphite lattice. The angle θ between the propagation direction of the rows and the HOPG reference axes [-1100] is -10 ± 2°in the monolayers of (*R*)-**1,3Ph** and (*R,R*)-diaminocyclohexane and+12 ± 3° for (*S*)-**1,3Ph** and (*S,S*)-amine (while the angles for the pure acids are -4 ± 2 and +5 ± 3, respectively, see Table 5.3).

Sequential deposition of the two compounds also leads to substrate-mediated diastereomeric complex formation (Figure 5.2). Domains of (*R*)-**1,3Ph** formed upon casting a droplet of the solution of (*R*)-**1,3Ph** in 1-phenyloctane onto the basal plane of HOPG disappear in time after addition of a droplet of a solution of (*R,R*)-diaminocyclohexane in 1-phenyloctane, as they are replaced gradually by domains composed of the complex (*R*)-**1,3Ph**/(*R,R*)-DACH . Therefore, the dynamics in the monolayers can be followed by STM in real time and the replacement of the surface-bound acid with the complex is fast (for the present case after 5 minutes). Two mechanisms could explain this process:

- (*R,R*)-diaminocyclohexane co-adsorbs at the liquid-solid interface and forms a complex with (*R*)-**1,3Ph**. Because of the larger unit cell of the diastereomeric complex, some (*R*)-**1,3Ph** desorbs into the liquid phase, which allows for the formation of *(R*)-**acid**/(*R,R*)-diaminocyclohexane domains.
- The diastereomeric complex is preformed in solution and takes the place of (*R*)-**1,3Ph** via competitive adsorption, mediated by the dynamics taking place at the liquid-solid interface.

At this stage it is not clear which mechanism predominates in the formation of the monolayers of the diastereomeric complex. If the preformed mixture contains a large excess of **1,3Ph**, domains of pure **1,3Ph** are also formed in addition to the

diastereomeric complex as presented in Figure 5.3. These results reflect the presence of at least three equilibriums (Scheme 5.2); the formation of the complex between acid and amine (in solution or at the surface) and the equilibrium between the two species (the pure acid and its complex) between the surface and the solution.

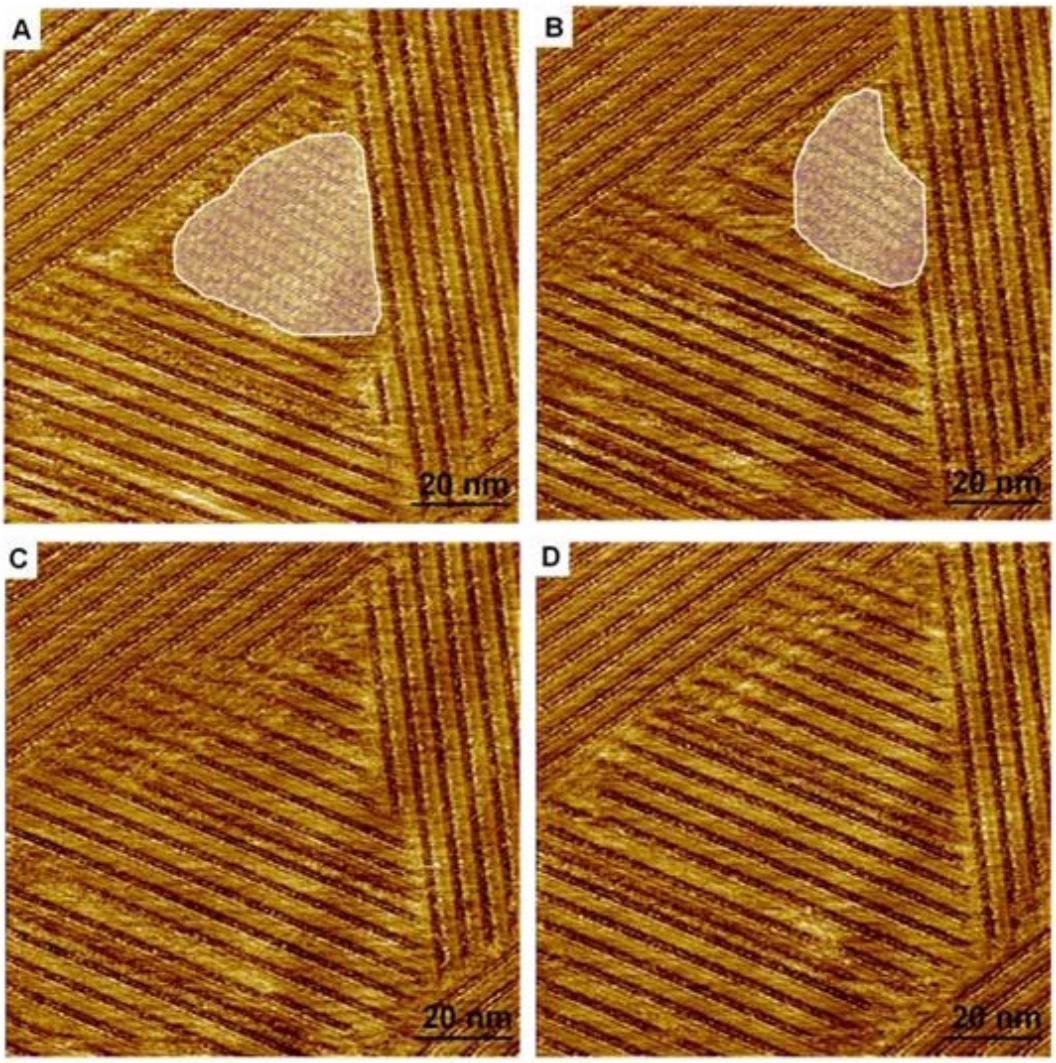

Figure 5.2: *A sequence of STM images zooming in on an area that contains both domains formed only by (R)-**1,3Ph** and (R)-**1,3Ph** +(R,R)-DACH at the 1-phenyloctane - HOPG interface. (R,R)-DACH was added after a monolayer of (R)-**1,3Ph** was formed. (I_{set} = 0.20 nA; V_{set} = 0.50 V). Domains marked in white contain only (R)-**1,3Ph**. The time gap between consecutive frames is 192, 256 and 385 seconds.*

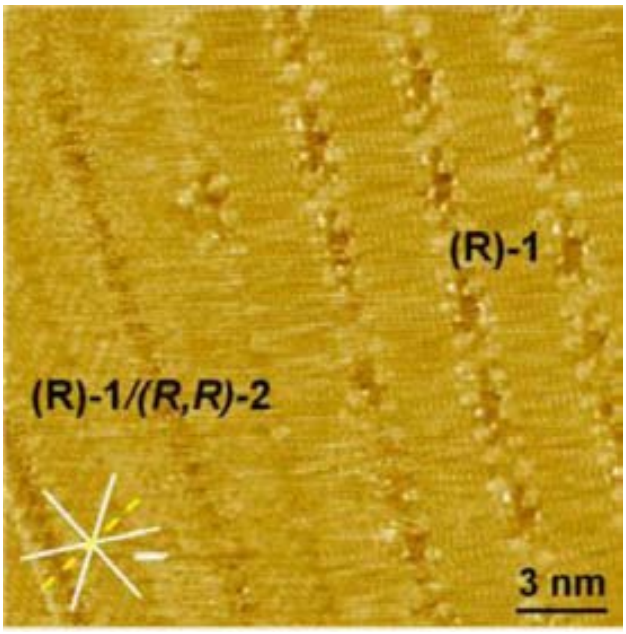

Figure 5.3: *STM images of monolayers at the 1-phenyloctane - HOPG interface formed upon premixing (R)-**1,3Ph** and (R,R)-DACH at a 66:1 ratio (I_{set} = 0.20 nA; V_{set} = 1.00 V). Concentration of **1,3Ph** is 7.6×10^{-3} M. White solid lines indicate graphite main symmetry axes. Yellow dashed lines indicate the selected graphite reference axis running perpendicular to one of the main symmetry axes. Domains of (R)-**1,3Ph**/(R,R)-amine and (R)-**1,3Ph** are formed, as indicated.*

Unlike the combinations of acids and amine described above, mixtures of unlike enantiomers (*R*)-**1,3Ph** and (*S*,*S*)-diaminocyclohexane**,** or (*S*)-**1,3Ph** and (*R*,*R*)-diaminocyclohexane at the same ratio of acid to amine as previously (2:1) do not lead to co-adsorption. Only monolayers of **1,3Ph** are observed in the two enantiomeric cases, with molecular packing and chiral expression identical to those of the enantiopure resorcinol derivatives alone. However, if the amount of diamine is increased ((*R*)-**1,3Ph**: (*S*,*S*)-amine ratio = 1:5), a new packing pattern is formed which is strong evidence that (*S*,*S*)-amine molecules are involved in monolayer formation with the (*R*)-**1,3Ph** acid (and similarly for the (*S*)-**1,3Ph**/(*R,R*)-amine pair). The new packing pattern is similar but clearly distinct to the one formed by (*S*)-**1,3Ph** and (*S*,*S*)-amine (see Figure 5.4). Based on the experimental evidence, it can be concluded that the surface-supported diastereomeric complexes (*R*)-**1,3Ph**/(*R,R*)-diaminocyclohexane and (*S*)-**1,3Ph**/(*S,S*)-diaminocyclohexane are more stable than (*R*)-**1,3Ph**/(*S,S*)-diaminocyclohexane and (*S*)-**1,3Ph**/(*R,R*)-diaminocyclohexane. This hypothesis was confirmed experimentally by performing resolution experiments (vide infra).

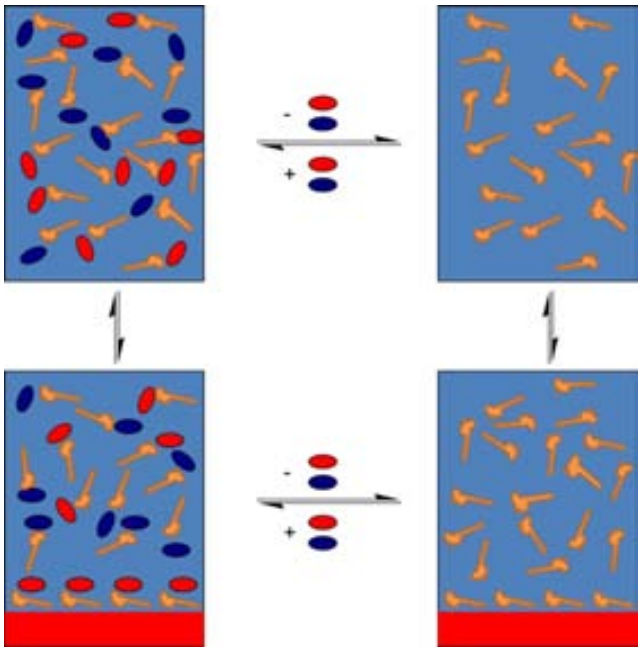

Scheme 5.2*: Illustration of equilibriums: the red and blue oval stands for two enantiomers of amine and orange hammer-like features symbolize the enantiopure resolving acid. Complexation of acid in solution (the equilibrium between the two rectangular on the top) and equilibrium of adsorption of acid at the graphite -1-phenyloctane interface (on the left) and between complex of acid and amine (on the right).*

In order to gain insight into the structure and energy characteristics of the absorbed diastereomeric complexes, in Roberto Lazzaroni's group (Université de Mons) a joint Molecular Mechanics/Molecular Dynamics (MM/MD) approach was used to model self-assembled monolayers of (*R*)-**1,3Ph** interacting with either (*R*,*R*)- or (*S*,*S*)-diaminocyclohexane (in a 2:1 ratio) on a graphite substrate. Structural parameters extracted from the MD were compared with the STM data. An in-depth analysis of the different contributions to energy-minimized geometric structures was then performed, with a special focus on the formation of hydrogen bonds that were anticipated to drive the formation of the self-assembled diastereomeric complexes.

The formation of monolayers on graphite was modelled with the DREIDING force field, which provides an accurate description of the hydrogen bonds. The initial geometries were built on the basis of the STM measurements. The calculations involved energy minimization of the STM inspired geometric structures followed by quenched MD simulations in the NVT ensemble (where **N**umber of molecules/atoms, **V**olume and **T**emperature is fixed for the calculation, and other parameters - energy, pressure can vary during experiment) at 25°C for 1 ns (with an energy minimization performed at

each picosecond of the MD run). The long-range non-bonded interactions were turned off with a cubic spline cut-off set at 18 Å. The assemblies were built by applying periodic boundary conditions on a unit cell containing two rows of ten (*R*)-**1,3Ph** resorcinol molecules, separated by a central row of ten (*R,R*)- or (*S,S*) diaminocyclohexane molecules, see Figures 5.4 and 5.5. Structural parameters were extracted from the MD trajectory, whereas the energy characterization was performed on the minimized structures of the quenched dynamics.

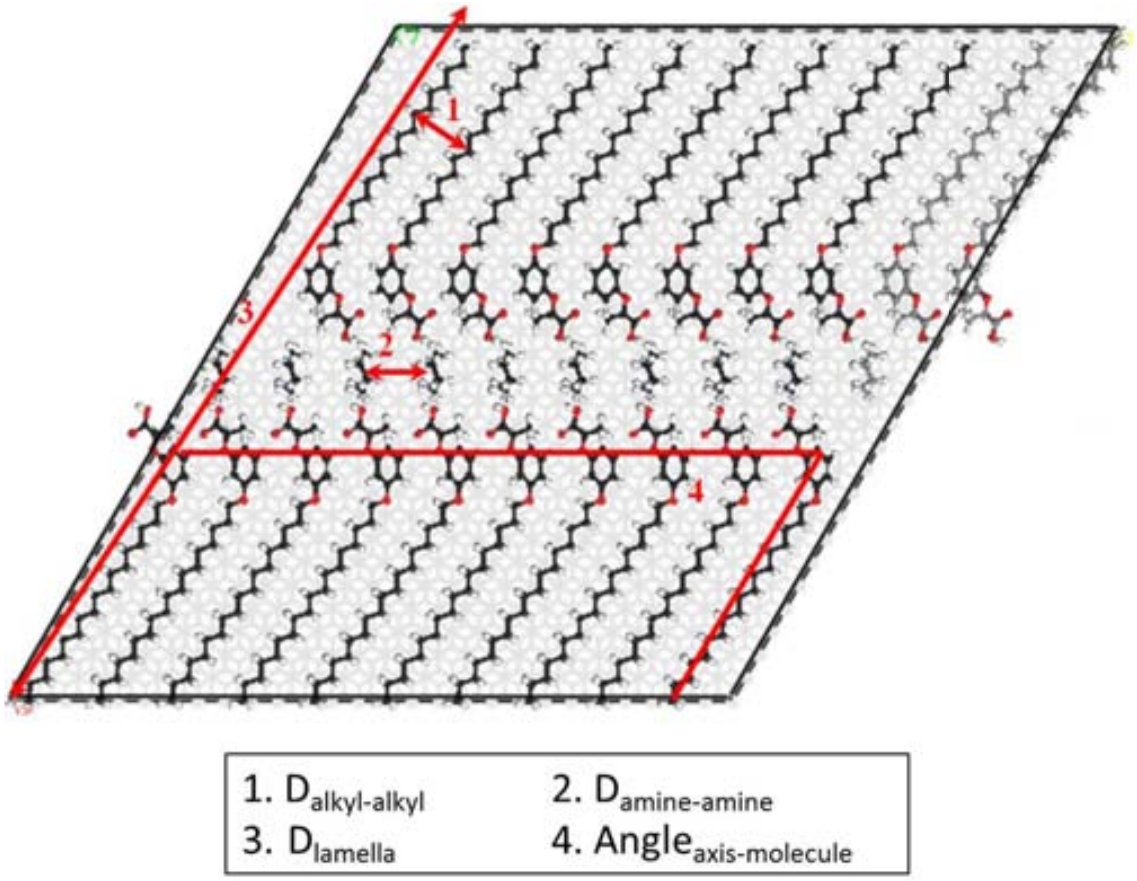

***Figure 5.4**: Structural parameters for minimized structure extracted from the MD simulations. "$D_{alkyl-alkyl}$" refers to the separation between alkyl chains of neighbouring resorcinol molecules; "$D_{amine-amine}$" refers to the distance between two neighbouring diamines; "$D_{lamella}$" is the lamella thickness (distance between two adjacent rows of resorcinol-diamine pairs); and "$Angle_{axis-molecule}$" is the angle formed by the resorcinol rows and their alkyl chains.*

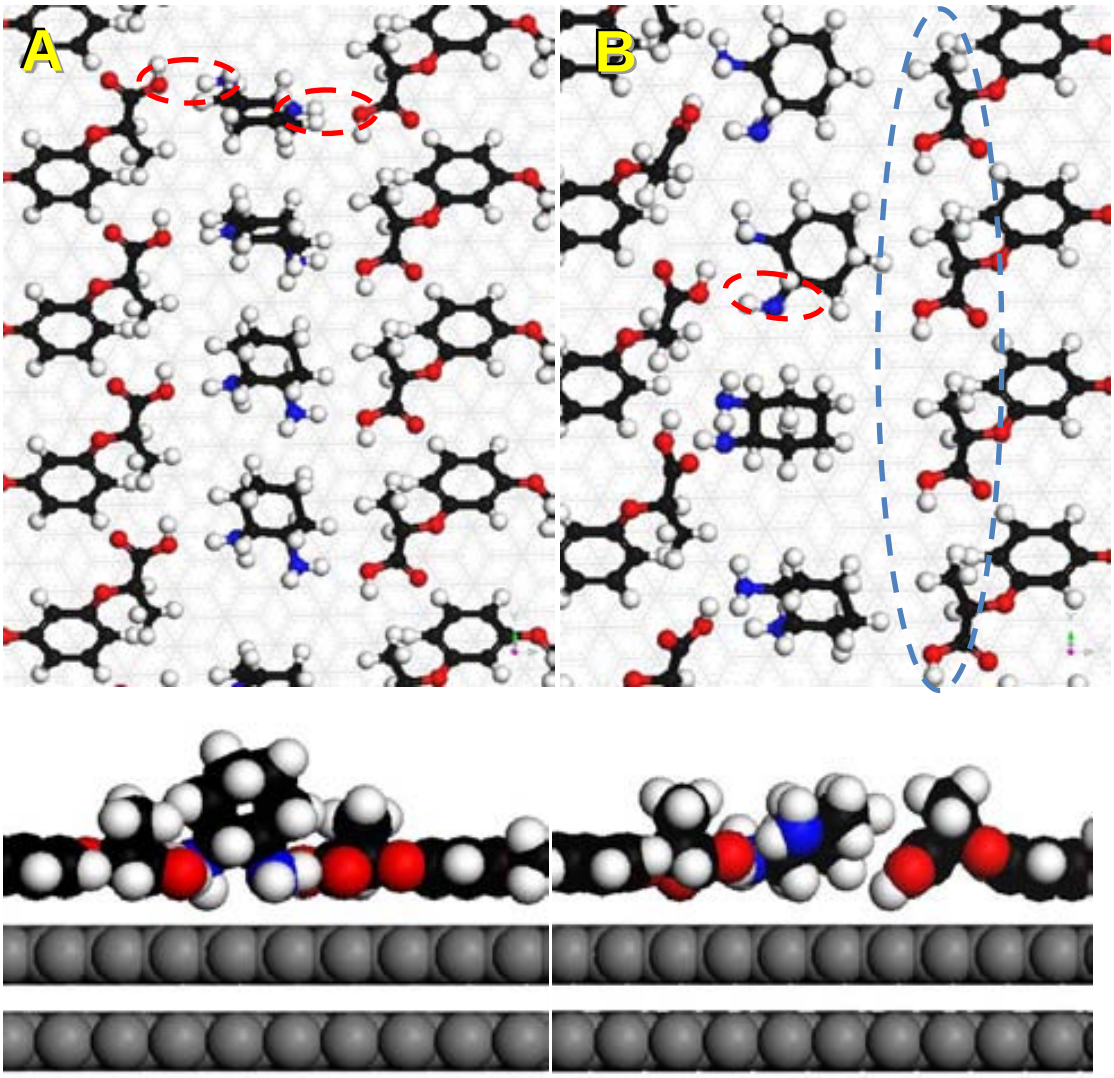

Figure 5.5: *Snapshots of representative structures (top view and side view) taken during the MD run (they are not energy minima but transient complexes) for A: (R)-**1,3Ph**/(R,R)-DACH and B:(R)-**1,3Ph**/(S,S)-DACH assemblies. The dashed red ellipses mark hydrogen bonds between the acid and amine molecules; the dashed blue ellipse points to the absence of hydrogen bonding between the row of amine and one row of acid molecules in the (R)-**1,3Ph**/(S,S)-DACH assembly.*

The structural parameters obtained from the force-field simulations are compared to the STM data in Table 5.1 (see Figure 5.4 for labelling).

Overall, there is very good agreement between the experimental and theoretical values for the lattice parameters characterizing the monolayers at the graphite surface, which validates the models proposed for the supramolecular organization of the chiral molecules on this substrate. In addition, the calculations shed light on the arrangement of the diaminocyclohexane in the diastereomeric combinations considered ((*R*)-

1,3Ph/(*R*,*R*)-diaminocyclohexanevs. (*R*)-**1,3Ph**/(*S*,*S*)-diaminocyclohexane), which cannot be directly assessed from the STM images (where only molecules of **1,3Ph** can be identified unambiguously). This is key information since the interactions between **1,3Ph** and the amine provide the stereoselective adsorption of one diastereomer. Not all the phenyl groups of **1,3Ph** lie parallel to the surface, which is consistent with the local variations in the STM contrast observed above these groups as a result of the tip of the microscope interacting with them.

Table 5.1: *Geometrical parameters measured (STM) and calculated (Dreiding modelling) for assemblies of (R)-**1,3Ph**/(R,R)-DACH and (R)-**1,3Ph**/(S,S)-DACH diastereomeric complexes on graphite.*

	(*R*)-**1,3Ph**/(*R*,*R*)-diaminocyclohexane		(*R*)-**1,3Ph**/(*S*,*S*)-diaminocyclohexane	
	Modelling	STM	Modelling	STM
$D_{alkyl\text{-}alkyl}$	0.51±0.08 nm	0.50±0.02 nm	0.51±0.07 nm	0.50±0.02 nm
$D_{amine\text{-}amine}$	0.70±0.06 nm	0.66±0.03 nm	0.68±0.05 nm	0.65±0.03 nm
$D_{lamella}$	5.21±0.17 nm	5.29±0.12 nm	5.15±0.12 nm	5.11±0.12 nm
$Angle_{axis\text{-}molecule}$	47.0±3.0°	40.1±2.4°	48.2±3.0°	59.0±1.9°

Representative snapshots of the MD simulations on the way to their energy minima are displayed in Figure 5.5. The most striking result is that while the (*R*,*R*)-diaminocyclohexane molecules can insert well in between two adjacent rows of (*R*)-**1,3Ph** forming an ordered hydrogen bonded array, the enantiomeric diamine cannot, owing to the spatial arrangement of its amino groups. The (*S*,*S*) amine can only form hydrogen bonds with one row of (*R*)-**1,3Ph**.

Because more hydrogen bonds form in the (*R*)-**1,3Ph**/(*R*,*R*)-diaminocyclohexane combination, this assembly is anticipated to be more stable than its diastereomeric (*R*)-**1,3Ph**/(*S*,*S*)-diaminocyclohexane counterpart. This supposition is confirmed by the energy analysis summarised in Table 5.2.

Table 5.2: *Interaction energies in assemblies of (R)-**1,3Ph**/(R,R)-DACH and (R)-**1,3Ph**/(S,S)-DACH complexes, and details of hydrogen bond contribution to the total energy. All energies are given per one molecule of DACH interacting with two (R)-**1,3Ph** molecules.*

Energy (kJ/mole)	(*R*)-**1,3Ph**+(*R*,*R*)-diaminocyclohexane	(*R*)-**1,3Ph**+(*S*,*S*)-diaminocyclohexane	$\Delta_{(R,R)\text{-}(S,S)}$
Total	-338.0	-333.5	-4.5
van der Waals	-310.7	-311.6	0.9
Electrostatic	-129.0	-125.4	-3.6
Hydrogen bond, total	-40.8	-38.5	-2.3
Hydrogen bond, **1,3Ph**-diaminocylohexane	-35.6	-30.1	-5.5
Hydrogen bond, **1,3Ph-1,3Ph**	-4.2	-5.6	1.4
Hydrogen bond, **amine-amine**	-1.0	-2.8	1.8

Thus, the molecular modelling study: (i) supports the experimental finding that the simultaneous co-adsorption of **1,3Ph**anddiaminocyclohexaneon graphite results in the development of stable assemblies based on a two-to-one complexes; (ii) provides structural information on the arrangement of the diaminocyclohexane in the assemblies, and (iii) relates the higher stability of the (*R*)-**1,3Ph**/(*R*,*R*)-diaminocyclohexane over the (*R*)-**1,3Ph**/(*S*,*S*)-diaminocyclohexane combination to the formation of a more dense **1,3Ph**-diaminocyclohexanone hydrogen bonding network.

Preferential substrate-mediated diastereomeric complex formation offers the opportunity to use one of the components as resolving agent at the liquid-solid interface. The true resolution experiments were performed (Scheme 5.3) for mixtures of enantiomers of the acid (amine resolving agent) or amine (acid resolving agent).

When the racemic acid **1,3Ph** was premixed with (*R*,*R*)-*trans*-diaminocyclohexane at a molar ratio of 2:1 - so that the amine could potentially act as a resolving agent for the acid – the STM data of the physisorbed complex shown that the monolayer is composed of domains of (*R*)-**1,3Ph**/(*R*,*R*)-diaminocyclohexane and domains of (*S*)-**1,3Ph**. Figure 5.6 shows an area at a moment where both these domains were imaged clearly (the disordered parts of the monolayer indicate that the system had not reached the

thermodynamic minimum at the time of imaging). Likewise, premixing of (*RS*)-**1,3Ph** with (*S,S*)-diaminocyclohexane leads to the exclusive formation of domains of (*S*)-**1,3Ph**/(*S,S*)-diaminocyclohexane and domains of pure (*R*)-**1,3Ph**. The situation in these experiments is complicated by the possibility of a mixed 2:1 complex where the two enantiomers of **1,3Ph** complex to one diamine molecule, which explains partially the larger disorder in this system. Mixing an excess of (*RS*)-**1,3Ph** with one of the diaminocyclohexane enantiomers, e.g. (*R,R*)-diaminocyclohexane, leads in addition to (*R*)-**1,3Ph**/(*R,R*)-diaminocyclohexane and (*S*)-**1,3Ph**domains, to the appearance of (*R*)-**1,3Ph**domains as shown in Figure 5.7. In this case, the non-complexed enantiomer remains on the surface.

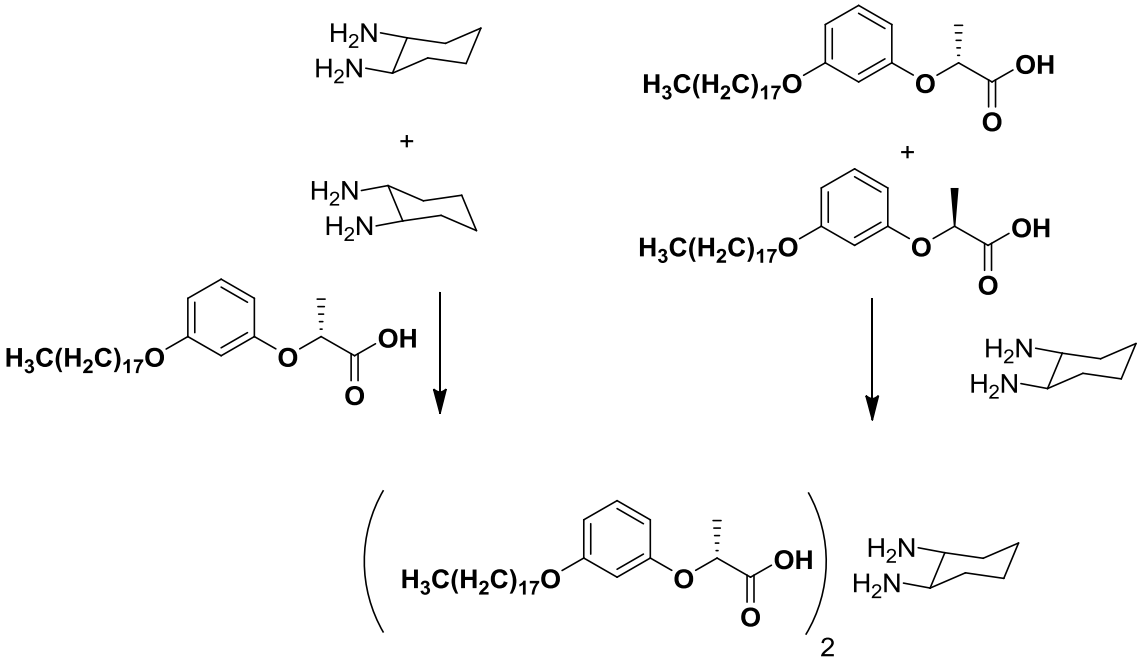

Scheme 5.3: *Two possibilities of resolution: acid resolving amines (on the left) or amine resolving acid (on the right)*

When **1,3Ph** is used as a resolving agent for *trans*-diaminocyclohexane, which does not form stable monolayer by itself at the liquid-solid interface, a true segregation can take place. To explore the ability of **1,3Ph** to selectively co-adsorb one of the enantiomers of *trans*-diaminocyclohexane, (*R*)-**1,3Ph** or (*S*)-**1,3Ph** were premixed with the combination of (*R,R*) and (*S,S*)-diamines. In general, adding both enantiomers of diaminocyclohexane to one of the enantiomers of **1,3Ph** (e.g. (*R*)-**1,3Ph**, concentration 7.6×10^{-3} M) leads exclusively to the anticipated two component pattern consisting of

(*R*)-**1,3Ph** and (*R,R*)-diaminocyclohexane for a solution composition with a ratio ranging from 1:10:10 up to 4:1:1, as revealed by the STM experiments (Figure 5.8 and 5.9), the lamellae are 5.0 ± 0.5 nm wide for 1:10:10 mixture and 5.3 ± 0.1 nm for the 4:1:1 one, and the angles with respect to the main graphite axes are -12 ± 5 degrees and -10 ± 2 degrees respectively.

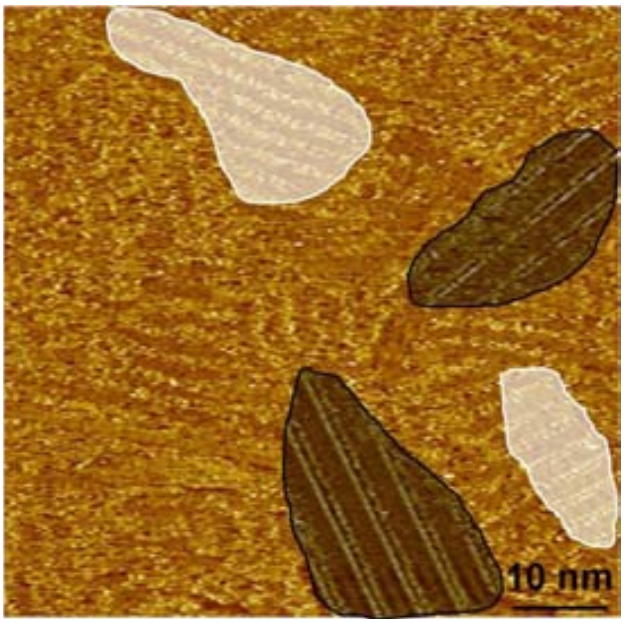

Figure 5.6: *STM image of monolayer at the 1-phenyloctane - HOPG interface formed upon mixing the racemate of* ***1,3Ph*** *and (R,R)-DACH at a ratio of 2:1. The monolayer contains domains of (S)-****1,3Ph****, and (R)-****1,3Ph****/(R,R)-DACH (I_{set} = 0.05 nA; V_{set} = 1.20 V).* ***(S)-1,3Ph****, and (R)-****1,3Ph****/(R,R)-DACH domains are marked in white and black, respectively.*

These experiments prove that the monolayer of acid can act as a resolving agent of the amine by preferential adsorption of one of the enantiomers. Only at a high excess of acid (*R*)-**1,3Ph** (e.g. 16:1:1 see Figure 5.8C; 4:1:1 Figure 5.8A and 5.8B) domains of the uncomplexed resorcinol derivative (*R*)-**1,3Ph** are observed. The adsorption of the non-matching enantiomer of amine (*S,S*)-diaminocyclohexane) was not noticed in any of the experiments. These results clearly show the capacity of (*R*)-**1,3Ph** to selectively co-adsorb one of the enantiomers of *trans*-diaminocyclohexane. Thus, acid resolves amine and amine resolves acid at the surface.

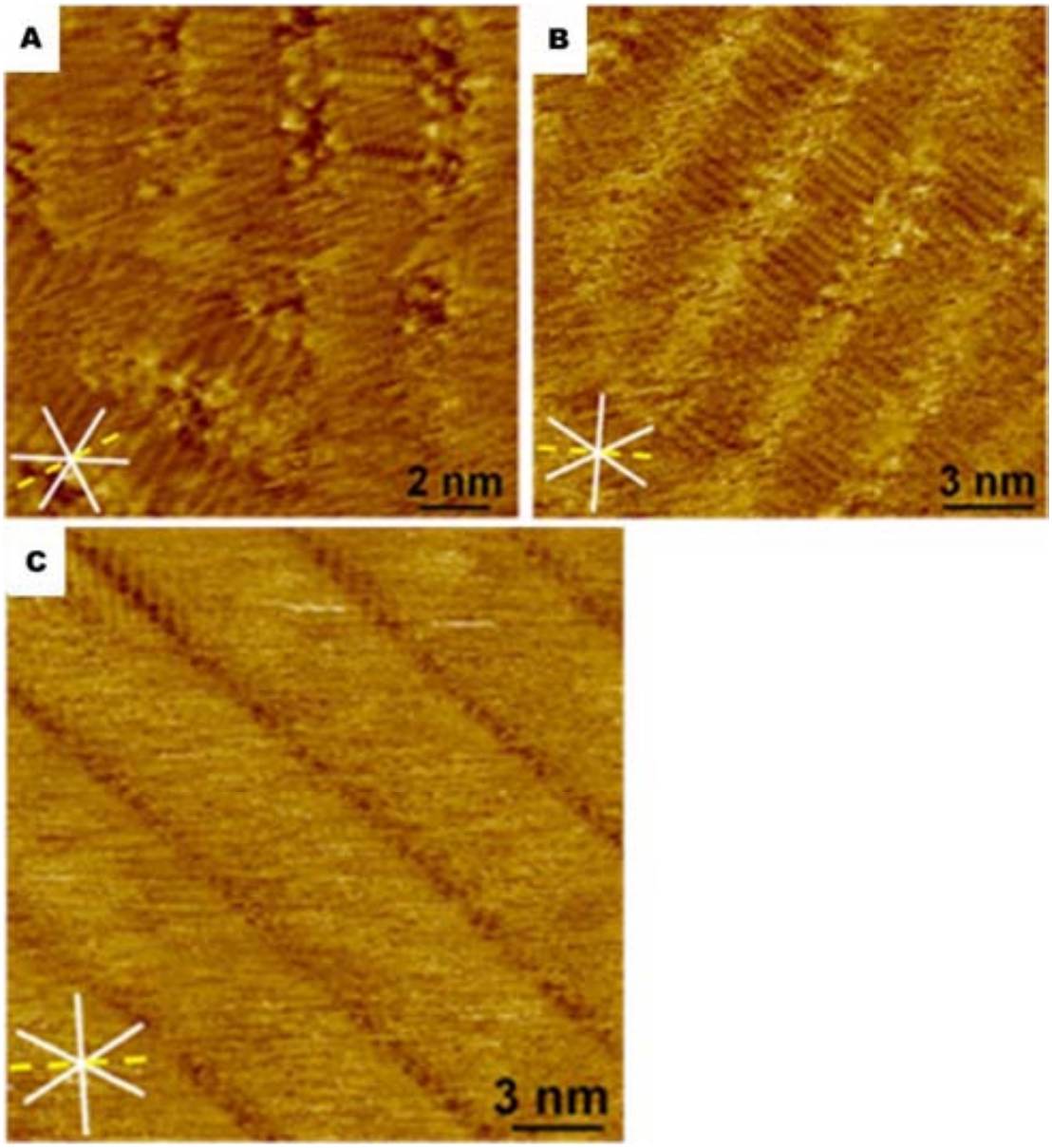

Figure 5.7: *STM images of monolayers formed upon premixing (R)-**1,3Ph**, (S)-**1,3Ph** and (R,R)-DACH (33:33:1) at the 1-phenyloctane - HOPG interface with the total concentration of **1,3Ph** 7.6×10^{-3} M. (A) A domain only contains (R)-**1,3Ph**(I_{set} = 0.20 nA; V_{set} = 0.70 V); (B) A domain only contains (S)-**1,3Ph**(I_{set} = 0.20 nA; V_{set} = 0.70 V); (C) A domain contains (R)-**1,3Ph**/(R,R)-DACH (I_{set} = 0.20 nA; V_{set} = 0.80 V). White solid lines indicate graphite main symmetry axes. Yellow dashed lines indicate the selected graphite reference axis running perpendicular to one of the main symmetry axes.*

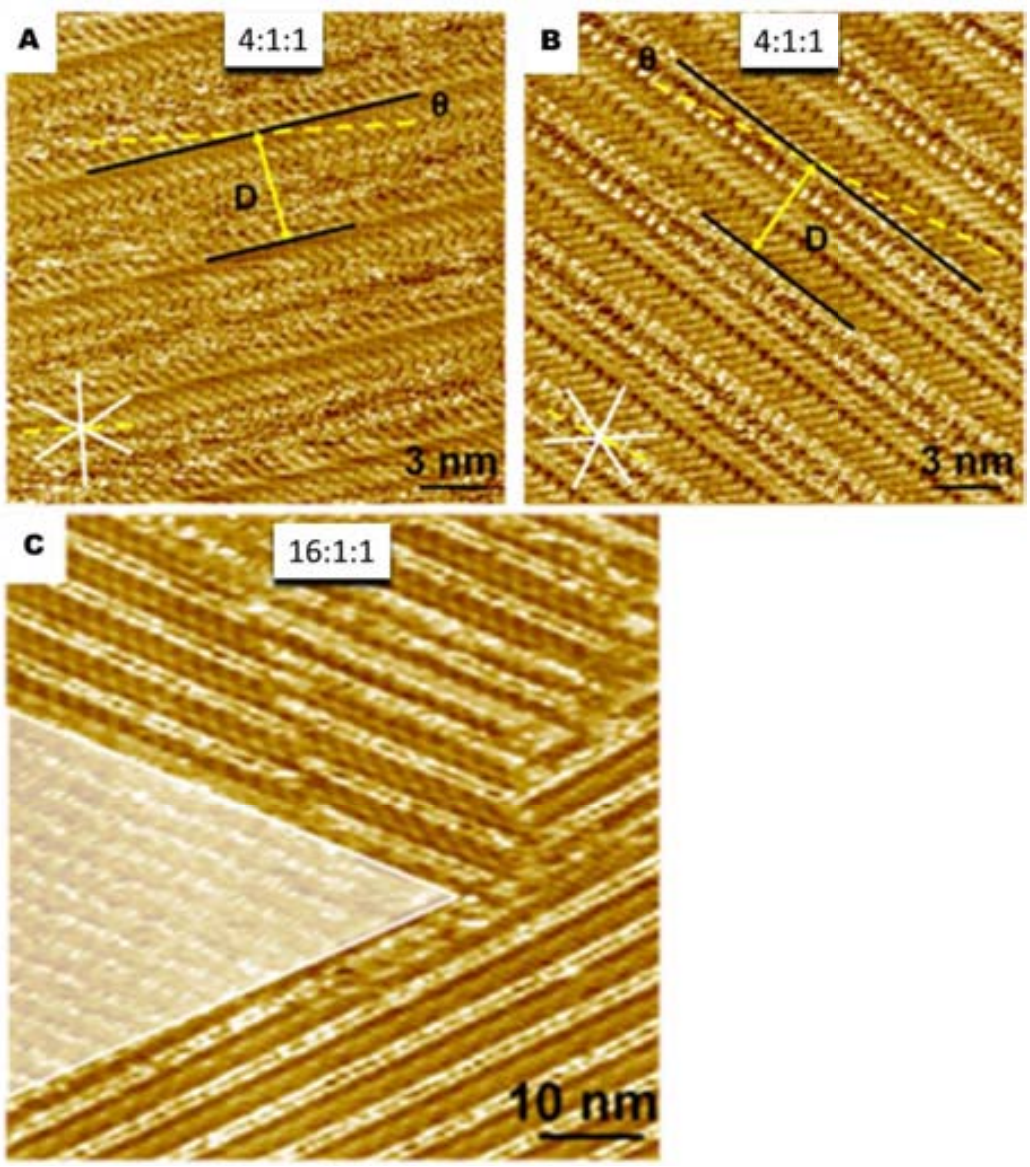

Figure 5.8: *STM images of monolayers formed upon premixing one enantiomer of* ***1,3Ph****, and the racemate of trans-DACH at the 1-phenyloctane - HOPG interface. The concentration of* ***1,3Ph*** *was* 7.6×10^{-3} *M. A) (R)-****1,3Ph*** *: (R,R)-DACH : (S,S)-DACH (4:1:1), B) (S)-****1,3Ph*** *: (R,R)-DACH : (S,S)-DACH (4:1:1) (*I_{set} *= 0.20 nA;* V_{set} *= 0.80 V for A and B). White solid lines indicate graphite main symmetry axes. Yellow dashed lines indicate the selected graphite reference axis running perpendicular to one of the main symmetry axes. Black solid lines indicate the direction of molecular rows. Double-headed yellow arrows show the width (D) of the bi-component rows. C) (R)-****1,3Ph*** *: (R,R)-DACH : (S,S)-DACH (16:1:1) (*I_{set} *= 0.25 nA;* V_{set} *= 0.50 V). (R)-****1,3Ph*** *domain is marked in white.*

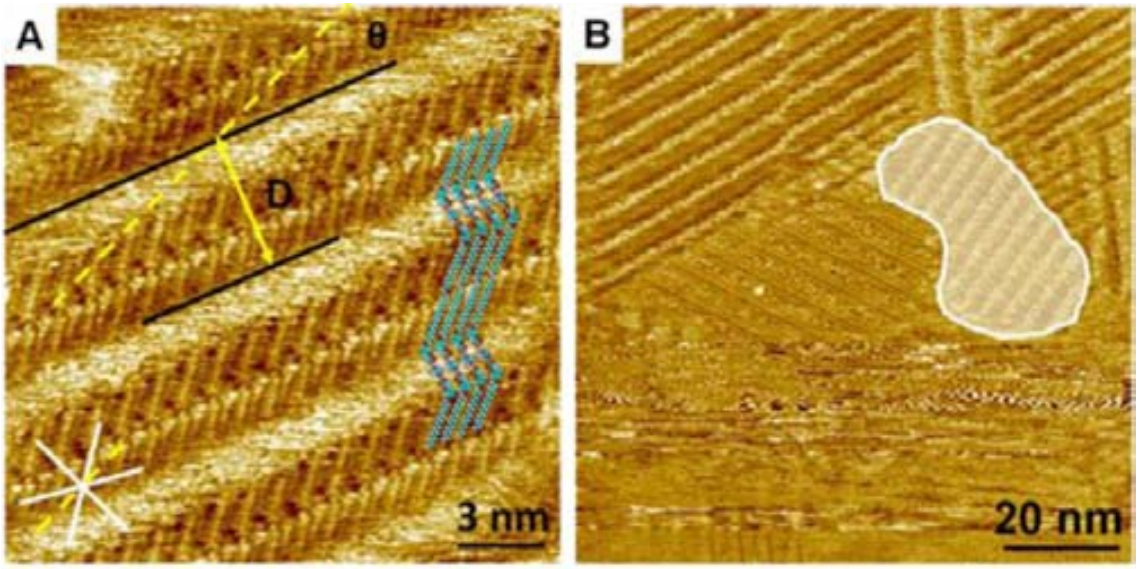

Figure 5.9: *STM images of monolayers formed upon premixing* ***1,3Ph*** *and DACH at the 1-phenyloctane - HOPG interface. The concentration of* ***1,3Ph*** *is* 7.6×10^{-3} *M. A) R-****1,3Ph****:(S,S)-DACH (1:5) (*I_{set} *= 0.20 nA;* V_{set} *= 0.80 V), B) R-****1,3Ph****:(S,S)-DACH (1:10) (*I_{set} *= 0.20 nA;* V_{set} *= 0.80 V), recorded 0.5 hour after deposition. White solid lines indicate graphite main symmetry axes. Yellow dashed lines indicate the selected graphite reference axis running perpendicular to one of the main symmetry axes. Black solid lines indicate the direction of molecular rows. Double-headed yellow arrows show the width (D) of the bi-component rows. Domain marked in white in B) contains only R-****1,3Ph****. Via a tentative molecular model,* ***1,3Ph*** *and DACH molecules are superimposed on the STM image to highlight their respective location.*

In the Figure 5.10 the high resolution image of the monolayer formed from a mixture of resorcinol derivative **1,3Ph** with (*R,R*) and (*S,S*)-*trans*-diaminocyclohexane mixed in proportion 1:10:10 on the graphite surface was captured. The structure is clearly the predicted one: A complex of two molecules of acid and diamine molecule in between are observed. The profiles proves the formation of complex **1,3Ph**-amine-**1,3Ph**.

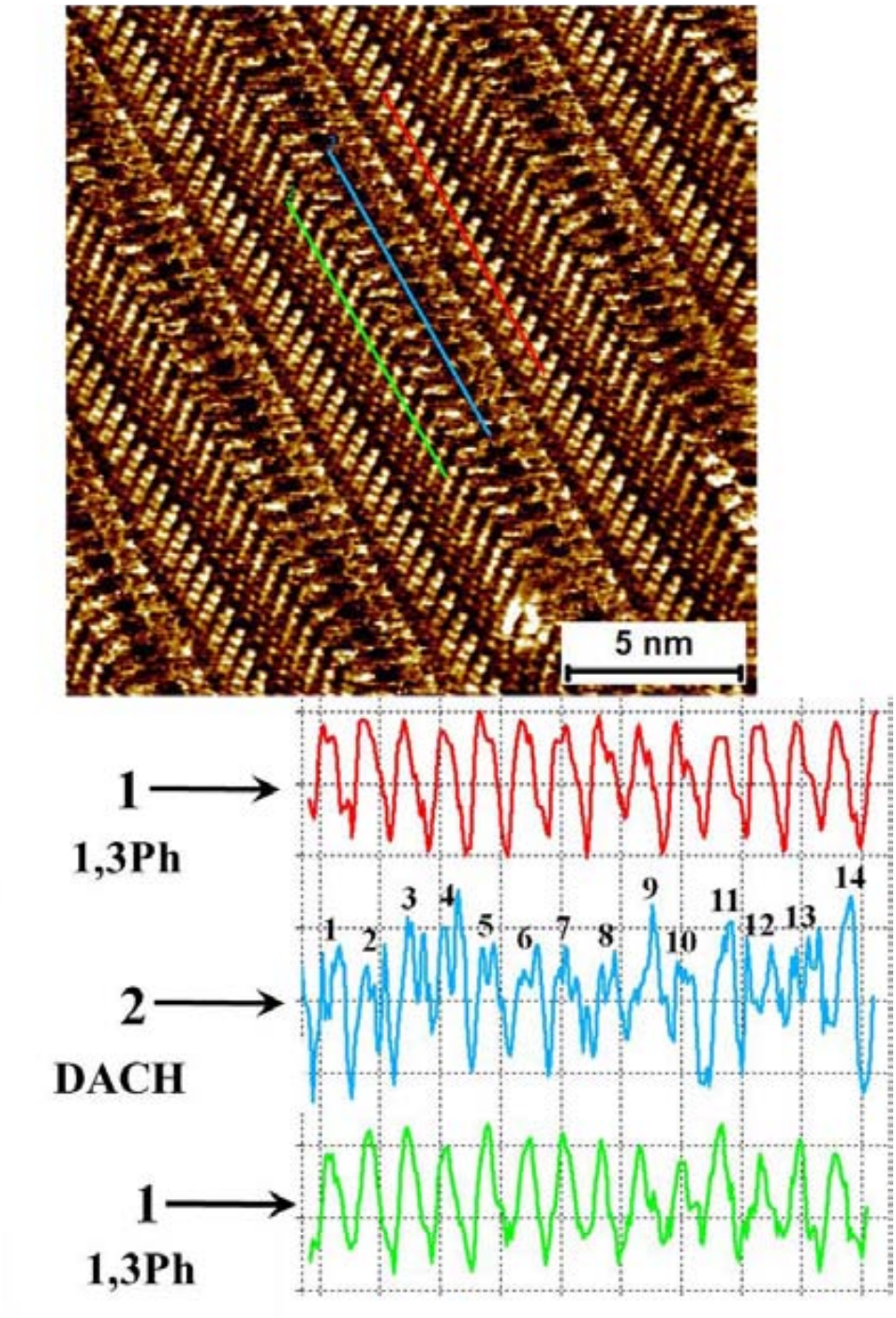

Figure 5.10: *STM images of monolayers showing (R)-**1,3Ph**/(R,R)-diaminocylohexane formed upon premixing (R)-**1,3Ph**, (R,R)-DACH and (S,S)-**1,3Ph** (1:10:10) at the 1-phenyloctane-HOPG interface. The total concentration of (R)-**1,3Ph** in solution was 7.6×10^{-3} M. (I_{set} = 0.15 nA; V_{set} = 0.85 V).The line profile analysis shows two lines (red and green) passing through the alkyl chain region of the row and one line (blue) passing through the centre of the row where the amine molecules are adsorbed. The line profiles obtained along these features clearly show the presence of 2:1 complex.*

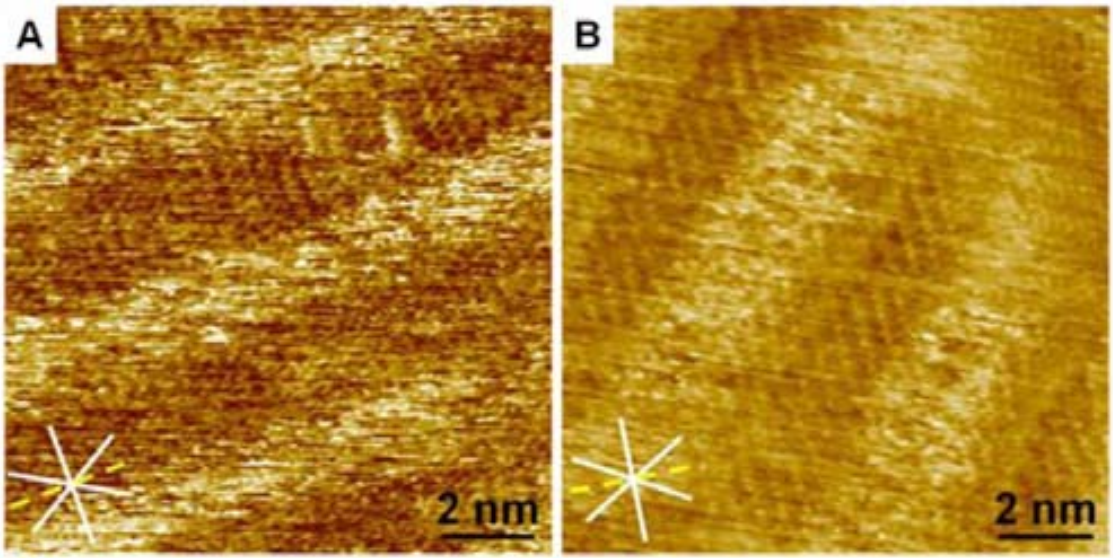

Figure 5.11: *STM images of monolayers formed upon premixing (R)-**1,3Ph**, (S)-**1,3Ph** and (S,S)-DACH (1:1:1) at the 1-phenyloctane - HOPG interface with the total concentration of **1,3Ph** 7.6×10^{-3} M. A: A domain only contains (R)-**1,3Ph** (I_{set} = 0.20 nA; V_{set} = 0.80 V); B: A domain contains (S)-**1,3Ph**/(S,S)-DACH (I_{set} = 0.25 nA; V_{set} = 0.80 V). White solid lines indicate graphite main symmetry axes. Yellow dashed lines indicate the selected graphite reference axis running perpendicular to one of the main symmetry axes.*

Table 5.3: *Structural characteristics of the monolayers. Width of adjacent rows (D), angle of row propagation direction with respect to the graphite reference axis (θ), domain composition [compound **1,3Ph**/DACH] and number of domains investigated. N is the number of domains analysed.*

Solution composition	D (nm)	θ(°)	Co-adsorption of amine	Domain composition	N
(*R*)-**1,3Ph**	3.7±0.2	-4±2	-	(*R*)-**1,3Ph**	13
(*S*)-**1,3Ph**	3.7±0.1	+5±3	-	(*S*)-**1,3Ph**	21
(*R*)-**1,3Ph**: (*S*)-**1,3Ph** (1:1)	3.8±0.1	-3±2	-	(*R*)-**1,3Ph**	28
	3.8±0.1	+3±2	-	(*S*)-**1,3Ph**	21
(*R*)-**1,3Ph**:(*S*,*S*)-DACH (2:1)	3.7±0.1	-4±2	No	(*R*)-**1,3Ph**	22
(*S*)-**1,3Ph**:(*R*,*R*)-diaminocyclohexane (2:1)	3.5±0.2	+4±3	No	(*S*)-**1,3Ph**	5
(*R*)-**1,3Ph**:(*R*,*R*)-DACH (2:1)	5.3±0.4	-10±2	Yes	(*R*)-**1,3Ph**/(*R*,*R*)-DACH	27
(*S*)-**1,3Ph**:(*S*,*S*)-DACH (2:1)	5.4±0.3	+12±3	Yes	(*S*)-**1,3Ph** /(*S*,*S*)-DACH	15
(*R*)-**1,3Ph**:(*R*,*R*)-DACH **:**(*S*,*S*)-DACH (4:1:1)	5.3±0.1	-10±2	Yes	(*R*)-**1,3Ph**/(*R*,*R*)-DACH	4
(*S*)-**1,3Ph**: (*R*,*R*)-DACH **:**(*S*,*S*)-DACH (4:1:1)	5.1±0.2	+10±3	Yes	(*S*)-**1,3Ph** /(*S*,*S*)-DACH	10
(*R*)-**1,3Ph**: (*R*,*R*)-DACH **:**(*S*,*S*)-DACH (1:1:1)	5.1±0.2	-10±3	Yes	(*R*)-**1,3Ph**/(*R*,*R*)-DACH	12
(*R*)-**1,3Ph**: (*R*,*R*)-DACH **:**(*S*,*S*)-DACH (1:10:10)	5.0±0.5	-12±5	Yes	(*R*)-**1,3Ph**/(*R*,*R*)-DACH	14
(*R*)-**1,3Ph**: (*R*,*R*)-DACH **:**(*S*,*S*)-DACH (16:1:1)	5.5±0.8	-14±4	Yes	(*R*)-**1,3Ph**/(*R*,*R*)-DACH	7
	3.7±0.4	-4±1	No	(*R*)-**1,3Ph**	2
(*R*)-**1,3Ph**: (*R*,*R*)-DACH **:**(*S*,*S*)-DACH (160:1:1)	3.6±0.2	-3±3	No	(*R*)-**1,3Ph**	12
(*R*)-**1,3Ph***:* (*S*)-**1,3Ph**:(*R*,*R*)-DACH *(1:1:1)*	3.7±0.1	+4±3	No	(*S*)-**1,3Ph**	8
	5.4±0.2	-9±3	Yes	(*R*)-**1,3Ph**/(*R*,*R*)-DACH	11
(*R*)-**1,3Ph***:* (*S*)-**1,3Ph**:(*S*,*S*)-DACH *(1:1:1)*	4.1±0.1	-1±1	No	(*R*)-**1,3Ph**	1
	5.4±0.2	+12±5	Yes	(*S*)-**1,3Ph** /(*S*,*S*)-DACH	2

***Table 5.4**: Structural characteristics of the monolayers at various solution compositions. Width of adjacent rows (D), angle of row propagation direction with respect to the graphite reference axis (θ), domain composition [compound **1,3Ph**/DACH] and number of domains investigated. N is the number of domains analysed.*

Solution composition	D (nm)	θ(°)	Co-Adsorption	Domain composition	N
(*R*)-**1,3Ph**: (*R*,*R*)-DACH (66:1)	3.8±0.1	-2±1	No	(*R*)-**1,3Ph**	12
	5.4±0.1	-12±3	Yes	*(R)*-**1,3Ph**/(*R*,*R*)-DACH	4
(*R*)-**1,3Ph**: (*S*)-**1,3Ph**: (*R*,*R*)-DACH (33:33:1)	4.0±0.2	-4±3	No	(*R*)-**1,3Ph**	2
	3.9±0.1	+1±1	No	(*S*)-**1,3Ph**	3
	5.0±0.1	-15±1	Yes	(*R*)-**1,3Ph**/(*R*,*R*)-DACH	1
(*R*)-**1,3Ph**: (*S*)-**1,3Ph**: (*S*,*S*)-DACH (33:33:1)	3.8±0.1	-4±2	No	(*R*)-**1,3Ph**	2
	3.7±0.1	+2±1	No	(*S*)-**1,3Ph**	1
	5.2±0.1	+11±1	Yes	(*S*)-**1,3Ph**/(*S*,*S*)-DACH	2
(*R*)-**1,3Ph**: (*S*,*S*)- DACH (1:5)	5.1±0.1	+19±2	Yes	(*R*)-**1,3Ph**/(*S*,*S*)-DACH	10

The diastereoselectivity detected in monolayers on the surface of graphite is the same as that observed in the bulk: When a classical resolution experiment was performed by combining (*R*)-resorcinol derivative **1,3Ph** with (*S*,*S*)-diaminocyclohexane and (*R*,*R*)-diaminocyclohexane in *tert*-butyl methyl ether, the resulting white solid proved to be a 1:1 complex of the (*R*)-enantiomers (the amine was present in 82% *ee*). (Figure 5.12).

On the other hand, no obvious diastereoselectivity was seen in solution: The NMR spectra of either 1:1 or 2:1 mixtures of (*R*)-**1,3Ph** and (*S*,*S*)-diaminocyclohexane or (*R*,*R*)-diaminocyclohexane were essentially indistinguishable (Figure 5.13). Therefore, it seems that the diastereoselectivity arises during the formation of the condensates, in the bulk crystal or on the surface, and is likely to be driven by the thermodynamics and symmetry of the ordered assemblies of molecules.

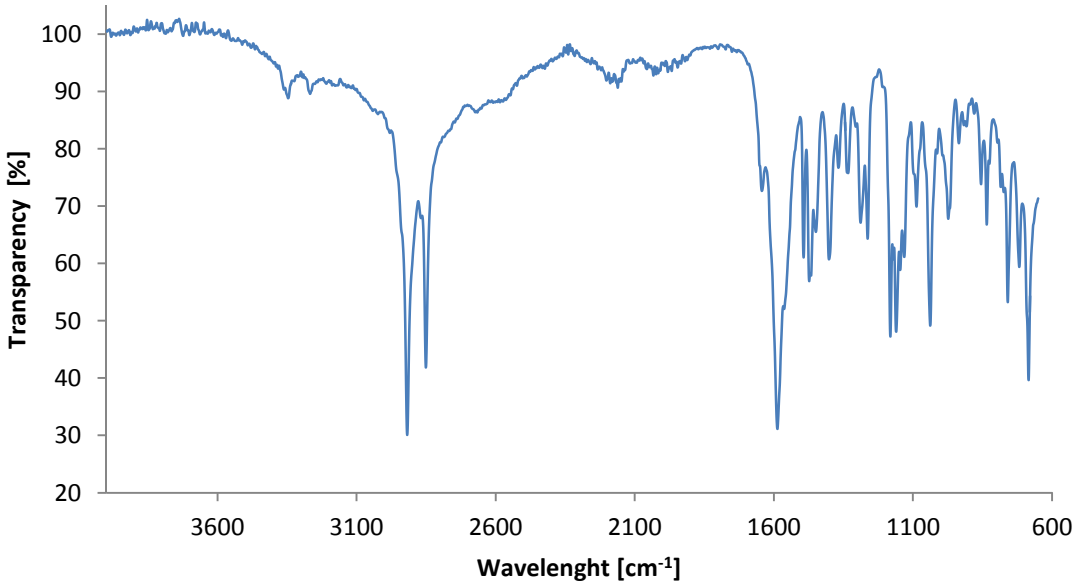

Figure 5.12: *Infrared spectrum of precipitate of (R)-**1,3Ph** with rac-diaminocyclohexane in tert-butyl methyl ether. In the spectrum there are strong peaks of carbonyl bond at 1587 cm^{-1}, C-H bond at 2918 and 2850 cm^{-1} and much less intense NH_2 peaks at 3246 and 3267 cm^{-1}.*

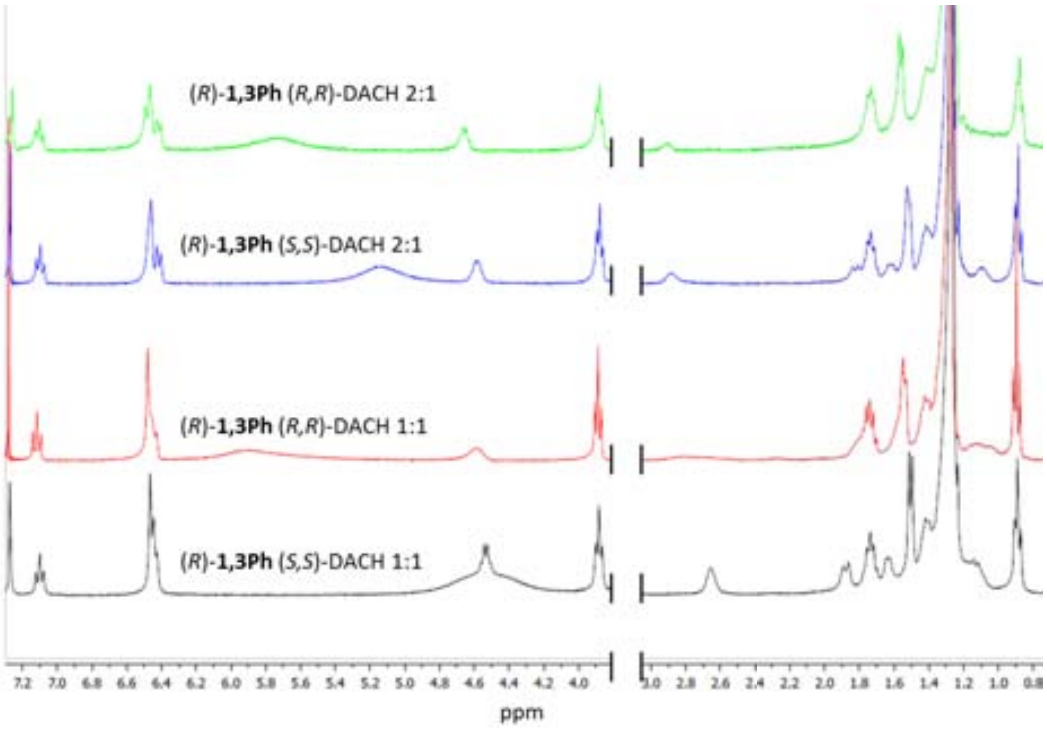

Figure 5.13: *^{1}H NMR spectra of mixtures of acid **1,3Ph** and DACH in deuterated chloroform.*

5.3 Self-assembly of 2,7-Dihydroxynaphthalene derivative 2,7Naph and trans-1,2-diaminocyclohexane

The acid **2,7Naph** was used for the same set of experiments as the homologue with the phenyl spacer because it has a similar bent shape to **1,3Ph** and it was envisaged that it might form isostructural layers. It is an important proof of principle because it would show that, once encountered, a particular packing geometry on a surface could lead to resolution of a given complementary compound.

The 1:1 mixture of (*R*,*R*)-*trans*-1,2-diaminocyclohexane and amphiphilic acid (*R*)-**2,7Naph** was also studied at the graphite-1-phenylocatane interface. It was found that in a similar manner to the resorcinol derivative **1,3Ph** there is formation of a complex which is readily adsorbed on the graphite surface. Representative images of this layer are presented in the Figure 5.14. The molecules of acid in this complex form straight lamellae in which the alkyl chains are not interdigitated, but tilted with the respect to the domain growth direction (unlike the case of the pure acid layers where interdigitation takes place). Each lamella is composed of two rows of acid molecules with aromatic parts of one row pointing towards the aromatic parts of the facing row. In between the aromatic moieties one can observe a darker area that is a not very well visualised with STM. This region is presumably occupied by the molecules of the diamine, which does not interact strongly with the surface, is not in the plane of the monolayer and therefore has a certain degree of freedom of movement, which causes the noise in the STM images.

The width of the lamellae that constitute the monolayer is 5.62 ± 0.14 nm, head to head distance is 0.66 ± 0.02 nm and chirality of the lamellae is -19.5 ± 0.7° with respect to main graphite axis [0010] and the alkyl chains are at an angle of 50.4 ± 1.7° with respect to the lamella growth direction. The dimers are Z-shaped, which is another form of expression of chirality of the monolayer.

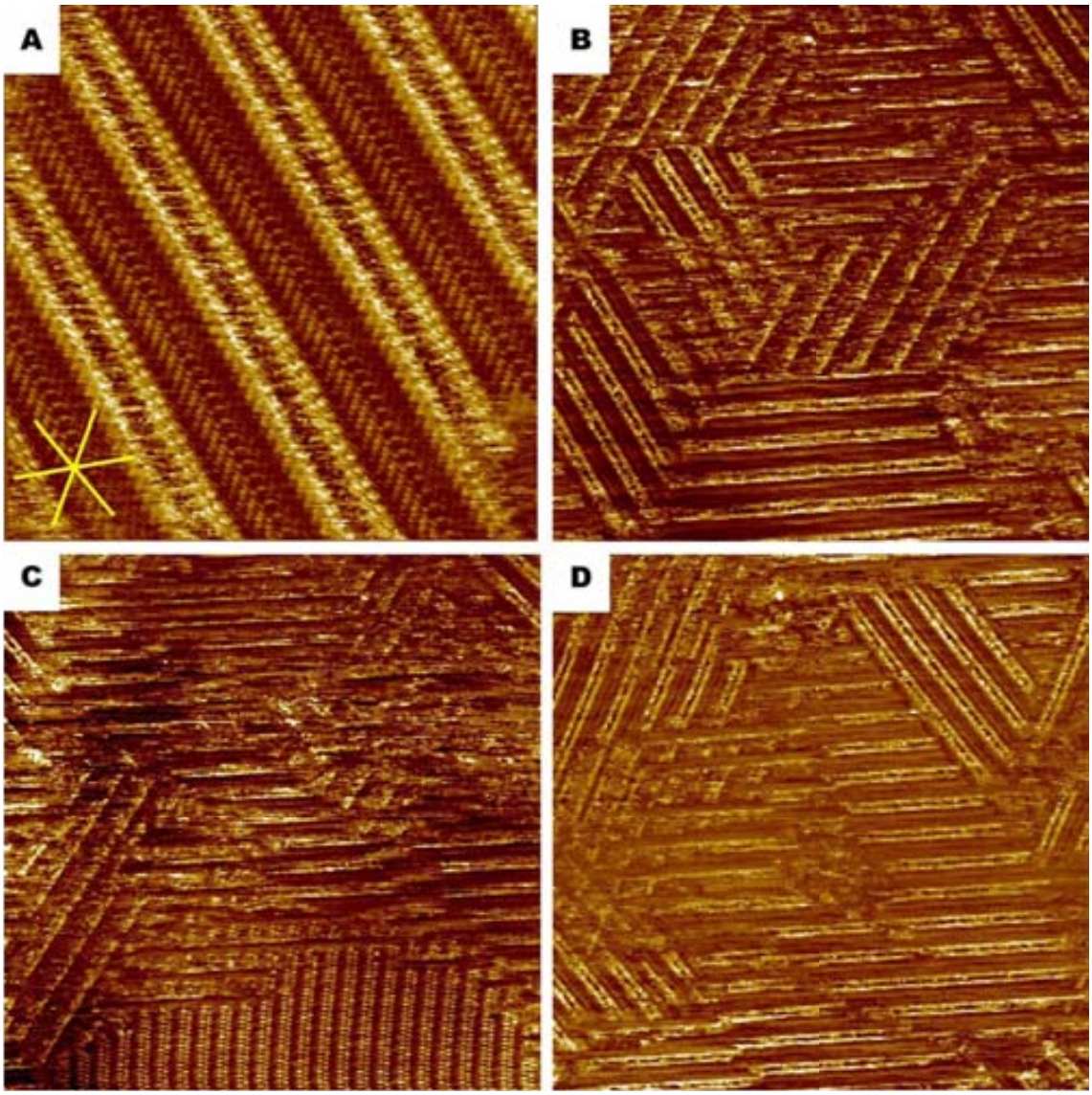

Figure 5.14: *STM images of monolayers formed by the (R)-**2,7Naph**, (R,R)-DACH (1:1) complex at the 1-phenyloctane-HOPG interface. The total concentration of (R)-**2,7Naph** in solution was 5.8×10^{-3} M. (A: 22.5x22.5 nm; B: 91x91 nm; C:98x98 nm; D:96.4x96.4 nm, I_{set} = 0.7 nA; V_{set} = -0.5 V for all the images).Image A shows a close up of the structure, the brightest stripes correspond to the area where the aromatic moieties are, and the fuzzy and dark area in between the aromatic parts is where the diamine molecules are located. Images B, C and D show the general structure of the monolayer. Multilayers are apparent in images B-D (seen as crossing lines). In image C the monolayer formed exclusively by acid (R)-**2,7Naph** can be observed in the bottom part of the image. Close by in the centre part of the image there is a layer of the complex growing on top of this domain.*

Images of multilayers and defects that were found in the STM images of the sample are shown in Figure 5.15. In the case of the multilayer it was found out that it has the

same structural parameters as the monolayer – the width, the chirality and the distance between molecules are very similar in all the images. Bearing this in mind, one could raise the question: Are the images that are considered a monolayer, as the Figure 5.14A - really a monolayer, or are they the top layer with some layers below it? In the Figure 5.14C one can observe the lamellae with good resolution in the STM image over the alkyl chains and poor resolution in between them. This effect might be caused by the molecules that are interacting atop of the layer visualised, but not yet forming complete overlayer.

The (*R*) enantiomer of **2,7Naph** shows quite different behaviour when mixed with the (*S*,*S*) enantiomer of *trans*-1,2-diaminocyclohexane.When this combination (1:1 ratio of acid to diamine) was studied by STM at the graphite-1-phenyloctane interface a quite disordered structure was evident, but after some time some ordered domains were observed. In this case the monolayer domains formed on the surface are rather small, the largest spotted was smaller than 1000 square nanometres, much smaller than domains of acid **2,7Naph** without DACH. However, the main feature in the monolayer is small domains with sides of 10-20 nm in length. The area in between these ordered domains is disordered, although in some cases lamellae that are not very straight and lack the high resolution of the ordered domain scan be observed, probably because of movement of the molecules on the surface. Figures 5.16 and 5.17 show typical images where these features can be appreciated.

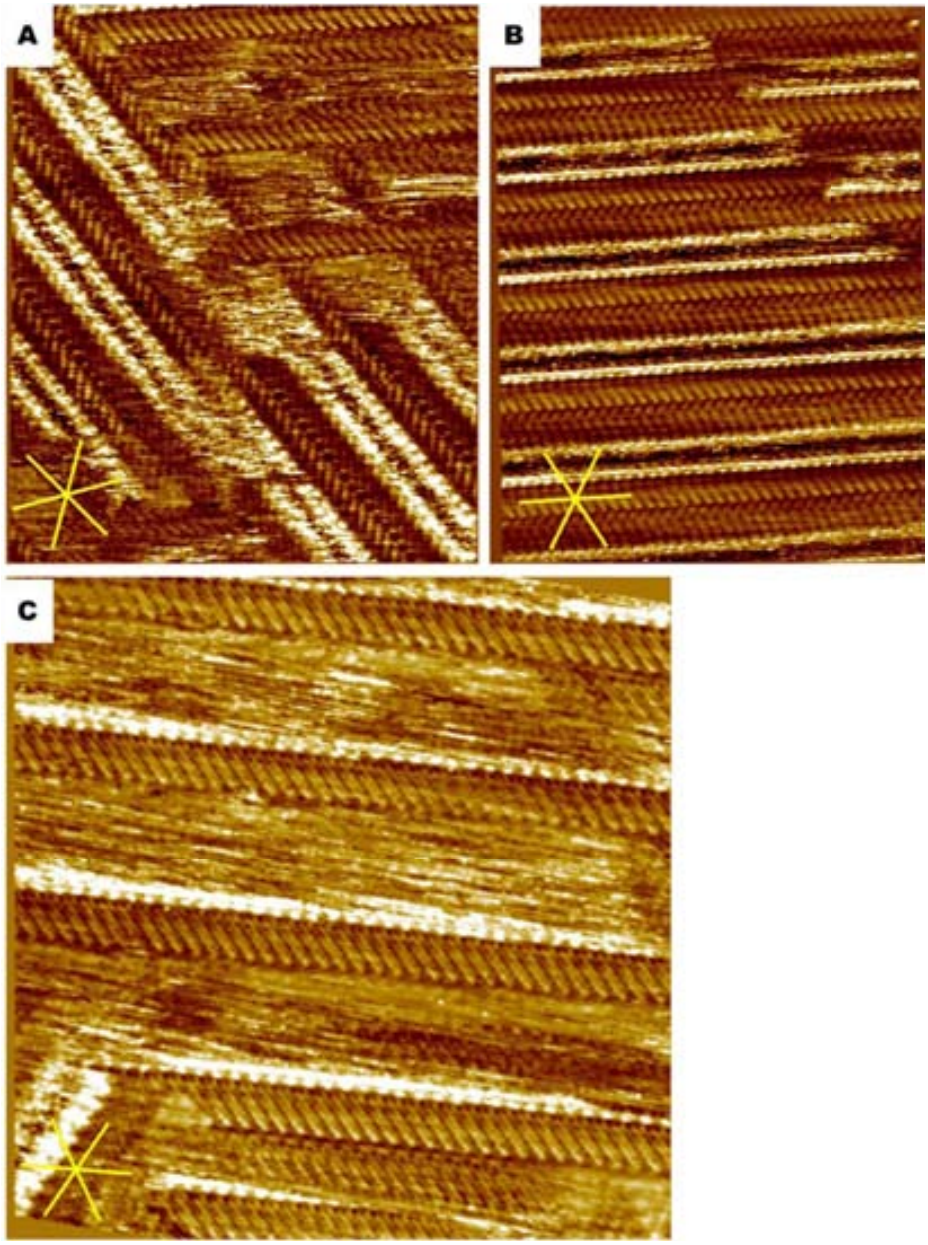

Figure 5.15: *STM images of monolayers showing (R)-**2,7Naph**/(R,R)-DACH formed upon premixing (R)-**2,7Naph**, (R,R)-DACH (1:1) at the 1-phenyloctane-HOPG interface. The total concentration of (R)-**2,7Naph** in solution was 5.8×10^{-3} M. (A: 24.1 x 28.5 nm; B: 24.2 x 31.0 nm; C: 23.8 x 25.3 nm, I_{set} = 0.7 nA; V_{set} = -0.5 V for all the images). Image A shows close up of the structure, it can be observed an overlayer in the right upper corner of the image growing on the lower layer. In image B a defect of the monolayer is shown, a kind of change of the direction of molecules in the same lamellae. In image C there is an overlayer grown on the top of the lamella that starts in left bottom corner of the image, the "shadow" of this lamella continue through the entire image. At the same time in the upper layer there is a good resolution of just one alkyl chains from each lamella, and there is fuzzy area in between. On the bottom of the image there is a kind of accumulation of alkyl chains without aromatic parts visible, probably they come from different layers.*

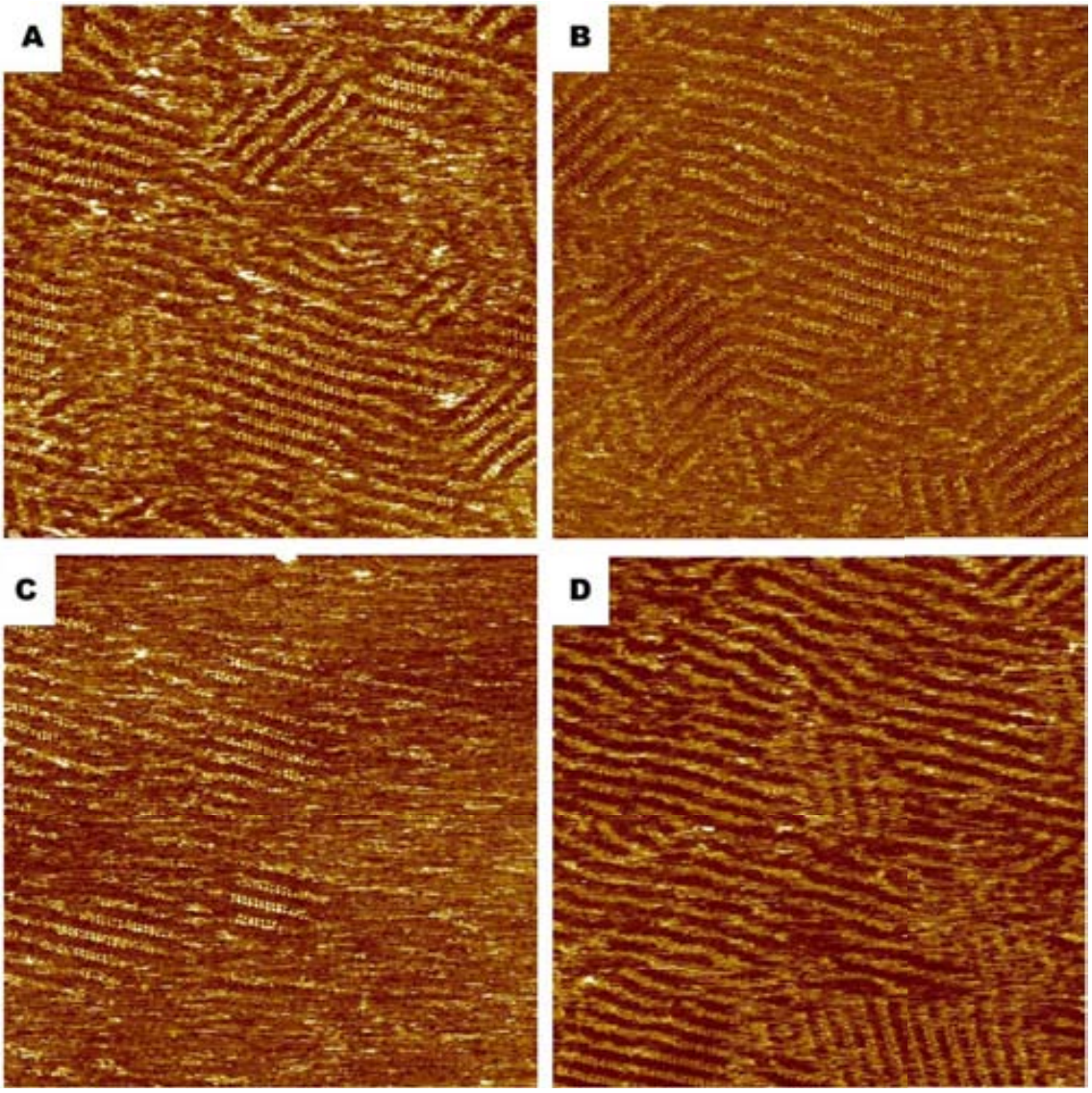

Figure 5.16: *STM images of monolayers formed upon premixing (R)-**2,7Naph**, (S,S)-DACH (1:1) at the 1-phenyloctane-HOPG interface. The total concentration of (R)-**2,7Naph** in solution was 5.8×10^{-3} M. (A: 96 x 96 nm,B:91.2 x 91.2 nm, C: 96.4 x 96.4 nm, D: 96.1 x 96.1 nm; I_{set} = 0.7 nA; V_{set} = -0.5 V for all the images).Image A shows the typical domains observed short time after deposition of the solution, where just below the centre of the image a domain composed exclusively by the molecules of (R)-**2,7Naph** is seen, as well as close to the top right corner of the image and at the left edge of the image. The main part of the monolayer is either completely disordered or has poorly defined lamellae. In image B one of the biggest domains seen can be observed in the centre of the zone. In image C there is surprising lamellae that are losing its resolution, as if something was attaching atop of the monolayer. In image D poorly defined lamellae are observed in the main, only on the bottom of the image one can see ordered monolayer formed by (R)-**2,7Naph**.*

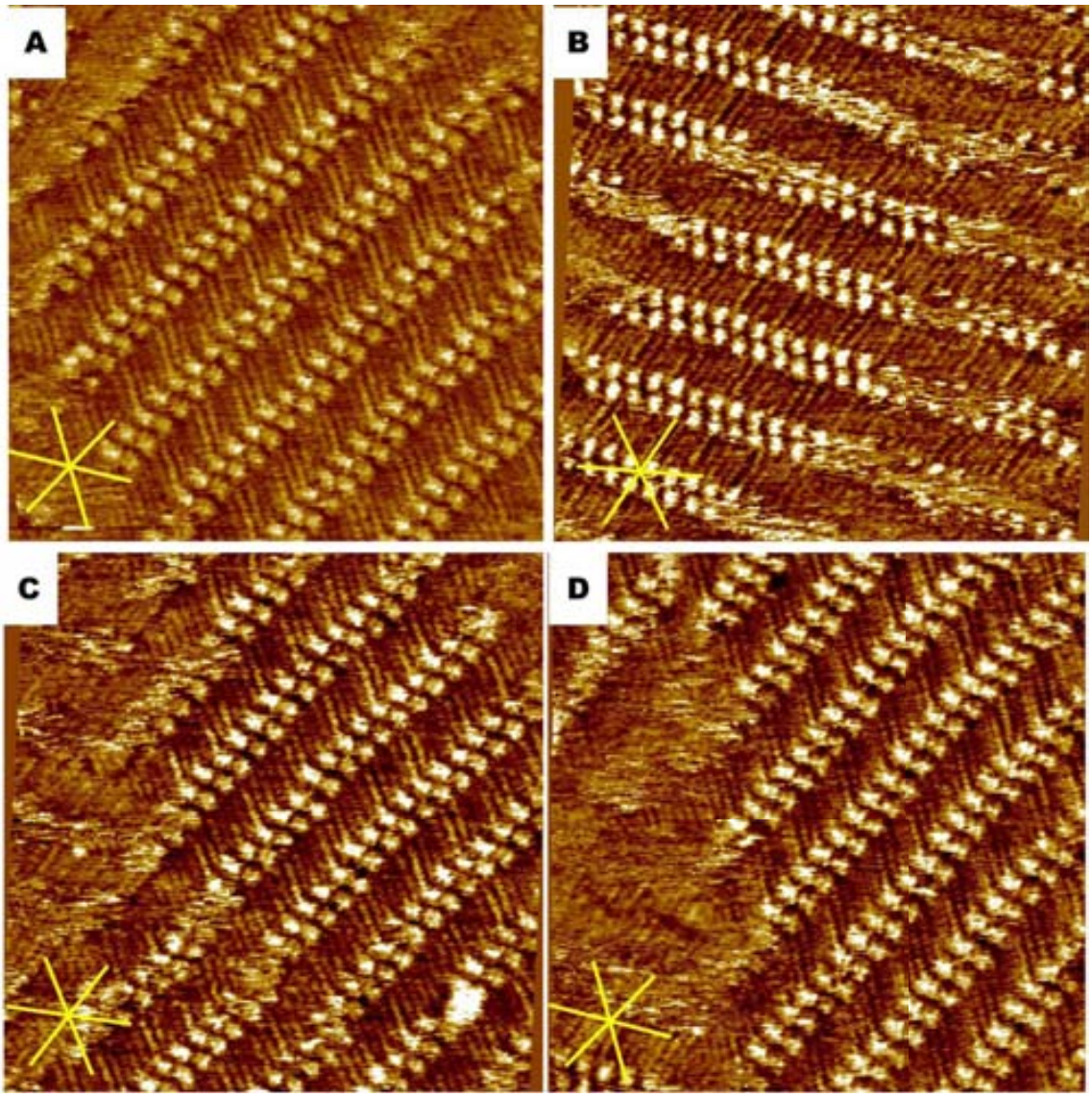

Figure 5.17: *Close-up STM images of monolayer showing (R)-**2,7Naph**/(S,S)-DACH formed upon premixing (R)-**2,7Naph**, (S,S)-DACH (1:1) at the 1-phenyloctane-HOPG interface. The total concentration of **2,7Naph** in solution was 5.8×10^{-3} M. (A: 23.2 x 23.2 nm; B: 24.9 x 24.9 nm; C: 22.8 x 22.8 nm, D: 23.9 x 23.9 nm; I_{set} = 0.7 nA; V_{set} = -0.5 V for all the images).Image A presents one of the biggest regular domains observed during the experiments. Image B shows a domain and on the right side there is something attached to the domain which causes noise in the image. At the same time the lamella size is expanding, so there is no good resolution in the area, but still the alkyl chains can be observed and one can recognize the position of most of the aromatic parts of the molecules. In the images C and D the boundary area is shown where one can still observe alkyl chains, but the head groups are totally fuzzy.*

The distance between the lamellae is 3.62 ± 0.15 nm, the head to head distance is 1.04 ± 0.05 nm and chirality +6.4 ± 3.0°. The distance values are very similar to those of lamellae composed exclusively by acid (*R*)-**2,7Naph** (respectively 3.56 ± 0.20 nm and

1.01 ± 0.06 nm), but the rotation with respect to the main graphite axis [0010] is the opposite, in the case of (*R*)-**2,7Naph** it is -7.47 ± 3.4º. So in this sample a switch of the chirality occurs by the addition of the (*S,S*)-*trans*-1,2-diaminocyclohexane. At the same time – and surely related to the previous observation – there is a change in the dimer type; S-shaped dimers are observed in the mixture of (*R*)-**2,7Naph**/(*S,S*) amineand Z-shaped dimers in the case of (*R*)-**2,7Naph**. In this case it seems that the amine inhibits the formation of large domains in the monolayer of (*R*)-**2,7Naph**, and favours the formation of a diastereomeric monolayer with inverted conformational chirality. Presumably, this diastereomeric conformation is not as stable as the pure acid in non-interacting medium (i.e. no amine), or because at the edges of domains a complex forms with the amine inducing the diastereomeric packing conformation, the inverted domains do not cover the entire surface as disordered areas are observed between them. At the same time poorly absorbed molecules can be observed, especially at domain edges, which may indicate that the complex of (*R*)-**2,7Naph**/(*S,S*) amine adsorbs on the surface, but there is no stable conformation of this complex at the graphite-1-phenyloctane interface under the conditions of the experiment.

Upon premixing and deposition of the racemic mixture of the acid **2,7Naph** and (*S,S*)-diaminocyclohexane, formation of a self-assembled monolayer was observed. The domains are not very large, the largest one was smaller than 30 x 30 nm, and not the entire surface was covered with the well-organized monolayer. The typical images are presented in the Figure 5.18 and 5.19. The structure observed is very similar to the SAM formed by molecules of **2,7Naph**, and no structures similar to those formed by (*R*)-**2,7Naph** and (*R,R*)-diaminocyclohexane, as in the Figures 5.14 and 5.15 were seen. Defects and noise were observed frequently in this sample, especially above the head groups what suggest that the molecules of acid in monolayer are interacting with the amine from the solution, however no stable structure involving amine was observed.

Unfortunately, due to the problems with visualising the graphite no correction was done on the captured images, so no reliable structural analysis could be done.

In the experiments the chiral recognition between (*R*)-**2,7Naph** and (*R,R*)-1,2-diaminocyclohexane was proved, and the curious switch of the chirality of monolayer formed by (*R*)-**2,7Naph** in the sample with (*R*)-acid **2,7Naph** and (*S,S*) amine. In the experiments using racemic mixture of acid with one enantiomer of amine no structure with amine was observed what might suggest that the complex is more stable in the

solution than at the graphite-1-phenyloctane interface. What is more, this is a proof that the analogue of the acid **1,3Ph** and bearing the same shape it is capable of forming isostructural domains. What is different is the observation of multilayers in the case of **2,7Naph**, and the behaviour with racemic mixture of acid – no complex was observed on the surface.

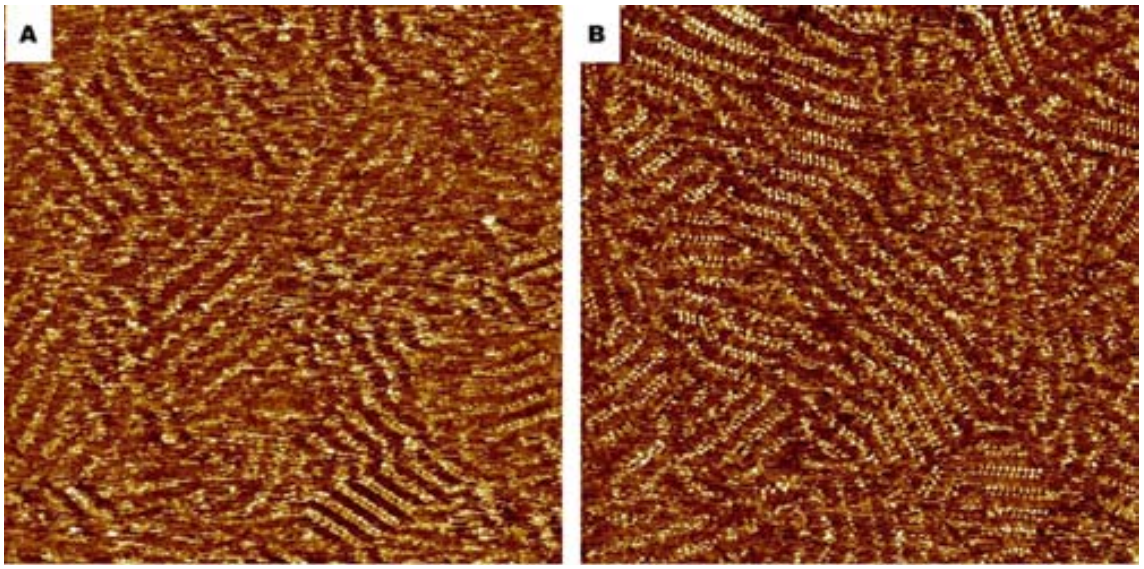

Figure 5.18: *STM images of monolayers showing racemic-**2,7Naph**/(S,S)-DACH formed upon premixing rcaemic-**2,7Naph**, (S,S)-DACH (1:1) at the 1-phenyloctane-HOPG interface. The total concentration of racemic-**2,7Naph**in solution was 5.8×10^{-3} M. (A: 90.4 x 90.4 nm, B: 90.4 x 90.4 nm; I_{set} = 0.7 nA; V_{set} = -0.5 V for all the images). In the images the general structure of monolayer is observed. In image A are with poorly defined domains, just in the bottom of image one domain with well-defined molecules of acid **2,7Naph**. In image B area with many well visualised domains, but as it is clearly seen there are separated by disordered area.*

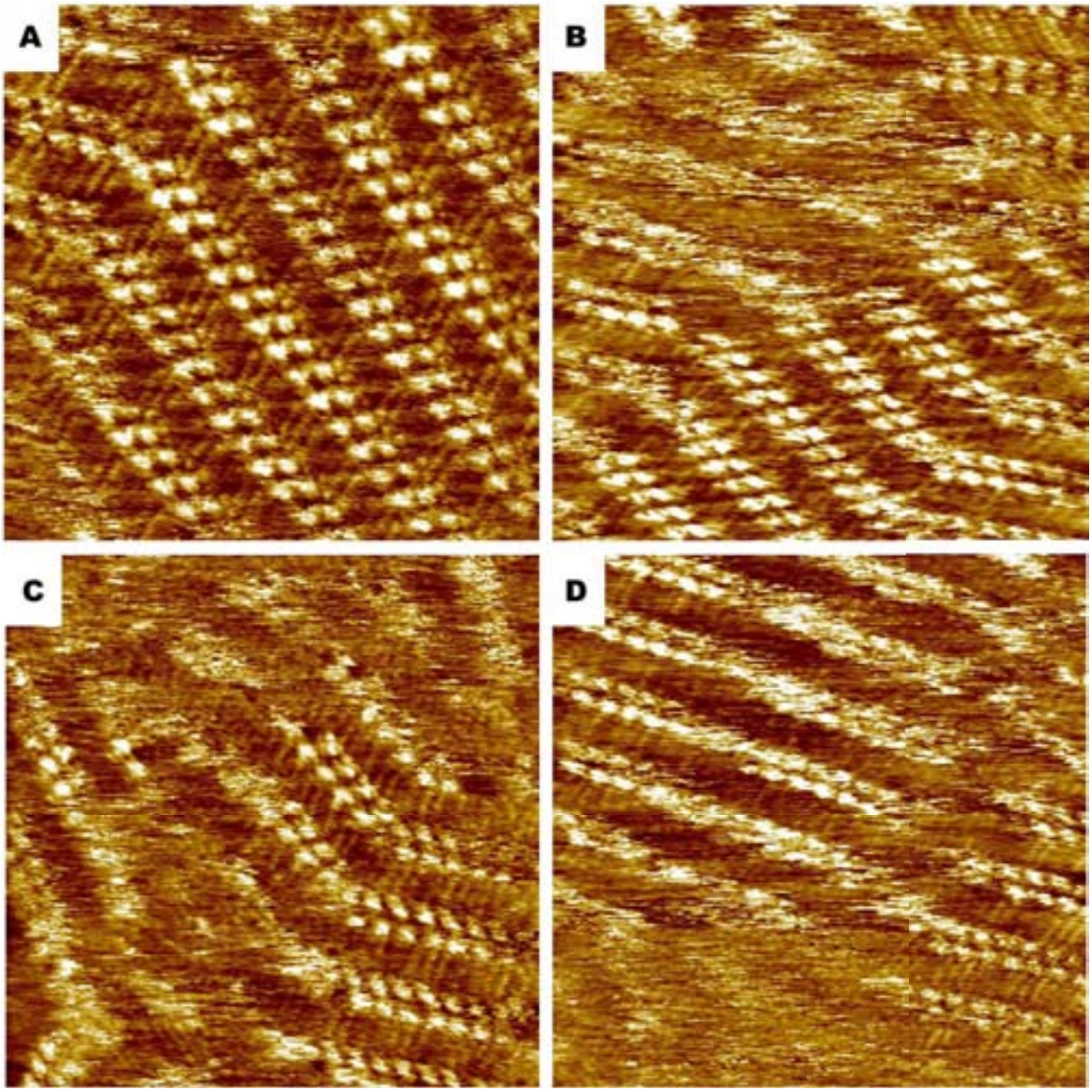

Figure 5.19: *Close-up STM images of monolayers showing racemic-**2,7Naph**/(S,S)-DACH formed upon premixing rcaemic-**2,7Naph**, (S,S)-DACH (1:1) at the 1-phenyloctane-HOPG interface. The total concentration of racemic-**2,7Naph** in solution was 5.8×10^{-3} M. (A: 18.9 x 18.9 nm ,B: 20.1 x 20.1 nm, C: 23.8 x 23.8 nm, D: 23.4x23.4 nm;; I_{set} = 0.7 nA; V_{set} = -0.5 V for all the images). In image A one of the largest observed domain. It can be observed that there are changes in the contrast on the aromatic parts of molecules, possibly something is interacting with carboxylic group of acid. In the images A B and C the S and Z shaped dimers are observed, this is indication that either both of the enantiomers of acid form the monolayer or there is a switch in the chirality of molecules on the surface. In image D changes of the contrast indicates that that there are molecules atop of the monolayer.*

5.4 Self-assembly of 1,5-Dihydroxynaphthalene derivative (S)-1,5Naph and trans-1,2-diaminocyclohexane

The derivative **1,5Naph** of 1,5-dihydroxynaphthalene has a quite different geometry to the previous lactate-derived surfactants used for the resolution of amines, in that, in principle, the main axis of the molecule can be linear, albeit that there is a slight shift in the axis between the alkyl chain and the lactate group.

The mixture of (*S*,*S*)-1,2-diaminocyclohexane and amphiphilic acid (*S*)-**1,5Naph** was also studied on the graphite-1-phenyloctane interface. While mixing the solution is 5.8×10^{-3} M of the two components (1:1) it was found that the complex precipitates, while both compounds separately are perfectly soluble at this concentration. Because of this feature the sample was diluted to 3.0×10^{-3}M in order to dissolve the complex. The solution was deposited on the graphite surface as before and imaged using the scanning tunnelling microscope. In the Figure 5.20 typical STM images are presented. There is a clear lamellar structure in the monolayer that is formed, but the domains are quite small; only a few of the observed domains occupied more than a few hundreds square nanometres. Within these small areas, the lamellae are straight and most of them are well defined. The structure is clearly distinct to that of (*S*)-**1,5Naph** on its own; the head groups form straight lines in the complex. Two different structures on the surface are seen; there is a one that does not involve interdigitation of the alkyl moieties, while the other one does involve interdigitation of the chains. Unfortunately, due to problems with drift and stability of the tip in the experimental conditions, possibly because of the poor solubility of the complex, there is insufficient resolution in the images for this mixture to measure the details of the structure.

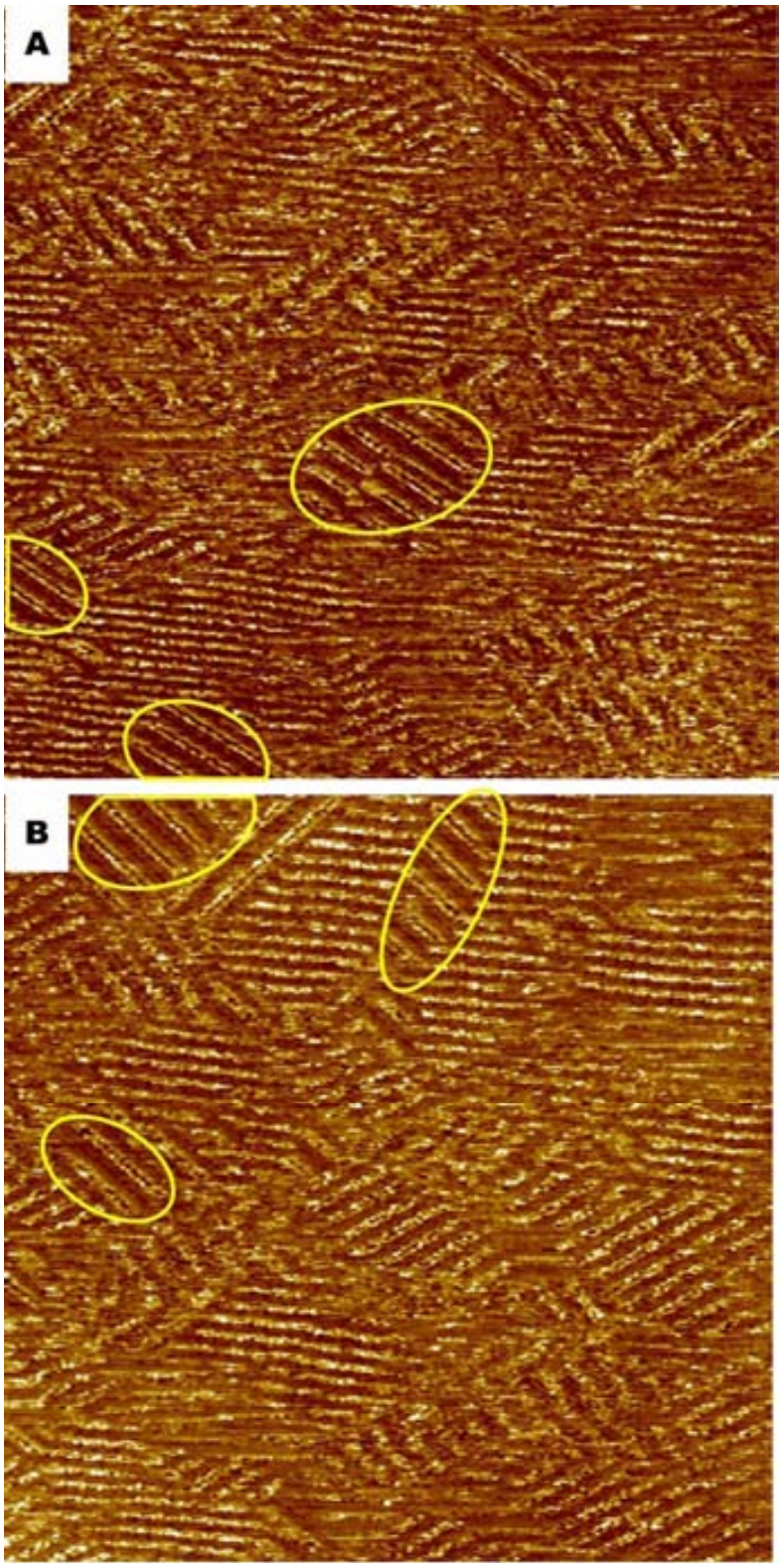

Figure 5.20: *STM images of monolayers showing (S)-**1,5Naph**/(S,S)-DACH formed upon premixing (S)-**1,5Naph**, (S,S)-DACH (1:1) at the 1-phenyloctane-HOPG interface. The total concentration of (S)-**1,5Naph**in solution was 3.0×10^{-3} M. (A: 94.8x94.8 nm ; B: 94.8x94.8 nm I_{set} = 0.7 nA; V_{set} = -0.5 V for both images). The wider lamellae, with alkyl chains not interdigitated are marked in yellow.*

The mixture of (*R,R*)- *trans*-1,2-diaminocyclohexane and amphiphilic acid (*S*)-**1,5Naph** also resulted in a solid complex upon mixing the solution at 5.8×10^{-3} M of the two components (1:1), despite the fact that both compounds separately are perfectly soluble at this concentration. Because of this difficulty the sample was diluted to 3.0×10^{-3}M in order to dissolve the complex. After deposition of the solution and bringing the microscope into feedback, a few minutes later the monolayer was observed using STM. It was found that large domains are formed, spreading over thousands of square nanometres, but at the same time smaller domains can be found and disordered areas in the other places (Figure 5.21 and 5.22). The domains are straight with alkyl chains interdigitated, the head groups are in line and it is possible to distinguish virtually every molecule. The molecular arrangement is not the one that was observed in the majority of images of acid **1,5Naph** on the surface, but it seems to be the same that was observed in few places for racemic mixture of acid **1,5Naph** and in the sample of acid on the surface (see chapter 4.5).

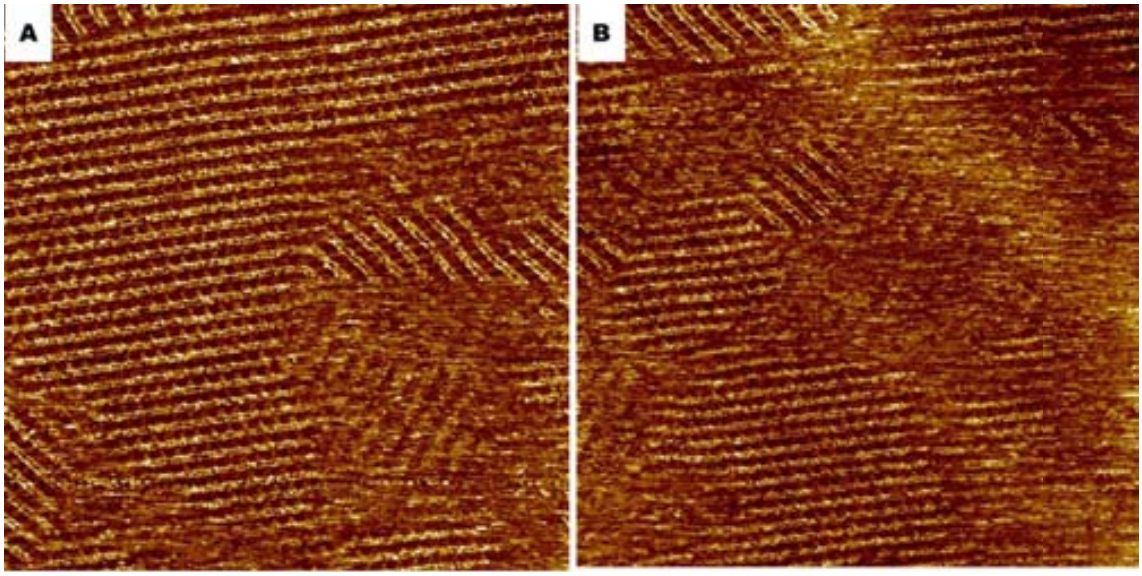

Figure 5.21: *STM images of monolayers showing (S)-**1,5Naph**/(R,R)-diaminocyclohexane formed upon premixing (S)-**1,5Naph**, (R,R)-DACH (1:1) at the 1-phenyloctane-HOPG interface. The total concentration of (S)-**1,5Naph** in solution was 3.0×10^{-3} M. (A: 97.6 x 97.6 nm; B: 100.2 x 100.2 nm; I_{set} = 0.7 nA; V_{set} = -0.5 V for both images). In image A one of the biggest domain is presented in the left and top part of the image, also there can be seen the other type of domain in the centre of the image a bit to the right. In image B one can see other domains surrounded by blurry area.*

Unfortunately, because of the problems with the stability of the tip and the drift of the

sample, the resolution was insufficient to determine the structural parameters of the monolayer.

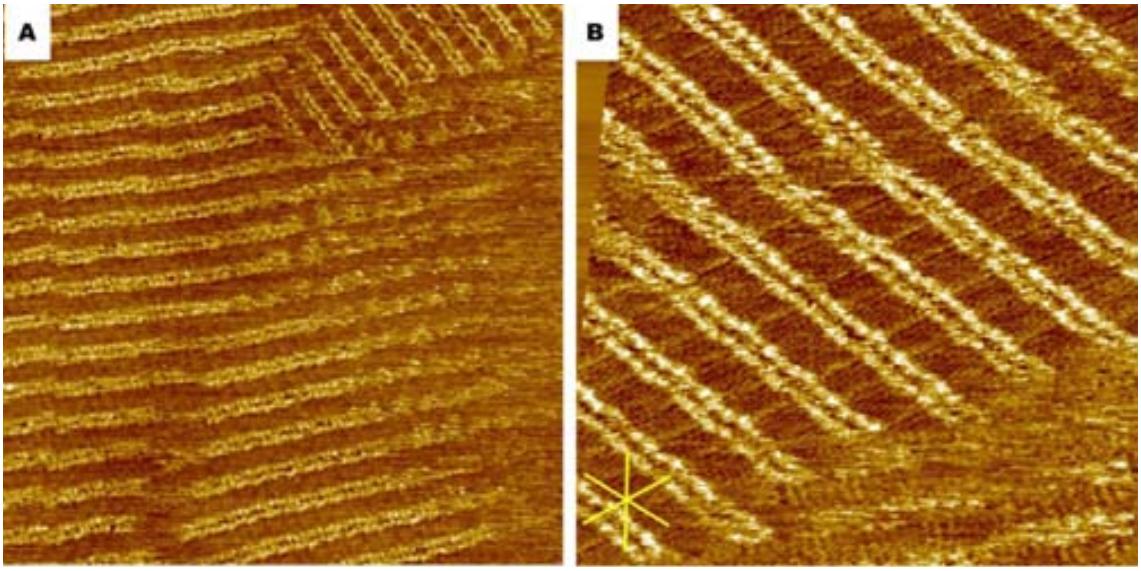

Figure 5.22: *STM images of monolayers showing (S)-**1,5Naph**/(R,R)-DACH formed upon premixing (S)-**1,5Naph**, (R,R)-DACH (1:1) at the 1-phenyloctane-HOPG interface. The total concentration of (S)-**1,5Naph** in solution was 3.0×10^{-3} M. (A: 82.1 x 82.1 nm; B: 23.4 x 23.4 nm; I_{set} = 0.7 nA; V_{set} = -0.5 V for both images). In image A there is intriguing effect of braking lamella, on the top of the image the lamella is complete, and on the bottom in the same domain there is a brake in the middle of it. Also the contrast in the left part of the image suggests formation of multilayers. In image B the close up of the structure is shown.*

Another measurement was performed using racemic **1,5Naph** and (*R,R*)-diaminocyclohexane. In this case the monolayer was observed, but again the monolayer is not visualised with very high resolution. The typical images are presented in the Figure 5.23. It can be seen immediately that the lamellar structure of the monolayer is formed, but the biggest domain does not present images with good resolution. In the close-up, in image B, the interdigitated alkyl chains are seen, but no detail of the aromatic part is observed. The lamella width was 3.69 ± 0.24 nm and the chirality measured was +25.5 ± 1.7° with respect to the [0010] graphite axis, it means that the structure is almost perpendicular to the main graphite axis, indicative, perhaps, of a pseudo-racemic structure.

The structures observed with STM for mixtures of **1,5Naph** and diaminocyclohexane cannot give clear answer about nature of interaction between the acid and amine, however no structure typical for the acid **1,5Naph**, as presented in the Figure 3.13 and

3.14A, was found in the mixtures with this amine. This observation leads to the conclusion that some kind of interaction between molecules of acid **1,5Naph** and diaminocyclohexane takes place, although it is not clear whether the observed SAM includes the amine, perhaps adsorbed above the plane of the layer – this situation could explain the lack of resolution in the aromatic parts of the surfactant. Alternatively, the acid group conformation could block an effective interaction with the DACH .

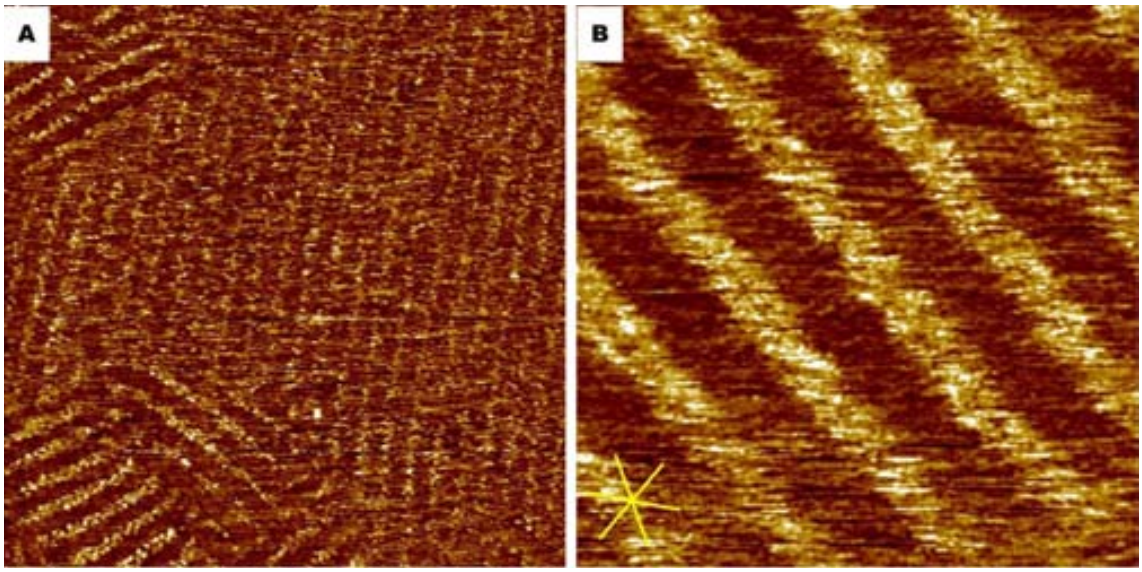

Figure 5.23: *STM images of monolayers showing rac-**1,5Naph**/(R,R)-DACH formed upon premixing rac-**1,5Naph**, (R,R)-DACH (1:1) at the 1-phenyloctane-HOPG interface. The total concentration of rac-**1,5Naph**in solution was 3.0×10^{-3} M. (A: 83.9 x 83.9 nm; B: 16.4 x 16.4 nm; I_{set} = 0.7 nA; V_{set} = -0.5 V for both images). In image A general view of lamella is presented. In image B the close up is shown.*

5.5 Self-assembly of Hydroquinone amphiphilic derivative (R)-1,4Ph and trans-1,2 diaminocyclohexane

The mixture of (*R,R*)- *trans*-1,2-diaminocyclohexane and amphiphile acid (*R*)**-1,4Ph** was also studied at the graphite-1-phenyloctane interface. As in previous samples the solution concentration equals 6.2×10^{-3} M for each of components and the ratio of acid to diamine was 1:1. Unlike the other cases it was very difficult to obtain any images of the monolayer of this complex, the only images captured are presented in the Figure 5.24.

The structure of the monolayer is obviously lamellar, but the lamellae are not very regular. There is a local fluctuation in the direction of the lamella. In the close up

presented in the Figure 5.24B one can see that there is interdigitation of the alkyl chains and there is a blurry, brighter area that separates them. The lamella chirality measured in this image is -26.1º with respect to the main graphite axis, while the width of the lamellae is 3.8 nm, which is more than the length of the molecule (3.2 nm). The pure acid forms monolayers which run along the graphite axes, and therefore a clear change of structure is observed, possibly as a result of complexation with the diamine. The change of organization of the monolayer, together with the fact that the lamella size is larger than one molecule but much shorter than two indicates that the diamine is incorporated in the self-assembled monolayer, even if it is not imaged clearly. However more evidence is necessary to prove the formation of complex on the surface.

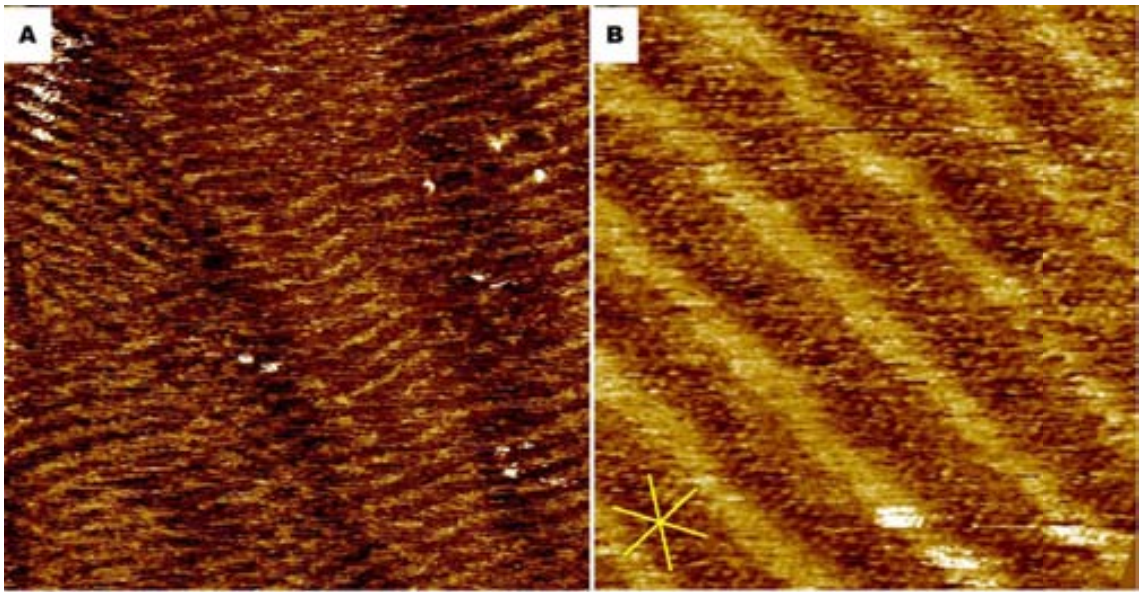

Figure 5.24: *STM images of upon premixing (R)-**1,4Ph** and (R,R)-DACH (1:1) at the 1-phenyloctane-HOPG interface. The total concentration of (R)-**1,4Ph** in solution was 6.2×10^{-3} M. (A: 96.4 x 96.4 nm; B: 18.2 x 19.7 nm; I_{set} = 0.7 nA; V_{set} = -0.5 V for both images). In image A the monolayer is observed, and a close up in image B.*

Also the diastereomeric complex of (*R,R*)-1,2-diaminocyclohexane and amphiphile acid (*S*)**-1,4Ph** was measured but no clear images were captured.

Therefore, it seems that the complex formed between **1,4Ph** and *trans*-1,2-diaminocyclohexane is not suited for the formation of stable monolayers on the surface of graphite. As no monolayer of **1,4Ph** was observed, it could be that the majority of molecules of acid is complexed in the solution, and this complex is not able to form stable structure on the surface of graphite, but more experiments are necessary to prove this hypothesis.

5.6 Diastereomer complexation experiments with other amines

The second series of experiments concerning the chiral recognition at the interface of graphite and 1-phenyloctane was dedicated to check the versatility and generality of the complexation at the interface by combining amphiphilic acids with various amines. The resorcinol derivative was chosen as the acid – because of its good selectivity and well behaved domain formation - and a variety of chiral amines were used, starting from a small ones (Figure 5.25) such as *cis*-1,2 diaminocyclohexane, *trans*-1,4 diaminocyclohexane, (*R*)-2-methylpiperazine and finishing with a chiral compounds used as a medicaments: Metoprolol, Atenolol and Verapamil were the molecules of choice here, their structure is presented respectively in Figure 5.30 and 5.41.

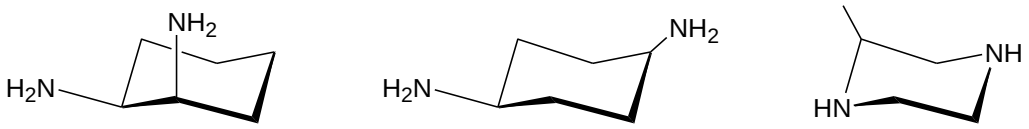

***cis*-1,2-diaminocyclohexane** ***1,4*-diaminocyclohexane** ***(R)-2*-methylpiperazine**

Figure 5.25: *Structure of cis-1,2-DACH and trans-1,4-DACH and (R)-2-methylpiperazine*

5.6.1 Self-assembly of (R)-1,3Ph and cis-1,2 diaminocyclohexane

The one to one mixture of *cis*-1,2-diaminocyclohexane and amphiphilic acid (*R*)-**1,3Ph** in 1-phenylocatane interface was deposited on graphite as in the previous cases. In this system the diamine is symmetric, because of the mirror plane that goes through the middle of molecule, however as there is always one axial and one equatorial amine group it can have, and has for most of the time, a chiral conformation. However, because of the low energetic barrier between the conformations it is impossible to separate the enantiomers at room temperature, the conformations convert one into the other constantly.

Upon deposition of *cis*-1,2-diaminocyclohexane and **1,3Ph** in phenyloctane on the graphite surface the formation of monolayer is observed by STM after a short while, although the structure is not very clear. In Figure 5.26 typical images are presented.

The structure is not very clear, but what can be observed are interdigitated alkyl chains and between them a blurry, bright area, which is not very straight. Domain

borders are not sharp at all. These features could be caused by the amine geometry; while one is attached to the acid lying in the monolayer another one could pointing out of this plane, and probably other molecules of acid are interacting with this molecule in an overlayer, which would cause noise in the STM image. To be able to prove this hypothesis images showing clearly areas with high resolution would be necessary, but under the conditions assayed such images were not forthcoming. In any case, the example serves to show the dramatic effect that stereochemistry can have on the structure and stability of the monolayers on graphite.

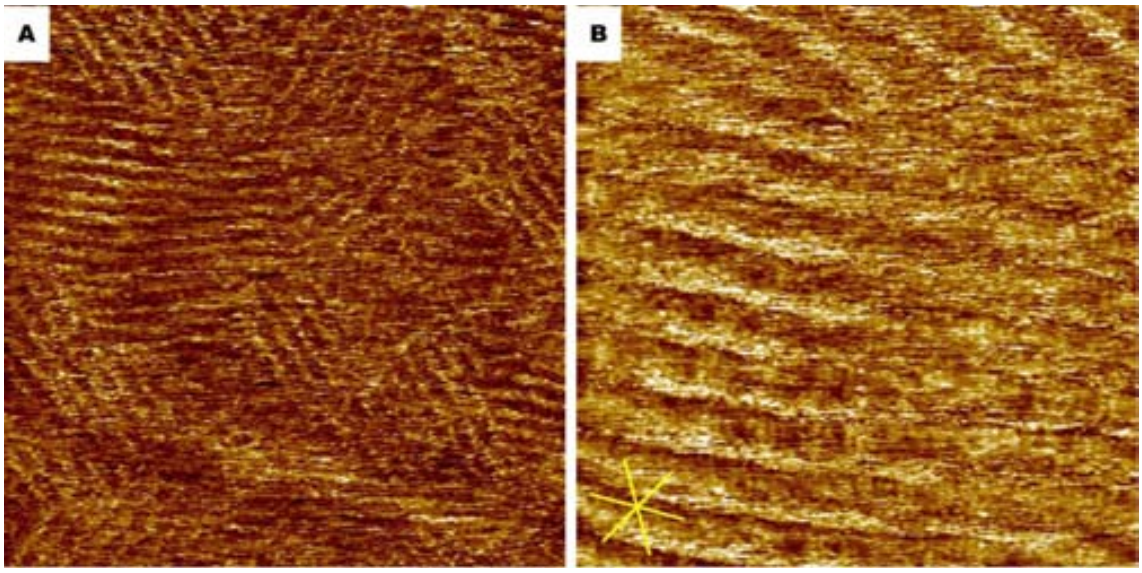

Figure 5.26: *STM images of monolayer showing (R)-**1,3Ph**/cis-DACH formed upon premixing (R)-**1,3Ph**, cis-DACH (1:1) at the 1-phenyloctane-HOPG interface. The total concentration of (R)-**1,3Ph** in solution was 6.2×10^{-3} M. (A: 96.4 x 96.4 nm; B: 24.6 x 24.6 nm; I_{set} = 0.7 nA; V_{set} = -0.5 V for both images).In image A one can observe the monolayer, composed by the small domains, and a close up in image B.*

5.6.2 Self-assembly of (R)-1,3Ph and trans-1,4-diaminocyclohexane

When the *trans*-1,4-diaminocyclohexane and (*R*)-**1,3Ph** mixture (1:1) in 1-phenyloctane was studied at the graphite surface well defined lamellae are formed. Figure 5.27 shows representative images. There is an obvious lamellar structure to the monolayer, with alkyl chains tilted by at approximately 50º with respect to the lamellar direction, which is quite straight. Slightly surprising is the gap between the lamellae, as seen in image in Figure 5.27B. It seems also that a multilayer system may be present, as

there are lamellae with different contrast (e.g. in Figure 5.27A there is an area where lamellae seem to overlay each other, although persistent noise aggravates good image taking).

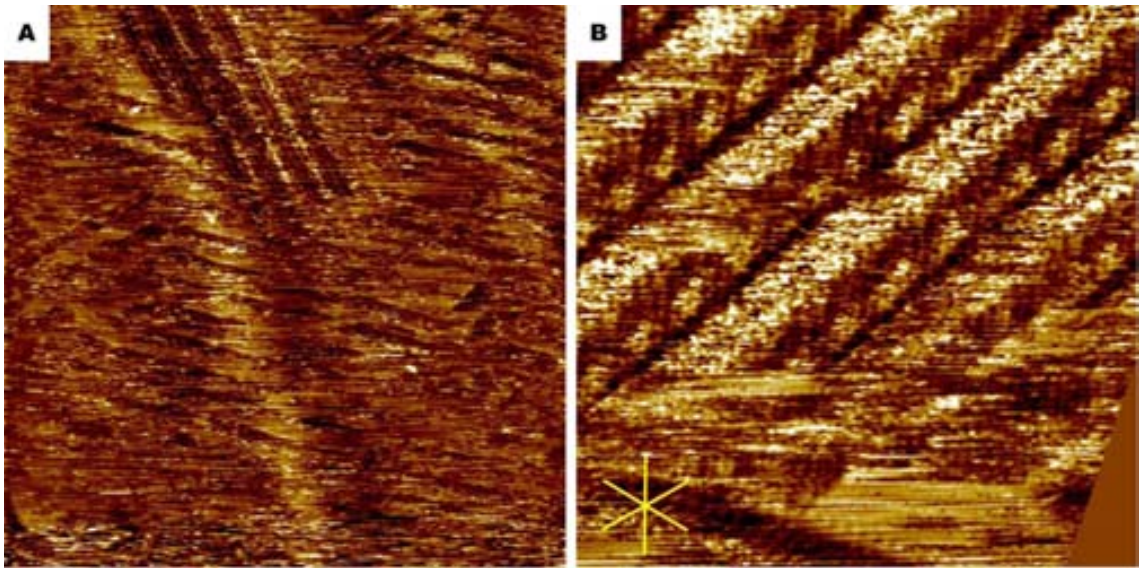

Figure 5.27: *STM images of monolayer showing (R)-**1,3Ph**/trans-1,4 DACH formed upon premixing (R)-**1,3Ph** and trans-1,4-DACH (1:1) at the 1-phenyloctane-HOPG interface. The total concentration of (R)-**1,3Ph** in solution was 6.2×10^{-3} M. (A: 90.4 x 90.4 nm; B: 23.3 x 23.3 nm; I_{set} = 0.7 nA; V_{set} = -0.5 V for both images). In image A the general view of the structure is presented, in the left part there is area where alkyl chains seems to cross with the other lamella. The different contrast in the lamella can be observed. In image B the close up of the structure is presented.*

The width of the lamellae formed in the monolayer is 5.19 ± 0.30 nm, the head to head distance is 0.66 ± 0.02 nm and the chirality of the layer with respect to the graphite reference axis is -13.5 ± 2.2°. The chiral twist of the lamellae with respect to the surface reference is therefore much greater than the pure acid, witnessing the clear formation of a complex (as does the width of the lamellae, only 3.7 nm for the pure acid), and is virtually the same as the complex formed with (*R,R*)-*trans*-1,2-diaminocyclohexane(5.29 nm).

Two other areas of the monolayer are shown in Figure 5.28 in close up. Although the parameters of both of them are very similar, the contrast of the molecules is distinct: The lamellae in the Figure 5.28A clearly have material on the top of them, which makes more than a half of the area of the lamellae blurry. In the image in Figure 5.28B there is also a blurry area where the aromatic parts and acid moieties lay, but the alkyl chains

are rather clear. The possible explanation of this phenomenon is that in the lamellae presented in image B, there are molecules of diamine adhered but wobbling on the top of the monolayer structure, while in image A, apart from these molecules, there are molecules of acid that get attached to the amine and are dislodged by the scanning tip during imaging.

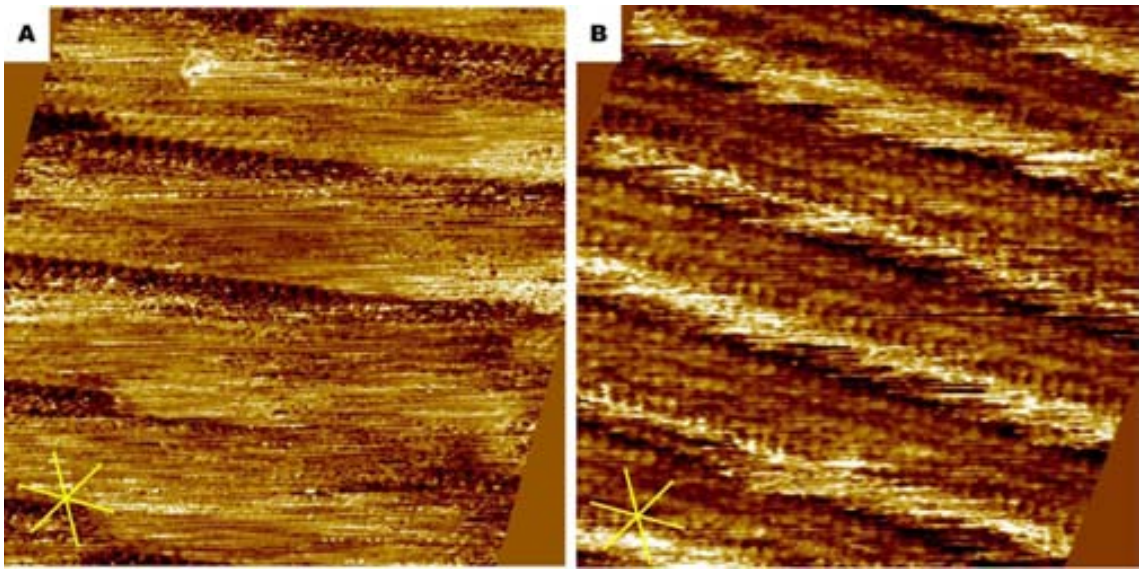

Figure 5.28: *STM images of monolayer showing (R)-**1,3Ph**/trans-1,4 DACH formed upon premixing (R)-**1,3Ph**, trans-1,4 DACH (1:1) at the 1-phenyloctane-HOPG interface. The total concentration of (R)-**1,3Ph**in solution was6.2×10^{-3} M. (A: 23.1 x 23.1 nm; B: 22.4 x 22.4 nm; I_{set} = 0.7 nA; V_{set} =-0.5 V for both images). The close up of two area shows the difference in the resolution, in image A only some of the alkyl chains can be observed, and in other areas the chains are covered, in image B the chains are clearly visualised, but the area where the head groups are located is very noisy.*

The formation of the monolayer of the complex of **1,3Ph** and the amine is evident in this experiment. Moreover there is some evidence for the formation of multilayers, but no high resolution images of the acid head groups and amine were captured, which might be caused either by movement of the molecules of amine during scanning or the interaction with the tip of the microscope with the layer. The monolayer appears very similar to the one formed by **1,3Ph** and *trans*-1,2-diaminocyclohexane and also the lamella width is almost the same 5.19 nm compared with 5.29 and 5.19 nm for either (*R*)-**1,3Ph**/(*R,R*) diaminocyclohexane or (*S*)-**1,3Ph**/(*S,S*) diaminocyclohexane.

5.6.3 Self-assembly of racemic 1,3Ph and (R)-2-methylpiperazine

The last of the series of experiments in this study of chiral recognition at the graphite surface for simple small amines involved the racemic resorcinol derivative **1,3Ph** and (*R*)-2-methylpiperazine. The racemic mixture of the amphiphile **1,3Ph** was used to check if there was a stereospecific interaction between it and the scalemic chiral amine. After deposition, some domains formed by molecules of acid **1,3Ph**, were observed, as presented in the Figure 5.29. Closer inspection of the images shows that the domain structure is not revealed clearly: There are places that distinguishing each molecule is very challenging. Also there are big disordered areas as in image A.

The problems with the stability of the monolayer and the tip precluded the registry of quality images, so a detailed description of the assembly cannot be given, although it is clear that the presence of the amine affects dramatically the organisation of the acid, because the images and behaviour are quite different to the pure material in which well-ordered domains are observed with no distortion of the STM images.

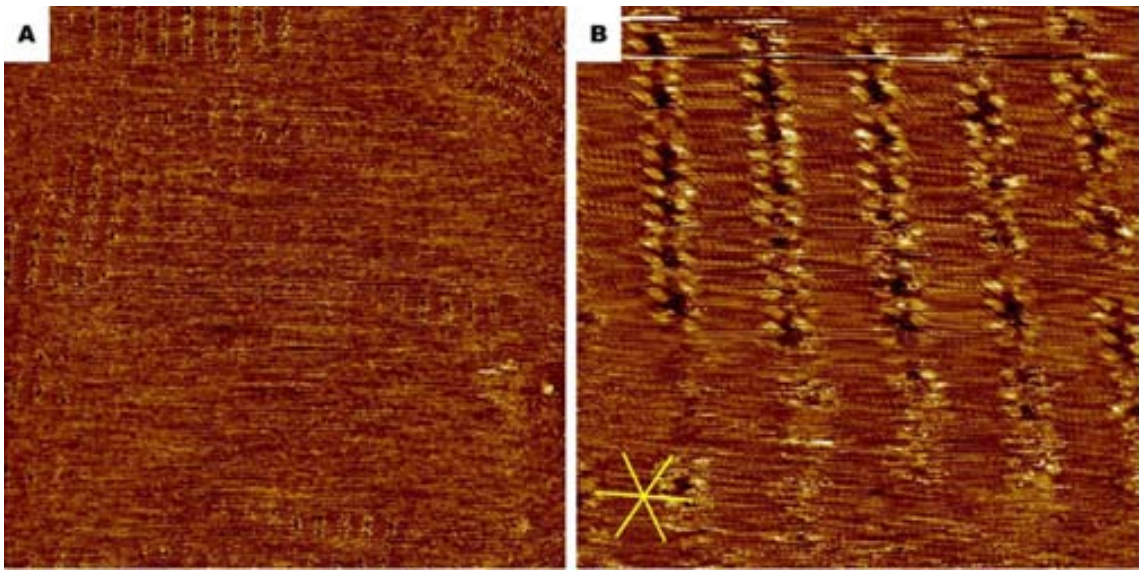

Figure 5.29: *STM images of monolayer showing (R)-**1,3Ph**/(R)-2-methylpiperazine formed upon premixing racemic-**1,3Ph**, (R)-2-methylpiperazine (1:1) at the 1-phenyloctane-HOPG interface. The total concentration of (R)-**1,3Ph** in solution was 6.2×10^{-3} M. (A: 90.4 x 90.4 nm; B: 20.1 x 20.1 nm; I_{set} = 0.7 nA; V_{set} = -0.5 V for both images). The general view of the self-assembly monolayer is presented in image A, where ordered and disordered area can be observed. Close up in image B, where some changes in the contrast are clear.*

5.6.4 Self-assembly of (S)-1,3Ph and Metoprolol

After showing that the amphiphilic derivative **1,3Ph** interacts with a variety of small amines, it was decided to check the abilities of chiral recognition on the surface of more complex molecules: Metoprolol was chosen, as it is a polyfunctional molecule of interest. It is a medicament used in the treatment of hypertension; it acts as a beta blocker (a medicine that blocks the receptors of adrenaline). The molecule is important for two reasons: it is available only as a racemate or a salt of racemate, and it has amine relatively close to the stereogenic centre. The structure of Metoprolol and Adrenaline are shown in the Figure 5.30.

The racemic Metoprolol used for experiments was bought (from Sigma Aldrich) as a salt of (+)-tartaric acid, and to obtain the free-base amine, the salt was dissolved in dichloromethane and the acid was extracted with an aqueous solution of sodium hydroxide. The organic phase was dried and evaporated to obtain racemic Metoprolol as colourless oil. The NMR analysis confirmed the structure.

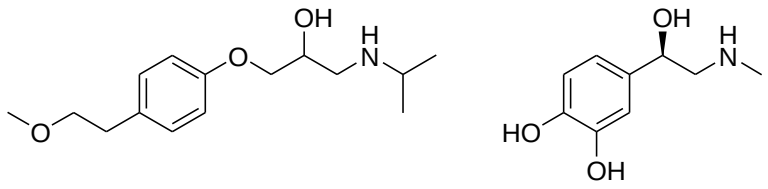

Metoprolol **Adrenaline**

Figure 5.30*. Structure of Metoprolol and Adrenaline, it can be seen that in both of molecules the stereogenic centre is two atoms away from amine.*

The mixture of amphiphilic acid (*S*)-**1,3Ph** and the racemic Metoprolol in 1-phenyloctane was deposited on the freshly prepared surface of graphite, and after 20 minutes a monolayer was observed with STM. The surface was covered with large domains spreading over thousands of square nanometres. The lamellae of this layer are straight, with alkyl chains tilted with respect to the lamella growth direction and the aromatic part is brighter in the middle of lamellae (Figure 5.31). The alkyl chains of two parallel rows are not interdigitated, but they are touching at their ends.

The lamellae formed are 5.07 ± 0.17 nm wide and the head to head distance (Figure 5.32) is 0.65 ± 0.04 nm. The chirality with respect to the graphite main axis is +13.0 ± 5.1° and the complex is Z-shaped. There is a curious effect evident in the image 5.32B, the change of the contrast in the unpaired lamella; the lower part is much better defined

than the upper one (this is not an effect of the tip otherwise the other lamellae should also be observed in the same way). Also it is worth comparing the contrast between the monolayer in images A and B, as in image B there is much more noise, just on the top of the aromatic head groups. It might be an indication that there are molecules attached to the monolayer that are not positionally stable enough to be visualised with STM.

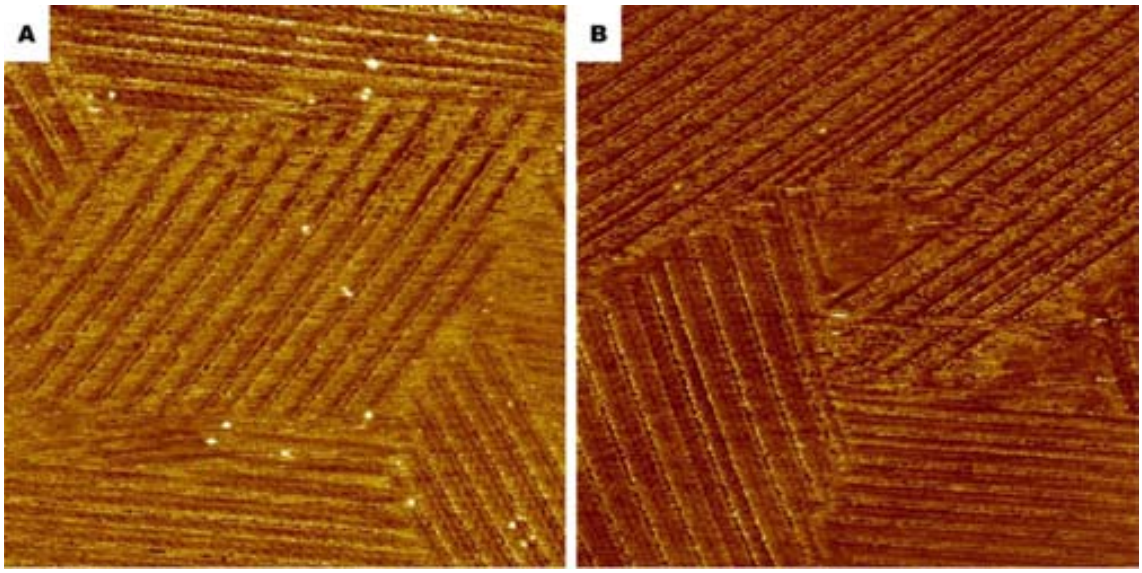

Figure 5.31: *STM images of monolayer showing (S)-**1,3Ph**/rac-Metoprolol(1:1) formed upon premixing at the 1-phenyloctane-HOPG interface. (A: 96.4 x 96.4 nm; B: 90.4 x 90.4 nm; I_{set} = 0.7 nA; V_{set} = -0.5 V for both images). The general view of the self-assembled monolayer in both of the images, in image B there is a curious defect in the domain; the lamella that starts above the centre of the image and goes close to the top left corner is much thinner than the rest of the lamellae.*

An unpaired lamella can be observed in Figure 5.32, a feature that is observed in almost every image. The so-called unpaired lamella is approximately 2.2 nm wide, alkyl chains are directed in the same way as the alkyl chains of the other lamellae. Probably the molecules of the resorcinol derivative **1,3Ph** in this unpaired lamella form a 1:1 complex through the hydrogen bond which blocks the possibility to interact between two molecules of resorcinol. In Figure 5.33 the proposed complex is presented.

Another interesting property of the structure observed in this system is the formation of multilayers, as presented in the Figure 5.34. In image A there is quite difference in contrast between the upper and lower layer. The formation of multilayer is not as surprising, when the structure of the Metoprolol is considered. As it was presented in the Figure 5.33 the hydrogen bonds probably are formed between the amine and

asymmetric hydroxyl of the compound, but the other two oxygen atoms are free to form hydrogen bonds. This property of the molecule might explain the changes in the contrast in Figure 5.32B, where noise appears just above some layers. It is possible that in those areas molecules of **1,3Ph** binds atop of the first layer and this way second layer starts forming.

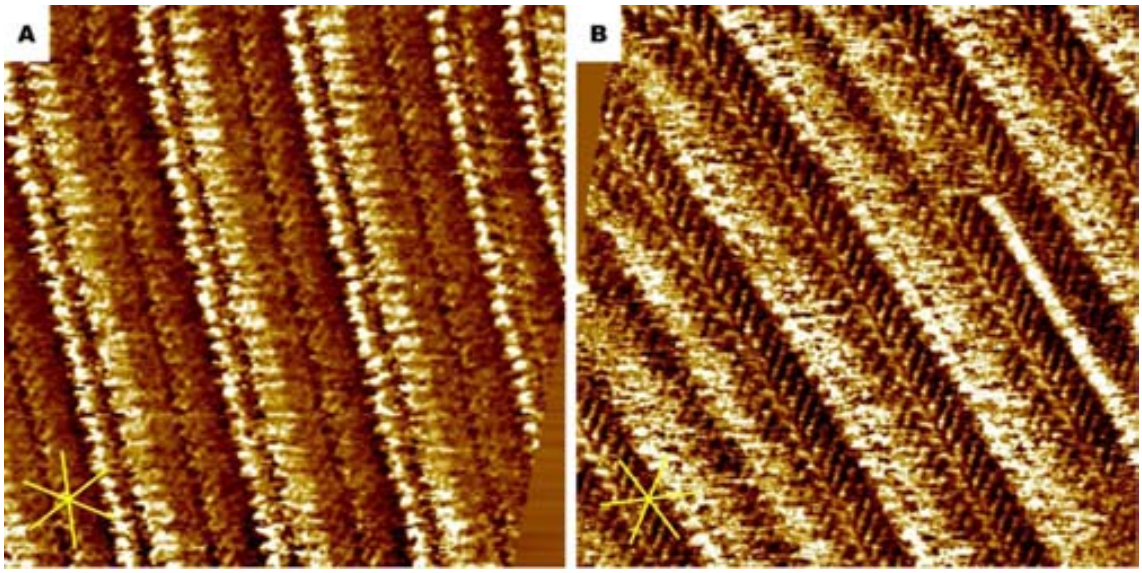

***Figure 5.32**: STM images of monolayer showing (S)-**1,3Ph**/rac-Metoprolol (1:1) formed upon premixing at the 1-phenyloctane-HOPG interface. (A: 20.0 x 20.0 nm ; B: 22.4 x 22.4 nm; I_{set} = 0.7 nA; V_{set} = -0.5 V for both images). The close up of the self-assembled monolayer in both of the images, in image A there is an "unpaired" lamella on the right of the image. In image B the same defect is in the lamella close to the top right corner.*

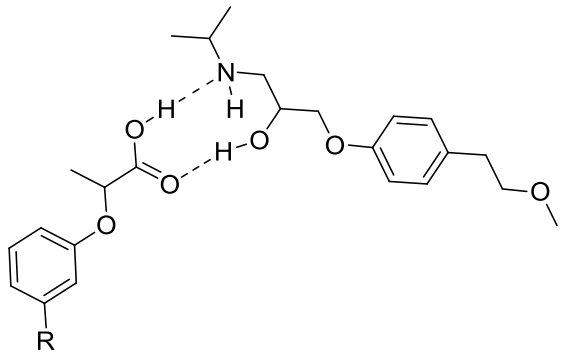

***Figure 5.33** The proposed structure of 1:1 complex between molecules of Metoprolol and acid **1,3Ph**.*

After performing the experiment with racemic Metoprolol, it was clear that there is some interaction between the acid **1,3Ph** and the drug molecule. To determine the nature

of the complex, it was decided to check separately the enantiomers of Metoprolol with the resorcinol derivative. To prepare optically pure compound preparative chiral HPLC was used as described previously,[52] and separated enantiomers were used for the study on the surface.

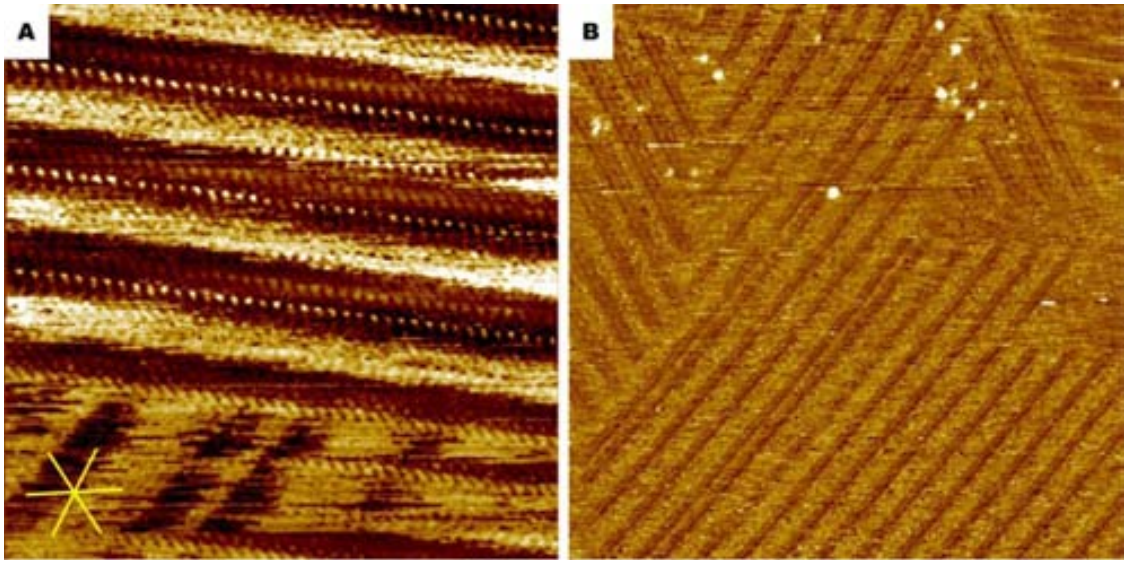

Figure 5.34: *STM images of monolayer of (S)-**1,3Ph**/rac-Metoprolol(1:1) formed upon premixing at the 1-phenyloctane-HOPG interface. (A: 26.3 x 26.3 nm; B: 90.4 x 90.4 nm; I_{set} = 0.7 nA; V_{set} = -0.5 V for both images). In image A the layer below is on the bottom part of the image, and in the right of the image the alkyl chain of upper part are clearly overlaying the structure. In image B there is lamella in the upper right corner of the image that is covered partially by the one that occupies the majority of the image.*

As the mixture of the (*R*)-**1,3Ph** and the (*R*) Metoprolol was deposited at the liquid solid interface, a monolayer was observed that was similar to the racemic mixture with large domains observed all over the surface. Figure 5.35 shows representative images of the self-assembled layer.

In the experiment some images were captured with clear evidence that the complex is capable of forming multilayers on the surface, as presented in the Figure 5.36.

[52] K. H. Kim,S. D Shin, J. H. Lee, S. C. Lee, J. S. Kang, W. Mar, S. P. Hong, H. J. Kim, *Arch. Pharm. Res.,* **2000**, *23*, 230.

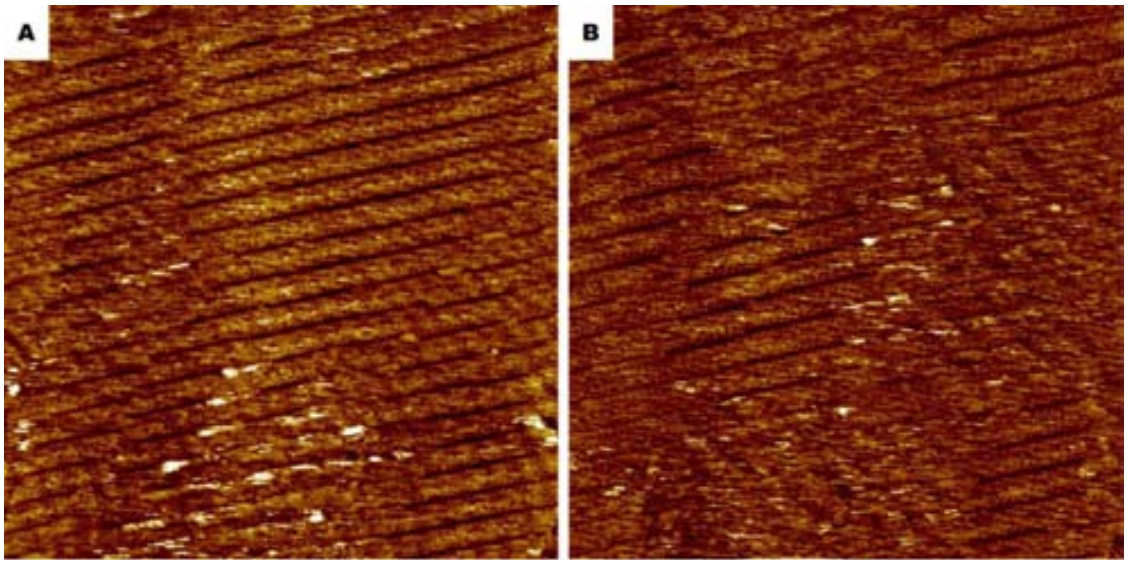

Figure 5.35: *STM images of monolayer of (R)-**1,3Ph**/(R)-Metoprolol(1:1) formed upon premixing at the 1-phenyloctane-HOPG interface. (A: 94.2 x 94.2 nm; B: 81.2 x 81.2 nm; I_{set} = 0.7 nA; V_{set} = -0.5 V for both images). In image A there is boundary area crossing the image from the top to the bottom left from the centre, where the lamellae from the right are not connecting to the left ones. In image B, a shadow of the layer that is lying below the one visualised in the right part of the image can be observed. Also the lamellae in the right upper corner have a defect – a kind of step in the alkyl chains.*

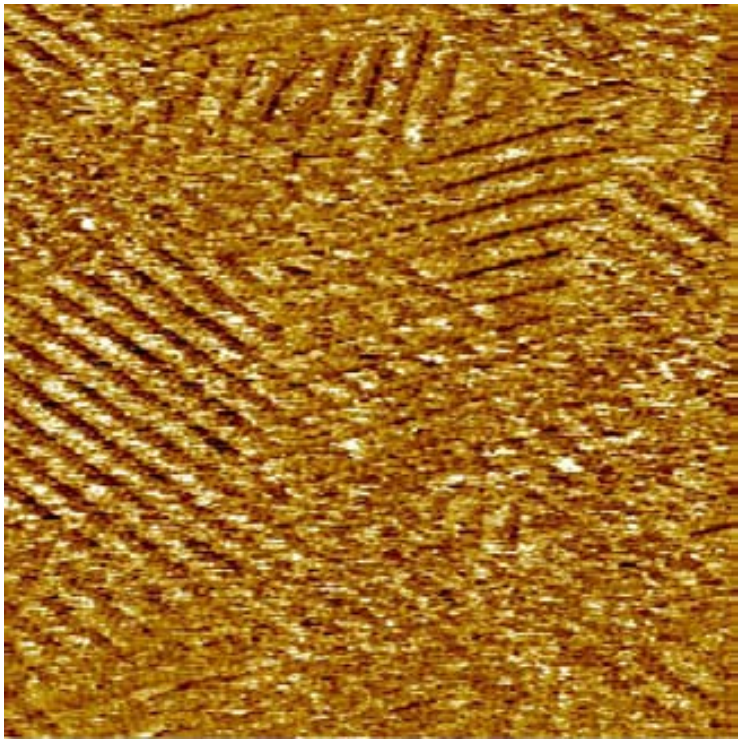

Figure 5.36: *STM image of monolayer showing (R)-**1,3Ph**/(R)-Metoprolol(1:1) formed upon premixing at the 1-phenyloctane-HOPG interface. (102.5 x 102.5 nm; I_{set} = 0.7 nA; V_{set} = -0.5 V). In the central part of the image the crossing lines indicates formation of multilayer.*

In Figure 5.37 close-up images of the monolayer are shown, evidencing the high resolution in the alkyl chains and the poorly resolved area around the polar region of the lamellae. What is surprising, compared with the other complexes of acid **1,3Ph** and amines on the surface, is that the alkyl chains clearly form pairs. The distance between the pairs is 1.11 ± 0.02 nm, which is less about 20% less than the double distance between the alkyl chains in the analogous structure like acid (*R*)-**1,3Ph** with amine (*R,R*)-diaminocyclohexane (in this SAM, the distance between alkyl chains equals 0.66 ± 0.03 nm).

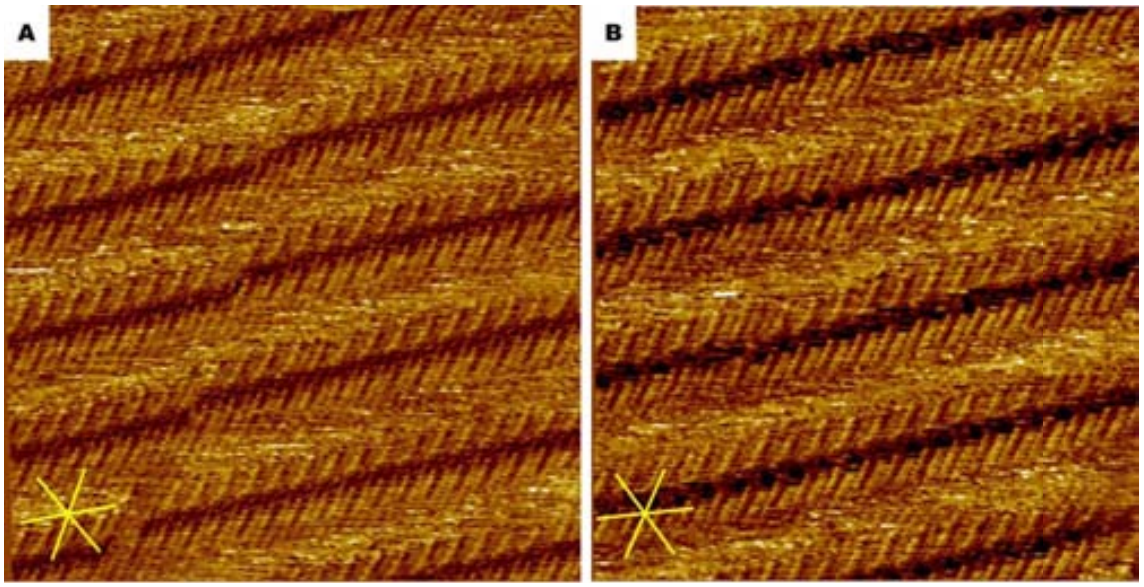

Figure 5.37: *STM images of monolayer showing (R)-**1,3Ph**/(R)-Metoprolol(1:1) formed upon premixing at the 1-phenyloctane-HOPG interface. (A: 19.8 x 19.8 nm; B: 20.2 x 20.2 nm; I_{set} = 0.7 nA; V_{set} = -0.5 V for both images) In image A there is surprising step in the lamellae. Also what is unexpected, that unlike the other structures seen, in this case the alkyl chains are paired. In image B it is shown, that in the paired alkyl chains one chain is always longer than the other. In the top lamella in the centre there is a defect, three alkyl chains joined together.*

The lamella formed is 4.97 ± 0.22 nm wide and the lamellar chirality with respect to the graphite main axis is -11.2 ± 1.8° and the complex is S-shaped. The lamella width is similar to the one obtained in experiment with (*S*)-**1,3Ph** and racemic Metoprolol (5.05 ± 0.17 nm), and the chirality has almost the same value, but with opposite sign (+13.0 ± 5.1°), as expected, since the other enantiomer of acid was used in this experiment. The only difference apart from rotation direction is the appearance of alkyl chain, in the experiment with (*R*)-**1,3Ph** and (*R*)-Metoprolol the alkyl chains comes in pairs what was not observed in the experiment of (*S*)-**1,3Ph** and racemic Metoprolol. Also the

"unpaired" lamella observed quite often in the sample of racemic Metoprolol are absent in the mixture of (*R*) acid with (*R*)-Metoprolol.

The (*S*) enantiomer of Metoprolol was mixed with acid (*R*)-**1,3Ph** in order to check if there is a diastereoselectivity in complex formation at the graphite 1-phenyloctane interface. After deposition within few minutes a monolayer could be observed. In this case the domains are not so large, there are a lot of defects and changes in the direction of lamellae. In Figure 5.38 typical images are presented. It can be observed that although majority of the monolayer is comprised of wide lamellae (with the alkyl chains not interdigitated and the aromatic area of the molecules blurry), there can still be observed quite a number of areas that are composed exclusively by molecules of acid (*R*)-**1,3Ph**.

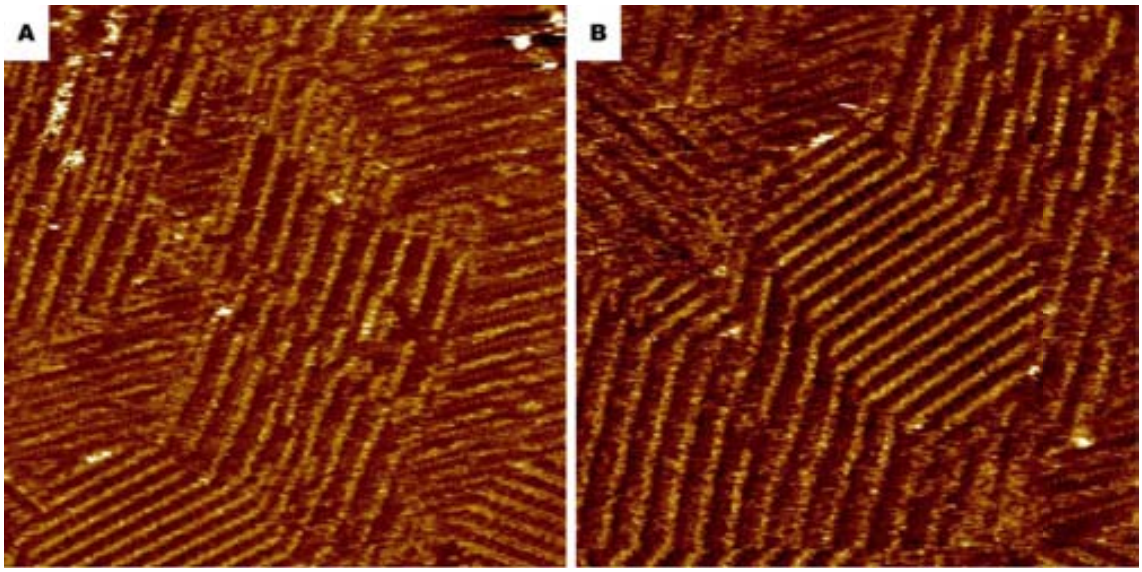

Figure 5.38: *STM images of monolayer showing general view of the self-assembly monolayer of (R)-**1,3Ph**/(S)-Metoprolol(1:1) formed upon premixing at the 1-phenyloctane-HOPG interface. (A: 96.9 x 96.9 nm; B: 96.9 x 96.9 nm; I_{set} = 0.7 nA; V_{set} = -0.5 V for both images). In the bottom of image A on the right and in the left down corner of the image are domains composed exclusively by molecules of acid **1,3Ph**. The rest of the domain in the image is a complex of **1,3Ph** and Metoprolol. In image B the domain in the centre with a narrow lamella is one made by acid **1,3Ph**.*

In the course of the experiment it was observed that the domains composed by acid **1,3Ph** are less stable than the domains of the complex. In some areas in a few minutes the process of desorption of molecules of acid and absorption of complex could be completed. In the Figure 5.39 there is an example of the process.

In Figure 5.40 the close-ups of the structure are presented. The parameters of this monolayer formed by complex of (*R*)-**1,3Ph** and (*S*)-Metoprolol on the surface are: 4.83 ± 0.43 nm width of lamella, rotation with respect to the main graphite axis [0010] is -8.9 ± 4.7°.The alkyl chains are doubled and separated by 1.18 ± 0.05 nm are forming S-shaped dimers. The angle between alkyl chain and lamella growth direction is 49.9 ± 2.7°. The values are similar to the parameters of self-assembly monolayer formed by (*R*)-**1,3Ph** acid with (*R*)-Metoprolol. The second type of lamellae, where head-groups appears as bright dots and alkyl chains are interdigitated were 3.57 ± 0.20 nm wide and chirality equals +4.9 ± 2.8°. These parameters and arrangement of molecules is similar to the monolayer formed exclusively by dimers of (*R*)-**1,3Ph** (3.68 ± 0.20 nm, -4.0 ± 1.9°), but the chirality is opposite to the one observed for (*R*)-**1,3Ph**. This reminds situation observed for the mixture of (*R*)-**2,7Naph** and (*S*,*S*)-diaminocyclohexane, where the amine induce switch of the chirality of the monolayer not taking part in the complex (see 5.3 section of this chapter).

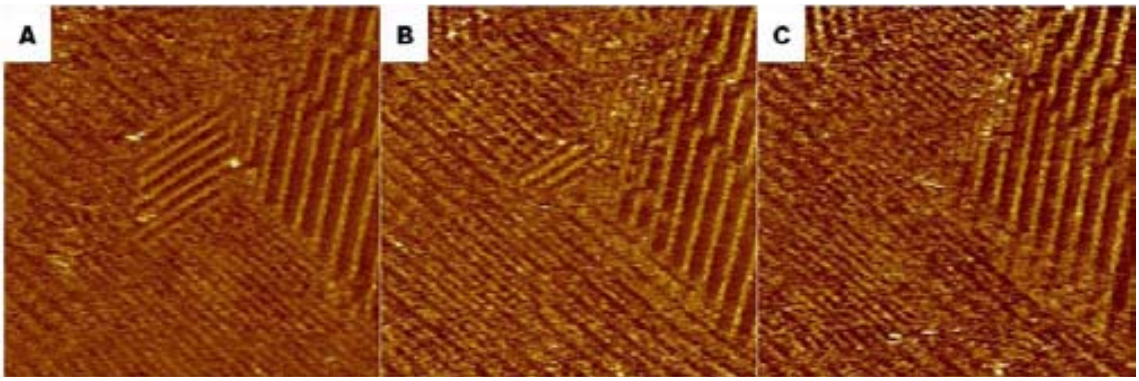

Figure 5.39: *STM images of monolayer showing (R)-**1,3Ph**/(S)-Metoprolol(1:1) formed upon premixing at the 1-phenyloctane-HOPG interface. (92.9 x 92.9 nm; I_{set} = 0.7 nA; V_{set} = -0.5 V for all of the images). Images were captured every 64 seconds. The domain of acid **1,3Ph** in the centre of the image is substituted by the complex of acid **1,3Ph** and Metoprolol.*

In the Table 5.5 there is comparison of parameters observed in experiments with Metoprolol. It is clear that the complex of **1,3Ph** and Metoprolol might be formed between any combination of chirality of these molecules, but the observation of dimers of uncomplexed acid (*R*)-**1,3Ph** on the surface in the experiment of (*R*) acid and (*S*)-Metoprolol and in general smaller and more disordered domains of complex is an indication that complex of (*R*) acid with (*S*) amine is not as strong or it is not forming as stable monolayer on the graphite as the other combination. Also the fact that the

structure observed in the sample of (*S*)-**1,3Ph** with racemic Metoprolol is the mirror image of the structure observed for (*R*)-**1,3Ph** and (*R*)-Metoprolol gives us the hint that this combination is more stable than the other, assuming that what is observed is the most stable structure in given condition.

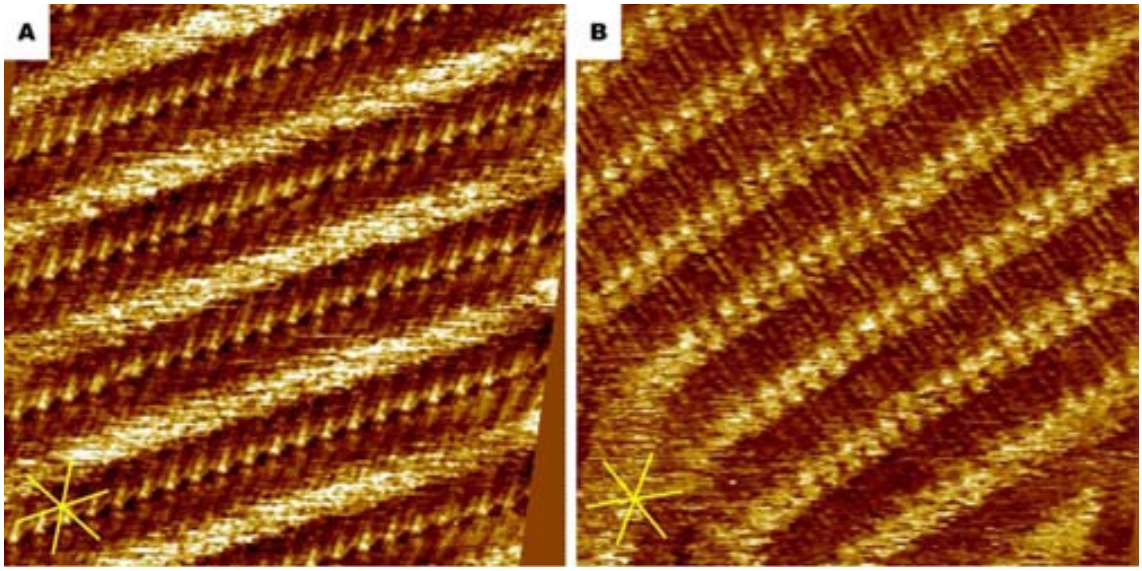

Figure 5.40: *STM images of monolayer showing (R)-**1,3Ph**/(S)-Metoprolol(1:1) formed upon premixing at the 1-phenyloctane-HOPG interface. (A: 23.5 x 23.5 nm; B: 22.1 x 22.1 nm; I_{set} = 0.7 nA; V_{set} = -0.5 V for all of the images). Image A shows the domain of complex of acid (R)-**1,3Ph** and (S)-Metoprolol. In image B the domain of (R)-**1,3Ph*** is observed.

Table 5.5*: Comparison data from different experiments with Metoprolol.*

	Lamella width [nm]	Head to head distance [nm]	Chirality	S/Z shaped
(*S*)-**1,3Ph**/rac-Metoprolol	5.05 ± 0.17	0.65 ± 0.04	+13.0 ± 5.1	Z
(*R*)-**1,3Ph**/(*R*)-Metoprolol	4.97 ± 0.22	1.11 ± 0.02*	-11.2 ± 1.8	S
(*R*)-**1,3Ph**/(*S*)-Metoprolol	4.83 ± 0.43	1.18 ± 0.05*	-8.9 ± 4.7	S
	3.57 ± 0.20	ND**	+4.9 ± 2.8	-***
(*R*)-**1,3Ph**	3.68 ± 0.20	0.98 ± 0.03	-4.0 ± 1.9	-***

*Chirality was measured with respect to the [0010] graphite axis. *Head to head distance is measured for doubled molecules. **Not determined, due to the limited number of high quality images of this kind of domain. ***dimers are perpendicular to the lamella growth direction*

5.6.5 Other experiments

Also experiments with mixtures of (*R*)-**1,3Ph** and, respectively, Atenolol and Verapamil in 1-phenyloctane (molar ratio was 1:1 in both cases) were performed. In Figure 5.41 the structure of the compounds is presented. In both cases a racemic mixture of the amine was used as free base. In order to liberate the hydrochloride salt of Verapamil, it was dissolved in water solution of sodium hydroxide and the organic compound was extracted with dichloromethane three times. The graphite with the drop of the mixture of acid and amine was placed in the microscope, but no formation of monolayer in either of the samples was registered. This observation, leads to conclusion that the acid interacts stronger with those molecules than with the surface, and in this way there are no molecules in the solution that are able to form stable monolayer on the surface. At the same time the complex formed by those molecules is more stable in solution than on the surface, what might be caused by conformation that is not compatible with flat surface (i.e. is not flat and alkyl chain is not able to interact with the surface on the whole length), or conformation of the complex is not able to form dense packed monolayer. It might be that there is complex absorbed on the surface, but due to the steric issues it is not able to pack a stable monolayer, and because of that molecules are moving on the surface during STM experiment.

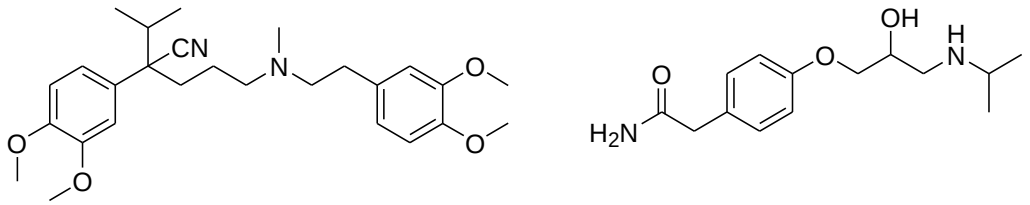

Verapamil **Atenolol**

Figure 5.41: *Structures of the Verapamil and Atenolol.*

5.7 Conclusions

Pasteurian diastereomeric resolution has been achieved at the liquid-solid interface in an equilibrating system thanks to the appropriate design of a resolving agent capable of interacting with the surface. The STM imaging provides clear evidence for the (competitive) formation and adsorption of diastereomeric complexes at the liquid-solid

interface. This approach allows enantioselective adsorption of one of the enantiomers at the liquid-solid interface. Chiral resorcinol derivative **1,3Ph** spontaneously resolves at the graphite-solvent interface, a feature which allows the study of its diastereomeric complexes with the *trans*-1,2-diaminocyclohexane, which co-adsorbs with **1,3Ph** in an enantioselective way. At a 2:1 molar ratio, the **1,3Ph**-diaminocyclohexane-**1,3Ph** trimer structures only appear for the homochiral combination. The resorcinol derivative can resolve in an enantioselective way a racemic mixture of chiral diaminocyclohexanes at the interface, thanks to the better formation of mixed hydrogen bonds between the corresponding enantiomers at the contact between the rows of adsorbed resorcinol and diamine molecules. Upon premixing the resolving agent (the resorcinol derivative) with the racemic mixture (the diaminocyclohexane), exclusively one of the diaminocyclohexane enantiomers is adsorbed as a diastereomeric complex on the achiral graphite substrate. The other enantiomer is left in solution. This discovery bodes well for the development of studies of diastereoselective phenomena at interfaces to deepen understanding of interfacial diastereomer complexes and their possible exploitation. The observation of Pasteurian resolution at an interface also opens the opportunity for the study of more complex resolution phenomena under similar conditions in dynamic systems. The results presented show the potential for STM to probe stereochemical processes usually associated with much larger scales, giving sub-molecular level information.

It has been proved also the molecular recognition at the graphite-1-phenyloctane interface between the homochiral combination of acid **2,7Naph** and diaminocyclohexane. Moreover there is evidence that this system is capable of forming multilayers. On the other hand, when diaminocyclohexane has opposite chirality than acid **2,7Naph**, it produces switch of the chirality of the monolayer of acid at the graphite-liquid interface. The experiments with **1,5Naph** and **1,4Ph** did not yield in any new structure, however no typical monolayer of uncomplexed molecules of acid were observed, what is clear indication that amine inhibits formation of most stable monolayer of those molecules at graphite- 1-phenyloctane interface.

It has been shown that the **1,3Ph** is able to form stable complex on the graphite-1-phenyloctane interface with both *cis* and *trans*-1,2-diaminocyclohexane, *trans*-1,4-diaminocylcohexane and with Metorpolol , moreover it is clear that there is some kind of interaction with all of the studied molecules, yet still more experiments need to be

performed to determine whether there is chiral recognition with all of the studied molecules. It should be pointed out that even in the case of (*R*)-2-methylpiperazine, Verapamil and Atenolol where no complex structure were found on the graphite surface, the chiral recognition in solution might take place. The experiments with Metoprolol proved that the chiral recognition with multifunctional and larger molecule can also take place, although there is not 100% selection of enantiomer there is preferential binding of one of them on the surface.

Chapter 6

Mixtures of amphiphilic acids as resolving agents at the graphite solvent interface

6.1 Introduction

The family technique for separation of enantiomers through salt formation – Dutch Resolution – is a powerful method because it increases the separation success rate in diastereomeric crystallisation.[53] Several possible explanations for the process exist, but a molecular level view of separation would help enormously to understand and allow a rational approach. Therefore, the family of acids used for diastereomeric recognition individually on the graphite surface were measured under Dutch resolution-type conditions under the same conditions. To do these experiments a mixture of structurally similar molecules will be used as a resolving agent. In our case the family of amphiphilic acids **2,7Naph**, **2,6Naph** and **1,5Naph** was the candidate, as the members of family are very similar in shape and the structures on the surface formed at the graphite 1-phenyloctane interface are similar in organisation, yet each form distinct monolayers. The experiments with mixtures of acids at the graphite surface described in Chapter 4 prove that the molecules can form mixed monolayers, and act as a structural reference point for the experiments described herewith. For this reason they are good candidates for a resolving agent family, as each of them can act differently in forming a monolayer on the graphite surface. The main objective of this study is to prove whether the mixtures of acids can improve chiral recognition on the surface.

6.2 General procedure

For the experiments a stock solution of all acids in 1-phenyloctane was prepared with the same concentration (3.0 mg/mL, 6.5 mM) as well as solutions of both enantiomers of *trans*-1,2 diaminocyclohexane (DACH) in 1-phenyloctane (8.0 mg/mL, 70 mM). For preparing the samples with the molar ratio 1:1:1, 20 µL of each acid and 2.0 µL of DACH solution was used, in a manner that the mixed sample concentration of each acid

[53] T. Vries, H. van Echten, J. Koek, W. ten Hoeve, R. M. Kellogg, Q. B. Broxterman, A. J.Minnard, S. van der Sluis, L. Hulshof, J. Kooistra, *Angew. Chem. Int Ed.*, **1998**, *37*, 2249.

was 3.1 mM and the concentration of DACH was 3.3 mM. The heated solutions of acid were premixed with DACH in Eppendorf vial and then applied to recently cleaved HOPG. As before, STM images were registered at room temperature with the Pt/Ir tip immersed in the solution.

6.3 Self-assembly of (R)-2,7Naph (S)-1,5Naph (R,R)-DACH

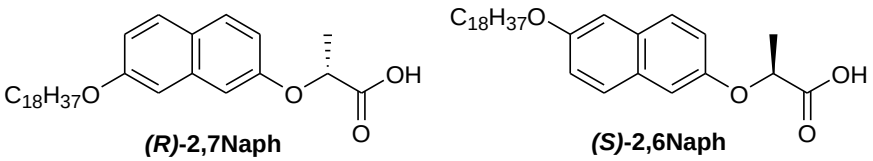

***(R)*-2,7Naph** ***(S)*-2,6Naph**

The mixture of acid (*R*)-**2,7Naph** and (*S*)-**1,5Naph** with (*R,R*)-DACH was studied on the surface of graphite in the same way as the diastereomeric complexes. In this complex mixture, the first domains formed within 20 minutes after deposition, and typical images are presented in Figure 6.1.

In this sample there is a quite complex situation where three different types of domains coexist at the graphite 1-phenyloctane interface (Figure 6.1A). One domain type is apparently composed exclusively by the pure acid (*R*)-**2,7Naph** which is not too large (approximately 20 x 20 nm); the biggest one found did not exceed a few hundred molecules. The width of the lamellae are 3.8 ± 0.4 nm, a value very close to that for the acid (*R*)-**2,7Naph** on its own (3.56 ± 0.20 nm). The chirality of the structure found in this mixed layer with respect to the main graphite axis is +0.6 ± 1.3°, compared with -7.4 ± 3.4° for the pure compound system, which at first sight is a bit surprising. However, the molecules of acid (*R*)-**2,7Naph** form S-shaped dimers on the surface in the case of the mixture, while in the sample of same acid measured on its own there is a Z-shaped dimer on the surface, similar effect of change of chirality was observed in the mixture of (*R*)-**2,7Naph** with (*S,S*)-DACH , described in Chapter 5. Therefore the diastereomeric inversed conformational chirality is present in the domain of this acid on the surface in the case of the mixture of acids with DACH . It should be pointed out that this well ordered domain is not isolated, but connects with less ordered areas with no clear break or jump in the lamellae except in terms of resolution (Figure 6.1 B). At the same time in the mixed acid sample (described in Chapter 4) no domain of this type was observed, while typical, Z-shaped SAM of (*R*)-**2,7Naph** was present. It is somehow

unexpected to find this kind of inverted structure in the mixture of two acids with amine, while neither in the mixture of those acids nor in the mixture of acid **2,7Naph** and DACH of given chirality this kind of arrangement was observed. The formation of this kind of inverted domain of acid **2,7Naph** seems to be strongly influenced by boundaries, the reversed domains converts smoothly into mixed domains as seen in the Figure 6.1B. As the other compound is acid **1,5Naph** of opposite chirality its influence has to result in inverted domain of (*R*)-**2,7Naph**.

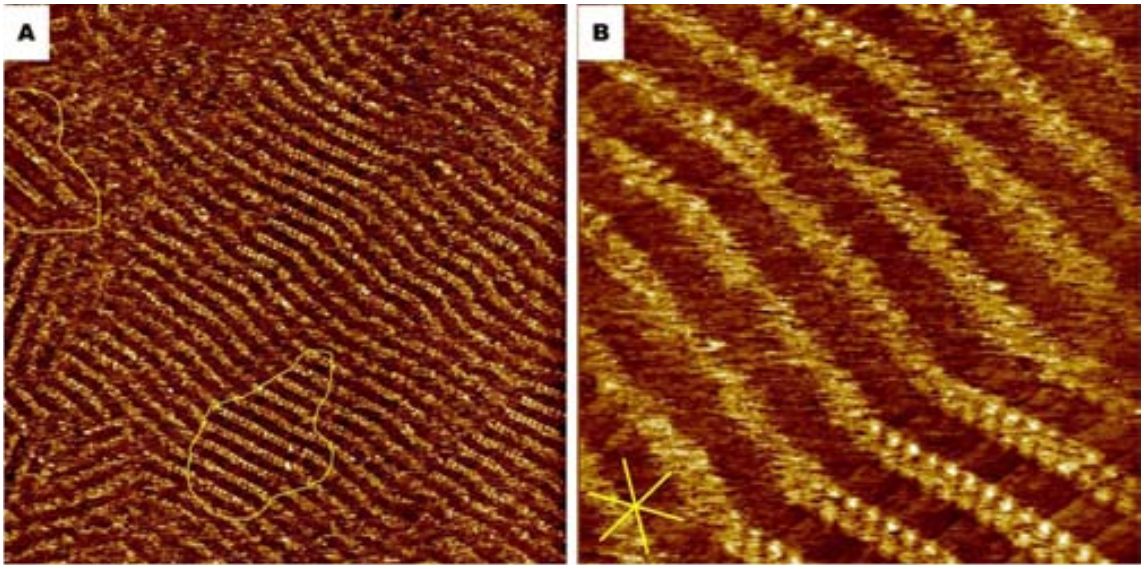

Figure 6.1: *STM images of the monolayer formed upon premixing (R)-**2,7Naph**, (S)-**1,5Naph** and (R,R)-DACH (1:1:1) at the 1-phenyloctane-HOPG interface. The concentration of each molecule in solution was 3.1 mM. (A: 100.0 x 100.0 nm; B: 26.9 x 26.9 nm; I_{set} = 0.2 nA; V_{set} = +0.8 V for both images). Image A shows a general view of the area, it can observed that there is a domain that is in parts very regular, with each bright spot a head group of the amphiphiles acid, one example is marked at the bottom of the image. At the same time this very well defined domain converts smoothly into a blurry domain that is not perfectly straight and each molecule cannot be distinguished. The close up of such an area – transition from very well ordered structure into the disordered to a certain level domain – is presented in image B. In image A at the left edge of the image area where the complex of acid (R)-**2,7Naph** and DACH (R,R)-DACH is marked.*

The second type of domain found in this mixture is composed of the molecules of both acids, as shown in the Figure 6.2. This type of structure extends over hundreds of nanometres in every direction as shown in the image in Figure 6.2A. The lamellae are generally straight, but locally they can change the direction of growth apparently at random. The region is characterised by interdigitation of the alkyl chains which are well

ordered and well resolved, and a lack of resolution of the aromatic part of the molecules, as presented in the Figure 6.2B. In some areas it was not possible to observe the alkyl chains as in the Figure 6.1B, but the image resolution in the region of the aromatic head groups is very poor, an effect that might be caused by the interaction of the acidic moieties with molecules of the DACH . This situation is curious for this type of molecule, in that in calamitic liquid crystals the chains are disordered and the head groups are better organised. In the present case, the octadecyl chain's interaction with the crystalline substrate means that an order is maintained in this segment of the molecule while the head group is left to adapt to the space it encounters in the mixed layer, leading to a dynamic situation. The mixed acid domain can convert smoothly into the domain of apparently pure acid (*R*)-**2,7Naph**.

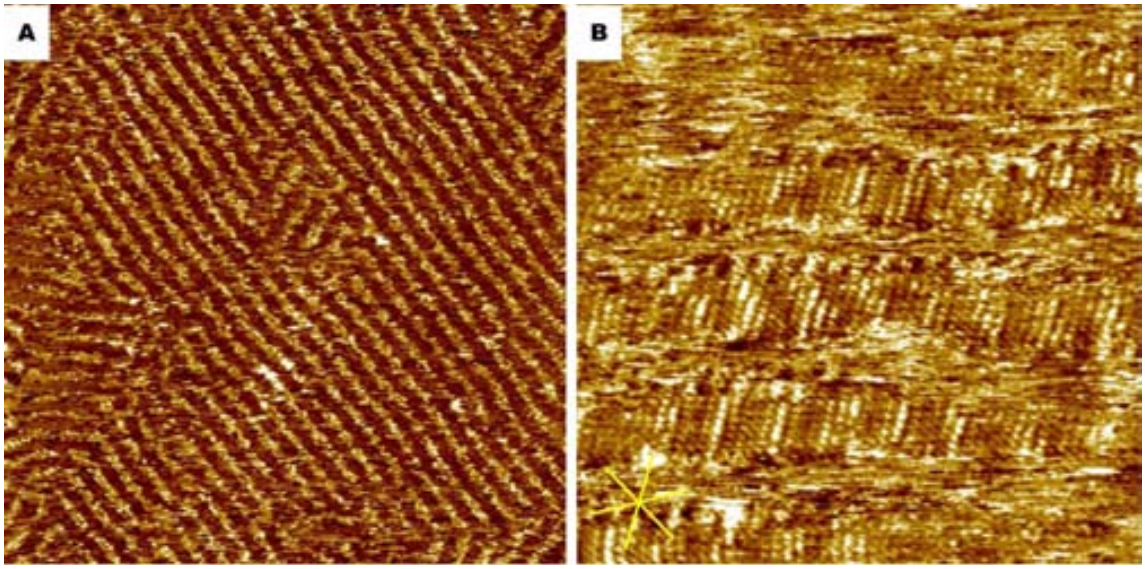

Figure 6.2: *STM images of a monolayer of mixed (R)-**2,7Naph**/(S)-**1,5Naph** at the 1-phenyloctane-HOPG interface, formed upon premixing (R)-**2,7Naph**, (S)-**1,5Naph** and (R,R)-DACH (1:1:1). The concentration of each molecule in solution was 3.1 mM. (A: 94.4 x 94.4 nm; B: 22.0 x 22.0 nm; I_{set} = 0.2 nA; V_{set} = +0.8 V for both images). In image A the general view of the structure is presented, in image B, a close up of the structure is shown. One can observe in both of the images that the structure is able to change direction locally. In image B the area in between the alkyl chains is blurry, and the horizontal lines in the image indicates that something was sticking to the tip during scanning, this is an indication that other molecules, presumably the DACH might be coordinated on the top of the structure.*

The parameters of the structure are: average lamella width 4.10 ± 0.54 nm; Chirality of the structure with respect to the surface main axis -27.0 ± 7.8°. This angle means that, unusually, the lamella growth direction is nearly perpendicular to the main graphite axis.

The third type of domain that is observed in this sample corresponds to the complex of acid (*R*)-**2,7Naph** and (*R*,*R*)-DACH as shown in Figure 6.3.

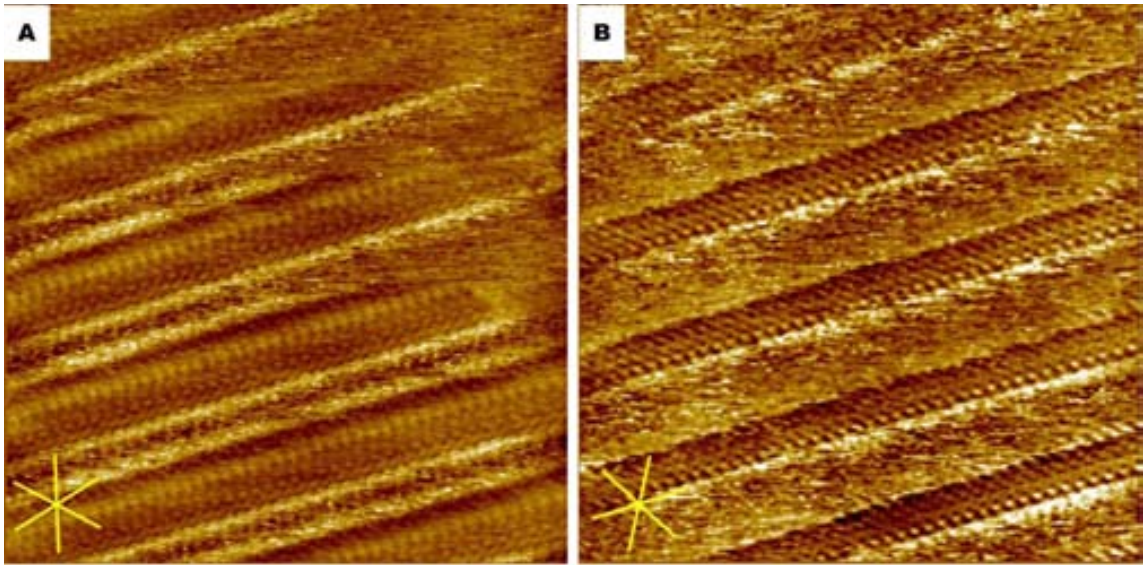

Figure 6.3: *STM images of a region showing the (R)-**2,7Naph**/(R,R)-DACH complex formed upon premixing (R)-**2,7Naph**, (S)-**1,5Naph** and (R,R)-DACH (1:1:1) at the 1-phenyloctane-HOPG interface. The concentration of each molecule in solution was 3.1 mM. (A: 27.0 x 27.0 nm; B: 26.3 x 26.3 nm; I_{set} = 0.2 nA; V_{set} = +0.8 V for both images). Image A shows well visualised domain, the bright stripe is where the aromatic parts are, the lines next to them are alkyl chains, and the blurry dark area between aromatic parts is where DACH is attached. In image B different contrast of the monolayer is presented, just one alkyl chain is visualised, while in the place where the other should be one cannot see almost anything, just noises. This effect might be caused by another layer of molecules that are attached on the top.*

The observed domains are rather small, not even reaching an area of 50 x 50 nm. In this case the lamellae are wider than for the pure acid **2,7Naph** regions, there is no interdigitation between alkyl chains and the aromatic parts of the molecules form two bright stripes with a darker area between them. The parameters measured for this type of domain in this system give a width of 5.76 ± 0.32 nm, a head to head distance (measured in just one image) of 0.66 nm and the chirality with respect to the main graphite axis was +17.4 ± 0.6°. All three parameters are similar to those of the monolayer of (*R*)-**2,7Naph** and (*R*,*R*)-DACH measured in previous experiments where only the two components were present (5.62 ± 0.14 nm; 0.66 ± 0.02 nm and +19.5 ± 0.7° respectively).

Another phenomena observed in this type of domains was the formation of multilayer

as shown in Figure 6.4. The multilayers are formed by complex of (*R*)-**2,7Naph**/(*R,R*)-DACH , those domains are not very large, or at least the parts that are identified as multilayers are usually few, up to 10 lamellae in width, and are surrounded by either disordered area or small domains of uncomplexed acid **2,7Naph**.

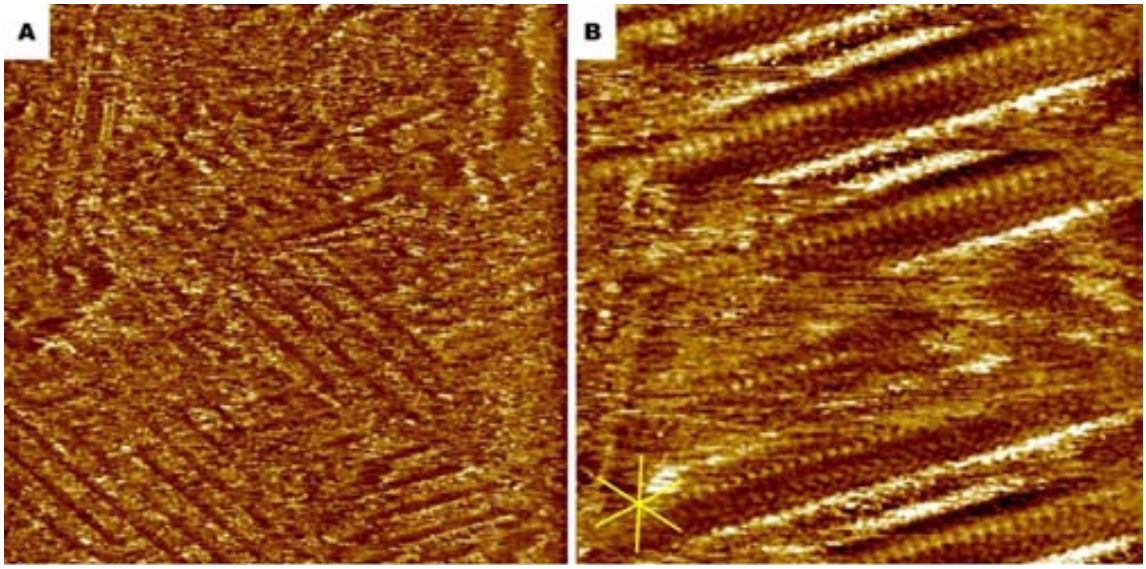

Figure 6.4: *STM images of a region containing a possible multilayer (R)-**2,7Naph**/(R,R)-DACH formed upon premixing (R)-**2,7Naph**, (S)-**1,5Naph** and (R,R)-DACH (1:1:1) at the 1-phenyloctane-HOPG interface. The concentration of each molecule in solution was 3.1 mM. (A: 107.0 x 107.0 nm; B: 27.0 x 27.0 nm; I_{set} = 0.2 nA; V_{set} = +0.8 V for both images). Image A presents the general view of the area, in the centre and bottom part of the image crossing lines of alkyl chains indicates the presence of multilayers. In image B there is the top domain in the top part of the image that is overlying the domain below next to the left edge of the image.*

In this mixture coexistence of three different ordered structures on the surface was observed, along with the presence of very poorly ordered regions. The formation of the complex (*R*)-**2,7Naph** and (*R,R*)-DACH was to be expected given its observation when the two components were combined alone, and it was found that this complex is formed under these conditions but is a minority surface species. The acid (*S*)-**1,5Naph** is not able to form a stable complex with (*R,R*)-DACH at the graphite 1-phenyloctane interface under the conditions of the experiment (see Chapter 5.4), and the main outcome is the formation of mixed monolayer (*R*)-**2,7Naph**/(*S*)-**1,5Naph**. It seems that this type of domain is more stable than that of (*S*)-**1,5Naph** on its own. However in some images one can observe that there might be some interaction between this type of domain and the DACH , judging by the very noisy contrast of this domains comparing

with mixed domains formed by molecules of both acids. (see Chapter 4.5)

The domain of acid (*R*)-**2,7Naph** which displays inverted pair chirality (observed S or Z shape) when compared with the pure compound is a bit surprising, since it has been demonstrated that this molecule forms a stable complex with the DACH at the surface (see Chapter 5.3). It is possible that the presence of the mixed monolayer stabilises small domains of the molecules of (*R*)-**2,7Naph** that can form locally its own areas, and the lamella chirality may inverted because of packing effects at the edge of the domains of the compound. Another possibility is that the (*S*)-**1,5Naph** inhibits forming expected monolayer, or gets involved in the monolayer forming mixed one, so just in case of inverted monolayer no molecules of **1,5Naph** are coabsorbed.

The monolayer is clearly different from the mixture of the two acids (see Chapter 4.5), in sample without DACH there was three different structures observed, domains of acid **2,7Naph**, mixed straight domains, with good resolution of the aromatic parts and disordered domains. When amine is present in the mixture, there are domains of acid **2,7Naph**/DACH complex, mixed monolayer, but with blurry aromatic part or inverted domains of **2,7Naph,** each of them different than either of the structure observed in mixture of acid. In any case, the presence of the (*S*)-**1,5Naph** clearly inhibits the formation of the complex between (*R*)-**2,7Naph** and DACH , and therefore the system would not aid in the resolution of solution-borne amine.

6.4 Self-assembly of (R)-2,7Naph (S)-1,5Naph (S,S)-DACH

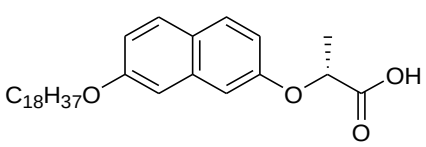

***(R)*-2,7Naph**

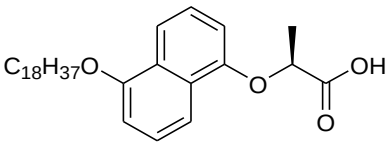

***(S)*-1,5Naph**

The same mixture of acids (*R*)-**2,7Naph**/(*S*)-**1,5Naph** but with the opposite enantiomer of the DACH , the (*S*,*S*), was deposited on the graphite to check the chiral recognition between the molecules in this complex kind of system. The images showing the kind of monolayer formed are shown in the Figure 6.5. One can observe that a variety of domains are formed; some spreading over thousands of nanometres and others that are very small, not reaching 10 nm in width and breadth. Some domains have very well defined boundaries, while others do not, lying next to the undefined, blurry

areas. These features are distinct from the mixture in which the (*R,R*) enantiomer of the DACH was used, but quite similar to those observed in the sample of (*R*)-**2,7Naph**/(*S*)-**1,5Naph** without amine.

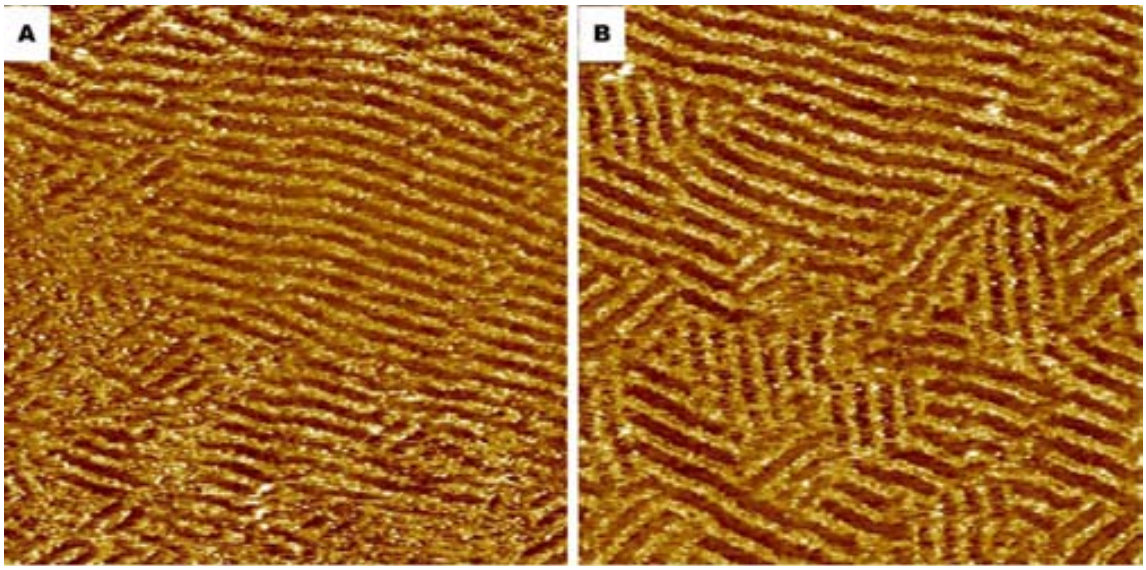

Figure 6.5: *STM images of the monolayer formed upon premixing (R)-**2,7Naph**, (S)-**1,5Naph** and (S,S)-DACH (1:1:1) at the 1-phenyloctane-HOPG interface. The concentration of each molecule in solution was 3.1 mM. (A: 96.5 x 96.5 nm; B: 93.4 x 93.4 nm; I_{set} = 0.2 nA; V_{set} = +0.8 V for both images). The general view of the monolayer is presented. In image A one of the larger domains is imaged, in the bottom and left part of the image undefined areas exist – this feature might be caused by some molecules of the DACH attached to the monolayer, or the molecules of acid that are not well organized. In image B a rather well defined domains are seen, but small, some of them not reaching 10 nm in width and breadth.*

Closer views of the superstructures reveal that there is a lamellar structure with interdigitation of the alkyl chains, but there is a lack of resolution of the aromatic parts of the molecules. Typical images are presented in the Figure 6.6. In general the monolayer is assigned as the mixed (*R*)-**2,7Naph**/(*S*)-**1,5Naph**, considering the interdigitated chains and the appearance of domain, although there are some domains without good resolution, which may indicate that there is either a movement of the molecules while interacting with graphite or there is another molecule involved on the top of the formed monolayer, and in this case the interaction with DACH is the most probable phenomenon.

The parameters of the observed structure are: lamella width 4.03 ± 0.21 nm what is very similar to the parameters obtained for mixed monolayer of (*R*)-**2,7Naph**/(*S*)-

1,5Naph, presented in Chapter 4.5. Chirality with respect to the perpendicular to main graphite axis equals +8.3 ± 10.5° and this result is a bit different with those obtained for the mixed monolayer without DACH (there the disordered domains were 4.41 ± 0.43 nm wide and - 2.3 ± 8.8° with respect to perpendicular to main graphite axes), but taking in account the significant error in both measurement of chirality it is hard to say if the structure is truly different. Moreover no clear domains of acid **2,7Naph** was spotted, as it was observed in the mixture of same two acids without amine or in the mixture of (*R*) acid **2,7Naph** with (*S,S*)-DACH . This is unexpected result, but it might be explained by differences of stability of the structure, mixed monolayer is more stable on the surface, while in the solution acid **2,7Naph** is interacting strongly with amine what limits its capability of forming stable monolayer. In the images where aromatic parts areas are noisy, apparently (*S,S*)-DACH interacts with mixed of monolayer what results in problems with visualisation using STM.

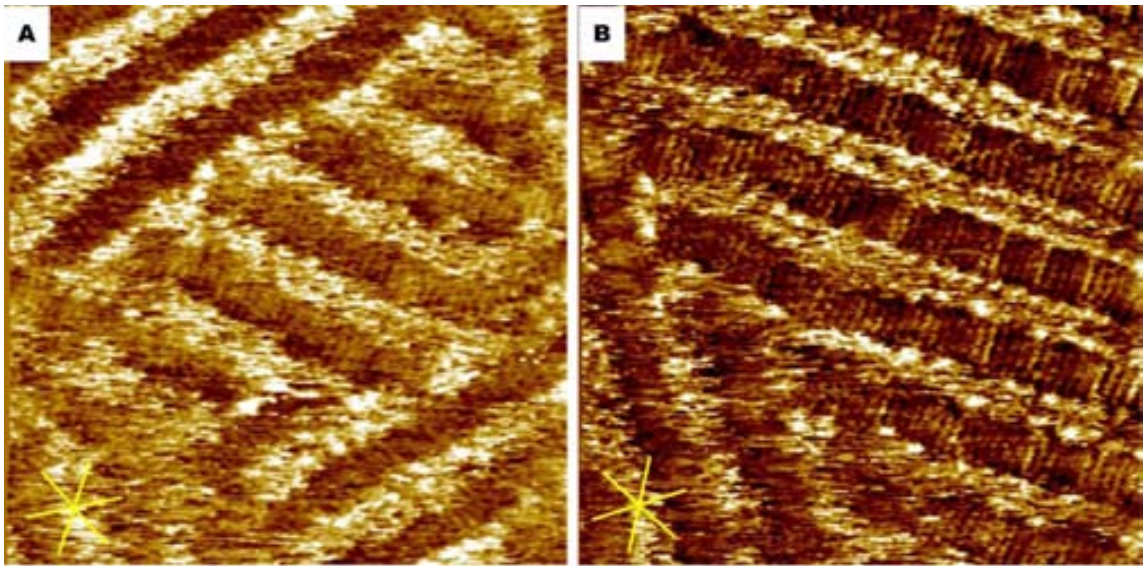

Figure 6.6: *STM images showing the mixed (R)-**2,7Naph**/(S)-**1,5Naph** monolayer formed upon premixing (R)-**2,7Naph**, (S)-**1,5Naph** and (S,S)-DACH (1:1:1) at the 1-phenyloctane-HOPG interface. The concentration of each molecule in solution was 3.1 mM. (A: 24.5 x 24.5 nm; B: 23.9 x 23.9 nm; I_{set} = 0.2 nA; V_{set} = +0.8 V for both images). The close up of the structure is presented. In both of the images there is a difference in the resolution of the neighbour domains, perhaps it is caused by the interactions with the tip or molecules of DACH .*

In any case, in common with the layers formed by the unlike enantiomers of **1,3Ph** and the DACH , no well-formed layers of the complex are observed.

6.5 Self-assembly of (S)-2,7Naph (R)-1,5Naph (R,R)-DACH

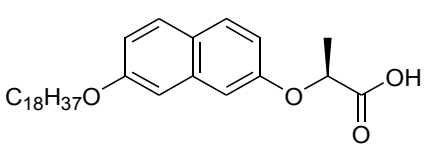

***(S)*-2,7Naph**

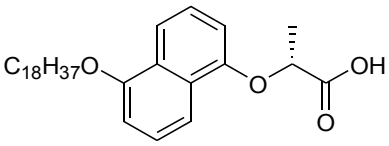

***(R)*-1,5Naph**

The mirror image experiment of the previous sample was checked and virtually the same structure was found. Representative images are shown in the Figure 6.7.

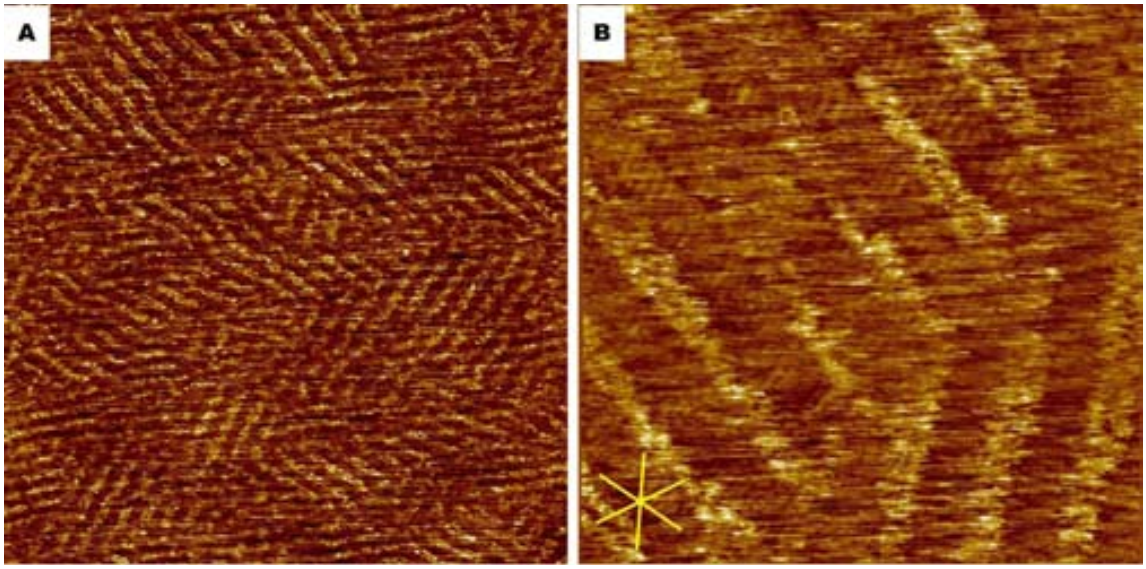

Figure 6.7: *STM images of the monolayer formed upon premixing (S)-**2,7Naph**, (R)-**1,5Naph** and (R,R)-DACH (1:1:1) at the 1-phenyloctane-HOPG interface showing mixed (S)-**2,7Naph**/(R)-**1,5Naph** domains. The concentration of each molecule in solution was 3.1 mM. (A: 96.4 x 96.4 nm; B: 25.4 x 25.4 nm; I_{set} = 0.2 nA; V_{set} = +0.8 V for both images). In image A the general view and in image B the close up of the structure*

The parameters measured in the sample were 4.23 ± 0.62 nm; chirality with respect to the perpendicular to main graphite axis equals +2.8 ± 4.8°, but it has to be mentioned that due to the instability of the tip and other problems during scanning not many images were captured and analysed. The monolayer width and chirality are very similar to the one observed for the mirror image sample. The lamella width is almost the same and the chirality is in + for both of the mirror image samples, but as there is significant variation of angle observed for those structures, and considering that the error bar is remarkable for both of them, it is understandable that there is not exact mirror image of the results between the mirror image samples. It has to be mentioned that the SAM formed by both of the samples are aligned within few degrees from perpendicular to main graphite axes.

6.6 Self-assembly of (R)-2,7Naph (R)-1,5Naph (R,R)-DACH

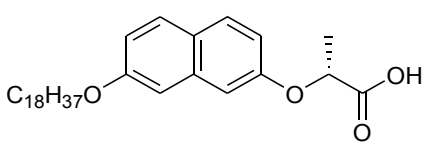

***(R)*-2,7Naph**

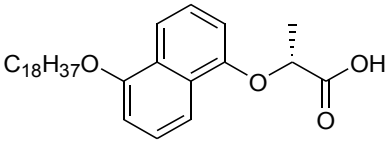

***(R)*-1,5Naph**

Also the mixture of the amphiphiles **2,7Naph** and **1,5Naph** of the same chirality (*R*) was measured with the (*R,R*) -DACH . After deposition on the surface, large domains were found with more than 100 nm in each direction, although smaller ones where also present. Typical STM images of the self-assembled monolayers are presented in Figure 6.8.

The lamellar structure is clear, but similar to the previous sample there are a number of defects in the lamellae, it seems like the general direction of growth is preserved, but locally it changes gently. Therefore the "two-dimensional crystal" type of layer is not formed, but instead a rather disordered structure over a large scale with orientational order.

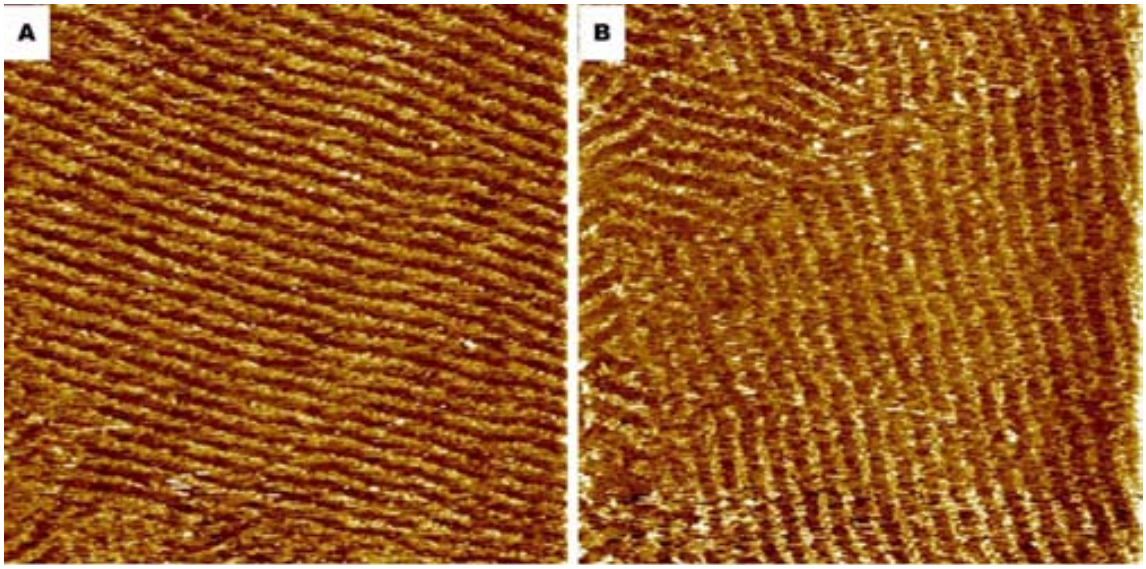

Figure 6.8: *STM images of monolayer showing mixed monolayer formed upon premixing (R)-**2,7Naph**, (R)-**1,5Naph** and (R,R)-DACH (1:1:1) at the 1-phenyloctane-HOPG interface. The concentration of each molecule in solution was 3.1 mM. (A: 103.8 x 103.8 nm; B: 91.3 x 91.3 nm; I_{set} = 0.2 nA; V_{set} = +0.8 V for both images). In image A and B large domains, in image B there are small domains with quite disordered structure.*

In Figure 6.9 a close up of the structure is presented, one can observe unusual changes

in the resolution of the lamellae: The alkyl chains are very well defined, clearly interdigitated, while the aromatic part of the molecule is blurry, in some areas almost no details of structure can be discerned. There is no sign of complex formation of (*R*)-**2,7Naph** and (*R,R*)-DACH , what was expected, the most possible explanation is that molecules of (*R*)-**1,5Naph** inhibits formation of complex monolayer on the surface.

The parameters of the observed structure are: lamella width 3.89 ± 0.26 nm; chirality with respect to the perpendicular to main graphite axis equals -4.6 ± 9.3°. Those values are very similar to the parameters of disordered SAM observed for these two acid without DACH , that were 3.99 ± 0.29 nm and -9.7 ± 6.7° respectively. At the same time, judging by the change of the contrast in the aromatic parts of the monolayer, it seems that there is some binding, or at least interaction between the DACH and acids absorbed on the surface, but this process seems to be posterior to the formation of the monolayer, as it is not influencing the parameters of monolayer.

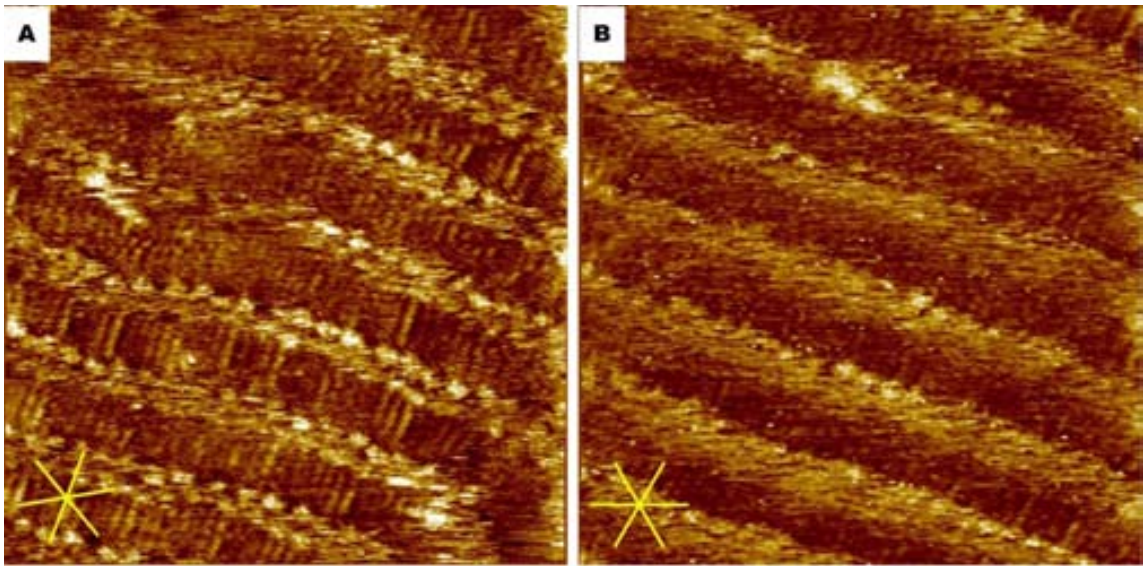

Figure 6.9: *STM images of monolayer showing close up of mixed (R)-**2,7Naph**/(R)-**1,5Naph** monolayer formed upon premixing (R)-**2,7Naph**, (R)-**1,5Naph** and (R,R)-DACH (1:1:1) at the 1-phenyloctane-HOPG interface. The concentration of each molecule in solution was 3.1 mM. (A: 22.3 x 22.3 nm; B: 22.3 x 22.3 nm; I_{set} = 0.2 nA; V_{set} = +0.8 V for both images). There is a curious change in the quality of image, in image A one can observe quite well all the head groups of the molecules at the bottom of the image, while in the top left of the image there is almost no resolution at all. In image B just a few naphthalene moieties can be recognized.*

6.7 Self-assembly of (R)-2,7Naph (R)-2,6Naph (R,R)-DACH

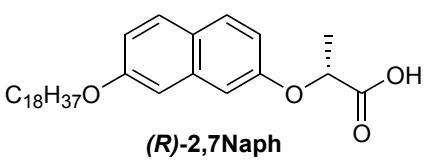

***(R)*-2,7Naph**

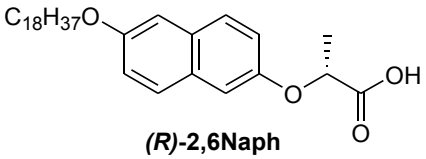

***(R)*-2,6Naph**

The mixture of acids (*R*)-**2,7Naph** and (*R*)-**2,6Naph** with (*R*,*R*)-DACH was also studied by STM at the graphite 1-phenyloctane interface. The first STM images were captured within 20 minutes after deposition of the mixture on the freshly-cleaved surface. The monolayer presents quite uniform contrast (with little to suggest binding of molecules on top of the monolayer) but rather disordered domains. Typical images of the monolayer are presented in the Figure 6.10.

A closer inspection of the monolayer with the STM allows one to appreciate that there is quite a high degree of irregularity in the structure of the lamellae, movement at the surface and much better image resolution of the alkyl chains compared with the aromatic parts of the component molecules. In the Figure 6.11 close up STM images of the monolayer structure are presented.

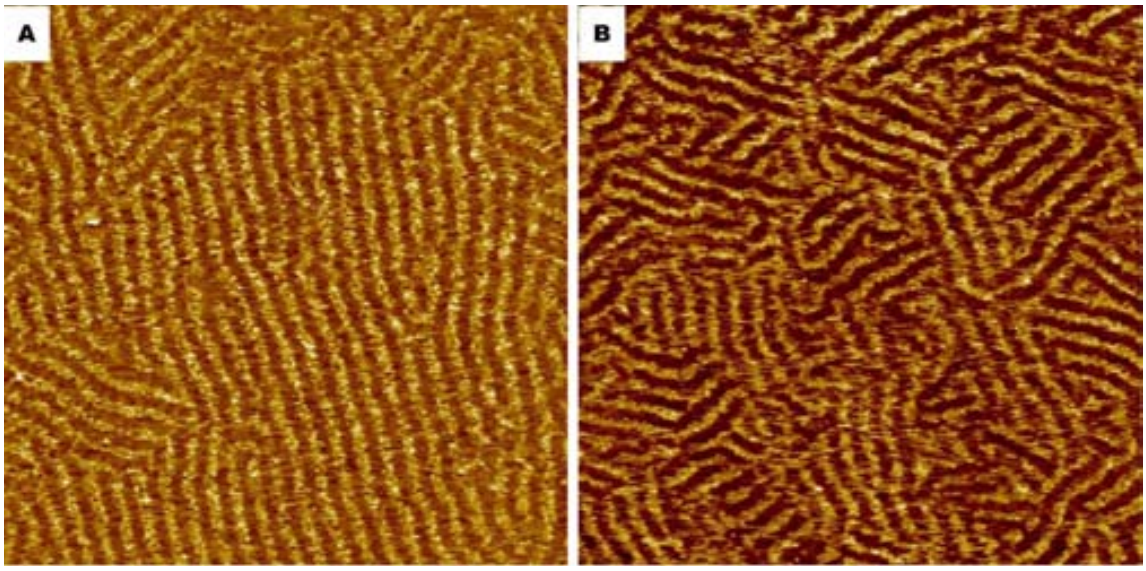

Figure 6.10: *STM images of the monolayer formed upon premixing (R)-**2,7Naph**, (R)-**2,6Naph** and (R,R)-DACH (1:1:1) at the 1-phenyloctane-HOPG interface. The concentration of each molecule in solution was 3.1 mM. (A: 99.1 x 99.1 nm; B: 96.2 x 96.2 nm; I_{set} = 0.2 nA; V_{set} = +0.8 V for both images). One of the largest observed domains in image A, and the area with small domains in image B. In this image one can see that there is quite a contrast in resolution between different domains, some are blurry and other very sharp.*

In this sample the mixture of acids can be seen, but the lack of high resolution in the aromatic region of the molecules might suggest that there is binding of DACH. The high resolution of the alkyl chains would suggest that there is not significant molecular motion within the monolayer. But again, the complex of acid **2,7Naph** with DACH was not observed, it seems not to be stable in these conditions at the graphite–1-phenyloctane interface.

The parameters of the observed structure are: lamella width 4.1 ± 0.1 nm; chirality with respect to the reference graphite axis equals -1.1 ± 8.1° and those values are similar to the parameters of mixed monolayer of acid (*R*)-**2,7Naph** and (*R*)-**2,6Naph** which were 4.2 ± 0.1 nm and lamella almost perpendicular to the main graphite axes (-24.9 ± 6.0°).

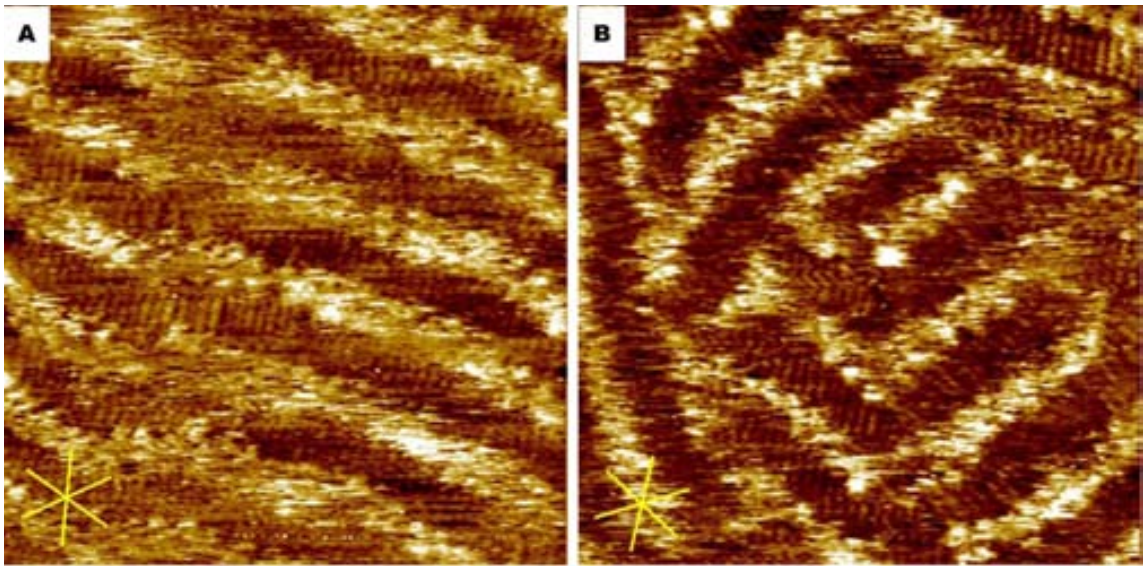

Figure 6.11: *STM images of monolayer showing mixed (R)-**2,7Naph**/(R)-**2,6Naph** monolayer formed upon premixing (R)-**2,7Naph**, (R)-**2,6Naph** and (R,R)-DACH (1:1:1) at the 1-phenyloctane-HOPG interface. The concentration of each molecule in solution was 3.1 mM. (A: 24.1 x 24.1 nm; B: 23.9 x 23.9 nm; I_{set} = 0.2 nA; V_{set} = +0.8 V for both images). In image A a close up of the monolayer structure is shown, witnessing the unexpected appearance of the same lamellae – in one area one can see well-resolved molecules and even aromatic heads of each molecule, while only a few nanometres further on there is blurry imaging and no details of the structure can be seen. In image B one of the smallest domains is presented, with a quite unusual bend in the alkyl chain in the centre of the image.*

6.8 Self-assembly of (R)-2,6Naph (R)-1,5Naph (R,R)-DACH

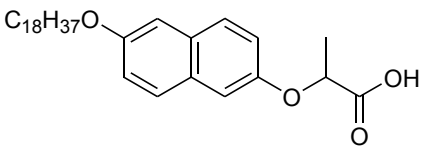

***(R)*-2,6Naph**

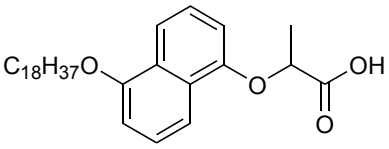

***(R)*-1,5Naph**

The mixture of the acids with the same stereogenic configuration (*R*)-**2,6Naph** and (*R*)-**1,5Naph** with (*R*,*R*)–DACH was also investigated to check the molecular recognition at the interface. Straight lamellae forming domains are observed once again, although not too large compared with domains formed by other mixtures presented in this chapter, the biggest one was smaller than 100 x 100 nm, and many of them had lateral dimensions less than 30 nm. The typical large scale STM images are presented in the Figure 6.12.

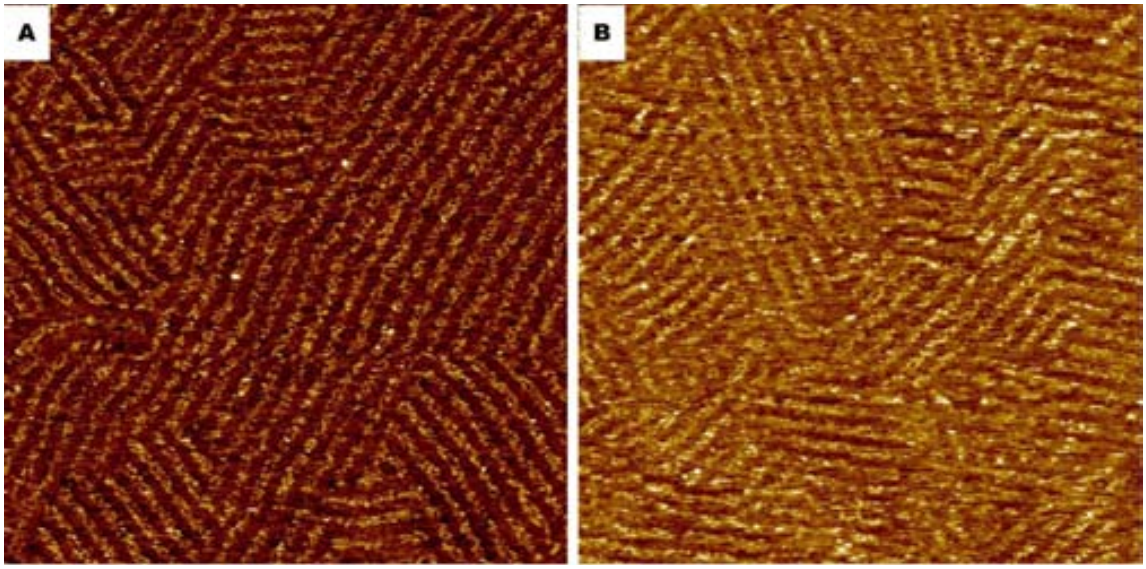

Figure 6.12: *STM images of monolayer formed upon premixing (R)-**2,6Naph**, (R)-**1,5Naph** and (R,R)-DACH (1:1:1) at the 1-phenyloctane-HOPG interface. The concentration of each molecule in solution was 3.1 mM. (A: 102.5 x 102.5 nm; B: 103.1 x 103.1 nm; I_{set} = 0.2 nA; V_{set} = +0.8 V for both images). The images present straight domains, except in a few areas with defects can be spotted, like in image A on the left edge where there is a domain that changes direction by approximately 60 degrees.*

In the close-up STM images (Figure 6.13) one can see that different structures can be found on the surface: Domains with no resolution in the head groups are observed,

probably caused by the interaction of molecules of DACH on top of the monolayer (Figure 6.13A). In other areas a quite disordered structure can be found, where areas with the head groups of molecules **2,6Naph** and **1,5Naph** imaged seemingly at random, but the interactions of alkyl chains apparently dominate in the formation of the monolayer. In the lamellae an irregular stripe of head groups, with jumps, and molecules separated by different distances, this type of structure is presented in the Figure 6.13B. Last type of structure observed in small areas is structures of acid **2,6Naph**, with characteristic jumps. The longest observed sequence of jumps consist of approximately 10 molecules is presented in the Figure 6.13A. It has to be mentioned that the structures can interconvert smoothly one in to the other in the same domain.

The average parameters of the observed structure are: lamella width 3.88 ± 0.24 nm; chirality with respect to the reference graphite axis equals +5.1 ± 5.4°. Values similar to those obtained for the other samples of two acid and DACH (i.e. (*R*)-**2,7Naph** (*R*)-**2,6Naph** (*R*,*R*)-DACH , but also others -lamella width is approximately 4 nm wide and the angle within is few degrees with respect to the perpendicular to the main graphite axis), where no formation of complex was observed.

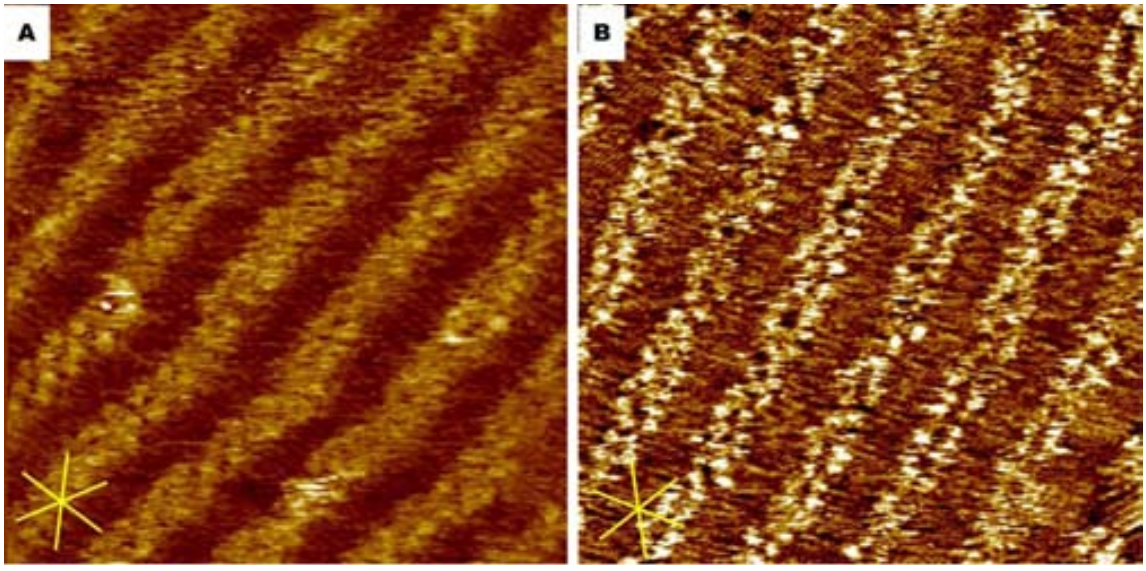

Figure 6.13: *STM images of monolayer showing mixed (R)-**2,6Naph**/(R)-**1,5Naph** monolayer formed upon premixing (R)-**2,6Naph**, (R)-**1,5Naph** and (R,R)-DACH (1:1:1) at the 1-phenyloctane-HOPG interface. The concentration of each molecule in solution was 3.1 mM. (A: 22.1 x 22.1 nm; B: 23.5x23.5 nm; I_{set} = 0.2 nA; V_{set} = +0.8 V for both images). In image A the area with acid **2,6Naph** is seen in the left part of the image, with the characteristic up-down pattern of the monolayers of this compound. In image B one can see each head group, except in a few areas where noise is observed over the head groups.*

6.9 Self-assembly of (R)-2,7Naph (R)-1,3Ph (R,R)-DACH

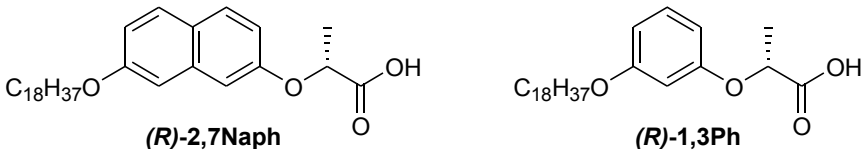

The last mixture measured in this series was the sample of acids (*R*)-**2,7Naph** and (*R*)-**1,3Ph** with (*R*,*R*)-DACH . In this case two types of monolayer structure can be observed with STM: A wide one, with no interdigitation of alkyl chains and a blurry area in between them and a domain with narrow and disordered lamellae. Typical STM images are presented in Figures 6.14 and 6.15.

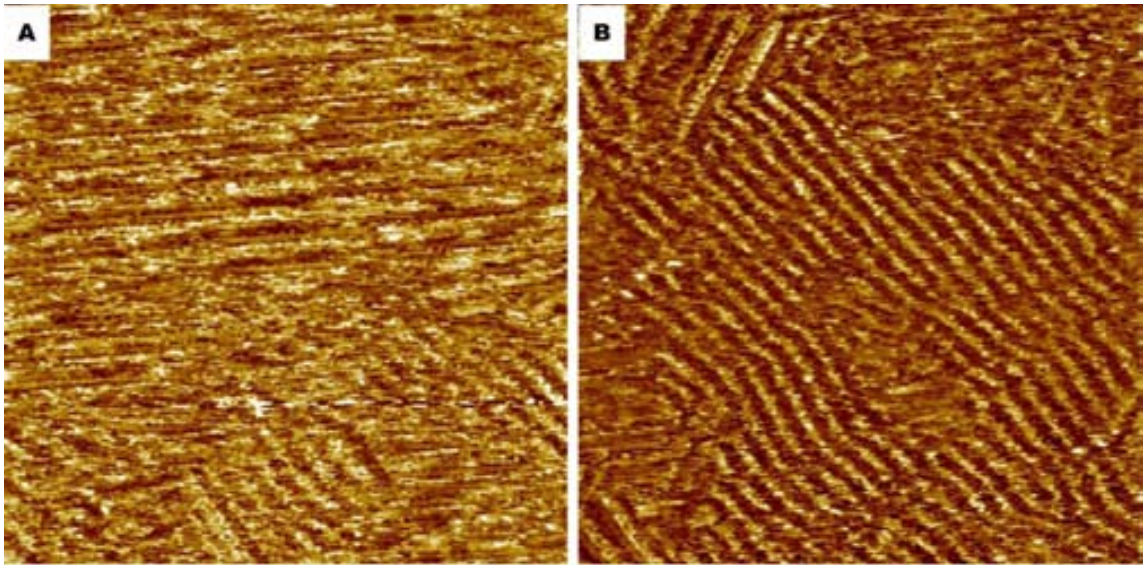

Figure 6.14: *STM images of a monolayer formed upon premixing (R)-**2,7Naph**, (R)-**1,3Ph** and (R,R)-DACH (1:1:1) at the 1-phenyloctane-HOPG interface. The concentration of each molecule in solution was 3.1 mM. (A: 95.9 x 95.9 nm; B: 97.4 x 97.4 nm; I_{set} = 0.2 nA; V_{set} = +0.8 V for both images). In image A one can observe a domain with wide, horizontal lamellae in the upper part of the image, while in the lower part narrow lamellae are observed. In image B the narrow domain dominates, while at the top and next to the left edge of the image one can observe the wide lamella.*

The wide domain seems to be very similar to the one observed for the complex (*R*)-**2,7Naph**/(*R*,*R*)-DACH , but as this complex is not significantly different in structure to the other possibility -(*R*)-**1,3Ph**/(*R*,*R*)-DACH -the composition of the monolayer cannot be determined judging solely by the images. At the same time the possibility of

formation of a mixed complex cannot be excluded, wherein each molecule of acid in a complex may be substituted by the other acid without influence on global organization of lamellae.

The narrow type of domain seems to be mixed monolayer of acids (*R*)-**2,7Naph**/(*R*)-**1,3Ph** as the structure is not absolutely straight. Locally lamellae change direction, but the overall direction is preserved. The resolution of the domain is not ideal, there is significant noise, especially in the aromatic part of lamellae, what might be an indication that molecules of DACH are interacting with already formed monolayer, although the position of DACH is not fixed, which causes the noise in the images.

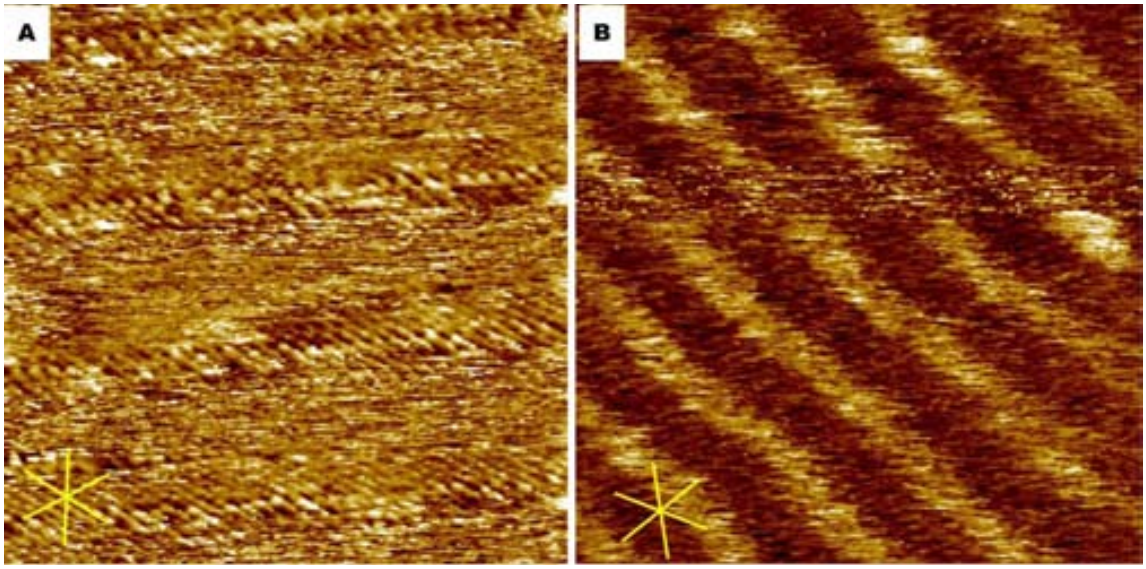

Figure 6.15: *STM images of monolayer showing the complex of acid (R)-**2,7Naph**/(R,R)-DACH in image A and mixed (R)-**2,7Naph**/(R)-**1,3Ph** monolayer in image B formed upon premixing (R)-**2,7Naph**, (R)-**1,3Ph** and (R,R)-DACH (1:1:1) at the 1-phenyloctane-HOPG interface. The concentration of each molecule in solution is 3.1 mM. (A: 20.1 x 20.1 nm; B: 20.0 x 20.0 nm; I_{set} = 0.2 nA; V_{set} = +0.8 V for both images). In image A complex of the acid with DACH is observed, the alkyl chains are seen but the aromatic parts of the molecules are very noisy, and in image B one can observe the mixed acid monolayer, above the centre of the image horizontal noise is due to the instability of the tip.*

The parameters of the only one measured narrow structure are: lamella width 3.6 nm; chirality with respect to the reference graphite axis +14.0 ± 3.0°. The lamella size is almost exactly the same as the one observed for the SAM formed by either **2,7Naph** or **1,3Ph** (3.56 nm and 3.7 nm respectively) and the angle is different to the one observed for either of the structures (-7.5 ± 3.4 and -4.0 ± 2.3 respectively), that suggests that

there is completely new structure, possibly containing a mixture of acids.

The other observed structure is remarkably different, the alkyl chains are bent at angle of approximately 50 degrees from lamella growth direction, not interdigitated and the lamella is wider than the other observed. The appearance is similar to the complex of **2,7Naph** with DACH or **1,3Ph** with DACH , unfortunately, due to the instability of the tip no images of complex with DACH were captured with graphite reference and because of that no analysis can be done on the structures.

6.10 Discussion

In the case of mixtures of acids with DACH, the formed structure changes dramatically, compared to either mixtures of acids or acid DACH samples. It is clear that for each three component sample there can be up to six different combinations of compound that can be found on the surface of graphite (assuming that DACH is not forming SAM and there is just one polymorph): acid A, acid B, mi x of acid A+B, acid A +DACH, acid B + DACH and mixture of acids with DACH. If it is taken in consideration that there can be different structures formed with different ratios of compound the number of possibilities multiplies.

In Table 6.1 the summary of observed structure is presented as well as the parameter of mixed acid domains described in Chapter 4.

The most commonly observed structure in these systems corresponded to domains containing a mixture of the two component acids, in which the aromatic part of the molecules appeared blurry, where the DACH might be interacting. The complex of acid with DACH was only observed in two experiments ((*R*)-**2,7Naph** (*S*)-**1,5Naph** with (*R*,*R*)-DACH and (*R*)-**2,7Naph** (*R*)-**1,3Ph** with (*R*,*R*)-DACH), which may indicate that the mixed monolayer of acids is more stable on the surface than the complex, or that the complex of DACH with acid is more soluble in this mixed system. In the case when molecules of acids possess the same chirality the formation of a mixed monolayer is preferred over formation of the complex, with one exception – the mixture of acid **1,3Ph** and **2,7Naph**, when probably the mixed monolayer of complex can be formed. In the case when there is a mixture of different chirality acids or mixture of acids that do not form stable complex on the surface on its own (**2,6Naph**, **1,5Naph**) no formation of complex on the surface was observed, instead mixed monolayer was found. The result is

somewhat surprising given the stability of the complex formed between like enantiomers for compounds (*R*)-**2,7Naph** and (*R*,*R*)-DACH (See chapter 5.3).

Table 6.1 *Comparison of the monolayer structures observed in STM of mixed acid and amine and mixed acid described in Chapter 4.*

	Lamella [nm]	Chirality	Composition
(*R*)-**2,7Naph** (*S*)-**1,5Naph** (*R*,*R*)-DACH	3.8±0.4	+0.6±1.3	(*R*)-**2,7Naph inverted**
	4.10±0.54	-27.0±7.8	(*R*)-**2,7Naph**/(*S*)-**1,5Naph**
	5.76±0.32	+17.4±0.6	(*R*)-**2,7Naph**/(*R*,*R*)-DACH
(*R*)-**2,7Naph** (*S*)-**1,5Naph** (*S*,*S*)-DACH	4.03±0.21	+8.3±10.5	(*R*)-**2,7Naph**/(*S*)-**1,5Naph**
(*S*)-**2,7Naph** (*R*)-**1,5Naph** (*R*,*R*)-DACH	4.23±0.62	+2.8±4.8	(*S*)-**2,7Naph**/(*R*)-**1,5Naph**
(*R*)-**2,7Naph** (*R*)-**1,5Naph** (*R*,*R*)-DACH	3.89±0.26	-4.6±9.3*	(*R*)-**2,7Naph**/(*R*)-**1,5Naph**
(*R*)-**2,7Naph** (*R*)-**2,6Naph** (*R*,*R*)-DACH	4.1±0.1	-1.1±8.1*	(*R*)-**2,7Naph**/(*R*)-**2,6Naph**
(*R*)-**2,6Naph** (*R*)-**1,5Naph** (*R*,*R*)-DACH	3.88±0.24	+5.1±5.4	(*R*)-**2,6Naph**/(*R*)-**1,5Naph**
(*R*)-**2,7Naph** (*R*)-**1,3Ph** (*R*,*R*)-DACH	3.6[a]	+14.0±3.0	(*R*)-**2,7Naph**/(*R*)-**1,3Ph**
	x[b]	x[b]	(*R*)-**2,7Naph**&/or (*R*)-**1,3Ph** /(*R*,*R*)-DACH
(*R*)-**2,7Naph**/(*S*)-**2,6Naph**	3.45	-3.6±1.8	(*R*)-**2,7Naph**
	4.44±0.28	-24.6±9.5	(*R*)-**2,7Naph**/(*S*)-**2,6Naph**
(*R*)-**2,7Naph**/(*R*)-**2,6Naph**	4.20±0.20	-28.9±4.8	(*R*)-**2,7Naph**/(*R*)-**2,6Naph**
(*R*)-**2,7Naph**/(*R*)-**1,5Naph**	3.48±0.13	-13.7±15.6	(*R*)-**2,7Naph**
	3.99±0.30	-9.7±6.8	(*R*)-**2,7Naph**/(*R*)-**1,5Naph**
(*R*)-**2,7Naph**/(*S*)-**1,5Naph**	3.72±015	-4.4±2.9	(*R*)-**2,7Naph**
	4.24±0.10	+3.1±4.2	(*R*)-**2,7Naph**/(*R*)-**1,5Naph**[c]
	4.41±0.43	+27.7±8.8	(*R*)-**2,7Naph**/(*S*)-**1,5Naph**[d]
(*R*)-**2,6Naph**/(*S*)-**1,5Naph**	4.22±0.42	-5.5±9.1	(*R*)-**2,6Naph**/(*S*)-**1,5Naph**
(*R*)-**2,6Naph**/(*R*)-**1,5Naph**	4.14±0.25	-24*	(*R*)-**2,6Naph**/(*R*)-**1,5Naph**

*Lamella refers to lamella width, chirality is measured with respect to main graphite axis with exception for the values give with *, in those cases it was measured with respect to perpendicular to main graphite axis. [a]Only one lamella measured. [b]No analysis was done, due to the instability of the tip during measurement of graphite [c]Straight mixed domains. [d]Wavy mixed domains.*

6.11 Conclusions

The amphiphile molecules of acid binds stronger to the surface than the amine-acid complex, in most of the cases what is observed with the STM is mixed monolayers of acids.

In some of the cases – mixtures of (*R*)-**2,7Naph** and (*S*)-**1,5Naph** and (*R,R*)-DACH and (*R*)-**2,7Naph** and (*R*)-**1,3Ph** and (*R,R*)-DACH, there is binding of amine, in the first case because of incompatibility of acids at the graphite- phenyloctane interface, this mixture simply is not as stable as the others. In the latter case the molecules of acids are very similar and at the same time both of them form stable complex on the graphite surface, so they form mixed monolayer of complex

In other cases what is observed is the formation of SAMs of mixed acids with possible interactions with amine atop of the formed domain. It is caused by much stronger interactions of acids with surface than with amine.

It seems likely that a mixture of acids which have very different interactions with the graphite surface will be necessary to generate ordered structures of diastereoisomers at this surface. The amine is not sufficiently specific in its binding to face a specific arrangement of the alkyl chains. A possible solution to this challenge could be the use of "Hydrotropes"[54] to aid resolution.

[54] M. H. Hatzopoulos, J. Eastoe, P. J. Dowding, S. E. Rogers, R. Heenan, R. Dyer, *Langmuir*, **2011**, *27*, 12346.

Chapter 7

Bulk phase behaviour of supramolecular diastereoisomers of the complex formed between a chiral amphiphilic acid and diaminocyclohexane.

7.1 Introduction

The mixing of components of the 2:1 complex formed between **1,3Ph** and diaminocyclohexane (Figure 7.1) is informative because it provides insight concerning the relative stability of the complexes, as well as their phase behaviour. This information could be used to identify crystalline complexes and could also identify materials which may be of use in other contexts. For example, it is known that complexes formed between acids and amines can give rise to supramolecular liquid crystals (LCs), wherein the components do not necessarily display this property.[22] The shape of acid and amine is an interesting one in this regard, as it could mimic a bent core type shape which is known to give a number of interesting LC phases.[55,56]

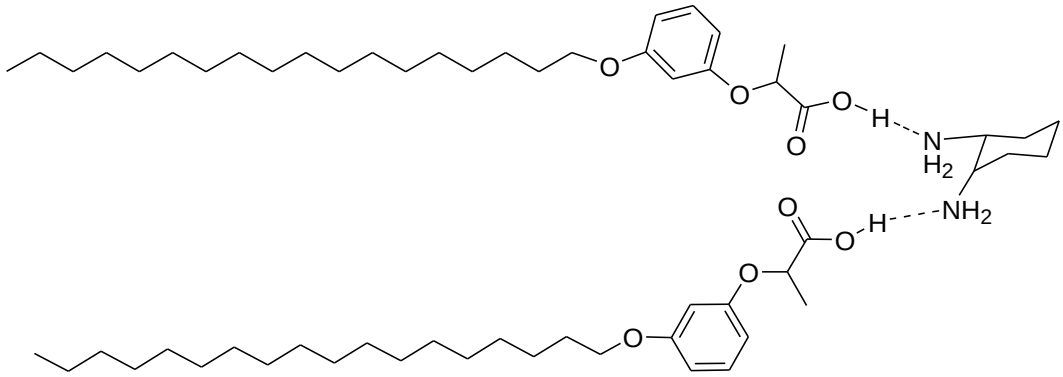

Figure 7.1*: The general structure of the supramolecular complex formed between* ***1,3Ph*** *and DACH*

[55] G. Pelzl, S. Diele, W. Weissflog, *Adv. Mater.*, **1999,** *11*, 707.
[56] R. A. Reddy, C. Tschierske, *J. Mater. Chem.*, **2006**, *16*, 907.

7.2 Sample preparation

The mixtures of **1,3Ph** and diaminocyclohexane were prepared by mixing THF solutions of the acid and amine, then the solvent was evaporated and the samples were melted in an oil bath at 120 ºC and then left to cool down in the oil bath overnight. Samples were left to age for a few days before the thermal analysis and diffraction experiments were carried out. In all the samples the molar ratio of acid to amine was 2 to 1. The samples were used for Differential Scanning Calorimetry (DSC) measurements, small angle X-ray scattering (SAXS) and wide angle X-ray scattering (WAXS) and their phase behaviour was checked with a polarising optical microscope (POM). The mixtures shown in Figure 7.2 were prepared.

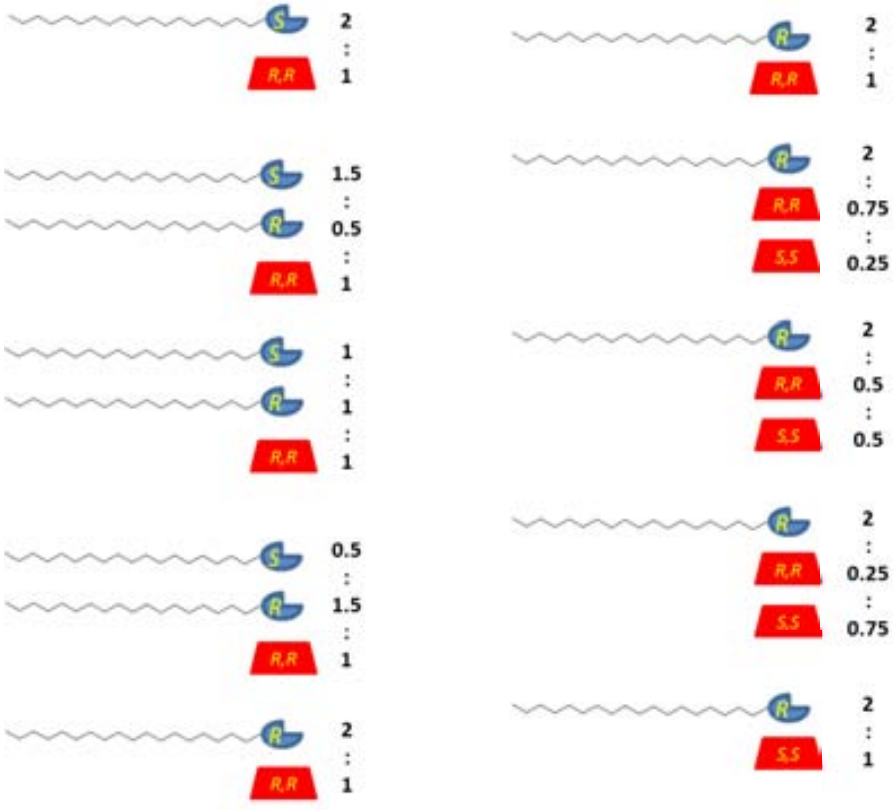

***Figure 7.2**: The proportions of compounds in the mixtures. The blue structure with tail stands for acid, and red trapezium is trans-1,2-diaminocyclohexane. The chirality of the compound is marked in yellow. In all of the samples overall proportion of acid to amine was 2:1.*

For the SAXS measurements, each sample was placed in a capillary which was sealed, then each sample was heated to 50, 55, 60, 65, 70, 75, 80, 85 and 90°C then equilibrated at each temperature for 10 minutes before measuring for the next 30

minutes. As three of the samples did not melt until 90°C, the measurements of those samples were repeated at 90, 95 100, 105, 110, 115 and 120°C. The intensity of the baseline in the spectra changes as a result of the compacting of the sample. At the beginning of the measurement the solid sample is mixed with the air, but when it melts the liquid flows downward in the capillary and air moves up, away from the beam. Because of this effect the spectra at higher temperatures have a lower baseline. The band in SAXS below 1 q/$nm^{-1}$is the reflection of the main beam, caused by the air in the glass capillary.

For DSC, samples were of approximately 3mg each of the mixture in question which was placed in the standard aluminium DSC pots, and were measured starting at 20°C, heated to 140°C at a rate of 5°C/min, then holding at 140°C for 10 minutes before cooling down to 20°C at a rate of 5°C/min. The cycle was repeated once again after 10minutes at 20ºC.

In the optical microscope a small amount of material was placed on a glass slide which was incorporated into a Linkam heating plate and the sample was warmed at a rate of 5°C/min. The heating was stopped manually during phase transition. All the images were taken with the light passing through crossed polarisers.

It should be noted that the system is in equilibrium between liquid and solid phase and in SAXS/WAXS just crystalline solid can be characterized, while in DSC the phase changes of the system is followed.

7.3 Summary of qualitative observations of aged samples under heating

In this section, the general characteristics of the different samples will be discussed so that the results presented can be interpreted within the context of the whole series of experiments. The mixtures of acid and amine prepared in the way described above were used for analysis after aging for a few days in a vial as a solid. All the data resulting from these experiments are given in Tables 7.1 and 7.2.

The X-ray diffractogram of acid **1,3Ph**, generated with Mercury software from the crystal structure of the compound is shown in Figure 7.3. The packing of this molecule is comprised of lamellae with interdigitated alkyl chains between them.[40] There is one main peak observed, at a q value of 1.77 that corresponds to the interplanar distance of 2.50 nm. It has to be mentioned that in the crystal structure there is a molecule of

DMSO involved in the packing of the head groups which are hydrogen bonded to it, that makes the interlayer pacing somewhat longer than would be the case of a pure compound.

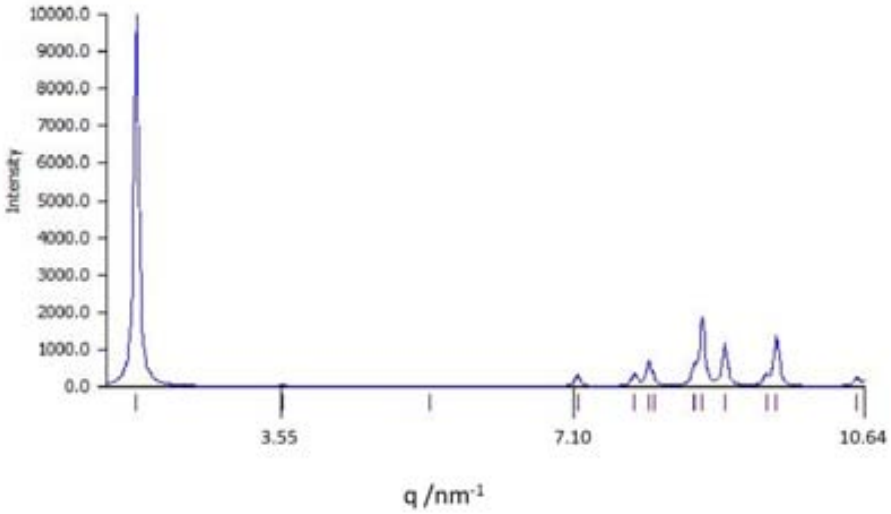

Figure 7.3 *X-ray diffractogram of acid* ***1,3Ph.DMSO****, generated from crystal structure* [3] *using Mercury software*

In the Figure 7.4 different possible structures for the **1,3Ph** DACH complexes are shown schematically. The packing presented in Figure 7.4A and 7.4D are the ones observed using STM in the monolayers of either **1,3Ph** DACH complex or **1,3Ph** alone. In Figure 7.4B, C and D there are different possible arrangements of a complex of **1,3Ph**-DACH presented, none of them was observed in STM and the interplanar distance marked in the Figure is an approximation based on models optimized in HyperChem. In packing A and B the inter-planar distance depends also on angle between the plane of the head-groups and the main vector described by the direction of the alkyl chains. In both of the packing models the angle α= 50° observed in STM was applied to calculate the distances, but as the restrictions of packing in 3D are different than in 2D the angle could vary and so the repetitive distance might change by several per cent.

For the samples where the one enantiomer of acid complexes diamine of varying chiral composition, the results obtained from the SAXS measurements seem to indicate that there is a well-defined complex in the samples containing pure (*R,R*)-diaminocyclohexane and the one where the racemic diamine is present. In these samples the SAXS peak appears at approximately 1.45 q/nm^{-1}, a value that corresponds to a distance of approximately 4.3 nm, which is closest to the packing presented in Figure

7.4C. In the sample with racemic amine there are additional peaks that indicate that there is a mixture of different structures in this sample which could arise from the different diastereoisomers that can occur. In the sample with a 3:1 ratio of the (*R,R*)- and (*S,S*)- amines there is a peak that corresponds to the distance of 3.37 nm, that coincides with the length of the molecule of acid **1,3Ph** (Figure 7.4D). This peak also appears in the sample where the ratio between (*R,R*)- and (*S,S*)-amines is 1:3 and the sample with a 3:1 ratio of (*R*)- to (*S*)-**1,3Ph** and the (*R,R*)-diamine. Quite similar peaks (at 3.25 nm or 3.50 nm) appear in all of the samples except the mixture of (*R*)-**1,3Ph** (*R,R*)-diaminocyclohexane. This observation might indicate that only the combination of molecules of (*R*)-**1,3Ph** and (*R,R*)-diamine can form stable periodic crystals containing lamellae; other combinations are mixtures of different structures.

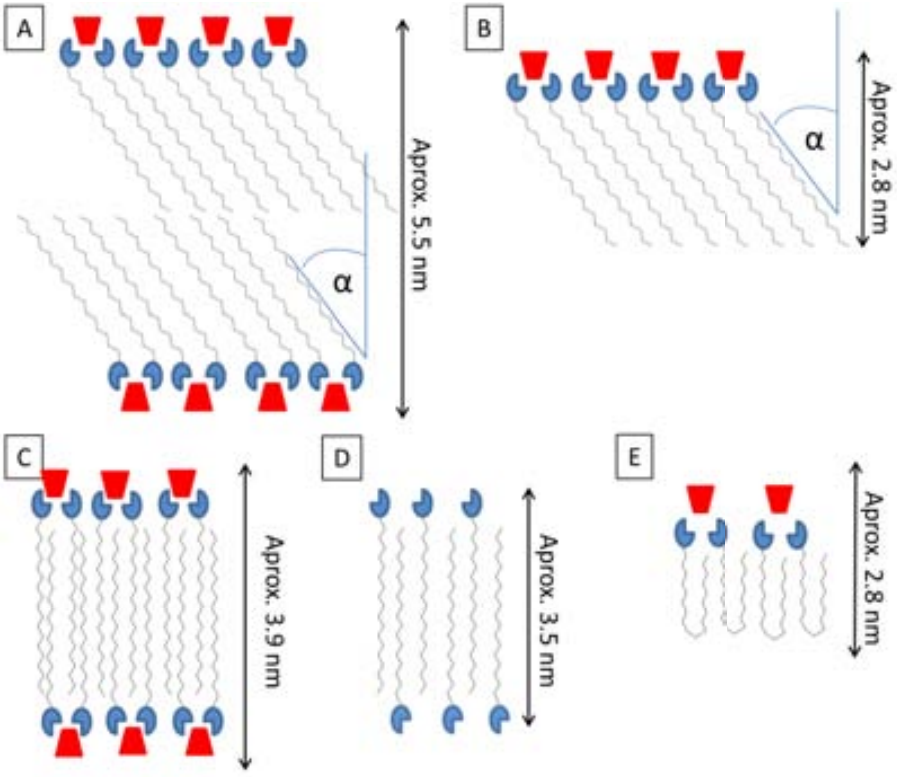

Figure 7.4: *Schematic draw of possible lamellar system of complex between acid (blue with tail) and diamine (red trapezium). The inter-planar distances are approximations based on the STM images of the complex at the graphite-1-phenyloctane interface, crystal structure of* ***1,3Ph***[49] *and modelling.*

Considering all the diffractograms no peak was found that could correspond to the distance of an ordered system without interdigitation of the alkyl chains (Figure 7.4A), the packing that is most common observed in SAMs on graphite (see section 5.2).

However, the peak observed at 4.3 nm could also be the interplanar distance of the complex presented in Figure 7.4A with alkyl chains tilted at 53 ° from the plane of head groups. Bearing in mind that in the monolayers chains are bent at 50 °this is a possible solution. The peak at 2.2 q/nm^{-1} that corresponds to 2.85 nm is observed in two of the samples, (*R*) acid with racemic amine and (*R*) acid with (*R,R*) and (*S,S*) DACH in a 0.75:0.25 ratio. This peak is not easy to explain; it could either be a structure with alkyl chains interdigitated and bent at some angle close to 50° (Figure 7.4B), or some structure with alkyl chains folded in half of its length (Figure 7.4D). A surprising fact in the observed system is the lack of the further peaks in SAXS that correspond to laminar systems, meaning that even though these lamellae are present they do not form part of a regular and perfectly periodic lamellar packing.

In the DSC measurements quite complex phase behaviour is observed in all the mixtures in the first heating cycle. In all of the samples a peak was observed at low temperature, in the range of 40 to 63°C that indicates first phase change, which is close to the melting point of the diaminocyclohexane (45°C). After this change in some of the samples ((*R*)-**1,3Ph** acid and (*R,R*)-DACH (*S,S*)-DACH (2:0.25:075), (*R*)-**1,3Ph** acid and (*S,S*)-DACH , all of the mixtures of acid (*R*) and (*S*)-**1,3Ph** and (*R,R*)-DACH) there is a negative peak in the DSC that indicates an exothermic process associated most probably with crystallization, a hypothesis backed up by the observation of crystallites with the optical microscope. Then the melting is observed in the form of broad peaks. In the case of sample (*R*)-**1,3Ph** acid and (*R,R*)-DACH the material shows as many as five peaks, which means that the material goes through various intermediate structures before melting. The peaks are broad in the case of mixtures of enantiomers of amine with one enantiomer of acid **1,3Ph**, but in the case of mixtures of enantiomers of the acid the samples give sharper peaks. In the second cycle of heating (carried out 5 minutes after the first heating cycle) just one peak was observed for all of the samples, the melting took place at the temperature 42-48°C.

The samples were studied using Infrared spectroscopy (Figures 7.5 and 7.6). This technique proved the formation of a complex between acid and amine– as in each of the samples a hydrogen bond is observed – the carbonyl band of the acid at approximately 1700 cm^{-1} is shifted to lower wavenumber and a broad band at approximately 2700 cm^{-1} corresponding to the NH bond is seen - but no clear difference between the different compositions of the mixtures is observed at the room temperature.

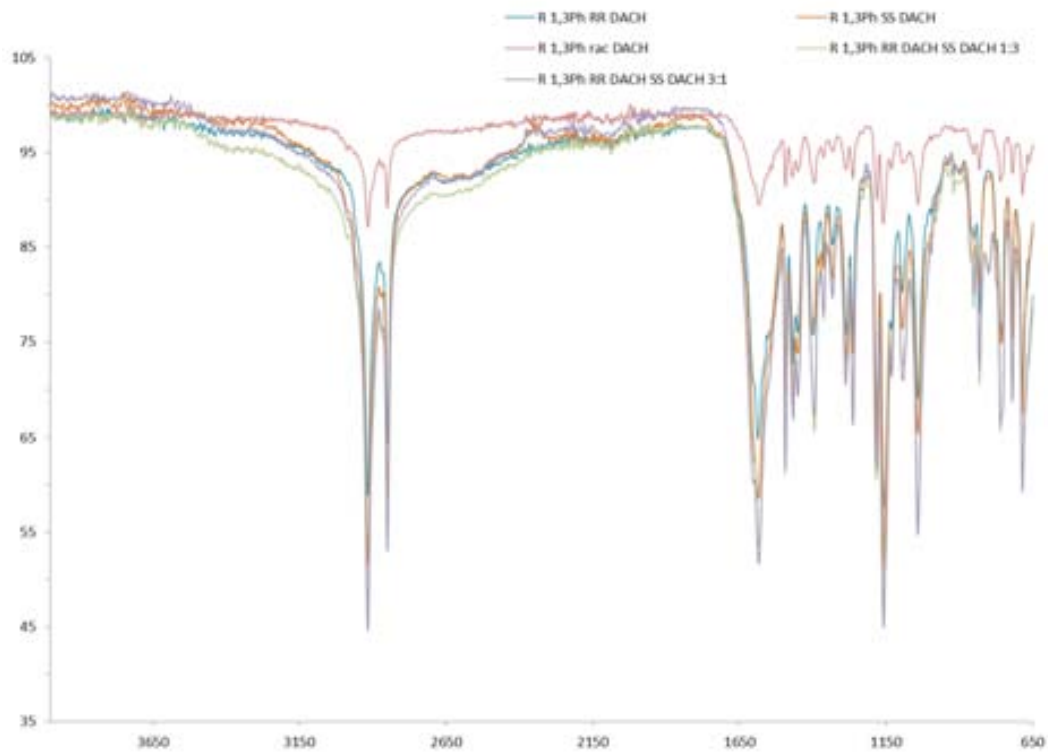

Figure 7.5: *Infrared spectra of 2:1 mixtures of acid (R)-**1,3Ph** and differing proportions of the enantiomers of DACH. At 1585 cm^{-1} there is the band of carbonyl group proving hydrogen bonding.*

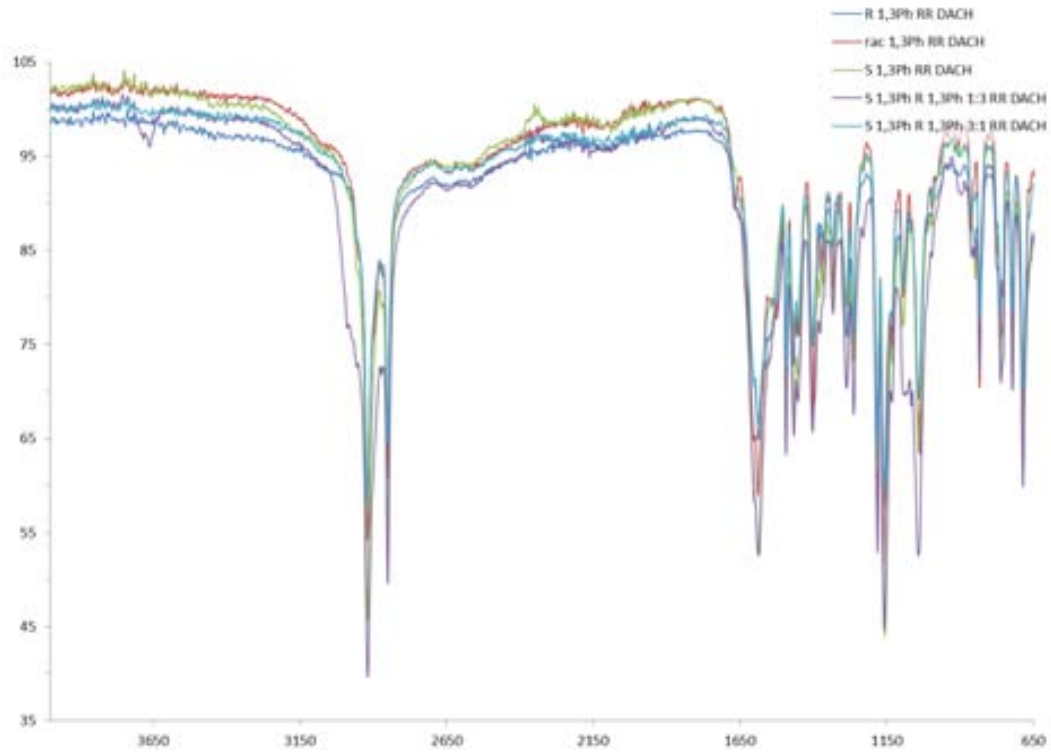

Figure 7.6: *Infrared spectra of 1:2 mixtures of (R,R)-DACH and differing proportions of the enantiomers of acid **1,3Ph**. At 1585 cm^{-1} there is the band of carbonyl group proving hydrogen bonding.*

In general the melting processes observed in SAXS occur at the same or slightly higher temperature compared with the DSC and optical microscope observations, just in one case, sample (*R*)-**1,3Ph** acid and (*S*,*S*)-DACH did not show melting at 90°C while in the DSC measurement it melted at 82ºC and in optical microscope at 84°C, values that match well the melting point of pure **1,3Ph** (82ºC).

Table 7.1: *Comparison of the SAXS data and phase transitions of the 2:1 mixtures of acid (R)-**1,3Ph** and differing proportions of the enantiomers of DACH from different techniques.*

Proportion (*R*,*R*)-to (*S*,*S*)	SAXS distances [nm]	SAXS melting point [°C]	DSC Transition onset [°C]	DSC phase transition peaks [°C]	DSC clearing point [°C]	DSC 2nd cycle phase transition peak [°C]	optical microscope phase transition (first value melting onset, last value clearing point) [°C]
100 : 0	4.3; 2.04	85-90	41	50; 62; 72; 80; 86	88	45	56; 84
75 : 25	3.37; 2.83; 1.78; 1.38; 1.2	80-85	43	58; 72	82	42	56; 76
50 : 50	4.3; 3.37; 2.83; 2.04; 1.78; 1.45; 1.38; 1.2	75-80	44	63; 71	79	42	x; 74
25 : 75	3.37; 1.46;	85-90	40	51; 80	83	48	55; 79
0 : 100	3.25; 1.46	90+	40	51; 82	89	45	x 84

x- onset of first phase change is not clear in POM

Table 7.2: *Comparison of the SAXS data and phase transitions of the 1:2 mixtures of (R,R)-DACH and differing proportions of the enantiomers of acid **1,3Ph** of from different techniques.*

Proportion (*R*)-to (*S*)	SAXS distances [nm]	SAXS melting point [°C]	DSC Transition onset [°C]	DSC phase transition peaks [°C]	DSC clearing point [°C]	DSC 2nd cycle phase transition peak [°C]	optical microscope phase transition (first value melting onset, last value clearing point) [°C]
0 : 100	4.07; 3.25; 1.46	85-90	40	51; 82	85	46	53; 82
25 : 75	3.51; 1.35	100-105	40	40; 46; 54; 96	103	47	x 100
50 : 50	3.50; 1.35	105-110	40	46; 105	106	47	x 103
75 : 25	3.40; 1.35	100-105	38	50; 84	102	45	53; 95
100 : 0	4.3; 2.04	85-90	41	50; 62; 72; 80; 86	88	45	56; 84

x- onset of first phase change is not clear in POM

7.4 (R)-1,3Ph acid (R,R)-diaminocyclohexane

The as-prepared sample of (*R*)-**1,3Ph** acid (*R,R*) -diaminocyclohexane is crystalline at room temperature as shown by the diffraction data (Figure 7.7). A laminar packing is present, as the secondary peak is observed (double of the first peak) in SAXS. A gradual melting is evident with a clearing point at around 85 ºC, after melting there is a broad band which indicates that the material is not completely amorphous, but contains small clusters, dimers, trimers etc. This peak is a correlation peak corresponding to a distance of approximately 3.1 nm and is seen to grow in intensity gradually from 60ºC.

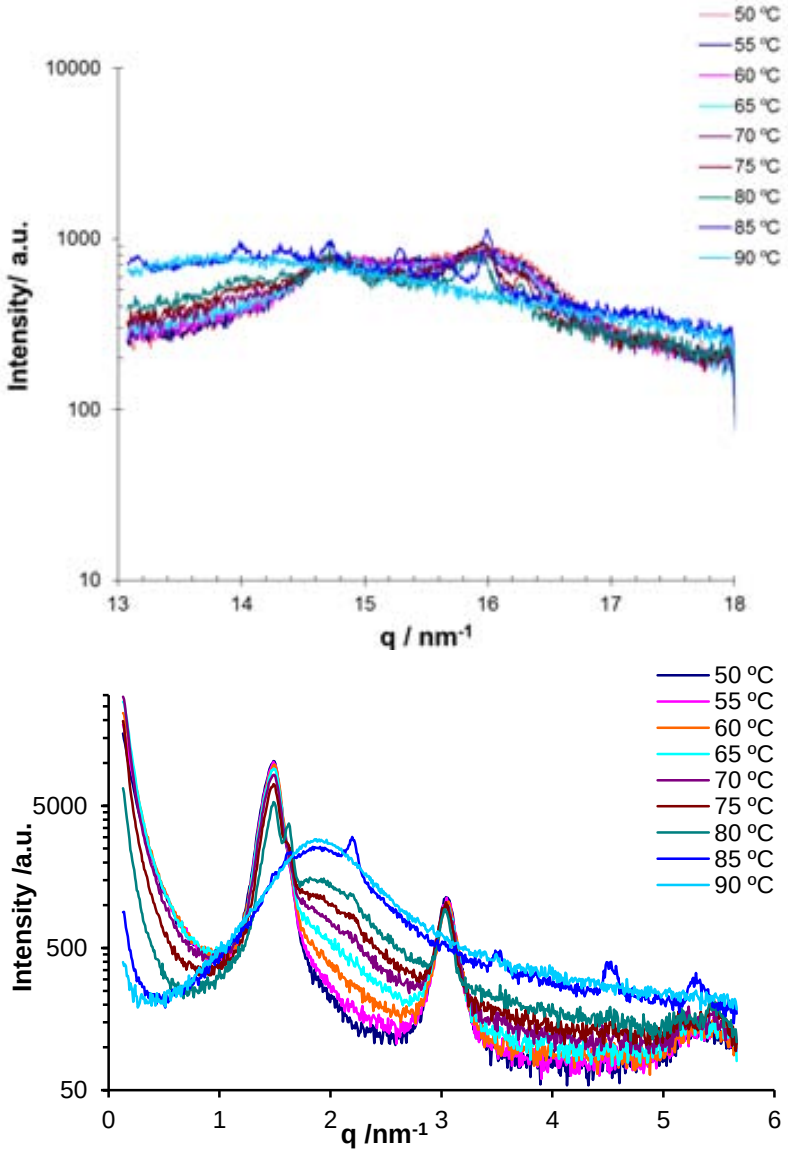

Figure 7.7: *WAXS and SAXS of the mixture of (R)-**1,3Ph** acid and (R,R)-DACH (2:1) bottom during heating*

In WAXS the peaks get sharper closer to the melting point, indicating a rearrangement of the material that is also evidenced in the polarising optical microscope measurements (see below). The distance between the layers is 4.2 nm which corresponds to the size of the complex of **1,3Ph** acid with amine, organisation A in Figure 7.4, however it could be also arrange as in C in the same Figure. The sample melts below 90°C, as at this temperature no peaks were observed in the WAXS.

In the DSC curves (Figure 7.8), the first cycle displays abroad range of phase transitions and melting phenomena between 50 and 88°C, with at least five maxima. The second heating cycle, in contrast, shows a very simple curve with a peak corresponding to the melting of the material occurring at about 45-46 ºC. The solidification is the same in both cycles and is observed in the cooling cycles at about 26 ºC.

In Figure 7.9 POM images of the sample are presented. Image A shows a micrograph captured at 45°C where the material as it was at room temperature, with no changes observed in the structure of the material. Image B captured at 56°C shows the result of the first phase change; the material gets partially liquid, so apparently there is a separation of phases. In micrograph C taken at 66°C the recovered crystalline structure can be observed, and this effect is even clearer in image D, recorded at 76°C. The sample truly melts at 83-84°C, that is presented in images E and F. Micrograph E just as the process starts, F just before melting is over.

It is clear that this sample is not homogeneous throughout the heating cycle; there are various possible phases as seen in the DSC curve. The phase changes start below 50°C and goes through some four stages until it finishes at 88°C where the homogeneous liquid is formed. In the POM the same process was observed, the samples starts melting at approximately 50°C, at 56°C it seems that more than a half of the material was liquid, but surprisingly it became crystalline again. There is minor change in appearance of the sample at 76°C when it is more shiny and then it starts melting again to clear at about 83-84°C, a temperature a bit lower than that observed in DSC and WAXS.

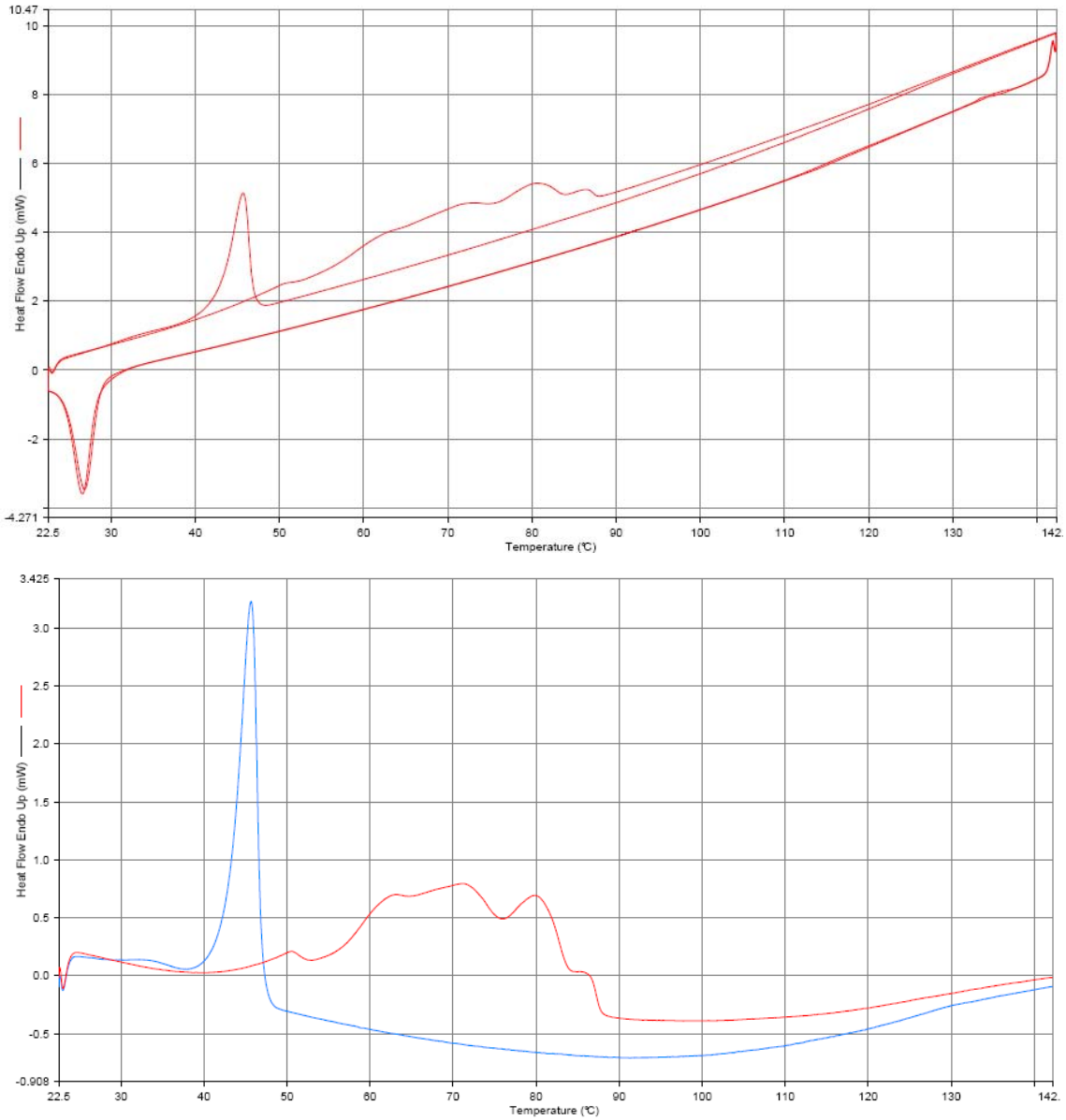

Figure 7.8: *Differential Scanning Calorimetric measurement of the sample of the mixture of (R)-**1,3Ph** acid and (R,R)-DACH (2:1), the sample was heated and cooled twice. In the first cycle the broad band of melting can be observed between 50 and 88°C, in the second heating the melting occurs at about 45-46 ºC. Solidifying is the same in both cycles and is observed at about 26 ºC in the cooling curves.*

Considering all of the data and comparing with STM results, where this combination of chirality of acid and amine gave the most stable structure on graphite 1-phenyloctane interface (see Chapter 5.2) it is expected to form a stable complex. Indeed the most pronounced peak in SAXS corresponds to the interplanar distance of 4.2 nm that is expected to be the size of the complex between acid and amine, which can be either model A or C in the Figure 7.4.

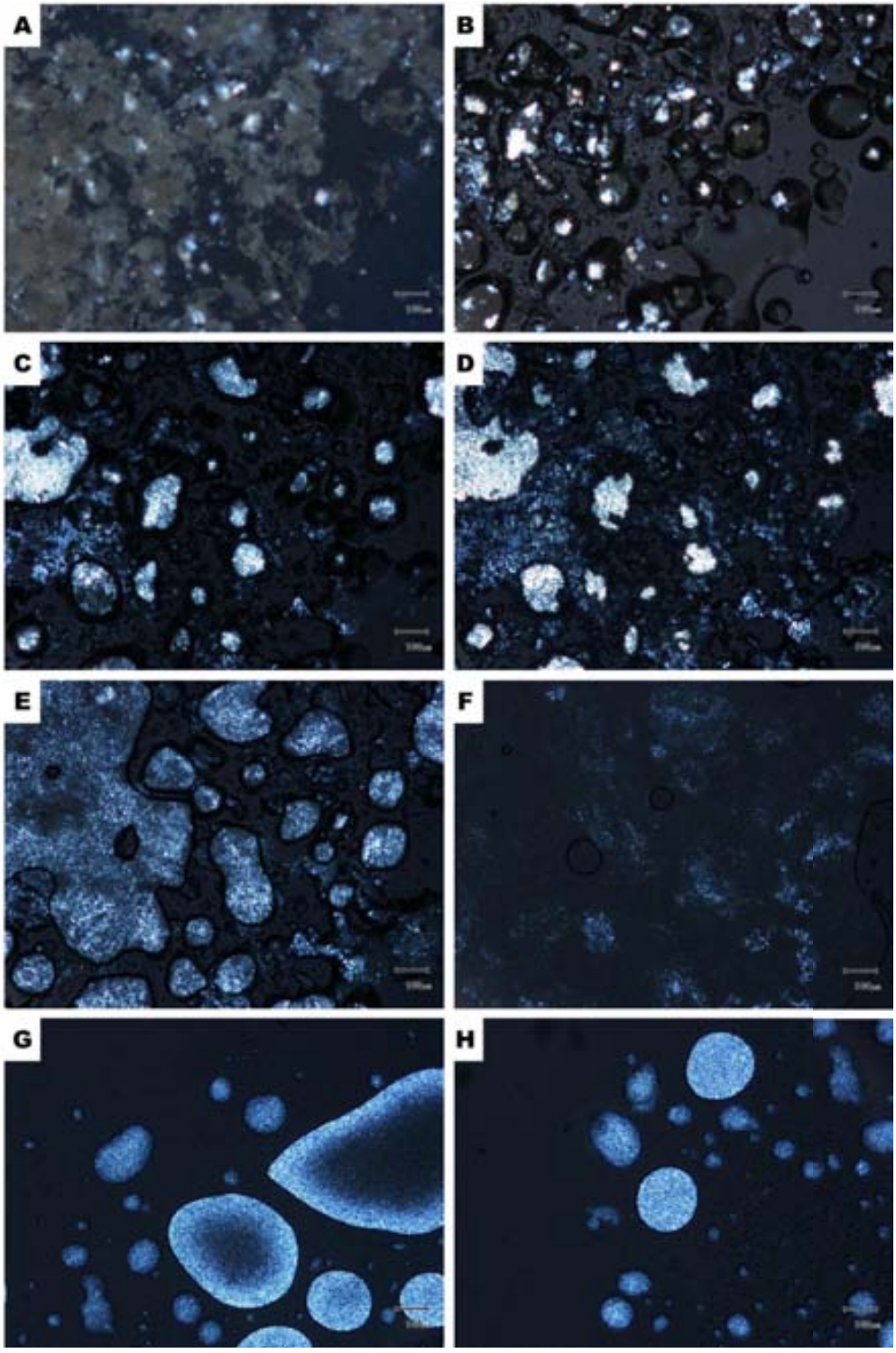

Figure 7.9: *Optical Microscope images of the mixture of (R)-**1,3Ph** acid and (R,R)-DACH (2:1). Image A, captured at 45°C shows the material as it was in room temperature, no changes observed in the structure of the material. Image B captured at 56°C shows first phase change, material gets partially liquid. Image C: at the temperature of 66°C recovered crystalline structure can be observed, and this effect is even clearer in image D, captured at 76°C. The sample truly melts at 83-84°C, what is presented in images E and F, image E just as the process starts, image F just before melting is over. Images G and H presents sample after fast cooling.*

7.5 (R)-1,3Ph acid, (R,R)-diaminocyclohexane and (S,S)-diaminocyclohexane (2:0.75:0.25)

The SAXS and WAXS patterns of the mixture of (*R*)-**1,3Ph** acid, (*R,R*)-diaminocyclohexane and (*S,S*)-diaminocyclohexane (2:0.75:0.25) are shown in Figure 7.10. The sample is crystalline, laminar, with two different distances between layers, 2.8 and 3.5 nm. The material melts at approximately at 80ºC. The spectrum in WAXS is difficult to interpret, a series of peaks occur indicative of a complex mixture of materials. The shift of the peaks in the SAXS and WAXS regions are an indication that the spacing between the lamellae in the material increase with increasing temperature, a feature not observed in the previous sample with enantiopure DACH.

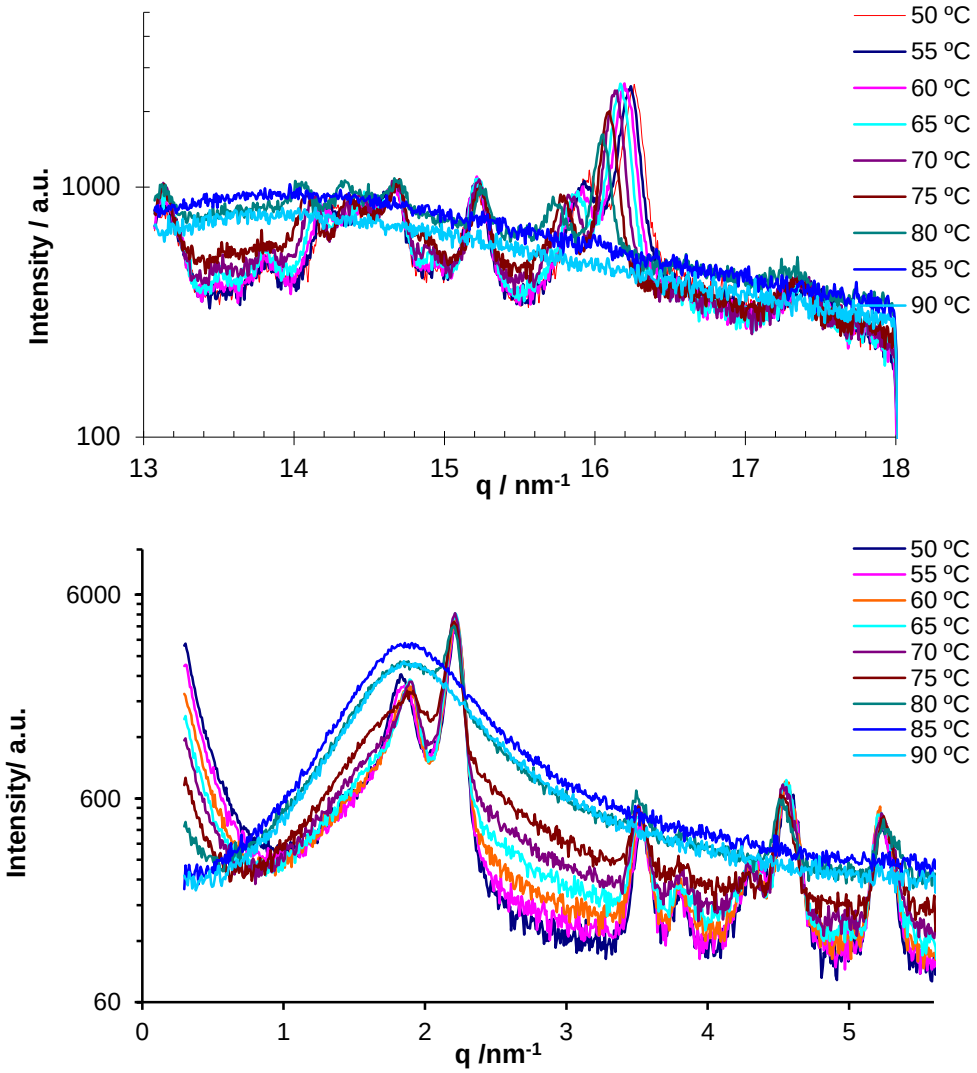

Figure 7.10: *WAXS (top) and SAXS (bottom) of the mixture of (R)-**1,3Ph** acid, (R,R)-DACH and (S,S)-DACH (2:0.75:0.25) in the heating cycle*

In the DSC measurements (Figure 7.11) the phase changes starts from approximately 49°C and the clearing point is at 82°C, with two maxima observed at 58°C and 72°C, a remarkably simpler behaviour to the mixture containing only (*R,R*)-DACH . It seems that there are two phases that coexist. In the second cycle of heating the melting one sharp peak at 42°C is observed, so another metastable phase forms during fast cooling.

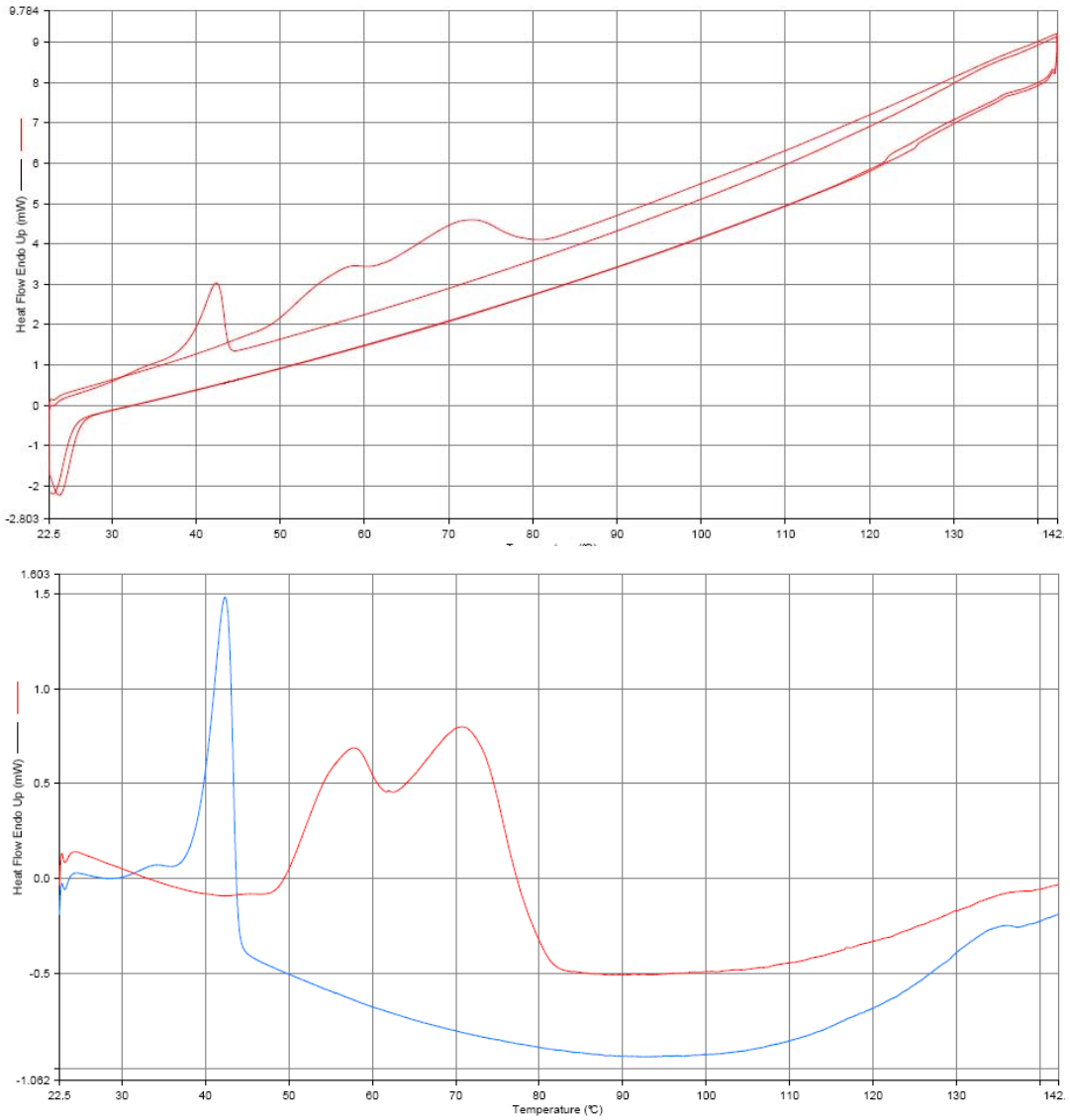

Figure 7.11: *DSC of the sample of (R)-**1,3Ph** acid, (R,R)-DACH and (S,S)-DACH (2:0.75:0.25): whole cycle (up) and corrected heating (down). In the heating one can see the difference between the first and second cycle, in the first one there are two broad peaks with maximum at 58°C and 72°C and the melting is over at about 82°C, in the second cycle there is just one sharp peak at 42°C.*

In the POM measurements (Figure 7.12) the melting starts at approximately 52°C, at 56°C (7.12B) the first change is observed where part of the material melts, and above

65°C (Figure 7.12 C, D and E) the second melting is observed, at 77°C melting is almost over (Figure 7.12F).

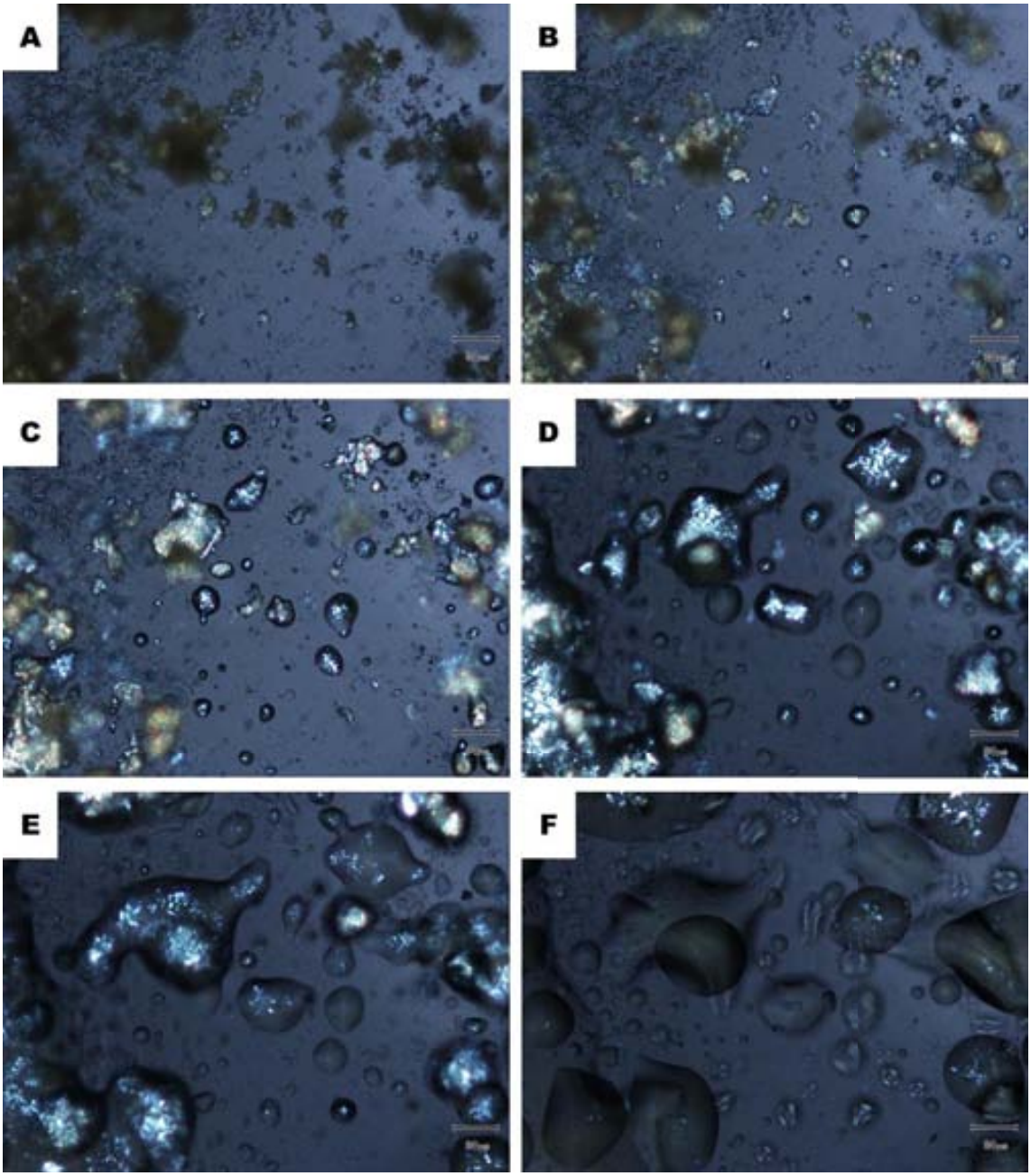

Figure 7.12: *Optical Micrographs of the mixture of (R)-**1,3Ph** acid and (R,R)-DACH (S,S)-DACH (2:0.75:0.25). Image A, captured at 50°C shows the material as it was in room temperature, no changes observed in the structure of the material. Image B captured at 56°C shows first phase change, material gets partially liquid. Images C (at 65°C), D (at 69°C) and E (at 72°C) show a progress in melting of material. The sample finally melts at a 74-77°C, that is presented in image F just before melting is over.*

Taking into consideration all of the data, clearly there are two different phases in this

mixture, one that melts at lower temperature (approximately 60-65°C, but melting is not sharp at all) with longer interplanar distance 3.5 nm. In SAXS, at 70°C and above this temperature, peaks of this structure disappear slowly. The second structure with a higher melting point melts above 70°C. At 80°C no signals in WAXS and very weak peaks in SAXS are observed, that could be an indication of liquid crystal behaviour. The clearing point is the same as melting in DSC, in POM the clearing point is observed at a slightly lower temperature.

7.6 (R)-1,3Ph acid and (rac) diaminocyclohexane (2:1)

The SAXS and WAXS data of (*R*)-**1,3Ph** acid and racemic diaminocyclohexane (2:1) are shown in Figure 7.13 and 7.14. A lot of peaks are observed compared with the other samples, and for this reason the spectrum is difficult to analyse, but the sample is crystalline. It melts at approximately 75°C. There are at least three principal structures with peaks at 1.44, 1.84 and 2.20 q/nm^{-1} that correspond to 4.35, 3.41 and 2.85 nm respectively. The peaks at 1.44 and smaller one at approximately 3 q/nm^{-1} disappear at temperature of 65°C, but in WAXS not big changes are observed until the melting at 75°C. The sample probably is a mixture of acid **1,3Ph** (Figure 7.4D) and acid amine complex (Figure 7.4A), and at higher temperature the amine becomes liquid and separated from crystalline acid (Figure 7.4D).

In cooling (Figure 7.14) the solidifying process can be followed, peaks are observed at 45 and 40°C in SAXS, while in WAXS no peaks are observed. The positions of peaks are: 1.53, 2.09, 3.03 q/nm^{-1} that correspond to 3.01 and 2.07 nm respectively. It is evident that the position of peaks does not coincide exactly with the ones observed before melting, and therefore confirms that (as for the other mixtures) the packing immediately after fast cooling is different to that after a long period standing at room temperature. Probably there packing is similar to the one presented in Figure 7.4B or 7.4E, however there is also possibility that racemic DACH (melting point 15°C) is trapped inside crystal structure of **1,3Ph** as a liquid.

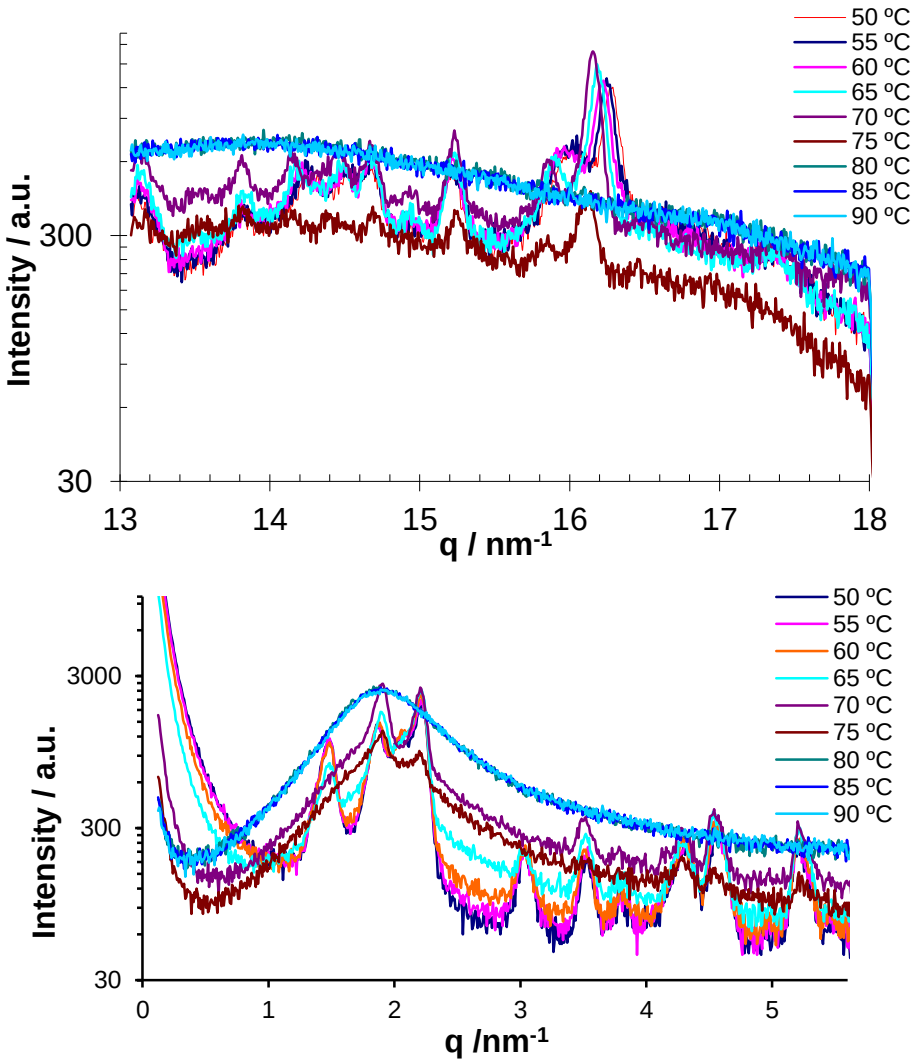

Figure 7.13: *WAXS and SAXS bottom during heating of (R)-**1,3Ph** acid and (rac)-DACH (2:1).*

In DSC (Figure 7.15) there is very broad peak observed for melting, starting at approximately 48°C and finishing at 79°C, with two maxima, at 63°C and at 71°C. Possibly there is the same structure that was observed in previous sample. Two maxima means that there are two phases, but bearing in mind the SAXS of the sample, the shoulder at approximately 55°C could be sign of existence of another phase transition.

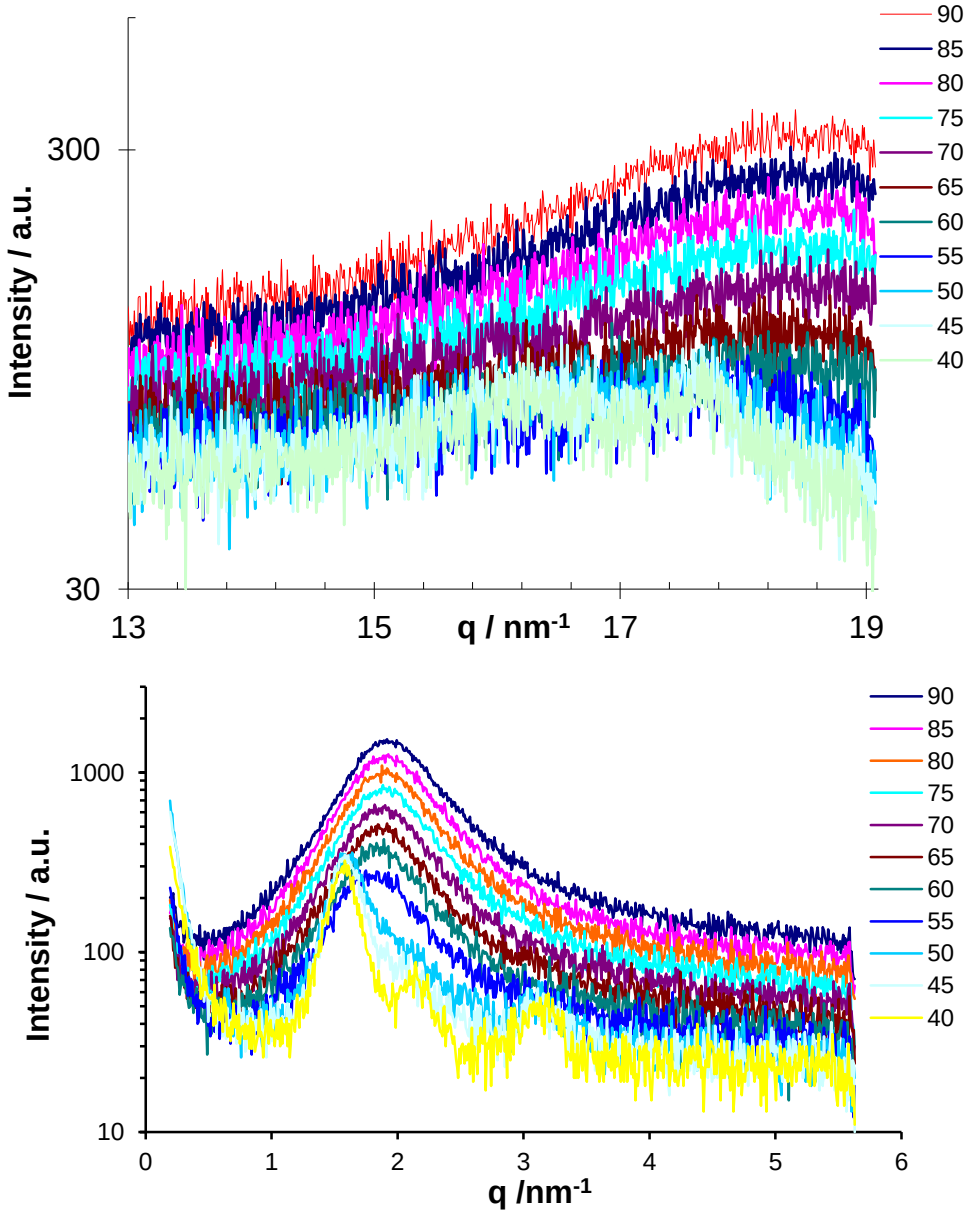

Figure 7.14: *WAXS and SAXS bottom during cooling of (R)-**1,3Ph** acid and (rac)-DACH (2:1).*

In the POM experiments (Figure 7.16) at 30°C the material appears as it was at room temperature, no changes were observed in the structure of the material. Image B captured at 51°C shows that material became more birefringent with increasing temperature. Then the first phase change is observed, the material gets partially liquid (Image C: at 58°C). In the next image, D, at 70°C the crystals are covered with liquid. The melting at 74°C is presented in the images E and F. The phase changes observed with the microscope are taking place consecutively so it is difficult to determine where each change starts and finish, as one might expect from the DSC curves. There are at least three processes observed: change from quite amorphous solid (image A) into

crystalline solid (images B and C), melting of part of the material (images C and D) and clearing point (images E and F).

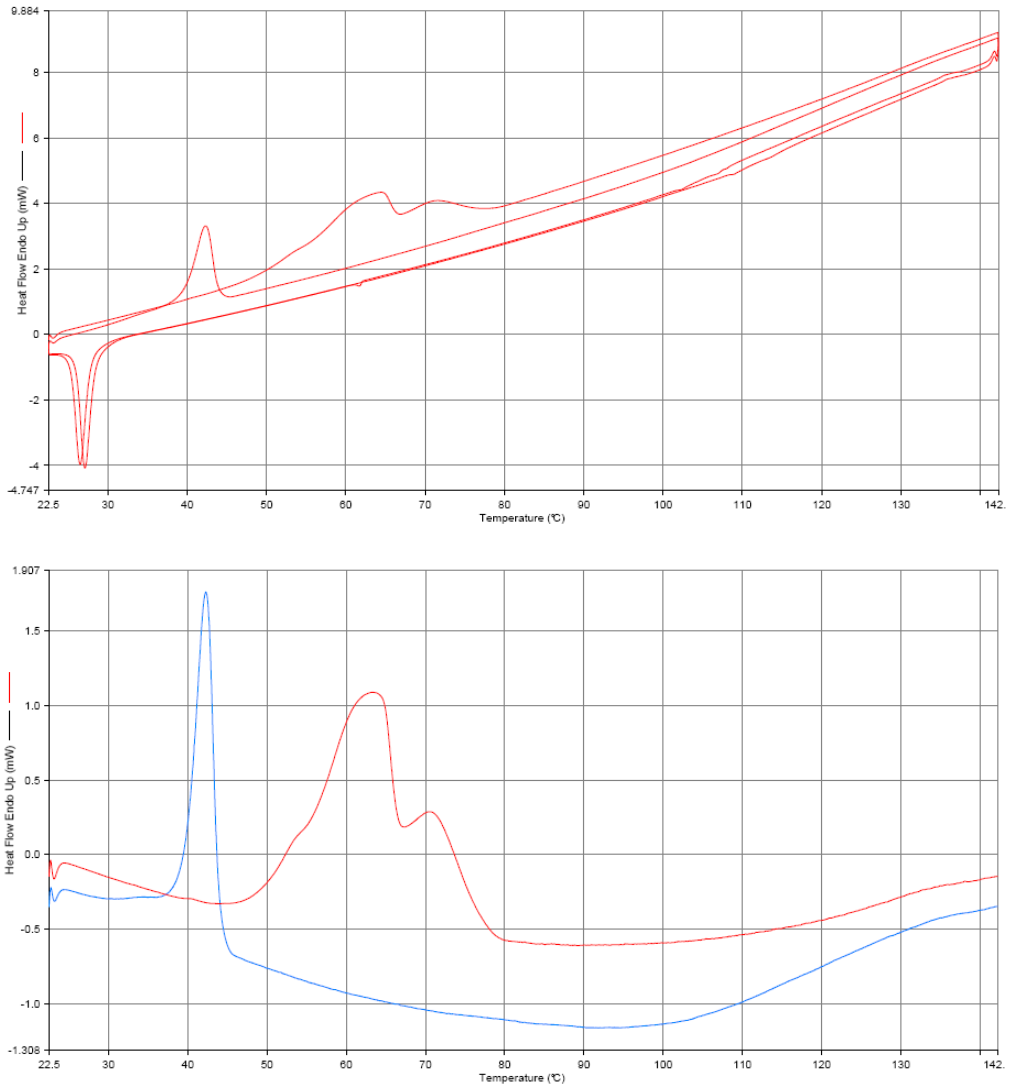

Figure 7.15: *DSC of the sample of (R)-**1,3Ph** acid and (rac) DACH (2:1), whole cycle (top) and corrected heating (bottom). In the heating curve one can see the difference between the first and second cycle, in the first one have two broad peaks with maxima at approximately 63°C and 71°C and the melting is over at about 82°C, in the second cycle there is just one sharp peak at 42°C.*

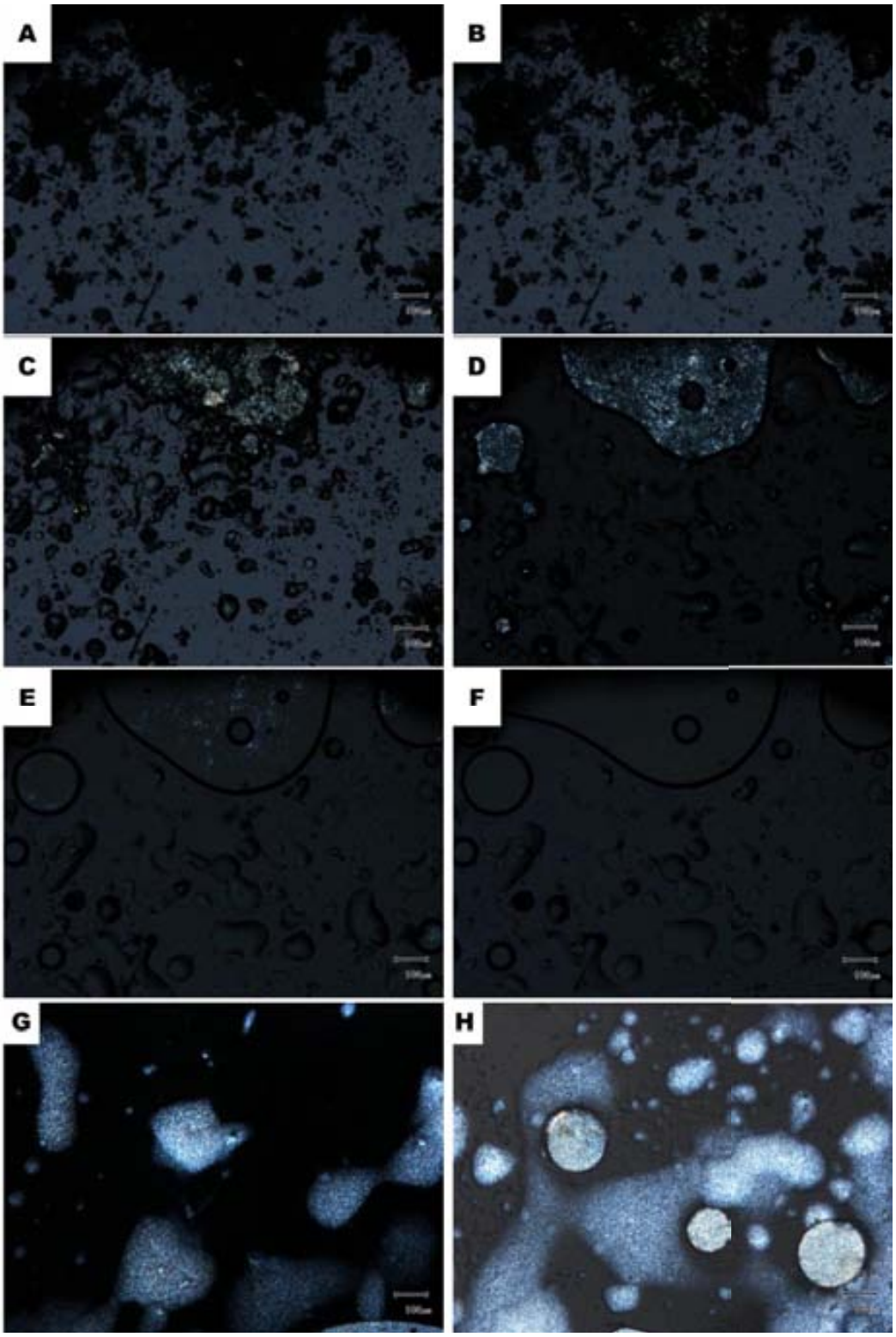

Figure 7.16: *Optical Microscope images of the mixture of (R)-**1,3Ph** acid and (rac)-DACH (2:1). Image A, captured at 30°C shows the material as it was in room temperature, no changes observed in the structure of the material. Image B captured at 51°C shows that material became more crystalline with temperature. Image C: at the temperature of 58°C material is partially liquid, in image D, at 70°C the crystals are covered with liquid. The melting at 74°C is presented in the images E and F. Images after cooling are presented in G and H.*

In the SAXS (Figure 7.13 and 7.14) this process also can be followed, as the peak at 1.44 q/nm^{-1} disappears at 70°C. The melting point observed in POM is a bit lower (74°C) than with other techniques (75 < mp < 80°C in SAXS and 78°C in DSC). Apart from this observation, there are a lot of peaks in the XRD measurements, the spectrum is difficult to analyse, but the sample is crystalline. There are at least three principal structures with peaks at 1.44, 1.84 and 2.20 q/nm^{-1} that correspond to 4.35, 3.41 and 3.11 nm respectively. The structures observed can be partially identified: as there are the same structure that was observed for mixture of (*R*) **1,3Ph** with (*R,R*) DACH . (most probably Figure 7.4A)

7.7 (R)-1,3Ph acid and (R,R)-diaminocyclohexane(S,S)-diaminocyclohexane (2:0.25:075)

The SAXS and WAXS of the mixture of (*R*)-**1,3Ph** acid and (*R,R*)/ (*S,S*)-diaminocyclohexane (2:0.25:075) is shown in the Figure 7.17. In the SAXS the peaks indicate that the structure is not laminar, it melts at about 85°C. The distance between layers is 3.3 nm which corresponds either to the complex of **1,3Ph** acid and amine (Figure 7.4B or E) or to the acid **1,3Ph** (Figure 7.4D) and second interplanar distance equals 1.46 nm. In the WAXS pattern there are three main peaks, at 13.79, 15.23 and 16.02- 16.08 nm^{-1}with side band at 16.40-16.56, that correspond to respectively 0.456, 0.413, 0.392-391 and 0.383-379 nm. In case of last two signals there is an unusual tendency, with higher temperature the interplanar distance gets shorter.

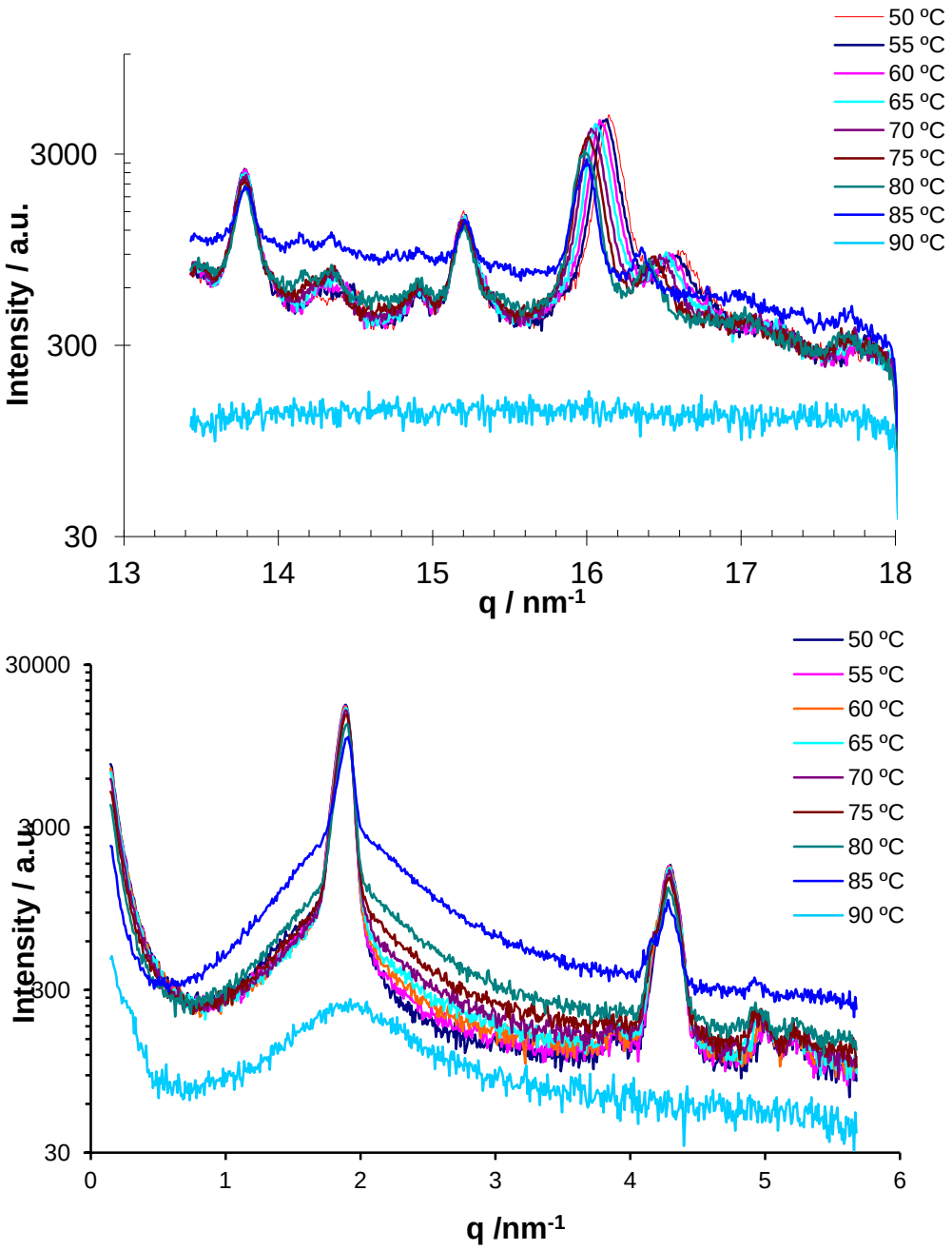

Figure 7.17: *WAXS top and SAXS bottom of mixture of (R)-**1,3Ph**acid and (R,R)-DACH (S,S)-DACH (2:0.25:075).*

In the DSC trace of the sample (Figure 7.18) two well separated peaks are observed with maxima at 50°C and 80°C, clearly there are two phase changes. During the second heating cycle, the sample shows one peak at 42°C.

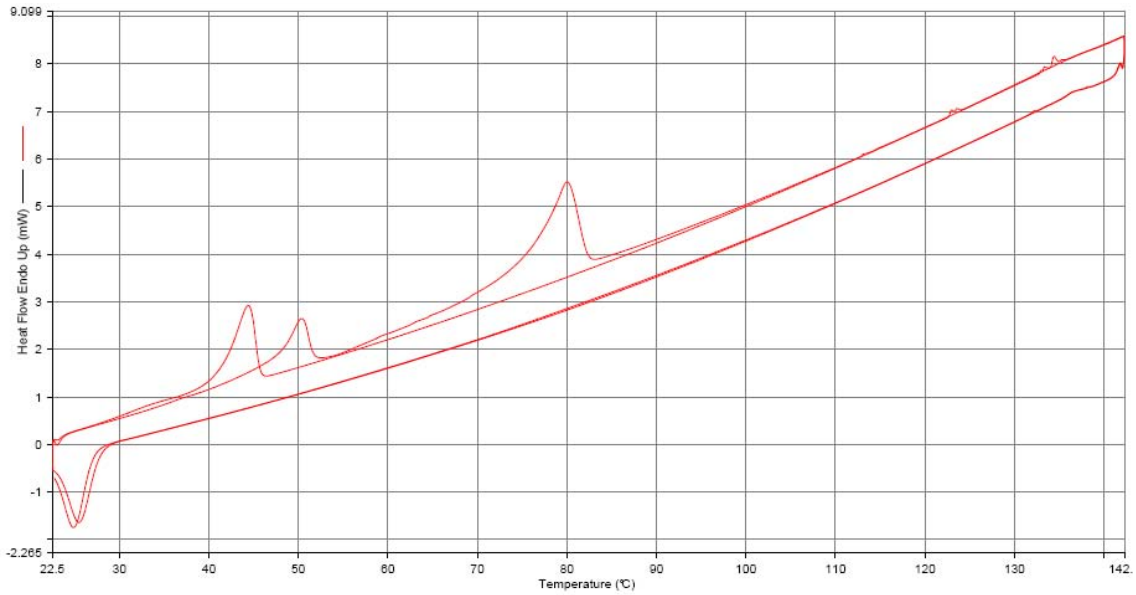

Figure 7.18: *DSC of the sample of (R)-**1,3Ph**acid and (R,R)-DACH (S,S)-DACH (2:0.25:075). In the heating one can see the difference between the first and second cycle, in the first one there are two peaks with maximum at about 50°C and 80°C, in the second cycle there is just one sharp peak at 42°C.*

In POM (Figure 7.19) the sample also shows two phase changes, the material became more crystalline in the first change (images A –D) and melting (images E-H). Clearing point is approximately at 80°C. In the SAXS one just can follow the second phase change, as there are no significant differences between spectra at 50°C and 80°C.

Taking in account that the melting point is close to the one observed for pure **1,3Ph**, and a similarity of peaks in XRD of **1,3Ph** and SAXS of this sample, most probably there is phase separation between acid and amine. This explanation is supported by DSC and POM measurement, where two separated phase changes are observed, first one at 50°C close to the melting point of DACH (40-43°C) and second one at 80°C close to the melting of acid (82°C).

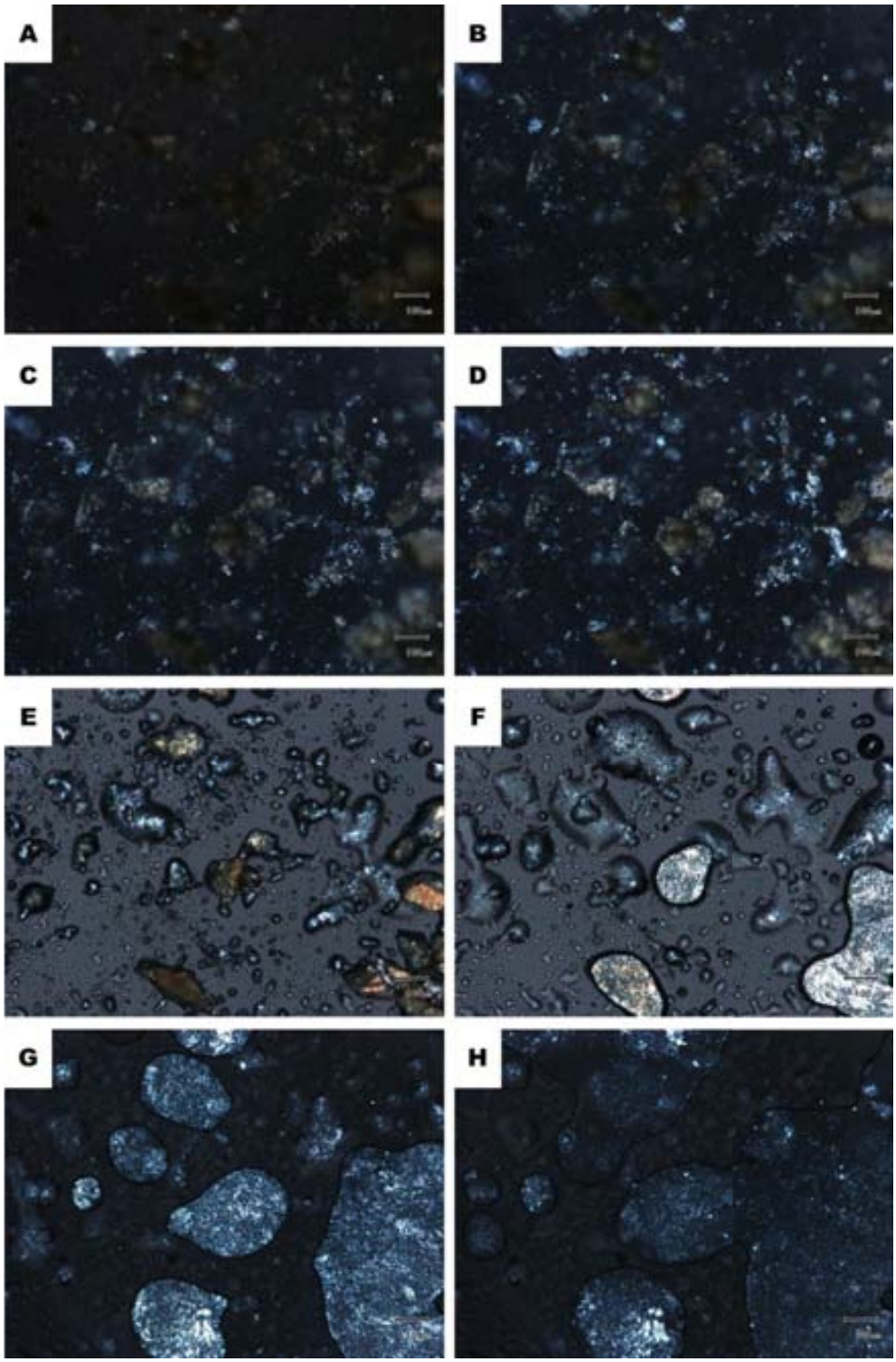

Figure 7.19:*Optical Microscope images of the mixture of (R)-**1,3Ph** acid and (R,R)-DACH (S,S)-DACH (2:0.25:075). Image A, captured at40°C shows the material as it was at room temperature, no changes observed in the structure of the material. Image B captured at 55°C shows the first phase change, the material becomes more crystalline. With the increasing temperature, the sample becomes brighter (images C at 63°C and D at 73°C). In image E at 77°Cthe meltingis started. The sample finally melts at a 78-80°C, that is presented in images F and G at 78°C and in image H at 79°C, just before last crystals disappears*

7.8 (R)-1,3Ph acid and (S,S)-diaminocyclohexane (2:1)

The as-prepared and matured sample of (*R*)-**1,3Ph** acid (*S,S*) -diaminocyclohexane is crystalline at room temperature as shown by the diffraction data (Figure 7.20). Melting was not observed in SAXS, although there is considerable peak broadening, so the clearing point has to be above 90°C. The distance between the layers is 3.25 nm which corresponds to the length of a molecule of acid. Another peak corresponds to a spacing of 1.46 nm. In WAXS, similarly to the sample described in section 7.7, there is just one structure observed, that does not melt until 90°C.

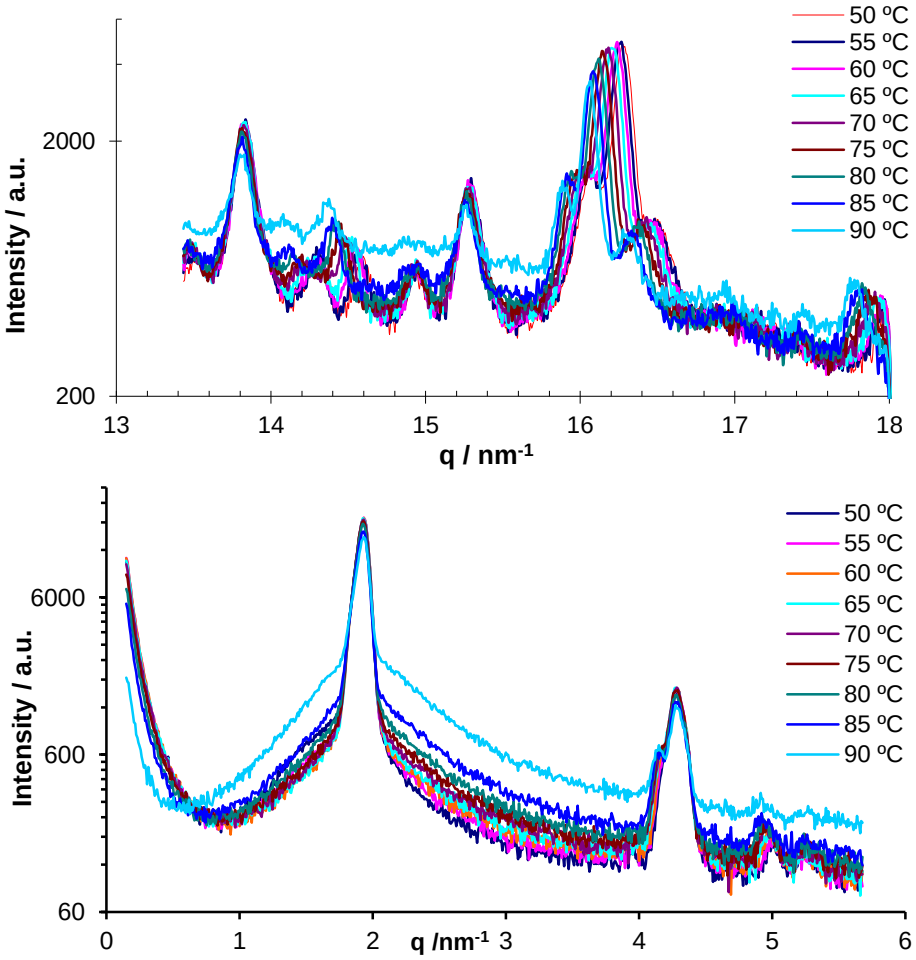

Figure 7.20: *WAXS top and SAXS bottom of the mixture of (R)-**1,3Ph** acid and (S,S)-DACH (2:1).*

In DSC (Figure 7.21) there two sharp peaks were observed with maxima at 52°C and 86°C, what is unusual compared with the other samples is an exothermic phase change just after the first phase change, probably the molecules reorganize into more stable structure that melts at 86°C.

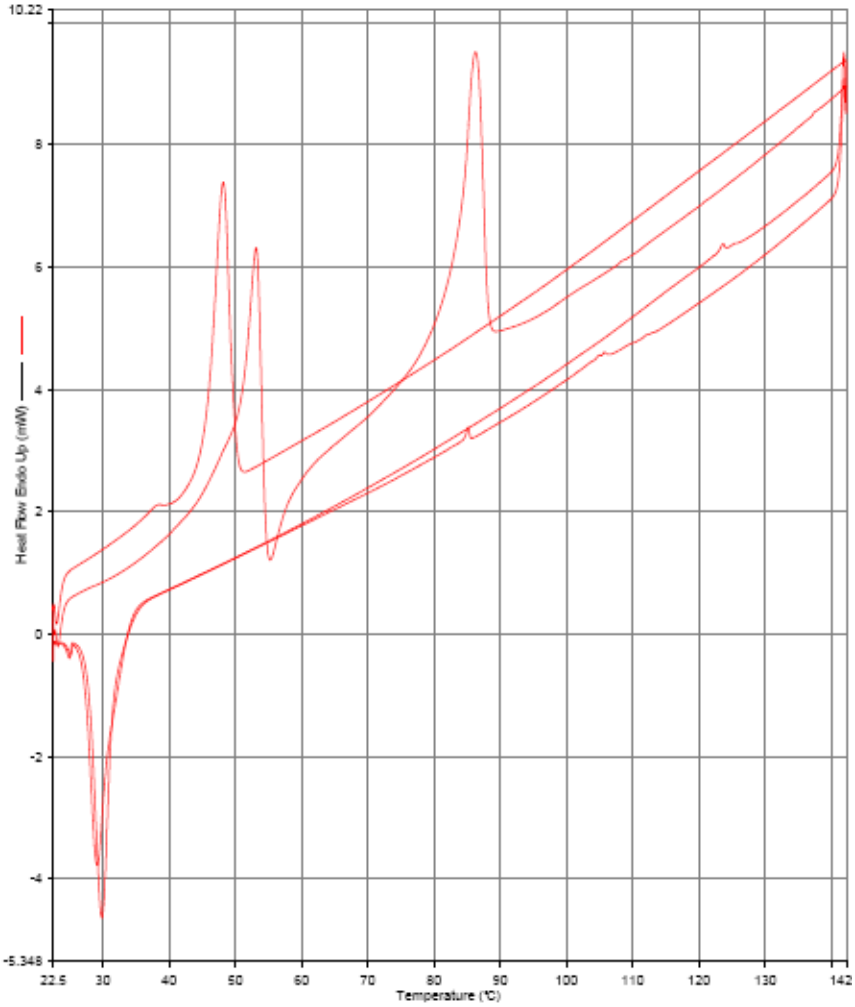

Figure 7.21: *DSC of the sample of (R)-**1,3Ph** acid and (S,S)-DACH (2:1). In the heating one can see the difference between the first and second cycle, in the first one there are peaks with maximum at approximately 52°C and 86°C, in the second cycle there is just one sharp peak at 48°C. There is a curious effect, after first phase transition at about 55°C the sample is exothermic seems like a crystallization after the first phase transition.*

In the DSC the clearing point is just below 90°C and in POM the clearing is observed at 86°C.

There is a significant discrepancy between the observed melting points in different techniques; in DSC and POM the material melts at 86 and 85°C respectively, while in SAXS the melting is not observed even at 90°C. Considering the peaks in SAXS there is either coexistence of separated structures of acid and amine in crystalline solid or a structure that can change the phase at approximately 52°C then exothermic phase change takes place and sample finally melts at 85-86°C. Taking in account that the melting point is just few degrees higher than the one observed for pure **1,3Ph**, and a of peaks in XRD of **1,3Ph** and SAXS of this sample, it can be assumed that the crystal

phase of acid **1,3Ph** is separated from amine phase.

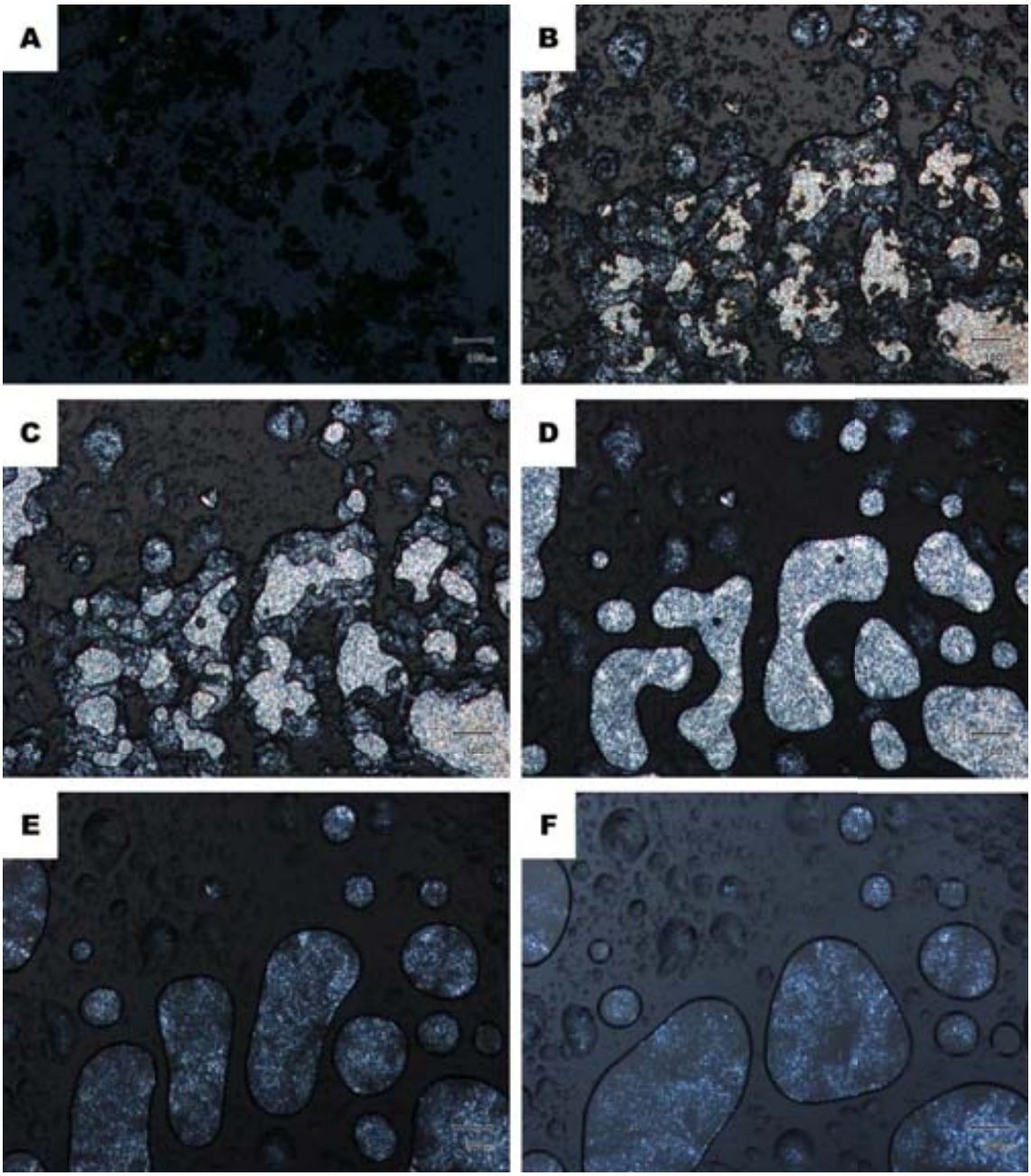

Figure 7.22: *Optical Microscope images of the mixture of (R)-**1,3Ph** and (S,S)-DACH (2:1). Image A, captured at 65°C shows the material after the first phase transition. Image B captured at 77°C shows the structure before the second transition. Image C at the temperature of 82°C when the material starts melting, image D at 83°C, shows the structure as it melts. The sample truly melts at 83-85°C, that is presented in images E and F, image E at 84.5°C, image F just before melting is over at 85°C.*

7.9 (S)-1,3Ph acid and (R,R)-diaminocyclohexane (2:1)

The mirror image of the preceding sample, that of (*S*)-**1,3Ph** acid (*R,R*) – diaminocyclohexane, is crystalline at room temperature as shown by the diffraction data (Figure 7.23). In SAXS there are three different peaks observed, the first at 1.51 q/nm^{-1}, second, stronger one at 1.89 q/nm^{-1} and the last one at 4.25 q/nm^{-1} that correspond to distance respectively 4.1 nm, 3.28 nm and 1.47 nm. During heating the first peak loses its intensity, and disappears at 80°C. Melting point of the sample takes place between85 and 90°C. The distance of 4.1 nm corresponds to the complex of acid **1,3Ph** with DACH and 3.28 nm is the length of molecules of acid **1,3Ph**.

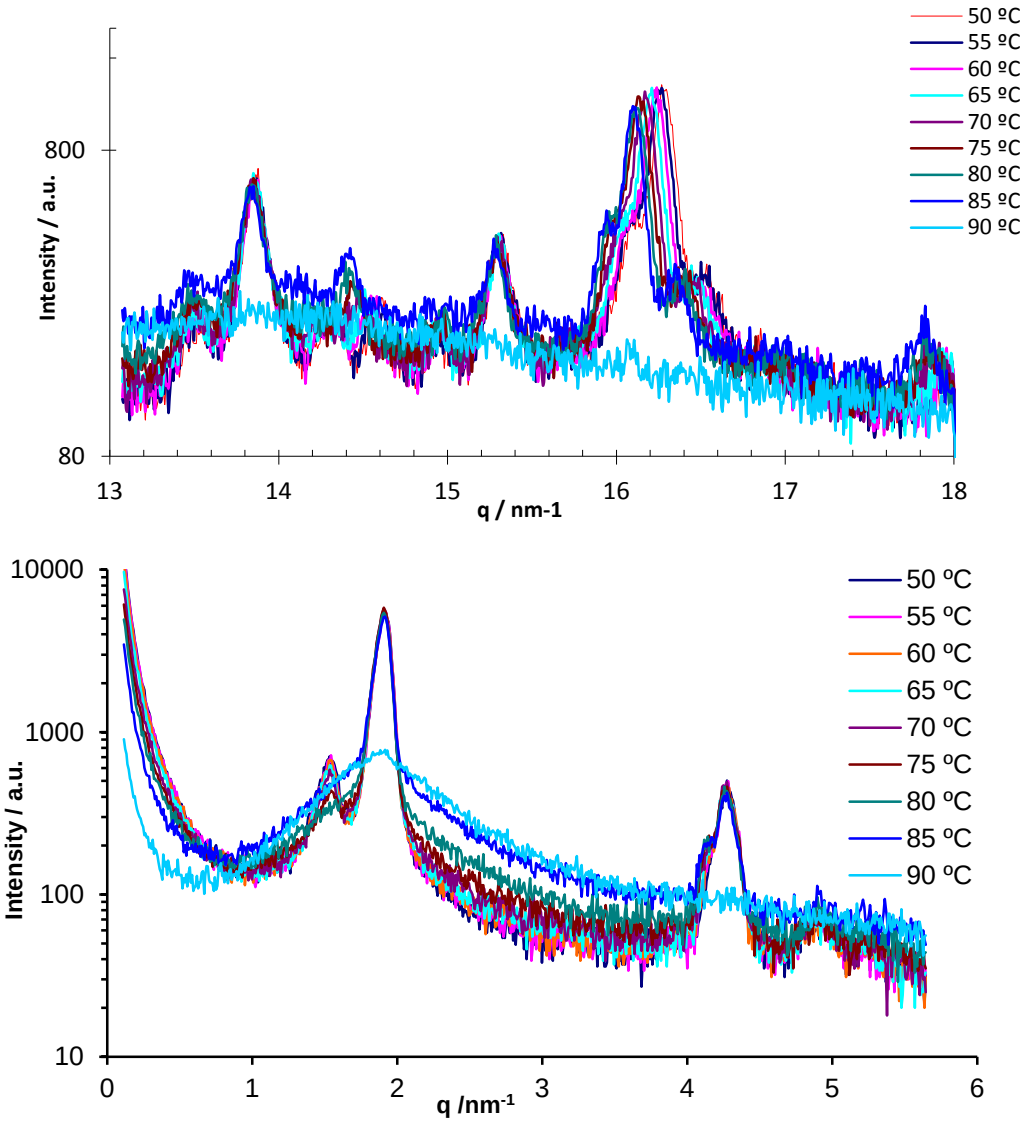

Figure 7.23: *WAXS top and SAXS bottom of the sample of (S)-**1,3Ph** acid and (R,R)-DACH (2:1)*

In DSC (Figure 7.24) there are two phase changes observed, one at 62°C, followed by small exothermic change, and then the melting of the material at 82°C takes place. The last phase change is most probably melting of the acid **1,3Ph**.

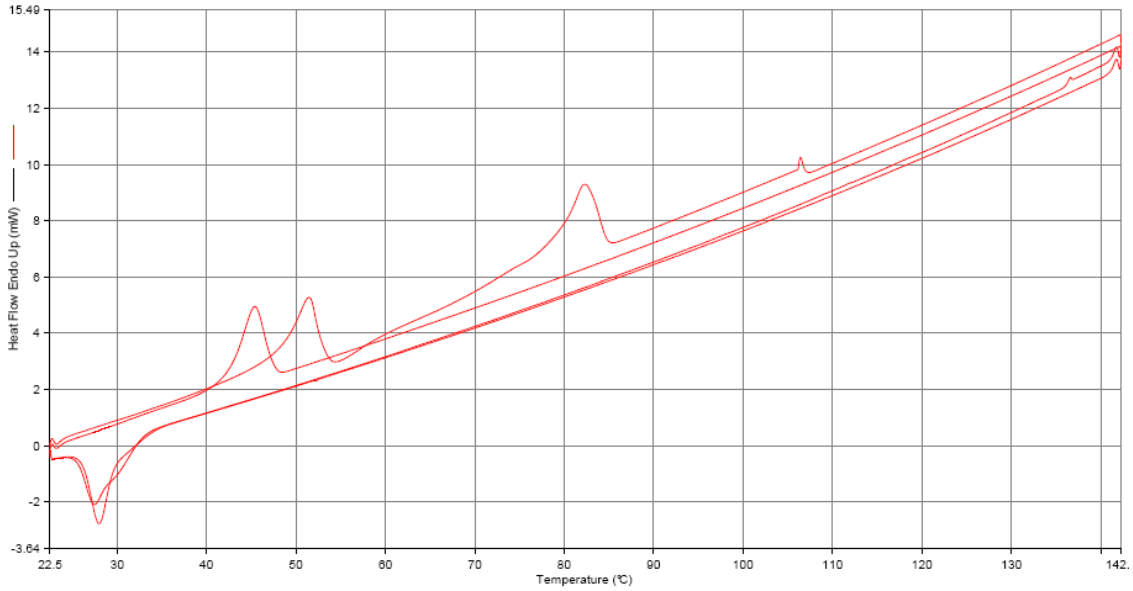

Figure 7.24: *DSC of the mixture of (S)-**1,3Ph** acid and (R,R)-DACH (2:1). The first phase change takes place at 62°C, after that one can observe the small area that goes below the line, this is exothermic crystallization. At 82°C the final melting is observed. In the second cycle melting occurs at 45°C. In the cooling the crystallization takes place at about 28°C in both first and the second cycle.*

In POM (Figure 7.25) the same two changes are observed, first at approximately 53°C (image B) the material becomes partially liquid, then it becomes more crystalline, as observed by shiny areas in polarised light (image C). Then the melting of the material takes place at 81-83°C (imaged D and E). This particular sample was checked after heating to prove whether the sample is crystalline or not after heating and fast cooling. In image F the sample is presented after 5 hours in room temperature, and clearly it is crystalline, as demonstrated with the mechanical scratch.

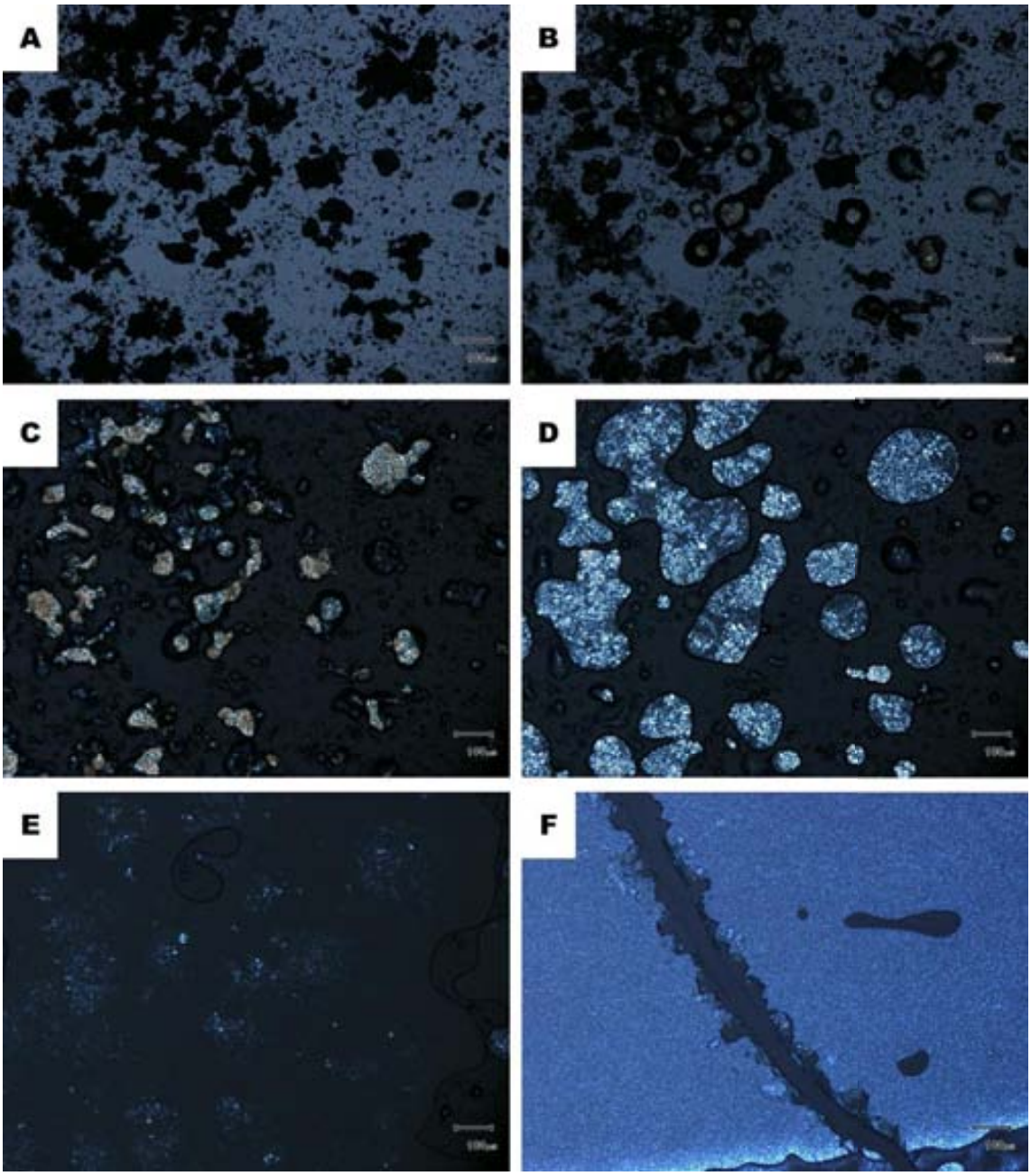

Figure 7.25: *Optical Microscope images of the mixture of (S)-**1,3Ph** acid and (R,R)-DACH (2:1). Image A, captured at 45°C shows the material as it was in room temperature, no changes observed in the structure of the material. Image B captured at 53°C shows that material partially melts and becomes more crystalline with temperature. Image C: at the temperature of 79°C material is partially liquid, before last phase change. In the images D and E, the melting of the material can be observed at 81°C and 83°C. In image F the material after cooling and 5h at RT is presented. The scratch going through the middle of the image was made mechanically to prove that the material is truly solid and crystalline.*

There is good agreement between the different techniques, as the changes observed in DSC and POM takes place at almost very same temperature, in SAXS the first change

could be the melting of the structure that gives peak at 1.51 q/nm^{-1},what is observed as the peak disappear. The clearing point is observed at slightly lower temperature (84°C) in POM than in DSC (86°C) and SAXS (85°C<mp <90°C).

Comparing with the mirror image sample described in section 7.8 there is an extra peak in SAXS observed at 1.51 q/nm^{-1} until 80°C, above this temperature the sample spectra are very similar, both DSC and POM melting point is observed at virtually same temperature. Clearly unlike the mirror image sample, here there is some kind of stable complex between acid and amine (Figure 7.4A), but it melts and above 80°C crystalline **1,3Ph** coexist with either liquid amine or amine –acid complex.

7.10 (S)-1,3Ph acid(R)-1,3Ph acid and (R,R)-diaminocyclohexane (1.5:0.5:1)

Samples(*S*)-**1,3Ph** acid (*R*)-**1,3Ph** acid and (*R,R*)-DACH (1.5:0.5:1), (*rac*)-**1,3Ph** acid and (*R,R*)-DACH (2:1) and (*S*)-**1,3Ph** acid (*R*)-**1,3Ph** acid and (*R,R*)-DACH (0.5:1.5:1) do not melt before 90°C , because of that the SAXS was measured also in the range 90-120°C. All the samples have a peak that corresponds to distance around 3.3 nm, and small one that corresponds to distance around 1.45 nm.

In SAXS (Figure 7.26) there are just two peaks, at 1.80 q/nm^{-1} and 4.56 q/nm^{-1} that correspond to 3.49 nm and 1.38 nm respectively. The melting takes place at approximately 110°C, a bit higher than observed with DSC and POM. In the WAXS one can observe that the distances between layers decreases with increasing temperature (peaks move to the right in the spectrum).This effect is not common, usually the separation increases. The position of the peak in the WAXS moves from 15.50 to 15.58 q/nm^{-1} that corresponds to distance of 0.405-0.403 nm.

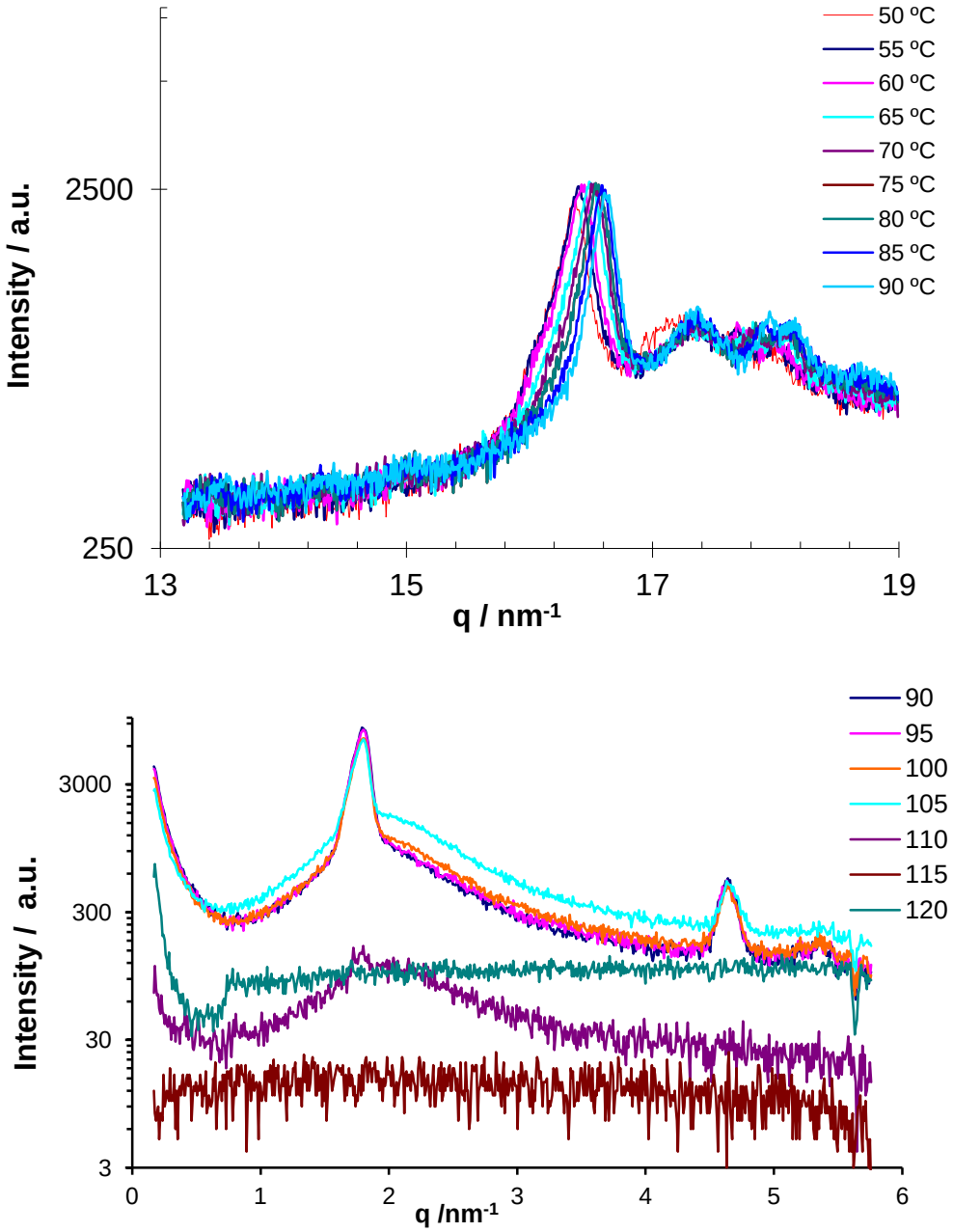

Figure 7.26: *WAXS top and SAXS bottom of the mixture of (S)-**1,3Ph** acid (R)-**1,3Ph** acid and (R,R)-DACH (1.5:0.5:1)*

In DSC (Figure 7.27) there are two broad peaks observed in the first heating, the first phase change starts at approximately 45°C and continuously takes place until 55°C. There is broad maximum at 52°C with another broad shoulder (probably another peak at 47°C). The final melting is very broad peak starting at approximately 75°C and finishes at 102°C, with a maximum at 96°C. The peak at 40°C is assigned to an impurity in this sample.

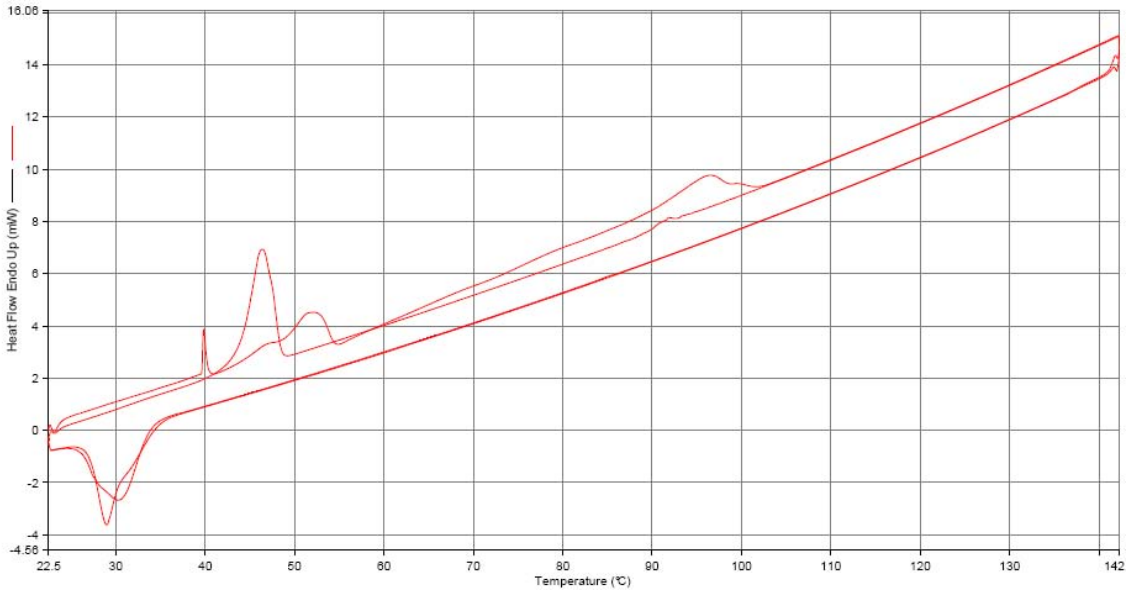

Figure 7.27: *DSC measurement of (S)-**1,3Ph** (R)-**1,3Ph** and (R,R)-DACH (1.5:0.5:1) The sample gives very sharp peak at 40°C (probably artefact), broad one at approximately 47°C which goes smoothly into another broad one with maximum at 52°C. The final melting is in the broad band with maximum at 96°C. The second cycle shows just one peak at 46°C. In the cooling there is just one peak with maximum at 28-30°C.*

In Figure 7.28 there are POM images that show how with increasing temperature sample becomes more crystalline (images B, C and D) at 53°C and higher. Then the melting of the material is presented, which takes place in the same range of temperatures as the second phase change in DSC (88-105°C). The sample after cooling down is presented in the last image.

The peaks observed in SAXS suggest that there is same arrangement of material as in the previous two samples – crystalline **1,3Ph**. On the other hand in DSC there are two peaks at 40-55°C and the last phase change takes place at significantly higher temperature (96°C), but it might be caused by chiral composition of the sample.

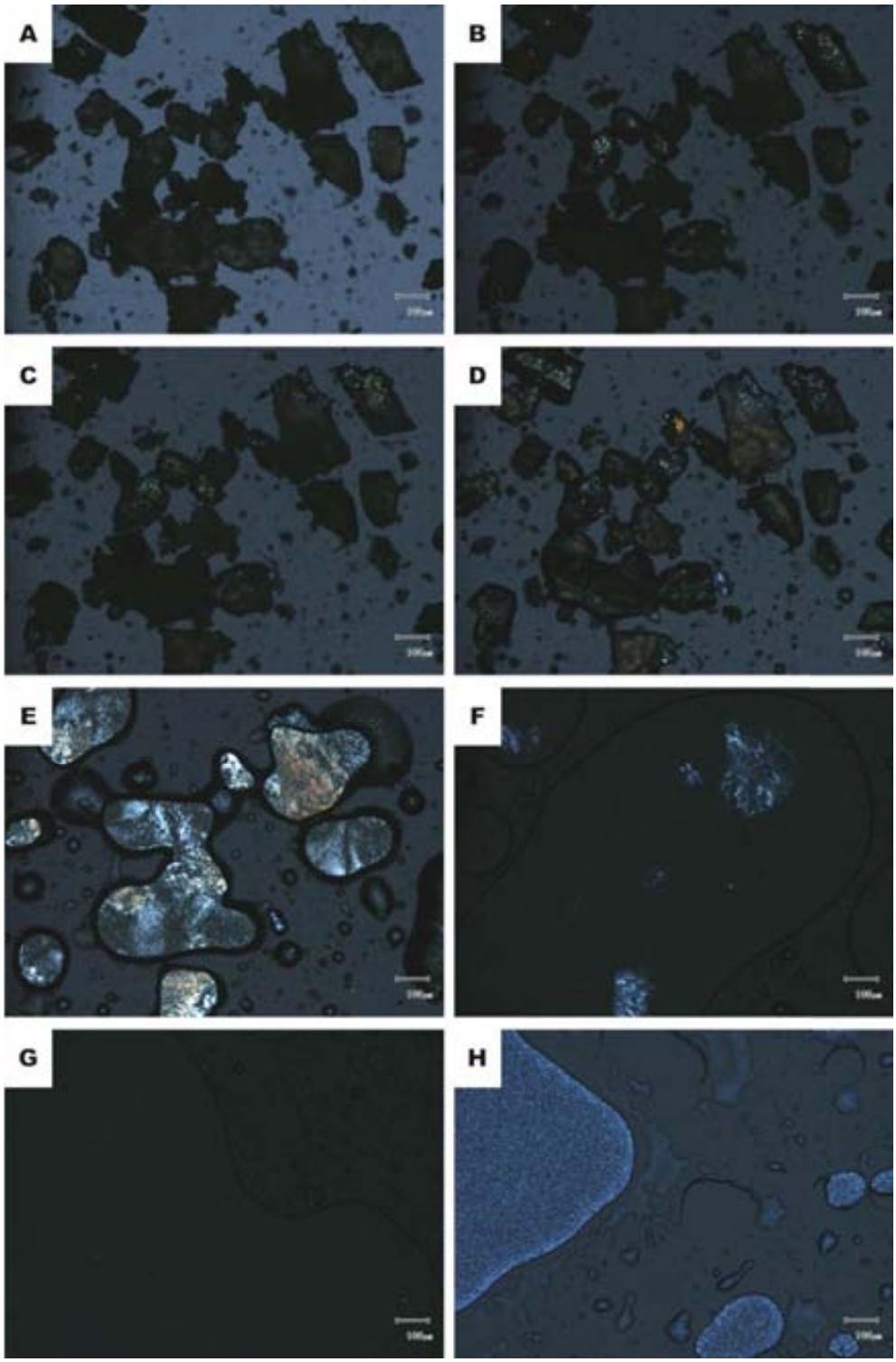

Figure 7.28: *Optical Microscope images of the mixture of (S)-**1,3Ph** acid (R)-**1,3Ph** acid and (R,R)-DACH (1.5:0.5:1). Image A, captured at 41°C shows the material as it was in room temperature, no changes observed in the structure of the material. Images B and C captured at 53°C and 60°C respectively shows that material becomes more crystalline with temperature. Image D: material before the melting at 88°C. Images E and F at 94°C and 100°C respectively, present melting of material. Image G captured at 105°C when the material is completely melted. Image H at RT after cooling.*

7.11 (rac)-1,3Ph acid and (R,R)-diaminocyclohexane (2:1)

The SAXS and WAXS of (*rac*)-**1,3Ph** acid (*R,R*) -diaminocyclohexane is shown in Figure 7.29. In SAXS there are two principal peaks, at 1.80 q/nm^{-1}and 4.65 q/nm^{-1} that correspond to 3.49 nm and 1.35 nm respectively. The position of the peak in WAXS are 13.99, 14.17, 14.86, 15.01 and 15.50 to 15.56 q/nm^{-1}, what correspond to 0.449, 0.443, 0.423, 0.419 and 0.405-0.404 nm respectively. The peaks in WAXS are moving slightly, the distances are bigger with temperature.

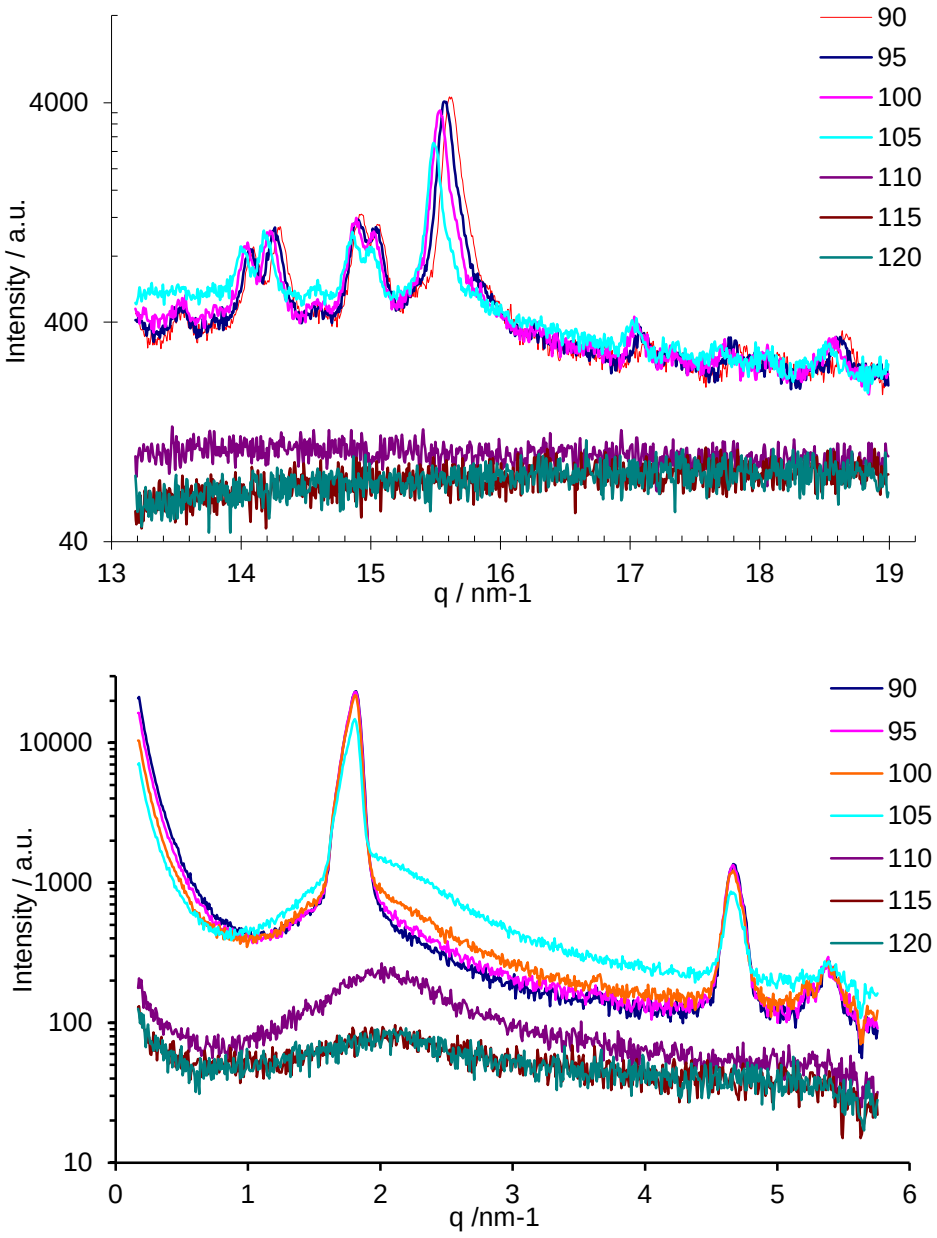

Figure 7.29: *WAXS top and SAXS bottom of the mixture of (rac)-**1,3Ph** acid and (R,R)-DACH (2:1)*

In DSC (Figure 7.30) the sample shows one small peak at 48°C and then the melting takes place from approximately 94°C until 106°C with maximum at 104°C.

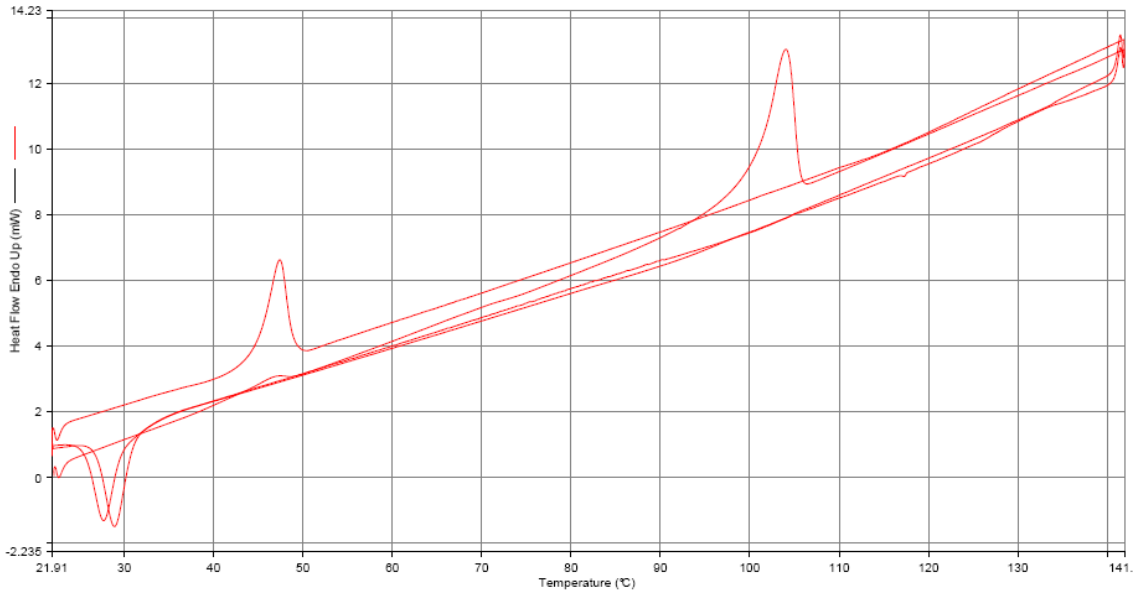

Figure 7.30: *DSC of the mixture of (rac)-**1,3Ph** acid and (R,R)-DACH (2:1). Sample shows small peak at 48°C and melting peak at 104°C. In the second cycle material melts at 48°C. In the cooling the crystallization is observed at 28 and 29°C.*

In POM (Figure 7.31) there is very little change observed until the melting starts at approximately 88°C, and it takes place until 103°C, slightly lower temperature than in DSC.

In SAXS the sample melts between 105°C and 110°C, few degrees higher than observed with DSC and POM. The packing of the solid seems to be the same as the previous three samples – crystalline **1,3Ph**, but again the melting point is higher than the others, but it might be caused by. What is surprising is the small intensity of the first peak in DSC.

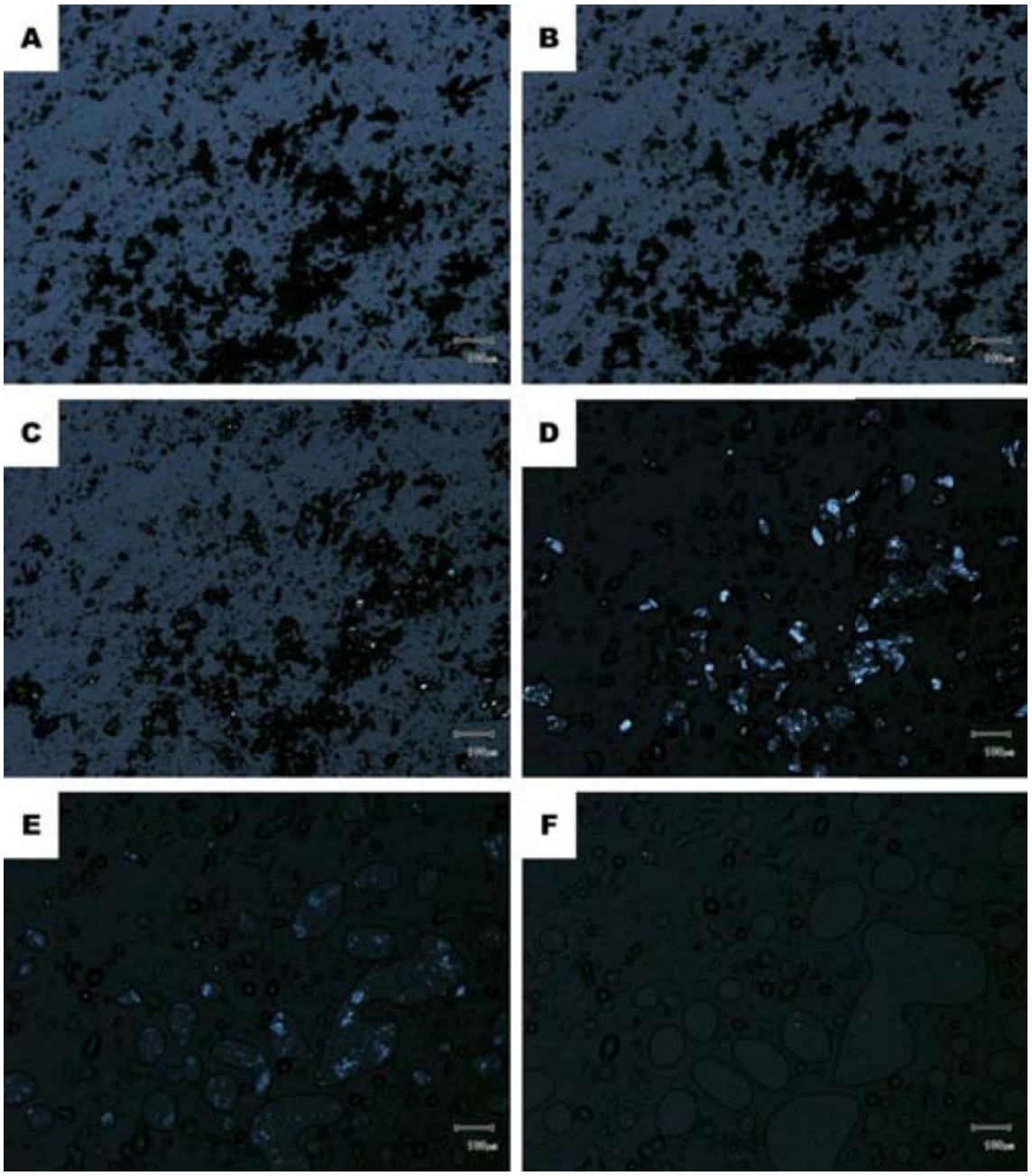

Figure 7.31: *Optical Microscope images of the mixture of (rac)* ***1,3Ph*** *acid and (R,R)-DACH (2:1). Image A, captured at 35°C shows the material as it was in room temperature, no changes observed in the structure of the material. Image B captured at 58°C shows virtually no change. Image C at the temperature of 88°C material is just before the melting starts. In the images D the partially liquid material can be observed at 101°C. In image E, at 102°C and F at 103°C the melting of the material is presented.*

7.12 (S)-1,3Ph acid(R)-1,3Ph acid and (R,R)-diaminocyclohexane (0.5:1.5:1)

SAXS and WAXS of (*S*)-**1,3Ph** acid (*R*)-**1,3Ph** acid and (*R,R*)-diaminocyclohexane (0.5:1.5:1) is shown in Figure 7.32. In SAXS there are two peaks observed, at 1.81 q/nm^{-1} and 4.61 q/nm^{-1} that corresponds to 3.4 nm and 1.35 nm. The position of the most pronounced peak in WAXS is 15.50 q/nm^{-1} at 95°C and 15.59 q/nm^{-1}at 90°C what correspond to 0.405 to 0.403 nm respectively.

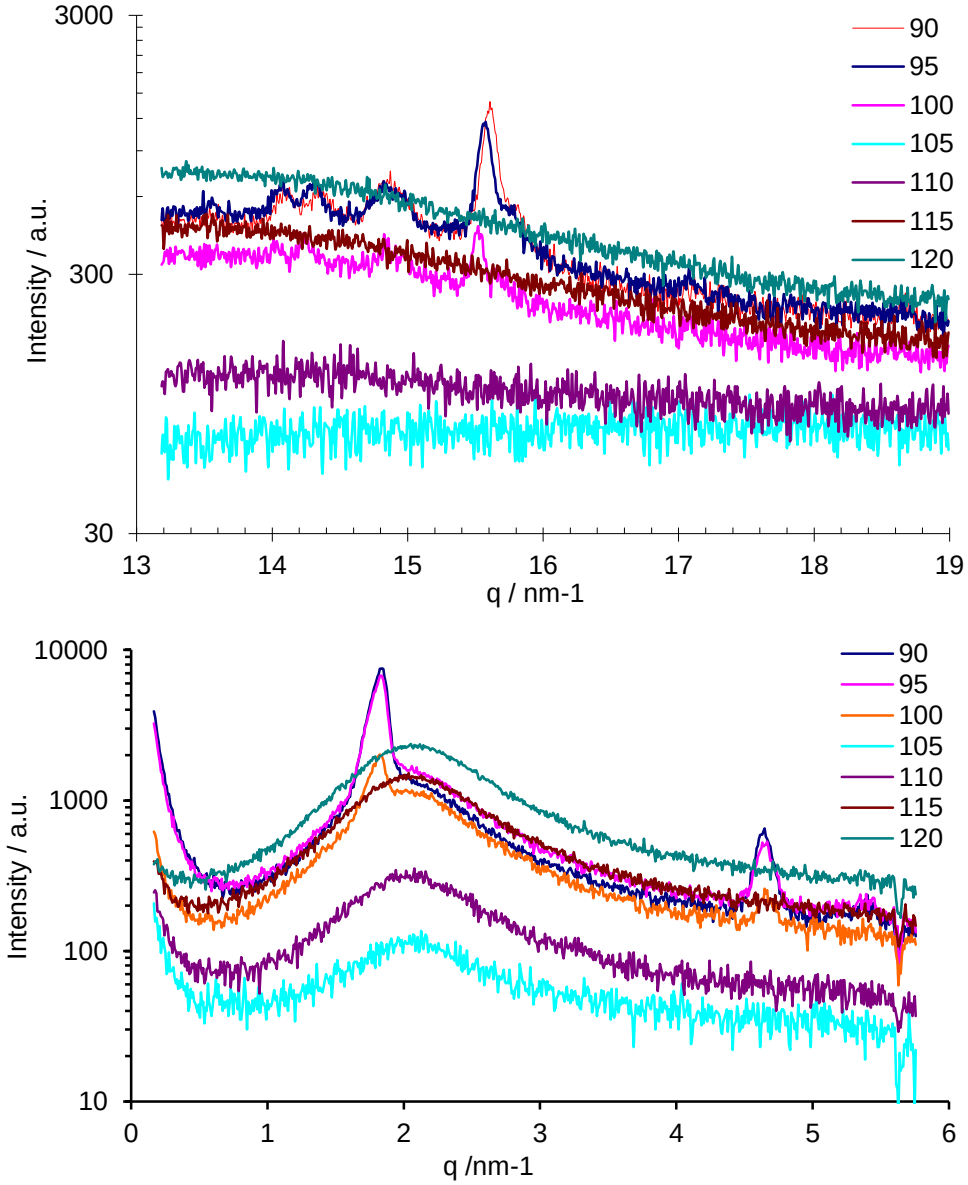

Figure 7.32: *WAXS top and SAXS bottom of (S)-**1,3Ph** acid (R)-**1,3Ph** acid and (R,R)-DACH (0.5:1.5:1)*

In DSC (Figure 7.33) there are two very broad bands observed, one at 45-53°C, and the second one at 65°C to 97°C. In the second cycle of heating just one structure is observed, at 45°C. In cooling the solidifying peak appears at approximately 25°C.

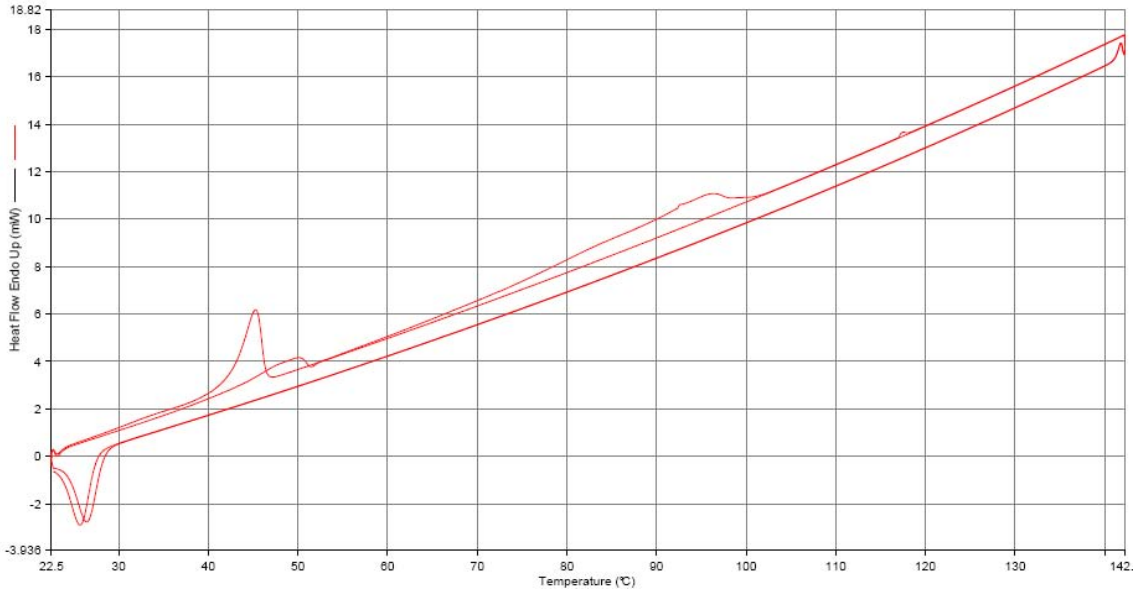

Figure 7.33: *DSC measurement of (S)-**1,3Ph** acid (R)-**1,3Ph** acid and (R,R)-DACH (0.5:1.5:1). The melting starts with very broad band at 45-52°C, then from approximately 65°C to 97°C the melting peak is observed. In the second cycle the second cycle melting takes place at 45°C. In the cooling crystallization peak appears at 25°C.*

In POM (Figure 7.34) the first phase change is not visualised very well, there just slight changes in contrast between images captured at room temperature, at 51°C (image A) and 84°C (image C). The melting is observed above 85°C, and the clearing point was observed at 99°C.

In SAXS peaks disappear at 105°C, so the melting point is observed a bit higher than in the DSC and POM.

The results shows that again there is just one principle structure observed in SAXS for all of the series of the sample of mixtures of enantiomers of acid **1,3Ph** and (*R,R*) diaminocyclohexane –crystalline **1,3Ph**. In this case the DSC shows surprises, as the phase changes are stretched, the second phase change takes place over 30°C.

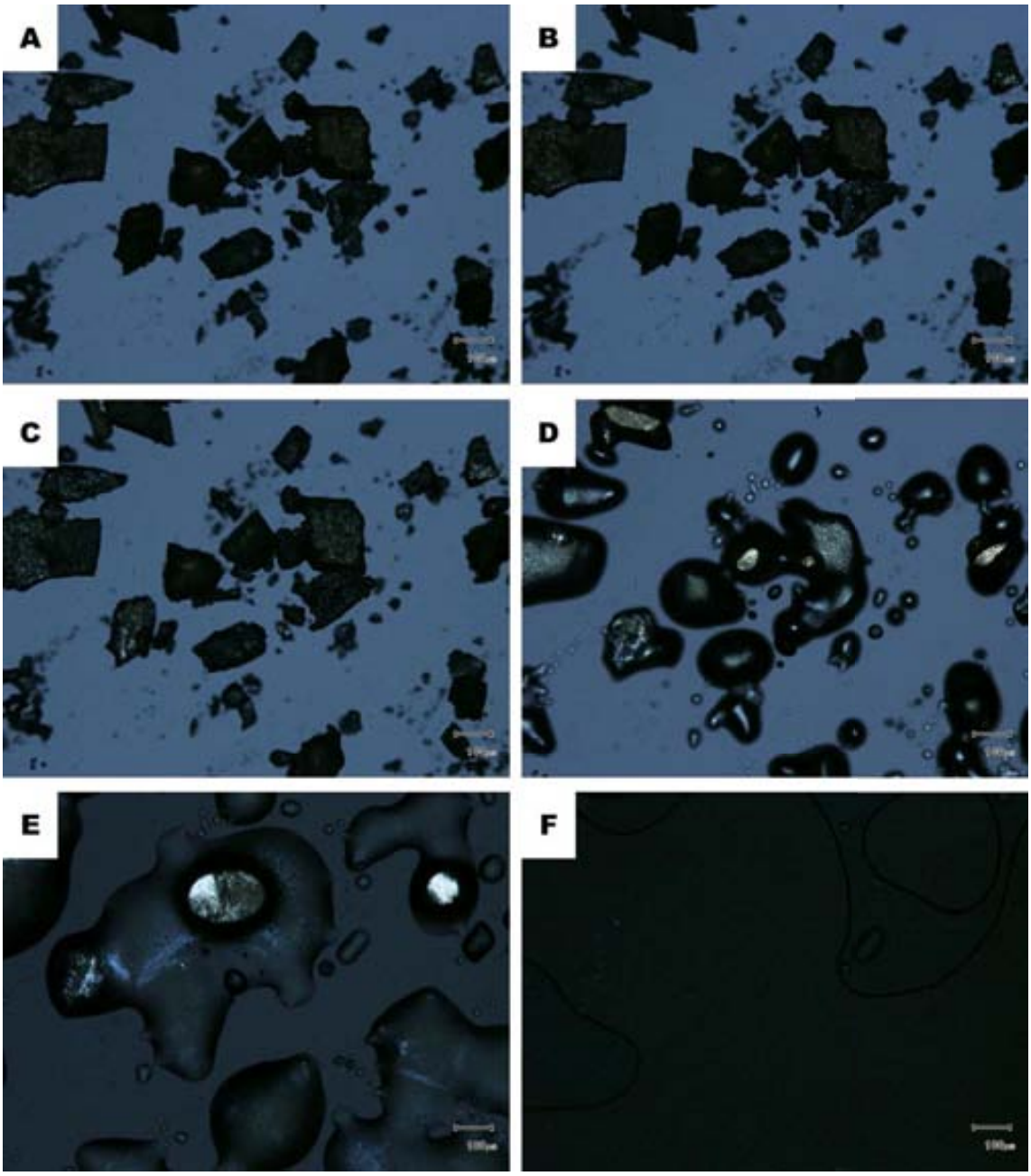

Figure 7.34: *Optical Microscope images of the mixture of (S)-**1,3Ph** acid (R)-**1,3Ph** acid and (R,R)-DACH (0.5:1.5:1). Image A, captured at 51°C shows the material as it was in room temperature, no changes observed in the structure of the material. Image B captured at 53.5°C shows that material become slightly brighter. Image C: at the temperature of 84°C material just before the melting occurs. in the images D and E, the melting of the material can be observed at 90.5°C and 94°C. In micrograph F shows polarised light image of the material after melting at 99°C.*

7.13 Conclusions

It is clear that the molecules of acid **1,3Ph** and diaminocyclohexane do recognize one another's chirality, as there are large differences in both thermal and structural characteristics observed in the materials that they form when distinct diastereoisomeric combinations are used to prepare them. The exact phase behaviour is not clear which makes it difficult to take clear conclusions about the nature of the crystals that are observed. The samples show strong hysteresis in their thermal behaviour, so the way that sample is prepared may influence the result. Equilibrating of the samples takes a period of approximately twelve hours (overnight) to reach the most thermodynamically stable form. All of the samples after melting in DSC shown low melting point (42 to 48°C) in the second cycle corresponding to a metastable (non-equilibrium) form of the mixtures.

There is no clear evidence of liquid crystal behaviour observed for the samples, something we had initially hoped for and expected. In all of the samples but (*R*)-**1,3Ph** acid and (*R,R*)-DACH there is uncommon effect observed in WAXS, the distances between molecules decreasing with temperature, somehow the structure seems to be better packed in higher than at lower temperature.

What is observed in DSC in samples (*R*)-**1,3Ph** acid and (*R,R*)-DACH, (*R*)-**1,3Ph** acid and (*rac*)-DACH and (*R*)-**1,3Ph** acid and (*R,R*)-DACH (*S,S*)-DACH (2:0.75:025) the peaks are joined together, as if the phase changes goes smoothly from one to the other. In the case of other samples there is clear separation between first phase change (at 40 – 52°C) and melting of the rest of the material (82°C melting point of enantiopure acid, 105°C highest melting point for **1,3Ph** –DACH mixtures). POM shows good agreement with the DSC data, and SAXS confirms the clearing point. As the peaks in SAXS coincide with the peaks in XRD of **1,3Ph** for the series of mixtures of enantiomers of **1,3Ph** and

In cooling there was just a three samples measured with SAXS, and two of them did not crystallize in the measured range 90–40°C, only the sample (*R*)-**1,3Ph** acid and (*rac*)-DACH at 40°C, shows peaks in SAXS, while in WAXS no peaks are observed, which indicates that there might be liquid crystal phase in this sample during cooling.

In the other samples DSC and polarised optical microscopy were used to observe the cooling process. During cooling in DSC just one phase change is observed at very

similar temperature for all of the samples, all of them crystallize between 23 and 30°C, and the process occurs in the same way in both first and second cycle of heating. In the optical microscope similar results were obtained, as all of the materials look similar in the optical microscope, just two of them are presented in the images. The material is crystalline at room temperature after standing, as proved by scratching it.

Chapter 8

General Conclusions

The following general conclusions one can draw from this thesis:

- The geometry of the molecule plays a key role in determining the structure of the SAMs. Bent core molecules **1,3Ph** and **2,7-Naph** form one stable type of chiral domains, while different polymorphs were discovered in case of compounds with linear geometry **1,5Naph**, **4,4'Biph** and **1,4Ph**. 1D crystals are formed by **2,6Naph.**
- The naphthalene derivatives are capable of forming stable mixed monolayers at the liquid solid interface. Just in particular cases of acids with different chirality of head group and different geometry of aromatic space, the separated domains of pure acid could be observed along with mixed ones. Also DSC and XRD measurements of bulk mixtures of acids confirmed capability of forming stable mixtures.
- Pasteurian diastereomeric resolution has been achieved at the liquid-solid interface: *trans*-1,2-diaminocyclohexane co-adsorbs with **1,3Ph** in an enantioselective way. At a 2:1 molar ratio, the **1,3Ph**-DACH-**1,3Ph** complex appear only for the homochiral combination. Upon premixing the resolving agent (**1,3Ph**) with the racemic mixture (DACH), exclusively one of the diaminocyclohexane enantiomers is adsorbed as a diastereomeric complex on the achiral graphite substrate, while the other enantiomer is left in solution.

  Chiral recognition at the graphite-1-phenyloctane interface between the homochiral combination of acid **2,7Naph** and diaminocyclohexane was proved, the system is capable of forming multilayers. The experiments with **1,5Naph** and **1,4Ph** did not yield in any new structure, however no typical monolayer of uncomplexed molecules of acid were observed, what is clear indication that amine inhibits formation of most stable monolayer of those molecules at graphite- 1-phenyloctane interface.

  The experiments with **1,3Ph** proved that amphiphilic acids are able to form stable complex with variety of molecules including Metoprolol,

multifunctional and larger molecule.

- The amphiphile molecules of acids bind stronger to the surface than the amine-acid complex, in most of the cases what is observed with the STM is mixed monolayers of acids.

  In the case of (*R*)-**2,7Naph** and (*R*)-**1,3Ph** and (*R,R*)-DACH, there is binding of amine, the molecules of acids are very similar and at the same time both of them form stable complex on the graphite surface, so they form mixed monolayer of complex

  In other cases what is observed is the formation of SAMs of mixed acids with possible interactions with amine atop of the formed domain. It is caused by much stronger interactions of acids with surface than with amine.
- Chiral recognition in a three dimensional system between **1,3Ph** and DACH causes large differences in thermal and structural behaviour for different combinations of chirality of molecules.

Chapter 9

Experimental Section

9.1 Techniques and instruments

9.1.1 Spectroscopy and spectrometry

Nuclear Magnetic Resonance Spectroscopy (NMR): NMR measurements were performed in solution in deuterated solvents at the Universitat Autonoma de Barcelona using Bruker Avance 360MHz and 250MHz instruments for ^{1}H NMR and 90MHz for ^{13}C NMR. The reference used in the spectra was tetramethylsilane or residual protonated solvent. Chemical shifts are reported in ppm (δ- scale). The usual abbreviation was used in the description of spectra: s for singlet, d for doublet, dd for double doublet, t for triplet, m for multiplet and br for broad signal.

Infrared Spectroscopy (IR): IR measurements were done using Perkin Elmer Spectrum One Fourier transform spectrometer. All measurements of the solid compounds were performed in attenuated total reflection mode (ATR).

Mass spectrometry (MS): Mass spectra were recorded using Bruker Ultrafle x II Matri x Assisted Laser Desorption Ionization/Time of Flight equipment, with positive ions pulse extraction at high power. The compounds were dissolved in chloroform or DCM and deposited onto the stainless steel plate.

9.1.2 Chromatography

Thin Layer Chromatography (TLC): The thin layer chromatography plates Merck 60 F^{25}_{4} were used to monitor reactions and detect compounds in the column chromatography. Plates were air dried and scrutinized under UV lamp, or developed either with an aqueous solution of $KMnO_4$ (3 g of $KMnO_4$, 20 g of K_2CO_3, 5 mL of 1M NaOH in 300 mL of H_2O) or with Cerium/Molybdenum acidic solution. (10 g $(NH_4)_3MoO_3$, 4 g of $Ce(SO_4)_2$ in 400 mL of 15% H_2SO_4), and then heated in stream of hot air.

Column chromatography: Column chromatography was performed at ambient pressure using SDS silica gel 60, (35-70 mesh).

Chiral High Performance Liquid Chromatography (HPLC): HPLC experiments were performed at analytical department of SYNCOM B.V. in Groningen.

9.1.3 Scanning Tunnelling Microscopy

Scanning Tunnelling Microscopy experiments were performed in Prof. Steven de Feyter`s laboratories in the Spectroscopy and Molecular Dynamics Department of the Katholieke Universiteit Leuven, Belgium. All experiments were done at a liquid-solid interface at room temperature (approximately 23ºC). Platinum/Iridium wire (80:20, 0.25 nm) was mechanically cut and used as the STM tip. Graphite (HOPG, grade ZYB, Advanced Ceramics Inc., Cleveland, OH) was cleaved before each experiment. STM was performed using Agilent MI 5100 Picoscan instrument. The close –up images of monolayer were corrected using the image of graphite, that was captured at I_{set} = 1 nA; V_{bias} = 0.001 V immediately after each image of monolayer. Drifts effect were corrected using Scanning Probe Image Processing (SPIP) software developed by Image Metrology Aps. The images were processed with plane correction using 3rd level Polynomial Fit Method: Least Mean Square Average Profile applied while loading. Only images with small drift were used for the analysis.

9.1.4 Small and Wide Angle X-Ray Diffraction

The experiments were performed on a Hecus X-ray Systems diffractometer in CID – CSIC in the collaboration with group of Jordi Esquena. The radiation was emitted from a Cu anode (wavelength = 0.154 nm) and the scattering was detected with a linear position sensitive detector OED-50M. The q range was approximately from 0.02 to 6 nm^{-1}, in the SAXS region and from 13 to 18 nm^{-1} in the Wide Angle X-ray Scattering (WAXS) region. Solid crystalline phases were studied by WAXS, using an Inel CPS 120 XRD instrument, which operates with Debye-Scherrer geometry. The scattering was detected with 120º curved detector, and the q range is between 1.4 and 70.6 nm^{-1}. The distance is calculated by the equation $d = 2\pi/q$ where q is the scattering vector corresponding to the first order peak. The temperature controller was a Peltier device.

9.1.5 Differential Scanning Calorimetry

DSC measurements were performed on Perkin Elmer DSC 8500 LAB SYS calorimeter, calibrated previously, with approximately 3mg of each sample in 25 µL aluminium capsule.

Melting Point Melting points were determined with SIMPIO equipment, produced by Bibby scientific and are uncorrected.

9.1.6 Optical Microscopy

The optical micrographs were captured with an Olympus BX51TRF Microscope using rotatable polarisers in transition mode with an Olympus digital camera. The variable temperature experiments were performed using LTS 350 Linkam heating plate.

9.1.7 Polarimetry

The optical rotation of the compounds was measured with Dr. Kernchen Propol polarimeter in 1 cm cell.

9.1.8 Reactants and solvents

Reagents and starting materials were used as obtained from SDS, Fluka, Sigma-Aldrich and Merck. The dry THF was distilled from metallic sodium under a nitrogen atmosphere.

9.2 Synthesis

9.2.1 *(S)*-Methyl 2-(7-hydroxy-naphthalen-2-yloxy)propionate

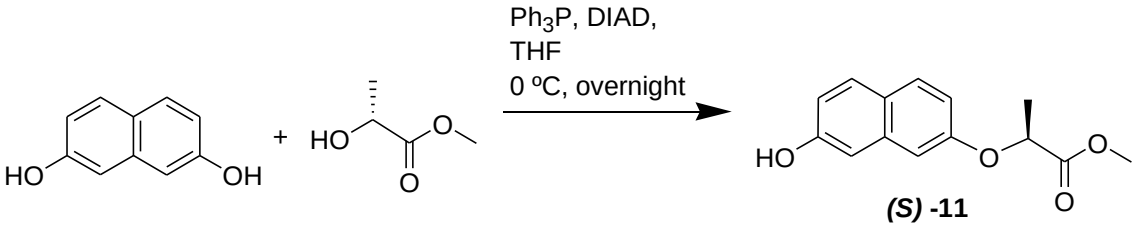

***(S)* -11**

2,7 Dihydroxynaphtalene (Aldrich, 3.0 g, 18.73 mmol), *(R)*-methyl lactate (Aldrich, 2.05 mL, 21.4 mmol) and triphenylphospine (Merck, 5.6 g, 21.4 mmol) were dissolved in dry THF (150 mL) and the mixture was cooled in an ice bath to 0ºC under atmosphere of nitrogen. A solution of diisopropylazidicarboxylate (DIAD) (Aldrich, 4.23 mL, 21.4 mmol) in 20 mL of THF was added drop wise to the previously mentioned cooled and stirred solution over a period of 15 minutes. The reaction was stirred overnight at 0ºC. After addition of water (50 mL), THF was removed in rotary evaporator and water was added and extracted two times with DCM. The organic phase was dried over Na_2SO_4 and the residue after evaporation of the solvent was purified by column chromatography on silica gel using 10-30 % vol. ethyl acetate in hexane to give 1.2 g of the desired product (26% yield).

M.F.: $C_{14}H_{14}O_4$; M.W.: 246.26; M.P.: 101-103 ºC; ^{1}H NMR (250 MHz, $CDCl_3$): 7,63 (t, *J*=7.9 Hz, 2H, ArH), 7.00 (m, 3H, ArH), 6.88 (d, *J*=2.8 Hz, 1H, ArH), 6.23 (br s, 1H,

-OH), 4.91 (q, *J*=6.8 Hz, 1H, -OC<u>H</u>CH_3COOCH_3), 3.77 (s, 3H, -$COOC\underline{H_3}$), 1.68 (d, *J*=6.9 Hz. –$OCHC\underline{H_3}COOMe$); ^{13}C NMR (100 MHz, $CDCl_3$): 173.0, 156.0, 154.1, 151.0, 135.6, 129.5, 124.6, 116.1, 108.8, 106.4, 72.5, 52.4, 18.5; FT- IR (ATR): 2922, 2851, 1707, 1623, 1529, 1483, 1446, 1434, 1384, 1313, 1293, 1235, 1199, 1166, 1137, 1095, 1051, 989, 967, 956, 859, 834, 818, 804, 759, 748 cm^{-1}.

9.2.2 *(S)*-Methyl 2-(7-octadecyloxy-naphthalen-2-yloxy)propionate

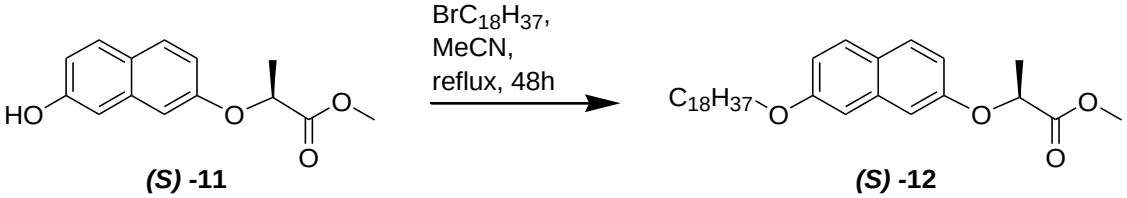

***(S)* -11** ***(S)* -12**

Pre dried ground K_2CO_3 (1.9 g, 13.7 mmol) was suspended in acetonitrile (100 mL) in a 3 neck round bottom flask and the mixture was degassed with a flow of nitrogen for 30 minutes. Then the lactate derivative *(S)*-**11** (850 mg, 3.4 mmol) was added as a solid, and the resulting solution was heated to reflu x under nitrogen. After 30 minutes, the reaction was cooled, and 1-bromooctadecane (Fluka, 1.2 mL, 3.6 mmol) was introduced as a liquid. The temperature of the mixture was then raised to gentle reflux, and these conditions were maintained for 48 hours.

The reaction mixture was filtered at the pump while it was still warm, and the residual solid was washed with warm acetonitrile. Immediately crystals had started to form in the filtered liquid, and after 30 minutes they were collected by filtration. After evaporating some of acetonitrile with a rotary evaporator from the filtrate, a further crop of crystals was obtained. The reaction gave 980 mg of white crystals (yield 57%).

M.F.: $C_{37}H_{50}O_4$; M.W.: 498.74; M.P.: 53-54 ºC; ^1H NMR (360 MHz, $CDCl_3$): 7.66 (m, 2H, ArH), 7.01 (m, 4H, ArH), 4.92 (q, *J*=6.6 Hz, 1H, -OC<u>H</u>CH_3COOMe), 4.06 (t, *J*=6.6 Hz, 2H -$OC\underline{H_2}(CH_2)_{16}CH_3$), 3.78 (s, 3H, -$COOC\underline{H_3}$), 1.85 (m, 2H, -$OCH_2\underline{CH_2}(CH_2)_{15}CH_3$), 1.69 (d, *J*=6.8 Hz. –$OCHC\underline{H_3}COOMe$), 1.48 (m, 2H, -$OCH_2CH_2\underline{CH_2}(CH_2)_{14}CH_3$), 1.26 (m, 28H, -O $CH_2CH_2CH_2\underline{(CH_2)_{14}}CH_3$), 0.90 (t, *J*=6.8 Hz, 3H, -$O(CH_2)_{17}\underline{CH_3}$); ^{13}C NMR (90 MHz, $CDCl_3$): 173.2, 158.2, 156.5, 136.1, 129.8, 129.4, 125.0, 117.4, 116.4, 107.5, 106.5, 73.1, 68.4, 52.8, 32.4 30.1-29.7, 26.5, 23.1, 19.1, 14.5; FT- IR (ATR): 2915, 2850, 1739, 1627, 1607, 1514, 1472, 1460, 1435, 1386, 1252, 1208, 1173, 1134, 1091, 1049, 967, 957, 925, 858, 834, 814, 796, 756, 716cm^{-1}.

9.2.3 *(S)*-2-(7-Octadecyloxy-naphthalen-2-yloxy)-propionic acid

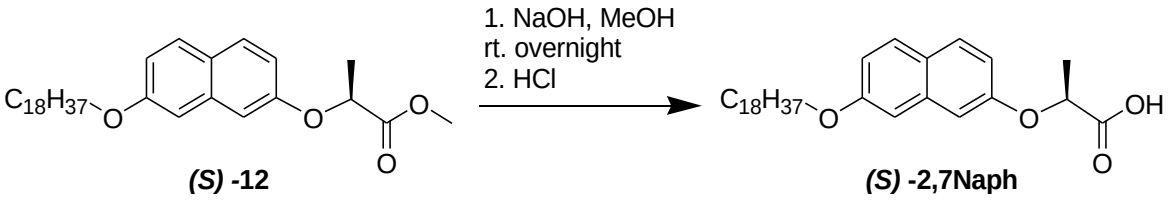

***(S)* -12** **(S) -2,7Naph**

To a solution of 910mg (1.8 mmol) of ester *(S)*-**12** in methanol (90 mL) was added 2N water solution of sodium hydroxide (3.6 mL, 7.2 mmol) and the mixture was stirred overnight at room temperature. The reaction mixture was concentrated, diluted with water and acidified to pH=2 with 2N hydrochloric acid. The acid compound was extracted with DCM two times and crystallized from acetonitrile to give the product. Crystallization from acetonitrile gave 420 mg of product and 100mg in the first and second crops, respectively. (Yield 59%)

M.F.: $C_{36}H_{48}O_4$; M.W.: 484.64; M.P.: 89-90 ºC; ^{1}H NMR (360 MHz, $CDCl_3$): 7.68 (m, 2H, ArH), 7.04 (m, 4H, ArH), 4.95 (q, *J*=6.8 Hz, 1H, -OC<u>H</u>CH_3COOH), 4.03 (t, *J*=6.3 Hz, 2H -OC<u>H_2</u>$(CH_2)_{16}CH_3$), 1.84 (m, 2H, -OCH_2<u>CH_2</u>$(CH_2)_{15}CH_3$), 1.73 (d, *J*=6.8 Hz. –OCHC<u>H_3</u>COOH), 1.48 (m, 2H, -OCH_2CH_2<u>CH_2</u>$(CH_2)_{14}CH_3$), 1.27 (m, 28H, -O $CH_2CH_2CH_2$<u>$(CH_2)_{14}$</u>CH_3), 0.90 (t, *J*=6.8 Hz, 3H, -$O(CH_2)_{17}$<u>CH_3</u>); ^{13}C NMR (90 MHz, $CDCl_3$): 177.8, 157.9, 155.6, 135.7, 129.6, 129.0, 124.7, 117.2, 115.8, 107.2, 106.0, 72.0, 68.0, 32.0, 29.7-29.3, 26.1, 22.7, 18.5, 14.1 MALDI-TOF MS m/z: calc. 484.36 found 484.27; FT- IR (ATR): 3238, 2916, 2850, 1760, 1628, 1514, 1471, 1458, 1435, 1388, 1326, 1250, 1213, 1202, 1170, 1143, 1121, 1094, 1041, 984, 956, 937, 854, 838, 797, 717, 665 cm^{-1}; HPLC: Chiralpack IA column, Heptane/IPA/TFA (97.3/2.5/0.2) 0.7ml/min, ee=96.0%

9.2.4 *(R)*-Methyl 2-(7-hydroxy-naphthalen-2-yloxy)propionate

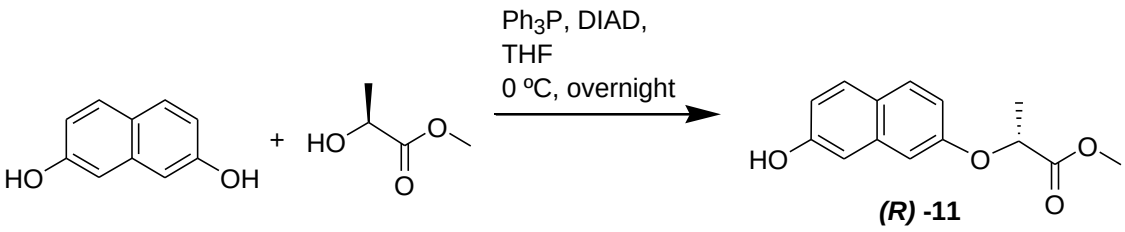

***(R)* -11**

The reaction was performed using same procedure as for *(S)*-**11** except with 5.0 g (34.7 mmol) of 2,7 dihydroxynaphtlene, 3.41 mL of (*S*)-methyl lactate (35.5 mmol), 9.3

g of triphenylphospine (35.5 mmol) and 7.05 mL of DIAD (35.5 mmol). Column chromatography on silica gel using 10-30 % vol. ethyl acetate in hexane afforded 2.2 g of product (27% yield).

M.F.: $C_{14}H_{14}O_4$; M.W.: 246.26; M.P.: 98-101 ºC; ^{1}H NMR (250 MHz, $CDCl_3$): 7.68 (t, *J*=8.3 Hz, 2H, ArH), 7.01 (m, 3H, ArH), 6.90 (d, *J*=2.9 Hz, 1H, ArH), 5.96 (br s, 1H, -OH), 4.94 (q, *J*=6.8 Hz, 1H, -OC<u>H</u>CH_3COOCH_3), 3.77 (s, 3H, -COOC<u>H$_3$</u>), 1.71 (d, 3H, *J*=6.9 Hz. –OCHC<u>H$_3$</u>COOMe); ^{13}C NMR (90 MHz, $CDCl_3$): 173.3, 156.0, 154.4, 151.0, 135.8, 129.6, 129.5, 124.7, 116.1, 116.0, 108.9, 106.5, 72.5, 52.6, 18.6; FT- IR (ATR): 3490, 3084, 2926, 2588, 2365, 2083, 1598, 1574, 1476, 1438, 1281, 1222, 1182, 1154, 1111, 1089, 1045, 1008, 912, 859, 773, 746, 728, 708, 674 cm^{-1}.

9.2.5 *(R)*-Methyl 2-(7-Octadecyloxy-naphthalen-2-yloxy)propionate

***(R)* -11** **(R) -12**

The reaction was carried out with 1.0 g (4.1 mmol) of *(R)*-**11** using same procedure as for the opposite enantiomer. The crude product was recrystallized from acetonitrile to give 1.3 g of white solid (yield 64%).

M.F.: $C_{37}H_{50}O_4$; M.W.: 498.74; M.P.: 67-68 ºC; ^{1}H NMR (250 MHz, $CDCl_3$): 7.63 (m, 2H, ArH), 6.96 (m, 4H, ArH), 4.89 (q, *J*=6.6 Hz, 1H, -OC<u>H</u>CH_3COOMe), 4.04 (t, *J*=6.3 Hz, 2H -OC<u>H$_2$</u>$(CH_2)_{16}CH_3$), 3.76 (s, 3H, -COOC<u>H$_3$</u>), 1.76 (m, 2H, -OCH_2<u>CH_2</u>$(CH_2)_{15}CH_3$), 1.67 (d, *J*=6.8 Hz. –OCHC<u>H$_3$</u>COOMe), 1.48 (m, 2H, -OCH_2CH_2<u>CH_2</u>$(CH_2)_{14}CH_3$), 1.26 (m, 28H, -O $CH_2CH_2CH_2$<u>$(CH_2)_{14}$</u>CH_3), 0.87 (t, *J*=6.8 Hz, 3H, -$O(CH_2)_{17}$<u>CH_3</u>); ^{13}C NMR (90 MHz, $CDCl_3$): 172.9, 157.8, 156.0, 135.7, 129.4, 129.0, 124.6, 116.0, 107.0, 106.1, 72.6, 68.0, 52.4, 31.9, 29.7-29.3, 26.1, 22.7, 18.7, 14.1; FT- IR (ATR): 2918, 2849, 1751, 1631, 1608, 1515, 1458, 1435, 1395, 1383, 1351, 1310, 1253, 1200, 1176, 1137, 1095, 1066, 1050, 1020, 998, 984, 967, 958, 930, 906, 860, 848, 822, 796, 753, 722, 674cm^{-1}

9.2.6 *(R)*-Methyl 2-(7-Octadecyloxy-naphthalen-2-yloxy)-propionic acid

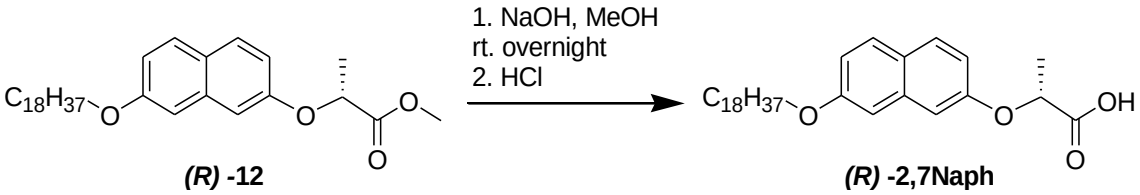

The reaction was performed using the same procedure as for *(S)*-**2,7 Naph**. 925 mg of starting material *(R)*-**12** (1.85 mmol) and 5 mL of 1N NaOH solution (5.0 mmol) was used for the reaction. Crystallization from methanol gave 490mg of product and 100mg was obtained in a second crop. (Total yield 66%)

M.F.: $C_{36}H_{48}O_4$; M.W.: 484.64; M.P.: 87-88 ºC ^{1}H NMR (250 MHz, $CDCl_3$): 7.65 (m, 2H, ArH), 7.02 (m, 4H, ArH), 4.92 (q, *J*=6.9 Hz, 1H, -OC<u>H</u>CH_3COOH), 4.01 (t, *J*=6.3 Hz, 2H -OC<u>H_2</u>$(CH_2)_{16}CH_3$), 1.82 (m, 2H, -OCH_2<u>CH_2</u>$(CH_2)_{15}CH_3$), 1.72 (d, *J*=6.8 Hz. –OCHC<u>H_3</u>COOH), 1.46 (m, 2H, -OCH_2CH_2<u>CH_2</u>$(CH_2)_{14}CH_3$), 1.27 (m, 28H, -O $CH_2CH_2CH_2$<u>$(CH_2)_{14}$</u>CH_3), 0.91 (t, *J*=6.8 Hz, 3H, -$O(CH_2)_{17}$<u>CH_3</u>); ^{13}C NMR (90 MHz, $CDCl_3$): 176.5, 157.9, 155.6, 135.7, 129.6, 129.0, 124.7, 117.2, 115.8, 107.2, 106.0, 68.0, 52.4, 31.9, 29.7-29.3, 26.1, 22.7, 18.5, 14.1; MALDI-TOF MS m/z: calc. 484.36 found 484.28; FT- IR (ATR): 2916, 2850, 1735, 1629, 1514, 1471, 1432, 1387, 1332, 1249, 1211, 1167, 1123, 1093, 1034, 982, 956, 853, 830, 716, 665 cm^{-1}; HPLC: Chiralpack IA column, Heptane/IPA/TFA (97.3/2.5/0.2) 0.7ml/min, ee=94.4%

9.2.7 *(R)*-Methyl 2-(6-Hydroxy-naphthalen-2-yloxy)propionate

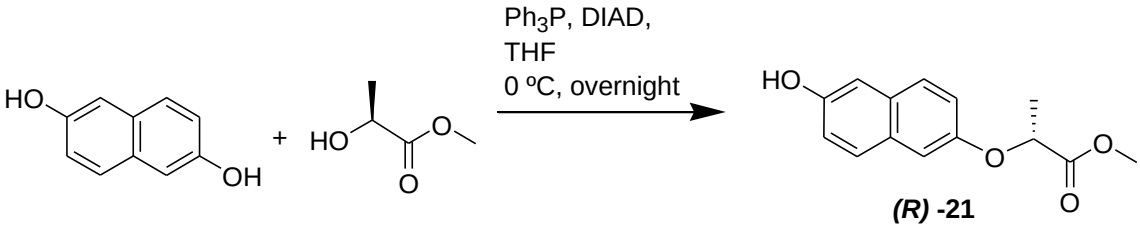

The reaction was performed using the same procedure as for *(S)*-**11** employing 1.8g of 2,6 dihydroxynaphthalene (11.2 mmol), 1.23 mL of *(S)*-methyl lactate (13.0 mmol), 3.4 g of triphenylphospine (13.0 mmol) and 2.55 mL of DIAD (13,0 mmol). Column chromatography on silica gel using 10-20 % vol. ethyl acetate in hexane to get 620 mg of product (24% yield).

M.F.: $C_{14}H_{14}O_4$; M.W.: 246.26;M.P.: 76-78 ºC; $[\alpha]^{25}_{546}$= +10.4 deg·cm²·g⁻¹

(C=0.077M CH_2Cl_2);^{1}H NMR (360 MHz, $CDCl_3$): 7.52 (t, *J*=7.8 Hz, 2H, ArH), 7.08 (m, 4H, ArH), 6.43 (br s, 1H, -OH), 4.91 (q, *J*=6.8 Hz, 1H, -OC<u>H</u>CH_3COOCH_3), 3.78 (s, 3H, -COOC<u>H_3</u>), 1.68 (d, *J*=7.2 Hz. –OCHC<u>H_3</u>COOMe);^{13}C NMR (100 MHz, $CDCl_3$): 173.3, 153.6, 152.5, 130.3, 129.1, 128.4, 128.0, 119.2, 118.3, 109.5, 108.0, 106.4, 72.6, 52.5, 21.9, 18.6; FT- IR (ATR): 3385, 2955, 1732, 1603, 1511, 1445, 1445, 1387, 1210, 1115, 1050, 980, 953, 855, 800, 736, 693, 659cm^{-1}

9.2.8 *(R)*-Methyl 2-(6-(octadecyloxy)naphthalen-2-yloxy)propionate

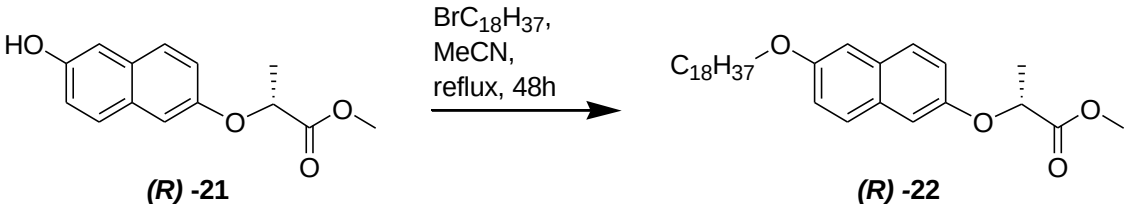

***(R)* -21** ***(R)* -22**

The reaction was performed in the analogical way as the preparation of compound *(S)*-**12**, using pre-dried ground K_2CO_3 (1.1 g, 8.04 mmol), *(R)*-**21** (480 mg, 2.01 mmol), 1-bromooctadecane (0.72 mL, 2.11 mmol) and acetonitrile (30 mL). Reaction gave 720 mg of white solid (yield 74%).

M.F.: $C_{37}H_{50}O_4$; M.W.: 498.74; M.P.: 76-78 ºC; $[\alpha]^{25}_{546}$= +4.12 deg·cm²·g^{-1} (C=0.015M CH_2Cl_2); ^{1}H NMR (360 MHz, $CDCl_3$): 7.62 (m, 2H, ArH), 7.10 (m, 4H, ArH), 4.90 (q, *J*=6.8 Hz, 1H, -OC<u>H</u>CH_3COOMe), 4.06 (t, *J*=6.6 Hz, 2H -OC<u>H_2</u>$(CH_2)_{16}CH_3$), 3.78 (s, 3H, -COOC<u>H_3</u>), 1.85 (m, 2H, -OCH$_2$<u>CH_2</u>$(CH_2)_{15}CH_3$), 1.69 (d, *J*=6.8 Hz. –OCHC<u>H_3</u>COOMe), 1.44 (m, 2H, -OCH$_2$CH$_2$<u>CH_2</u>$(CH_2)_{14}CH_3$), 1.28 (m, 28H, -O $CH_2CH_2CH_2$<u>$(CH_2)_{14}$</u>CH_3), 0.90 (t, *J*=6.8 Hz, 3H, -O$(CH_2)_{17}$<u>CH_3</u>); ^{13}C NMR (90 MHz, $CDCl_3$): 172.8, 155.9, 153.8, 130.2, 129.3, 128.3, 128.1, 119.4, 119.0, 108.1, 106.7, 72.7, 68.0, 52.3, 31.9, 29.7-29.3, 26.0, 22.6, 18.6, 14.1; FT- IR (ATR): 2955, 2915, 2848, 1734, 1605, 1510, 1462, 1441, 1398, 1376, 1310, 1264, 1232, 1170, 1123, 1099, 1054, 1035, 987, 953, 846, 835, 805, 755, 719, 697cm^{-1}

9.2.9 *(R)*-2-(6-Octadecyloxy-naphthalen-2-yloxy)-propionic acid

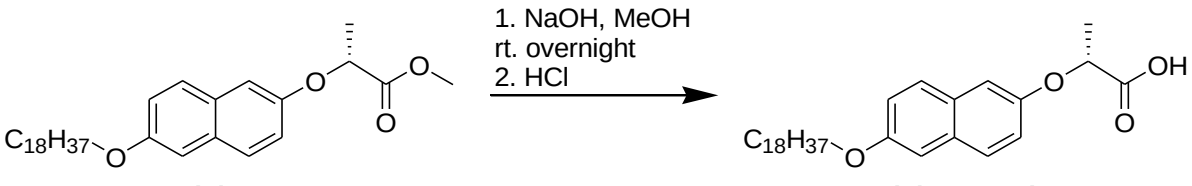

***(R)* -22** ***(R)* -2,6Naph**

Saponification was performed using typical procedure as described for (S)-**2,7Naph**. In the reaction 680 mg of ester *(R)*-**22** (1.36 mmol), 2N aqueous solution of NaOH (2 mL, 4.0 mmol) and methanol (50 mL) was used. The crude compound was crystallized from acetonitrile to give 455 mg of product. (Yield 69%)

M.F.: $C_{36}H_{48}O_4$; M.W.: 484.64; M.P.: 103-104ºC; $[\alpha]^{25}_{546}$= -4.82 deg·cm²·g⁻¹ (C=0.012M CH_2Cl_2); ^{1}H NMR (360 MHz, $CDCl_3$): 7.63 (m, 2H, ArH), 7.12 (m, 4H, ArH), 5.32 (s, 1H. –COOH), 4.93 (q, *J*=6.8 Hz, 1H, -OCHCH$_3$COOH), 4.06 (t, *J*=6.5 Hz, 2H -OCH$_2$(CH$_2$)$_{16}$CH$_3$), 1.85 (m, 2H, -OCH$_2$CH$_2$(CH$_2$)$_{15}$CH$_3$), 1.72 (d, *J*=6.8 Hz. –OCHCH$_3$COOH), 1.47 (m, 2H, -OCH$_2$CH$_2$CH$_2$(CH$_2$)$_{14}$CH$_3$), 1.27 (m, 28H, -O CH$_2$CH$_2$CH$_2$(CH$_2$)$_{14}$CH$_3$), 0.90 (t, *J*=6.8 Hz, 3H, -O(CH$_2$)$_{17}$CH$_3$); ^{13}C NMR (90 MHz, $CDCl_3$): 176.2, 156.1, 153.4, 130.5, 129.3, 128.5, 128.2, 119.6, 118.9, 108.8, 106.9, 72.5, 68.1, 31.9, 29.7-29.3, 26.1, 22.7, 18.4, 14.1; MALDI-TOF MS m/z: calc. 484.36 found 484.30; FT- IR (ATR): 3576, 2917, 2850, 1724, 1604, 1509, 1463, 1395, 1309, 1232, 1167, 1120, 1137, 1120, 1035, 972, 953, 848, 809, 792, 753, 718, 661 cm^{-1}

9.2.10 *(S)*-Methyl 2-(6-hydroxynaphthalen-2-yloxy)propionate

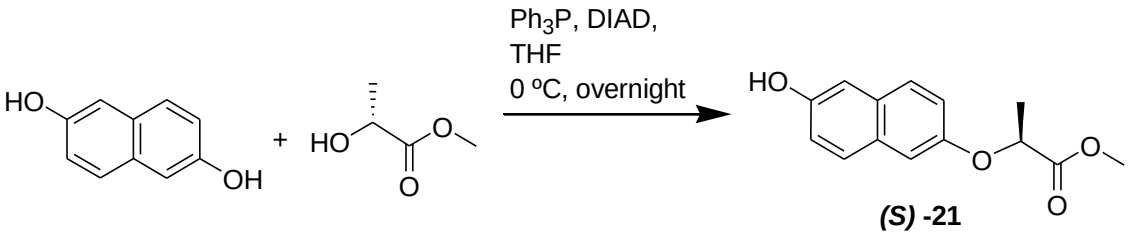

***(S)* -21**

The compound was prepared in the same way and with the same amounts of reagents as for the enantiomer *(R)* except using *(R)*-methyl lactate as the alcohol. The product was afforded in 23% yield as a white solid (600 mg).

M.F.: $C_{14}H_{14}O_4$; M.W.: 246.26; M.P.: 85-87 ºC; $[\alpha]^{25}_{546}$= -11.3 deg·cm²·g⁻¹ (C=0.047M CH_2Cl_2); ^{1}H NMR (250 MHz, $CDCl_3$): 7.53 (m, 2H, ArH), 7.09 (m, 4H, ArH), 5.48 (br s, 1H, -OH), 4.92 (q, *J*=6.8 Hz, 1H, -OCHCH$_3$COOCH$_3$), 3.81 (s, 3H, -COOCH$_3$), 1.70 (d, *J*=6.8 Hz. –OCHCH$_3$COOMe); ^{13}C NMR (62.5 MHz, $CDCl_3$): 173.3, 156.5, 155.0, 134.5, 133.1, 127.9, 115.6, 115.2, 72.6, 52.6, 18.6; FT- IR (ATR) 3391, 2945, 1726, 1600, 1524, 1470, 1437, 1385, 1327, 1267, 1207, 1179, 1159, 1136, 1114, 1094, 1052, 980, 951, 850, 802, 748, 692cm^{-1}

9.2.11 *(S)*-Methyl 2-(6-(octadecyloxy)naphthalen-2-yloxy)propionate

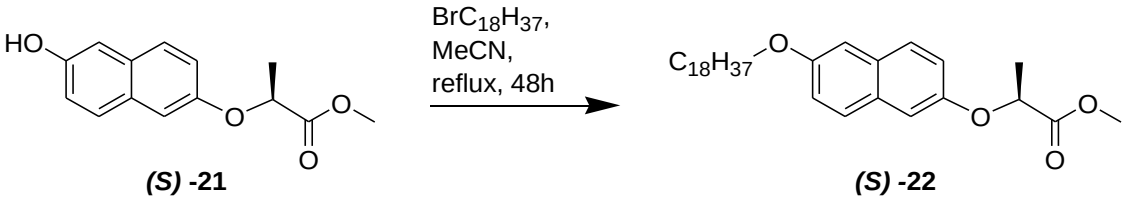

***(S)* -21** ***(S)* -22**

The compound was prepared in an analogous way to the enantiomer *(R)* from 550 mg of (*S*)-**21** (2.2 mmol) and using 0.79 mL of 1-bromooctadecane (2.3 mmol), giving 630 mg of the product as a white solid (Yield 65%).

M.F.: $C_{37}H_{50}O_4$; M.W.: 498.74; M.P.: 78-79 ºC; $[\alpha]^{25}_{546}$= -4.44 deg·cm²·g⁻¹ (C=0.021M CH_2Cl_2); ^{1}H NMR (360 MHz, $CDCl_3$): 7.62 (m, 2H, ArH), 7.12 (m, 4H, ArH), 4.90 (q, *J*=6.8 Hz, 1H, -OC<u>H</u>CH_3COOMe), 4.05 (t, *J*=6.5 Hz, 2H -OC<u>H_2</u>$(CH_2)_{16}CH_3$), 3.78 (s, 3H, -COOC<u>H_3</u>), 1.88 (m, 2H, -OCH_2C<u>H_2</u>$(CH_2)_{15}CH_3$), 1.68 (d, *J*=6.8 Hz. –OCHC<u>H_3</u>COOMe), 1.48 (m, 2H, -OCH_2CH_2<u>CH_2</u>$(CH_2)_{14}CH_3$), 1.28 (m, 28H, -O $CH_2CH_2CH_2$<u>$(CH_2)_{14}$</u>CH_3), 0.90 (t, *J*=6.8 Hz, 3H, -O$(CH_2)_{17}$<u>CH_3</u>); ^{13}C NMR (90 MHz, $CDCl_3$): 172.9, 155.9, 153.9, 130.3, 129.4, 128.4, 128.2, 119.4, 119.0, 108.2, 106.8, 72.8, 68.0, 52.4, 31.9, 29.7-29.3, 26.1, 22.7, 18.7, 14.1; FT- IR (ATR) 2955, 2915, 2848, 1735, 1605, 1511, 1463, 1399, 1311, 1264, 1232, 1170, 1123, 1099, 1054, 1035, 987, 953, 846, 835, 805, 755, 719, 697cm^{-1}

9.2.12 *(S)* -2-(6-Octadecyloxy-naphthalen-2-yloxy)-propionic acid

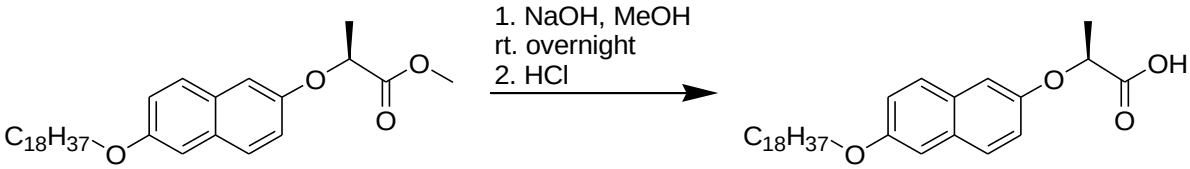

***(S)* -22** ***(S)* -2,6Naph**

The compound was prepared in the same way as for the enantiomer *(R)*. For the reaction 200 mg (0.40 mmol) of starting material *(S)*-**22** and 1.3 mL of 1N NaOH solution (1.3 mmol) was used. Crystallization from acetonitrile gave 130 mg of product (Yield 69%)

M.F.: $C_{36}H_{48}O_4$; M.W.: 484.64; M.P.: 104-105 ºC; $[\alpha]^{25}_{546}$= - 5.3 deg·cm²·g⁻¹ (C=0.0069M CH_2Cl_2); ^{1}H NMR (360 MHz, $CDCl_3$): 7.64 (m, 2H, ArH), 7.12 (m, 4H, ArH) 4.92 (q, *J*=6.8 Hz, 1H, -OC<u>H</u>CH_3COOH), 4.06 (t, *J*=6.6 Hz, 2H -

$OC\underline{H_2}(CH_2)_{16}CH_3$), 1.85 (m, 2H, -$OCH_2\underline{CH_2}(CH_2)_{15}CH_3$), 1.72 (d, *J*=6.8 Hz. –$OCHC\underline{H_3}COOH$), 1.48 (m, 2H, -$OCH_2CH_2\underline{CH_2}(CH_2)_{14}CH_3$), 1.27 (m, 28H, -O $CH_2CH_2CH_2(\underline{CH_2})_{14}CH_3$), 0.90 (t, *J*=7.0 Hz, 3H, -$O(CH_2)_{17}\underline{CH_3}$); ^{13}C NMR (90 MHz, $CDCl_3$): 177.2, 156.1, 153.5, 130.5, 129.3, 128.5, 128.3, 119.6, 118.9, 108.7, 106.9, 72.5, 68.2, 31.9, 29.7-29.3, 26.1, 22.7, 18.4, 14.1; MALDI-TOF MS m/z: calc. 484.36 found 484.32; FT- IR (ATR) 3587, 2917, 2850, 1724, 1604, 1509, 1463, 1395, 1379, 1309, 1233, 1167, 1138, 1120, 1035, 972, 953, 848, 809, 792, 753, 718, 661cm^{-1}

9.2.13 *(R)*-Methyl 2-(5-hydroxy-naphthalen-1-yloxy)propionate

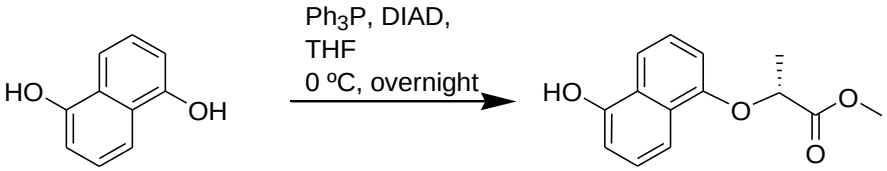

***(R)* -31**

The compound was prepared using the protocol described for *(S)*-**11**, with 3.0 g (18.73 mmol) of 1.5 dihydroxynaphthalene, 2.04 mL of *(S)*-methyl lactate (21.4 mmol), 5.6 g of triphenylphosphine (21.4 mmol) and 4.23 mL of DIAD (21.4 mmol). Column chromatography on silica gel using 10-30 % vol. ethyl acetate in hexane, and then ethyl acetate (1-3% vol.) in dichloromethane gave 800 mg of product (17% yield).

M.F.: $C_{14}H_{14}O_4$; M.W.: 246.26; M.P.: 158-160 ºC; ^{1}H NMR (360 MHz, $CDCl_3$): 7.94 (d, J_1=8.5 Hz, 1H, ArH), 7.79 (d, *J*=8.5 Hz, 1H, ArH) 7.08 (q, *J*=8.3 Hz, 4H, ArH), 6.85 (d, *J*=7.3 Hz, 1H, ArH), 6.73 (d, *J*=7.4 Hz, 1H, ArH) 4.96 (q, *J*=6.8 Hz, 1H, -$OC\underline{H}CH_3COOCH_3$), 3.78 (s, 3H, -$COOC\underline{H_3}$), 1.77 (d, *J*=6.9 Hz. –$OCHC\underline{H_3}COOMe$); ^{13}C NMR (62.5 MHz, $CDCl_3$): 173.3, 153.7, 151.7, 126.0, 125.8, 125.2, 115.3, 110.0, 106.7, 73.5 52.8, 19.0; FT- IR (ATR): 3359, 2981, 2956, 2933, 1716, 1597, 1519, 1451, 1431, 1412, 1373, 1356, 1273, 1231, 1211, 1163, 1149, 1128, 1095, 1070, 1052, 967, 891, 881, 767, 734, 696, 682, 662cm^{-1}

9.2.14 *(R)*-Methyl 2-(5-Octadecyloxy-naphthalen-1-yloxy)propionate

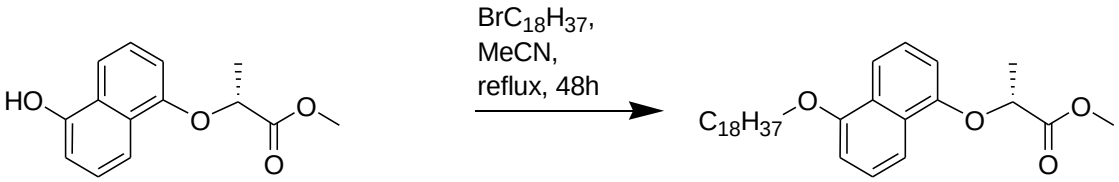

***(R)* -31** ***(R)* -32**

The reaction was performed in the same way as for *(S)*-**12**, using 700 mg of *(R)*-**31** (2.8 mmol) and 1.0 ml of 1-bromooctadecane (3.0 mmol) in 40mL of acetonitrile. Active carbon was used to remove impurities, leaving 240 mg of white solid after crystallization from acetonitrile. (yield 18%).

M.F.: $C_{37}H_{50}O_4$; M.W.: 498.74; M.P.: 79-80 ºC; ^{1}H NMR (360 MHz, $CDCl_3$): 7.91 (d, *J*=8.4 Hz 2H, ArH), 7.39 (t, *J*=8.2Hz, 1H, ArH), 7.32 (t, *J*=8.1Hz, 1H, ArH) 6.85 (d, *J*=7.8Hz, 1H, ArH) 6.74 (d, *J*=7.8Hz, 1H, ArH) 4.95 (q, *J*=6.8 Hz, 1H, -OC<u>H</u>CH_3COOMe), 4.13 (t, *J*=6.6 Hz, 2H -OC<u>H_2</u>$(CH_2)_{16}CH_3$), 3.77 (s, 3H, -COOC<u>H_3</u>), 1.95 (m, 2H, -OCH_2<u>CH_2</u>$(CH_2)_{15}CH_3$), 1.76 (d, *J*=6.8 Hz. –OCHC<u>H_3</u>COOMe), 1.55 (m, 2H, -OCH_2CH_2<u>CH_2</u>$(CH_2)_{14}CH_3$), 1.28 (m, 28H, -$OCH_2CH_2CH_2$<u>$(CH_2)_{14}$</u>CH_3), 0.90 (t, *J*=6.8 Hz, 3H, -$O(CH_2)_{17}$<u>CH_3</u>); ^{13}C NMR (90 MHz, $CDCl_3$): 172.8, 154.7, 153.3, 127.0, 126.8, 125.4, 124.7, 115.5, 114.2, 106.4, 105.5, 73.0, 68.2, 52.3, 34.0, 32.8, 32.0, 29.7, 28.8, 26.3, 22.7, 18.7, 14.1; FT- IR (ATR): 2955, 2918, 2849, 2161, 1732, 1594, 1508, 1468, 1418, 1386, 1343, 1310, 1266, 1216, 1191, 1177, 1131, 1099, 1086, 1073, 1058, 1028, 977, 943, 878, 832, 776, 720, 671, 662cm^{-1}

9.2.15 *(R)*-2-(5-Octadecyloxy-naphthalen-1-yloxy)-propionic acid

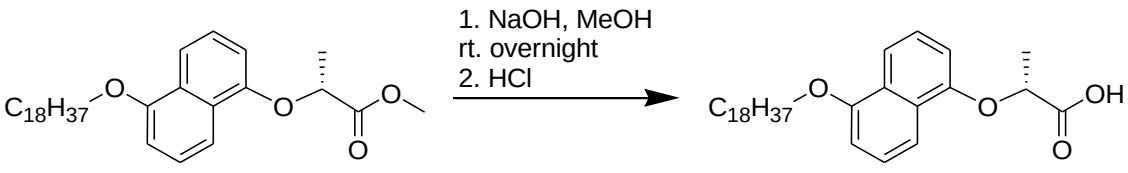

***(R)* -32** ***(R)* -1,5Naph**

The title compound was prepared in the same way as *(S)*-**2,7Naph**, using 210 mg (0.42 mmol) of starting material *(R)*-**32** and 1.3 mL (1.3 mmol) of 1N NaOH solution for reaction. Crystallization of the product from acetonitrile gave 110 mg. (Yield 54%)

M.F.: $C_{36}H_{48}O_4$; M.W.: 484.64; M.P.: 100-101 ºC; ^{1}H NMR (360 MHz, $CDCl_3$): 7.95 (d, *J*=8.4 Hz 1H, ArH), 7.89 (d, *J*=8.8 Hz 1H, ArH), 7.40 (t, *J*=8.0Hz, 1H, ArH), 7.34 (t,

J=8.2Hz, 1H, ArH) 6.86 (d, *J*=7.5Hz, 1H, ArH), 6.79 (d, *J*=7.8Hz, 1H, ArH) 4.99 (q, *J*=6.8 Hz, 1H, -OC<u>H</u>CH_3COOH), 4.15 (t, *J*=6.6 Hz, 2H -OC<u>H_2</u>$(CH_2)_{16}CH_3$), 1.95 (m, 2H, -OCH_2<u>CH_2</u>$(CH_2)_{15}CH_3$), 1.79 (d, *J*=6.8 Hz, 3H –OCHC<u>H_3</u>COOH), 1.57 (m, 2H, -OCH_2CH_2<u>CH_2</u>$(CH_2)_{14}CH_3$), 1.29 (m, 28H, -O $CH_2CH_2CH_2$<u>$(CH_2)_{14}$</u>CH_3), 0.91 (t, *J*=7.0 Hz, 3H, -$O(CH_2)_{17}$<u>CH_3</u>); ^{13}C NMR (90 MHz, $CDCl_3$): 177.0, 154.7, 152.8, 127.1, 126.9, 125.6, 124.6, 115.9, 114.0, 106.8, 105.6, 72.7, 68.3, 31.9, 29.7-29.3, 26.3, 22.7, 18.5, 14.1; FT- IR (ATR) 3119, 2915, 2849, 1713, 1678, 1596, 1509, 1470, 1418, 1387, 1346, 1319, 1264, 1215, 1178, 1132, 1101, 1074, 1055, 1047, 1026, 953, 887, 767, 719, 669cm^{-1}; HPLC: Chiralpack IB column, Heptane/IPA/TFA (97.3/2.5/0.2) 0.7ml/min, ee=99.0%

9.2.16 *(S)*-Methyl 2-(5-hydroxy-naphthalen-1-yloxy)propionate

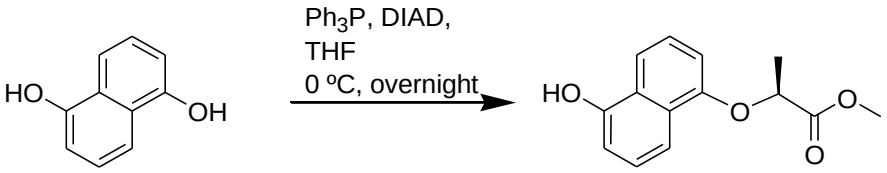

***(S)* -31**

As for *(S)*-**11**, 3.00 g of 1.5 dihydroxynaphthalene (19 mmol), 1.8 mL of *(R)*-methyl lactate (21 mmol), 5.60 g of triphenylphospine (21 mmol)and 4.2 mL of DIAD (21 mmol) were reacted together. Column chromatography of the crude product on silica gel using 10-30 % vol. ethyl acetate in hexane followed by ethyl acetate (1-3% vol.) in dichloromethane gave 950 mg of the desired product *(S)*- **31** (21% yield).

M.F.: $C_{14}H_{14}O_4$; M.W.: 246.26; M.P.: 156-161 ºC; ^{1}H NMR (360 MHz, $CDCl_3$): 7.94 (d, J_1=8.5 Hz, 1H, ArH), 7.80 (d, *J*=8.5 Hz, 1H, ArH) 7.31 (q, *J*=8.3 Hz, 4H, ArH), 6.85 (d, *J*=7.3 Hz, 1H, ArH), 6.72 (d, *J*=7.2 Hz, 1H, ArH) 4.96 (q, *J*=6.9 Hz, 1H, -OC<u>H</u>CH_3COOCH_3), 3.78 (s, 3H, -COOC<u>H_3</u>), 1.77 (d, *J*=6.9 Hz. –OCHC<u>H_3</u>COOMe); ^{13}C NMR (90 MHz, $CDCl_3$): 173.3, 153.8, 151.6, 125.8, 125.3, 115.3, 110.0, 106.7, 73.5, 52.8, 19.1; FT- IR (ATR): 3360, 1717, 1596, 1519, 1450, 1412, 1361, 1273, 1231, 1211, 1163, 1149, 1128, 1096, 1052, 974, 891, 768, 682cm^{-1}

9.2.17 *(S)*–Methyl-2-(5-octadecyloxy-naphthalen-1-yloxy)propionate

***(S)* -31** ***(S)* -32**

As for *(S)*-**12**, *(S)* -**31** (820 mg 3.3 mmol) in 50mL of acetonitrile was reacted with octadecylbromide (1.2 mL, 3.5 mmol). The product was isolated as a yellowish solid by crystallisation from acetonitrile (950 mg, yield 59%).

M.F.: $C_{37}H_{50}O_4$; M.W.: 498.74; M.P.: 79-80 ºC ^{1}H NMR (360 MHz, $CDCl_3$): 7.91 (d, *J*=8.6 Hz 2H, ArH), 7.39 (t, *J*=8.2Hz, 1H, ArH), 7.32 (t, *J*=8.1Hz, 1H, ArH) 6.86 (d, *J*=7.9Hz, 1H, ArH) 6.74 (d, *J*=7.8Hz, 1H, ArH) 4.95 (q, *J*=6.8 Hz, 1H, -OC<u>H</u>CH_3COOMe), 4.13 (t, *J*=6.6 Hz, 2H -OC<u>H_2</u>$(CH_2)_{16}CH_3$), 3.77 (s, 3H, -COOC<u>H_3</u>), 1.94 (m, 2H, -OCH_2<u>CH_2</u>$(CH_2)_{15}CH_3$), 1.76 (d, *J*=6.8 Hz. –OCHC<u>H_3</u>COOMe), 1.55 (m, 2H, -OCH_2CH_2<u>CH_2</u>$(CH_2)_{14}CH_3$), 1.28 (m, 28H, -O $CH_2CH_2CH_2$<u>$(CH_2)_{14}$</u>CH_3), 0.92 (t, *J*=6.8 Hz, 3H, -$O(CH_2)_{17}$<u>CH_3</u>); ^{13}C NMR (90 MHz, $CDCl_3$): 173.2, 155.1, 153.7, 127.3, 122.8, 125.0, 115.9, 114.6, 106.8, 105.9, 73.5, 68.6, 52.7, 32.3, 30.1-29.7, 26.7, 23.1, 19.1, 14.4; FT- IR (ATR): 2917, 2849, 2159, 1732, 1594, 1508, 1467, 1418, 1386, 1343, 1310, 1266, 1216, 1177, 1131, 1099, 1086, 1073, 1059, 1028, 977, 943, 878, 832, 776, 720, 671, 662 cm^{-1}

9.2.18 *(S)*-2-(5-Octadecyloxy-naphthalen-1-yloxy)-propionic acid

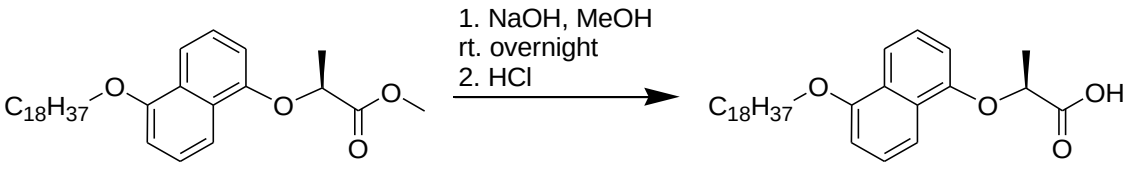

***(S)* -32** ***(S)* -1,5Naph**

The title compound was prepared in a a similar way to *(S)*-**2,7Naph**, but using 410 mg of starting material *(S)*-**32** (0.82 mmol) and 2.5 mL of 1N NaOH solution (2.5 mmol) for reaction. Crystallization of the crude product from acetonitrile gave 254mg of white solid. (Yield 64%)

M.F.: $C_{36}H_{48}O_4$; M.W.: 484.64; M.P.: 99-101 ºC; ^{1}H NMR (360 MHz, $CDCl_3$): 7.94 (d, *J*=8.6 Hz 2H, ArH), 7.86 (d, *J*=8.6Hz, 1H, ArH), 7.40 (t, *J*=7.6Hz, 1H, ArH) 7.36 (t,

J=7.6Hz, 1H, ArH) 6.86 (d, *J*=7.9Hz, 1H, ArH) 6.79 (d, *J*=7.8Hz, 1H, ArH) 4.99 (q, *J*=6.8 Hz, 1H, -OC<u>H</u>CH_3COOH), 4.13 (t, *J*=6.6 Hz, 2H -OC<u>H_2</u>$(CH_2)_{16}CH_3$), 1.92 (m, 2H, -OCH_2<u>CH_2</u>$(CH_2)_{15}CH_3$), 1.79 (d, *J*=6.8 Hz. –OCHC<u>H_3</u>COOH), 1.57 (m, 2H, -OCH_2CH_2<u>CH_2</u>$(CH_2)_{14}CH_3$), 1.28 (m, 28H, -O $CH_2CH_2CH_2$<u>$(CH_2)_{14}$</u>CH_3), 0.90 (t, *J*=7.0 Hz, 3H, -$O(CH_2)_{17}$<u>CH_3</u>); ^{13}C NMR (90 MHz, $CDCl_3$): 177.0, 154.7, 152.8, 126.8, 125.7, 124.6, 115.9, 113.9, 106.6, 105.5, 72.6, 68.2, 31.9, 29.7-29.3, 26.3, 22.7, 18.5, 14.1; MALDI-TOF MS m/z: calc. 484.36 found 484.28; FT- IR (ATR): 3065, 2917, 2850, 1713, 1596, 1509, 1470, 1418, 1387, 1319, 1264, 1215, 1177, 1133, 1103, 1074, 1056, 1026, 954, 881, 767, 719, 669 cm^{-1}; HPLC: Chiralpack IB column, Heptane/IPA/TFA (97.3/2.5/0.2) 0.7ml/min, ee=99.9%

9.2.19 *(S)*-Methyl 2-(4'-hydroxy-biphenyl-4-yloxy)propionate

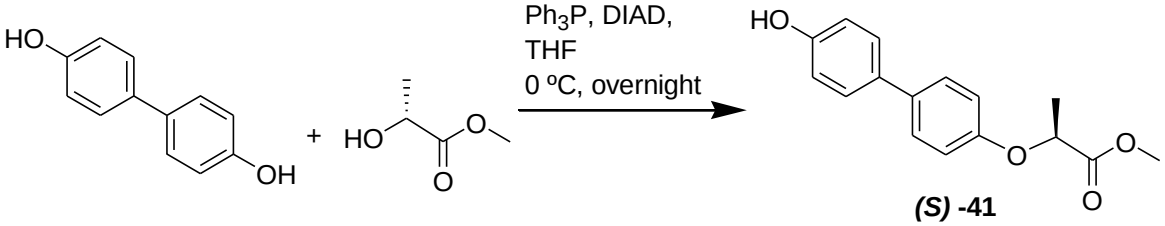

***(S)* -41**

The reaction was carried out using the same procedure as for the other lactate derivatives, using 4.0 g of 4,4'-biphenol (Aldrich, 21 mmol), 2.1 mL of *(R)*- methyl lactate (26 mmol), 6.7 g of triphenylphosphine (26 mmol) and 5.0 mL of DIAD (26 mmol). Column chromatography on silica gel using 10-30 % vol. ethyl acetate in hexane, and then 1-3% vol. ethyl acetate in dichloromethane to get 2.1 g of product as a white solid (37% yield).

M.F.: $C_{16}H_{16}O_4$; M.W.: 272.30; M.P.: 136-139 ºC; ^{1}H NMR (360 MHz, $CDCl_3$): 7.47 (m, 4H, ArH), 6.95 (dd, J_1=8.8 Hz, J_2=10.3 Hz, 4H, ArH), 4.82 (q, *J*=7.0 Hz, 1H, -OC<u>H</u>CH_3COOCH_3), 3.79 (s, 3H, -COOC<u>H_3</u>), 1.69 (d, *J*=6.9 Hz. –OCHC<u>H_3</u>COOMe); ^{13}C NMR (90 MHz, $CDCl_3$): 173.3, 156.5, 155.0, 134.5, 133.0, 127.9, 127.8, 115.6, 115.3 72.6 52.6, 18.7; FT- IR (ATR): 3362, 2923, 1726, 1610, 1496, 1443, 1407, 1346, 1265, 1229, 1173, 1130, 1103, 1051, 971, 943, 820, 762, 731cm^{-1}

9.2.20 *(S)*-Methyl 2-(4'-octadecyloxy-biphenyl-4-yloxy)propionate

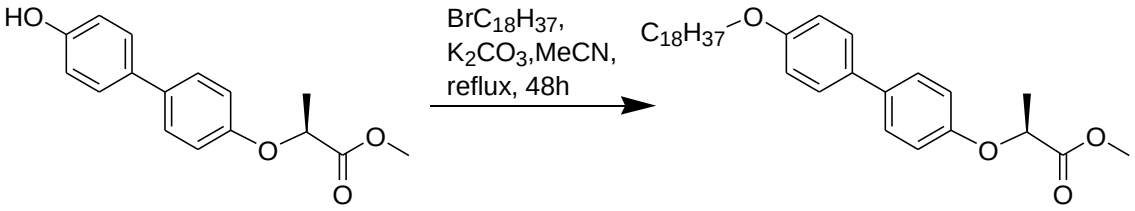

***(S)* -41** **(S) -42**

The reaction was carried out in a same way as described for *(S)*-**12** with 1.5 g of *(S)*-**41** (5.5 mmol) and 2.0mL of 1-bromooctadecane (5.8 mmol) in 70mL of acetonitrile. 1.95 g of white solid was obtained from the reaction after purification by crystallisation (yield 68%).

M.F.: $C_{39}H_{52}O_4$; M.W.: 524.39; M.P.: >300 ºC ^{1}H NMR (360 MHz, $CDCl_3$): 7.47 (m, 4H, ArH), 6.95 (m, 4H, ArH) 4.82 (q, *J*=6.8 Hz, 1H, -OC<u>H</u>CH_3COOCH_3), 4.00 (t, *J*=6.6 Hz, 2H -OC<u>H_2</u>$(CH_2)_{16}CH_3$), 3.80 (s, 3H, -COOC<u>H_3</u>), 1.81 (m, 2H, -OCH_2<u>CH_2</u>$(CH_2)_{15}CH_3$), 1.66 (d, *J*=6.8 Hz. 3H, –OCHC<u>H_3</u>COOMe), 1.49 (m, 2H, -O CH_2CH_2<u>CH_2</u>$(CH_2)_{14}CH_3$), 1.29 (m, 28H, -O $CH_2CH_2CH_2$<u>$(CH_2)_{14}$</u>CH_3), 0.91 (t, *J*=6.8 Hz, 3H, -$O(CH_2)_{17}$<u>CH_3</u>); ^{13}C NMR (90 MHz, $CDCl_3$): 172.7, 158.4, 156.6, 134.5, 133.0, 127.8, 115.3, 114.7, 72.7, 68.0, 52.4, 31.9, 29.7-29.3, 26.1, 22.7, 18.6, 14.1; FT- IR (ATR): 2917, 2849, 1743, 1605, 1499, 1473, 1394, 1269, 1244, 1218, 1176, 1130, 1100, 1036, 982, 822, 761, 719, 701cm^{-1}

9.2.21*(S)*-2-(4'-Octadecyloxy-biphenyl-4-yloxy)-propionic acid

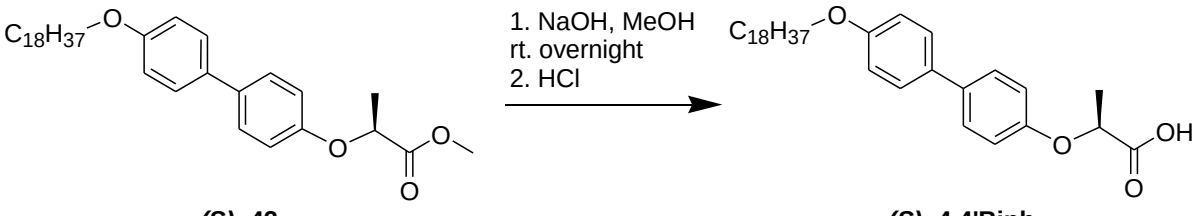

***(S)* -42** ***(S)* -4,4'Biph**

Using the usual saponification conditions with 1.6 g of starting material *(S)*-**42** (3.0 mmol) and 9 mL of 1N NaOH solution (9 mmol) were reacted, and after extraction and crystallization from acetonitrile 640 mg. (Yield 41%) of product was obtained.

M.F.: $C_{38}H_{50}O_4$; M.W.: 510.75; M.P.: 122-126 ºC; ^{1}H NMR (360 MHz, $CDCl_3$): 7.48 (m, 4H, ArH), 6.97 (m, 4H, ArH), 4.86 (q, *J*=6.8 Hz, 1H, -OC<u>H</u>CH_3COOH), 4.00 (t, *J*=6.6 Hz, 2H -OC<u>H_2</u>$(CH_2)_{16}CH_3$), 1.83 (m, 2H, -OCH_2<u>CH_2</u>$(CH_2)_{15}CH_3$), 1.70 (d, *J*=6.8 Hz. –OCHC<u>H_3</u>COOH), 1.46 (m, 2H, -OCH_2CH_2<u>CH_2</u>$(CH_2)_{14}CH_3$), 1.28 (m, 28H, -O

$CH_2CH_2CH_2(\underline{CH_2})_{14}CH_3$), 0.90 (t, *J*=7.0 Hz, 3H, -O$(CH_2)_{17}\underline{CH_3}$); ^{13}C NMR (90 MHz, $CDCl_3$): 128.3, 128.2, 115.9, 115.1, 32.3, 30.1-29.8, 23.1, 14.5; MALDI-TOF MS m/z: calc. 510.37 found 510.31; FT- IR (ATR): 3038, 2917, 2850, 1742, 1607, 1586, 1499, 1474, 1462, 1396, 1372, 1285, 1266, 1241, 1177, 1132, 1109, 1036, 943, 818, 729, 718, 663 cm^{-1}; HPLC: Chiralpack IA column, Heptane/EtOH/TFA (94.8/5.0/0.2) 0.7ml/min, ee=93.0%

9.2.22*(R)*–Butyl 2-(4'-octadecyloxy-biphenyl-4-yloxy)propionate

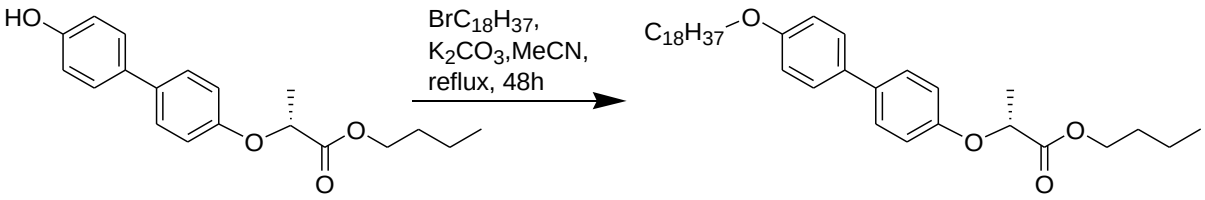

***(R)* -41L** **(R) -42L**

Compound *(R)*-**41L** (1.5 g, 4.8 mmol), prepared as described previously,[39] was reacted with octadecylbromide (1.7 mL, 5.0 mmol) in a similar way to the homologues in 70mL of acetonitrile. The product was isolated as a white solid (1.82 g, yield: 67%).

M.F.: $C_{37}H_{58}O_4$; M.W.; 566.85; M.P.: 75-78 ºC; ^{1}H NMR (360 MHz, $CDCl_3$): 7.45 (m, 4H, ArH), 6.94 (m, 4H, ArH) 4.80 (q, *J*=6.8 Hz, 1H, -OC$\underline{H}$$CH_3$$COOCH_2$-), 4.20 (m, 2H, -COOC$\underline{H_2}$$CH_2CH_2CH_3$), 4.00 (t, *J*=6.6 Hz, 2H -OC$\underline{H_2}$$(CH_2)_{16}CH_3$), 1.83 (m, 2H, -OC$H_2\underline{CH_2}$$(CH_2)_{15}CH_3$), 1.77 (d, *J*=6.8 Hz, 3H –OCHC$\underline{H_3}$COOBu), 1.65-1.30 (m, 34H, -OCH_2CH_2(C$\underline{H_2}$$)_{15}CH_3$+-COOC$H_2$(C$\underline{H_2}$$)_2CH_3$), 0.90 (m, 6H, -O$(CH_2)_{17}\underline{CH_3}$+ -COO$(CH_2)_3\underline{CH_3}$); ^{13}C NMR (90 MHz, $CDCl_3$): 172.3, 158.4, 156.6, 134.4, 133.1, 127.7, 115.3, 114.7, 72.7, 68.0, 65.1, 31.9 30.5, 29.7-29.3, 26.1, 22.7, 18.9, 18.6, 14.1, 13.6; FT- IR (ATR): 2956, 2917, 2849, 1752, 1607, 1570, 1498, 1474, 1464, 1393, 1379, 1270, 1240, 1192, 1176, 1116, 1053, 1037, 998, 949, 825, 807, 755, 728, 720cm^{-1}

9.2.23*(R)*-2-(4'-Octadecyloxy-biphenyl-4-yloxy)-propionic acid

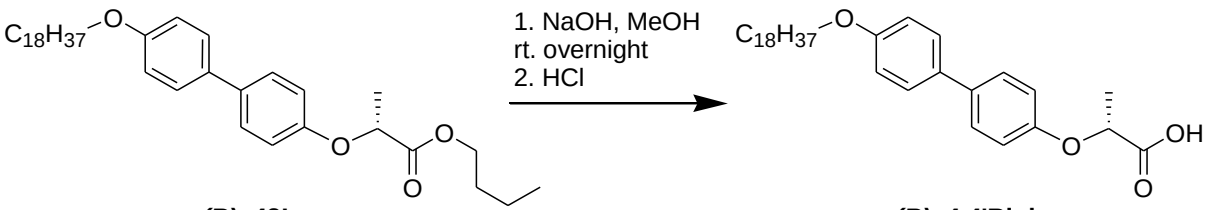

***(R)* -42L** ***(R)* -4,4'Biph**

The reaction was performed using same procedure as for*(S)*-**2,7Naph**, 1.0 g (1.8 mmol) of starting material *(R)*-**42L** and 5.5 mL of 1N NaOH (5.5 mmol) solution was used for reaction. Crystallization from acetonitrile gave 530mg of white product. (Yield 59%)

M.F.: $C_{38}H_{50}O_4$; M.W.: 510.75; M.P.: 123-125 ºC; ^{1}H NMR (360 MHz, $CDCl_3$): 7.47 (m, 4H, ArH), 6.96 (m, 4H, ArH), 4.85 (q, *J*=6.8 Hz, 1H, -OC<u>H</u>CH_3COOH), 4.00 (t, *J*=6.6 Hz, 2H -OC<u>H_2</u>$(CH_2)_{16}CH_3$), 1.83 (m, 2H, -OCH_2<u>CH_2</u>$(CH_2)_{15}CH_3$), 1.70 (d, *J*=6.8 Hz. –OCHC<u>H_3</u>COOH), 1.46 (m, 2H, -OCH_2CH_2<u>CH_2</u>$(CH_2)_{14}CH_3$), 1.28 (m, 28H, -O $CH_2CH_2CH_2$<u>$(CH_2)_{14}$</u>CH_3), 0.90 (t, *J*=7.0 Hz, 3H, -$O(CH_2)_{17}$<u>CH_3</u>); ^{13}C NMR (90 MHz, $CDCl_3$): 158.5, 132.9, 127.9, 127.7, 115.7, 114.9, 72.6, 68.2, 31.9, 29.7-29.3, 26.0, 22.6, 18.3, 14.4; MALDI-TOF MS m/z: calc. 510.37 found 510.34; FT- IR (ATR): 2956, 2917, 2850, 1743, 1717, 1607, 1586, 1499, 1474, 1463, 1395, 1285, 1241, 1177, 1109, 1036, 942, 811, 729, 718 cm^{-1}; HPLC: Chiralpack IA column, Heptane/EtOH/TFA (94.8/5.0/0.2) 0.7ml/min, ee=90.5%

9.2.24 1-Benzyloxy-4-octadecyloxy-benzene

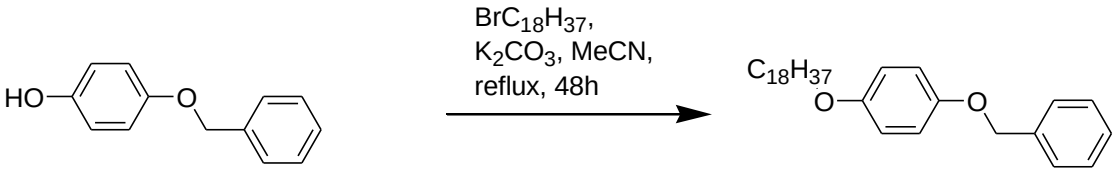

51

The reaction procedure was same as for the preparation of *(S)*-**12**. For the reaction 16 g of pre-dried ground K_2CO_3 (118 mmol), 5.0 g of 4-(benzyloxy)phenol (Aldrich, 25 mmol), 200 mL of acetonitrile and 9.5 mL 1-bromooctadecane (28 mmol) was used. The total amount of product obtained was 10.5 g (89% yield).

M.F.: $C_{31}H_{48}O_2$; M.W.: 452.71; M.P.: 84-87 ºC; ^{1}H NMR (250 MHz, $CDCl_3$): 7.45-7.30 (m, 5H, ArH), 6.80-6.96 (m, 4H, ArH), 5.05 (s, 2H, Ar<u>CH_2</u>O-), 3.93 (t, *J*=6.5 Hz, 2H, -O<u>CH_2</u>$(CH_2)_{16}CH_3$), 1.80-1.72 (m, 2H, -OCH_2<u>CH_2</u>$(CH_2)_{15}CH_3$), 1.44-1.40 (m, 2H, -OCH_2CH_2<u>CH_2</u>$(CH_2)_{14}CH_3$), 1.29 (m, 28H, -O $CH_2CH_2CH_2$<u>$(CH_2)_{14}$</u>CH_3), 0.88 (t, *J*=6.8 Hz, 3H, -$O(CH_2)_{17}$<u>CH_3</u>); ^{13}C NMR (90 MHz, $CDCl_3$): 153.6, 152.9, 137.4, 128.4, 127.7, 127.3, 115.8, 115.4, 70.7, 68.6, 33.7, 32.8, 31.9, 29.7-29.3, 28.7, 28.1, 26.0, 22.6, 14.0; FT- IR (ATR):2956, 2916, 2873, 2848, 2535, 2025, 1625, 1510, 1473, 1463, 1418, 1384, 1290, 1239, 1226, 1113, 1081, 1023, 945, 911, 866, 824, 777, 733, 719, 691cm^{-1}

9.2.25 4-Octadecyloxy-phenol

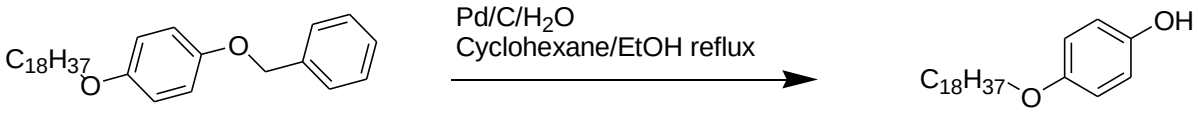

51 **52**

The starting material (14 g, 30 mmol) was placed in a 1 L round-bottom flask and the cyclohexene (145 mL), ethanol (360 mL) and palladium on Degussa carbon (Aldrich, 20% wt. Pd/C/H_2O, 2.1 g, 3 mmol) were added. The mixture was brought to reflu x in an oil bath, under argon inlet. After 6h at reflux, the mixture was allowed to cool and was filtered through celite and was washed with ethanol (400 mL). Evaporation of the solvent afforded crude product, which and after crystallization from hexane gave 5.8 g of pure product (54% yield).

M.F.: $C_{24}H_{42}O_2$; M.W.: 362.59; M.P.: 93-95 ºC; ^{1}H NMR (250 MHz, $CDCl_3$): 6.72-6.81 (m, 4H, ArH), 4.39 (s, 1H, HO-), 3.90 (t, *J*=6.5 Hz, 2H, -O$CH_2(CH_2)_{16}CH_3$), 1.80-1.72 (m, 2H, -O$CH_2CH_2(CH_2)_{15}CH_3$), 1.44-1.40 (m, 2H, -O$CH_2CH_2CH_2(CH_2)_{14}CH_3$), 1.27 (m, 28H, -O $CH_2CH_2CH_2(CH_2)_{14}CH_3$), 0.88 (t, *J*=6.7 Hz, 3H, -O$(CH_2)_{17}CH_3$); ^{13}C NMR (90 MHz, $CDCl_3$): 153.4, 149.3, 116.0, 115.7, 68.8, 31.9, 29.7-29.3, 26.0, 22.7, 14.1; FT- IR (ATR) 3437, 3393, 2955, 2917, 2850, 1518, 1473, 1463, 1398, 1373, 1299, 1243, 1170, 1106, 1057, 1039, 1025, 1011, 828, 818, 770, 727, 719, 555, 528cm^{-1}

9.2.26 *(R)*-Methyl 2-(4-octadecyloxy-phenoxy)propionate

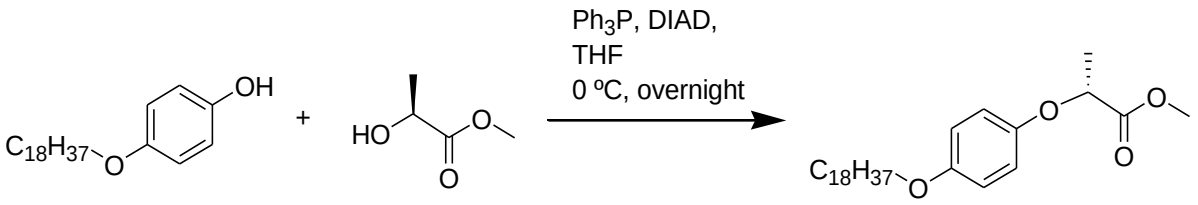

52 ***(R)* -53**

The reaction was carried out using procedure as for *(S)*-**11**, with 1.4 g of 4-(Octadecyloxy)phenol (3.9 mmol), 0.44 mL of *(S)*-methyl lactate (4.6 mmol) and 1.2 g of triphenylphosphine (4.6 mmol), 0.92 mL of DIAD (0.91 ml 4.6 mmol) and dry THF (100 mL). Column chromatography on silica gel using 10-30 % vol. ethyl acetate in hexane gave the crude product, that was crystallized from methanol to give 1.05 g of white solid (Yield 61%).

M.F.: $C_{28}H_{48}O_4$; M.W.: 448.68; M.P.: 66-67 ºC ^{1}H NMR (250 MHz, $CDCl_3$): 6.80 (s,

4H, ArH), 4.68 (q, *J*=6.5 Hz, 1H, -OC<u>H</u>CH_3COOMe), 3.89 (t, *J*=6.2 Hz, 2H -O<u>CH_2</u>$(CH_2)_{16}CH_3$), 3.76 (s, 3H, -COOC<u>H_3</u>), 1.75 (m, 2H, -OCH_2<u>CH_2</u>$(CH_2)_{15}CH_3$), 1.60 (d, *J*=6.9 Hz, 3H –OCHC<u>H_3</u>COOMe), 1.42 (m, 2H, -OCH_2CH_2<u>CH_2</u>$(CH_2)_{14}CH_3$), 1.26 (m, 28H, -O $CH_2CH_2CH_2$<u>$(CH_2)_{14}$</u>CH_3), 0.88 (t, *J*=6.7 Hz, 3H, -$O(CH_2)_{17}$<u>CH_3</u>); ^{13}C NMR (90 MHz, $CDCl_3$): 172.9, 154.0, 151.5, 116.5, 115.4, 73.6, 68.5, 52.3, 31.9, 29.7-29.4, 26.0, 22.7, 18.7, 14.1; FT- IR (ATR): 2955, 2918, 2849, 2190, 2020, 1731, 1507, 1475, 1463, 1448, 1393, 1381, 1342, 1318, 1280, 1234, 1222, 1134, 1115, 1097, 1051, 1036, 1021, 976, 948, 840, 825, 763, 722, 692, 662cm^{-1}

9.2.27 *(R)*-2-(4-Octadecyloxy-phenoxy)-propionic acid

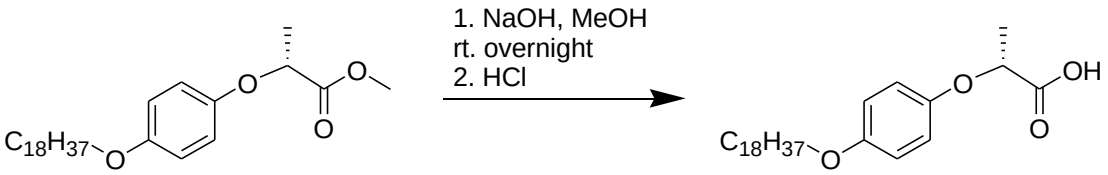

***(R)* -53** **(R) -1,4Ph**

Reaction procedure was the same as for the saponification of *(S)*-**2,7Naph**. In the reaction 600 mg of *(R)*-**53**(600 mg, 1.33 mmol), 2N water solution of sodium hydroxide (2.1 mL, 4.2 mmol) and methanol (150 mL) was used. Crystallization from methanol afforded 340 mg of white solid (yield 59%).

M.F.: $C_{27}H_{46}O_4$; M.W.: 434.65; M.P.: 87-88 ºC; ^{1}H NMR (250 MHz, $CDCl_3$): 6.79 (m, 4H, ArH), 4.68 (q, *J*=6.8 Hz, 1H, -OC<u>H</u>CH_3COOH), 3.88 (t, *J*=6.3 Hz, 2H -O<u>CH_2</u>$(CH_2)_{16}CH_3$), 3.76 (s, 3H, -COOC<u>H_3</u>), 1.75 (m, 2H, -OCH_2<u>CH_2</u>$(CH_2)_{15}CH_3$), 1.60 (d, *J*=7.0 Hz. –OCHC<u>H_3</u>COOMe), 1.42 (m, 2H, -OCH_2CH_2<u>CH_2</u>$(CH_2)_{14}CH_3$), 1.23 (m, 28H, -O $CH_2CH_2CH_2$<u>$(CH_2)_{14}$</u>CH_3), 0.88 (t, *J*=6.6 Hz, 3H, -$O(CH_2)_{17}$<u>CH_3</u>); ^{13}C NMR (90 MHz, $CDCl_3$): 176.4, 154.5, 151.0, 116.8, 115.5, 73.5, 68.6, 52.2, 31.9, 29.7-29.3, 26.0, 22.7, 18.3, 14.1; TOF MS m/z: calc. 434.36 found 434.23; FT- IR (ATR): 2956, 2915, 2849, 1703, 1510, 1470, 1387, 1333, 1286, 1233, 1141, 1115, 1097, 1071, 1037, 1025, 934, 819, 764, 718, 692, 674 cm^{-1}; HPLC: Chiralpack IA column, Heptane/IPA/TFA (97.3/2.5/0.2) 0.7ml/min, ee=98.2%

9.2.28 *(S)*-Methyl 2-(4-octadecyloxy-phenoxy)propionate

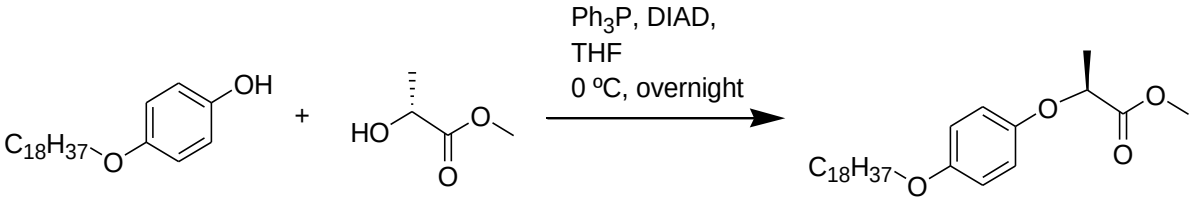

52 ***(S)* -53**

Compound *(S)*-**53** was prepared in the same way as the opposite enantiomer and with the same amounts of reagents, but with the other enantiomer of methyl lactate. After purification 1.12 g of white solid was obtained (Yield 65%).

M.F.: $C_{28}H_{48}O_4$; M.W.: 448.68; M.P.: 64-65 ºC; ^{1}H NMR (250 MHz, $CDCl_3$): 6.80 (s, 4H, ArH), 4.68 (q, *J*=6.5 Hz, 1H, -OC<u>H</u>CH_3COOMe), 3.89 (t, *J*=6.2 Hz, 2H -OC<u>H_2</u>$(CH_2)_{16}CH_3$), 3.76 (s, 3H, -COOC<u>H_3</u>), 1.75 (m, 2H, -OCH_2<u>CH_2</u>$(CH_2)_{15}CH_3$), 1.61 (d, *J*=6.8 Hz, 3H, –OCHC<u>H_3</u>COOMe), 1.42 (m, 2H, -OCH_2CH_2<u>CH_2</u>$(CH_2)_{14}CH_3$), 1.26 (m, 28H, -O $CH_2CH_2CH_2$<u>$(CH_2)_{14}$</u>CH_3), 0.88 (t, *J*=6.7 Hz, 3H, -$O(CH_2)_{17}$<u>CH_3</u>); ^{13}C NMR (90 MHz, $CDCl_3$): 173.0, 154.0, 151.5, 116.5, 115.4, 73.6, 68.5, 52.2, 31.9, 29.7-29.3, 26.0, 22.7, 18.6, 14.1; FT- IR (ATR): 2957, 2921, 2850, 1732, 1508, 1476, 1465, 1393, 1382, 1342, 1319, 1283, 1235, 1223, 1135, 1115, 1098, 1052, 1022, 977, 828, 763, 722, 662, 549, 525cm^{-1}

9.2.29 *(S)* -2-(4-Octadecyloxy-phenoxy)-propionic acid

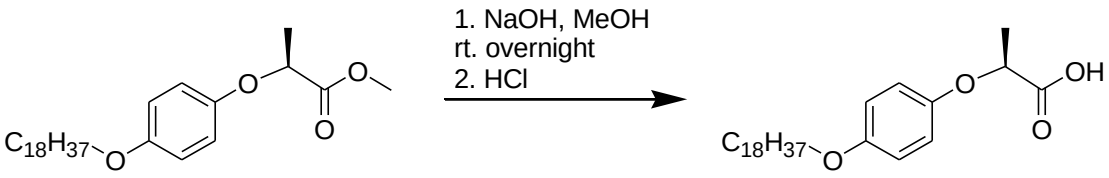

***(S)* -53** ***(S)* -1,4Ph**

The acid *(S)*-**1,4Ph** was prepared employing the same procedure as for the other enantiomer, but with 1.05g *(S)*-**53**(2.3 mmol)and 7.5 mL of 1N water solution of sodium hydroxide (7.5 mmol)in methanol (250 mL). Crystallization from methanol gave 551 mg of white solid (yield 55%).

M.F.: $C_{27}H_{46}O_4$; M.W.: 434.65; M.P.: 91-92 ºC;^{1}H NMR (250 MHz, $CDCl_3$): 6.79 (m, 4H, ArH), 4.68 (q, *J*=6.8 Hz, 1H, -OC<u>H</u>CH_3COOH), 3.88 (t, *J*=6.3 Hz, 2H -OC<u>H_2</u>$(CH_2)_{16}CH_3$), 3.76 (s, 3H, -COOC<u>H_3</u>), 1.75 (m, 2H, -OCH_2<u>CH_2</u>$(CH_2)_{15}CH_3$), 1.60 (d, *J*=7.0 Hz. –OCHC<u>H_3</u>COOH), 1.42 (m, 2H, -OCH_2CH_2<u>CH_2</u>$(CH_2)_{14}CH_3$), 1.23 (m,

28H, -O $CH_2CH_2CH_2(\underline{CH_2})_{14}CH_3$), 0.88 (t, *J*=6.6 Hz, 3H, -O$(CH_2)_{17}\underline{CH_3}$); ^{13}C NMR (90 MHz, $CDCl_3$): 176.4, 154.5, 151.0, 116.8, 115.5, 73.5, 68.6, 52.2, 31.9, 29.7-29.3, 26.0, 22.7, 18.3, 14.1; MALDI-TOF MS m/z: calc. 434.36 found 434.23; FT- IR (ATR): 2915, 2849, 1704, 1510, 1470, 1387, 1371, 1334, 1286, 1232, 1140, 1117, 1096, 1071, 1037, 1025, 967, 933, 818, 780, 764, 717, 673 cm^{-1}; HPLC: Chiralpack IA column, Heptane/IPA/TFA (97.3/2.5/0.2) 0.7ml/min, ee=98.8%

9.2.30 Bulk complex formed between 1,3-Ph and diaminocyclohexane in Resolution Experiment

A mixture of the (*R*)-resorcinol derivative **1,3-Ph** (105.0 mg, 0.24 mmol), (*S,S*)-diaminocyclohexane(13.5mg, 0.12mmol) and (*R,R*)-diaminocyclohexane (13.8mg, 0.12 mmol) were dissolved in *tert*-butyl methyl ether (Fluka analytical, >98%, 10 mL) by heating to approximately 50°C. A white, amorphous balls (71 mg), formed, and was characterized as the 1:1 complex of the (*R*)-**1,3-Ph**with (*R,R*)-diaminocyclohexane. Chiral HPLC analysis indicated the majority presence of (*R,R*)-diaminocyclohexane (*ee* = 82%). M.P.: 68-72°C (melting point of the acid**1,3Ph** is 80ºC, and the diaminocyclohexane is 45 ºC). ^{1}H NMR (360MHz, $CDCl_3$) 7.11 (t, 1H), 6.45-6.49 (m, 3H), 4.55 (q, 1H), 3.91 (t, 2H), 3.21 (bs, 4H), 2.60 (m, 2H), 1.90 (m, 2H), 1.76 (m, 2H), 1.67 (d, 3H), 1.28 (m, 28H), 1.11 (m, 2H), 0.93 (t, 3H) ppm. FT- IR (ATR): 3345, 3266, 2917, 2850, 2161, 2032, 1642, 1587, 1493, 1472, 1449, 1401, 1367, 1333, 1288, 1262, 1181, 1170, 1160, 1145, 1131, 1087, 1037, 973, 935, 907, 855, 834, 784, 759, 717, 684 cm^{-1}

Chapter 10
Bibliography

1 G. H. Wagnière, *On Chirality and the Universal Asymmetry*, Verlag Helvetica Chimica Acta, Zurich, Wiley-VCH, **2007**.

2 A. Guijarro, M. Yus, *The Origin of Chirality in the Molecules of Life*, RSC Publishing, **2009**.

3 (a) E. Francotte, W. Lindner (eds) *Chirality in Drug Research*, Wiley-VCH, **2006**. (b) A. Mannschreck, R. Kiesswetter, E. von Angerer, *J. Chem. Ed*., **2007**, *84*, 2012.

4 (a) J. Zhang, M. T. Albelda, Y. Liu, J. W. Canary, *Chirality*, **2005**, *17*, 404. (b) D. B. Amabilino, *Nanoscale Chirality*. Special issue of *Chem. Soc. Rev.*, **2009**, *38*, issue 3. (c) D. B. Amabilino, *Chirality at the Nanoscale*, Wiley-VCH, **2009**. (d) Y. Wang, J. Xu, Y. Wang, H. Chen, *Chem. Soc. Rev.*, **2013**, *42*, 2930.

5 R. Raval, *Chem. Soc. Rev*. **2009**, *38*, 707.

6 M. Parschau, R. Fasel, K. H. Ernst, *Cryst. Growth Des*., **2008**, *8*, 1890.

7 L. Pérez-García, D. B. Amabilino, *Chem. Soc. Rev.*, **2002**, *31*, 342.

8 L. Pérez-García, D. B. Amabilino, *Chem. Soc. Rev.*, **2007**, *36*, 941.

9 Note that formally a solid solution is a random mixture of two compounds in a crystal lattice, so that the lattice spacing does not change irrespective of the local composition. A pseudoracemate can be considered a type of solid solution, but in this Thesis it shall be used as a term for a specific case where there is partial ordering of enantiomers (which could be in rows or sheets) but these structures do not repeat in the lattice (Figure 1.1).

10 D. M. Walba, E. Körblova, R. Shao, J. E. Maclennan, D. R. Link, M. A. Glaser, N. A. Clark, *J. Phys. Org. Chem.*, **2000**, *13*, 830.

11 K. E. Plass, A. L. Grzesiak, A. J. Matzger, *Acc. Chem. Res*., **2007**, *40*, 287.

12 E. Pidcock, *Chem. Comm.*,**2005**, 3457.

13 T. Matsuura, H. Koshima, *J. Photochem. Photobiol. C-Photochem. Rev.*, **2005**, *6*, 7.

14 (a) C. P. Brock, W. B. Schweizer, J. D.Dunitz, *J. Am. Chem. Soc.*, **1991**, *113*, 9811.

(b) J. Jacques, A. Collet, S. H. Wilen, *Enantiomers, Racemates,and Resolutions*, John Wiley & Sons: New York, **1981,** 23. (c) C. P. Price, A. J. Matzger, *J. Org. Chem.*, **2005**, *70*, 1.

15 (a) D. G.. Yablon, L. C. Giancarlo, G. W. Flynn, *J. Phys. Chem. B*, **2000**, *104*, 7627. (b) F. Tao, S. L. Bernasek, *J. Phys. Chem. B*, **2005**, *109*, 6233. (c) A. M. Berg, D. L. Patrick, *Angew. Chem., Int. Ed.*, **2005**, *44*, 1821.

16 (a) W. Mamdouh, H. Uji-i, A. E. Dulcey, V. Percec, S. De Feyter, F. C. De Schryver, *Langmuir*, **2004**, *20*, 7678. (b) W. Mamdouh, H. Uji-i, A. Gesquiere, S. De Feyter,; D. B. Amabilino, M. M. S. Abdel-Mottaleb, J. Veciana, F. C. De Schryver, *Langmuir*, **2004**, *20*, 9628. (c) I. Weissbuch, M. Berfeld, W. Bouwman, K. Kjaer, J. Als-Nielsen, M. Lahav, L. Leiserowitz, *J. Am. Chem. Soc.*, **1997**, *119*, 933. (d) S. De Feyter, A. Gesquiere, P. C. M. Grim, F. C. De Schryver, S. Valiyaveettil, C. Meiners, M. Sieffert, K. Mullen, *Langmuir*, **1999**, *15*, 2817.

17 (a) L. Pasteur *C. R. Acad. Sci.*, **1853**, *37*, 162. (b) L. Pasteur *Ann. Chim. (Paris)*, **1853**, *38*, 437. (c) J. Jacques, A. Collet, S. H. Wilen, *Enantiomers, racemates and resolutions*. Malabar, FL: Krieger Publishing Company, **1994**. (d) E. Fogassy, M. Nógrádi, D. Kozma, G.. Egri, E. Pálovics, V. Kiss, *Org. Biomol. Chem.*, **2006**, *4*, 3011. (e) F. Faigl, E. Fogassy, M. Nógrádi, E. Pálovics, J. Schindler, *Tetrahedron: Asymmetry*, **2008**, *19*, 519.

18 W. Marckwald, A. McKenzie, *Ber. Dtsch. Chem. Ges.*,**1899**, *32*, 2130.

19 W. J. Pope, S. J. Peachy, *J. Chem Soc.*,**1899**, *75*, 1066.

20 D. Kozma, Ed., *CRC Handbook of Optical Resolutions via Diastereomeric Salt Formation*, CRC Press, New York, **2002**.

21 G.. Coquerel, D. B. Amabilino, *The Nanoscale Aspects of Chirality in Crystal Growth: Structure and Heterogeneous Equilibria* in *Chirality at the Nanoscale* 305-348 Amabilino, D.B. Ed., Wiley-VCH, Weinheim, **2009**.

22 (a) T. Vries, H. van Echten, J. Koek, W. ten Hoeve, R. M. Kellogg, Q. B. Broxterman, A. J. Minnard, S. Van der Sluis, L. Hulshof, J. Kooistra, *Angew. Chem. Int Ed.*, **1998**, *37*, 2249. (b) Q. B. Broxterman, E. van Echten, L. A. Hulshof, B. Kaptein, R. M. Kellogg, A. J. Minnaard, T. R. Vries, H. Wynberg, *Chemistry Today*, **1998**, *16*, 34. (c) A. Collet, *Angew. Chem. Int Ed.*, **1998**, *37*, 3239. (d) R. M. Kellogg, B. Kaptein, T. R. Vries, *Top. Curr. Chem.*, **2007**, *269*, 159.

23 (a) I. Weissbuch, I. Kuzmenko, M.Berfeld, L.Leiserowitz, M. Lahav, *J. Phys. Org. Chem.*, **2000**, *13*, 426. (b) I. Weissbuch, M. Lahav, *Chem. Rev.* **2011**, *111*, 3236.

24 M.Böhringer, W. D. Schneider, R. Berndt,*Surf. Rev. Lett.*, **2000**, *7*, 661.

25 Q.Chen, N. V. Richardson,*Nature. Mat.*, **2003**, *2*, 324.

26 Y. Mastai, *Chem. Soc. Rev.*, **2009**, *38*, 772.

27 M. Linares, A. Minoia, P. Brocorens, D. Beljonne, R. Lazzaroni, *Chem. Soc. Rev.*, **2009**, *38*, 806.

28 (a) M. Böhringer, K. Morgenstern, W. D. Schneider, R. Berndt, *Angew. Chem. Int. Ed.*, **1999**, *38*, 821. (b) M. O. Lorenzo, C. J. Baddeley, C. Muryn, R. Raval, *Nature*, **2000**, *404*, 376. (c) J. D. Mougous, A. J. Brackley, K. Foland, R. T. Baker, D. L. Patrick, *Phys. Rev. Lett.*, **2000**, *84*, 2742. (d) A. Kühnle, T. R. Linderoth, B. Hammer, F. Besenbacher, *Nature*, **2001**, *415*, 891. (e) A. Mugarza, N. Lorente, P. Ordejon, C. Krull, S. Stepanow, M. L. Bockquet, J. Fraxedas, G.. Ceballos, P. Gambardella, *Phys. Rev. Lett.*, **2010**, *105*, 115 702. (f) H. L. Tierney, C. J. Murphy, E. C. H. Sykes, *Phys. Rev. Lett.*, **2011**, *106*, 010 801. (g) J. A. A. W. Elemans, I. De Cat, H. Xu, S. De Feyter, *Chem. Soc. Rev*., **2009**, *38*, 722. (h) R. Gutzler, T. Sirtl, J. F. Dienstmaier, K. Mahata, W. M. Heckl, M. Schmittel, M. J. Lackinger, *J. Am. Chem. Soc.*, **2010**, *132*, 5084. (i) R. Madueno, M. T. Raisanen, C. Silien, M. Buck, *Nature*, **2008**, *454*, 618. (j) D. M. Ceres, J. K. Barton, *J. Am. Chem. Soc*., **2003**, *125*, 14964. (k) D. M. Cyr, B. Venkataraman, G. W. Flynn, *Chem. Mater.* **1996**, *8*, 1600. (l) Q. H. Yuan, C. J. Yan, H. J.Yan, L. J. Wan, B. H. Northrop, H. Jude, P. J. Stang, *J. Am. Chem. Soc.*, **2008**, *130*, 8878. (m) D. P. E. Smith, J. K. H. Horber, G. Binnig, H. Nejoh, *Nature*, **1990**, *344*, 641. (n) S. De Feyter, A. Gesquiere, M. M. Abdel-Mottaleb, P. C. M. Grim, F. C. De Schryver, C.Meiners, M. Sieffert, S. Valiyaveettil, K. Mullen, *Acc. Chem. Res.*, **2000**, *33*, 520. (o) L. Askadskaya, J. P. Rabe, *Phys. Rev. Lett.*, **1992**, *69*, 1395. (q) L. Liu, L. Zhang, X. Mao, L. Niu, Y. Yang, C. Wang, *NanoLett.*, **2009**, *9*, 4066. (r) S. De Feyter, P. . M. Grim, M. Rücker, P. Vanoppen, C. Meiners, M. Sieffert, S. Valiyaveettil, K. Müllen, F. C. De Schryver, *Angew. Chem. Int. Ed.* **1998**, *37*, 1223. (s) V. Humblot, S. M. Barlow, R. Raval, *Prog. Surf. Sci.* **2004**, *76*, 1. (t) S. Romer, B. Behzadi, R. Fasel, K.-H. Ernst, *Chem. Eur. J.* **2005**, *11*, 4149. (u) M. Lingenfelder, G. Tomba, G. Costantini, L. C. Ciacchi, A. De Vita, K. Kern, *Angew. Chem.* **2007**, *119*, 4576--4579; *Angew. Chem. Int. Ed.* **2007**, *46*, 4492. (v)

N. Katsonis, E. Lacaze, B. L. Feringa, *J. Mater. Chem.* **2008**, *18*, 2065. (w) I. Paci, *J. Phys. Chem. C* **2010**, *114*, 19425. (w) A. Robin, P. Iavicoli, K. Wurst, M. S. Dyer, S. Haq, D. B. Amabilino, R. Raval, *Cryst. Growth Des.* **2010**, *10*, 4516. (x) E. V. Iski, H. L. Tierney, A. D. Jewell, E. C. H. Sykes, *Chem. Eur. J.* **2011**, *17*, 7205. (y) M. M. Knudsen, N. Kalashnyk, F. Masini, J. R. Cramer, E. Lægsgaard, F. Besenbacher, T. R. Linderoth, K. V. Gothelf, *J. Am. Chem. Soc.* **2011**, *133*, 4896. (z) M. Stöhr, S. Boz, M. Schär, M.-T. Nguyen, C. A. Pignedoli, D. Passerone, W. B. Schweizer, C. Thilgen, T. A. Jung, F. Diederich, *Angew. Chem. Int. Ed.* **2011**, *50*, 9982.

29 (a) A. Gesquiere, P. Jonkheijm, A. P. H. J. Schenning, E. Mena-Osteritz, P. Bauerle, S. De Feyter, F. C. De Schryver, E.W. Meijer, *J. Mater. Chem*., **2003**, *13*, 2164. (b) P. Jonkheijm, A. Miura, M. Zdanowska, F. J. M. Hoeben, S. De Feyter, A. P. H. J. Schenning, F. C. De Schryver, E.W. Meijer, *Angew. Chem. Int. Ed*., **2004**, *43*, 74. (c) A. Miura, P. Jonkheijm, S. De Feyter, A.P.H.J. Schenning, E. W. Meijer, F. C. De Schryver, *Small*, **2005**, *1*, 131. (d) A. Gesquiere, P. Jonkheijm, F. J. M. Hoeben, A. P. H. J. Schenning, S. De Feyter, F. C. De Schryver, E. W. Meijer, *Nano Lett*., **2004**, *4*, 1175. (e) M. Linares, P. Iavicoli, K. Psychogyiopoulou, D. Beljonne, S. De Feyter, D. B. Amabilino, R. Lazzaroni, *Langmuir,* **2008**, *24*, 9566.

30 D. G. Yablon, J. S. Guo, D. Knapp, H. B. Fang, G. W. Flynn, *J Phys. Chem. B,* **2001**, *105*, 4313.

31 S. De Feyter, A. Gesquiere, P. C. M. Grim, F. C. De Schryver, S. Valiyaveettil, C. Meiners, M. Sieffert, K. Mullen, *Langmuir*, **1999**, *15*, 2817.

32 (a) F. Stevens, D. J. Dyer, D. M. Walba, *Angew. Chem. Int. Ed.*, **1996**, *35*, 900. (b) P. Qian, H. Nanjo, T. Yokoyama, T. M. Suzuki, *Chem. Lett.*, **1998**, *11*, 1133. (c) P. Qian, H. Nanjo, T. Yokoyama, T.M. Suzuki, K. Akasaka H. Orhui, *Chem. Commun*., **2000**, 2021.

33 Z. Guo, I. De Cat, B. Van Averbeke, J. Lin, G. Wang, H. Xu, R. Lazzaroni, D. Beljonne, E. W. Meijer, A. P. H. J. Schenning, S. De Feyter, *J. Am. Chem. Soc.* **2011**, *133*, 17764.

34 (a) S. De Feyter, A. Miura, S. Yao, Z. Chen, F. Wurthner, P. Jonkheijm, A. P. H. J. Schenning, E. W. Meijer, F. C. De Schryver, *NanoLett.*, **2005**, *5*, 77. (b) A. Gesquiere, P. Jonkheijm, F. J. M. Hoeben, A. P. H. J. Schenning, S. De Feyter, F.

C. De Schryver, E. W. Meijer, *NanoLett.,* **2004**, *4*, 1175. (c) F. J. M. Hoeben, J. Zhang, C. C. Lee, M. J. Pouderoijen, M. Wolffs, F. Wurthner, A. P. H. J. Schenning, E. W. Meijer, S. De Feyter, *Chem.-Eur. J.*, **2008**, *14*, 8579. (d) P. Jonkheijm, A. Miura, M. Zdanowska, F. J. M. Hoeben, S. De Feyter, A. P. H. J. Schenning, F. C. De Schryver, E. W. Meijer, *Angew. Chem., Int. Ed.*, **2004**, *43*, 74. (e) A. Miura, P. Jonkheijm, S. De Feyter, A. P. H. J. Schenning, E. W. Meijer, F. C. De Schryver, *Small,***2005**, *1*, 131. (f) H. Uji-i, A. Miura, A. Schenning, E. W. Meijer, Z. J. Chen, F. Wurthner, F. C. De Schryver, M. Van der Auweraer, S. De Feyter, *ChemPhysChem*, **2005**, *6*, 2389. (g) A. P. H. J. Schenning, E. W. Meijer, *Chem. Commun.*,**2005**, 3245. (h) Q. Chen, T. Chen, D. Wang, H. B. Liu, Y. L.Li, L. J.Wan, *Proc. Natl. Acad. Sci. U.S.A.,* **2010**, *107*, 2769. (i) D. Gonzalez-Rodríguez, P. G. A. Janssen, R. Martín-Rapun, I. De Cat, S. De Feyter, A. P. H. J. Schenning, E. W. Meijer, *J. Am. Chem. Soc.,* **2010**, *132*, 4710. (j) P. Jonkheijm, P. Van der Shoot, A. P. H. J .Schenning, E. W. Meijer, *Science*, **2006**, *313*, 80.

35 S. Yagai, Y. Goto, X. Lin, T. Karatsu, A. Kitamura, D. Kuzuhara, H. Yamada, Y. Kikkawa, A. Saeki, S. Seki, *Angew. Chem. Int. Ed.*,**2012**, *51*, 6643.

36 O. Mitsunobu, Y. Yamada, *Bull. Chem. Soc. Japan,* **1967**, *40*, 2380.

37 W. J. Saletra, H. Xu, T. Vosch, S. De Feyter, D. B. Amablino, *CrystEngComm*, **2011**, *13*, 5578.

38 (a) L. Xu, X. Miao, B. Zha, W. Deng, *Chem. Asian J*., **2013**, *8*, 926. (b) N. T. N. Ha, T. G. Gopakumar, M. Hietschold, *Surf. Sci.,* **2013**, *607*, 68. (c) J. F. Dienstmaier, K. Mahata, H. Walch, W. M. Heckl, M. Schmittel, M. Lackinger, *Langmuir*, **2010**, *26*, 10708. (d) R. Gutzler, T. Sirtl, J. F. Dienstmaier, K. Mahata, W. M. Heckl, M. Schmittel, M. Lackinger, *J. Am. Chem. Soc.*, **2010**, *132,* 5084. (e) J.-H. Kim, K. Tahara, J. Jung, S. de Feyter, Y. Tobe, Y. Kim, M. Kawai, *J. Phys. Chem. C*, **2012**, *116*, 17082. (f) S. Lei, K. Tahara, F. C. De Schryver, M. van der Auweraer, Y. Tobe, S. de Feyter, *Angew. Chem. Int. Ed.*, **2008**, *47*, 2964.

39 D. B. Amabilino, J.-L. Serrano, T. Sierra, J. Veciana, *Mendeleev Commun.* **2004**, 256.

40 S. De Feyter, A. Gesquiére, K. Wurst, D. Amabilino, J. Veciana, F. C. De Schryver, *Angew. Chem. Int. Ed.*, **2001**, *40*, 3217.

41 P. Iavicoli, H. Xu, T. Keszthelyi, J. Telegdi, K. Wurst, B. Van Averbeke, W.J. Saletra, A. Minoia, D. Beljonne, R. Lazzaroni, S. De Feyter, D.B. Amabilino, *Chirality*, **2012,** *24*, 155.

42 M. Lundquist, *ChimicaScripta*, **1971**, *1*, 197.

43 R. M. Kellogg, J. W. Nieuwenhuijzen, K. Pouwer, T. R. Vries, Q. B. Broxterman, R. F. P. Grimbergen, B. Kaptein, R. M. La Crois, E. de Wever, K. Zwaagstra, A. C. van der Laan, *Synthesis*, **2003**, *10*, 1623.

44 K. Ekelund, E. Sparr, J. Engblom, H. Wennerström, S. Engström, *Langmuir,* **1999**, *15*, 6946.

45 A. K. Panda, K. Nag, R. R. Harbottle, F. Possmayer, N. O. Petersen, *Colloids Surfaces A,* **2004**, *247*, 9.

46 B. M. Ocko, M. S. Kelley, A. T. Nikova, D. K. Schwartz *Langmuir* **2002,** *18*, 9810.

47 H. J. Lehmler, M. Jay, P. M. Bummer, *Langmuir,* **2000**, *16*, 10161.

48 S. E. Qaqish, S. G. Urquhart, U. Lanke, S. M. K. Brunet, M. F. Paige, *Langmuir,* **2009**, *25*, 7401.

49 C. A. Hunter, J. K. M. Sanders, *J. Am. Chem. Soc.*, **1990**, *112*, 5525.

50 (a) K. H. Ernst, *Top. Curr. Chem*., **2006**, *265*, 209. (b) V. Demers-Carpentier, G. Goubert, F. Masini, R. Lafleur-Lambert, R., Y. Dong, S. Lavoie, G. Mahieu, J., Boukouvalas, H. L. Gao, A. M. H. Rasmussen, L. Ferrighi, Y. X. Pan, B. Hammer, P. H. McBreen, *Science,* **2011**, *334*, 776. (c) T. E. Jones, C. J. Baddeley, *Surf. Sci.* **2002**, *519*, 237. (d) Y. Wei, K. Kannappan, G. W. Flynn, M. B. Zimmt, *J. Am. Chem. Soc.* **2004**, *126*, 5318. (e) N. Liu, S. Haq, G. R. Darling, R. Raval, *Angew. Chem. Int. Ed.* **2007**, *46*, 7613. (f) W. Xiao, X. Feng, P. Ruffieux, O. Gröning, K. Müllen, R. Fasel, *J. Am. Chem. Soc.* **2008**, *130*, 8910. (g) U. Schlickum, R. Decker, F. Klappenberger, G. Zoppellaro, S. Klyatskaya, W. Auwärter, S. Neppl, K. Kern, H. Brune, M. Ruben, J. V. Barth, *J. Am. Chem. Soc.* **2008**, *130*, 11778. (h) S. Haq, N. Liu, V. Humblot, A. P. J. Jansen, R. Raval, *Nat. Chem.* **2009**, *1*, 409. (i) L. Burkholder, D. Stacchiola, J. A. Boscoboinik, W. T. Tysoe, *J. Phys. Chem. C* **2009**, *113*, 13877. (j) P. Iavicoli, H. Xu, L. N. Feldborg, M. Linares, M. Paradinas, S. Stafström, C. Ocal, B. Nieto-Ortega, J. Casado, J. T. López Navarrete, R. Lazzaroni, S. De Feyter, D. B. Amabilino, *J. Am. Chem. Soc.* **2010**, *132*, 9350. (k) M. E. Cañas-Ventura, K. Aït-Mansour, P. Ruffieux, R.

Rieger, K. Müllen, H. Brune, R. Fasel, *ACS NANO* **2011**, *5*, 457. (l) F. Masini, N. Kalashnyk, M. M. Knudsen, J. R. Cramer, E. Lægsgaard, F. Besenbacher, K. V. Gothelf, T. R. Linderoth, *J. Am. Chem. Soc.* **2011**, *133*, 13910. (m) J. Liu, T. Chen, X. Deng, D. Wang, J. Pei, L. J. Wan, *J. Am. Chem. Soc.* **2011**, *133*, 21010. (n) K. Tahara, H. Yamaga, E. Ghijsens, K. Inukai, J. Adisoejoso, M. O. Blunt, S. De Feyter, Y. Tobe, *Nat. Chem.* **2011**, *3*, 714. (o) I. De Cat, Z. Guo, S. J. George, E. W. Meijer, A. P. H. J. Schenning, S. De Feyter, *J. Am. Chem. Soc.* **2012**, *134*, 3171.

50 K. H. Kim, S. D. Shin, J. H. Lee, S. C. Lee, J. S. Kang, W. Mar, S. P. Hong, H. J. Kim, *Arch. Pharm. Res.*, **2000**, *23*, 230.

51 H. Xu, W. J. Saletra, P. Iavicoli, B. van Averbeke, E. Ghijsens, K. S. Mali, A. P. H. J. Schenning, D. Beljonne, R. Lazzaroni, D. B. Amablino, S. de Feyter, *Angew. Chem. Int. Ed.*, **2012**, *51*, 11981.

51 C. M. Paleos, D. Tsiourvas, *Angew. Chem.Int.*, **1995**, *34*, 1696.

52 M. H. Hatzopoulos, J. Eastoe, P. J. Dowding, S. E. Rogers, R. Heenan, R. Dyer, *Langmuir*, **2011**, *27*, 12346.

53 G. Pelzl, S. Diele, W. Weissflog, *Adv. Mater.*, **1999,** *11*, 707.

54 R. A. Reddy, C. Tschierske, *J. Mater. Chem.***2006**, *16*, 907.